HELLENIC ASTRONOMICAL SOCIETY

PROCEEDINGS

6th HELLENIC ASTRONOMICAL CONFERENCE

Penteli, Athens, Greece, 15-17 September 2003

Sun and Heliosphere

Stars & Stellar Systems

Extragalactic Astronomy

High Energy Astrophysics

Cosmology, Relativity & Relativistic Astrophysics

Galactic Dynamics & Chaotic Dynamical Systems

Infrastructure of Astronomy in Greece

History & Teaching of Astronomy

Edited by

PAUL G. LASKARIDES

ATHENS March 2004

Proceedings of the

6th ASTRONOMICAL CONFERENCE

of Hel.A.S.

PUBLISHED BY
The Hellenic Astronomical Society

PRINTED BY
The Editing Office of the University of Athens, Greece

Hellenic Astronomical Society e-mail: elaset@astro.auth.gr

ISBN 960-88092-0-7

Hellenic Astronomical Society (Hel.A.S.)

Proceedings of the

6th ASTRONOMICAL CONFERENCE

15 – 17 September 2003, Penteli, Athens, Greece

Edited by Paul G. Laskarides

Athens 2004

COUNCIL OF Hel.A.S.

Scientific Organizing Committee

P. Laskarides (Chairman, Univ.of Athens), S. Persides (Thessaloniki U.), C. Goudis (IAA-NOA & Patras U.), N. Kylafis (Crete U.), K. Tsinganos (Athens U.), I. Daglis (NOA Athens), K. Kokkotas(Thessaloniki U.), A. Mastichiadis (Athens U.), L. Vlahos (Thessaloniki U.), N. Voglis (R.C.A.A.M. Academy of Athens), E. Plionis (IAA-NOA Athens), E. Antonopoulou (Athens U.), M. Kontizas (Athens U.),D. Hatzidimitriou (Crete U.), E. Theodossiou (Athens U.), E. Danezis (Athens U.), M. Mathioudakis(Queens U., Belfast) P. Patsis (R.C.A.A.M. Academy of Athens)

Local Organizing Committee

from I.A.A. of the National Observatory of Athens

C. Goudis (chairman)
E. Kontizas, A. Dapergolas, I. Georgantopoulos, P. Boumis, E. Xilouris,
I. Bellas-Velidis, N. Matsopoulos

Sponsors:

National Observatory of Athens
University of Athens
Achaia Clauss, Hewlett Packard
Streamtrade K. Nomikos
Municipality of Kalavryta
Kalavryta Ski Centre

This Volume has been published by the Editing Office of the University of Athens, a generous offer of the Vice-Rector of this University, Professor D. Asimakopoulos

Preface

The 6th Conference of the Hellenic Astronomical Society was held at the Penteli Astronomical station of the Institute of Astronomy and Astrophysics (IAA) of the National Observatory of Athens (NOA), from 15th to 17th of September 2003. This Conference was a high point in the history of Hel.A.S. since it was attended by the largest so far number of participants, especially young ones (graduate or undergraduate students of the Greek and foreign Universities). We all feel that their active participation guarantees the future of our Society. Also, a small number of internationally acclaimed invited speakers added their prestige to the very good work, as a whole, that was presented during the Conference by the Greek members of our Society and by their collaborators here and abroad.

As you probably know, the financial situation of our Society did not permit the edition of the Proceedings and the plan was to have them posted on the electronic site of our Society as it was done with the 5th Conference. It was a pleasant surprise for all of us to hear the Vice-Rector of the University of Athens, Professor Demosthenis Asimakopoulos, during his official address, to promise the editing of the Proceedings by the Editing Office of the University of Athens. This offer made possible the printing of this volume and we all thank him for his offer. This surprise, however, brought some problems to us, since we were not prepared to collect the papers. The speakers were not ready (and some of them not even willing) to write a paper. So the initial deadline of November 15th was extended again and again in our desire to include as many papers in the proceedings as possible. The compilation of the volume was delayed even further since we had to deal with much different kind of files (some of them impossible to convert).

I want to thank all of those who submitted their papers for publication. I am sorry that some of the speakers chose not to write one. For those, I have included in the Proceedings the abstracts they submitted before the Conference.

As President of the Society, I take the opportunity to thank officially for one more time the members of the Scientific Organizing Committee, the members of the Local Organizing Committee as well as all the graduate students working in the I.A.A. of the N.O.A. and the clerks of this Institute for their contribution to the success of this Conference.

Paul G. Laskarides
Editor

Penteli Station of the National Observatory of Athens

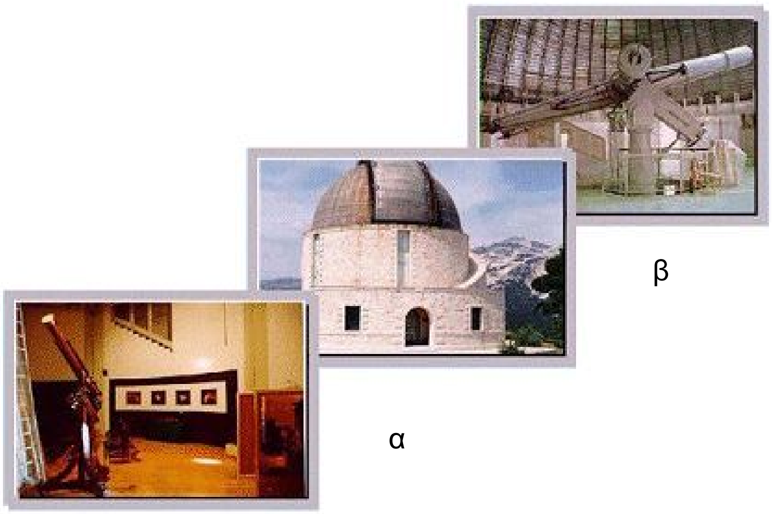

β

α

The Hel.A.S. Invited Speaker Talks and the proceedings of half of the parallel sessions took place at the Visitors' Center of the Institute of Astronomy and Astrophysics of the National Observatory of Athens (α) in the dome and under the operation plateau of the 26" Newall telescope (β).

TABLE OF CONTENTS

ABSTRACTS OF POSTER PAPERS

SESSION II – STARS AND STELLAR SYSTEMS

ABSTRACTS OF POSTER PAPERS

SESSION VI – DYNAMICAL ASTRONOMY AND CHAOTIC DYNAMICAL SYSTEMS

ABSTRACTS OF POSTER PAPERS

SESSION VII – INFRASTRUCTURE OF ASTRONOMY IN GREECE

ABSTRACTS OF POSTER PAPERS

HELAS INVITED SPEAKER

SESSION VIII - HISTORY OF ASTRONOMY TEACHING OF ASTRONOMY

ABSTRACTS OF POSTER PAPERS

HELLENIC ASTRONOMICAL SOCIETY

INVITED REVIEW

UNIVERSAL MAGNETIC RECONNECTION AND CORONAL HEATING

E. N. Parker

Dept. of Physics, University of Chicago

UNIVERSAL MAGNETIC RECONNECTION AND CORONAL HEATING*

E.N. Parker,
Dept. of Physics, University of Chicago

I Introduction

Almost all stars exhibit X-ray emission, implying gases in the temperature range $10^6 - 10^7$ K and densities of $10^8 - 10^{11}$ions/cm^3 in the outer atmosphere. Such hot gases must be trapped in re-entrant magnetic fields, i.e. bipolar or more complicated form, with both ends of the field rooted in the star. Presumably the high temperature arises from some combination of dissipation of magnetohydrodynamic (MHD) waves and the direct dissipation of magnetic free energy through rapid reconnection (flares, microflares, and nanoflares. We point out that rapid reconnection and nanoflaring is expected throughout the bipolar fields through the spontaneous formation of surfaces of tangential discontinuity (TD's) in the interwoven topology of the field lines.

The purpose of this writing is to review the theoretical basis for the spontaneous formation of TD's in magnetic field topologies lacking the special symmetries of the familiar continuous solutions (Parker, 1972, 1988, 1994). The TD's form as the entangled field relaxes to static equilibrium.

II Conditions for Static Equilibrium

Consider the simple case of an initial uniform field B extending in the z-direction through an ideal fluid lacking electrical resistivity between the end plates z = 0 and z = L. The system extends uniformly without bound in the transverse x and y directions. The end plates are without resistivity and can be mapped incompressibly within each surface z = 0 and z = L in any way desired.

At time t = 0 introduce the two dimensional incompressible fluid motion

$$v_x = +vkz\frac{\partial\psi}{\partial y}, v_y = -vkz\frac{\partial\psi}{\partial x}, v_z = 0 \tag{1}$$

where $\psi = \psi(x, y, kzt)$. The end plate z = 0 remains rigid, while the end plate z = L is subject to the mapping velocity described by the stream function $\psi(x, y, kLt)$. The function $\psi(x, y, kzt)$ and its derivatives are bounded, smooth and continuous. The fluid motion described by ψ carries the initial uniform field B into the generally interwoven entangled field

$$B_x = +Bkt\frac{\partial\psi}{\partial y}, B_y = -Bkt\frac{\partial\psi}{\partial x}, B_z = 0 \tag{2}$$

in a time t. This interwoven field is bounded, smooth, and continuous, of course.

It should be emphasized that, apart from being bounded, smooth and continuous, there are no restrictions on the mechanical manipulation of the fluid and field described by ψ. Thus the field topology may take any desired swirling intertwining topological form, although there can be no

---

* HelAS Invited Speaker
Proceedings 6[th] Hellenic Astronomical Society Conference, 15-17 September 2003, Penteli, Athens, Greece

knots, of course, because both ends of each field line remain tied to the end plates. This fact of arbitrary interweaving of the field lines plays a crucial role in considering the possibility of continuous equilibrium solutions.

The fluid motion is shut off after a time t = τ and the end plate z = L subsequently held rigid while the fluid throughout 0 < z < L is released so that the system can relax to the lowest available energy state of **B**. A small viscosity is introduced into the fluid to consume the associated decline of magnetic free energy, so that the field relaxes asymptotically to equilibrium.

To fix ideas, the mechanical manipulation $\psi(x, y, kzt)$ introduces a characteristic scale and correlation length λ in the x and y directions, so that the final equilibrium field has the same transverse correlation length λ. There is no mean transverse field on larger scales, and the statistical properties of the transverse field are homogeneous throughout $-\infty < x, y < +\infty$.

The fluid pressure p is maintained at some uniform value at the end plates. Then since $\mathbf{B} \cdot \nabla p = 0$, it follows that $\nabla p = 0$ throughout. Hence the Maxwell stress tensor

$$M_{ij} = -\delta_{ij} \frac{B^2}{8\pi} + \frac{B_i B_j}{4\pi} \tag{3}$$

in the field $B_i(x_k)$ is in equilibrium with itself, with

$$\frac{\partial M_{ij}}{\partial x_j} = 0 \;, \tag{4}$$

implying the general condition

$$\nabla \times \mathbf{B} = \alpha \mathbf{B}, \tag{5}$$

where the scalar function α represents the degree of swirling or torsion in the magnetic field. It should be appreciated that, in spite of its simple appearance, equation (5) is not linear in **B**, because α depends on **B**.

III Torsion Coefficient α

Before investigating the special properties of equation (5), consider the physical implications of the torsion coefficient α (**r**). The divergence of equation (5) yields $\mathbf{B} \cdot \nabla \alpha = 0$, from which it follows that α (**r**) is constant along each field line. The essential point is that α (**r**) is a measure of the local circulation, or swirl, of magnetic field around each field line, and that is constant along each field line, from z = 0 to z = L. It is curious, then, that the mechanical manipulation $\psi(x, y, kzt)$ of the field lines can vary arbitrarily along the interlacing flux bundles, switching from swirling and spiraling with one helicity to the opposite and back, as many times as desired. How, then, is the fixed swirl represented by α (**r**) to match the variable spiraling of the field line itself? We return to that question in the sequel. For the present, note that the magnetic circulation C(R) around a small circle of radius R centered on a point P on a given field line leads to

$$C(R) = \oint d\mathbf{s} \cdot \mathbf{B}$$

$$=\alpha_P\Phi_P \tag{6}$$

where we have used Stokes theorem, and $\Phi_P = \pi R^2 B_P$ represents the magnetic flux through the circle. It follows that $\alpha_P = C(R)/\Phi_P$. That is to say, the torsion coefficient α represents the local magnetic circulation per unit flux through a small circle centered on the given field line. Note, then, that, with $\mathbf{B}\cdot\nabla\alpha = 0$, the circulation per unit flux has the same value everywhere along the field line.

Another point is that the torque T(R) transmitted along the field across the circle R by the Maxwell stress is also constant along the field line if the radius R varies along the line so that the flux Φ_P through the circle is constant, with

$$\mathrm{T(R)} = \frac{\Phi_P{}^2\alpha_P}{16\pi^2} \tag{7}$$

$$= \frac{\Phi_P C(R)}{16\pi^2} \ . \tag{8}$$

The torque per unit flux depends only on C(R).

.

IV Mathematical Properties of $\nabla\times\mathbf{B} = \alpha\mathbf{B}$

Consider the mathematical properties of equation (5) that lead to the formation of TD's in all but the most carefully selected field topologies. The essential point is that equation (5) is a partial differential equation with mixed characteristics. For instance, the curl of equation (5) can be written as

$$\mathbf{B}\times\nabla\alpha = \nabla^2\mathbf{B} + \alpha^2\mathbf{B} \ . \tag{9}$$

The properties of this equation are determined by the highest derivatives, viz. $\nabla^2\mathbf{B}$, from which it looks like a quasilinear elliptic equation. The equation has two families of complex characteristics. On the other hand, the divergence of equation (5), together with the condition that $\nabla\cdot\mathbf{B} = 0$, yields

$$\mathbf{B}\cdot\nabla\alpha = 0 \tag{10}$$

already noted. It is evident by inspection that α is constant along each field line, which is to say that the field lines represent a family of real characteristics. Thus the field direction may vary discontinuously from one field line to the next. It is evident, from the required continuity of the magnetic pressure $B^2/8\pi$ for equilibirum, that the magnitude of the field must be continuous from one field line to the next. The simplest example is the planar magnetic field with uniform magnitude B,

$$\mathrm{B}_x = \mathrm{B}\cos\theta(z), \mathrm{B}_y = \mathrm{B}\sin\theta(z)$$

where the arbitrary function $\theta(z)$ may be discontinuous in any way desired. The torsion coefficient α is equal to $-\theta'(z)$, which is not defined on the points of discontinuity.

Now the surface of tangential discontinuity – the TD – is the geometrical surface defined by the contact of two regions of continuous field on either side. Hence the TD has no physical content. The field is not defined on the TD nor is any field gradient defined.

V Simplifying the Problem

To investigate the final asymptotic equilibrium solution into which the magnetic field of equation (2) relaxes, it is convenient to simplify the problem through the uniform dilatation of the system in the z-direction by some large factor Q (>>1). This preserves the swirling topology of the field described by equation (2) and has no effect on the z-component of that field, while it expands the transverse components B_x and B_y, reducing them by the factor $\varepsilon \equiv 1/Q$<<1. The magnetic field can then be written as $\varepsilon \mathrm{B} b_x, \varepsilon \mathrm{B} b_y, \mathrm{B}(1+\varepsilon b_z)$, where the dimensionless field b_i is of the order of unity. Stretching the field pattern in the z-direction reduces $\partial/\partial z$ by the factor ε, so that $\partial/\partial z$ is small $O(\varepsilon)$ compared to $\partial/\partial x$ and $\partial/\partial y$. Write $\varsigma = \varepsilon z$ so that $\partial/\partial\varsigma$ is of the same general order as $\partial/\partial x$ and $\partial/\partial y$. The three components of equation (5) and the divergence condition reduce to

$$\varepsilon \frac{\partial b_y}{\partial \varsigma} - \frac{\partial b_z}{\partial y} = -\alpha b_x, \tag{11}$$

$$\varepsilon \frac{\partial b_x}{\partial \varsigma} - \frac{\partial b_z}{\partial x} = +\alpha b_y, \tag{12}$$

$$\varepsilon \left(\frac{\partial b_y}{\partial x} - \frac{\partial b_x}{\partial y} \right) = +\alpha (1 + \varepsilon b_z), \tag{13}$$

$$\frac{\partial b_x}{\partial x} + \frac{\partial b_y}{\partial y} + \varepsilon \frac{\partial b_z}{\partial \varsigma} = 0, \tag{14}$$

respectively. Equations (11) and (12) indicate that b_z is small $O(\varepsilon)$ compared to b_x and b_z. This reflects the fact that the Maxwell stresses in the transverse field components, of the general order of $\varepsilon^2 B^2/8\pi$, are balanced by the perturbation $2\varepsilon B^2 b_z/8\pi$ in the pressure of the z-component of the field. So, neglecting terms $O(\varepsilon^2)$ compared to one, equation (14) implies that b_x and b_y can be described in terms of a vector potential or stream function ϕ,

$$b_x = +\frac{\partial \phi}{\partial y}, b_y = -\frac{\partial \phi}{\partial x}. \tag{15}$$

Equation (13) requires that α be small $O(\varepsilon)$, so write $\alpha = \varepsilon a$. Equation (13) becomes

$$a = -\left(\frac{\partial^2 \phi}{\partial x^2} + \frac{\partial^2 \phi}{\partial y^2} \right). \tag{16}$$

Equation (10) can then be written

$$\frac{\partial a}{\partial \varsigma} = \frac{\partial \phi}{\partial x}\frac{\partial a}{\partial y} - \frac{\partial \phi}{\partial y}\frac{\partial a}{\partial x}. \tag{17}$$

It was pointed out by Van Ballegooijen (1985) that equations (15) – (17) have exactly the same form as the vorticity equations for the 2D flow of an inviscid incompressible fluid. For in that case the velocity can be written in terms of a stream function Ψ ,

$$v_x = +\frac{\partial \Psi}{\partial y}, v_y = -\frac{\partial \Psi}{\partial x} , \tag{18}$$

so that the vorticity is

$$\omega = \frac{\partial v_y}{\partial x} - \frac{\partial v_x}{\partial y}$$

$$= -\left(\frac{\partial^2 \Psi}{\partial x^2} + \frac{\partial^2 \Psi}{\partial y^2} \right). \tag{19}$$

The vorticity equation reduces to $d\omega / dt = 0$, or

$$\frac{\partial \omega}{\partial t} = \frac{\partial \Psi}{\partial x}\frac{\partial \omega}{\partial y} - \frac{\partial \Psi}{\partial y}\frac{\partial \omega}{\partial x} . \tag{20}$$

Thus the torsion coefficient $a(x, y, \varsigma)$ varies with ς along the field in exactly the same way that the vorticity $\omega(x, y, t)$ varies with time.

The essential point is that the specification of *a* at any surface $\varsigma = constant$ projects along the field lines and determines *a* for all ς , in the same way that specification of the vorticity on any surface *t* = *constant* projects along the stream lines and determines ω for all *t*. The torsion coefficient *a* evolves along the field in the same way as the vorticity evolves with the passage of time, about which we have some knowledge (cf. Kraichnan and Montgomery, 1980).

VI Limitations of Continuous Solutions

Consider the limitations of continuous solutions of equation (17) when confronted with the arbitrary succession of field topologies of equation (2). The most conspicuous contradiction arises when the swirling pattern represents the braiding of three flux bundles. That involves each bundle wrapping successively first one way and then the other way about each of its two companion bundles. The two opposite wrappings in a given bundle are identical except for the sign of the helicity of the wrapping. However, equations (2), (10), and (17) do not allow the opposite sign. So there are no continuous solutions for any interweaving of the field lines involving anything like the braiding topology, in which the wrapping of a flux bundle around neighboring flux bundles changes sign anywhere along the field. On the other hand, the wrapping topology imposed by the mechanical manipulation $\psi(x, y, kzt)$ is free to reverse the helicity in any way desired.

Another way to demonstrate the contradiction is to imagine special extended patterns of field line wrapping, with topologies that vary along the field in ways that cannot be duplicated by solutions of the 2D vorticity equation. For instance, suppose that the swirling and wrapping, prescribed by $\psi(x, y, kzt)$, has the transverse correlation length λ , as already mentioned. That is to say, the local topological pattern, prescribed arbitrarily by $\psi(x, y, kzt)$, involves a strong swirling eddy with characteristic transverse scale λ and a scale λ / ε along the field. This eddy pattern is then repeated *m* times (*m*>>1) along the field for a distance $O(m\lambda / \varepsilon)$, from $z = 0$ to $z = O(m\lambda / \varepsilon)$.

Suppose then that an unrelated eddy topology begins at $z = O(m\lambda / \varepsilon)$ and is repeated *m* times from $z = O(m\lambda / \varepsilon)$ to $z = O(2m\lambda / \varepsilon)$. Then another eddy topology takes over and is repeated *m* times, from $z = O(2m\lambda / \varepsilon)$ to $z = O(3m\lambda / \varepsilon)$, etc., so that n unrelated arbitrary swirling topological patterns are successively imposed across the distance *L*, where, then, $nm\lambda / \varepsilon = L$.

The footpoints of the field, at $z = 0$ and $z = L$, are then held fixed and the field is allowed to relax to the lowest available energy state, preserving the topology of the field lines. The final asymptotic equilibrium is described by the "vorticity" equation (17) or (20). It should be recognized that the relaxation to equilibrium involves torsional Alfven waves propagating back and forth along the field lines as each eddy pattern tugs on its neighbors. Thus a twist in one eddy pattern may unwind and extend itself along the entire field, from z = 0 to z = L, or it may be blocked by the interlacing of the neighboring patterns, so that it extends only a short distance into the next pattern. In either case the interior of each region $O(m\lambda / \varepsilon)$ remains more or less periodic on the basic scale λ / ε.

Now two questions come immediately to mind. The first is whether the vorticity equation has continuous solutions that accommodate the approximate repetition *m* times of an arbitrarily designed swirling eddy topology. The second question is whether, having passed through *m* repetitions of one arbitrarily chosen swirling pattern, the solution of the vorticity equation can switch to another arbitrarily specified and unrelated swirling eddy pattern. Recall that the first pattern repeats *m* times as it projects along the field lines for the distance $O(m\lambda / \varepsilon)$ and then must anticipate the next arbitrary eddy pattern, which, somehow it repeats m times, before switching to yet another arbitrarily specified swirl, etc.

It would appear that the answer to the first question is negative in almost all cases, because only special vorticity patterns repeat themselves. Any given pattern tends to be unstable, evolving into other forms. A truly stationary pattern requires $\omega = \omega(\Psi)$ or $a = a(\phi)$. So repetition m times seems to be out of the question for a eddy of arbitrary topology.

The answer to the second question is generally negative too, because the arbitrary vorticity pattern (of which there are infinitely many choices) throughout out one interval $O(m\lambda / \varepsilon)$ cannot very well anticipate the unrelated pattern (of which there are infinitely many choices) in the next interval $O(m\lambda / \varepsilon)$.

In fact the long term solutions of the 2D vorticity equation have been investigated at some length (see Kraichnan and Montgomery, 1980, and references therein). The essential point is that the solutions created by an initial pattern of eddies with specified correlation length λ, corresponding to wave number k_0, take on the properties of turbulence, with a cascade of kinetic energy to small wave numbers and enstrophy to large wave numbers from the initial k_0. This is quite unlike the arbitrary sequence of interweaving patterns all with basic wave number k_0 imposed by $\psi(x, y, kzt)$.

VII Resolving the Contradiction

It would appear that a complex field line topology arbitrarily imposed by $\psi(x, y, kzt)$ cannot be represented by continuous solutions of the equilibrium vorticity equation (17) or (20). On the other hand, a stable equilibrium exists because all the field lines are tied at both ends to the end plates, $z = 0$ and $z = L$. The tension along each field line shortens the lines as much as the interwoven topology allows without cutting across other lines. And there we find the lowest available energy state, i.e. a stable static equilibrium.

The contradiction arises from the invariance of the torsion coefficient α (representing the local circulation or swirl along each field line as prescribed by equation (10)), while the swirling topology of the field lines passes through diverse unrelated patterns along the way (Parker, 1972, 1994). Resolution of the contradiction arises through introduction of an additional degree of freedom in the torsion of the field, viz. the appearance of the surface of tangential discontinuity, or TD, across which there is arbitrary torsion, i.e. the field direction differs by a finite amount on opposite sides of the TD. The change in field direction across a TD is not restricted by equation (10) because the TD is only the geometrical surface of contact between two regions of continuous field, as already noted. Hence the TD contains no magnetic field and α is undefined. So equation (10) cannot apply, and the rotation of the field direction across the TD is not restricted. Hence, the TD resolves the contradiction, and we expect to find TD's in any equilibrium field configuration in which there is a change in the topological swirl of the field anywhere along the field.

The general statement is that in almost all field line topologies, static equilibrium involves internal TD's. There is no known way at present to define just how simple the field topology must be to avoid a TD. However, the set of all topologies necessary and sufficient for entirely continuous fields is obviously of measure zero compared to the set of all the more complex field line topologies. The *optical analogy* for the field lines in an equilibrium field (Parker, 1991, 1994) illustrates sufficient conditions for the formation of a TD, thereby helping to determine at what point in topological complexity the TD's occur.

VIII The Optical Analogy

Consider a magnetic field described by a scalar potential function $\varphi(\mathbf{r})$, so that

$$B_i = +\frac{\partial \varphi}{\partial x_i} \tag{21}$$

The equation for the field lines can be written

$$\frac{dx_i}{ds} = \frac{1}{B}\frac{\partial \varphi}{\partial x_i}, \tag{22}$$

where ds is an element of arc length along the field line, and B is the magnitude of the field, $B^2 = (\nabla \varphi)^2$. Note, then, that the eikonal equation for the ray paths of a wave $\exp i\beta(\mathbf{r})$ in an index of refraction $n(\mathbf{r})$ is

$$\frac{dx_i}{ds} = \frac{1}{n}\frac{\partial \beta}{\partial x_i}, \tag{23}$$

(cf Born and Wolf, 1975). It is evident from equations (22) and (23) that the field lines follow the same path as the ray paths in an optical medium with index of refraction *n* proportional to the magnitude *B*. Thus, knowing the magnitude $B(\mathbf{r})$ makes it possible to compute the path of a field line connecting any two points 1 and 2 without further information about the field, e.g. the three field components necessary to compute the path from equation (22).

The force-free field described by equation (5) is not curl free and cannot be written as the gradient of a scalar function. However, consider the two dimensional space represented by a single flux surface $\Sigma(\Gamma)$ defined by any arbitrary curve Γ extending across the field B_i. The magnetic field in the two dimensional space Σ has no curl, because if it had a curl, that curl would be perpendicular to Σ. However, the equilibrium equation (5) asserts that $\nabla \times \mathbf{B}$ has no component perpendicular to Σ. Hence, the field in the two dimensional space Σ is curl free and can be written as the gradient of a scalar, as in equation (21). It follows, therefore, that each field line in Σ follows the same path as an optical ray path in a medium with index of refraction proportional to the field magnitude $B(\mathbf{r})$. Not only does this provide an elementary physical picture of the field line paths, but it also provides the handy mathematical formalisms developed for geometrical optics, e.g. Fermat's principle, that the path between points 1 and 2 are given by the extrema of $\int dsB$, or

$$\delta \int dsB(\mathbf{r}) = 0 . \tag{24}$$

Thus Euler's equations apply. In the simple case that Σ is a flat surface throughout the region between points 1 and 2, use the local Cartesian coordinates x and y, so that $ds = \left[(dx)^2 + (dy^2)\right]^{1/2}$. Euler's equation can then be written

$$\frac{y''}{1+y'^2} + y' \frac{\partial \ln B}{\partial x} - \frac{\partial \ln B}{\partial y} = 0 \tag{25}$$

for the ray path $y = y(x)$, choosing x to be the independent variable. A variety of examples of field line refraction can be found in the literature (Parker, 1994).

IX Creation of a TD

Consider the effect on the field lines in a flux surface Σ arising from a localized maximum in *B*. The two points 1 and 2 lie on a line passing straight across the maximum. Let point 1 be a distance h_1 from the maximum and point 2 a distance h_2 on the opposite side of the maximum. With the dimension D of the localized maximum small compared to h_1,h_2, it is readily apparent from Fig. 4a that the total distance s_1+s_2 to pass around the maximum, rather than cutting straight across, is

$$s_1 + s_2 = \left(D^2 + h_1{}^2\right)^{1/2} + \left(D^2 + h_2{}^2\right)^{1/2}$$

$$\cong h_1 + h_2 + \frac{D^2}{2}\left(\frac{1}{h_1} + \frac{1}{h_2}\right) + \dots .$$

The optical path length is then the ambient field magnitude *B* multiplied by this distance. Denoting the field magnitude throughout the maximum by $B + \Delta B$, the optical path length across the center of the maximum is approximately

$$B[(h_1 - D) + (h_2 - D)] + 2(B + \Delta B)D = B(h_1 + h_2) + 2\Delta BD\,.$$

The field line passes across the maximum for sufficiently small ΔB, but passes around to the side of the maximum when that optical path length is less than the path across the maximum, for

$$\frac{\Delta B}{B} > \frac{D}{4}\left(\frac{1}{h_1} + \frac{1}{h_2}\right)\,. \tag{26}$$

In the simple case that $h_1 = h_2 = h$, the requirement for avoiding the maximum is

$$\frac{\Delta B}{B} > \frac{D}{2h}\,. \tag{27}$$

For a localized region of increased field strength ($D<<h$) only a slight fluctuation ΔB in the field strength is required.

The result of field lines passing around the maximum is a gap in the flux surface Σ Neighboring flux surfaces are similarly affected, resulting in a gap through a finite thickness of field. The continuous fields on either side of the layer of gapped field push through the gap and meet, forming a TD where they meet because they are not generally parallel to each other. A number of examples can be found in the literature (Parker, 1994, Chapter 7).

X Conclusion

Magnetic fields are generated in stars and galaxies by disordered convection, so that the field line topology is untidy, i.e.interwoven in arbitrary and complex ways. Equilibrium is closely approached in the magnetic fields in the tenuous outer atmospheres of stars, where the Alfven speed is large compared to the rate of convective deformation of the fields, so that a close approach to equilibrium occurs.

There is always some slight electrical resistivity, so the system cannot relax all the way to the idealized tangential singularities required for equilibrium. As a result the fields are continually pushed toward the ideal singularities by the Maxwell stresses, but the increasing field gradients and electric current density are limited by the nonvanishing resistivity. This is, of course, the essence of rapid reconnection. We expect that resistive instabilities develop along the incipient TD's, which then play host to local regions of rapid reconnection and nanoflaring. It would appear that this is a major contribution to heating the X-ray emitting portions of the solar corona, and, by inference, the X-ray coronas of other stars.(Parker, 1983,1988,1994, Chapter 11).

References

Born, M. and Wolf, E. 1975, *Principles of optics*, Pergamon Press, Oxford, Fifth edition, chapter 3.

Kraichnan, R. H. and Montgomery, D. 1980, Two dimensional turbulence, *Rep. Prog. Phys.*, **43**, 547-619.

Parker, E. N. 1972, Topological dissipation and the small-scale fields in turbulent gases, *Astrophys. J.*, **174**, 499-510.

Parker, E. N. 1983,Magnetic neutral sheets in evolving fields. II Formation of the solar corona, *Astrophys. J.*, **264**, 642-647.

Parker, E. N. 1988, Nanoflares and the solar X-ray corona, *Astrophys. J.*, **330**, 474-479.

Parker, E. N. 1991, The optical analogy for vector fields, *Phys. Fluids B*, **3**, 2652-2659.

Parker, E.N. 1994, *Spontaneous current sheets in magnetic fields*, Oxford University Press, New York.

Van Ballegooijen, A. A. 1985, Electric currents in the solar corona and the existence of magnetostatic equilibrium, *Astrophys. J.*, **298**, 421-430.

Session I

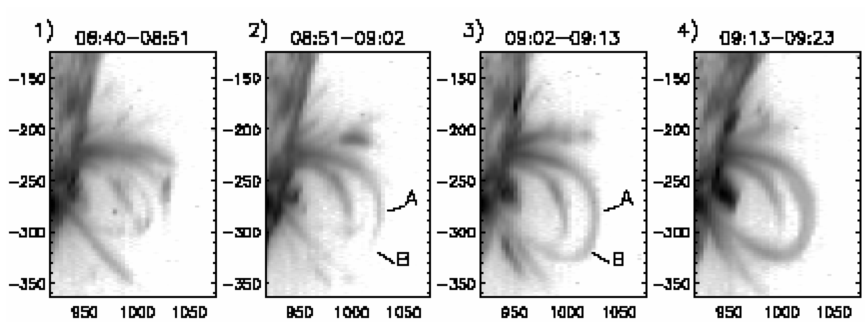

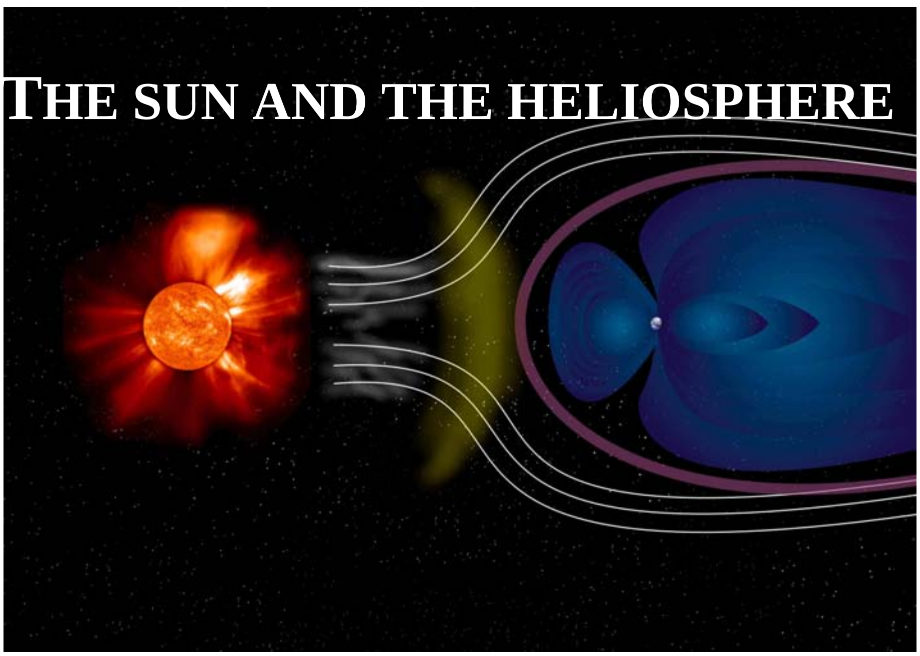

Conveners: I. Daglis and L. Vlahos

STATISTICAL PROPERTIES OF FLARING AND SUB-FLARING ACTIVITY IN THE SOLAR ATMOSPHERE*

Manolis K. Georgoulis
The Johns Hopkins University Applied Physics Laboratory, 11100 Johns Hopkins Rd., Laurel, MD 20723,

ABSTRACT: We review the observational, theoretical, and numerical efforts to interpret the statistical behavior of solar flares and sub-flares, and their role to coronal heating. The observed X-ray flares cannot heat the corona. The role of smaller-scale events is still inconclusive, although very recent observational evidence may shed light to the controversy. Statistical and classical modeling reproduces the statistics of large flares. Part of these models also predict a statistical behavior for the small-scale events consistent with that of Parker's nanoflares if these events indeed heat the solar corona.

1. INTRODUCTION

Solar flares are spectacular explosive phenomena in the solar active-region atmosphere that release enormous amounts of energy (10^{29} *erg* - 10^{32} *erg*) in very short timescales, of the order of *min*. The source of the released energy is thought to be the magnetic field in the solar atmosphere which, via a process called *magnetic reconnection*, is able to rearrange rapidly and release explosively magnetic energy stored gradually on much larger timescales. The released magnetic energy in solar (and stellar) flares accounts for three fundamental processes: *(i)* Radiation spanning over much of the electromagnetic spectrum, *(ii)* particle acceleration, and *(iii)* heating of the stellar atmospheres (see the pedagogic descriptions of Priest 1982; Benz 1993; Schrijver & Zwaan 2000, and references therein). In this review we will focus on the third process, known for the Sun as the *coronal heating* problem, whose proper understanding remains elusive for more than sixty years. Coronal heating is probably the most challenging problem of modern solar physics. The Sun maintains an effective photospheric "surface" temperature of ~ 5800 *K*. After a brief decrease to a minimum of ~ 4300 *K* shortly above the photosphere, the temperature increases from gradually to exponentially to reach an average of ~ $2 \, x \, 10^6$ *K* in the quiet, non- flaring corona (Withbroe & Noyes 1977). The source of this enormous energy input, estimated to vary between 5×10^5 $erg \, cm^{-2} s^{-1}$ and 10^7 $erg \, cm^{-2} s^{-1}$, is largely unknown. Estimations of the photospheric Poynting flux injected to the corona from the solar interior indicate that the deposited power is more than enough to sustain a hot corona, the problem being how to effectively dissipate this energy (e.g. Heyvaerts 2000). An established result is that solar flares are too few to provide the required power, although the local plasma temperature in the flaring corona may easily reach 1 - 2×10^7 *K*. This has driven researchers to consider other heating processes, such as wave heating (Narain & Ulmschneider 1996 for a review). These mechanisms are also problematic, however, and hence they cannot be considered the main power providers in the corona (Parker 1991). The purpose of this review is to focus on energy dissipation events and their contribution to coronal heating. We will show that coronal heating through flares is essentially a *statistical* problem. Synoptic observations of large numbers of flares reveal a strongly preferential statistical behavior. The origin and the cause of this behavior will be the

---

* Main Session Invited Review

Proceedings 6th Hellenic Astronomical Society Conference, 15-17 September 2003, Penteli, Athens, Greece

main aims of the following sections. Moreover, we will discuss specific requirements that need to be fulfilled if flares are to account for coronal heating.

2. OBSERVATIONS AND PROPERTIES OF FLARES AND SUB-FLARES

The prevailing viewpoint regarding the onset of a flare is that magnetic reconnection takes place in highly unstable current concentrations, called *current sheets*, which are formed in areas of sharp discontinuities in the magnetic topology. The post-flare configuration includes a canceled, or disrupted, current sheet, or ensemble of current sheets, with less stored energy than in the pre-flare stage. The energy difference is the dissipated energy during the flare. The spatial dimensions of current sheets are thought to

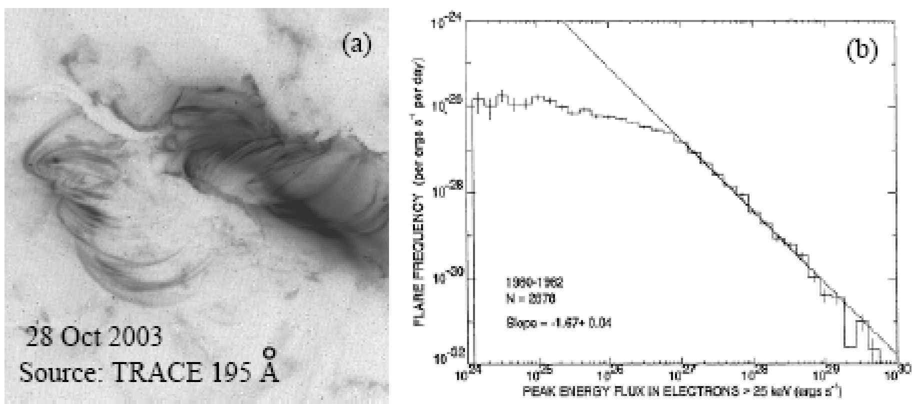

Figure 1. (a) *View of the recent X-17 flare of October 28, 2003 (the third largest X-flare on record).* (b) *Frequency distribution of the peak flare energies for* 2878 *events recorded by SMM/HXRBS between 1980 and1982 (Crosby et al. 1993)*

be very small, of the order of a few *m* to a few *km*, or even a few *cm* (Kraichnan 1965)! These spatial scales are well beyond the resolution of the present, or the conceived in the near future, observing instruments. Therefore, flares are detected by their consequences, i.e. the intense emission in various wavelengths. The flare emission "illuminates" the corresponding magnetic topology, known to consist of *coronal magnetic loops*. This is a topology of immense *complexity* (Fig. 1a). Excellent reviews on the morphology of the flaring volume can be found in Švestka et al. (1992) and Aschwanden (2002). Besides the morphological complexity in the flaring volume, any measured expression of the "size" of a flare, such as the flare duration, peak luminosity, or total released energy, is found to obey well-defined statistical laws. In Fig. 1b we show the differential distribution function of a large number of X-ray peak flare energies, compiled by Crosby et al. (1993). We notice that a power-law of the form

$$\frac{dN(E)}{dE} \propto E^{-\alpha}, \tag{1}$$

where E is the peak flare energy, $N(E)$ is the number of flares with energy between E and $E \pm dE$, and α is the power-law index, extends over three orders of magnitude in E. The deviation from the power law in the low-energy part of the distribution is because of the decreased instrumental sensitivity for small flares, which results in an under-sampling of these events. Deviations are also possible in the high-energy part of the distribution because of poor statistics, or due to an upper limit in the flare energies (Kucera et al. 1997). Nevertheless, robust, extended power laws in the distributions of the total energy, peak energy, duration, rise and decay times of flares have been found in numerous studies (e.g., Lin et al. 1984; Dennis 1985; Crosby et al. 1993; Lee et al. 1993; Biesecker 1994; Bromund et al. 1995; Crosby et al. 1998; Georgoulis et al. 2001). The above parameters are also interrelated via power laws. Power-law indices α appear to be remarkably robust, ranging between [1.4, 1.6], [1.6, 1.95], and [2.1, 2.5] for the total energy, the peak energy, and the total duration of flares, respectively. Another observational result, although not as robust and a subject of debate, is that the "waiting times", i.e. the quiescent times between flares, obey time-dependent Poisson statistics (Wheatland & Litvinenko 2002 and references therein). This implies that flares are nearly independent events in time, although one should not rule out sporadic cases of *sympathetic flaring* between adjacent magnetic con- figurations. The scaling laws in the distribution functions of flare energies offer an easy way to calculate the total flaring contribution to coronal heating, by integrating distributions similar to the one of Fig. 1b. It is found that the total flaring energy falls short by about an order of magnitude to explain the hot corona (Longcope & Noonan 2000 and references therein). Flares are massive energy providers, but at the same time they are statistically unimportant because of their small occurrence frequencies. As the number of flares is inversely proportional to their energy (Fig. 1b), interest was soon placed to small flares, also called *microflares*, with the hope that their large numbers might make these events statistically significant for coronal heating. Microflares with energies $\geq 10^{27}$ *erg* are observed in both X-rays and the extreme ultraviolet (EUV). Assuming that a power law of the form (1) in the flare energies holds in the interval |*Emin,Emax*|, then the total flaring energy contribution is

$$EN(E) \propto \frac{1}{2-a}\left(\frac{1}{E_{max}^{a-2}} - \frac{1}{E_{min}^{a-2}}\right) \tag{2}$$

From Eq. (2) it is evident that for microflares and small-scale events to be statistically significant, the power-law index α has to be > 2 (Hudson 1991). For α < 2 and *Emax* >> *Emin* one finds

$$EN(E) \simeq E_{max}^{2-a},$$

so large flares are the major energy providers. Since large flares are statistically unimportant, it is meaningless to examine the contribution of microflares.
For α > 2 and *Emax* >> *Emin*, however,

$$EN(E) \simeq \frac{1}{E_{min}^{a-2}},$$

which implies that the bulk of the thermal energy comes from small-scale events. The observed power-law index $\alpha \sim 1.5$ is well below 2, so if the distribution of Fig. 1b extends to smaller energies with the same power-law index, then coronal heating cannot be achieved by flares. If, however, the power law steepens as energy decreases, then small flares might heat the corona. Georgoulis & Vlahos (1998) and Georgoulis (2000), for example, have shown that for the observed distribution of Fig. 1b a power law in the undetected low-energy part extending between 10^{24} *erg* and 10^{27} *erg* with an index $\alpha \sim 3$ is able to account for the energy deficit.

E. N. Parker, with a long list of seminal papers and an illustrative book (Parker 1979) contributed substantially to our understanding of solar magnetic fields and their instabilities.

The filamentary nature of the emerged magnetic fields in the solar atmosphere, as well as the tangling of the field lines due to random photospheric shuffling of the magnetic footpoints may lead to frequent *tangential discontinuities* in the magnetic field configuration (Parker 1972, 1983, 1988, 1989, 1991). When these discontinuities are relaxed, they give rise to

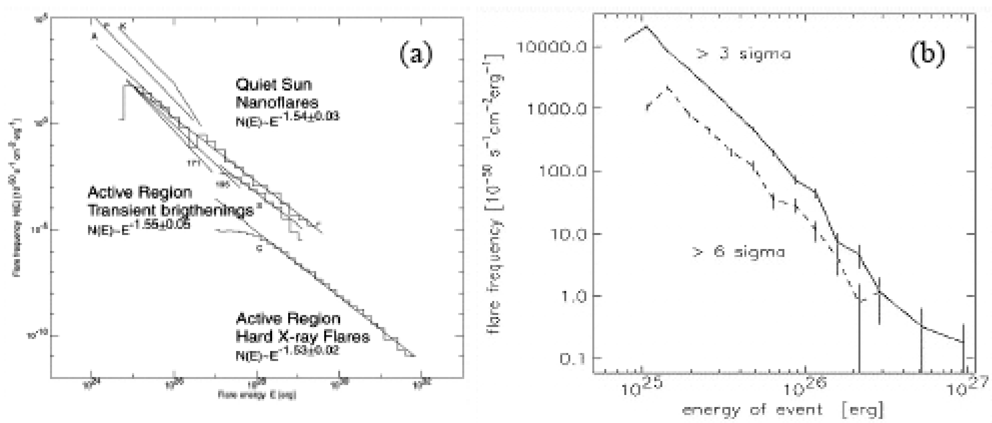

Figure 2. *The controversy in nanoflare statistics:(a)The results of several studies compiled by Aschwanden & Parnell (2002). In all cases, α < 2. (b) The results of Benz & Krucker (2002), where 2.3 < α < 2.6.*

elemental flaring events, called *nanoflares*, with energy content ~ 10^{24} *erg* and duration ~ 100 *s*. Parker (1988) estimated that a number of ~ 10^5 nanoflares might be present anywhere in the corona at any given time. The total amount of the released energy can then sustain a hot corona. In essence, Parker argued that swarms of nanoflares may be the building blocks of the entire X-ray corona.

2. SEARCHING FOR NANOFLARES: A HEATED DEBATE

Parker's predictions and Hudson's (1991) suggested nanoflare statistics sparked an unprecedented "hunt" for these tiny events. Theoretically, these events should be essentially thermal, lacking a hard X-ray component, so their contribution to the coronal energetics should be centered around heating. The latest X-ray and EUV imagers, such as *Yohkoh*/SXT, SOHO/EIT, and TRACE provided numerous observations of bright points and transient brightenings, which served as nanoflare candidates. The limit of detectable energies by the end of 1990s was pushed down to a few 10^{24} *erg* - 10^{25} *erg*. Numerous studies focused on the statistics of the above X-ray and EUV events. This research effort is ongoing and far from being completed, but its current status can be summarized as follows:

(1) The observed X-ray events do not obey "nanoflare statistics" (Shimizu 1995; Lee et al. 1995; Feldman et al. 1997). Their statistics are essentially identical to those of the large hard X-ray flares.
(2) The behavior of the observed EUV events is unclear: Several studies suggest power laws similar to those of flares (Berghmans et al. 1998; Aschwanden 1999; Aschwanden et al. 2000; Aschwanden & Parnell 2002; see Fig. 2a), while others find steep power laws with indices α > 2 (Krucker & Benz 1998; Parnell & Jupp 2000; Aletti et al. 2000; Benz & Krucker 2002; see Fig. 2b).

In terms of heating power, let it be emphasized that the required thermal energy input is yet to be explained. It cannot be explained by the observed X-ray events, while the observed EUV events, independently of their statistics, are not frequent enough to heat the corona. If $\alpha > 2$ for EUV events, we need to examine the contribution of even smaller energies. Some authors, such as S. Krucker and A. Benz, suggest that this might be the case, while others, such as M. Aschwanden, coin the above results "the end of the nanoflare story" (Trimble & Aschwanden 2003). Aschwanden and collaborators attribute the steep power laws to a temperature bias due to the narrow temperature filters of the

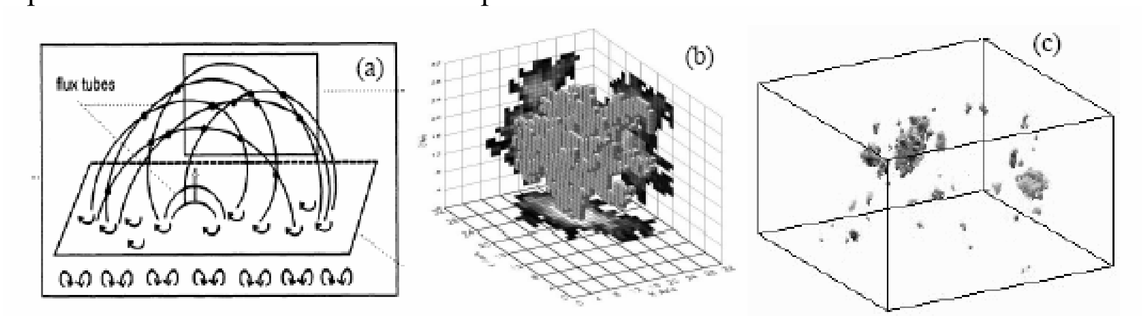

Figure 3. *Concepts of the SOC Statistical Flare models:* (a) *The external driver (Anastasiadis & Vlahos 1994).* (b) *Fractal avalanche triggered by a domino effect in the SOC state (McIntosh & Charbonneau 2001).* (c) *Scale-invariance of avalanche sizes (from the Statistical Flare model of M. Georgoulis & L. Vlahos).*

EUV instruments (Aschwanden & Charbonneau 2002), and to the neglected fractality of the emitting volume (McIntosh & Charbonneau 2001). Benz and Krucker argue that the previous authors impose selection criteria that lead to severe under-sampling of the low-energy events, thus suppressing the actual statistics. Georgoulis et al. (2001) performed a sampling test on a *deka - keV* flare data set and found that when focusing solely on low-energy events the power-law index is significantly steeper than the one obtained when focusing solely on high-energy events. They concluded that selective under-sampling is an important effect and that power laws may steepen as the energy decreases, thus fulfilling the nanoflaring requirements for coronal heating. Nenertheless, much more effort is required before any definitive conclusion is to be reached.

3. THE MODELERS' RESPONSE: STATISTICAL FLARE MODELS

The new trends in flare research triggered a rigorous parallel effort in modeling flares and dissipative phenomena in the solar atmosphere. The "traditional"magnetohydrodynamical (MHD) simulations were found inadequate to address the statistical problem because they are too time-consuming to produce sufficient statistics and they simulate very localized areas. A new array of flare models, hereafter called *Statistical Flare models*, were developed. These models include an early stochastic energy build-up and release model (Rosner & Vaiana 1978), the Self-Organized Critical (SOC), or avalanche, models (Georgoulis 2000; Charbonneau et al. 2001 for a review), the "logistic" avalanche model (Aschwanden et al. 1998), percolation models (e.g. MacKinnon et al. 1996), and models of reconnecting current sheets and large-scale reconnection (e.g. Litvinenko 1996, Wheatland & Craig 2003). Of particular interest and arguably the most successful Statistical Flare models are the SOC (avalanche) models, embedded in discrete cellular automata lattices. Based on the concept of Self-Organized Criticality (Bak 1996 for a review), these models both reproduced the observed statistical properties of flares and provided a physical understanding of flare onset. In the SOC view, solar active regions are externally driven non-linear dynamical systems. The driver of the dynamics is the random photospheric shuffling and the emergence of new magnetic flux from the solar interior (Fig. 3a). As the system evolves, energy is gradually stored into a complex network of *minimally stable* configurations. Each structure with minimal stability releases its stored energy when an instability is locally triggered. Instabilities occur when a *critical threshold* is crossed. If a single instability sets in, then further instabilities are triggered in the network of minimally unstable volumes via a *domino effect*, giving rise to an avalanche of energy release (Fig. 3b). The energy release process is fragmented, with a small timescale compared to the timescale of energy storage, like in actual solar flares (Vlahos 1994). The system is gradually selforganized through a sequence of meta-stable states into a final, statistically stable SOC state, where events of all sizes are expected (Figure 3c). The system's self-organization and the critical behavior with respect to the critical threshold are responsible for the scale-invariant, self-similar statistics of the results. The outcome is intermittency and extended power laws in the energy release process. Power laws are indicative of a common triggering behavior of events, independently from the events' size. Selforganization in solar active regions may be the outcome of the fully developed turbulence thought to be acting in the solar atmosphere (Biskamp 1993 for a review), while the critical threshold might refer to a critical value of the current density in current sheets (Einaudi et al. 1996), the excession of the Parker angle in tangential discontinuities (Parker 1983), or strong field gradients required for three-dimensional magnetic reconnection (Priest et al. 2003).

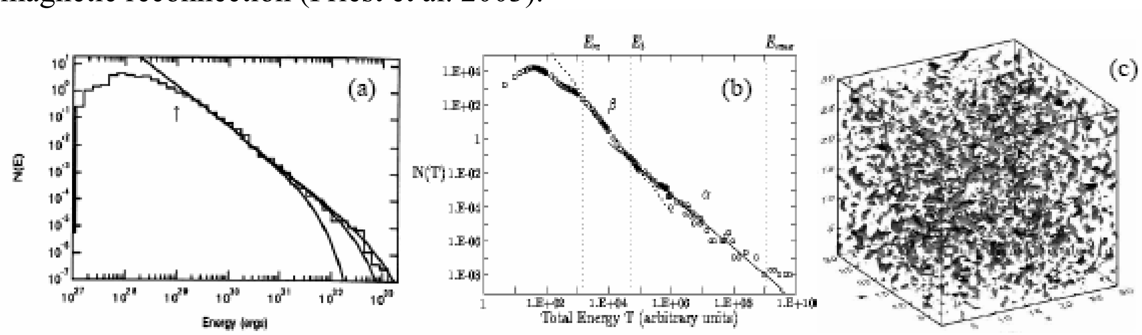

Figure 4. *Results of the SOC Statistical Flare models:* (a) *Comparison with flare observations (Lu et al. 1993). The histogram refers to the observations, while the power laws with the rollovers refer to the results of the SOC model.* (b) *The dual power-law behavior for nanoflares and flares, predicted by the SOC model of Georgoulis & Vlahos (1998). Nanoflares obey a power law with index β > 2.* (c) *The electric current density in the extended cellular automaton model of Isliker et al. (2001). Notice the fragmentation in current sheets.*

SOC was applied to solar flares by Lu & Hamilton (1991), Lu et al. (1993), Lu (1995a, b, c) and was modified or generalized by Vlahos et al. (1995), Georgoulis et al. (1995), Galsgaard (1996), and Georgoulis & Vlahos (1996, 1998). A comparison between the results of a SOC flare model and flare observations is given in Fig. 4a. M. Georgoulis and L. Vlahos extended the cellular automata rules to include anisotropic instability criteria and a variable driver. The result was a steepening of the power laws in low energies, such that the low-energy part of the distributions obeys nanoflare statistics (Fig. 4b). This result is yet to be confirmed observationally. If confirmed, it will signal a possible significant contribution of nanoflares to coronal heating, together with a plausible physical justification. Despite the success of the SOC Statistical Flare models, their physical background needs to be enhanced in order to mimic more closely the actual active region atmosphere. Attempts to reconcile the MHD formulation with SOC cellular automata were carried out by Anastasiadis et al. (1997), Vassiliadis et al. (1998), Chou (1999), Longcope & Noonan (2000), Isliker et al. (2000, 2001), Vlahos et al. (2002), Krasnoselskikh et al. (2002), Podladchikova et al. (2002), and Buchlin et al. (2003). In particular, Isliker et al. (2001) derived an extremely complex coronal volume, fragmented by myriads of unstable current sheets (Fig. 4c). Other attempts addressed the statistics of MHD turbulent models, embedded in one- and two-dimensional geometries (Dmitruk et al. 1998; Georgoulis et al. 1998; Einaudi & Velli 1999; Galtier 1999). An encouraging result is that power laws and intermittency are obtained in MHD models, as well. The power-law indices are similar to those of flares. In one case (Galtier 1999) the distributions showed a dual power law with a steeper component in lower energies. The relevance of SOC with MHD turbulence is also an issue of debate and an ongoing research topic. There are indications, for example, that SOC models driven in a continuum, rather than a discrete, limit resemble the dynamics of MHD turbulent systems (Liu et al. 2002).

5. NEW NANOFLARE CANDIDATES?

The lack of solid observational evidence (*§*3) precludes any conclusion on whether nanoflares heat the corona. On the other hand, only few models (Georgoulis & Vlahos 1996, 1998; Galtier 1999; Georgoulis et al. 2001) predict that power laws steepen as the energy decreases. As research reaches a stalemate, however, the advent of new, very high-resolution observations suggests that the search for nanoflares should be extended toward more directions than previously thought. In the following, we refer to additional nanoflare candidates that might finally solve the coronal heating puzzle:

Schrijver & Title (2002) uncovered a tremendous complexity in the corona: “Fault lines” exist in the solar atmosphere and the coronal loops exhibit a “tectonic” behavior. Myriads of topological discontinuities exist on the interfaces between different connectivity patterns (called *separatrices* by Démoulin & Priest 1997) and evolve simultaneously and independently. Complexity is enhanced by the random photospheric shuffling and may give rise to vast numbers of nanoflares. The mechanism is found to be equally effective (or more effective) in the quiet corona, in line with Parker’s assertions about the abundance of nanoflares. Georgoulis et al. (2002) identified hundreds of *Ha* brightenings (Ellerman bombs) in the low chromosphere of an emerging flux region over a period of a few *hr*. These events were found to heat the surrounding chromosphere and even the base of the transition region in the active region (Schmieder at al. 2004). Ellerman bombs are reconnection events, occurring in topological discontinuities of the magnetic field (Pariat et al. 2003). Preliminary results suggest that they obey nanoflare statistics, i.e. power laws with indices $a > 2$.

Tziotziou et al. (2003 and in this volume) have uncovered a fine chromospheric structure with numerous spicules and bi-directional velocity fields that are strongly reminiscent of magnetic reconnection. This also implies a very high frequency of magnetic reconnection in the low solar atmosphere. Vourlidas & Korendyke (2003) analyzed very high6 resolution data of the upper chromosphere in both an active region and the quiet Sun. The *Lya* images uncover a tremendous small-scale activity in the upper chromosphere. This activity is equally present in the quiet and the active-region atmosphere, also in line with Parker’s nanoflares.

6. CONCLUSIONS

Despite major recent advances in our observational, modeling, and computational capabilities, a definitive answer to the coronal heating question remains elusive. It is yet to be clarified whether nanoflares are important for coronal heating. The observed Xray flares and sub-flares are not sufficient to heat the solar corona. The role of the EUV events is still unclear, as the impact of various biases is unknown. Moreover, new observations suggest new directions for the study of dissipative phenomena in the solar corona. The Sun continues to surprise us as the instrumental resolution increases; it appears unlikely that the observed complexity will subside in smaller spatial scales. In view of forthcoming developments, it is only fair to comment that “this is not the end of the nanoflare story”, thus paraphrasing Trimble & Aschwanden (2003). Modeling should proceed in concert with observations. Statistical Flare models in general and SOC models in particular must be shielded with more physics to capture the dynamics and the turbulent nature of the energy dissipation. One envisions an arsenal of MHD and Statistical Flare models that act complementary; MHD models that highlight the microphysics of the energy release process, and statistical models that reproduce the macroscopic behavior of the dynamics in the solar corona.

ACKNOWLEDGMENTS: I am grateful to Prof. L. Vlahos for his sage advice and mentoring during and after the completion of my PhD thesis. I also thank the Organizers of the 6*th* HELAS Conference for their invitation and for giving me the opportunity to provide this review.

REFERENCES

Aletti, V., Velli, M., Bocchialini, K., Einaudi, G., Georgoulis, M., & Vial, J.-C., 2000, ApJ, 544, 550
Anastasiadis, A., & Vlahos, L. 1994, ApJ, 428, 819
Anastasiadis, A., Vlahos, L., & Georgoulis, M., 1997, ApJ, 489, 367
Aschwanden, M. J., 1999, SoPh, 190, 233
Aschwanden, M. J., 2002, SSRv, 101, 1
Aschwanden, M. J., & Charbonneau, P., 2002, ApJ, 566, L59
Aschwanden, M. J., Dennis, B. R., & Benz, A. O., 1998, ApJ, 497, 972
Aschwanden, M. J., & Parnell, C. E., 2002, ApJ, 572, 1048
Aschwanden, M. J., Tarbell, T. D., Nightingale, R. W., Schrijver, C. J., Title, A., Kankelborg, C. C., Martens, P., & Warren, H. P., 2000, ApJ, 535, 1047
Bak, P., 1996, How Nature Works, Springer Verlag: New York
Benz, A. O., Plasma Astrophysics; Kinetic Processes in Solar and Stellar Coronae, 1993, Kluwer: Dordrecht
Benz, A. O., & Krucker, S., 2002, ApJ, 568, 413
Berghmans, D., Clette, F., & Moses, D., 1998, A&A, 336, 1039
Biesecker, D., 1994, Ph. D. Thesis, University of New Hampshire
Biskamp, D., 1993, Nonlinear Magnetohydrodynamics, Cambridge Univ. Press: Cambridge Bromund, K. R., McTiernan, J. M., & Kane, S., R., 1995, ApJ, 455, 733
Buchlin, E., Aletti, V., Galtier, S., Velli, M., Einaudi, G., & Vial, J.-C., 2003, A&A, 406, 1061 Charbonneau, P., McIntosh, S. W., Liu, H.-L., & Bogdan, Th. J., 2001, SoPh, 203, 321
Chou, Y.-P., 1999, ApJ, 527, 958
Crosby, N. B., Aschwanden, M. J., & Dennis, B. R., 1993, SoPh, 143, 275
Crosby, N. B., Vilmer, N., Lund, N., & Sunyaev, R., 1998, A&A, 334, 299
Démoulin, P., Priest, E. R., 1997, SoPh, 175, 123
Dennis, B. R., 1985, SoPh, 100, 465
Dmitruk, P., Gómez, D. O., & DeLuca, E. E., 1998, ApJ, 505, 974
Einaudi, G., & Velli, M., 1999, Phys. Plasmas, 6(11), 4146
Einaudi, G., Velli, M., Politano, H., & Pouquet, A., 1996, ApJ, 457, L113
Feldman, U., Doschek, G. A., & Klimchuk, J. A., 1997, ApJ, 474, 511
Galsgaard, K., 1996, A&A, 315, 312 Galtier, S., 1999, ApJ, 521, 483
Georgoulis, M. K., 2000, Ph. D. Thesis, University of Thessaloniki Georgoulis, M., Kluiving, R., & Vlahos, L., 1995, Physica A, 218, 191

Georgoulis, M. K., Rust, D. M., Bernasconi, P. N., & Schmieder, B., 2002, ApJ, 575, 506 Georgoulis, M. K., Velli, M., & Einaudi, G., 1998, ApJ, 497, 957
Georgoulis, M. K., Vilmer, N., & Crosby, N. B., 2001, A&A, 367, 326
Georgoulis, M. K., & Vlahos, L., 1996, ApJ, 469, L135
Georgoulis, M. K., & Vlahos, L., 1998, A&A, 336, 721
Heyvaerts, J., 2000, In Introduction to MHD (eds.: Rozelot, J. P., Klein, L., & Vial, J.-C.), CNRS Summer School on Solar Astrophysics, LNP, 553, 1 Hudson, H. S., 1991, SoPh, 133, 357
Isliker, H., Anastasiadis, A., & Vlahos, L., 2000, A&A, 363, 1143
Isliker, H., Anastasiadis, A., & Vlahos, L., 2001, A&A, 377, 1068
Kraichnan, R. H., 1965, Phys. Fluids, 8, 1385
Krasnoselskikh, V., Podladchikova, O., Lefebvre, B., & Vilmer, N., 2002, A&A, 382, 699 Krucker, S. & Benz, A. O., 1998, ApJ, 501, L213
Kucera, T. A., Dennis, B. R., Schwartz, R. A., & Shaw, D., 1997, ApJ, 475, 338
Lee, T. T., Petrosian, V., & McTiernan, J. M., 1993, ApJ, 412, 401
Lee, T. T., Petrosian, V., & McTiernan, J. M., 1995, ApJ, 418, 915
Lin, R. P., Schwartz, R. A., Kane, S. R., Pelling, R. M., & Hurley, K. C., 1984, ApJ, 283, 421 Litvinenko, Y. E., 1996, SoPh, 167, 321
Liu, H.-L., Charbonneau, P., Pouquet, A., Bogdan, Th., & McIntosh, S., 2002, Phys. Rev. E., 66, 6111
Longcope, D. W., & Noonan, E. J., 2000, ApJ, 542, 1088
Lu, E. T., 1995a, ApJ, 446, L109
Lu, E. T., 1995b, ApJ, 447, L416
Lu, E. T., 1995c, PRL, 74, L2511
Lu, E. T., & Hamilton, R. J., 1991, ApJ, 380, L89
Lu, E. T., Hamilton, R. J., McTiernan, J. M., & Bromund, K. R., 1993, ApJ, 412, 841
McIntosh, S. W., & Charbonneau, P., 2001, ApJ, 563, L135
MacKinnon, A. L., Macpherson, K. P., & Vlahos, L., 1996, A&A, 310, L9
Narain, U., & Ulmschenider, P., 1996, SSRv, 75, 453
Pariat,E.,Aulanier,G.,Schmieder, B.,Georgoulis,M. K.,Rust,D.M.,& Bernasconi,P.N.,2003, ApJ, to be submitted
Parker, E. N., 1972, ApJ, 474, 499
Parker, E. N., 1979, Cosmical Magnetic Fields, Oxford Univ. Press
Parker, E. N., 1983, ApJ, 264, 642
Parker, E. N., 1988, ApJ, 330, 474
Parker, E. N., 1989, SoPh, 121, 271
Parker, E. N., 1991, ApJ, 376, 355
Parnell, C. E., & Jupp, P. E., 2000, ApJ, 529, 554
Podladchikova, O., Dudol de Wit, T., Krasnoselskikh, V., & Lefebvre, B., 2002, A&A, 382, 713
Priest, E. R., 1982, Solar Magnetohydrodynamics, Reidel: Dordrecht
Priest, E. R., Hornig, G., & Pontin, D. I., 2003, JGR, 108, A7, 1285
Rosner, R., & Vaiana, G., 1978, ApJ, 222, 1104
Schmieder, B., Rust, D. M., Georgoulis, M. K., Démoulin, P., & Bernasconi, P. N., 2004, ApJ, 601, in press
Schrijver, C. J., & Title, A. M., 2002, SoPh, 207, 223
Schrijver, C. J., & Zwaan, C., 2000, Solar and Stellar Magnetic Activity, Cambridge Univ. Press: New York Shimizu, T., 1995, PASJ, 47, 251 ¸
Švestka, Z., Jackson, B. V., & Machado, M. E., 1992, In Eruptive Solar Flares (eds.: ¸Švestka, Z., Jackson, B. V., & Machado, M. E.), Procs. IAU Coll. 133, LNP, 399, 409
Trimble, V., & Aschwanden, M. J., 2003, PASP, 115, 514
Tziotziou, K., Tsiropoula, G., & Mein, P., 2003, A&A, 402, 361
Vassiliadis, D., Anastasiadis, A., Georgoulis, M., & Vlahos, L., 1998, ApJ, 509, L53
Vlahos, L., 1994, SSRv, 68, 39
Vlahos, L., Fragos, T., Isliker, H., & Georgoulis, M., 2002, ApJ, 575, L87
Vlahos, L., Georgoulis, M., Kluiving, R., & Paschos, P., 1995, A&A, 299, 897
Vourlidas, A., & Korendyke, C., 2003, AAS/SPD Meeting #34, 20.09
Wheatland, M. S., & Craig, I. J. D., 2003, ApJ, 595, 458
Wheatland, M. S., & Litvinenko, Y. E., 2002, SoPh, 211, 255
Withbroe, G. L., & Noyes, R. W., 1977, ARA&A, 15, 363

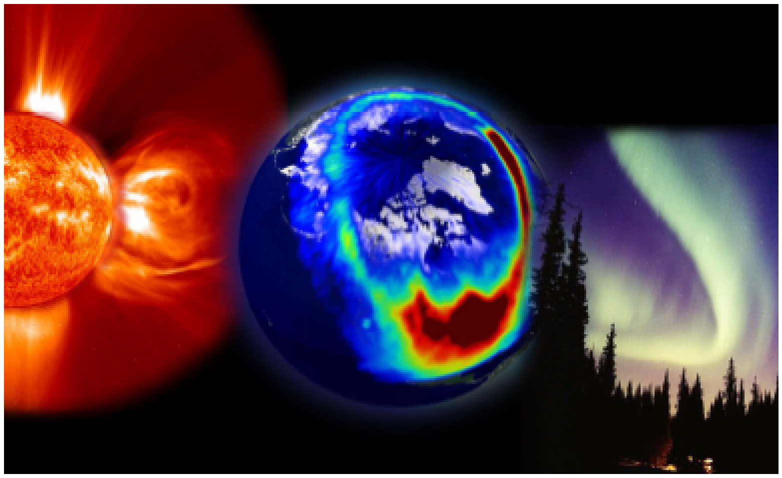

STUDY OF A SOLAR ACTIVE REGION LOOP USING EUV SPECTRA*

C. Gontikakis[1], G. J. D. Petrie [2,3], H. C. Dara[1] and K. Tsinganos[2]

[1]Academy of Athens, Research Center of Astronomy and Applied Mathematics, GR-106 73 Athens Greece.
[2]IASA and Section of Astrophysics, Astronomy and Mechanics, Department of Physics, University of Athens, Greece
[3]High Altitude Observatory, National Center for Atmospheric Research PO Box 3000 Boulder, USA

ABSTRACT

We analyse a coronal loop observed with the *Normal Incidence Spectrometer* (NIS), which is part of the *Coronal Diagnostic Spectrometer* (CDS) on board the *Solar and Heliospheric Observatory* (SOHO) satellite. The measured dopplershifts and proper motions along the selected loop strongly indicate unidirectional flows. With the Emission Measure Loci we estimate the temperature along the loop to be about 380 000 K.

1 INTRODUCTION

Coronal loops seem to be, in all length scales, the basic feature of the solar corona. It is widely accepted that the understanding of these features, will bring us closer to the heating mechanism of the corona. Recently, Petrie *et al.* (2003), comparing a steady 2D-MHD loop model with observations of EUV loops, noticed that the flows have an important influence on the energy balance. This means that flows, along with temperature and density, are the physical quantities that should be carefully determined in order to proceed in constraining the loop heating function. The flows in active region loop systems can be very complex to study quantitatively, however the analysed observations of CDS supply a unique opportunity to study them, even though CDS wasn't designed to study motions.

2 OBSERVATIONS, DATA REDUCTION AND FLOWS IN O V 630 Å

On October 26 and 27, 1999, CDS/NIS observed the active region 8737 at the S-W limb of the Sun, executing 218 scans with a 10 minute cadence (Fredvik *et al.* 2002). Each slit exposure recorded simultaneously six spectral lines emitted by the ions: He I, O III, O V, Ne VI, Mg IX, and Fe XVI at the wavelengths 584 Å599 Å, 630 Å, 562 Å, 368 Å and 361 Å, sampling the solar atmosphere in temperatures of the upper chromosphere, the transition region and the corona. We corrected the data for the CCD bias, flatfield, burn-in effects and cosmic rays (see Del-Zanna 2003a for an introduction to the CDS data reduction). We applied a fitting routine to each individual profile to produce intensity and dopplershift maps in the O V line. As the images were taken after the SOHO recovery, we had to take into account the change of the PSF of the spectrometer, which produces line profiles that do not have a Gaussian shape (Thompson, 1999). The dopplershift maps were corrected for the geometric distortion. As we don't have a wavelength calibration on-board, we made the

* *Proceedings 6th Hellenic Astronomical Society Conference, 15-17 September 2003, Penteli, Athens, Greece*

assumption that the dopplershift is equal to zero at a quiet region very close to the limb. Figure 1 presents 4 consecutive images, indicating the formation of the selected loop where we can track the motion along its length, as well as the corresponding Doppler maps. In an effort to study the physical parameters along the loop, we then sampled the loop in the 09:13-09:23 raster (see Fig. 2). For each spectral profile selected along the loop, we chose up to 4 more profiles nearby, but outside, of the loop (Fig 2. panel 2). We subtracted the mean of these nearby profiles from the loop ones, to correct for the background.

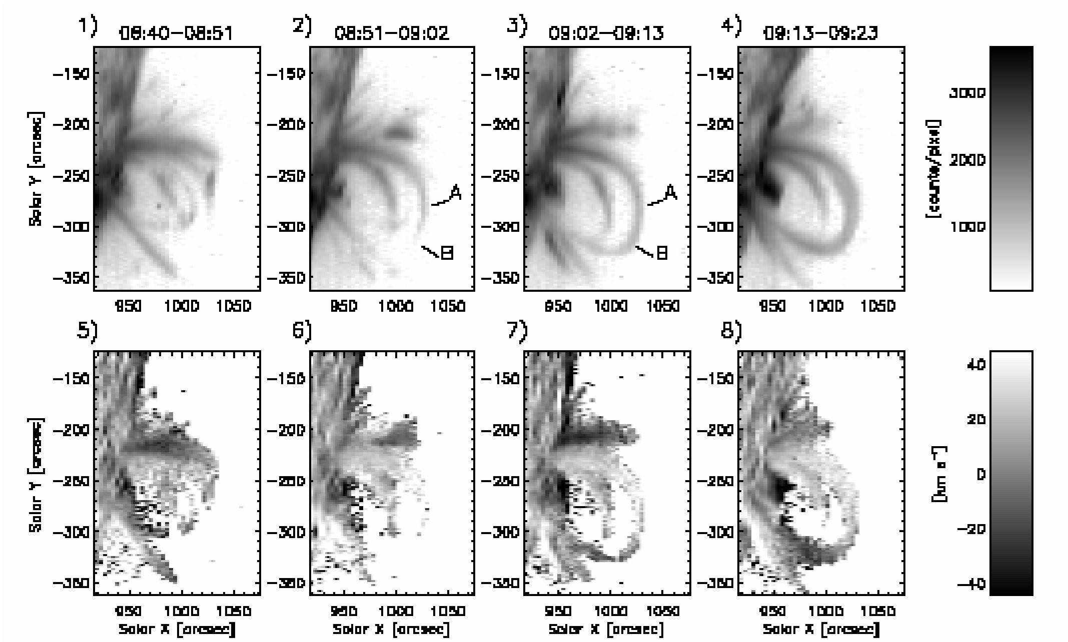

Figure 1*: Total line intensity maps (first row) and the corresponding dopplergrams (second row) in O V 630 °A (formed at about 250 000 K) showing the evolution of the active region. The segments A and B in panels 2 and 3 show the selected loop. The loop evolution in panels 2 and 3 and the corresponding dopplergrams (6 and 7) indicate that the loop is replenished from its northen footpoint by a unidirectional flow. The first row images indicate proper motions of the order of ± 6 ±km* s^{-1}.

The background in our case is composed of photons that are emitted along the line of sight (l.o.s.) but out of the loop (the plasma is optically thin), and from those of the off-band scattered light (Brekke *et al.* 2000). The fitting of the corrected profiles provide the dopplershift and the total intensity along the loop (see Fig. 2 panels 4,5).

3 EMISSION MEASURE LOCI ANALYSIS ALONG THE LOOP.

In Fig. 3, the images for the six spectral lines recorded during the 09:13-09:23 raster are presented. We looked if the loop morphology that we analysed in O V is also present in the other images of Fig. 3. This seems to be the case for Ne VI. However, we cannot see the loop in O III and in He I we see only its footpoints. In the hotter lines of Mg IX 368 Å, and Fe XVI 361 Å, no loop features seem co-spatial with the O V one. Therefore, we assume that the considered loop plasma emits only in the temperature range of the O V 630 Å and the Ne VI 562 Å lines. As for O V, we computed the total intensity of the Ne VI line along the loop. We derived the contribution functions G(T) for the two ions using the CHIANTI package

(Dere *et al.* 1997), considering hybrid abundance for the solar corona (Fludra & Schmelz 1999) and assuming that the plasma is in ionization equilibrium, we applied the Arnaud & Rothenflung (1985) ionization fractions. For each point along the loop, we computed the Emission Measure function of the temperature $EM(T) = I/G(T)$, where (I) is the total intensity and, assuming that the plasma along the l.o.s. is isothermal and using the emission.

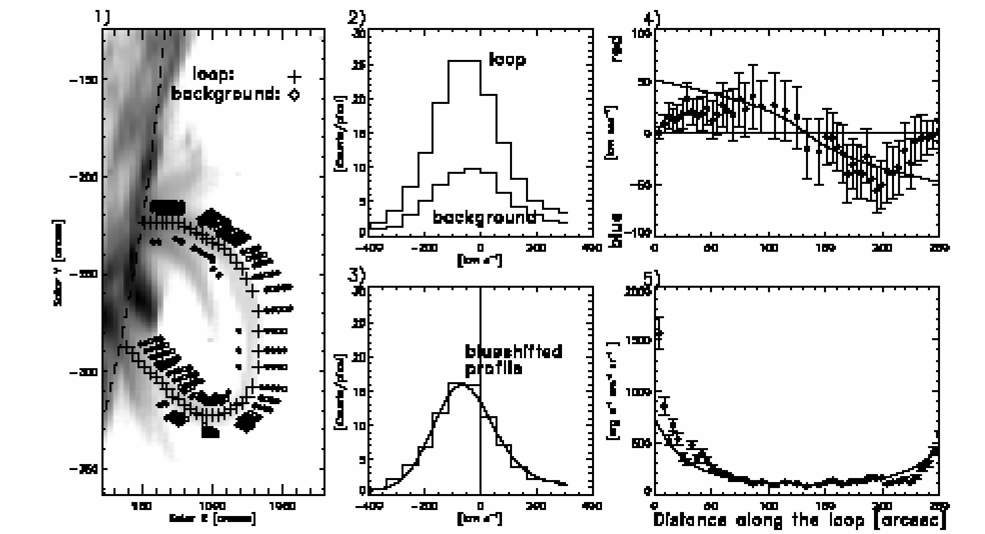

Figure 2: *A thorough study of the loop in O V 630 Å. In panel 1, crosses are the sampling points along the loop and diamonds are the corresponding background ones. Panel 2 shows one spectral profile taken on the loop and the corresponding background one, (dispersion axis is in km s^{-1}). Panel 3 is the loop profile of panel 2 after background subtraction, fitted to compute total intensity and dopplershift. Panel 4, shows the dopplershift along the loop (starting from the northen footpoint). Even with the large error bars (dispersion pixel size=56 km s^{-1}) a clear variation of the dopplershift from red (positive velocities) to blue shift is present. Panel 5 shows the flux emitted from the loop plasma along the loop in physical units. In panels 4 and 5, the thick lines represent an attempt to fit the data with the results from an MHD computation (see the Discussion for a brief comment).*

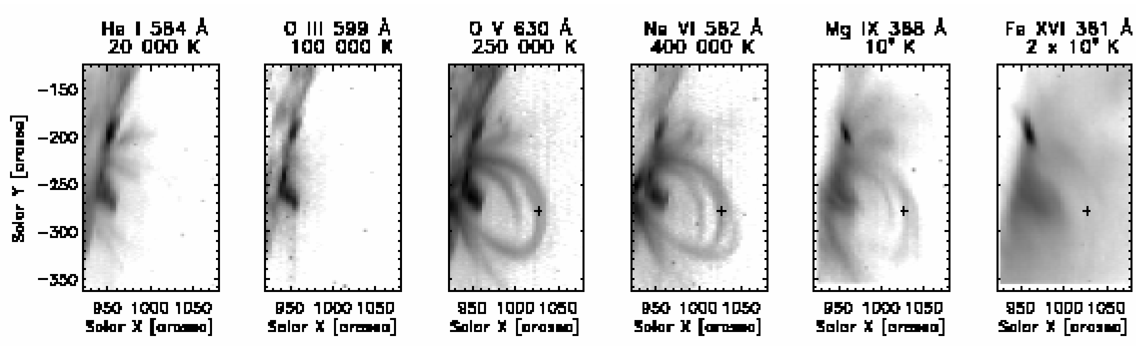

Figure 3: *Images from all spectral lines observed during the 09:13-09:23 raster ordered with increasing temperature of maximum ion concentration. The Mg IX and Fe XVI images coalignment was corrected to account for the spatial offset between NIS-1 (308-379 Å) and NIS-2 (513-633 Å) parts of the CDS detector. The cross at (1026.7", -279"), shows that the loops of Mg IX are not exactly co-spatial with the O V, and Ne VI ones.*

measure loci for the two spectral lines, we estimated the value of the temperature along the loop (see Del Zanna 2003b and references therein for details on EM loci). The error bars on the calculated temperature were estimated by the statistical uncertainties on the total intensity

4 DISCUSSION

The dopplershifts (Fig. 2) and proper motions (Fig. 1) strongly indicate a unidirectional flow along the selected loop. The temperature along the loop can also be estimated at first order.

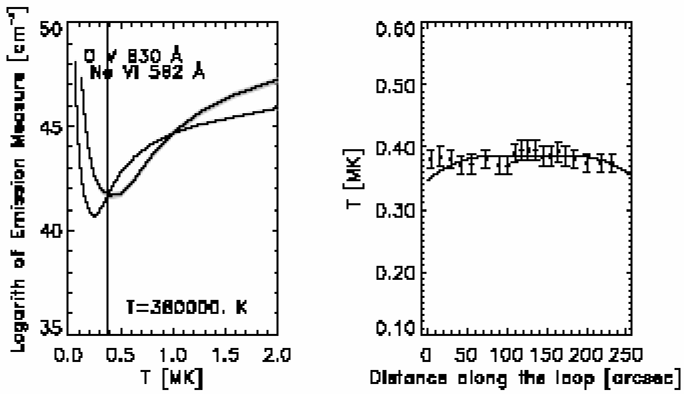

Figure 4: *Derivation of the temperature using the Emission Measure Loci technique. In the first panel, the emission measures for O V 630 Å and Ne VI 562 Å for a given part of the loop are plotted as functions of temperature. The first crossing point indicates a prospective temperature and emission measure of the plasma. The right panel shows the derived temperature along the loop. The grey contour of the emission measure curves and the error bars on the temperature are computed from the fitting process. In panel 2 we show the computed temperature from the MHD model.*

It seems that near the loop top, we have slightly hotter plasma. We proceed to a fitting of our measurements with an analytical 2D-MHD model of coronal loops (see Petrie *et al.* 2003 and Petrie *et al.* this issue). Given the loop dimensions, the model computes the flow, the mass density, temperature and heating along the loop, for a given shape of the magnetic field. Using an estimation of the loop geometry, we reproduced the l.o.s. velocity (Fig. 2 panel 4) and from the computed electron density and temperature (plotted in Fig. 4 panel 2), the O V flux along the loop (Fig. 2 panel 5). The loop heating function, is stronger at the footpoints of the loop, especially the upflow one. In a future work, we will include the other observed spectral lines and we will further study the results of the model.

ACKNOWLEDGMENTS

CG and GP acknowledge funding by the EU Research Training Network PLATON, contract number HPRN-CT-2000-00153. CG also acknowledges support from the Research Comittee of the Academy of Athens and the Costopoulos Foundation. We also thank T. Fredvik for reading the manuscript.

REFERENCES

Arnaud M. and Rothenflug R., 1985, A&AS, 60, 425

Brekke P., ThompsonW.T., Woods T.N., Eparvier F.G., 2000, ApJ, 536, 959
Dere K.P., Landi E., Mason H.E., Monsignori Fossi B.C., Young P.R., 1997, A&AS, 125, 149
Fludra A. and Schmelz J.T., 1999, A&A, 348, 286
Fredvik T., Kjeldseth-Moe O., Haugan S.V.H., Brekke P., Gurman J.B., Wilhelm K., 2002, AdSpR, 30, 635
Harrison R.A., *et al.* 1995, Solar Phys., 162, 233
Petrie G.J.D., Gontikakis C., Dara H.C., Tsinganos K., Aschwanden M.J., 2003, A&A, 409, 1065
Petrie G.J.D., Gontikakis C., Dara H.C., Tsinganos K., Aschwanden M.J., this issue
ThompsonW.T., CDS Software note No 53, http://solg2.bnsc.rl.ac.uk/software/notes.shtml
Del Zanna G., 2003a, http://www.medoc-ias.u-psud.fr/workshops/atelierTOSTISP.html
Del Zanna G., 2003b, A&A, 406, L5

BASIC ASPECTS OF THE COLLISIONLESS KINETIC THEORY OF THE SOLAR WIND*

I. Zouganelis, N. Meyer-Vernet, M. Maksimovic and K. Issautier

Laboratoire d'Etudes Spatiales et d'Instrumentation en Astrophysique (LESIA), Observatoire de Paris, 5, place Jules Janssen, F-92195 Meudon Cedex, France

Abstract: An important assumption inherent to the usual fluid solar wind models is that the plasma is dominated by collisions. Therefore the fluid approach implies that the particles velocity distribution functions are rather close to a Maxwellian. However the observed solar wind electron distributions depart from nearly isotropic Maxwellians, indicating the limited validity of this hypothesis. The high velocity particles forming the tail of these distribution functions have an enhanced phase space density compared to a Maxwellian. In this work, we present a recent kinetic collisionless model of the solar wind acceleration, which assumes non-thermal electron velocity distributions in the low corona. The suprathermal electrons are modelled by superimposing to a Maxwellian core either a hot Maxwellian or a hot generalized lorentzian (kappa) function. Such a model is suggested by the fact that suprathermal electrons are nearly collisionless in the wind acceleration region (the mean free path is of the order of 1AU) and thus should not be in equilibrium, a fact which seems to be confirmed by recent measurements in the corona. This model is able to reproduce the transonic solutions of the high speed solar wind without assuming unreasonably large coronal temperatures or additional heating of the outer region of the corona, as it is needed in fluid models. The theoretical properties of plasma parameters such as density, speed and temperature are compared with in situ measurements provided by the Ulysses spacecraft.

* *Proceedings 6th Hellenic Astronomical Society Conference, 15-17 September 2003, Penteli, Athens, Greece*

2D MHD modelling of heated coronal loops compared to TRACE observations

G.J.D. Petrie[1], C. Gontikakis[2], H.C. Dara[2], K. Tsinganos[1], and M.J. Aschwanden[3]

[1]*IASA and Section of Astrophysics, Astronomy and Mechanics, Department of Physics, University of Athens, Panepistimiopolis, GR-157 84 Zografos, Athens, Greece*

[2]*Academy of Athens, Research Center of Astronomy and Mathematics, GR-106 73 Athens, Greece*

[3]*Lockheed Martin, Solar and Astrophysics Lab. L9-41, Bldg. 252, 3251 Hanover Street, Palo Alto CA 94304*

Abstract

An analytical MHD model of coronal loops with compressible flows and including heating is compared to observational data. We calculate models whose loop length, shape, plasma density, temperature and velocity profiles are fitted to loops observed with TRACE. A synthetic emission profile is also calculated and fitted to the observed emission pattern. The consistently calculated heating profile is concentrated at the foot points and is influenced by the flow, being biased towards the upflow foot point.

1 Introduction

A coronal loop is an important localised structure which connects the photosphere to the corona through the transition region and may thus be studied to gain information about the heating of the corona as a whole. To date heated loop studies have generally included only hydrostatic or hydrodynamic models. These are one-dimensional in the sense that they do not model the cross-field force balance: forces are only balanced along the loop. However, in the highly magnetised and sparse coronal plasma the magnetic field is likely to have a significant direct effect on the statics or dynamics of such a curved structure as a coronal loop, while plasma flow, even at such sub-Alfvénic velocities as 20 km/s (Dara et al., 2002), may have an effect on the heating balance. Moreover, the geometrical details may have an impact on the energy profile of the loop, via the potential energy, and therefore on the heating model. The models in this paper include two-dimensional geometry, compressible MHD plasma flow in uniform gravity and heating in single consistent exact solutions and thereby give a first opportunity to investigate these effects.

2 The Analytical Model

The *dynamics* of flows in solar coronal loops may be described to zeroth order by the well known set of steady ($\partial/\partial t = 0$) ideal hydromagnetic equations:

$$\rho\,(\mathbf{V}\cdot\nabla)\,\mathbf{V} = \frac{1}{4\pi}(\nabla\times\mathbf{B})\times\mathbf{B} - \nabla P - \rho g\hat{Z}\,, \tag{1}$$

$$\nabla\cdot\mathbf{B} = \mathbf{0}\,,\quad \nabla\cdot(\rho\mathbf{V}) = \mathbf{0}\,,\quad \nabla\times(\mathbf{V}\times\mathbf{B}) = \mathbf{0}\,, \tag{2}$$

where $\mathbf{B}$, $\mathbf{V}$, $-g\hat{Z}$ denote the magnetic, velocity and (uniform) external gravity fields while ρ and P the gas density and pressure. The *energetics* of the flow on

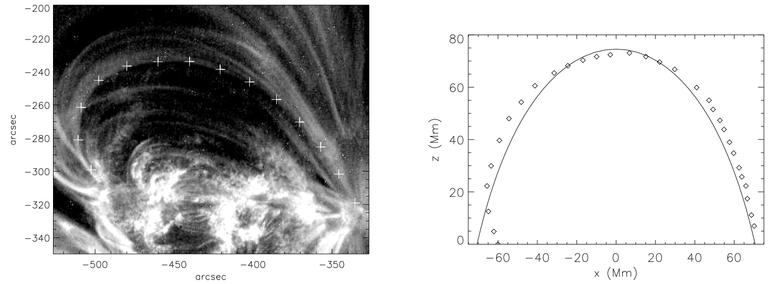

Figure 1: An MHD model of a loop observed by TRACE fitted to observational data: shown are the TRACE image of the loop system with the loop of interest contained within crosses (left picture) and the model field line (solid line) fitted to the observed line, represented by diamonds (right picture) in the X-Z plane.

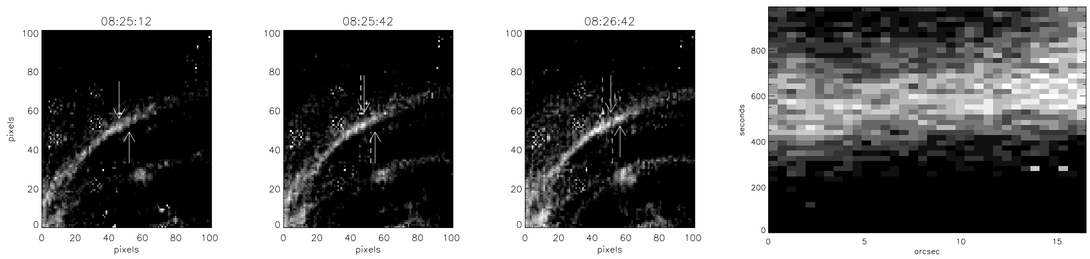

Figure 2: Proper motions along the loop shown in Fig. 1. We show in the first three pictures a part of the loop in three 171 Å images close in sequence, showing the displacement of two blobs of material indicated by arrows. The dashed lines in the second and third pictures show the initial positions of the two blobs. The mean velocity we calculate is of the order of 30 km/sec. We show in the fourth picture the evolution of the intensity along another segment of the loop (horizontal axis) versus time (vertical axis). Black represents unenhanced loop emission and shades of grey represent enhanced emission. This variation of intensity travelling toward the right foot point of the loop may be associated with a flow along the loop. We can estimate roughly from this figure a velocity of 40-50 km/sec.

the other hand is governed by the first law of thermodynamics :

$$q = \rho \mathbf{V} \cdot \left[\nabla \left(\frac{1}{\Gamma - 1} \frac{P}{\rho} \right) + P \nabla \frac{1}{\rho} \right] , \tag{3}$$

where q is the net volumetric rate of some energy input/output, while $\Gamma = c_p/c_v$ with c_p and c_v the specific heats for an ideal gas. Assuming the loop is planar and translationally self-similar, the system of equations (1) - (2) can be solved to give ρ, P, $\mathbf{V}$ and $\mathbf{B}$ (see Petrie et al., 2002, where the many solutions are summarised in Table 1), then one may determine the volumetric rate of thermal energy from Eq.(3).

Next, we balance the energy in the loop; the net volumetric rate of heating input/output q, the net radiation L_R, the heat conduction energy $\nabla \cdot \mathbf{F}_C$, where $\mathbf{F}_C$ is the heat flux due to conduction, and the unknown remaining heating E_H,

$$q = E_H + L_R - \nabla \cdot \mathbf{F}_C. \tag{4}$$

The net heat in/out q is calculated from the MHD model using the first law of thermodynamics Eq. 3, while the radiation L_R is given by $L_R = -(n/2)^2 Q(T)$, as in Rosner et al. (1978), where n is the particle number density (we assume that the plasma is fully ionised) and $Q(T)$ is a function of T. The thermal conduction energy is calculated assuming that conduction is mainly along the field, using the expression

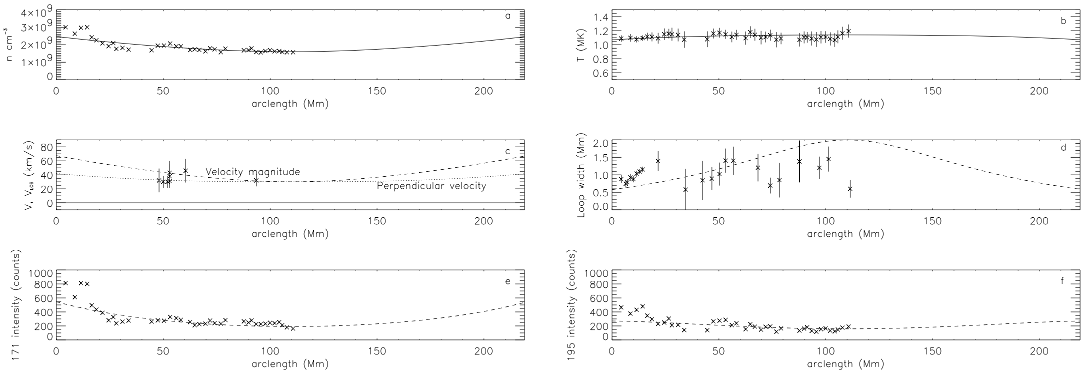

Figure 3: Shown are (a) the particle number density, (b) the temperature, (c) the flow velocity, (d) the loop width and (e) the 171 Å and (f) the 195 Å emission patterns compared with the synthetic forward-modelled emission from the MHD model. The forward-modelled emission patterns are computed using the TRACE response functions. All are graphed against arc length along the field line of the loop shown in Fig. 1. In these plots, the observed values are represented by x symbols and the model by the lines. In the velocity plot the modulus $|\mathbf{V}|$ is graphed with a dashed line while a simulated perpendicular velocity profile is represented by a dotted line.

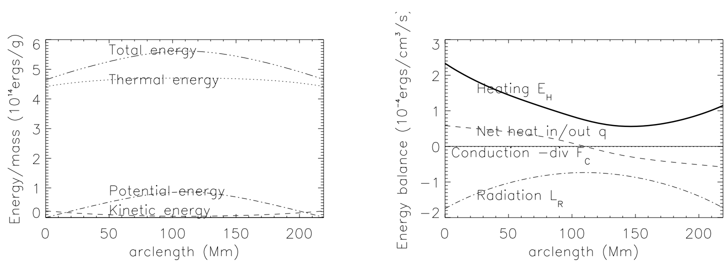

Figure 4: Shown are (left) the breakdown of the energy integral along the loop and (right) the volumetric energy rate along the loop graphed against arc length along the loop. In the heating plot, the net heat in/out is represented by the dashed line, the radiative losses by the dot-dashed line, the losses due to conduction by the dotted line, and the remaining heating by the thick solid line. Except for a small region near the apex, radiative losses are larger than conductive losses. The heating profile is largely dominated by radiative losses but, influenced by the flow, it is not symmetrical, but is concentrated at the inflow foot point.

$$-\nabla \cdot \mathbf{F}_C = \frac{d}{ds}\left(\kappa_{||}\frac{dT}{ds}\right) - \frac{\kappa_{||}}{B}\frac{dB}{ds}\frac{dT}{ds}, \tag{5}$$

where subscripts $||$ indicate values and derivatives along the field line, and B's variation along the field line is taken into account (Priest, 1982).

3 Observations, data reduction and loop diagnostics

We used observations from TRACE in the 195 Å, and 171 Å bands taken on 24-26 October 1999. The instrument was pointing on a well-defined isolated loop system (see Fig. 1, top left picture) with field of view 768×768 pixels, pixel size 0.5 Å . We applied the following corrections: we subtracted the readout pedestal and the dark current, we cleaned out the pixels damaged due to cosmic-rays and we extracted the CCD readout noise. In order to derive the geometry of the loop as well as the physical parameters we followed Aschwanden et al., (1999). We used the STEREO package (Aschwanden et al., 1999), which is part of the solar software (SSW) in order to reproduce the geometry of the loops.

As the lines used are optically thin, we took great precautions to extract the background emission. We sampled only half of the loop starting from the left foot point as, the other part is too faint and cannot safely be separated from the background. We fitted with a Gaussian function the intensity profile across the loop at selected positions. The full width at half maximum of the Gaussians functions resulting from the fit is taken as the width of the loop at these positions. We also computed the temperature and the emission measure using a filter ratio technique with the 171 Å and 195 Å filters. We derived the mean electron density n_e at each point along the loop using the relation $n_e = \sqrt{EM/w}$ where w is the average of the loop width.

We tried to measure the proper motions, if any, of the loop plasma. We centered the 171 Å every 30 sec. images and made a movie with them. In Fig. 2 we show a part of the loop in three 171 Å images close in sequence, showing the displacement of two blobs of material indicated by arrows. Since half a pixel is the minimum displacement and it corresponds to a velocity of 17 km/s, we consider this as the error of the measurements. The measurement is very subjective, but since quite some points are measured and most of their velocities are within the range of 30-40 km/s we believe that this value is close to the real velocity. The mean velocity that we calculate is of the order of 30 km/sec. We show in the bottom picture of Fig. 2 the evolution of the intensity along another segment of the loop plotted against time. We can estimate roughly from this picture a velocity of 40-50 km/sec. It is unlikely that the observed "proper motions" are wave disturbances since 30-50 km/s is below the smallest possible wave speed, the tube speed, which is approximately equal to the sound speed at around 120 km/s.

4 Discussion

Figs. 1, 3 and 4 show the results of the model of the loop under consideration (see the captions for details). The model indicates that plasma flow has a strong influence on the location of the loop heating: the heating is concentrated at the foot points and is biased towards the upflow foot point. In Petrie et al. (2003) we calculate further examples modelling data from SoHO/CDS and SoHO/SUMER and further details of the dynamics are given.

Acknowledgments

GP and CG acknowledge funding by the EU Research Training Network PLATON, contract number HPRN-CT-2000-00153. CG also acknowledges support from the Research Comittee of the Academy of Athens and the Costopoulos Foundation. We would like to thank C.E. Alissandrakis and H. Peter for software support.

References

Aschwanden, M.J., Newmark, J.S., Delaboudiniere, J-P., Neupert, W.M., Klimchuk, J.A., Gary, G.A., Portier-Fozzani, F., Zucker, A., 1999, ApJ, 515, 842

Dara, H.C., Gontikakis, C., Zachariadis, Th., Tsiropoula, G., Alissandrakis, C.E., Vial, J.-C., 2002, in Proceedings of the Second Solar Cycle and Space Weather Euroconference, ESA SP-477, 95

Petrie, G.J.D., Vlahakis, N. and Tsinganos, K., 2002, A&A, 382, 1081

Petrie, G.J.D., Gontikakis, C., Dara, H.C., Tsinganos, K., Aschwanden, M.J., 2003, A&A, 409, 1065

Priest, E.R., 1982, *Solar Magnetohydrodynamics*, Reidel

Rosner, R., Tucker, W.H. and Vaiana, G.S., 1978, ApJ, 220, 643

CORONAL LOOP HEATING BY NANOFLARES: SOME OBSERVATIONAL IMPLICATIONS*

S. Patsourakos[1] and J. A. Klimchuk
Naval Research Laboratory, Space Science Division, Washinton, DC 20375-5352, USA

ABSTRACT

Coronal heating by nanoflares occurring at sub-resolution elements is a potential candidate for the heating of coronal loops. We address here this conjecture by the means of time-dependent hydrodynamic simulations of nanoflares occurring at sub-resolution strands. We find that such processes can capture two of the most important observed properties of coronal loops: the over and underdensities with respect to static equilibrium and the broad Differential Emission Measure distributions.

1. INTRODUCTION

The solar corona is threaded by numerous coronal loops filled with plasma attaining temperatures of few million K (for a review see the book of Bray et al. 1991). Why these loops are hot represents a cornerstone problem not only for solar physics but also for the discipline of Sun-Earth Connections, given the fact that coronal loops are major contributors of the Sun's variable output in the EUB and SXR.

There has been a big deal of theoretical effort to explain the heating in coronal loops (e.g., Mandrini et al. 2001 for a review). One of the major candidates for coronal heating invokes nanoflares (Parker 1988)l. Nanoflares are impulsive releases of very small amounts of energy (of the order of 10^{24} erg), many orders of magnitude smaller than the energy of a "normal" flare. Random, slow motions of the foot-points of coronal loops in the photosphere make the magnetic field in the corona entangled and braided and increase the energy. When the angle between adjacent misaligned flux tubes reaches a threshold a nanoflare occurs and the surplus energy is released.

Nanoflares occurring at cross-sections that are below the best spatial resolution currently available (≈ 1 arcsec in the EUV), are repeated on time-scales of the order of the cooling time of coronal plasma (≈ few 1000s) to meet the heating requirements of "macroscopic" coronal loops. In the frame of the above picture (Cargill 1994; Klimchuk and Gargill 2001) the observed coronal loops are made up of a large number of unresolved strands (hundreds or thousands) which are heated by nanoflares in an impulsive way and then cool down. The combination of the emissions of the ensemble of strands, at different stages of heating and cooling, makes up the "macroscopic" observed loop.

In the recent years and with the advent of several space-borne missions (YOHKOH, SOHO, TRACE) delivering high quality data, a new picture for coronal loops emerged (e.g., Aschwanden, Schrijver and Alexander 2001; Winebarger, Warren and Mariska 2003). Two

---

* *Proceedings 6th Hellenic Astronomical Society Conference, 15-17 September 2003, Penteli, Athens, Greece*
[1] also Center for Earth Observing and Space Research, Institute for Computational Sciences, George Mason University, Fairfax, VA 22030, USA

of the most important properties of coronal loops concern their densities and the thermal distribution of plasma obtained in them. It is that coronal loops seen in the in the EUV in temperatures of 1-2 MK are overdense 2-2000 times with respect to static equilibrium theory, whereas they are underdense when seen in "hotter" emission (T> 2 MK) in SXR (Winebarger et al. 2003). In the frame of static equilibrium theory (e.g., Rosner, Tucher and Vaiana 1978) loops are steady (time independent) structures characterized by force and energy balance in the absence of flow. It seems that steady flows cannot help to explain the bulk of the observations (Patsourakos, Klimchuk and McNeice 2004). Spectroscopic observations of coronal loops have shown that they can be characterized by broad differential emission measure (DEM) distributions (e.g., Schmelz et al. 2001).

The above observations call for: (1) time-dependent heating and (2) multi-thermal plasmas in coronal loops. It is thus that impulsive nanoflare heating at sub-resolution strands could be a possibility for explaining these observations. With this work we address the above issues by the means of hydrodynamic simulations of nanoflares. In Section 2 we describe the numerical model we used and the details of our calculations In Section 3 we give our results and our conclusions.

2. NUMERICAL MODEL

Given the fact that the solar corona is a highly conducting low β medium, the magnetic field confines the plasma within flux tubes, and the plasma can be described with 1D hydrodynamics. The time-dependent single-fluid equations for conservation of mass, momentum and energy along a coronal loop are:

$$\frac{\partial \rho}{\partial t} + \frac{\partial}{\partial s}(\rho \upsilon) = 0, \tag{1}$$

$$\frac{\partial}{\partial t}(\rho \upsilon) + \frac{\partial}{\partial s}(\rho \upsilon^2) = \rho g_{\|}(s) - \frac{\partial P}{\partial s}, \tag{2}$$

$$\left[\left(E + P \right) \upsilon \right] = \rho \upsilon g_{\|}(s) + \frac{\partial}{\partial s}\left(k_0 T^{5/2} \frac{\partial T}{\partial s} \right) - n^2 \Lambda(T) + H, \tag{3}$$

and

$$E = \frac{1}{2}\rho \upsilon^2 + \frac{P}{\gamma - 1}, \tag{4}$$

where we have assumed that loops have a constant cross section, as supported by observations of both EUV and SXR loops (Watko and Klimchuk 2000; Klimchuk 2000). In the above equations, s corresponds to the distance along the loop from the "left" base of the model; ρ = 1.67 x 10^{-24} x n is the mass density assuming a fully ionized hydrogen plasma with n being the electron number density; υ is the plasma flow velocity; T is the plasma temperature; $P = 2nkT$ is the pressure from the ideal gas law; $\kappa_0 = 10^{-6}$ is the coefficient of thermal conduction; $\gamma = 5/3$ is the ratio of the specific heats; H is the volumetric heating rate; $\Lambda(T)$ is the optically thin radiation loss function, and $g_{\|}(s)$ is the component of gravity parallel to the loop axis.

The coronal part of our loop is taken to be semicircular with a full length L = 150 Mm, typical of observed EUV and SXR loops. Attached to each end of the coronal semicircle is a 60 Mm chromospheric section.

We adopt an optically thin radiative loss function $\Lambda(T)$ that has a piecewise continuous power-law form as given by Klimchuk and Cargill (2001). The loss function drops precipitously to zero between 30,000 and 29,500 K, guaranteeing that the model chromosphere is approximately isothermal within the temperature range. A more realistic treatment would require optically thick radiative transfer and is unnecessary for studying the properties of the coronal part of the loop. All that we demand of the chromosphere is that it provides a source and sink of mass through the processes of chromospheric evaporation and condensation.

Equations (1) to (3) are solved using our state-of-art 1D hydrodynamic code we call Adaptively Refined Godunov Solver (ARGOS), described in detail in Antiochos et al. (1999). Two aspects of ARGOS make it particularly well suited for studying coronal and transition region dynamics. First, the time-dependent solution is advanced using a second-order Godunov scheme with a MUSCL limiter, which is one of the most robust numerical schemes for studying 1D hydrodynamics. Second, ARGOS employs the PAEAMESH parallel adaptive mesh refinement (AMR) package, which dynamically refines or derefines the grid based on the local density variations. For the applications described in this paper, the minimum grid spacing is roughly 25 km and is adequate for resolving the small spatial scales of the transition region. Rigid wall boundary conditions are applied at the ends of the flux tube. Our model chromosphere is many gravitational scale heights thick [$H_g(T = 30{,}000\text{K}) \approx$ 1500 Mm] so that the boundary conditions have negligible influence on the plasma dynamics in the transition region and corona and so that the height of the chromosphere is not affected by the depletion and accumulation of mass.

3. RESULTS AND DISCUSSION

For the loop described above we first calculated a static equilibrium solution. We applied a heating that is uniform in space and constant in time and we let the system evolve to a static equilibrium. The equilibrium loop had an apex temperature of ≈ 2.5 MK and was used as an initial condition for the nanoflare calculations reported below. Given that we: (1) apply very strong heating and (2) consider many nanoflares, the choice of the initial condition does not impact the evolution of the loop.

We then ejected 60 successive nanoflares into the loop. The nanoflares were modeled by applying a spatially uniform heating every 3800 s, with each nanoflare lasting 250 s. The heating $H = H_{nano}$ associated with each nanoflare was selected randomly from the interval 0.002 – 0.06 erg cm^{-3} s^{-1} and remained constant during each nanoflare. In the intervals between consecutive nanoflares no other additional heating was applied. Considering a sub-resolution (say 100 km^2) cross-sectional area of the applied nanoflares, their duration, and the employed H_{nano} leads to energies falling into the nanoflare regime. Therefore the "loop" considered here is formerly equivalent to a sub-resolution strand in a "macroscopic" loop. The convolution of a large number of such strands makes up the "macroscopic" loops.

From the solution of Equations (1) – (3) we had the temporal evolution of the density and temperature along the loop. We calculated the spatial averages of n and T in the upper 2/3 of the loop.

In Figure 1 we plot the ration $n_{nanoflare}/n_{static}$ of the calculated densities to the density of the static loop with the same temperature for all the nanoflares considered here. The latter were calculated using the scaling law of Rosner et al. (1978) relating n and T for static loops. We first note that for any given T, $n_{nanoflare}/n_{statiac}$ varies substantially. This results from the fact that we considered nanoflaraes with different energies. Second, we observe that $n_{nanoflar}e/n_{static}$ is smaller than 1 (i.e., the loop is underdense) for temperatures higher than ≈ 2 MK, corresponding to SXR observations, but that it is larger than 1 (i.e., the loop is overdense) for lower temperatures, corresponding to EUV observations. This kind of bifurcated behavior is in good agreement with the observations (Winebarger et al. 2003). Moreover the resulting $n_{nanoflare}/ns_{tatic}$ fall withinthe range of the observed over and underdensities.

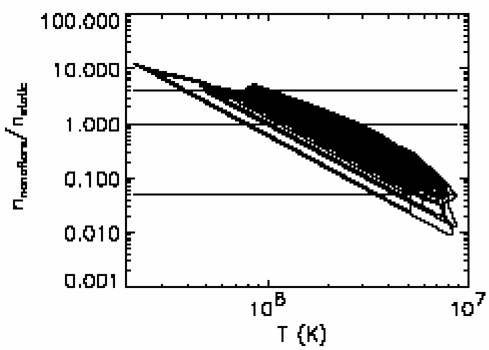

Figure 1. *Ratio of the loop density from the nanoflare calculations to the density of a static loop at the same temperature for all the 60 nanoflares considered here. The upper and lower horizontal lines observed loop density to the density of a static loop with the same temperatures for loops with the same length as the loop used in our calculations.*

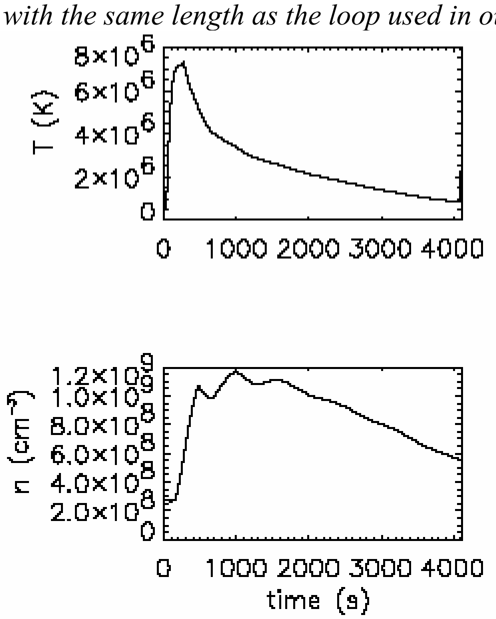

Figure 2. Time – evolution of the average temperature (upper panel) and density (lower panel) for a sample nanoflare.

To understand this behavior we show in Figure 2 the evolution of the average temperature and density for a sample nanoflare. In the first 250 s, the time during which the nanoflare heating is “on”, we note that both temperature and density are increasing. The temperature increase is due to the intense and impulsive nanoflare heating whereas the density increase is dye to the intense and impulsive nanoflare heating whereas the density increase is due to the evaporation of dense chromospheric material into the loop. After the heating is turned off the loop starts to cool down. It fast cools down by conduction. This results in an increase of the density due to chromospheric evaporation, while the temperature is falling. It is thus that the cooling loop would be underdense with respect to a static loop (static equilibrium predicts that $n \propto T^2$) with the same temperature. Then, when the loop temperature is low enough (< 2 MK), the loop cools down by radiation. The density now drops, since mass drains from the corona into the foot points, but this occurs at smaller rate than for the temperature. We thus have that the loop would be overdense with respect to a static loop at the same temperature.

We then calculated the *DEM* distribution from the average *n* and *T* averaged over both space and time. The *DEM* is defined as:

$$DEM(T) = n^2 dh / dt, \tag{5}$$

with *dh* the extent of the loop along the line of sight (taken as 2000 K which is a typical loop diameter). For calculating *DEM* we first defined a grid in *T* with a step of 0.3 in *logT* and then found the densities corresponding to each temperature bin *dT*. *DEM* thus provides a measure of the amount of plasma at a given temperature.

The resulting *DEM* is in Figure 3. It has a roughly symmetric shape and a significant width in *T* in the range ≈ $10^{5.5} - 10^{6.5}$ K which is consistent with the observations of Schmelz et al. (2001). Nanoflares lead to broad *DEM* in multi-stranded loops because a any given time there are strands in the loop at different stages (i.e., temperatures) of their cooling/heating. It is therefore that plasma can be found at many different temperatures which in turn is reflected in broad EM distributions.

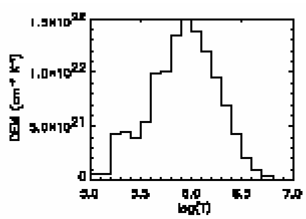

Figure 3. *DEM* distribution for the 60 nanoflares considered in this work.

Our results are very promising for explaining the over and underdensities and the broad *DEM* of coronal loops. Nanoflares at sub-resolution strands qualitatively capture also some other important properties of coronal loops such as flat intensity filter ratios, lifetimes and net redshifts. We plan to carry out more detailed comparisons of similar models with loop observations.

ACKNOWLEDGMENTS : Research supported by NASA and ONR.

RERERENCES

Antiochos, S.K., MacNeice, P.J., Spicer,D.S., and Klimchuk, J.A. 1999, ApJ, 512, 985
Aschwanden, M.J., Schrijver, C.J., and Alexander, D. 2001, ApJ, 550,1036
Bray, R.J., Cram, L.E., Durrant, C.J. and Loughead, R.E. 1991, Plasma Loops in the Solar Corona (Cambridge: Cambridge Univ. Press)
Cargill, P.J. 1994, ApJ, 422, 381
Klimchuk, J.A. 2000, Sol. Phys., 193, 53
Klimchuk, J.A., and Cargill, P.J. 2001, ApJ, 553, 440
Mandrini, C.H., Demoulin, P. and Klimchuk, J.A. 2001, ApJ, 530, 999
Parker, E.N. 1988, ApJ, 330, 474
Patsourakos, S., Klimchuk, J.A., and MacNeice, P.J. 2004, ApJ, in press
Rosner, R., Tucker, W.H. and Vaiana, G.S. 1978, ApJ, 220, 643
Schmelz, J.T. et al. 2001, ApJ, 556, 896
Watko, J.A., and Klimchuk, J.A. 2000, Sol. Phys. 193, 77
Winebarger, A.R., Warren, H.P., and Mariska, J.T. 2003, ApJ, 587, 439

ON THE APPLICATION OF NUMERICAL BIFURCATION ANALYSIS VERSUS LINEAR STABILITY THEORY TO CORONAL LOOP EQUILIBRIA*

Z. Romeou[1] and T. Neukirch[2]

[1] Center for Astrophysics, University of Central Lancashire, Preston, PR1 2HE, U.K.
[2] School of Mathematics and Statistics, University of St Andrews, St Andrews, U.K.

ABSTRACT
In the present work we investigate the connection between linear MHD stability thresholds and equilibrium bifurcation points for axisymmetric straight flux tube models of line-tied coronal loops. We further discuss the importance of this study for models of solar eruptive processes where the onset of the eruption is identified with the bifurcation of an equilibrium sequence, as well as in future investigations of bifurcations in 3D cases and their interpretation in terms of solar activity.

1 INTRODUCTION
MHD instabilities of coronal loops have been suggested for a long time as a possible mechanism for explaining solar eruptive phenomena like flares (e.g. Priest, 1982; Priest & Forbes, 2002). The concept is to drive a stable tube unstable by slow changes of the boundary conditions. In the context of MHD linear analysis this means that at least one MHD mode becomes unstable at a certain instability threshold. If the system is modelled by a sequence of equilibria it is expected that the linear instability point corresponds to a bifurcation point of the equilibrium theory. In the present paper we investigate how far this assumption holds, e.g whether the points of linear instability of rotationally symmetric straight line-tied flux tubes have a one-to-one correspondence with the bifurcation points of equilibrium sequences.
For this study we used the well known Gold-Hoyle equilibrium class of axisymmetric magnetic flux tubes (Gold & Hoyle, 1960), which can be considered as straight analogues of coronal loops and for which results are readily available in the literature (e.g Hood & Priest, 1979; De Bruyne & Hood 1992). We have used two different ways of calculating the equilibrium sequences, namely Grad-Shafranov theory and Euler potentials.
The related physical background is presented in Section 1, in Section 2 we briefly discuss the numerical method used to calculate the equilibrium sequences and to determine their bifurcation points and branches, in Section 3 the results of these calculations are presented and discussed and Section 5 summarises and concludes.

2 THE PHYSICAL BACKGROUND
In the theory of straight axisymmetric flux tubes which are often used to model coronal loops the magnetic field can be conveniently written as

$$\mathrm{B}_0 = \nabla A \times \nabla \phi + B_\phi \mathrm{e}_\phi \tag{1}$$

resulting in the *Grad-Shafranov* equation for rotational symmetry in cylindrical coordinates

$$-\nabla \cdot \left(\frac{1}{r^2} \nabla A \right) = \mu_0 \frac{\mathrm{d}p}{\mathrm{d}A} + \frac{1}{r^2} b_\phi \frac{\mathrm{d}b_\phi}{\mathrm{d}A} \tag{2}$$

* *Proceedings of the 6th Hellenic Astronomical Society Conference, 15-17 September 2003, Penteli, Greece*

where $b_\phi(r,z) = rB_\phi(r,z) = G(A_0(r,z))$. The equilibrium selected for this analysis is the constant twist Gold-Hoyle field. For this class of axisymmetric equilibria $A_0^{G\text{-}H}$ gets the form

$$A_0^{G\text{-}H} = \frac{\lambda}{2}\ln(1+r^2) \tag{3}$$

Pressure is given by

$$p(A) = \frac{1}{2}\left(1-\lambda^2\right)\exp\left(-\frac{4A}{\lambda}\right) \tag{4}$$

For this field, it has been found with different methods that for lying-tying conditions and for the force-free case, there is a critical loop length $L/b \approx 2.5\pi$ for the m = 1 kink mode. The non-force-free case was investigated in De Bruyne and Hood (1989), where a sufficient condition for stability and the instability region for localized modes ($m \to \infty$) were calculated. De Bruyne and Hood (1992) derived linear stability thresholds for the whole range of m values depending on the loop length L, and we will use their results for the m = 0 mode.
An alternative approach is offered within the *Euler Potentials* representation where the magnetic field is determined by two scalar α and β, such that

$$\mathrm{B} = \nabla\alpha \times \nabla\beta. \tag{5}$$

As the system is axisymmetric, we introduce $\widetilde{\beta} = -\frac{1}{\lambda}z$ by $\beta = \widetilde{\beta} + \phi$ where ϕ is the coordinate of invariance in our system of cylindrical coordinates r, ϕ, z . We then get

$$\mathrm{B} = \nabla\alpha \times \nabla\widetilde{\beta} + \nabla\alpha \times \nabla\phi. \tag{6}$$

We can compare this with the Grad-Shafranov theory by noticing that α is the same function as the flux function A . For the starting equilibrium solution, we have $\alpha = A_{G\text{-}H} = \frac{1}{2}\lambda\ln\left(1-r^2\right)$.
The profile for the other Euler potential, $\widetilde{\beta}$ will be determined so that it is consistent with this choice of α , and the boundary conditions of the Gold-Hoyle solution, namely $\widetilde{\beta} = -\frac{1}{\lambda}z$. We now need to solve the following two coupled nonlinear equations

$$\nabla\widetilde{\beta}\cdot\nabla\times(\nabla\alpha\times\nabla\widetilde{\beta}) - \nabla\cdot\left(\frac{1}{r^2}\nabla\alpha\right) = \frac{dp}{dA}, \tag{7}$$

$$\nabla\alpha\cdot\nabla\times(\nabla\widetilde{\beta}\times\nabla\alpha) = 0. \tag{8}$$

3 THE NUMERICAL METHOD

The numerical method we use solves the force balance equation (in either the Grad-Shafranov or the Euler potential form) with a predictor-corrector continuation scheme proposed by Keller (1977). The code solves the resulting partial differential equations by using a Ritz-Galerkin method which provides a built-in stability criterion, (see Schindler et al., 1983). The discretization is done by finite elements and Gauss elimination with pivoting is used for the inversion of the discritized matrix. The 2D version of the code uses triangle elements with six node points and quadratic shape functions. We have recently developed a 3D version of the code which uses cubic elements with eight node points and trilinear shape functions. A 3D version of the code is presently in the testing phase (see Romeou and Neukirch, 2002, and references there in).

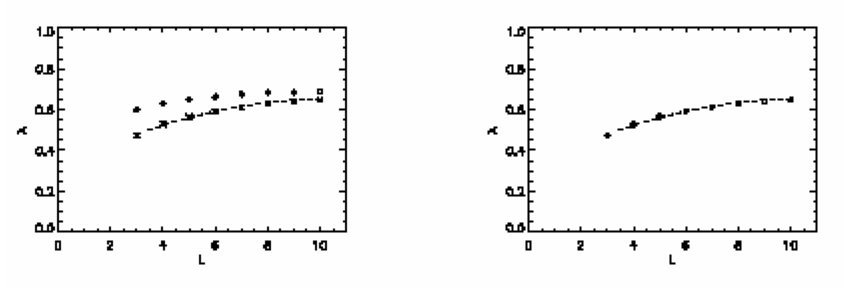

Figure 1: The left column shows the first (◊) and the second (×) set of bifurcation points for the G-S case. It is the second and not the first set that falls onto the m = 0 instability curve (dashed line) derived by linear stability analysis. The right column refers to the Euler potential case and shows that in this case it is the first (◊) bifurcation point that corresponds to the linear instability threshold of the m = 0-mode derived by De Bruyne & Hood (1992) (dashed line).

4 RESULTS AND DISCUSSION

We used the same computational domain as Longbottom et al. (1996), namely a cylinder with $0 \le r \le R$ and $0 \le z \le L$. We set R = 8 and L = 3, 4, 5, 6, 7, 8, 10 for the Grad-Shafranov case and L = 3, 5, 7 for the E.P case. The imposed boundary conditions were $A = A_{G-H}$ on all boundaries in the Grad-Shafranov case and $a = A_{G-H}$ and $\widetilde{\beta} = -\frac{1}{\lambda} z$ in the E.P case. We calculated equilibrium sequences for each value of L starting from λ = 1 and following the branches towards values of $\lambda < 1$.

The values of λ at the first two bifurcations points encountered in the Grad-Shafranov case are compared with the linear instability thresholds for the m = 0 mode as derived by De Bruyne and Hood (1992) in Fig. 1 (left column). It is obvious that the instability corresponds to the second and not the first bifurcation point, if counted in the direction of decreasing λ. The reason for this behaviour can be found by calculating the bifurcating branches and investigating the spatial structure of A along these branches. As an example we show the bifurcation diagram for the case $\lambda = 7$ in Fig. 2 (middle column).

The spatial structure of A for example solutions on the two bifurcating branches is shown in Fig. 2, (side columns). Obviously the z-dependence of A on the first branch is of $\sin(\pi z/L)$ -type whereas the second branch has a $\sin(2\pi z/L)$ behaviour.

The linear stability analysis for line-tied boundary conditions performed by De Bruyne and Hood (1992) predicts a $\sin(2\pi z/L)$ dependence on z for the m = 0-mode. The profile of the magnetic field lines for the two bifurcating branches shows that it is the branch of the second bifurcation point that confirms this result.

The results for the Euler potential case are shown in Fig. 1, right column. In this case it is the first bifurcation point detected by the code that coincides with the m = 0-mode instability threshold of De Bruyne and Hood (1992).

This behaviour can be understood by comparing the mode structure of linear stability analysis with the structure of the calculated bifurcating branch. Whereas for the line-tied stability analysis the perturbation must vanish on the boundaries, the G-S theory requires only the component perpedicular to the poloidal magnetic field to be fixed. Therefore existence of additional critical points is possible.

No additional bifurcations have been found when Euler potentials are used, possibly because the further constraint for the $\widetilde{\beta}$ Euler potential that has to be imposed on the boundaries does not allow the development of this additional mode.

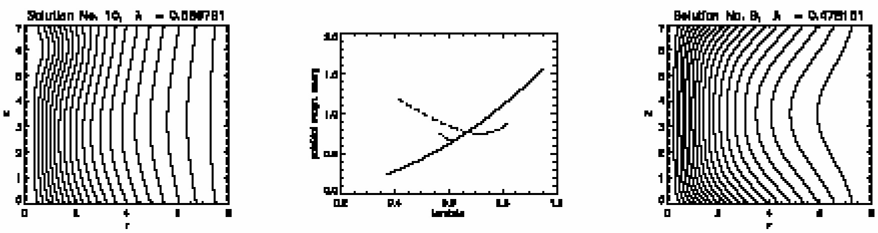

Figure 2: The middle column shows solution diagrams for the L = 7 case. The full line represents the basic G-H branch onto which we overplotted in dashed and dash-dotted lines the bifurcation branches for the first two bifurcations, counting from right to left. The side columns show magnetic flux contours for the corresponding branches. The left column corresponds to the left bifurcating branch (2nd bifurcation point) while the right column corresponds to the right branch (1st bifurcation point).

5 CONCLUSIONS

We have used an axisymmetric predictor-corrector continuation code to investigate the connection between bifurcations of MHD equilibrium sequences and the stability threshold predicted by linear stability theory for line-tied equilibria. It was found that depending on the way the equilibrium sequences are calculated (Grad-Shafranov theory or Euler potentials) the bifurcation structure changes. In the first case, it was shown that not the first bifurcation point but the second one coincides with the linear stability threshold of the m = 0 sausage instability. On the contrary, in the Euler potential case, applying the same numerical bifurcation method leeds to results consistent with the predictions of linear stability theory. This agreement between linear stability and E.P. results makes them very important and most favourable candidates for future 3D studies, not necessarily assuming symmetry, where a thorough analytical theory as to which bifurcations are the correct ones and can be interpreted as onsets of solar eruptive processes is not as yet available.

Acknowledgments

The authors thank Alan Hood for useful discussions. This work has been partially supported by the European Community's Human Potential programme under contract number HPRN-CT-2000-00153, PLATON.

REFERENCES

De Bruyne P. and Hood A.W., 1989, Solar Phys., 123, 241
De Bruyne P. and Hood A.W., 1992, Solar Phys., 142, 87
Gold T. and Hoyle F., 1960, MNRAS 120, 89
Hood A.W. and Priest E.R., 1979, Solar Phys., 64, 303
Keller H.B., 1977, in Rabinowitz P.H. (ed.) Applications of Bifurcation Theory, Academic Press, New York, p.359
Priest E.R., 1982, Solar Magnetohydrodynamics, D.Reidel, Dordrecht
Priest E.R. and Forbes T.G., 2002, A& AR 10, 313
Romeou Z. and Neukirch T., 2002, JASTP 64, 639
Schindler K. et al, 1983, Solar Phys., 87, 103

DEPENDENCE OF THE DECAY PHASE OF SOLAR ENERGETIC ELECTRON EVENTS ON THE LARGE-SCALE IMF STRUCTURE: *ACE* OBSERVATIONS[•]

Emmanuel T. Sarris and Olga E. Malandraki[2]

Space Research Laboratory, Democritus University of Thrace, Xanthi 67100, Greece

Abstract. Using recent measurements of energetic electrons (≥ 38 keV) by the *ACE*/EPAM experiment, we examine the dependence of the characteristic decay time of two impulsive solar electron events on the large-scale structure of the Interplanetary Magnetic Field (IMF) within which the electrons are emitted. The technique of mapping the solar wind and extrapolating the frozen-in magnetic field is used to obtain the large-scale IMF structure within and beyond the location of the ACE spacecraft. We find that the electron event that occurred within a converging IMF structure exhibits a remarkably longer decay phase compared to the electron event observed inside a diverging IMF configuration. The observations provide strong evidence for the location of magnetic "barriers" in space beyond 1 AU and their role in determining the decay phase of solar energetic electron events and the establishment and maintenance of particle reservoirs in the Heliosphere.

1. Introduction

Early in the spacecraft era it was shown that, following many solar events, the Heliosphere within about 1 AU became nearly uniformly filled with energetic particles [*McCracken et al.,* 1967; *McKibben*, 1972]. *Roelof et al* [1992] showed that a charged particle reservoir fills the inner Heliosphere out to ~3.5 AU following intense solar activity, with the density in the reservoir slowly decaying over time. However, the exact interplanetary conditions that contribute to the establishment and maintenance of these particle reservoirs following solar events remain unknown. In this paper, we examine the dependence of the characteristic decay time scale for two impulsive solar electron events on the large-scale structure of the IMF and its implications for particle containment and the formation of particle reservoirs in space. Fine time resolution measurements of magnetically deflected electrons (DE) measured by the B detector of the CA60 telescope of the EPAM experiment (Electron Proton, and Alpha Monitor) onboard *ACE* are utilized. A full description of the EPAM experiment has been given by *Gold et al.* [1998]. Solar wind data were provided by the *ACE*/SWEPAM experiment described in detail by *McComas et al.* [1998].

2. Observations and Data Analysis

Figure 1 shows 1-minute averages of the differential intensity of 53-103 keV electrons as measured by the *ACE*/EPAM experiment for the interval from 0600-1600 UT, April 30, 2001 (DOY 120), during which a major impulsive solar electron event is detected. The exponential decay of the electron event has a characteristic decay time scale of ~ 10 minutes. This is typical for the decay phase of the so-called 'scatter-free' electron events [*Lin*, 1970] in which the electron intensities drop down to ~1/e of their peak value in a few tens of minutes. This event was associated with a soft X-ray flare (class C2.2) [*Solar Geophysical data*, http://sgd.ngdc.noaa.gov/sgd/jsp/solarindex.jsp, 2001]. Inspection of the pitch angle distributions (PADs) shows that strong unidirectional anisotropies are persistently observed after the onset of the event (Figure 2*a*), consistent with a relatively 'scatter-free' electron propagation [*Haggerty and Roelof,* 2002].

[•] *Proceedings 6th Hellenic Astronomical Society Conference, 15-17 September 2003, Penteli, Athens, Greece*

[2] *Also at National Observatory of Athens, Institute for Space Applications and Remote Sensing, Athens, Greece.*

In Figure 3, we map the measured solar wind (*ACE*/SWEPAM experiment) and the frozen-in magnetic field to the Carrington connection longitude at the solar corona [*Nolte and Roelof,* 1973] in order to obtain a picture of the large scale solar wind stream and IMF

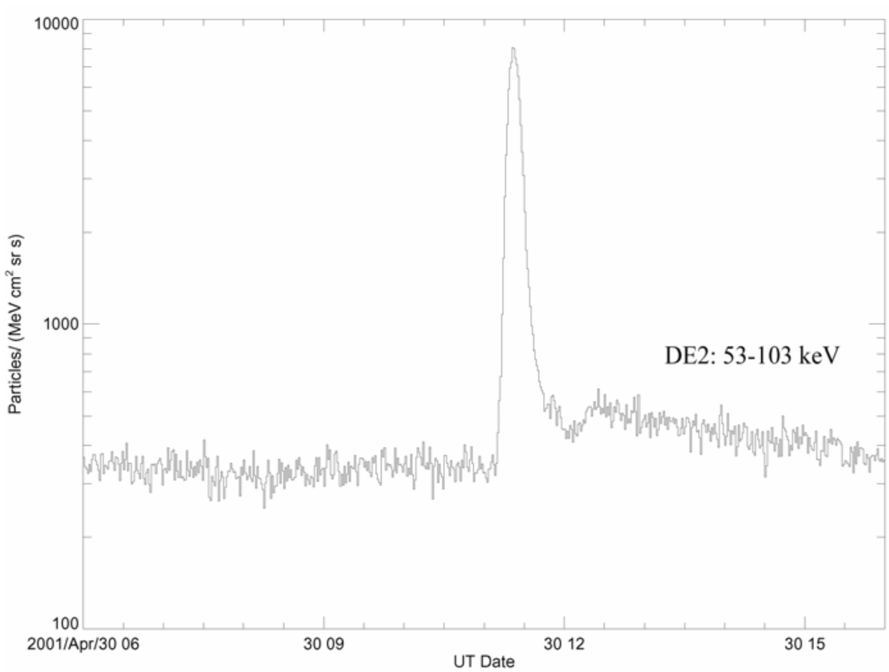

Figure 1. High-resolution time-intensity profile of an energetic (53-103 keV) electron event observed on April 30, 2001 at 1 AU by *ACE*/EPAM.

structure within and beyond the radial distance of *ACE* during the electron event. The relationship between Carrington connection longitude L and distance R from the Sun is given by the equation $L(t) = L_o(t) + (\Omega/V)\,R$, where $L_o(t)$ is the Carrington longitude of *ACE* at the time of observation, Ω the solar sidereal rotation, and V the measured solar wind speed. In this representation, the time marked on the horizontal line at 1 AU runs from right to left as the spacecraft crosses the streamlines which are fixed to the Sun. Figure 3 shows that the energetic electrons observed on April 30 (DOY 120) were injected within a clearly diverging configuration of the large scale structure of the IMF to distances well beyond ~3 AU.

In Figure 4, we present differential intensities of energetic electrons (53-103 keV) obtained by the *ACE*/EPAM experiment from 1800 UT, July 9, 2002 (DOY 190) to July 11, 2002 (DOY 192), during an impulsive solar electron event that exhibits remarkably different characteristics than the

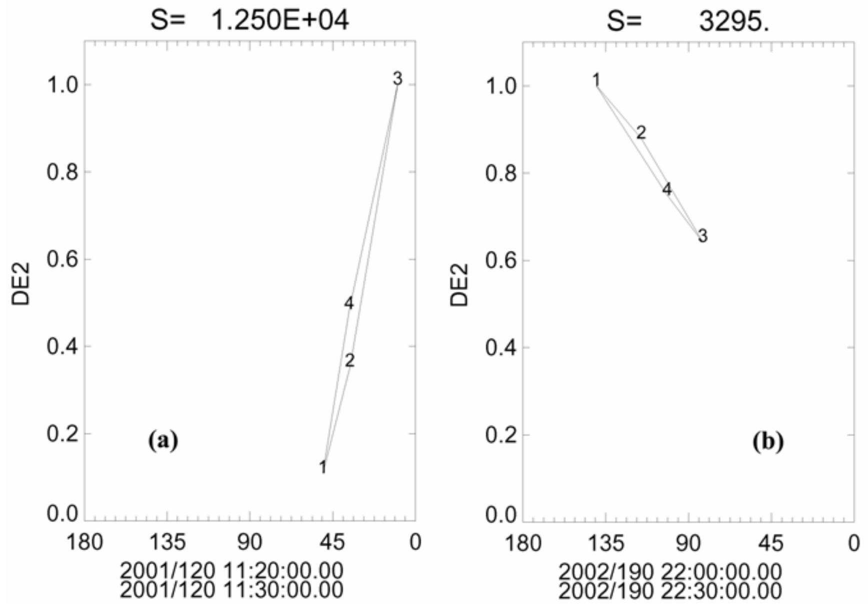

Figure 2. Pitch-angle distribution snapshots for the two solar electron events (DE2: 53-103 keV). Normalized differential flux is plotted versus pitch angle. The accumulation interval is indicated below each graph; on top of the figure, S indicates the maximal flux to which the distribution is normalized.

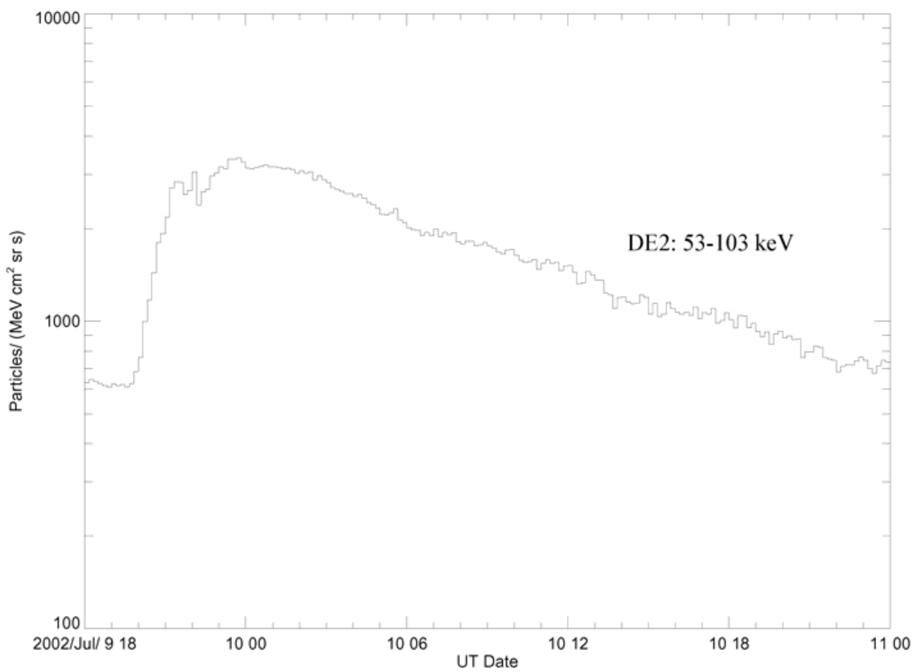

Figure 4. Fine time resolution measurements of the intensities of energetic electrons (53-103 keV) by *ACE*/EPAM during the solar electron event observed in July 2002.

previous one. The observed e-folding flux decay time of this electron event is ~ 14 hrs. After the event onset *ACE* detects strong unidirectional electron PADs (Figure 2*b),* indicating the electrons are streaming away from the Sun, that evolve to isotropic distributions in ~ 3 hrs. We have examined the configuration of the interplanetary medium during the electron event, incorporating again the technique of mapping the observed solar wind back to the solar corona, as presented in Figure 5. The streamlines within which the electrons were emitted are intersected beyond 1 AU by a faster solar wind stream. Colliding solar wind streams originating at different parts of the solar corona give rise to extended regions with compressed magnetic field. It is important to know the presence and location of these magnetic constrictions since they act as reflecting magnetic mirrors along the path of the injected energetic electrons [*Sarris et al.,* 1983; *Malandraki et al.,* 1997]. The distance along the spiral flux tube from *ACE* to the magnetic constriction for the July 9, 2002 electron event is computed to be ~2.7 AU beyond the s/c.

2. Discussion

In order to investigate the physical reasons that lead to the formation of particle reservoirs in the interplanetary space we have studied two impulsive solar energetic electron events observed by the *ACE*/EPAM experiment under clearly diverging and converging configurations of the large-scale IMF structure. Our observations demonstrate that the July 9, 2002 electron event was observed within flux tubes that were strongly converging with a following faster solar wind stream. It is estimated that a magnetic constriction was formed at a distance of ~ 2.7 AU along the magnetic flux tube beyond the location of *ACE*; this had a strong effect on the electron transport by damming the particle outflow in its immediate vicinity. Hence, the energetic electrons are “semi-trapped” within a magnetic bottle, bouncing back and forth between mirrors located near the Sun and beyond *ACE*. The observed long decay phase of the electron event with the unusually large (~ 14 hours) e-folding time scale is determined by the various leakage processes, which operate on the trapped energetic electrons. First, electrons leak through the magnetic bottleneck by diffusing into the loss cone due to small-angle pitch angle scattering. This takes place during their propagation in between the magnetic mirrors, as evidenced by the isotropic PADs observed during the decay phase of the electron event. Furthermore, electrons drifting across the highly inhomogeneous magnetic fields prevailing at the stream-stream interaction region, as well as near the Sun, can escape onto field lines outside the containment region. The flux decay rate of the electron event is thus dominated by the rate of electron leakage from the containment region. It is noted that *Bieber et al.* [2002] successfully simulated the intensity and anisotropy profiles of high energy solar particles during the Bastille Day event, incorporating the model of focused transport through a presumed magnetic bottleneck formed by a CME ~ 0.3 AU beyond the Earth’s orbit.

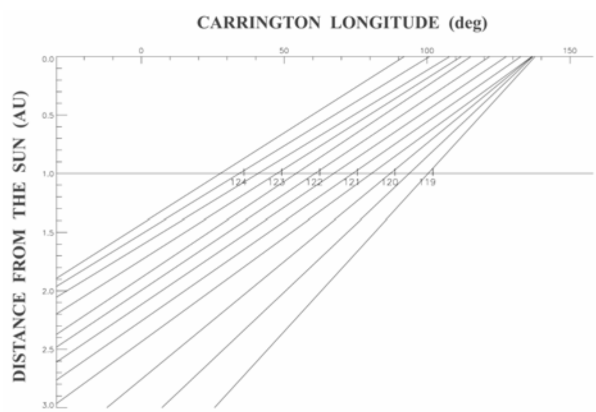

Figure 3. Mapping of the observed solar wind to the Carrington connection longitude at the solar corona during the solar electron event of April 30, 2001.

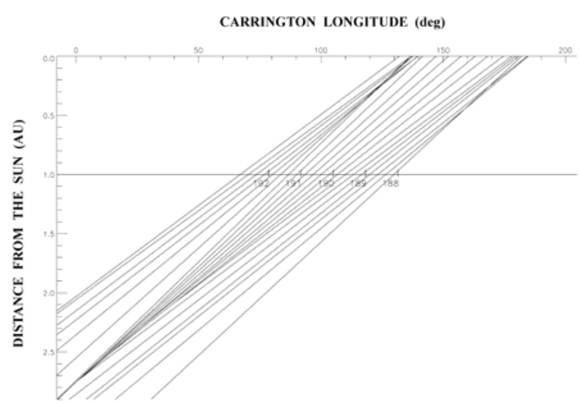

Figure 5. Mapping of the observed solar wind to the Carrington connection longitude at the solar corona during the solar electron event of July 9, 2002.

On the contrary, the April 30, 2001 electron event occurred in a configuration of the interplanetary medium with diverging streamlines and shows dramatically different features. For the exponential decay of the electron event the e-folding time of the electron intensities is only ~ 10 min. In this case, no large-scale magnetic constriction or stream-stream interaction is anticipated in the nearby interplanetary space. Thus, the energetic electrons following their impulsive injection at the

Sun are able to “freely escape” along the IMF over distances of ~ 10 AU and their intensities decay quickly filling up a huge region of space.

These observations provide strong evidence for the physical mechanisms that determine the decay rate of solar energetic electron events and the establishment and maintenance of particle reservoirs in the Heliosphere, based on the inferred locations of magnetic “barriers” in space beyond 1 AU.

Acknowledgements. We are thankful to our HI-SCALE team colleagues for their support and encouragement. We also thank the *ACE* SWEPAM instrument team and the ACE Science Center for providing the *ACE* data. O.E.M. acknowledges support from the State Scholarships Foundation (I.K.Y.) through a Post-Doctoral Fellowship.

References

Bieber, J. W., et al., *Astrophys. J., 567,* 622, 2002
Gold, R. E., et al., *Space Sci. Reviews, 86,* 541, 1998.
Haggerty, D. K., and E. C. Roelof, *Astrophys. J., 579,* 841, 2002.
Lin, R. P., *Solar Phys.,15*, 453, 1970.
Malandraki, O. E., et al., *Proc. 25th Int. Cosmic Ray Conf.,* Durban, S. Africa, 1, 281, 1997.
McComas, D. J., et al., *Space Sci. Reviews, 86,* 563, 1998.
McCracken, K. G., et al., *J. Geophys. Res., 72,* 4293, 1967.
McKibben, R. B., *J. Geophys. Res., 77,* 3957, 1972.
Nolte, J. T., and E. C. Roelof, *Solar Phys., 33*, 241, 1973.
Roelof, E. C., et al., *Geophys. Res. Lett., 19,* 1243, 1992.
Sarris, E. T., et al., *Solar Phys., 83*, 51, 1983.

THE NONLINEAR DYNAMICS OF THE MAGNETOSPHERE AND ITS IMPLICATIONS FOR SPACE WEATHER FORECASTING*

Isidoros Doxas[1]

University of Colorado Wendell Horton, University of Texas

Abstract: With the advent of Space Weather research and forecasting, the question of assimilating magnetospheric data into numerical forecast models becomes an important one. Contrary to tropospheric weather, where tens of thousands of data points are available, the much greater space of the magnetosphere is covered by only a small number of satellites. It is therefore becoming increasingly important to develop reduced models of the magnetospheric dynamics as driven by the solar wind, to aid us in developing reliable numerical forecast models with only a limited amount of data. Such efforts have been going on for over twenty years, and we will review some of the methods used and the results obtained to date, in particular as they relate to reduced representations of the magnetospheric dynamics.

[1] Main Session Invited Speaker

ON THE NATURE OF CHROMOSPHERIC UMBRAL FLASHES AND RUNNING PENUMBRAL WAVES

K.Tziotziou[1], G.Tsiropoula[2] , N.Mein[3] and P.Mein[3]

(1) Sterrekundig Instituut, Universiteit Utrecht, The Netherlands
(2) Institute for Space Applications and Remote Sensing, National Observatory of Athens, Greece
(3) LESIA, Observatoire de Paris, France

Abstract: Two dimensional, high cadence (8 sec), simultaneous Ha and CaII 8542 Å observations of umbral flashes and running penumbral waves in a sunspot at the chromospheric level have been analysed. The data were obtained on October 4, 2001 with the Multichannel Subtractive Double Pass (MSDP) spectrograph mounted on The German VTT telescope at Teide Observatory on Tenerife. Spectrograms, Doppler velocity movies, time slices, and wavelet analysis power maps are used to study the physical characteristics and the temporal behaviour of umbral flashes and running penumbral waves and to demonstrate that are closely related oscillatory phenomena, exhibiting however different oscillatory periods. We study the nature of umbral flashes and penumbral waves and further elaborate on the suggestion that flash brightenings are caused by shocked material which is combined with a coherent wave spreading over the entire sunspot.

* *Proceedings 6th Hellenic Astronomical Society Conference, 15-17 September 2003, Penteli, Athens, Greece*

TRACING THE MAGNETIC TOPOLOGY OF THE JULY 2000 CORONAL MASS EJECTION EVENT AT 62º SOUTH HELIOLATITUDE BY MEANS OF *ULYSSES*/HI-SCALE > 38 KeV ELECTRON OBSERVATIONS*

O. E. Malandraki[1,2], E. T. Sarris[1], P. Trochoutsos[1] and G. Tsiropoula[2]

[1] *Space Research Laboratory, Democritus University of Thrace, Xanthi, 67100, Greece*
[2] *National Observatory of Athens, ISARS, Penteli, Athens, 15236, Greece*

Abstract. We present results from a study of the energetic particle characteristics in the vicinity and during the traversal of an Interplanetary Coronal Mass Ejection (ICME) event observed by *Ulysses,* the unique s/c that is probing the heliosphere in 3-D, in July 2000 at 62º S heliographic latitude and ~ 3.2 AU helioradius. The still unsolved problem of whether ICMEs have been detached from the solar corona or are still magnetically anchored to it when they arrive at the s/c is rigorously tackled.

1. Introduction

Sarris and Krimigis (1982) have obtained the first estimates of the spatial extent of magnetic loops to distances ~ 3.5 AU from the Sun. Occasionally, the onset of a solar particle event is observed by a spacecraft located inside an ICME (Farrugia et al., 1993; Malandraki et al., 2000b, 2002). Such observations imply that the field lines embedded within the ICME structure remained connected to the Sun after the CME lift-off in the solar corona. Furthermore, the *Ulysses* observations presented by Malandraki et al. (2000a, 2001) strongly suggest the existence of both open and closed Interplanetary Magnetic Field (IMF) topologies rooted to the Sun within several ICMEs, probably resulting from 3-D magnetic reconnection at the Sun (Gosling et al. 1995). Moreover, more rarely, ICMEs are observed to involve more complex intertwined structures including regions both connected to and disconnected from the Sun (Malandraki et al. 2001). In this paper, we use solar flare energetic electron fluxes (E_e > 38 keV) injected by the large solar flare of X5.7 class which occurred on July 14, 2000 (Bastille day event) in order to probe the large-scale structure and topology of the IMF embedded within a well-identified ICME structure detected by *Ulysses* near solar maximum at 62º S heliolatitude. The angular distributions of the intensities of the energetic electrons as measured by the *Ulysses*/HI-SCALE instrument (Lanzerotti et al., 1992) are also utilized.

2. Observations and Data Analysis

An overview of the hourly and spin-averaged differential intensities of electrons in four energy channels (38-315 keV) as measured by the WART B detector head of the HI-SCALE experiment from 4-28 July, 2000 is presented in Fig. 1. An ICME, bounded by vertical traces C (Commencement) and E (End), began at 00:00 UT on July 15 and ended at 02:00 UT on July 16 (see Table I of Gosling and Forsyth, 2001). The ICME was observed during a major solar flare electron event.

In Fig. 2, we focus on the ICME and its vicinity. On the top panel, 30-min averaged electron intensities are shown for the interval 11-18 July, 2000. The three lower panels

* *Proceedings 6th Hellenic Astronomical Society Conference, 15-17 September 2003, Penteli, Athens, Greece*

present hourly-averaged magnetic field magnitude and direction in the RTN coordinate system. The ICME consisted an isolated magnetic field structure. A noteworthy feature is the very stable nature of the magnetic field inside the ICME compared to the turbulent field observed outside. The magnetic field magnitude remains nearly the same and the azimuth angle is constant throughout the ICME, whereas the observation of a smooth rotation in the field polar angle is a signature that the ICME has a flux rope structure (Gosling and Forsyth, 2001).

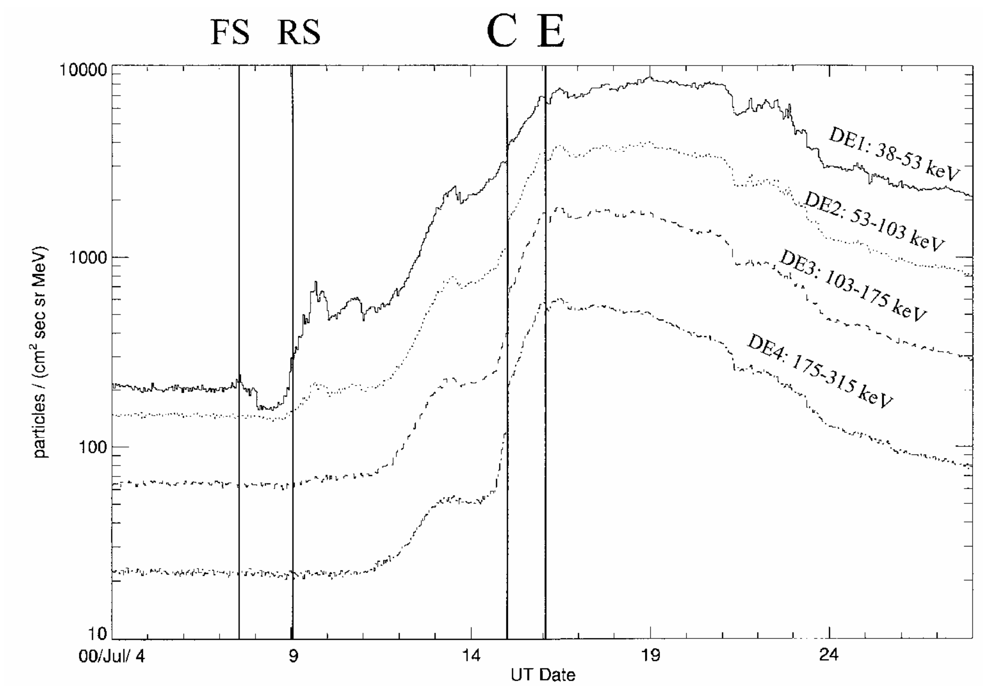

Figure 1. An ICME was observed by *Ulysses* at 62º south heliolatitude during the major solar electron event associated with the Bastille day solar flare.

The electron fluxes in the higher energy channels start an additional rise at 16:00 UT on July 14. During this period *Ulysses* was located at 62º S heliolatitude, at 3.2 AU helioradius and 116º east from the Earth. Using the measured solar wind velocity of 580 km/sec by the SWOOPS experiment onboard *Ulysses* at the onset of the event, the Parker spiral connecting *Ulysses* to the Sun was computed to be ~ 3.7 AU long and mapped back to S62W19 on the visible hemisphere of the Sun as viewed from the Earth. The transit time for a 175-315 keV electron with a 60º pitch angle along the ~ 3.7 AU long spirals is 1.5 hrs. Thus an injection time at the Sun at 14:30 UT on July 14 would be implied. On July 14, active region 9077 on the Sun produced the large Bastille day solar flare of X5.7 intensity (white light Ha importance 3B) which started at 10:03 UT and was located at N22 W07 and also a much less intense 1N/M3.7 solar flare at N20 W08 starting at 13:44 UT (Fig. 2, arrows on top panel). Obviously, there was a difference of 84º in heliolatitude between the magnetic connection of *Ulysses* to the Sun and the flare locations. The delayed onset and slow risetime of the electron event are to be expected from the consistently ‘poor’ nominal connection with the flare latitudes. The energetic electrons must have undergone drifts across the highly inhomogeneous fields near the Sun before reaching the *Ulysses* footpoint and escaping in space, populating this high latitude ICME.

Representative snapshots of the pitch-angle distributions (PADs) detected throughout the ICME and its vicinity are presented in Fig. 3. Normalized differential flux is plotted versus the pitch angle. J on top indicates the maximal flux to which the distribution is normalized. The time interval is indicated below each graph. The first three columns in Fig. 3 show snapshots of the isotropic PADs observed by *Ulysses* after the onset of the electron event outside the ICME. *Ulysses* detects a transition after entering the ICME: isotropic PADs outside suddenly switch to unidirectional inside, indicating electrons streaming away from the Sun are observed inside the ICME. Furthermore, upon entry into the ICME and coincident with the dramatic change in the electron PADs an abrupt and discontinuous increase in the particle intensities is observed (Fig. 2). We believe this indicates that the magnetic connection of *Ulysses* to the flare locations is greatly improved inside the ICME. Unidirectional PADs persist for 4 hrs inside the ICME. PADs show a clear tendency to unidirectionality till 16:00 UT on July 15. From that time till exit from the ICME *Ulysses* detected distinct unidirectional anisotropy in the PADs indicating electrons streaming away from the Sun were observed. The PADs become isotropic upon exit of the s/c from the ICME.

1. Summary and Conclusions

We have examined the electron intensities and directional distributions observed by the *Ulysses*/HI-SCALE experiment during the traversal and in the neighborhood of an ICME in July 2000. The ICME was observed during the risephase of a major electron event associated with intense flaring activity at the Sun (the Bastille Day solar flare). This implies a constant magnetic connection of the ICME to the Sun. Our observations indicate that energetic electrons injected by solar flares at the Sun and reaching the *Ulysses* footpoint are channeled by the ICME and propagate freely along the ICME magnetic field lines to 62º S heliolatitude. Thus, on the basis of the presented energetic particle observations, we conclude that open field lines rooted to the Sun at only one end are threading through this high latitude ICME.

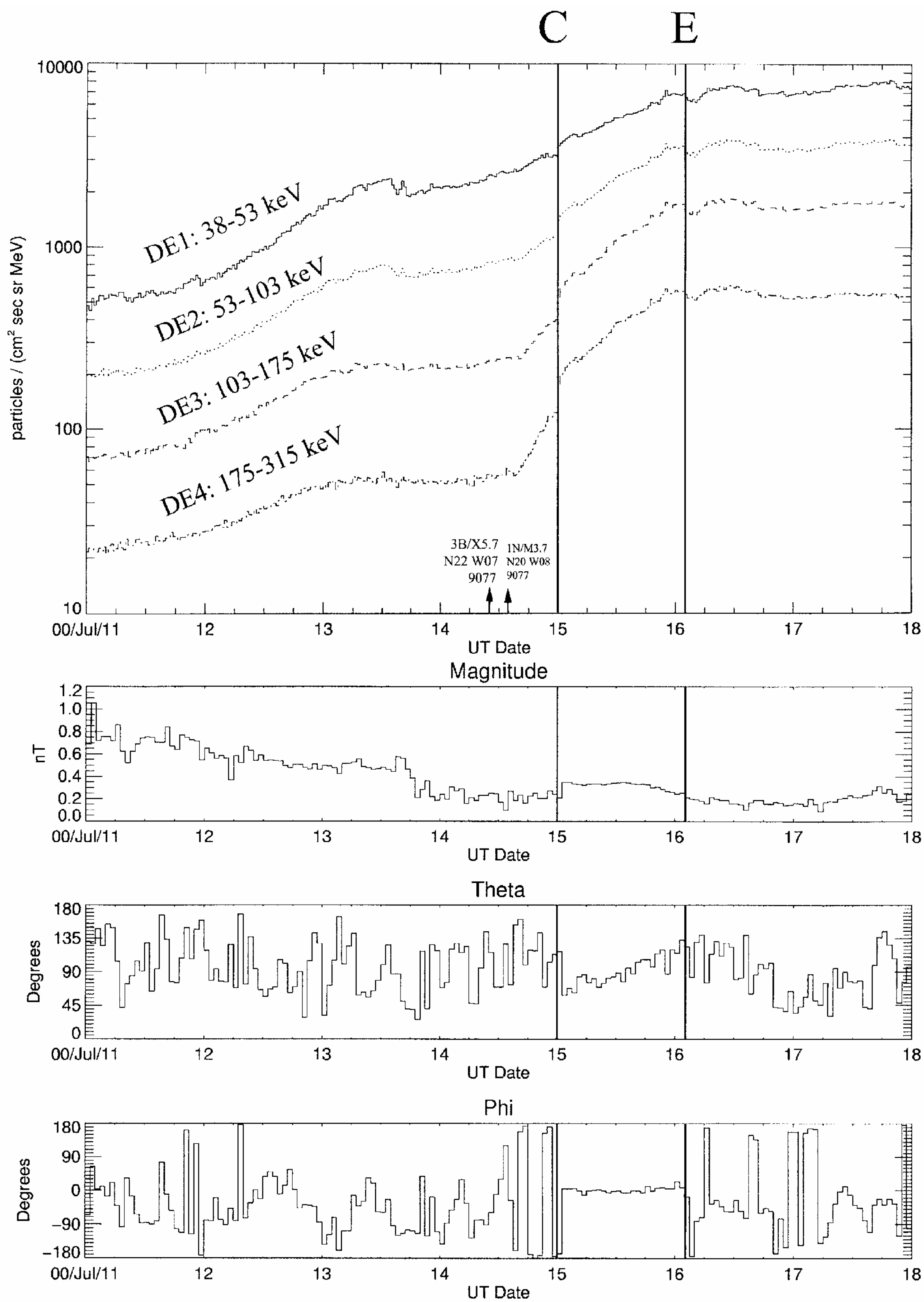

Figure 2. *Ulysses* energetic electron and magnetic field data in the vicinity and during the traversal of the ICME observed in July 2000. An abrupt and discontinuous increase in the particle intensities is observed upon entry of *Ulysses* inside the ICME.

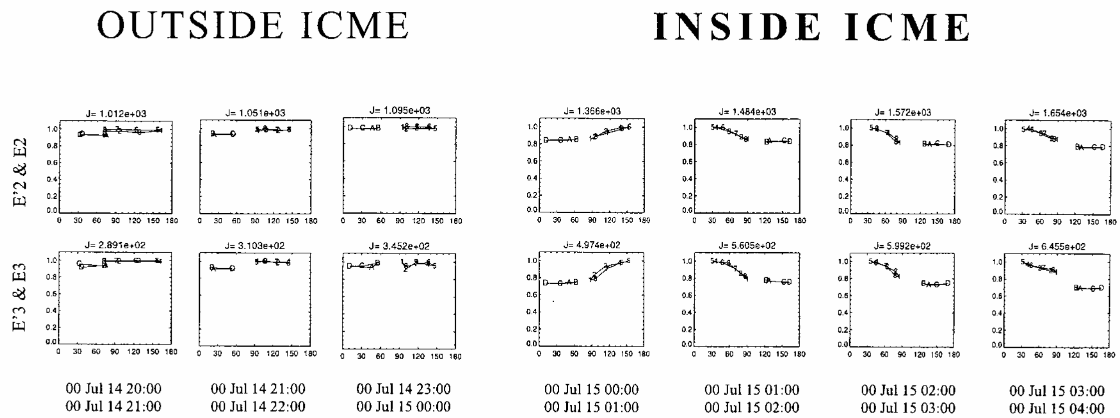

Figure 3. Representative snapshots of the electron pitch-angle distributions observed inside and outside the high latitude ICME by the *Ulysses*/HI-SCALE instrument in July 2000.

Acknowledgements. We are thankful to our HI-SCALE team colleagues for their support and encouragement. O.E.M. acknowledges support from the State Scholarships Foundation (I.K.Y.) through a Post-Doctoral Fellowship.

References

Farrugia C. J., Burlaga L. F., Osherovich V. A., Richardson I. G., Freeman M. P., Lepping R. P., Lazarus A. J., *J. Geophys. Res*., 98, 7621, 1993.

Gosling J. T., Birn J., Hesse M., *Geophys. Res. Lett.,* 22, 869, 1995.

Gosling J. T., Forsyth R. J., *Space Sci. Rev*., 97, 87, 2001.

Lanzerotti L. J., Gold R. E., Anderson K. A., Armstrong T. P., Lin R. P., Krimigis S. M., Pick M., Roelof E. C., Sarris E. T., Simnett G. M., Frain W. E., *Astron. Astrophys. Suppl. Ser.,* 92, 349, 1992.

Malandraki O. E., Sarris E. T., Trochoutsos P., *Ann. Geophysicae*, 18, 129, 2000a.

Malandraki O. E., Sarris E. T., Kasotakis G., Sidiropoulos N., *Adv. Space Res*., 26/5, 875, 2000b.

Malandraki O. E., Sarris E. T., Lanzerotti L. J., Maclennan C. G., Pick M., Tsiropoula G., *Space Sci. Rev*., 97, 263, 2001.

Malandraki O. E., Sarris E. T., Trochoutsos P., Tsiropoula G., Pick M., *J. Atmos. Sol.- Ter. Phys.,* 64/5-6, 517, 2002.

Sarris E. T., Krimigis S. M., *Geophys. Res. Lett*., 9, 167, 1982.

TRANSPORT AND ACCELERATION OF IONS DURING STORM-TIME SUBSTORMS*

F.-A. Metallinou[1], I. A. Daglis[2], D. Delcourt[3] and J.-H. Seiradakis[1]

[1]University of Thessaloniki, Department of Physics, Section of Astrophysics, Astronomy and Mechanics, GR-540 06, Thessaloniki, Greece
[2]National Observatory of Athens, Institute for Space Applications and Remote Sensing, GR-152 36 Penteli, Greece
[3]Centre d'Etude des Environnements Terrestre et Planetaires, Centre National de la Recherche Scientifique, Saint-Maur des Fosses, France

Abstract: This is a study of life-history of charged particles in the magnetosphere, aiming to assess the role of substorm ion acceleration in storm-time ring current growth. The global enhancement of the magnetospheric convection electric field and the localized induced electric field that develops in the nightside magnetosphere during substorms, are the major mechanisms that inject plasma to the inner magnetosphere. We clarify the relative influence of the above two mechanisms to the ring current development. The tree- dimensional model that is used, can give insight on energy transfer processes, particle acceleration, and non- adiabatic effects of particle orbits. Mass-dependence effects on particle trajectories and energisation are also investigated. Particular emphasis is given on the impulsive transport and energisation of ionosphere-originating ions during substorms and on their subsequent injection into the ring current.

AN UNEXPLORED ATMOSPHERE; THE CASE OF VENUS IN VIEW OF THE ARRIVAL OF VENUS EXPRESS.

M. E. Koukouli
Atmospheric, Oceanic and Planetary Physics, Oxford University

Abstract: Shrouded by the thick clouds of a hot and dense atmosphere, Venus - Earth`s close neighbour in space - remained mysterious until recent decades. The fleet of American and Russian spacecraft that visited her in the late 60s and 70s generated far more questions about the atmospheric composition, chemistry, structure, dynamics, surface- atmosphere interactions, than provided us with a comprehensive knowledge of the conditions on the planet. Twenty years later, the Venus Express (Vex) European Space Agency (ESA) mission to Venus, due to launch in November 2005, will aim to complete a global and detailed investigation of Venus` atmospheric composition, chemistry and dynamics, and plasma environment from orbit, and address several important aspects of geology and surface physics. The scientific goals of the mission include the study of the atmospheric structure between 40 and 180 km by means of thermal IR sounding, the atmospheric composition between 0 and 180 km by high resolution spectroscopy via nadir and solar/stellar occultations geometry, the atmospheric dynamics between 50 and 120 km via cloud-tracking in the UV, the plasma environment and its interaction with the solar wind via in situ measurements and the physical properties of the surface via radar sounding and thermal mapping. In this talk we will expound upon the open questions about our neighbouring planet and provide the scientific background that justifies the renewed interest in understanding this complex yet fascinating atmosphere and the crucial significance in a comparative planetology context for understanding long-term climatic evolution processes on Earth.

* *Proceedings 6th Hellenic Astronomical Society Conference, 15-17 September 2003, Penteli, Athens, Greece*

THE ROLE OF SUBSTORMS IN ION ACCELERATION DURING GEOSPACE MAGNETIC STORMS*

I. A. Daglis[1], Y. Kamide[2], D. Delcourt[3], and F.-A. Metallinou[4,1]

1. Institute for Space Applications & Remote Sensing, National Observatory of Athens, Greece
2. Solar-Terrestrial Environment Laboratory, Nagoya University, Japan
3. Centre d'étude des Environnements Terrestre et Planétaires, Saint-Maur des Fossés, France
4. Department of Physics, University of Thessaloniki, Greece

Abstract: Acceleration of charged particles is an essential ingredient of both magnetospheric substorms and geospace magnetic storms and a critical part of space weather. In the case of geospace storms, the ultimate result of particle acceleration is a bulk flow of electric charge through the inner magnetosphere, commonly known as the ring current. Syun Ichi Akasofu and Sydney Chapman, two of the early pioneers in space physics, postulated that the bulk acceleration of particles during storms is rather the accumulative result of partial acceleration during consecutive substorms. This paradigm has been heavily disputed during recent years. The new case is that substorm acceleration may be sufficient to produce individual high energy particles that create auroras and possibly harm spacecraft, but it cannot produce the massive acceleration that constitutes a storm. This paper is a critical review of the long standing issue of the storm substorm relationship, or the capability or necessity of substorms in facilitating or driving the build up of the storm time ring current. We mainly address the physical effect itself, i.e. the bulk acceleration of particles, and not the diagnostic of the process, i.e. the Dst index, which is rather often the case. Within the framework of particle acceleration, substorms retain their storm importance due to the potential of substorm-induced impulsive electric fields in the massive ion acceleration needed for the storm-time ring current buildup.

1. Introduction

The magnetosphere of the Earth has the capability to rapidly accelerate charged particles to high energies over short times and distances. Acceleration of charged particles is an essential ingredient of both magnetospheric substorms and geospace magnetic storms. Syun-Ichi Akasofu and Sydney Chapman, two of the early pioneers in space physics, had postulated that the bulk acceleration of particles during storms is the additive result of fractional acceleration during consecutive substorms (Chapman, 1962; Akasofu, 1968). This paradigm has been disputed during recent years. A new line of thought is that substorm acceleration may be sufficient to produce individual high-energy particles, but it cannot produce the massive acceleration that builds-up the storm-time ring current, i.e. the belt of energized ions drifting around the Earth and producing global geomagnetic disturbances on the ground (Daglis, 2001). In other words, it has been suggested that substorm occurrence during storms is incidental and does not have any causal relation to storm development (Kamide, 1992; Siscoe, 1997).

It is noteworthy that the substorm dispute relates to two coupled, yet distinct issues, which are often confused: the effects of substorms on the ring current growth and the effects of substorms on *Dst* variations. It is useful to remember that the ring current growth is the way a storm materializes, while the *Dst* variations is the method a storm is measured. Regrettably, most studies have addressed the effects of substorms on *Dst* variations; that is, most efforts have concentrated on the diagnostics rather than on the physical processes themselves.

The present paper addresses the dispute on the storm-substorm relationship and, in particular,

* *Proceedings 6th Hellenic Astronomical Society Conference, 15-17 September 2003, Penteli, Athens, Greece*

the question of substorm effects on the bulk particle acceleration that leads to the build-up of the storm-time ring current.

2. The Dispute on the Storm-Substorm Relation

Previous studies addressing the storm-substorm dispute have mainly focused on two diagnostics of the storm-substorm relation:

i) the degree of correlation between geospace magnetic storm development and auroral electrojet activity / large-scale magnetospheric convection.

ii) the influence of magnetospheric substorm expansion on the *Dst* variations.

The parameters involved in i) are the global storm disturbance index *Dst*; the rectified solar wind electric field (vB_s), representing the rate of dayside reconnection and nightside convection, i.e. external driving; and the westward auroral electrojet index *AL*, representing the intensity of substorm expansion, i.e. internal driving.

Approach ii) also involved the *AL* and *Dst* indices, in an effort to investigate the storm response (in terms of *Dst* variations) at substorm expansion onset. Iyemori and Rao (1996) studied a total of 28 geospace storms "containing" substorm expansion onsets identifiable through mid-latitude geomagnetic disturbance indices. As an indicator of the storm intensity they used the *SYM-H* index, which is essentially a high-time resolution (1-min) *Dst* index. The authors found out that substorm expansion onsets were accompanied by negative *SYM-H* responses in some cases and by positive responses in other cases. The authors concluded that the ring current development is not the result of the frequent occurrence of substorms, but the result of enhanced convection caused by large southward IMF.

Regarding the apparent lack of *Dst* response to substorm expansion, Daglis et al. (2000) examined the intense storm of June 5, 1991 and reached different conclusions. Daglis et al. examined the second main phase of this particular storm with respect to substorm occurrence, *Dst* variations and compositional variations. They showed that the *Dst* change rate increased after substorm occurrence, indicating a significant substorm influence on storm development. The relative abundance of O^+ ions in the ring current also increased after substorm occurrence. This is consistent with a large body of observations, which show that distinct, large compositional changes accompany the main phase of intense storms. The implications of O^+ flux enhancements for the storm-substorm relationship are elaborated in the next section.

3. Substorms and Storm-Time Ion Acceleration

Both geospace magnetic storms and magnetospheric substorms are characterized by the efficient acceleration of ions and their subsequent injection into the inner magnetosphere. However, non-storm substorms are of notably inferior efficiency in the quantity and the extent of inward penetration of accelerated particles, when compared to magnetic storms.

As already mentioned, recent studies have questioned the traditional Chapman-Akasofu perception of substorms as "individual, indispensable parts of a storm", i.e. the necessity of substorm occurrence for storm development. The anti-substorm attitude is based on the *a priori* assumption that storm-time substorms do not differ from non-storm substorms, hence the "inability" of non-storm substorms to produce significant ring currents, condemns all substorms to "storm-impotence". However, there are no sound research results that could justify this assumption and therefore it is still too premature to dismiss substorms as particle accelerating processes significant for the ring current.

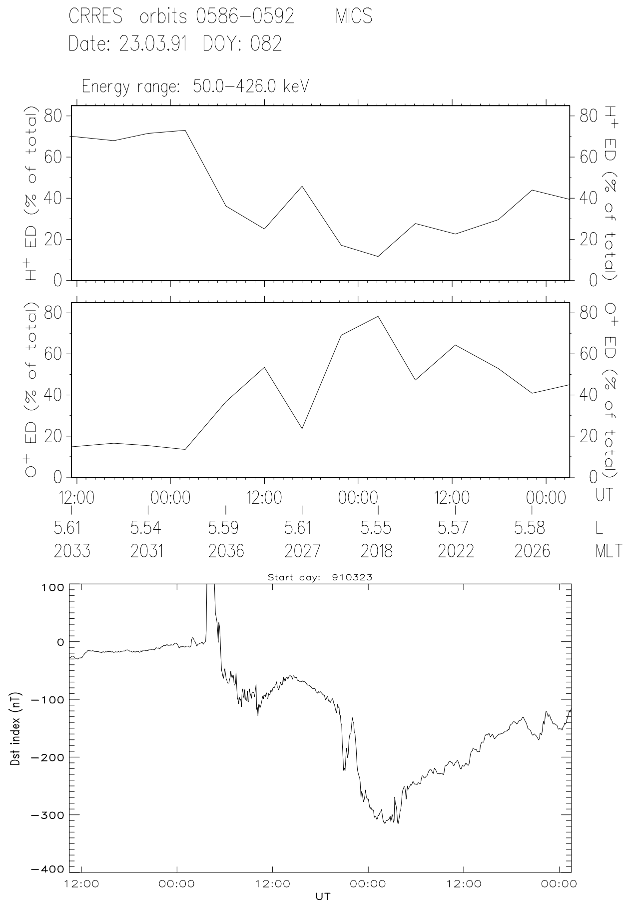

Fig. 1. Spacecraft measurements have demonstrated that O^+ ions dominate the inner magnetosphere during the main phase of intense storms. During the March 23-25, 1991 storm O^+ ions contributed nearly 80% of the ring current energy density at storm maximum (Daglis, 1997; Daglis et al., 1999). This figure shows the time profile of the H^+ (top panel) and O^+ (middle panel) contribution to the total ion energy density in the *L*-range 5-6. The bottom panel shows the time profile of the 5-min resolution *Dst* index. It is remarkable that the *Dst* minima are concurrent with O^+ maxima, implying that the ring current intensifications are due to the acceleration and transport of new ionospheric ions into the inner magnetosphere.

This dispute actually points to the relative efficiency of the large-scale convection electric field and of the substorm-associated impulsive electric fields in accelerating and transporting ions into the ring current. Short-lived impulsive electric fields reported in the literature are induced by magnetic field reconfigurations at substorm onset: i.e., “dipolarizations” from stretched tail-like to dipole-like configuration. Wygant et al. (1998) observed strong impulsive electric fields with amplitudes of up to 20 mV/m, which is more than three times the largest convection electric field. Consequently, substorm induced electric fields can indeed compete with the convection electric field in ion acceleration during storm development: they may be episodic, but they are much stronger.

To reach a firm conclusion in this issue, it is imperative to assess the efficiency of substorm induced electric fields in ring current development. The problem has been addressed by a number of different model studies, with opposing results. While Fok et al. (1996) had suggested that the substorm contribution was subtle, and possibly negative to the development of a ring current, a more recent study by Fok et al. (1999) suggested that the substorm-associated induced electric fields significantly enhance the ring current by redistributing plasma pressure earthward.

We have approached this issue connecting it to another aspect of substorm/storm development in the inner magnetosphere, namely the significant, and at times major, compositional changes. Massive outflow and preferential acceleration of ionospheric O^+ ions is outstanding during intense storms (Figure 1), when the oxygen to proton energy density ratio can reach values of up to 400% (Daglis, 1997; Daglis et al., 1999).

Actually the O^+ abundance increases with the intensity of the storms (Daglis, 1997). This is also a feature of magnetospheric substorms, certified by relevant studies with measurements from the AMPTE and CRRES missions (Daglis et al., 1994, 1996). The close correlation of O^+ energy density enhancements with enhancements of the auroral electrojet intensity led Daglis and Axford (1996) to suggest a fast response of the ionosphere to increased magnetospheric activity.

Consequently, we have to consider and explain the efficient acceleration of originally cold O^+ ions to ring current energies. The O^+ acceleration is moreover preferential with regard to H^+ and He^{++} (Daglis and Axford, 1996) and therefore cannot be due to simple convection. Delcourt (2002) investigated single-particle dynamics in simulations of magnetic field dipolarizations, which revealed prominent short-lived acceleration of plasma sheet ions during the expansion phase of substorms. He showed that under the effect of the transient impulsive electric fields induced by relaxation of the magnetic field lines, ions with gyro-periods comparable to the field variation time scale can experience dramatic non-adiabatic heating. For a 1-min magnetic transition, low-energy O^+ ions originating from the terrestrial ionosphere are found to be accelerated up to a few hundreds of keV during earthward injection. These ions evidently can provide a significant part of the ring current. This tells us that inductive electric fields, and therefore substorms, are indeed important for the storm-time ion acceleration and ring current dynamics.

The reason we focus on O^+ ions is their important role in storm-substorm relationship, Observations and modeling studies have indicated a feedback between O^+ injections and substorm breakups moving progressively duskward and earthward (Baker et al., 1985; Rothwell et al., 1988). Such a feedback will substantially contribute to a rapid enhancement of the ring current. This feature is also consistent with the penetration of intense electric fields to low altitudes during intense storms (Wygant et al., 1998). It is further consistent with a relatively old storm study (Konradi et al., 1976), which had shown that the substorm injection boundary was displaced earthward with each successive substorm during the storm.

If we will combine model predictions with observations, and furthermore consider the fact that O^+ abundance increases with storm size (Daglis, 1997), we will conclude with a scenario of feedback between enhanced O^+-feeding of the plasma sheet and/or the inner magnetosphere and series of intense substorms occurring at progressively lower *L*-shells. Such a combination of successive substorms and continuous O^+ supply can facilitate successive inward penetration of substorm ion injections, consistent with the model of Rothwell et al., (1988) and with the observations reported by Daglis (1997) and Konradi et al. (1976). Successive inward penetration of substorm injections will result in the transport of increasingly more energetic ions into the inner magnetosphere, leading to the intensification of the ring current. This scenario can explain why some substorms seem to influence the storm-time ring current growth, while others don't: substorms resulting in weak inward penetration of injections will not contribute much to the ring current growth. An experimental verification will be possible through detailed global imaging of storms with sufficient composition information.

4. Discussion

We have tried to outline the storm-substorm dispute in the limited space of this paper. The main argument against substorm significance for storm development has been the weak correlation between *Dst* and *AL* time series, combined with the assumption that *AL* is the most appropriate "substorm index". However, as pointed out by a number of authors (e.g., Kamide and Akasofu, 1983), the *AL* index has an inherent deficiency: it is not reliable during intense geospace storms. As auroral electrojets expand equatorwards during intense storms, the *AE* ground magnetogram stations will not provide the actual value of the electrojet intensity, because they miss a significant part of the electrojets, which will be larger the greater the storm is. In other words, the greater the storm, the worse the underestimate of the auroral electrojet (substorm) intensity will be. Thus, prudence in drawing conclusions from studies based on such simplifying tools is imperative.

In an effort to avoid statistical studies, which smooth out features of individual events, Daglis et al. (1998) compared a storm-time substorm and a non-storm substorm with approximately the same size (as measured by the *AL* index). Their results show that there are indeed differences between the two kinds of substorms, especially concerning compositional characteristics. Although compositional changes do occur in both cases, the storm-time substorm features more intense and temporally longer-lived changes than the non-storm substorm. O^+ provides 80% of the total energy density in the storm-time substorm, but only 15% of it in the non-storm substorm.

Storm-time mass loading of the inner magnetosphere by extraordinarily high fluxes of ionospheric O^+ has been demonstrated for intense storms (Daglis, 1997; Daglis et al., 2003). An implication of mass loading, which is of critical importance to the storm-substorm relationship, is the feedback between O^+ abundance and the location of substorm expansions/intensifications. Both observational and modeling studies have shown that in the presence of high O^+ fluxes, substorm breakups move progressively duskward and earthward (Baker et al., 1985; Rothwell et al., 1988). The physical reason behind this property of O^+ ions is their ability in driving plasma instabilities critical for substorm breakup (e.g., Lakhina, 2001).

Near-Earth substorm onsets are associated with magnetic field dipolarization and impulsive induced electric fields that reach very high values during intense geospace storms (Wygant et al., 1998). Consequently, the increasing abundance of O^+ ions during storms can lead to progressively earthward substorm breakups, permitting the transport and acceleration of ions to ever lower altitudes, leading to a stronger ring current and establishing a feedback between O^+ extraction/acceleration and earthward displacement of substorm breakups. Frequent, successive substorm breakups at lower altitudes can further facilitate particle access to the inner magnetosphere and promote ring current build-up. An accumulative effect of successive substorm occurrence on ring current build-up was suggested by Daglis (2001) and was later confirmed by studies of integrated storm and substorm indices (Ahn et al., 2002; Metallinou et al., 2002).

Motivated by studies suggesting the lack of storm-substorm relationship, Sun and Akasofu (2000) suggested that it is more appropriate to examine the relationship between the corrected ring current intensity *Dst** and the upward field-aligned current density, instead of the standard *Dst* and *AE* indices. The authors proposed the new approach in order to accommodate the dominance of ionospheric ions in the ring current during intense storms. Sun and Akasofu showed that the directly driven component (DD) of the upward field-aligned currents is poorly correlated to the corrected *Dst* index (correlation coefficient of 0.33), while the unloading component (UL) correlates much stronger (correlation coefficient of 0.81). This indicates that the upward field-aligned currents during substorms play an important role in the formation of the ring current. Sun and Akasofu further concluded that the poor correlation between DD and *Dst* indicates that the formation of the ring current is not the result of enhanced convection. The strong correlation between UL and *Dst*, on the other side, is consistent with the observational evidence that the magnetosphere-ionosphere coupling plays an important role in the ring current growth.

5. Summary

The paper has addressed the storm-substorm relationship with an emphasis on the particle acceleration that is necessary for the build-up of the storm-time ring current.
The foundations of the storm-substorm dispute lie in correlation studies between auroral electrojet indices and the *Dst* index. While early studies showed a causal relationship between substorms and storms, more refined investigations that followed, have questioned this relationship. These investigations concluded that storms are the result of large-scale magnetospheric convection, with no effect from substorm occurrence.

Time has come to investigate the physical processes themselves instead of their diagnostics. The critical process in this case is particle acceleration leading to the storm-time ring current build-up. The role of substorm induced impulsive electric fields is presumably decisive for obtaining the massive ion acceleration needed for storms. A small number of studies have investigated this aspect, showing that indeed substorm particle acceleration is very efficient, and that large-scale convection and substorm dipolarizations do cooperate to inject plasma energy more deeply into the magnetosphere than either would individually. Furthermore, the fact that intense storms tend to be dominated by ionospheric O^+ ions has to be accommodated by any storm theory, and simple convection does not give this preferential O^+ heating. More detailed studies on this issue are underway.

REFERENCES

Ahn, B.-H., et al., Universal time variation of the Dst index and the relationship between the cumulative AL and Dst indices during geomagnetic storms, *J. Geophys. Res.*, 107 (A11), 1409, doi:10.1029/ 2002JA009257, 2002.

Akasofu, S. -I., *Polar and Magnetospheric Substorms*. Boston, MA: D. Reidel, 1968.

Baker, D. N., et al., The role of heavy ions in the localization of substorm disturbances on March 22, 1979: CDAW 6, *J. Geophys. Res.*, *90*, 1273-1281, 1985.

Chapman, S., Earth storms: Retrospect and prospect, *J. Phys. Soc. Japan*, *17*, Suppl. A-I, 6-16, 1962.

Daglis, I. A., The role of magnetosphere-ionosphere coupling in magnetic storm dynamics, in *Magnetic Storms*, *Geophys. Monogr. Ser.*, 98, edited by B. T. Tsurutani, W. D. Gonzalez, Y. Kamide, and J. K. Arballo, pp. 107-116, AGU, Washington, DC, 1997.

Daglis, I.A., The storm-time ring current, *Space Sci. Rev.*, *98*, 343-363, 2001.

Daglis, I. A., and W. I. Axford, Fast ionospheric response to enhanced activity in geospace: Ion feeding of the inner magnetotail, *J. Geophys. Res.*, *101,* 5047-5065, 1996.

Daglis, I. A., S. Livi, E. T. Sarris, and B. Wilken, Energy density of ionospheric and solar wind origin ions in the near-Earth magnetotail during substorms, *J. Geophys. Res.*, *99,* 5691-5703, 1994.

Daglis, I. A., et al., Auroral ionospheric ion feeding of the inner plasma sheet during substorms, *J. Geomagn. Geoelectr.*, *48*, 729-739, 1996.

Daglis, I. A., et al., Ion composition in the inner magnetosphere: Its importance and its potential role as a discriminator between storm-time substorms and non-storm substorms, in *Fourth International Conference on Substorms* (*ICS-4*), edited by S. Kokubun and Y. Kamide, pp. 767-772, Terra/Kluwer Publications, Tokyo, 1998.

Daglis, I. A., et al., Variations of the ion composition during a large magnetic storm and their consequences, *Phys. Chem. Earth*, *24*, 229-232, 1999.

Daglis, I. A., *et al*., Fine structure of the storm-substorm relationship, *Adv. Space Res.*, 25 (12), 2369-2372, 2000.

Daglis, I. A., et al., Intense space storms: Critical issues and open disputes, *J. Geophys. Res.*, *108* (A5), 1208, doi:10.102/ 2002JA009722, 2003.

Delcourt, D. C., Particle acceleration by inductive electric fields in the inner magnetosphere, *J. Atmos. Sol. Terr. Phys.*, *64*, 551–559, 2002.

Fok, M.-C., T. E. Moore, and M. E. Greenspan, Ring current development during storm main phase, *J. Geophys. Res.*, *101*, 15,311-15,322, 1996.

Fok, M.-C., T. E. Moore, and D. C. Delcourt, Modeling of inner plasma sheet and ring current during substorms, *J. Geophys. Res.*, *104*, 14,557-14,569, 1999.

Iyemori, T., and D. R. K. Rao, Decay of the *Dst* field of geomagnetic disturbance after substorm onset and its implication to storm-substorm relation, *Ann. Geophys.*, *14*, 608-618, 1996.

Kamide, Y., Is substorm occurrence a necessary condition for a magnetic storm?, *J. Geomagn. Geoelectr.*, *44*, 109-117, 1992.

Kamide, Y., and S.-I. Akasofu, Notes on the auroral electrojet indices, *Rev. Geophys. Space Phys.*, *21*, 1647-1656, 1983.

Konradi, A., C.L. Semar, and T.A Fritz, Injection boundary dynamics during a geomagnetic storm, *J. Geophys. Res.*, *81*, 3851-3865, 1976.

Lakhina, G. S., Role of helicon modes in the injection of oxygen ions in the ring current, *J. Atmos. Sol. Terr. Phys.*, *63*, 481-487, 2001.

Metallinou, F.-A., I. A. Daglis, and J.-H. Seiradakis, Study of the relation between storms and substorms in the terrestrial magnetosphere, in *Proceedings of the Fifth Astronomical Conference of The Hellenic Astronomical Society*, ed. by D. Hatzidimitriou, Univ. of Crete, 2002. Available at: http://astrophysics.physics.uoc.gr/conf/proceedings.htm

Rothwell, P. L., L. P. Block, M. B. Silevitch, and C.-G. Fälthammar, A new model for substorm onsets: The pre-breakup and triggering regimes, *Geophys. Res. Lett.*, *15*, 1279-1282, 1988.

Siscoe, G. L., Big storms make little storms, *Nature*, *390*, p. 448, 1997.

Sun, W., and S.-I. Akasofu, On the formation of the storm-time ring current belt, *J. Geophys. Res.*, *105*, 5411-5418, 2000.

Wygant, J., et al., Experimental evidence on the role of the large spatial electric field in creating the ring current, *J. Geophys. Res.*, *103*, 29,527-29,544, 1998.

FINE RADIO STRUCTURES DURING A MAJOR SOLAR EVENT OBSERVED WITH ARTEMIS IV*

P. Tsitsipis[4], A.Kontogeorgos[4], C. Caroubalos[1], X. Moussas[2], C. E. Alissandrakis [3], A. Hillaris[2], P. Preka-Papadema[2], J. Polygiannakis[2], J.-L. Bougeret[5], G. Dumas[5], C. Perche[5]

[1] Dep. of Informatics, Un. of Athens
[2] Astrophysics, Astronomy and Mechanics, Un. of Athens
[3] Section of Astro-Geophysics, Physics, Un. of Ioannina, Ioannina
[4] Department of Electronics, TEI of Lamia, Lamia, Greece
[5] LESIA, Observatoire de Paris, Meudon

Abstract : We analyse the fine structure of the type IV radio burst, during the main phase of the 14th July 2000 major event recorded by the radiospectrograph ARTEMIS-IV, in the 110- 650 MHz (10Hz sampling rate) and the 270-450 MHz (100Hz rate) range. In this report we focus on variations in frequency drift rate and repetition rate of fibres bursts. A pronounced asymmetry between the number of bursts with positive and negative frequency drift is noted at certain time periods. These variations follow closely the evolution of the magnetic structure associated with the major solar event and the onset of the corresponding Coronal Mass Ejection. We also present fine structure observed during several other events. We have recently constructed a new antenna and aquisition system and ARTEMIS IV records 100 spectra every second in thew range of 20 MHz to 650 MHz (1.2BG every day).

THE ROLE OF SPICULES IN THE MASS BALANCE AND ENERGY BUDGET OF THE SOLAR ATMOSPHERE

G. Tsiropoula[1] and K. Tziotziou[2]

[1]National Observatory of Athens, Institute of Space Applications and Remote Sensing, P. Penteli, Greece
[2]Universiteit Utrecht, Sterrekunding Institute, Postbus 80000, 3508 TA Utrecht, The Netherlands

Abstract: High-resolution Hα observations of a solar region containing several mottles (spicules) were obtained with the Multichannel Subtractive Double Pass Spectrograph (MSDP). The temporal and spatial variations of the line-of- sight velocity provide strong indication that the mechanism responsible for the driving of the observed flows is magnetic reconnection. Apart from the line-of- sight velocity, application of the cloud model permits the derivation of several other parameters. The temporal evolution of these parameters provides reasonable estimates of the role of these structures in the mass and energy balance of the solar atmosphere.

* *Proceedings 6[th] Hellenic Astronomical Society Conference, 15-17 September 2003, Penteli, Athens, Greece*

MAGNETIC CLOUDS: A SUBJECT OF SPACE WEATHER PREDICTION*

A. Geranios (1), M. Vandas (2)

(1) Nuclear and Particle Physics Section, Department of Physics, University of Athens, Greece.
(2) Astronomical Institute, Academy of Sciences, Bocni II 1401, 14131 Praha 4, Czech Republic.

ABSTRACT

A magnetic cloud is a transient ejection in the solar wind defined by relatively strong magnetic fields, a large and smooth rotation of the magnetic field direction over approximately 0.25AU at 1AU and a low proton temperature.
Magnetic clouds are ideal objects for solar-terrestrial studies because of their simplicity and their extended time intervals of southward and northward magnetic fields. Magnetic clouds constitute a significant subset of coronal mass ejections with remarkable characteristics in the interplanetary medium and a strong influence on the Earth's magnetosphere, giving rise to geomagnetic storms. Therefore, they can be used as a subject for space weather predictions.
We present a set of observed magnetic clouds in the interplanetary space and compare their characteristics with proposed theoretical models. The evolution of such a cloud from the neighbourhood of the sun up to the earth is numerically simulated also for the case of the presence of a faster moving shock front. Its influence on the magnetosphere can be seen by the triggered geomagnetic storms.

INTRODUCTION

Magnetic clouds are specific regions in the solar wind, which exhibit the following properties: 1. The magnetic field direction rotates smoothly through a large angle during an interval of the order of one day; 2. The magnetic field strength is higher than in surroundings; and 3. The temperature is lower than average [1,2]. The rotation of magnetic field and the temperature decrease inside clouds indicate that magnetic clouds represent a closed magnetic

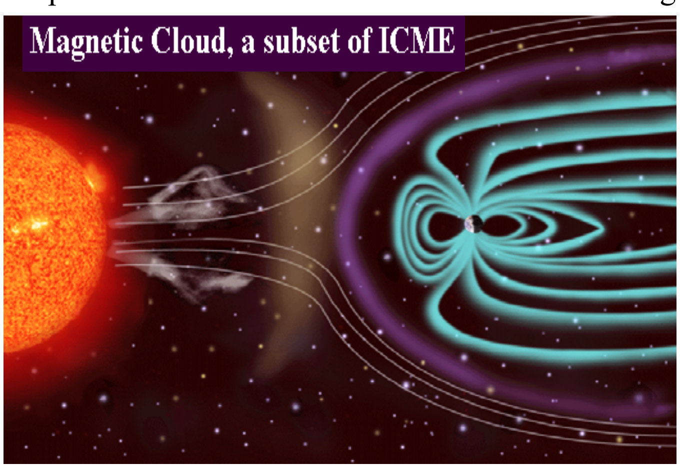

Fig. 1 *Formation of magnetic cloud in interplanetary space (not scaled).*

* *Proceedings 6th Hellenic Astronomical Society Conference, 15-17 September 2003, Penteli, Athens, Greece*

field configuration, which isolates them from ambient plasma to some extent and thus suppresses the heat transport from the hot solar corona. The topology of the magnetic field inside clouds is under intensive examinations. There are two basic concepts of magnetic cloud structure, a loop rooted at the sun (Fig. 2a), and a closed plasmoid detached from the solar corona (spheroidal, Fig. 2b).

Burlaga et al. [3] have suggested a cylindrical model as a basis for the comparison with measured data. The physical reason for this was that a magnetic cloud as a loop could locally be described with the cylindrical solution.

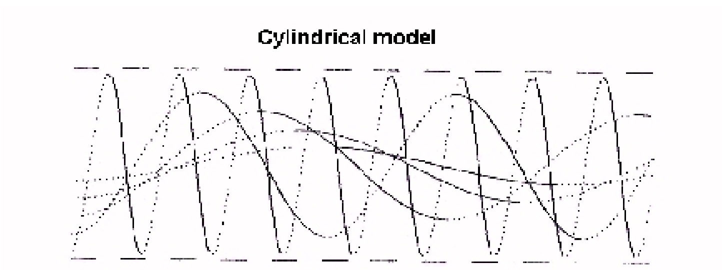

Fig. 2a *Cylindrical model*

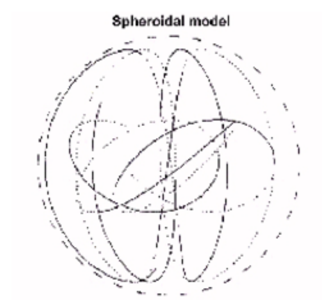

Fig. 2b *Spheroidal model*

They have brought several indices in favor of a loop configuration for a several cases and have reached quite good results in matching the angles of the magnetic field vector (θ to the ecliptic plane, φ in the ecliptic plane), but fits of the magnetic field magnitude (B) are not very good (Fig. 3). Magnetic field profiles are often non-symmetric and the ratio of maximum to boundary magnitude sometimes exceeds 2 contrary to the cylindrical solution. These facts have led us to examine other solutions, namely spheroidal ones (representing plasmoids, Fig. 2b). Spheroidal models are based on a solution in [4] and are described in details in [5]. Spheroidal clouds have a z-axial symmetry with the corresponding semi-axis c and the other semi-axes a, the oblateness is $\varepsilon=(a-c)/a$; we speak about oblate ($\varepsilon>0$), spherical ($\varepsilon=0$), or prolate ($e<0$) clouds.

EVOLUTION OF MAGNETIC CLOUDS

Several years ago it is performed [6] MHD simulations of a propagating flux rope in the inner heliosphere in two dimensions. The flux rope was perpendicular to the computational domain. A model of the flux rope was a cylinder with a constant-α force-free field inside. For three dimensional simulations we followed the same way, only the cylinder was replaced by a toroid; initially, a constant-α force-free field was inside the toroid and the external field was a potential field around a toroid, described in [7]. During injection of the toroid, only the magnetic field was perturbed at the inner boundary, other quantities remained unchanged. The simulation was made for several inclinations of the flux rope to the ecliptic plane. Figure 4a shows a shape of a flux rope when its leading edge (apex) crossed 1 AU.

The flux rope was injected with 0^0 inclination to the ecliptic plane. Labels in figure 4a identify parts of the flux rope, the apex and two legs (western and eastern). The upper insert of Fig. 4a shows the distribution of the magnetic field intensity inside the flux rope in the ecliptic plane for the apex region of cloud. A technique in 2.5 dimensional calculations was used [8] to simulate magnetic cloud propagation. A magnetic cloud was modeled as a circular cross section of a toroidal flux rope, perpendicular to the computational plane, with this plane (equatorial or meridional). The simulations showed an asymmetric expansion of magnetic clouds and their deflection in a unipolar ambient magnetic field from the radial propagation. Vandas et al [9] studied an interaction of a shock wave with a magnetic cloud. The magnetic cloud became very compressed in the radial direction, its magnetic field intensified, which increased its geoeffectiveness (Fig. 4b).

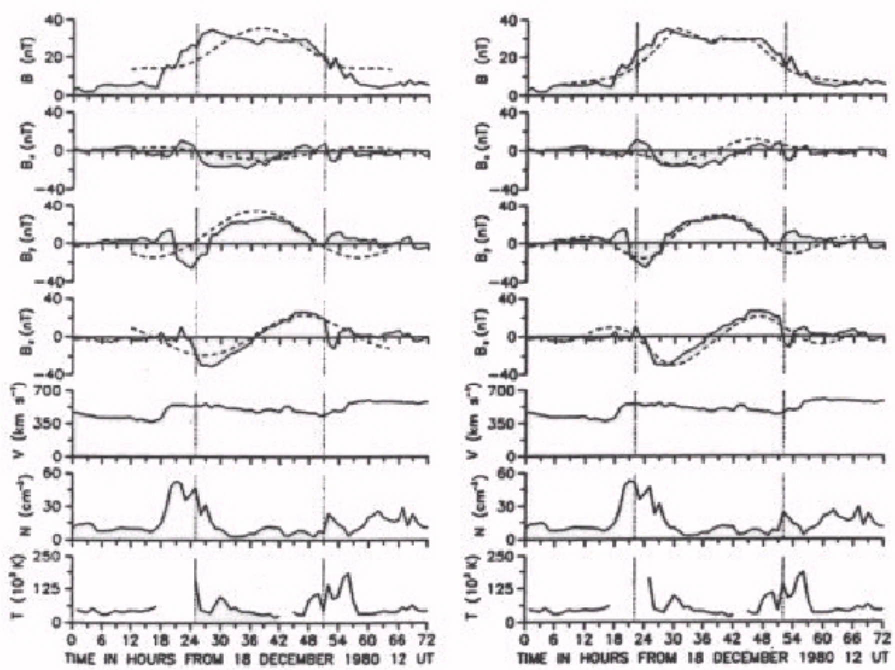

Fig. 3. The magnetic cloud 14 from LJB. The left part shows the fit by the cylindrical model; the right part shows the fit by the oblate cloud. The parameters of the fits are given in Table 1.

Fig. 3 *From top: B, B_x, B_y, B_z, V, d, T, for both models (left cylindrical, right spheroidal). Dotted lines are the fits of the two models to the data (continuous line).*

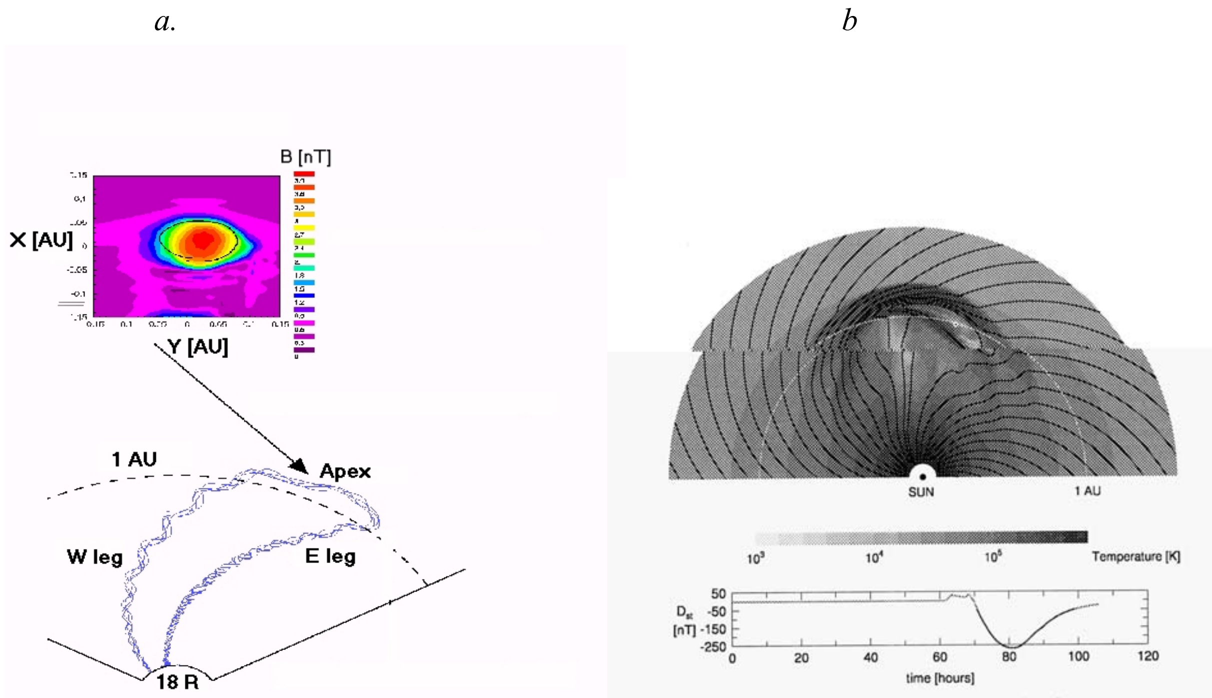

Fig. 4a Flux rope in the ecliptic plane as a result of numerical simulations. The upper insert shows the distribution of the magnetic field intensity inside the flux rope in the ecliptic plane for the apex region of cloud.

Fig. 4b Magnetic field lines and temperature distribution in the ecliptic plane when a magnetic cloud reached 1 AU. The magnetic cloud was overtaken by a shock wave from a pressure and velocity pulse. The magnetic cloud became more geoeffective (D_{st} value)

CONCLUSION

The geoeffectiveness of magnetic clouds is simulated in the case of a propagating cylindrical cloud perpendicular to the ecliptic plane, which is overtaken by a fast moving shock wave. When the magnetic field of the cloud is southward it annihilates with the northward geomagnetic field dropping the D_{st} to high negative values. This fact may create strong geomagnetic storms with several impacts on humans and environs. For instance, adding to astronauts and aviation staff radiation doses, damaging HV-transformators, accelerating the corrosion of pipelines, confusing electronic control systems, and other phenomena.

References

[1] Geranios, A., A Search for the Origin of Very Low Electron Temperatures. Planet. Space Sci., 26, 571, 1978.
[2] Burlaga, L., E. Sittler, F. Mariani and R. Schwenn, Magnetic loop behind an interplanetary shock: Voyager, Helios and IMP-8 observations, J. Geophys. Res. 86, 6673, 1981.
[3] Burlaga, L., R. Lepping and J. Jones, Global configuration of a magnetic cloud, Phys. Of Magn. Flux Ropes, ed. E. Priest, L. Lee and C. Russel, AGU Geophys. Monograph 58, 373, 1990.
[4] Ivanov, K., and A. Hashiladze, Interplanetary spheromaks, Geomagn. Aeron. 25, 377, 1985.
[5] Vandas, M., S. Fischer and A. Geranios, Spheroidal models of magnetic clouds. Proc. 1st SOLTIP Symposium, Liblice 1991.
[6] Vandas, M., S. Fischer, M. Dryer, Z. Smith and Detman, T. Simulation of magnetic cloud propagation in the inner heliosphere in 2 dimensions 1. A loop perpendicular to the ecliptic plane. J. Geophys. Res. 100, 12285, 1995.
[7] Romashets, E. and Vandas, M. Propagation of a toroidal magnetic cloud through the inner heliosphere. Adv. Space Res. 29, 313, 2002.
[8] Vandas, M., S. Fischer, M. Dryer, Z. Smith, T. Detman. Simulation of magnetic cloud propagation in the inner Heleiosphere in 2-dimensions. 1. A loop perpendicular to the ecliptic plane. J. Geophys. Res. 100, 12285, 1995.
[9] Vandas, M., S. Fischer, M. Dryer, Z. Smith, T. Detman, and A. Geranios. MHD simulation of an interaction of a shock wave with a magnetic cloud. J. Geophys. Res. 102, 22295, 1997.

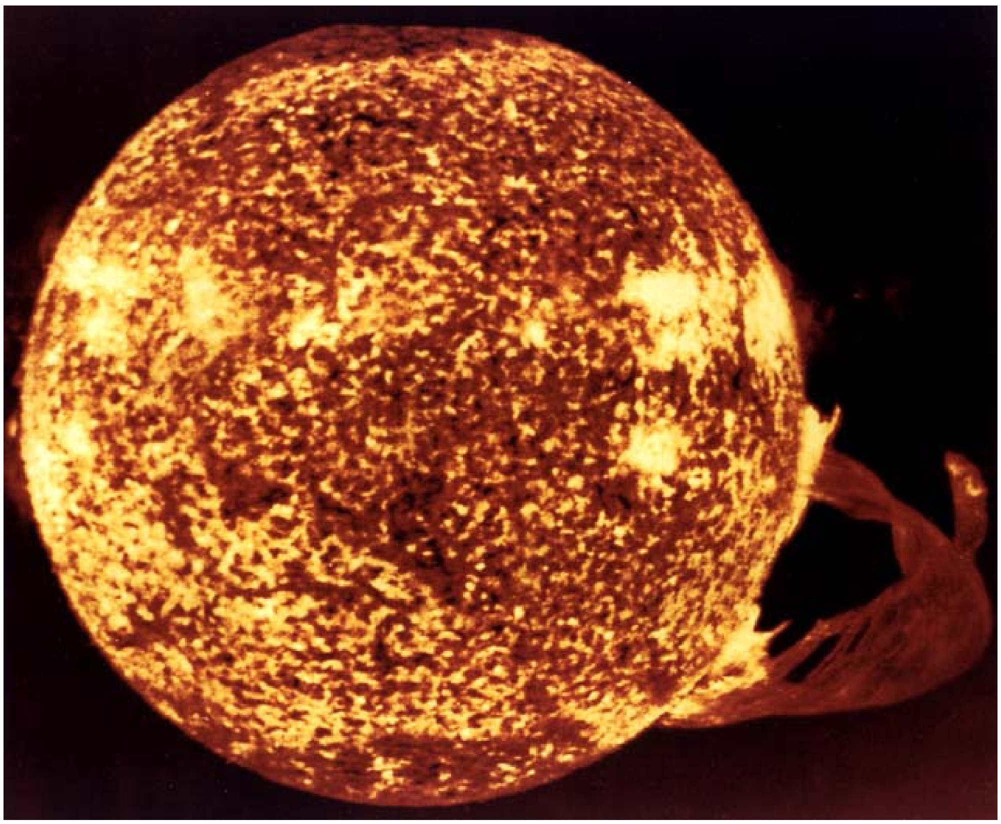

ENERGETIC PARTICLE ACCELERATION AND RADIATION IN EVOLVING COMPLEX ACTIVE REGIONS*

A.Anastasiadis[1], C. Gontikakis[2], N. Vilmer[3], and L. Vlahos[4]

[1]National Observatory of Athens, Institute for Space Applications and Remote Sensing, 152 36 Penteli, GREECE
[2] Research Center for Astronomy and Applied Mathematics, Academy of Athens, GREECE
[3]LESIA, Observatoire de Paris-Meudon, 92195 Meudon Cedex, FRANCE
4 Department of Physics, University of Thessaloniki, 54124 Thessaloniki, GREECE

ABSTRACT

We present a model for the acceleration and radiation of solar energetic particles (electrons) in an evolving active region. The spatio - temporal evolution of the active region is calculated using a Cellular Automaton (CA) model for the energy release process. The acceleration of electrons is due to the presence of randomly placed, localized electric fields. We calculate the resulting kinetic energy distributions of the particles and their emitted X-ray radiation spectra, using the thick target approximation, by performing a parametric study with respect to number of electric fields present and the thermal temperature of the initially injected distribution.

1. INTRODUCTION

During the last two decades, due to the existence of several space-born solar instruments together with a number of ground based solar telescopes, a number of statistical studies of the solar flaring activity has been performed (for review see Vilmer 1993; Vilmer & Mackinnon 2003). These studies established that the frequency distributions of impulsive events (e.g. solar flares, X-ray bright points) as a function of total energy, peak luminosity and duration are well defined power laws, extending over several orders of magnitude. Several qualitative models have been developed in order to model the dynamic evolution of solar flares (for reviews see Vlahos 1996; Bastian & Vlahos 1997) following the above observational evidence. These models revealed the necessity to study and understand the global behavior of the evolution of the complex active regions and particle acceleration in such a complex environment.

The theoretical work for studying the evolution and the dynamics of complex active regions followed, in general, two different approaches:

(1). MHD numerical simulations (e.g. Galsgaard & Nordlund 1996; Einaudi et al. 1996; Georgoulis et al. 1998). According to these models, random shearing motions of the magnetic field lines at the photospheric boundary lead to the formation of current sheets inside the active region, where magnetic reconnection occurs. The MHD approach gives detailed insight into the smallscale processes (i.e. magnetic reconnection) in active regions, but has difficulty modelling the complexity of entire active regions and solar flares.

(2). Cellular Automata (CA) models either based on Self Organized Criticality (SOC), (e.g. Lu & Hamilton 1991; Lu et al. 1993; Vlahos et al. 1995; Georgoulis & Vlahos 1996; 1998) or in percolation theory (i.e. probabilistic CA models) (e.g. MacKinnon et al. 1996; Vlahos et al. 2002). In these models the continuous loading of the active regions with new magnetic flux can produce several magnetic discontinuities. Simple rules were applied for the redistribution of

* *Proceedings 6th Hellenic Astronomical Society Conference, 15-17 September 2003, Penteli, Athens, Greece*

magnetic fields and the release of magnetic energy at these discontinuities. The CA models can rapidly and efficiently treat the complexity of spatially extended, large systems but they face problems describing in details the small scale processes occurring.

Recently several efforts have been done to connect the two complementary approaches (the MHD simulations and the CA models). Isliker et al. (1998; 2000) revealed the role of several components of CA models, such as the physical interpretations of the grid-variable, the nature of the energy release process and the role of diffusivity. These efforts leaded to a construction of a new type of CA models for solar flares (Isliker et al. 2001) which are compatible to MHD theory and produce statistical results in agreement with the observations. In addition to the above efforts, hybrid models, which are intermediate between CA models and full MHD and reduced MHD models, have been constructed mainly to account for the coronal heating problem (e.g. Einaudi & Velli 1999; Buchlin et al. 2003).

The most common approach for the particle acceleration models proposed for solar flares (for review on acceleration models see Anastasiadis 2002) is the decoupling of the different processes (i.e. the energy release, the acceleration, the transport and radiation). It is clear that in any effort to develop global models for solar flares, one must consider the coupling between different processes, from energy release process to particle acceleration, transport and radiation. This is not an easy task as these processes have different time and spatial scales and usually are acting simultaneously.

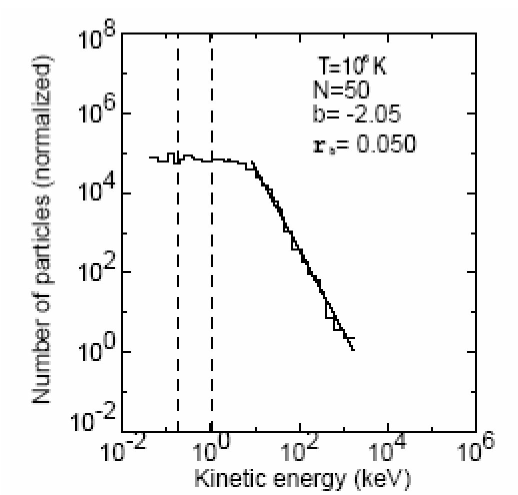

Figure 1. The average kinetic energy distribution of electrons accelerated for the case of N = 50 *and T*1 = 106 *K. The fit is given by Eq. 7 and the vertical dashed lines indicate the injected kinetic energy range.*

The main goal of this work, is to connect the energy release process during solar flares, through a cellular automaton model, with the particle acceleration and radiation processes and to compare our results with the observations. In the next section we outline the basic rules of the CA model, used for the calculation of the energy release time series. In Section 3, the acceleration model is presented, followed by the computed energy distribution of electrons and the corresponding X-ray radiation flux. Finally we discuss the possible extensions of this work.

2. THE CA MODEL FOR ENERGY RELEASE

For the study of the energy release process we use a 3- D Cellular Automaton (CA) model based on the Self - Organized Criticality (SOC). For a detailed description of the CA model see Vlahos et al. (1995) and Georgoulis & Vlahos (1998). The basic rules of the CA model are: (1) Initial loading (2) Ongoing random loading with increment δB given by the equation:

$$prob(\delta B) \approx (\delta B)^{-5/3} \tag{1}$$

(3) Relaxation process due to reconnection of magnetic field, leading to the generation of Reconnecting Current Sheets (RCS), according to the equation:

$$\vec{\nabla} \times \mathrm{B} \approx J \tag{2}$$

(4) The energy release is calculated using:

$$\in \approx \left(B_i - \frac{6}{7} B_{cr} \right)^2 \tag{3}$$

where B_i is the value of the magnetic field of given grid point i, which is becoming unstable when $B_i \geq$ ¸ B_{cr}, with B_{cr} been a critical value of the magnetic field.
An energy release time series ($\in ^2(t)$) can be constructed, using Eq. 3. This time series obeys a double power-law frequency distribution and also exhibits a scale-invariant behavior and encloses a self - similar nature.

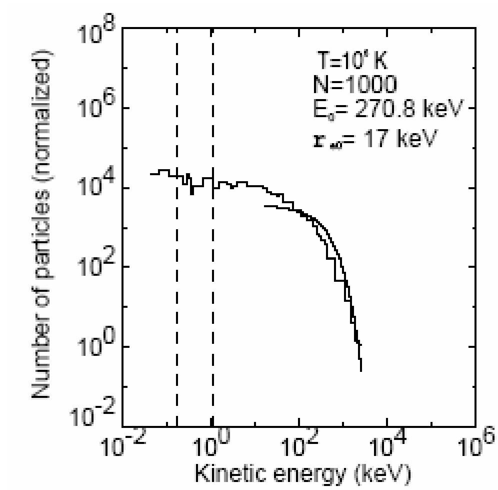

Figure 2. Same as Fig. 1, but for N = 1000. *The fit is given by Eq. 8.*

3. DESCRIPTION OF THE MODEL

In order to estimate the electric field strength in each RCS, we follow the calculation of Litvinenko (1996), using the Amp`ere law, with the assumption that a particle flow towards the RCS is produced by the electric drift. The electric field in given by the equation:

$$E = \frac{B^2}{4\pi en\Delta l} \tag{4}$$

where Δl is the maximum length over which the particles are accelerated and the ambient plasma has a density of $n = 10^{10}$ cm^{-3}. As the released energy calculated by the CA model is $\in ^2(t) \sim B^2(t)$ (i.e. Eq. 3), we can produce a virtual electric field time series ($E(t)$) from the energy release time series using Eq. 4 for the electric field. Each injected electron enters into the acceleration volume and interacts

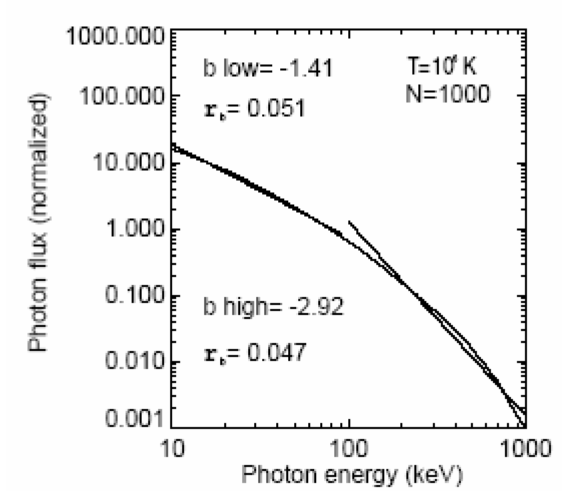

Figure 3. The calculated X-ray radiation spectrum of the resulting electron distribution given in Fig. 2. The fitting was performed in two energy ranges 10-100 keV and 100- 1000 keV and is given by power-laws.

successively with N randomly selected elements of the electric field time series. At each electron-RCS interaction, the kinetic energy change of an electron is given by the relation:

$$\Delta E_k = \pm \alpha e E(t) \Delta l \tag{5}$$

where the plus (minus) sign corresponds to in (out of) phase interaction, e is the electron charge and $\Delta l = 10^3$ cm. The parameter α is selected randomly to vary between zero and one at each electron - RCS interaction. A more detailed description of the acceleration model can be found in Anastasiadis et al. (1997). Our aim is to calculate the final kinetic energy distribution of the electrons, by performing a parametric study according to N, and to compute the resulting X-ray radiation flux using the thick target approximation.

4. RESULTS

According to our model, each electron performs a free flight between RCS of variable strength. We follow the interaction of a Maxwellian type velocity distribution of electrons, given by the form:

$$f(\upsilon) = \frac{n}{(2\pi)^{1/2} V_e} exp\left(-\frac{\upsilon^2}{2V_e^2}\right) \tag{6}$$

We inject electrons with initial velocity in the range $2 \leq (\upsilon/V_e) \leq 5$, where V_e is the thermal velocity and n is the ambient plasma density. We consider two different temperatures: $T_1 = 10^6$ K corresponding to $V_{e1} = 3.88 \times 10^8$ cm s^{-1} and $T_2 = 10^7$ K corresponding to $V_{e2} = 1.23 \times 10^9$ cm s^{-1}. The resulting thermal kinetic energies are 43 eV and 430 eV, respectively.

We are interested in calculating the average resulting electron distributions, in order to eliminate any effects of the random numbers, by performing a parametric study with respect to the maximum number N. Note that this parameter can be considered as a rough measure of the maximum trapping time of the injected electron distribution.

In Fig. 1 and 2 we present the numerically evaluated kinetic energy distribution (average of 10 sample runs) for $N = 50$ and $N = 1000$ respectively for the case of $T_1 = 10^6$ K. All of our resulting average kinetic energy distributions can be fitted for kinetic energies above 10 keV, either with a power law function of the form:

$$F(E_k) \approx E_k^{-b} \tag{7}$$

or with an exponential function of the form:

$$F(E_k) \approx exp\left(-\frac{E_k}{E_0}\right) \tag{8}$$

Our results suggest that, as the maximum number of interactions (*N*) increases, it affects the shape of the energy distribution, which begins to diverge from a well defined power law and an exponential tail is starting to develop. In addition to the acceleration process we compute the resulting X-ray radiation flux. In order to do so we choose to consider as a first approach, that energetic electrons produce thick target radiation (for details see Brown 1971). In Fig 3 the X-ray spectrum produced by the electron distribution of Fig 2 is shown. The fitting was done by a power law in the energy ranges 10 -100 keV (considered as the low energy part) and 100 - 1000 keV (considered as the high energy part). In Fig. 4 we present in a form of scatter plots our results for the power law index of the calculated X-ray spectra in respect to the maximum number *N* for the two temperatures used. For the low energy range (10 - 100 keV) the mean value of the index is -1.45 for $T_1 = 10^6$ K and -1.47 for $T_2 = 10^7$ K, as for the high energy part (100 - 1000 keV) the mean values are -2.96 and -3.08 respectively.

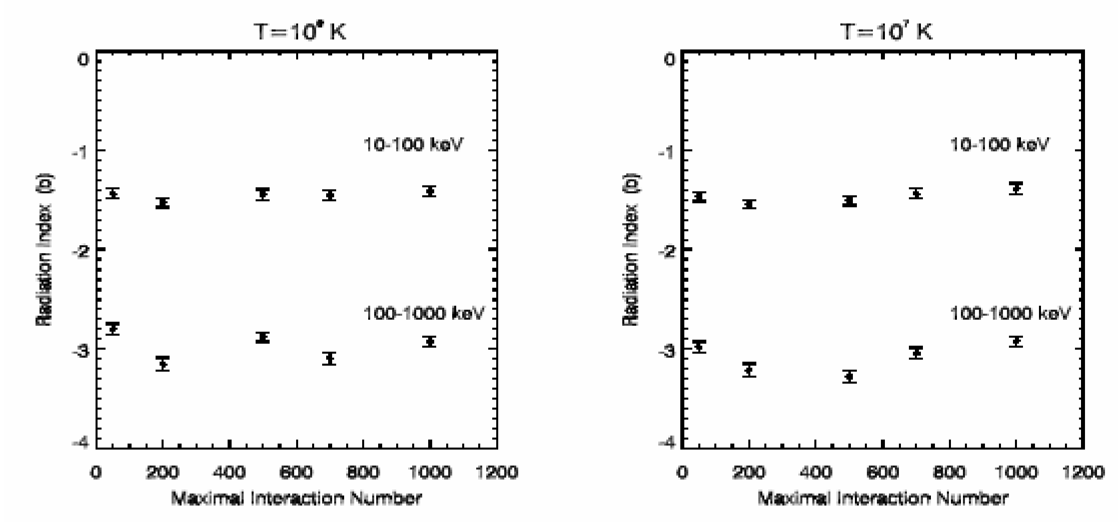

Figure 4. Scatter plots summarizing our results concerning the power law index of the emitted X-ray radiation in respect to the maximum number N for the two temperatures used.

5. SUMMARY AND DISCUSSION

In this work, the connection of the energy release process with the acceleration environment is attempted. Using a CA model, the turbulent driver of the convection zone (i.e. the random on going loading of the CA) is connected with the energy distribution of the accelerated particles. Our results for the kinetic energy distributions of electrons show a power-law or an exponential behavior depending upon their maximum number of interactions *N*. In addition, the X-ray radiation flux, using the computed kinetic energy distributions, was presented. The predicted spectra could be consistent with some observations (at least for the higher part of the predicted spectrum where Coulomb energy losses play a less significant role). The hardness of the predicted spectrum above 100 keV may be consistent with what is observed but a consistent photon flux should also be produced.

More work is clearly needed in the future if we want to incorporate the transport of the particles and to include 4 the radiation losses due to collisions inside the acceleration volume (i.e. use of the thin target emission). This approach can be done if we considered the newly develop CA model -named extended CA- (X-CA) (Isliker et al. 2001), taking advantage the consistent calculation of the magnetic and electric fields in the simulation box. In this direction, studies for the case a random walk process in a environment which has fractal properties, like the one produced by the CA models are currently under way (see Isliker & Vlahos 2003). We believe that much effort should be put in developing global models for the study of the solar corona, that can couple the different processes, occurring in different time and spacial scales. This approach will open a new highly promising and challenging field for solar physics research.

Acknowledgments: We would like to thank Dr. H. Isliker and Dr. M. Georgoulis for many stimulating discussions on cellular automata models and their applications to solar flares. CG would also like to thank the Research Comittee of the Academy of Athens for their support. This work was partially supported by the Greek General Secretariat for Research and Technology.

REFERENCES

Anastasiadis, A. 2002, J. Atmosph. Solar - Terrestr. Phys., 64(5-6), 481
Anastasiadis, A., Vlahos, L., & Georgoulis, M. K. 1997, ApJ, 489, 367
Bastian, T. S., & Vlahos, L. 1997, in Lecture Notes in Physics, Vol. 483, ed. G. Trottet, (Springer-Verlag), 68
Brown, J. C. 1971, Sol. Phys., 18, 489
Buchlin, E., Aletti, V., Galtier, S., Velli, M., et al. 2003, A&A, 406, 1061
Einaudi, G., & Velli, M. 1999, Phys. Plasmas, 6, 4146
Einaudi, G., Velli, M., Politano, H., & Pouquet, A. 1996, ApJ, 457, L13
Galsgaard, K., & Nordlund, A. 1996, J. Geophys. Res., 101, 13445
Georgoulis, M., & Vlahos, L. 1996, ApJ, 469, L135
Georgoulis, M., & Vlahos, L. 1998, A&A, 336, 721
Georgoulis, M., Velli, M., & Einaudi, G. 1998, ApJ, 497, 957
Isliker, H., & Vlahos, L. 2003, Pys. Rev. E, 67, 026413
Isliker, H., Anastasiadis, A., & Vlahos, L. 2000, A&A, 361, 1134
Isliker, H., Anastasiadis, A., & Vlahos, L. 2001, A&A, 377, 1068
Isliker, H., Anastasiadis, A., Vassiliadis, D., & Vlahos, L. 1988, A&A, 309, 1085
Lu, E. T., & Hamilton, R. J. 1991, ApJ, 380, L89
Lu, E. T., Hamilton, R. J., McTierman, J. M., & Bromund, K. R. 1993, ApJ, 412, 841
Litvinenko, Y. E. 1996, ApJ, 462, 997
MacKinnon, A. L., Macpherson, K. P., & Vlahos, L., 1996, A&A, 310, L9
Vilmer, N. 1993, Adv. Space Res., 13(9), 221
Vilmer, N., & MacKinnon, A. L. 2003, in Energy Conversion and Particle Acceleration, ed. K.-L. Klein, (Springer-Verlag), 127
Vilmer, N., & Trottet, G. 1997, in Lecture Notes in Physics, Vol. 483, ed. G. Trottet,(Berlin:Springer-Verlag), 28
Vlahos, L. 1996, in Radio Emission from the Stars and the Sun, ASP Confer. Ser., 93, ed. A. R. Taylor and J. M. Paredes (ASP Press), 355
Vlahos, L., Fragos, T., Isliker, H., & Georgoulis, M. 2002, ApJ, 575, L87
Vlahos, L., Georgoulis, M. K., Kluiving, R., & Paschos, P. 1995, A&A, 299, 897

*ABSTRACTS OF PAPERS POSTED DURING THE PROCEEDINGS OF THE SESSION "THE SUN AND THE HELIOSPHERE"**

DISTINCT SHOCK ACCELERATION PROCESSES - EVALUATION OF THE MAGNETIC TRAP DIMENSIONS FORMED UPSTREAM OF THE INTERPLANETARY SHOCK ON 147 DAY, 1991, USING MEASUREMENTS OF ULYSSES

P.K. Marhavilas, E.T. Sarris and G.C. Anagnostopoulos
Space Research Lab., Demokritos University of Thrace

Abstract: We analyze the acceleration signatures of energetic ions (E>50 keV) and electrons (E>30 keV) being observed on day 147 of the year 1991 UT, in the vicinity of the surface of a fast-mode quasi-perpendicular interplanetary hydromagnetic shock, using fine time resolution measurements by the HI-SCALE instrument onboard the Ulysses spacecraft (s/c). The observations present strong evidence for the acceleration of energetic particles trapped within magnetic structures on the surface of the fast-mode shock. We discuss the flux-times profiles and particle distributions near the shock in the context of previous theoretical studies and models. Moreover we are in the procedure of evaluating the width L and amplitude A of the magnetic structure by using HI-SCALE measurements and a sinusoidal form geometry.

STUDY OF 40 SOLAR ENERGETIC EVENTS BASED ON GOES, LASCO AND ARTEMIS IV DATA (1998-2000)

E. Mitsakou, C. Vassiliou, X. Moussas, J. Polygiannakis, A. Hillaris, P. Preka-Papadema,
Department of Physics, University of Athens,
Caroubalos, C.,
Department of Informatics, University of Athens,
C. E. Alissandrakis,
Department of Physics,University of Ioannina,
P. Tsitsipis, A. Kontogeorgos,
Technological Education Institute of Lamia,
J.-L. Bougeret, G. Dumas, C. Perche.
Observatoire de Paris

Abstract: We are studying 40 solar energetic events; the basic data set consists of all type II, IV and II/IV metric radio bursts recorded by the Artemis IV radiospectrograph during the time interval 1998-2000. These are supplemented by CME data, from the LASCO CME lists, and GOES SXR data, from NOAA. The analysis of the combined data sets is presented and compared with previously established results, regarding the spatial and temporal association between the occurrences of radio bursts flares and CMEs.

* *Proceedings 6th Hellenic Astronomical Society Conference, 15-17 September 2003, Penteli, Athens, Greece*

*ABSTRACTS OF PAPERS POSTED DURING THE PROCEEDINGS OF THE SESSION "THE SUN AND THE HELIOSPHERE"**

SOLAR PHYSICS FROM SPACE FOR THE NEXT SOLAR CYCLE

Angelos Vourlidas,
Naval Research Lab
Spiros Patsourakos,
Naval Research Lab - George Mason University

Abstract: The blooming of solar physics research that started with the SOHO launch in 1995 is going to continue in the next solar cycle. NASA is preparing a formidable array of space-based instruments for launch in 2005-2007 aboard the Solar-B, STEREO and SDO satellites. The Naval Research Laboratory plays a major role in all three missions by proving instrumentation (EIS/Solar-B, SECCHI/STEREO & SHARPP/SDO), analysis support and theoretical modeling. Here, we provide a brief description of the three missions, describe the scientific objectives and capabilities of the NRL instruments, and comment of the data products and the available analysis tools. Note that the data from the NASA missions will amount to several GBytes/day and will be freely available within a few minutes from their downlink. It is, therefore, important, that the international solar physics community is well informed on the contents and characteristics of the data in order to formulate the best data browsing/mining/analysis strategies and to exploit these soon-to-come immense databases to the maximum possible extent. The Solar Physics programs at NRL are supported by NASA, ONR and AF/STP grants

A FLUID DESCRIPTION OF DIRECTIONAL ENERGETIC PARTICLE FLUX OBSERVATIONS

J. M. Polygiannakis, A. Alevizos, X. Moussas
Section of Astrophysics, Astronomy and Mechanics, Department of Physics, Univ. of Athens

Abstract: We propose that, whenever directional flux measurements of a population of particles (e.g. solar energetic particles, cosmic rays, solar wind plasma) of well-defined energy resolution are available, new macroscopic fluid-like quantities (namely the energy depended analog of density, mean velocity, anisotropic pressure, temperature and heat flux) can be rigorously estimated, thus describing the sub-flux referring to that energy range in fluid terms. Exact, closed relations for these quantities as functions of lower order spherical harmonics coefficients are analytically derived, offering a new interpretation of the anisotropy flux components in fluid terms. The first order anisotropy vector can be interpreted as the direction of the population's mean velocity and, for strongly isotropic distributions, the direction of heat flux. Indicative applications are presented, using energetic particle flux measurements of Ulysses spacecraft. The number density of energetic particles increases together with the density of the solar wind at times and this is an indication that the energetic particles are probably part of the solar wind plasma. At other times energetic particle density increases when the solar wind density decreases and this is probably an indication of local acceleration, as it happens in shocks.

* *Proceedings 6th Hellenic Astronomical Society Conference, 15-17 September 2003, Penteli, Athens, Greece*

*ABSTRACTS OF PAPERS POSTED DURING THE PROCEEDINGS OF THE SESSION "THE SUN AND THE HELIOSPHERE"**

THE SHAPE AND TIME VARIATIONS OF THE HELIOSPHERE AND LONGTERM MODULATION OF COSMIC RAYS

G. Exarhos [1,2] and X. Moussas[1]
[1] Section of Astrophysics, Astronomy and Mechanics, Department of Physics, Univ. of Athens,
[2] Siemens A.E., Promitheos 12 Nea Kifisia, Athens, Greece

Abstract: We study the temporal variation of cosmic rays with various simple models of a spherical heliosphere, made of concentric shells with variable magnetic field and size (several variations). We calculate the cosmic ray temporal and latitudinal variations and their latitudinal and radial gradients using a realistic model based on actual spacecraft data. We also study the size and shape of the heliosphere using Ulysses data since launch and OMNI data for the last 40 years. We also estimate the size and shape of the Alfven and sonic solar surfaces, which vary with heliolatitude and time. We use 1AU spacecraft data for the last three solar cycles for the time dependence of the heliospheric radius and Ulysses data for the 3D shape of the heliosphere. Results: the cosmic ray modulation follows well the variations of the radius of the heliosphere, which varies periodically with the solar cycle between 80 and 150 AUs and the variations of the interplanetary magnetic field and that the shape of the heliosphere is slightly anisotropic (north-south difference) due to the differences in the flow of the solar wind No significant difference of the shape has been observed between solar minimum and solar maximum conditions. The IMF and the magnetic filed in all the heliosphere varies substantially. We have also studied the shape of the Alfven and sonic surfaces of the Sun under solar minimum and solar maximum conditions.

THE NORTHERN BOW SHOCK AND ELECTRON FORESHOCK OF MARS BASED ON MARS GLOBAL SURVEYOR DATA

N. Sergis, X. Moussas
Section of Astrophysics, Astronomy and Mechanics, Department of Physics, Univ. of Athens

Abstract: A very smooth and almost time invariable bow shock of Mars is revealed using Mars Global Surveyor's data. The bow shock position has been identified using magnetic and electron flux data obtained by the Mars Global Surveyor Magnetometer and Electron Reflectometer (MAG/ER) experiment. We analyze the time period between days 87 and 255 of 1998. The ionospheric crossings were also estimated and its surface is presented in 3D. The results are presented in the Areocentric reference system without any assumption of axial symmetry around the Mars-Sun axis.

* *Proceedings 6th Hellenic Astronomical Society Conference, 15-17 September 2003, Penteli, Athens, Greece*

*ABSTRACTS OF PAPERS POSTED DURING THE PROCEEDINGS OF THE SESSION "THE SUN AND THE HELIOSPHERE"**

STATISTICS ON THE OCCURRENCE OF SOLAR RADIO BURSTS (TYPE II AND IV) AND THEIR RELATION WITH CMES AND FLARES COVERING THE TIME INTERVAL 1996-2001 (RISING AND MAXIMUM PHASE OF SOLAR CYCLE 23)

Georgiou M., Preka-Papadema P., Moussas X., Polygiannakis J. and Hillaris A.
Section of Astrophysics, Astronomy and Mechanics, Department. of Physics, Univ. of Athens,

Abstract: A CME consists of a sudden expulsion of a dense cloud of magnetized plasma from the sun to interplanetary medium. It is a result of a rearrangement of large-scale coronal magnetic structures. The observations suggest that it is associated with the magnetically closed regions where the coronal plasma is initially trapped. Active regions, eruptive filaments, flares, metric type II and IV radio bursts and X-ray events have been associated with CMEs. However, the association has turned out to be so complex that, to this day, the exact relationship is still hotly debated. In this paper, we present a comparison of all the observed type II and IV solar radio bursts and the associated CMEs as well flares covering the time interval 1996-2001. We used radio bursts were recorded by different instruments, CMEs observed by SOHO/LASCO satellite and flares by GOES as well as ground based observatories. Solar wind large-scale disturbances caused by CMEs typically reach the Earth in 3 or 4 days and may cause geomagnetic storms if they have the appropriate magnetic field orientation. Thus, the understanding of the processes involved in the relation of type II and IV radio bursts with the launch of CMEs is important for the prediction of geomagnetic activity and space weather.

STUDY ON THE SPATIAL AND TEMPORAL OCCURRENCE RATE OF Hα SOLAR FLARES AND THEIR ASSOCIATION WITH HALO CMES DURING THE RISING AND MAXIMUM PHASE OF THE SOLAR CYCLE 23 (1994- 2001)

Pothitakis G[1]., Preka-Papadema P[1]., Petropoulos B[2]., Moussas X.[1], Polygiannakis J.[1], and Hillaris A[1].
[1] Section of Astrophysics, Astronomy and Mechanics, Department of Physics, Univ. of Athens,
[2] Research Center for Astronomy and Applied Mathematics, Academy of Athens

Abstract: We analyze the Hα solar flare occurrence rate during the rising and maximum phase of the solar cycle 23 using daily values. The distribution of flares in space and time is examined to verify the existence of a few sites of unusually strong solar activity (hot spots) and its probable variation during the solar cycle. Recently, several authors have reported some temporal and spatial association either with GOES X-ray flares or with eruptive filaments. Moreover, some CMEs characteristics change during the solar cycle, while others remain unchanged. We study the possible association of Hα flares and CMEs with emphasis on Halo CMEs during the examined time period and we discussed on the related geomagnetic activity.

* *Proceedings 6th Hellenic Astronomical Society Conference, 15-17 September 2003, Penteli, Athens, Greece*

ABSTRACTS OF PAPERS POSTED DURING THE PROCEEDINGS OF THE SESSION "THE SUN AND THE HELIOSPHERE"[*]

SPACE STORM MEASUREMENTS OF 17 AND 21 APRIL 2002 FORBUSH EFFECTS FROM ARTEMIS-IV SOLAR RADIO-SPECTROGRAPH, ATHENS NEUTRON MONITOR STATION AND CORONAS-F SATELLITE

C. Caroubalos[1], X. Moussas[1], P. Preka-Papadema[1], A. Hillaris[1], I. Polygiannakis[1], H. Mavromichalaki[1], C. Sarlanis[1], G. Souvatzoglou[1], M. Gerontidou[1], C. Plainaki[1], S. Tatsis[1], S.N.Kuznetsov[2], I. N. Myagkova[2], K. Kudela[3]

[1] Dept. of Physics, University of Athens,

[2] Scobeltsyn Institute of Nuclear Physics, Moscow State University, Moscow Russia

[3] Institute of Experimental Physics, SAS, Kosice, Slovakia

Abstract: Transient solar activity causes interplanetary and geomagnetic phenomena, cosmic ray storms and perturbed space weather, the study of which requires joint observations of different parameters. A preliminary analysis of a sequence of strong solar and interplanetary events such as solar flares, type II and IV radio bursts and CMEs, recorded by ARTEMIS-IV solar radio spectrograph as well as Forbush effects recorded within the NM energy range, related to geomagnetic storms in April 2002, has been performed. We also use data from the SONG instrument on board CORONAS-F satellite (fluxes of protons Ep>90 MeV and electrons Ep>60 MeV) and associated disturbances due to coronal mass ejections. The Athens Neutron monitor station (cut-off rigidity 8.53 GV) provides measurements of the hadronic component of the cosmic-ray intensity in real time presentation of current data suitable for space investigations. The influence of interplanetary medium conditions on the cosmic ray flux is analyzed and discussed. The observed time sequence of events of this time period indicates that the initiation of CMEs is closely related to type II and IV radio bursts and strong solar flares.

PRELIMINARY RESULTS FROM SECIS OBSERVATIONS OF THE 2001 ECLIPSE

A.C. Katsiyannis

Department of Pure and Applied Physics, Queen's University Belfast

Abstract: The Solar Eclipse Coronal Imaging System (SECIS) has been modified and used to observe the 2001 total solar eclipse from Zambia. A higher signal-to-noise ratio was achieved as a much broader green filter was used and a new alignment method was applied to the 8000 images taken during observations. These changes have led to better quality data and the authors would like to present some preliminary results that confirm previous detections of oscillation by SECIS during the 1999 total solar eclipse. The June 2001 total solar eclipse was observed using the SECIS instrument. The 8000 frames obtained were firstly corrected using dark and sky flat frames and then aligned to an accuracy of 0.05 pixels using automated software written for this purpose. The noise of the data set was reduced by applying the à Trous algorithm and wavelet analysis was used to detect oscillations. Statistical analysis of the oscillations detected in the moon disk and outer coronal areas allowed an estimation of atmospheric effects. A coronal loop of Active Region NOAA 9513 was found to contain a larger number of detections of intensity oscillations than expected. Additionally, these oscillations are distributed inside or alongside the loop, while the distribution of detections in other areas is isotropic. These preliminary results confirm the instrument's ability to detect MHD oscillations and their presence in the data set of the 2001 observations.

[*] *Proceedings 6th Hellenic Astronomical Society Conference, 15-17 September 2003, Penteli, Athens, Greece*

*ABSTRACTS OF PAPERS POSTED DURING THE PROCEEDINGS OF THE SESSION "THE SUN AND THE HELIOSPHERE"**

LORENTZ FORCES AND HELICITY DIAGNOSTICS IN SOLAR ACTIVE REGIONS, BASED ON A FAST RESOLUTION OF THE AZIMUTHAL AMBIGUITY IN SOLAR VECTOR MAGNETOGRAMS

Manolis K. Georgoulis, Barry J. LaBonte, and David M. Rust
The Johns Hopkins University Applied Physics Laboratory, 11100 Johns Hopkins Rd., Laurel

Abstract: We have developed a fast, fully automatic analysis package that expedites substantially the processing of solar vector magnetograms. This tool may be very useful in both existing and imminent ground-based and spaceborne solar projects, as well as in demanding Space Weather applications, such as are and geomagnetic storm prediction from coronal mass ejections. Given an active-region vector magnetogram, the implementation code performs the following tasks: *(i)* It resolves the azimuthal ambiguity of 180*o* in the magnetogram, *(ii)* it calculates the vertical Lorentz force and a lower limit of the non-field-aligned electric current density on the resolved magnetogram, and *(iii)* it estimates the magnetic helicity budget in the active region. The resolution of the 180*o*-ambiguity is obtained by a semi-analytical *structure minimization* technique, where we seek to minimize the complexity of the magnetic configuration. The required computation is only a small fraction of the one required by existing methods. For the first time, our technique is disentangled from any explicit use of potential / linear force-free magnetic extrapolations. Moreover, our results are in excellent agreement with the results of sophisticated, but impractically slow, techniques. The ambiguity resolution provides an approximate vertical gradient of the magnetic field strength. We show how this information leads directly to the calculation of the vertical Lorentz force on the plane of the observations. This further leads to a calculation of a lower limit of the non-field-aligned electric current density. Forced areas in an active region are identified quantitatively for the first time. We show that the magnetic configurations on the active-region solar photosphere are strongly forced. The above innovations allow the development of a technique to calculate the relative magnetic helicity budget in an active region. The method only assumes knowledge of the potential photospheric field and of a representative overall value of the force-free parameter for the active region. Based on the linear force-free approximation, the method tracks the coronal magnetic field lines in the active region thus providing an estimate of the relative magnetic helicity. The technique is currently applied to flaring active regions, prolific in coronal mass ejections, in an attempt to detect any signature of the flares or of the magnetic fields ejected in the heliosphere.

THE CYCLES OF THE SUNSPOTS IN REGARD WITH THE CONJUGATION OF THE PLANETS.

G. Leivadiotis, X. Mousas
Section of Astrophysics, Astronomy and Mechanics, Department of Physics,
University of Athens, Greece

Abstract: The relation of the main cycles of the sunspots timeseries with the conjugation of the planets is examined. We define a specific tidal function by taking into account all the planets including the initial conditions of their rotation round the Sun. The periodicities of this function are compared with the cycles of the sunspots.

* *Proceedings 6th Hellenic Astronomical Society Conference, 15-17 September 2003, Penteli, Athens, Greece*

Session II

STARS
AND STELLAR SYSTEMS

Conveners: E. Antonopoulou and M. Mathioudakis

PROBING YOUNG STELLAR OBJECTS AT AU SCALES UNDERSTANDING THE DRIVING AND HEATING MECHANISMS OF T -TAURI JETS*

Antonio Chrysostomou and Michihiro Takami
Centre for Astrophysics Research, Science & Technology Research Centre,
University of Hertfordshire, Hatfield, HERTS AL10 9AB

ABSTRACT

In this review we present our recent work investigating the physical conditions of jets from T-Tauri stars. We ask whether the heating and driving mechanism of protostellar jets is any better understood and summarise other work which places our research in context. Some of our recent results are discussed. An introduction to the technique of spectro-astrometry is provided.

1. INTRODUCTION

It is now understood that the accretion and outflow of material onto and from young stellar objects (YSOs) are intimately connected – it seems that one cannot proceed without the other. The correlation of UV excess and forbidden-line emission, which trace accretion and outflow respectively, suggests a physical link between these two phenomena [15]. It is thus important to study jets from YSOs as, apart from the star itself, they are an observable consequence of star formation.

The progress of star formation research has dictated that the circumstellar environment within 10 AU of the YSO is a very important region to study as it is here that disk material is accreted onto the protostar and launched into the jet. Jets in particular have generated a lot of interest in the literature (see the review in [12] for an example). In this present review, we summarise some of the important issues in this research and discuss the progress that has been made.

1.1. THE STAR FORMATION-OUTFLOW CONNECTION

For star formation to occur, it is clear that accretion is necessary but the need for outflows is not so straightforward to explain. What is certain is that jets and outflows are an ubiquitous signature of the star formation process and their action has important consequences. Outflows inject energy into, and can generate turbulence within, molecular clouds; the shocks that are subsequently created in the parent molecular cloud may trigger new instances of star formation; and perhaps their ultimate importance lies in the possibility that outflows and jets provide a means by which angular momentum may be removed from the circumstellar disk, thereby allowing accretion onto the protostar to proceed. However, despite their importance, we possess a poor understanding of YSO jets. For instance, it is not clear to us what physics is responsible for driving circumstellar material over such large distances and speeds?

Which objects are the most appropriate to study this phenomenon? The most powerful jets are generated at the earliest stages of a YSOs evolution – the so-called Class 0 and Class I YSOs. However, these are deeply embedded and dust enshrouded objects making it difficult

* Main Session Invited Review

Proceedings of the 6th Hellenic Astronomical Society Conference, 15-17 September 2003, Penteli, Greece

to observe the diagnostic emission lines found in the optical and near-infrared. The more evolved Class II objects are readily observed in the optical (in fact, the T-Tauri class of YSO is defined by its bright, optical light) but as most of the envelope material has either been accreted onto the protostar or cleared away, it is rare to find these objects driving jets. Hence, we are forced to conduct our research on objects which are arguably less than ideal and which probably represent special cases in the general population.

The observations clearly indicate that jets are launched from a region very close to the YSO, say within a radius of 1-10 AU, and the forbidden-emission line (FEL) regions tracing the jets extend out to ~ 1000 AU [10]. The jets remain remarkably well collimated over this distance [11]. Davis et al. [9] showed that the FEL region is generally more extended in Class I objects than in Class II. Intriguingly, Davis et al. [8] also showed that molecular hydrogen (H_2) emission jets in Class I YSOs are also, most likely, launched from the circumstellar disk from within a region very close to the protostar.

How jets are heated has also become a topic of much debate. Somehow the high temperatures necessary to excite the FEL region and sustain the ionisation fraction [1] needs to be generated and maintained in the jets. Currently, there are four heating mechanisms which are being debated on in the literature:

- *Shock heating*: shocks in the jet may be generated through instabilities in the flow or as a consequence of a time variable ejection mechanism. Models show that specific line ratios are able to distinguish between shocks and ambipolar diffusion models [17].
- *Ambipolar diffusion*: in the presence of a dynamically important magnetic field, ions in the gas will remain “frozen” to the field lines. Forcing ions and neutrals to flow past each other will cause friction and thereby heat the gas.
- *Turbulence*: the same instabilities and time dependencies which generate the shocks may also drive turbulence within the jet and thereby provide a source of heating. Understanding of turbulent shocks is still very much in its infancy.
- *X-ray heating*: TTauri stars are known X-ray emitters [14] although it is not clear that the X-ray luminosities are sufficient to reproduce the required ionisation fractions.

In the following sections we discuss our progress in these matters and briefly explain the technique of spectro-astrometry which we have used as a tool to aid our research.

2. SPECTRO-ASTROMETRY AS A PROBE OF YSOs AT AU SCALES

Over the last decade we have witnessed a dramatic increase in the detail that imaging instruments can provide us with. Arguably, the *Hubble Space Telescope* (*HST*) and adaptive optics on large telescopes has done the most to generate such information and interest in high resolution astronomy, revealing the complicated structure around young stars and galaxies alike. We have been able to directly probe the circumstellar environments of star forming regions, seeing the structure of some disks and jets for the first time [18]. Regardless of the variety of opening angles seen, it has been shown that the jets remain relatively well and uniformly collimated [11].

Despite these advances, neither the *HST* nor adaptive optics on large telescopes can reach the spatial limits required to probe at the 10 AU scale. With the nearest star forming regions being some 150 pc distant, 10 AU corresponds to ~ 0.05″. This means that the jet/wind launching region as well as the interaction region between circumstellar companions and the disk remain unobtainable to us. Milli-arcsecond observational accuracy is required.

Spectro-astrometry is not a new innovation, and requires no special instrumentation. It is improvements in the precision of instruments that has allowed us to probe regions down to

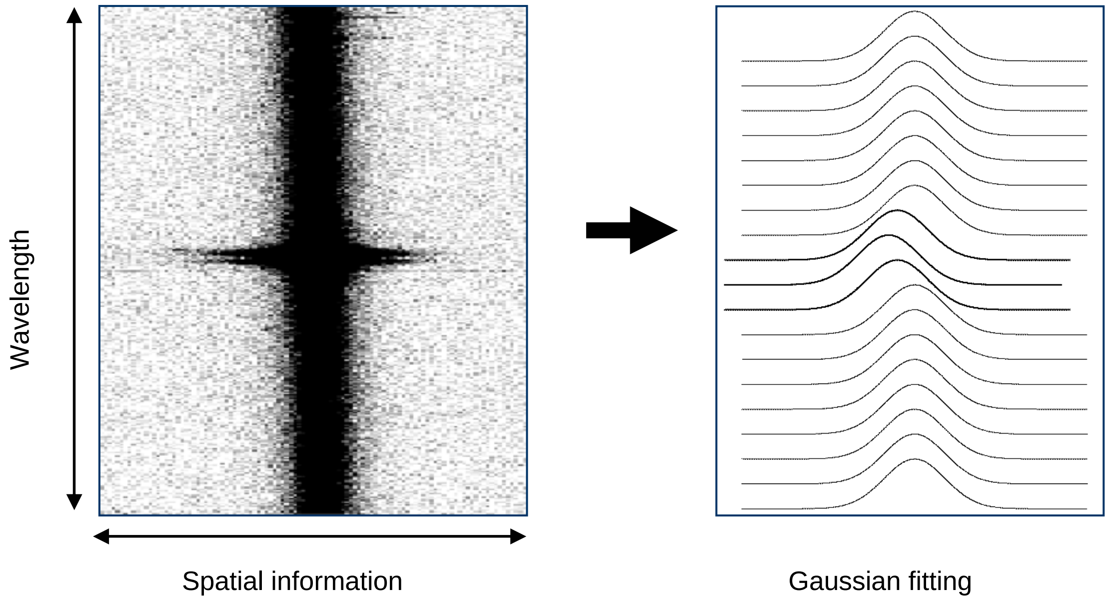

Figure 1: *The technique of spectro-astrometry. A long-slit spectrum is taken and the seeing position along the slit is measured using Gaussian fitting routines. Any asymmetry between line and continuum radiation become evident and the positional displacement relative to the continuum is measured. A relative position rather than absolute position is measured.*

milli-arcsecond scales. A standard long slit spectrograph which returns good sampling of the seeing profile is all that is required. The technique is explained in greater detail in [4] and [22], but simply, four spectra are observed at position angles separated by 90°. To determine the positional displacements (see Figure 1) in the N-S and E-W directions, fits to the seeing profile are made for each spectrum to determine the seeing centroid and the results taken at 0° and 180° are subtracted from each other and the same for positional displacements measured for 90° and 270°. This ensures that any instrumental effects (e.g. flexure in the instrument) are removed[1] while real displacements change sign. If there are any jets or companion stars present responsible for the line emission, the centroid position of the line will then differ from that at the continuum. It should be noted that spectro-astrometry returns just the relative positions, not the absolute positions. As such, each position spectrum has its continuum position arbitrarily adjusted to zero.

The measured positional accuracy depends on the seeing size and the photon number, N, at each wavelength. The detection limit is given by [22],

$$\sigma \propto \frac{\text{FWHM}}{\sqrt{N}} \text{ milli-arcseconds} \tag{1.1}$$

where FWHM is the full-width at half maximum of the seeing, and the constant of proportionality is ~ 0.5. This implies that a combination of arcsecond seeing and 3×10^4 photons, an accuracy of ~ 2 milli-arcseconds is achievable.

This represents a significant advance since the technique was first introduced [5]; more recent work [16] measured the displacement of FEL emission in T-Tauri stars down to 0.1″ scales. We have had a number of successes with this technique, including the detection of a number of binaries and outflows, the orbital motion of a binary (see Figure 2), the discovery of a gap in the circumstellar disk of the T-Tauri star RU Lupi through our observation of a bipolar Hα flow within 5 AU of the star, whereas for the FEL emission seen further out only

[1] Displacements due to real structure will have opposite signs, whereas instrumental deficiencies will remain constant.

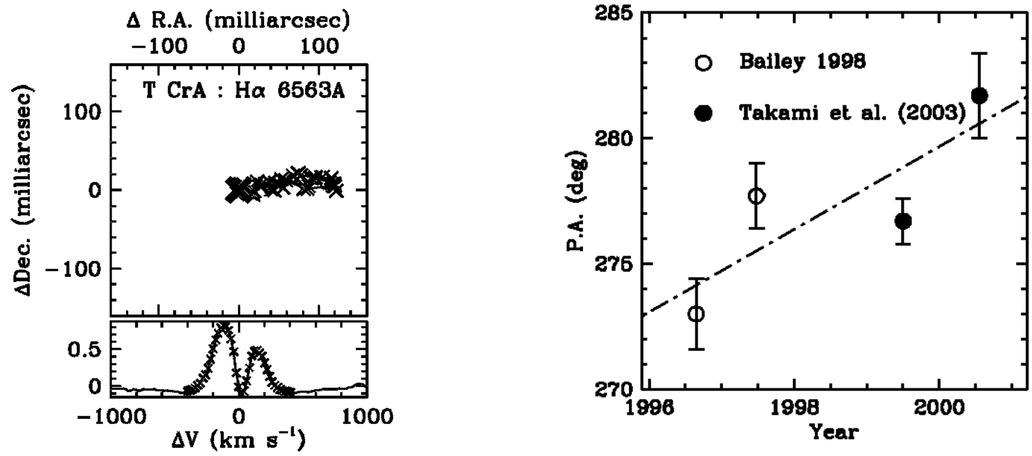

Figure 2 : *Detection of the orbital motion of the young T-Tauri star, T Cra [22]. The left panel shows our spectro-astrometric results. The total, velocity resolved Hα spectrum is shown below a graph of the 2D positional displacement as measured from the E-W and N-W spectra. The cross in the centre gives the position of the continuum emission. The graph clearly shows that the Hα emission comes from a companion currently at a position angle more than 270°. The right panel shows the positional angle measured at different epochs since 1998. Analysis reveals an orbital motion of 2°/yr (projected onto the plane of the sky), a binary separation of > 140 milli arcseconds with stellar masses > 0.2* $M_{\odot}$.

a monopolar flow is seen. The presence of a dip in the mid-infrared SED of RU Lupi corroborates our conclusion of the presence of a disk gap, most probably formed through tidal interactions with a companion.
Our major spectro-astrometric results to date are laid out in more detail in [20], [22], [4].

3. DG TAU: A CASE STUDY FOR JETS

Forbidden lines in T-Tauri stars arise from outflowing gas and often exhibit two blue-shifted components [16]. These correspond to low and high velocity components (LVC and HVC) to the jet. Different densities and temperatures determined for the LVC and HVC suggests a distinct origin for the two components, which most authors ascribe to a slow disk wind and a fast jet, respectively [13]. However, Bacciotti et al. [2] have argued that the HVC and LVC are just two manifestations of the same phenomenon – a disk wind whose velocity decays with radius.
DG Tau and its jet is one of the best studied T-Tauri stars. Despite its classification, it has a very energetic jet and a flat SED, attributes more similar to a Class I YSO than a Class II, and as such may represent a transition object between these two classes. Nevertheless, due to the attention it has gained it has become a prototypical example of a T-Tauri jet and a unique laboratory for testing theories and models of T-Tauri jets.

3.1. THE JET HEATING MECHANISM

Lavalley-Fouquet et al. [17] studied the optical line ratios from the jet and compared them to predictions based on ambipolar diffusion and shock models. Using a number of diagnostic line ratios, this analysis showed that the optical emission was clearly best explained in the context of shock heating.
Recently, we used the 8.2m Subaru telescope to observe DG Tau and obtained the first measurements of the HeI 1.083 μm line from within a jet in a T-Tauri star (see Figure 3 and [21] for more details). The high velocity component of the HeI line (found at similar

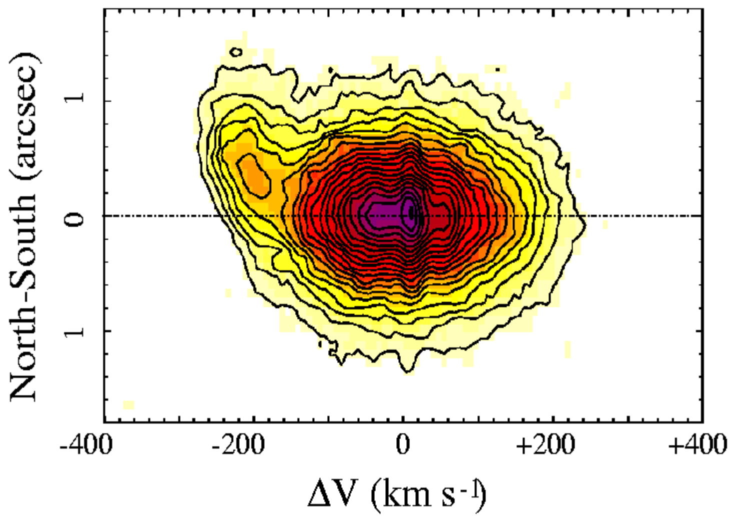

Figure 3 : *Continuum subtracted position-velocity diagram of the HeI 1.083 μm line from DG Tau along a slit placed at a position angle of N-S. The high velocity component at -200 km/s is seen to extend at least 1″ to the north. The dotted line at 0″ displacement represents the continuum position. The data also show a dominant, unresolved, component with a FWZI of ~ 500 km/s which likely arises from magnetospheric accretion columns.*

velocities to other FEL transitions identified with the HVC) clearly extends along the jet. The presence of such a high excitation line, requiring ~ 20 eV ($T_{ex} \sim 10^5$ K), restricts its origin to a region of either high temperature or intense ionising radiation. Ambipolar diffusion may be able to produce the necessary temperatures but inferred densities of $n_e \sim 10^5$ cm^{-3} are not likely to explain the presence of such a highly excited line [17]. In the face of other supporting evidence, such as the presence of other highly excited lines such as [OIII] in the spectrum of DG Tau [6], we agree with the findings of Lavalley et al. that shock heating is the most likely candidate for exciting this line and thus heating the jet.

3.2. THE JET-DRIVING MECHANISM

There are currently two competing models which attempt to explain how material from an accretion disk is channelled and accelerated into a jet. Both, disk-driven MHD models and the so-called X-wind model, rely on a combination of magnetic and centrifugal forces to drive and accelerate the disk material into a jet.

Numerical simulations of disk-driven models predict the presence of collimated jets, increased excitation towards the jet axis and that the disk material is accelerated off the surface of the accretion disk along magnetic field lines, rather like “beads on a wire”. Simulations of X-wind models show similar excitation and collimation characteristics but it is magnetic forces very close to the star, of the order of the stellar radius, which drive protostar-bound disk material into the jet.

Observations of DG Tau have gone a long way in helping us to understand the jet-driving mechanism (at least for this object!). The velocity structure of the LVC is seen to decrease as a function of distance from the jet axis [2]. This ‘onion-like’ or layered velocity structure is as predicted by disk-driven models with the high-velocity components closer to the axis and the low-velocity components spread out wider. Evidence for the high velocity components has been quite forthcoming with observations of the HVC and jets abound in the literature.

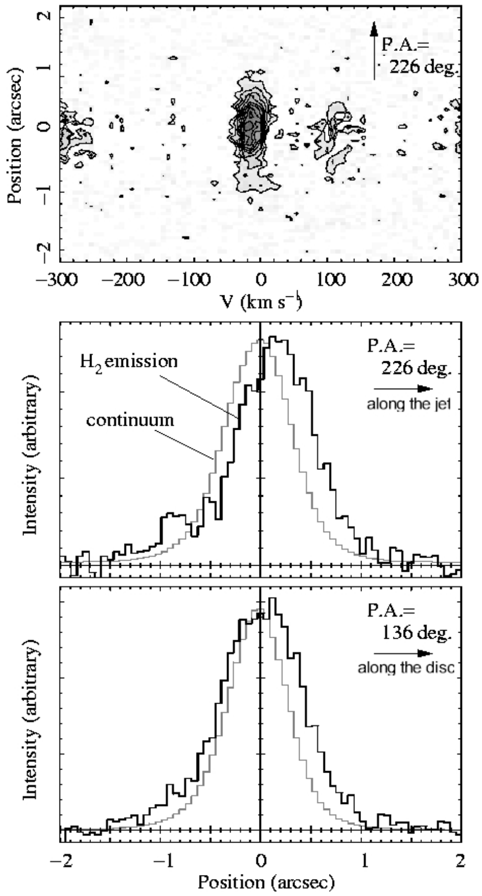

Figure 4 : *(top) Continuum subtracted position-velocity diagram of the H_2 1-0 S(1) 2.1218 μm emission line. The slit is at a position angle of 226°, parallel with the jet axis. (middle) Intensity distribution of the H_2 emission along the slit relative to the continuum. The offset from the star is clearly seen. (bottom) Intensity distribution of the H_2 emission along the disk direction showing that the H_2 emission comes from a more expansive region than the continuum.*

Recently, the detection of faint, wide-angled winds[2] [8] has broadened the debate – both disk-driven and X-wind models are capable of generating wide-angled winds.

Furthermore, for the first time a warm molecular (H_2) wind was recently detected from DG Tau [23] using the Subaru Telescope (Figure 4). The H_2 is seen coming from the jet at a distance of 0.2″ from the star and with a typical width of 0.6″. *HST* observations of the LVC [2] show that at a distance of 0.2″ from the star, the radial velocity is ~ 60 km/s on axis and ~ 30 km/s at a radius of 0.2″ from the axis. Extrapolating this velocity field to the radius of the H_2 wind, we might expect an observed radial velocity of ~ 15 km/s, in excellent agreement with the data.

Since most of the envelope material has been blown away, the only reservoir for the H_2 emission that remains is the circumstellar disk itself. This probably suggests that the wind is disk-driven as in X-wind models the flow originates from a few stellar radii [19]. The disk-driven model can more easily explain the presence of the H_2 molecules in the outflow, but the X-wind may have trouble as it is not clear whether any H_2 molecules could survive so close to the central protostar. Further modelling is called for, and perhaps one in which a hybrid X-wind/disk-driven model is at the heart of the jet driving mechanism.

It is clear that to make progress astronomers need to decide which model is most appropriate for driving jets and outflows, but this should be done with direct reference to the observations.

3.3. DO JETS REMOVE ANGULAR MOMENTUM?

Arguably, this is perhaps the most important question in star formation research. For a number of decades the problem that conservation of angular momentum poses for the formation of stars was understood to be a major hurdle for the theory. The discovery of jets and outflows fuelled speculation that these astonishing phenomena were directly responsible for removing the excess angular momentum from the circumstellar disk and thus allowing the protostar to accrete mass. This supposition only grew stronger as further observational work demonstrated an almost perfect correlation between the presence of outflow and star formation – one could not proceed without the other it seemed.

Proof of this, however, has been hard to come by due to the fact that the instrumentation available have not had the necessary precision. The last few years have seen a dramatic improvement with the first tentative detection of jet rotation made in the outflow of the

[2] Albeit these observations were made towards more embedded and younger Class I objects than the T-Tauri stars.

Herbig-Haro object, HH212 [7], albeit at relatively large distances from the source. A global rotation of the flow of a few km/s was deduced from measurements of the H_2 1-0 S(1) line with a sense of rotation consistent with the rotation of the circumstellar disk [25].
Bacciotti et al. [3] used *HST/STIS*, with 0.1″ resolution, to measure systemic velocity shifts in the line emission near the base of the DG Tau jet. The advantage here over the HH212 study is that the jet would not have suffered any strong interactions with the environment. Evidence for rotation of the jet is seen, and in the same sense as rotation of the circumstellar disk [24].

4. CONCLUSIONS

Perhaps the most interesting and important question to ask after describing this work is, 'Have we learned anything?' In conclusion, I outline below some of the problems and questions we were (and in some cases still are) faced with and what, if anything, we have learned.

– *How do we observe at the small scale lengths required to probe the central regions of protostars where the physics of outflow, accretion and planet formation are most complicated?*

  This is the first hurdle to overcome in our research and it is clear that a complimentary approach is necessary. We have shown that spectro-astrometry is a powerful technique which can probe regions which facilities like the *HST* cannot reach. In the future, the advent of optical interferometry, in particular through the VLTI in the next 5-10 years, will revolutionise what we think we understand today.

– *What is the dominant heating mechanism for jets?*

  The competing theories are still competing! Most of the evidence presented here and in other places seems to be in favour of shocks in the jet/wind as the likely heating mechanism. However, further observations of a more statistically significant sample are required before a clearer picture and understanding can be developed.

– *What is the driving mechanism for protostellar jets?*

  A similar scenario to the above applies for this question. The evidence seems to be in favour of the disk-driven models over the X-wind models. However, once hybrid X-wind/disk-driven models are developed and properly analysed, it may be difficult to discriminate between the two. It should be noted that in the absence of any clear and definitive predictions it will be hard to answer this question until the first VLTI results come through.

– *How is angular momentum removed from the accretion disk?*

  It's the outflow, as we always knew it would be!!!

REFERENCES

[1] Bacciotti F., & Eislöffel J., 1999, A&A, 342, 717
[2] Bacciotti F., Mundt R., Ray T.P., Eislöffel J., Solf J., Camenzind M., 2000, ApJ, 537, L49
[3] Bacciotti F., Ray T.P., Mundt R., Eislöffel J., Solf J., 2002, ApJ, 576, 222
[4] Bailey J.A., 1998, MNRAS, 301, 161
[5] Beckers J.M., 1981, Lowell Observatory Bulletin, 9, 165
[6] Cohen M., & Fuller G.A., 1985, ApJ, 296, 620
[7] Davis C.J., Berndsen A., Smith M.D., Chrysostomou A., Hobson J., 2002, MNRAS, 314, 241
[8] Davis C.J., Stern L., Ray T.P., Chrysostomou A., 2002, A&A, 382, 1021

[9] Davis C.J., Whelan E., Ray T.P., Chrysostomou A., 2003, A&A, 397, 693
[10] Dougados C., Cabrit S., Lavalley C., Ménard F., 2000, A&A, 357, 61
[11] Dougados C., Cabrit S., Lavalley-Fouquet C., 2002, in Emission Lines from Jet Flows, RMxAA, 13, 43
[12] Edwards S., 2003, ApSS, 287, 47
[13] Eislöffel J., Mundt R., Ray T.P., Rodríguez L.F., 2000, in Protostars & Planets IV, ed. V. Mannings, A.P. Boss & S.S. Russell (Tuscon: Univ. Arizona Press), 815
[14] Fiegelson E.D., & Montmerle T., 1999, ARAA, 37, 363
[15] Hartigan P., Edwards S., & Ghandour L., 1995, ApJ, 452, 736
[16] Hirth G.A., Mundt R., & Solf J., 1997, A&AS, 126, 437
[17] Lavalley-Fouquet C., Cabrit S., Dougados C., 2000, A&A, 356, L41
[18] Padgett D.L., Brandner W., Stapelfeldt K.R., Strom S.E., Terebey S., Koerner D., 1999, AJ, 117, 1490
[19] Shu F.H., Najita J.R., Shang H., & Li Z.-Y., 2000, in Protostars & Planets IV, ed. V. Mannings, A.P. Boss & S.S. Russell (Tuscon: Univ. Arizona Press), 789
[20] Takami M., Bailey J.A., Gledhill T.M., Chrysostomou A., Hough J.H., 2001, MNRAS, 323, 177
[21] Takami M., Chrysostomou A., Bailey J.A., Gledhill T.M., Tamura M., Terada H., 2002, ApJ, 568, L53
[22] Takami M., Bailey J.A., Chrysostomou A., 2003, A&A, 397, 675
[23] Takami M., Chrysostomou A., Ray T.P., Davis C.J., Dent W.R.F., Bailey J.A., Tamura M., Terada H., 2004, A&A, in press
[24] Testi L., Bacciotti F., Sargeant A.I., Ray T.P., Eislöffel J., 2002, A&A, 349, L31
[25] Wiseman J., Wooten A., Zinnecker H., McCaughrean M., 2001, ApJ, 550, L87

CCD PHOTOMETRY AND MODELLING OF THE ECLIPSING BINARY SYSTEM V417 Aql*

K.D. Gazeas, P.G. Niarchos, V.N. Manimanis
Section of Astrophysics, Astronomy and Mechanics, Department of Physics,
University of Athens, Greece

Abstract. The first BVRI CCD photometric observations of the eclipsing binary V417 Aql are presented. The light curves, obtained at the Kryonerion Astronomical Station, are analyzed and new geometric and photometric elements are derived. These elements are combined with the available spectroscopic data, to yield the absolute system parameters.

1. INTRODUCTION

The eclipsing binary V417 Aql (BD +52°4202, GSC 4904:0531, PPM 168201) was first discovered by Hoffmeister (1935). Soloviev (1937) classified it as a W UMa variable with a period of 0.37 days. Koch (1974) identified it as a strongly interacting solar type binary system. Since then, various studies were published, giving times of minima and a long term O-C diagram. More than 70 epochs of minimum light are available in the literature. An analysis of observations in U, B and V filters was made by Samec et al. (1997), who gave the system parameters as well as the first 3D model. The mass ratio was found spectroscopically to be q=0.362 (Lu & Rucinski, 1999).

A detailed orbital period investigation was presented by Qian (2003), based on the analysis of all the existed O-C values. It was shown that the period change of the binary system is continuous, leading to the conclusion that V417 Aql is either a member of a triple system with an invisible companion or there is a strong magnetic activity in the system, which is common for the solar-like components of close binaries.
Our observations show that V417 Aql has indeed a magnetic activity, which is obvious from the O'Connell effect in the light curves. In our analysis, it was necessary to assume the existence of cool spots on both components.

2. OBSERVATIONS

The ground-based observations of V417 Aql were made in two consecutive nights on July 13 and 14, 2002. The instruments used were the 1.22 m Cassegrain reflector at the Kryonerion Astronomical Station of the National Observatory of Athens, Greece, and a Photometrics CH250 CCD camera, equipped with a set U, B, V, R and I Bessell filters.

A total number of 632 frames were obtained in all filters, covering 4 minima (2 primary and 2 secondary). The images were processed with the AIP4WIN program of Berry & Burnell (2000).

Differential magnitudes were used to determine the standard deviation of our measurements, which is 0.005 mag in all bands used (B, V, R, I). From the light curves it is clear that V417 Aql is a contact eclipsing binary of W UMa type. The two maxima have not the same height with differences of about 0.030 mag in B, 0.025 mag in V, 0.020 mag in R, and 0.015 mag in I. On the other hand, the minima have negligible differences in depths.

---

* *Proceedings of the 6th Hellenic Astronomical Society Conference, 15-17 September 2003, Penteli, Greece*

3. LIGHT CURVE ANALYSIS

Although we succeeded to observe complete light curves, it was not possible to compute a new ephemeris, since only one secondary minimum was observed. The time of this minimum was computed by the method of Kwee & van Woerden (1956) and its value (the mean value in the four filters B, V, R and I) is: Min II (HJD) = 2452469.5570 ±0.0083.

For the phase diagrams we have used the following ephemeris given by Samec (1997):

$$\text{Min I (HJD)} = 2445554.7240 + 0^{d}.3703114 \times E \qquad (1)$$

Our light curves were analyzed with the Wilson-Devinney DC program, running in Mode 3. One hundred normal points were formed from our observations for each filter. Due to the profound asymmetries between the two maxima we had to assume the existence of at least one cool spot on the secondary component of the system. In the beginning of our solution it was assumed that no spots were present on the surface of the stars, and we performed the unspotted solution by omitting the observations around the secondary (lower) maximum between phases of 0.65 and 0.85.

Table 1. Light curve solutions for V417 Aql.

Parameter	**Mode 3 (unspotted)**	**Mode 3 (spotted)**
φ	0.0031 ± 0.0002	0.0031 ± 0.0002
i (degrees)	81.69 ± 0.27	81.82 ± 0.09
T_1 (K)	6250*	6250*
T_2 (K)	6527 ± 9	6402 ± 4
Ω_1	2.4832 ± 0.0044	2.4902 ± 0.0458
Ω_2	2.4832 ± 0.0044	2.4902 ± 0.0458
$q = m_2/m_1$	0.362*	0.362*
% overcontact	52%	49%
$L_1/(L_1+L_2)$ (B)	0.6377 ± 0.0025	0.6404 ± 0.0044
$L_1/(L_1+L_2)$ (V)	0.6523 ± 0.0021	0.6526 ± 0.0016
$L_1/(L_1+L_2)$ (R)	0.6417 ± 0.0016	0.6423 ± 0.0015
$L_1/(L_1+L_2)$ (I)	0.6498 ± 0.0015	0.6515 ± 0.0020
r_1 (vol)	0.5040 ± 0.0007	0.5019 ± 0.0010
r_2 (vol)	0.3308 ± 0.0007	0.3285 ± 0.0010
$\Sigma\, w(res)^2$	0.0303	0.0358

- assumed

The spectroscopic mass ratio q=0.362±0.007 (Lu & Rucinski 1999) was chosen as a fixed parameter. The free parameters to be determined by the program were the following: the phase of conjunction φ, the inclination i, the temperature of the secondary star T2, the surface potentials Ω (both Ω1 and Ω2) and the non-normalized monochromatic luminosities of the primary (L1) for the four filters. The temperature T1 had a fixed value (from spectroscopic observations). The usual values from the literature were used for the coefficients of gravity darkening. The limb darkening coefficients were taken from the new tables of Claret (2000) (bolometric values) and Claret, Díaz-Cordovés & Giménez (1995), according to the spectral type and the wavelength of observation. The third light was assumed equal to zero. The results are given in the second column of Table 1. The errors given are standard deviations.

In the second step of our analysis we used all the data, assuming that there are cool spots in both components (spotted solution), in longitude of 90±20 and 270±20 degrees and latitude of 90 degrees, for the sake of simplicity in the calculations. The radii of the spots were 18 and 14 degrees and the temperature factors 0.82 and 0.85, respectively. The results of the spotted solution are given in the third column of Table 1. The errors given are standard deviations

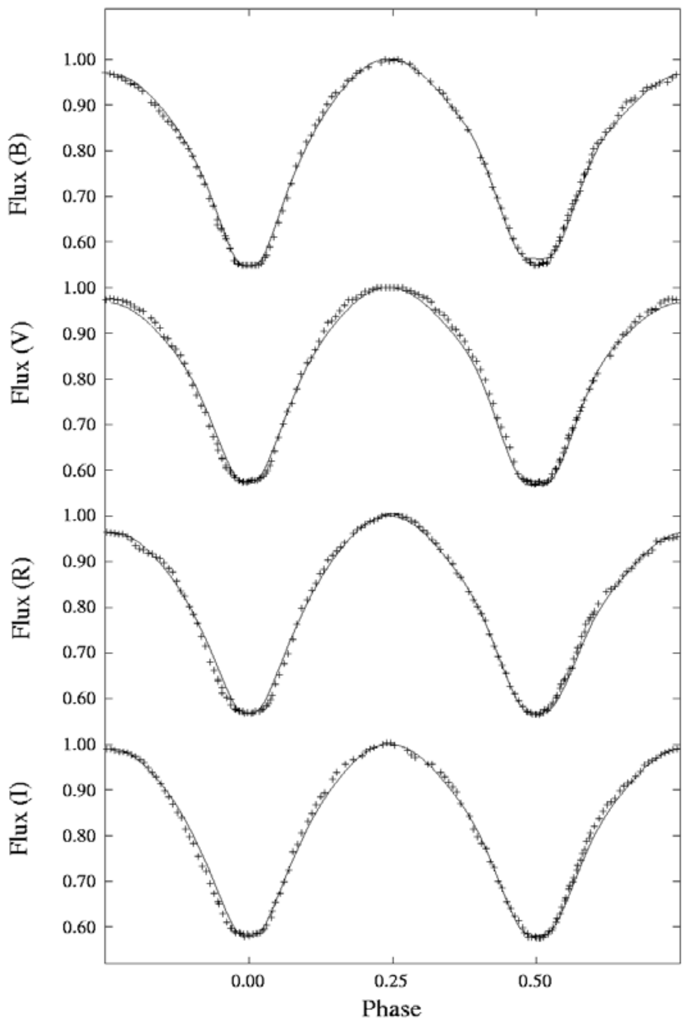

The derived parameters were used to construct a theoretical light curve, which is shown along with the observed light curves in Fig. 1.

.

The elements of Table 1 are combined with the available spectroscopic data to compute the following absolute physical parameters in solar units (radii, masses and luminosities) of V417 Aql, which are: $R1=1.355\pm0.012R_\odot$, $R2=0.887\pm0.016R_\odot$, $M1=1.418\pm0.153M_\odot$, $M2=0.513\pm0.055M_\odot$, $L1=2.527\pm0.046L_\odot$, $L2=1.192\pm0.043L_\odot$.

The absolute bolometric magnitudes are: M(bol)1=3.742, M(bol)2=4.558.

4. EVOLUTIONARY STATE

In Figure 2 we show the Mass-Radius diagram and the positions of the two components on it. The two lines represent the ZAMS and TAMS limits for single Main Sequence stars as they were published by Vandenberg (1985). V417 Aql has a G0V type primary and a F9V type secondary component, according to Samec (1997). It can be seen that both stars are well above the TAMS line, a fact supporting the idea that both stars are evolved. This result is also supported by the small orbital period and the almost equal temperatures of the two components.

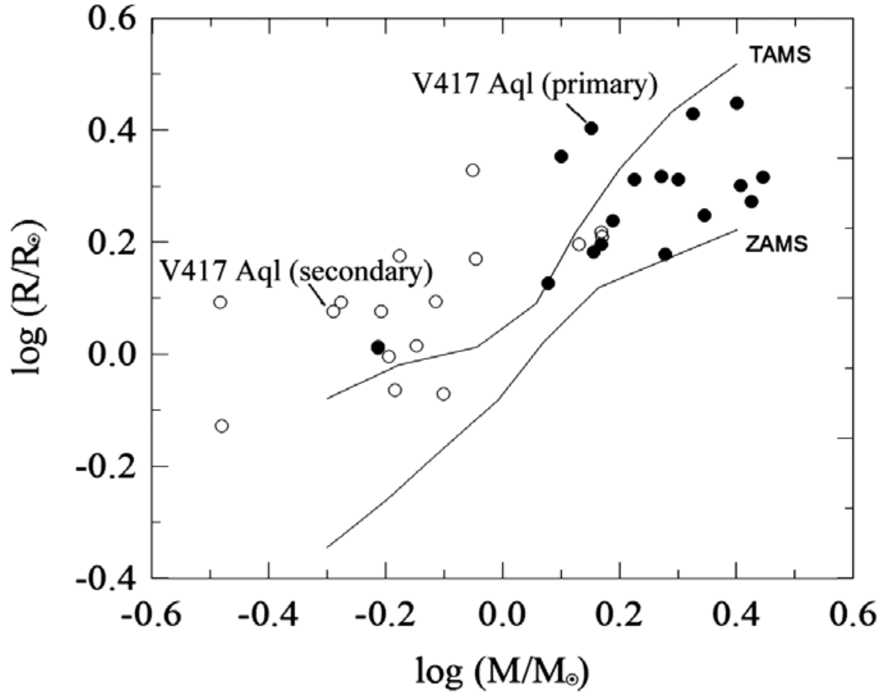

Figure 2. The M-R diagram and the position of the two components of V417 Aql.

5. SUMMARY AND CONCLUSIONS

It is clear from Fig. 1 that the observed light curves of V417 Aql are rather symmetrical with no noticeable irregular variations. There is a small difference in the depths of the two minima indicating different surface temperatures of the two components. Such a light curve is typical for W-type contact systems of W UMa type. The light curve analysis shows a highly contact configuration with a fill-out factor 49%. Our solution with assumed spectroscopic mass-ratio is quite similar to the solution given by Samec (1997), which was based on photometry alone, but differs significantly in the values of the fill-out factor. The results obtained from the present photometric solution were used to calculate the absolute system parameters and build the model of V417 Aql.

REFERENCES

Berry, R., Burnell, J. 2000, The Handbook of Astronomical Image Processing, Willmann-Bell, Richmond (Virginia).
Claret, A., 2000, A&A, 363, 1081
Claret, A., Díaz-Cordovés, J., Giménez, A., 1995, A&AS, 114, 247.
Hoffmeister, C., 1935, Astr. Nach., 255, 403
Koch, R., 1974, AJ, 79, 34
Kwee, K. K., van Woerden, H., 1956, Bull. Astron. Inst. of Netherlands, 12, 327.
Lu, W.X., Rucinski, S.M., 1999, AJ, 188, 515
Qian, S., 2003, A&A, 400, 649
Samec, R.G., 1997, AJ, 113, 401
Soloviev, A. 1937, Tadjik Obs. Circ., No. 22
Vanderberg, D.A., 1985, ApJS, 58, 711

THE FIRST VRI LIGHT CURVES AND ANALYSIS OF THE ECLIPSING BINARY CC SERPENTIS*

V.N. Manimanis, P.G. Niarchos, K.D. Gazeas
Department of Astrophysics, Astronomy and Mechanics, Faculty of Physics, National and Kapodistrian University of Athens

ABSTRACT

The first complete CCD light curves of the eclipsing binary system CC Serpentis with an A6 primary have been obtained in the V, R and I filters in two nights in April 2003 with the 40-cm telescope of the University of Athens Observatory. The light curves are analyzed with the W-D program in order to determine the geometrical and physical parameters of the system. These parameters are used together with the available spectroscopic data to compute the absolute elements of the system in order to estimate its evolutionary status.

1. INTRODUCTION

The variable CC Serpentis (= AN 41.1935 = Prager 3936) has been observed by very few observers, who used photoelectric photometers to record mainly times of minima (Pohl & Kizilirmak 1975, Agerer & Hübscher 1996 & 2000 and Agerer, Dahm & Hübscher 1999). Koch (1974) gives for the system a (B–V) value of +0.38, corresponding to a primary of spectral type A6, and a relatively low unreddened CN index of 0.176. Hilditch & Hill (1975) observed the system during mid-eclipse using the four-color (Strömgren) photometric system, while Rucinski (1983) studied properties of violet and ultraviolet spectral distributions from Strömgren observations. Brancewicz & Dworak (1980) include it in their catalogue of parameters as a W UMa-type binary system, i.e. one with an overcontact configuration, although they cite a very large temperature difference of 1550 K between its components and percentages of filling up of the Roche lobes 99% and 98% for the primary and secondary, respectively. Giuricin et al. (1983) include it in their statistical paper. Shaw (1994) includes it in his second catalogue of near-contact systems as a possible contact system.

2. THE OBSERVATIONS

The CCD observations of CC Serpentis were made in only two nights, on April 23 and 30, 2003. The instruments used were the 40-cm Cassegrain telescope of the University of Athens Observatory and an SBIG-8 CCD camera. The three Bessell V, R and I filters were used. The CCD images obtained were processed with the AIP4WIN photometry program of Berry & Burnell (2000).

The stars GSC 1494-1212 (V = 10,1) and GSC 1494-1082 (V = 11,1) were used as comparison and check stars, respectively. In total 202 yellow, 204 red and 200 infrared observations were obtained during the two nights. The probable error of a single observation was estimated to be ± 0.008 mag in infrared, ± 0.010 mag in red and ± 0.012 mag in yellow.

3. LIGHT CURVE SOLUTION

We first solved the light curves assuming that there are no spots on the components of the system. From an inspection of the curves, especially the one in filter R, we decided that the

* *Proceedings of the 6th Hellenic Astronomical Society Conference, 15-17 September 2003, Penteli, Greece*

observations in the phase interval 0.65 to 0.90 should be excluded, as this part of the light curve seems to be affected by the presence of spots. All observational points for each color were used in the analysis. The subscripts 1 and 2 refer to the star being eclipsed at primary and secondary minimum, respectively. The 1996 version of the Wilson-Devinney code was used in the light curve analysis.

Table 1: Unspotted light curve solution of CC Serpentis

Parameter	**Mode 3 solution**
φ_o	0.0015 ± 0.0002
i (°)	76.52 ± 0.21
T_1 (K)	7850*
T_2 (K)	7145 ± 17
g_1 , g_2	1.0*, 0.32*
A_1 , A_2	1.0*, 0.5*
Ω_1 (= Ω_2)	2.7402 ± 0.0177
$q = M_2/M_1$	0.45501 ± 0.0102
$L_1/(L_1+L_2)$ (V)	0.7419 ± 0.0405
$L_1/(L_1+L_2)$ (R)	0.7328 ± 0.0401
$L_1/(L_1+L_2)$ (I)	0.7195 ± 0.0395
X_1 , X_2 (bolom.)	0.605*, 0.541*
X_1 , X_2 (V)	0.614*, 0.619*
X_1 , X_2 (R)	0.489*, 0.515*
X_1 , X_2 (I)	0.388*, 0.434*
degree of overcontact	17.6%
r_1 (volume)	0.4625 ± 0.0027
r_1 (pole)	0.4306 ± 0.0023
r_1 (side)	0.4603 ± 0.0028
r_1 (back)	0.4912 ± 0.0025
r_2 (volume)	0.4143 ± 0.0064
r_2 (pole)	0.3013 ± 0.0052
r_2 (side)	0.3157 ± 0.0065
r_2 (back)	0.3546 ± 0.0118
Σ w(res)^2	0.1026

* assumed

Since no double-line spectroscopy was available, a “q-search” gave a starting value of q = 0.45. A preliminary set of the other input parameters was selected from the catalogue by Brancewicz & Dworak (1980). The results converged with the Mode 3 of the program; Modes 4 and 5 were also tried without achieving convergence. The adjustable parameters were the conjunction phase φ, the inclination i, the temperature T_2 of the secondary component, the non-dimensional surface potential Ω_1 (Modes 3 and 5), or Ω_2 (Mode 4), and the non-normalized monochromatic luminosity L_1. The fixed parameter was the temperature T_1 (from spectroscopic observations). Assumed values for gravity and limb darkening, and bolometric albedos, according to the spectral types of the components, were used. Third light was assumed to be zero. The results are given in Table 1. The errors given are the calculated standard deviations.

The parameters found in the unspotted solution were subsequently used in the *Binary Maker 2.0* program (Bradstreet 1993) to model the light curves with spots. We placed only one cool spot on the surface of the secondary, since the temperature of the primary is too high to allow spots in theory. The spot modelling has been derived by fitting the theoretical to the observational curves. The parameters of the spot are: Latitude 0°, longitude 115°, spot radius 24° and temperature factor 0.82.

Theoretical light curves based on the spot model and along with the observed ones are shown in Fig. 1. A three-dimensional model of the system with the spot visible at phase 0.75 is given in Fig. 2, along with a surface outline of the system.

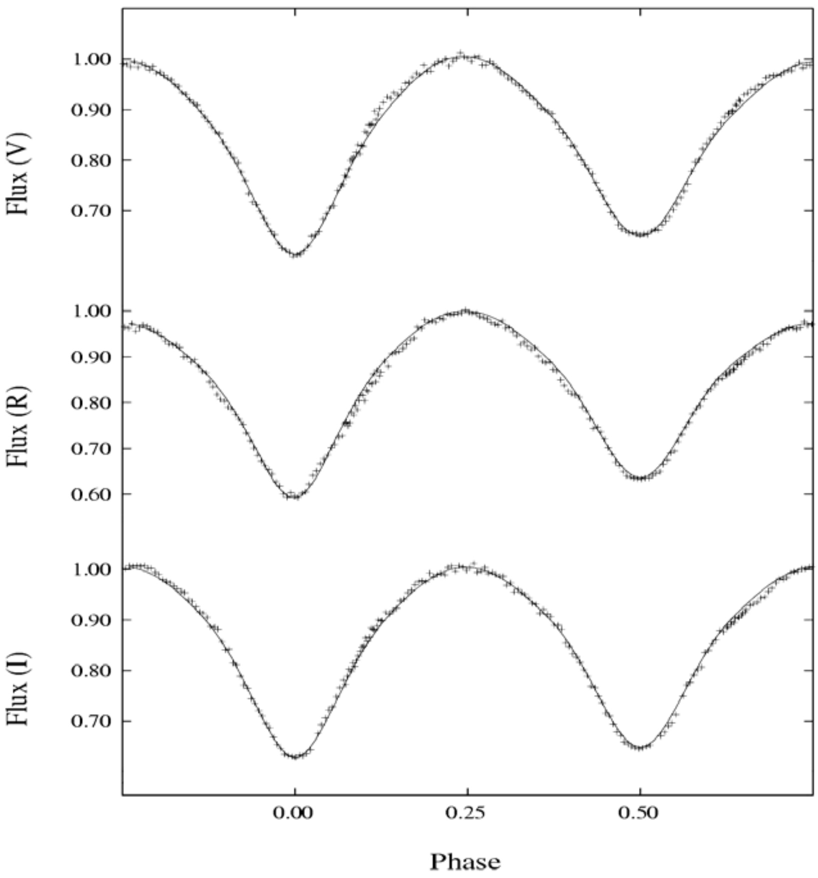

Fig. 1**.** *The observational points and theoretical light curves for our spot model (Mode 3).*

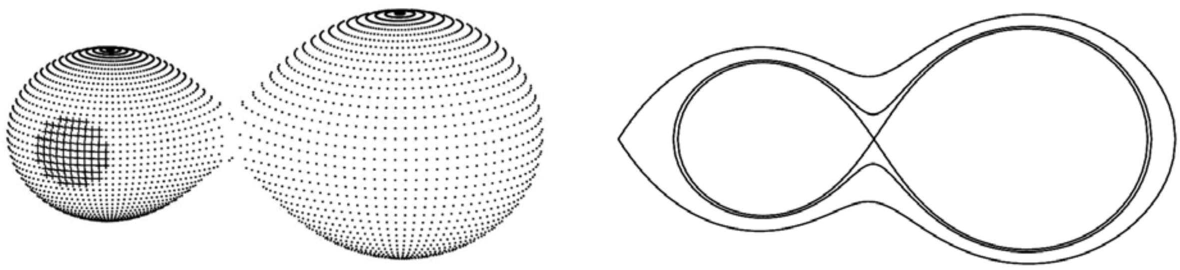

Fig. 2**.** *A three-dimensional model of CC Serpentis at phase 0.75 (left) and a surface outline of the system (right).*

4. ABSOLUTE ELEMENTS

From our solution and the spectral type of the system, we obtained the following absolute elements in solar units: $R_1 = 1.87 \pm 0.02$, $R_2 = 1.67 \pm 0.03$, $L_1 = 11.93 \pm 0.52$, $L_2 = 6.57 \pm 0.20$, $M_1 = 2.28 \pm 0.14$, $M_2 = 1.04 \pm 0.07$ Also, the bolometric absolute magnitudes $M_{bol(1)} = 2.06$ and $M_{bol(2)} = 2.71$.

5. SUMMARY AND CONCLUSIONS

From the results obtained using the WD program it seems more probable that the system of CC Serpentis is an overcontact one, so it should not be included in the catalogues of near-contact binaries. The large surface temperature, which prompted Shaw to include it in his list, must be explained in some other way. The evolutionary status of the star places it in the middle between the ZAMS and TAMS lines of the H-R diagram, a position similar with that of other W-UMa type systems.

REFERENCES

Agerer F., Dahm M., Hübscher J. 1999, *IBVS* No. 4712
Agerer F., Hübscher J. 1996, *IBVS* No. 4383
Agerer F., Hübscher J. 2000, *IBVS* No. 4912
Berry R., Burnell J. 2000, *The Handbook of Astronomical Image Processing*, Richmond: Willmann-Bell
Bradstreet D.H. 1993, *Binary Maker 2.0* User Manual
Brancewicz H.K., Dworak T.Z. 1980, *Acta Astronomica* **30**, 501
Giuricin G., Mardirossian F., Mezzetti M. 1983, *A&A Suppl. Series* **54**, 211
Hilditch R.W., Hill G. 1975, *Mem. R. Astron. Soc.* **79**, 101
Koch R.H. 1974, *AJ* **79**, 34
Pohl E., Kizilirmak A. 1975, *IBVS* No. 1053
Rucinski, S.M. 1983, *A&A* **127**, 84
Shaw J.S. 1994, *Mem. S. A. Ital.* **65**, 95

MHD OUTFLOW THEORIES. APPLICATIONS TO JETS FROM YOUNG STELLAR OBJECTS[*]

C. Sauty[1]
Université Paris 7, A.P.C., Observatoire de Paris, L.U.Th., 92190 Meudon, France
K. Tsinganos
University of Athens, Phys. Dept., Sect. of Astronomy, Astrophysics and Mechanics, Athens, Greece
E. Trussoni
I.N.A.F.,Osservatorio Astronomico di Torino, Strada Osservatorio 20,10025 Pino Torinese(TO), Italy

ABSTRACT

Jets are an ubiquitous ingredient of low mass star formation. Analytical models of such outflows show the following evolutionary sequence of jet presence. *First*, ejection may start at a very early stage of star formation (class 0 objects). *Second*, the ejection region evolves from the external part of the accretion disk towards the central star (class 1 and 2) in the form of a disk wind. *Third*, for TTauri stars (class 2) with low mass accreting rates, the star and the inner 2 or 3 stellar radii of the disk may account for most of the ejection. *Finally*, as the disk evaporates the jet naturally evolves into a solar-like type of wind.

I. INTRODUCTION

Outflows are widely observed in Young Stellar Objects (YSOs) and more specifically during low mass star formation, in the form of very well collimated jets. See the review on jet observations by Chrysostomou, this volume. Proto-stars and pre main-sequence low mass stars are usually classified in different broad classes from 0 to 3. Jets from classes 0 to 2 are usually very powerful and collimated and being usually associated with accretion disks (Fig. 1).

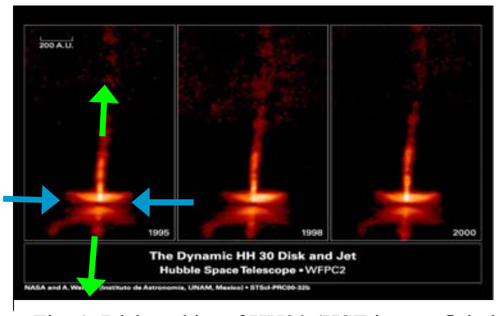

Fig. 1. Disk and jet of HH30 (HST image @ hubble.esa.int). Accretion proceeds in the equatorial plane (arrows in) while ejection is along the polar axis (arrows out).

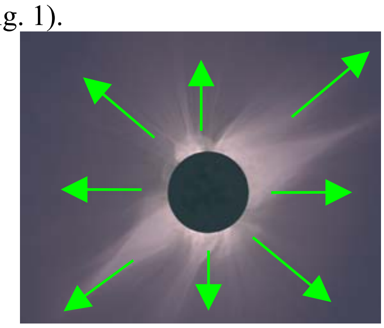

Fig. 2. The solar corona (1991 eclipse from Albers et al. Boulder @ www.solarsview.com). Ejection takes place all around the sun (arrows out).

However, the mass loss rate usually decreases with time, while velocity increases. Conversely, collimation seems to have a more complicated evolution. While class 0 jets are not very well collimated, class 1 jets are tightly collimated in a cylindrical structure and collimation even seems to increase further as we move to class 2 objects. In the following we summarize first the basic mechanisms at work in accelerating and collimating winds into jets. Then given the different existing models and how they best fit the various stages of the jet evolution, we suggest a scenario for the evolution of jets into winds where the ejection occurs closer and closer to the central object with a decrease of the magnetic efficiency in both accelerating and collimating the outflow.

II. BASIC MECHANISMS

Though jets are three dimensional and evolving with time, their secular evolution and their average properties can be understood assuming bipolarity, axisymmetry and steadiness. HH212 and the Solar Wind during the minimum of solar activity are some of the best examples in that respect. Of course

[*] Main Session Invited Speaker

Proceedings of the 6th Hellenic Astronomical Society Conference, 15-17 September 2003, Penteli, Greece

we cannot ignore the fact that jets also exist around binaries, or warped disks, and that the asymmetry of the environment, the presence of turbulence or transient features like coronal mass ejections and bursts may affect those two assumptions, providing several exceptions to their main trend. Nevertheless, the current understanding is that in most objects a fast and low density wind collimates into a jet in the case of a young star, surrounded by a fatter and slower component closer to the equatorial plane (Figs. 1 and 2).

Thus, in order to explain the launching and collimation of jets, stationary and axisymmetric MHD models of disk-winds and X-winds have been widely developed in the past, both analytically (e.g. Blandford & Payne, 1982, Vlahakis et al. 2000, Sauty et al. 2004, and references therein) and numerically (e.g. Casse & Keppens, 2002, Kudoh et al., 1998, Bogovalov & Tsinganos 2001), to cite only a few. Though the emphasis has usually been put on magnetic acceleration and collimation of jets, both magnetic and thermal effects are at play in those objects. The difference between those two types of models is the main source responsible for the ejection. While disk-wind models assume that the plasma outflows from the outer Keplerian part of the disk, X-wind models assume instead that it comes from the boundary of the disk with the stellar magnetosphere and the stellar corona itself. Of course in reality it is likely that both exist simultaneously, while one may prevail over the other depending on the stage of the evolution.

In Slow Magnetic Rotators like the Sun, acceleration is thermally, radiatively or wave driven, which roughly speaking amounts to say that there is a global "pressure" gradient that pushes the wind outwards from the central corona, as shown in Fig. 3. Conversely, in Fast Magnetic Rotators like YSOs, the launching may be predominantly magnetic, at least outside the polar axis. The presence of strong toroidal magnetic fields acting as a uncoiling spring can account for the transient ejections (Shibata & Uchida, 1990). However, magnetic acceleration in steady ejection is probably due to the strong initial poloidal field which forces the fluid to corotate up to the Alfvén point. The wind is then magneto-centrifugally driven like the familiar bead on a wire picture of Blandford & Payne (1982), Fig. 4.

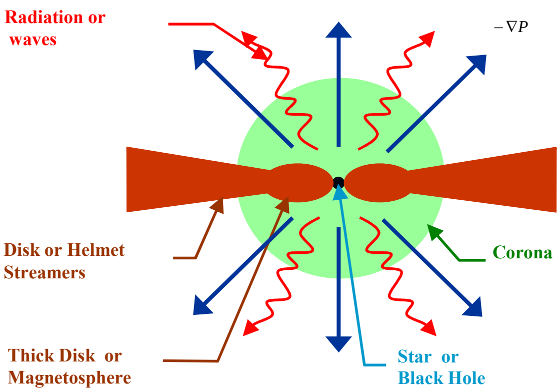

Fig. 3. ''Pressure'' driven wind

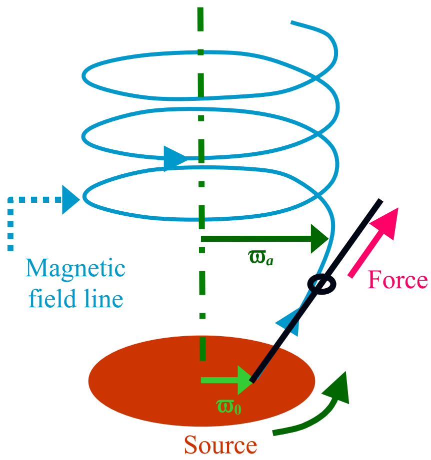

Fig. 4. Magnetocentrifugally driven wind

Both types of mechanisms may be at work also in collimating the outflow. Under-pressured jets with an increasing pressure as we move away of the central polar axis can be thermally confined by the tranverse pressure gradient pushing towards the axis (Fig. 5). This mechanism alone seems usually rather inefficient to produce very well collimated jets on large scales, where the pressure decreases significantly. Moreover, it cannot work in over-pressured jets. Conversely, pinching by the magnetic hoop stress can self-collimate the central part of the jet if it carries a poloidal current which eventually closes in the outer layers, or outside of the jet in the surrounding medium. In that case the toroidal magnetic field beyond the Alfvén point can sustain the flow against the centrifugal decollimating force and/or the pressure gradient, if it is an overpressured outflow (Fig. 6.).

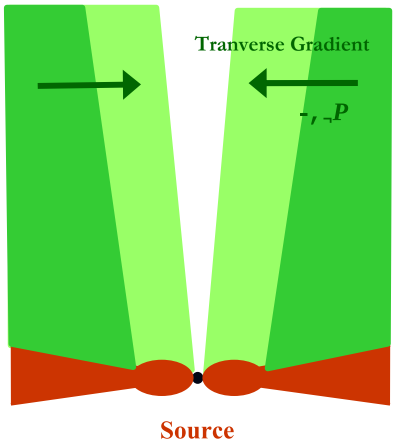

Fig. 5. Thermal confinement of an under-pressured jet

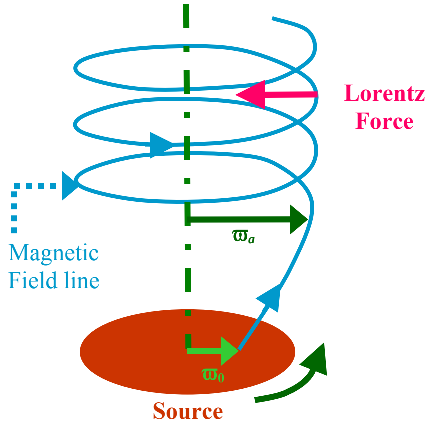

Fig. 6. Magnetic hoop-stress for the self-collimation of the jet.

II. WHAT CAN WE LEARN ABOUT THE JET EVOLUTION ?

II.1 Class 0 jets

In class 0 objects (André et al., 1993), the protostar is strongly embedded and the jet is very powerfull ($\dot{M}_{\mathrm{wind}} \sim 10^{-6} M_{\mathrm{sun}}/yr$ or higher) but rather slow (a few 10 km/s). As these objects seem to be in a very early stage, there is no obvious evidence that the star itself is already formed. In fact it has been shown in Contopoulos & Sauty (2000), that ejection may occur as soon as the centrifugal disk forms, even if accretion does not proceed towards the center.

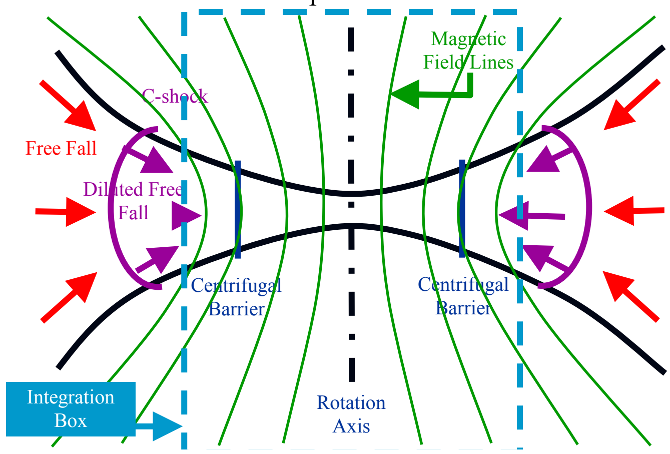

Fig. 7. Sketch of a disk driven jet for Class 0 objects showing the crucial role of the boundary

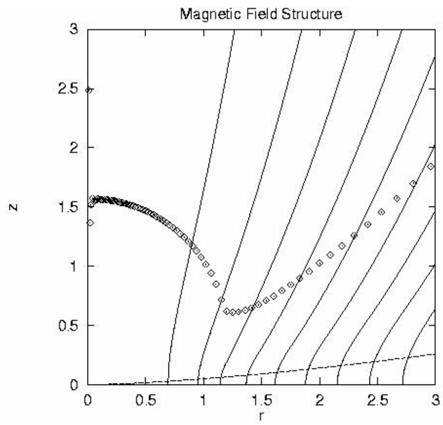

Fig. 8 Class 0 jet : computed potential field lines in the poloidal plane (solid) and the sonic surface (dots).

The idea is to take into account the diluted free fall of the matter beyond the centrifugal barrier (see Fig. 7) that drags the magnetic field inwards because of ambipolar diffusion. Then the geometry of a potential field can be calculated in the magnetosphere of the disk (Fig. 8) and it may be shown that this bending is enough to have magnetocentrifugal acceleration. Almost 40% of the gas is ejected in the transition region between the diluted free fall and the static disk below the centrifugal barrier. Below this barrier, gravity is exactly balanced by the centrifugal term and the magnetic field is vertical on the equatorial plane. Of course ejection is even more efficient if there is some mechanism (viscosity or magnetized outflow) to remove angular momentum. Then the magnetic fields may be accreted in the inner disk and bend even more. The mechanism proposed by Henriksen et al. (see Lery et al, 1999) of plasma circulating around the central part is somewhat similar despite the different treatment of the diluted free fall which is supposed to be ideal MHD.

II.2 Class 1 and class 2 jets with high accretion rates

In the next stage of class 1 and 2 objects, jets become much less powerful ($\dot{M}_{\rm wind} \sim 10^{-7}$ down to $10^{-8} M_{\rm sun}/yr$) but the velocities are already very high (a few 100 km/s). Though jets are very well collimated, they have rather large widths of a few tens of A.U. They may be produced by the inner part of the disk in the form of an X-wind (Shang et al. 2003) but because they widen so much it would imply rather strong magnetic fields at the foot points. Conversely disk wind models may be fairly adapted to them (see Dougados et al., this volume), although cold wind models like the one proposed by Ferreira (1997) fail at reproducing the high mass loss rate. The presence of a hot corona on top of the disk (Casse & Ferreira 2000) is needed. Moreover all those solutions refocalize onto the axis and can be valid only if terminated by a shock (Ferro-Fontan & Gomez de Castro, 2003). However, this can be done only if the true fast magnetosonic surface is crossed, which acts as an MHD horizon (Bogovalov, 1994, Tsinganos et al. 1996). Otherwise the perturbation of the shock may propagate upwind and destroy the solution. Such consistent solutions including a hot disk-corona and crossing all relevant critical points in the flow have been demonstrated in Vlahakis et al. (2000).

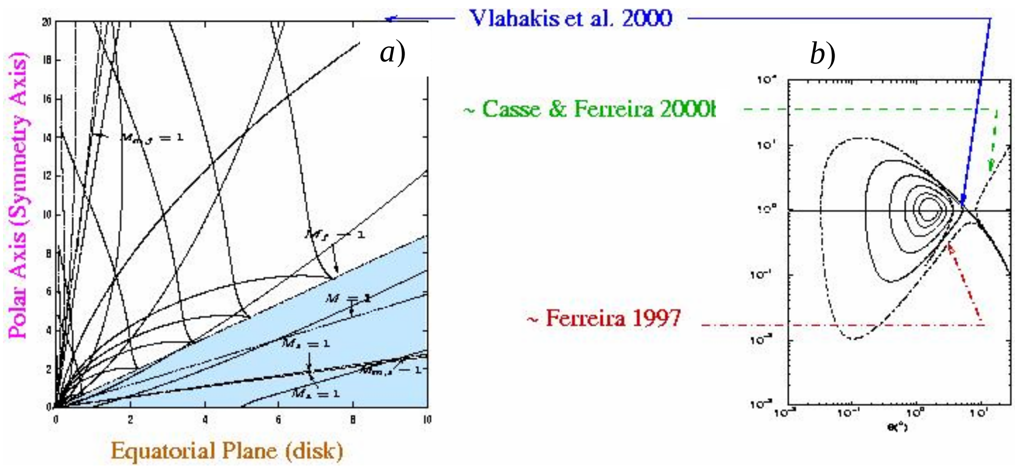

Fig. 9. Disk driven Jets for Class 1 and 2 objects with a consistent solution crossing all critical surfaces. In *a*) the poloidal fieldlines and the characteristics of the flow are displayed while in *b*) the topology around the fast magnetosonic point.

It remains to be shown how such solutions connect to the accretion disk. However, the cold plasma solution (Ferreira, 1997) is a breeze type solution and the hot plama solution of Casse & Ferreira (2000) is a terminated-type of solution. So by tuning the parameters of the hot disk corona (temperature and extension) such solutions should exist, which validates the relevance of disk-wind models.

In any case, from the theoretical point of view (a disk wind solution is not valid onto the axis) and the observational one (existence of multicomponent velocities in the jet), an X-wind or a stellar wind should also exist inside the inner part of the disk wind. This inner part can be collimated by the outer one as suggested by Bogovalov & Tsinganos (2001). Alhough this part may not be dominant in the class 1 and 2 objects with high accretion rates, it may become crucial for class 2 objects with low accretion rates.

II.3 From class 2 jets with low accretion rates to stellar winds

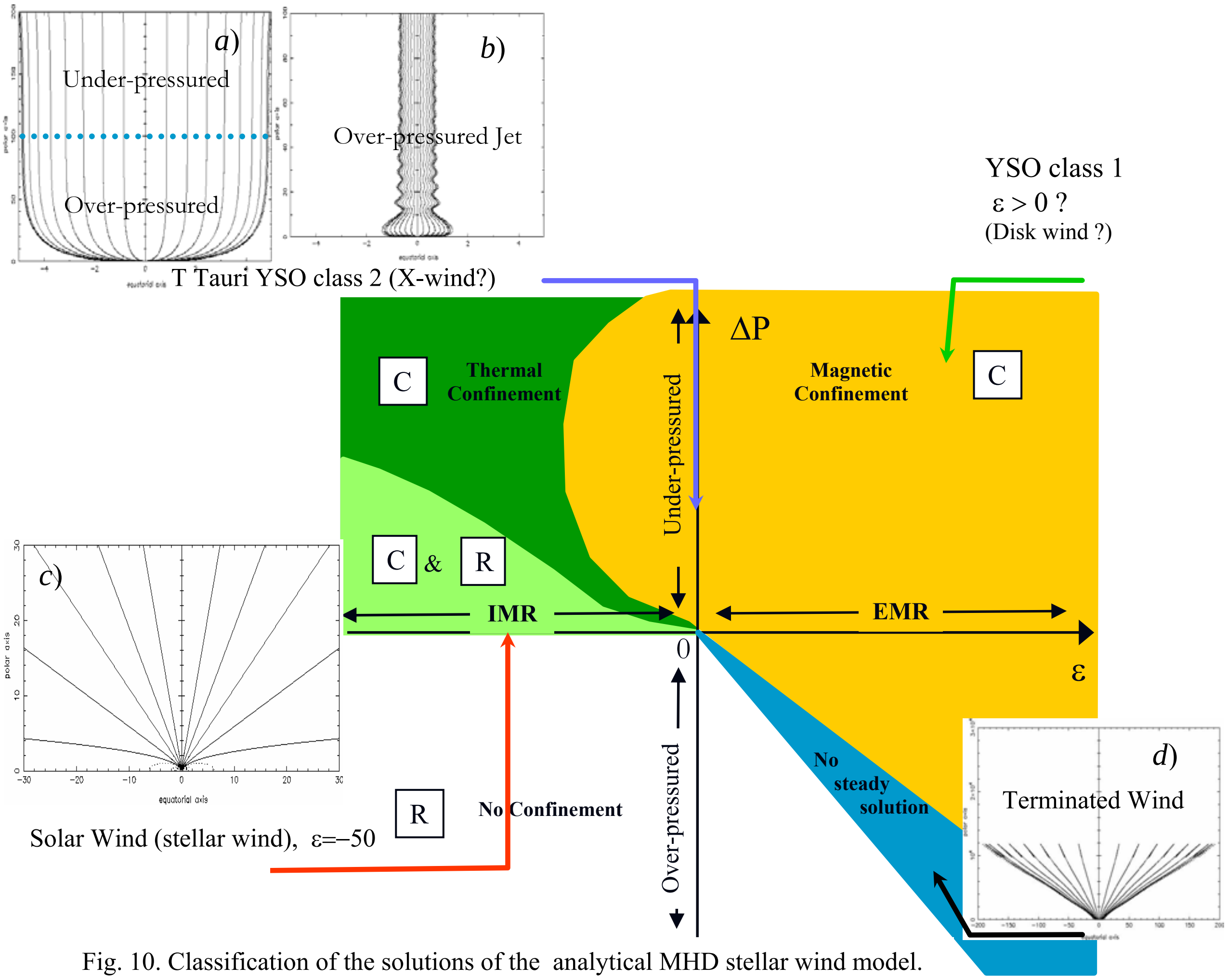

Fig. 10. Classification of the solutions of the analytical MHD stellar wind model.
R: solutions with radial asymptots, C: solutions with cylindrical asymptots.

In the last stages of class 2 jets, the flow becomes weaker ($\dot{M}_{wind} \sim 10^{-9} M_{sun}/yr$) and the width of the jet is usually unresolved, although the terminal velocities remain high. Such jets may be modelled with X-wind models. Such a type of model has been proposed and explored analytically in Sauty et al. (1999, 2002, 2004) using meridionally self-similar solutions. However the geometry of the flow is an output of the computation, as shown in Fig. 10. Thus, the same model is able to produce cylindrically collimated jets (Figs. 10*a*,*b*, domain labelled C), radial winds (as the solar wind, Fig. 10*c*, domain labelled R), or terminated flows (Fig. 10*d*). Such different solutions have been classified according to two parameters. First (vertical axis of Fig. 10), some solutions are under-pressured at the base (pressure increasing away from the axis, $\Delta P > 0$, possible thermal confinement) or over-pressured (pressure decreasing away from the axis, $\Delta P < 0$, no thermal confinement). Second (horizontal axis, ε, of Fig. 10), outflow solutions can be associated either with an efficient magnetic rotator ($\varepsilon > 0$) such that they are magnetically collimated by the toroidal field, or an inefficient magnetic rotator ($\varepsilon < 0$).

Specific application of this model has been done (Meliani, 2001) to the jet of RY Tau showing recollimation at 38 A.U. where a UV shock is observed. However the solution displayed in Fig. 10*b*) has a rather high effective temperature and a rather low mass loss rate for Classical TTauri Stars (CTTS). However by simply tuning the pressure, the same parameters give a second solution (Fig. 10*a*) without recollimation but which shows a transition from under to over pressured flow around 100 AU, typical of the distance where most jets become visible. Such a solution has a decreasing temperature from 10^5 K down to 10^3 K asymptotically and a mass loss rate of $\dot{M}_{wind} \sim 10^{-9} M_{sun}/yr$ ejected from 1.5 stellar radii of the disk around the stellar magnetosphere. This is a typical morphology of an X-wind solution and the same solution applies within some scaling factors to other CTTS like lk C15, DE Tau, GK Tau, DR Tau and IP Tau. For all those CTTS the typical magnetic rotator efficiency is of the order of 0, certainly below what we could find for a Class 1 jet. Moreover the part of jet ejected from the star itself corresponds to a mass loss rate of $\dot{M}_{wind} \sim 10^{-10} M_{sun}/yr$ which could be a typical value for a Weak TTauri Star (WTTS). Thus the same model may explain the dichotomy between CTTS and WTTS, because in CTTS the disk is connected to the central magnetosphere while in WTTS the disk is absent or not connected to the star.

Finally the same model can also reproduce quite successfully the structure of the solar wind close to the Sun using Ulysses data (Lima et al., 2001) at 1 A.U. In this case the efficiency of the magnetic rotator is much lower ($\varepsilon \approx -50$) showing no collimation even at large distances.

III. Conclusions: scenario for the evolution of Jets

The above brief overview of the different models applied to jets and winds from objects of Class 0 to main sequence stars seems to favour the following scenario. As time passes the jet becomes less and less collimated because the magnetic efficiency decreases also. However, up to Class 2 objects the radius of the jet decreases and the jet looses power because the source of the ejection moves from the outer edge of the Keplerian disk towards the star until eventually the disk evaporates and the jet becomes a stellar wind (see Fig. 11 for a sketch).

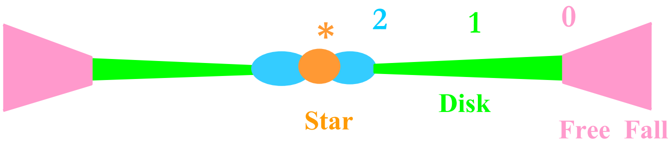

Fig. 11. Scenario for the evolution of the source of the jet in time.

Acknowledgments. We acknowledge our collaborators who participated in some of the results presented in this review, in alphabetic order, S. Bogovalov, I. Contopoulos, J. Lima, Z. Meliani, N. Vlahakis.

References

André P., Ward-Thompson D., Barsony M., 1993, ApJ, 406, 122
Blandford R.D., Payne D.G., 1982, MNRAS, 199, 883
Bogovalov S.V., 1994, MNRAS, 270, 721
Bogovalov S.V., Tsinganos K., 2001, MNRAS, 325, 249
Casse F., Ferreira J., 2000, A&A, 361, 1178
Casse F., Keppens R., 2002, ApJ, 581, 988
Contopoulos I., Sauty C., 2001, A&A, 365, 165
Ferreira J., 1997, A&A, 319, 340
Ferro-Fontan C., Gomez de Castro A.I., 2003, MNRAS, 342, 427
Kudoh T., Matsumoto R., Shibata K., ApJ, 508, 186
Lery T., Henriksen R.N., Fiege J., 1999, A&A, 350, 254
Lima J.J.G. et al., 2001, ESA SP-493, 269
Meliani Z., 2001, Master degree, University Paris 7
Sauty C., Tsinganos K., Trussoni E., 1999, A&A, 348, 327
Sauty C., Trussoni E., Tsinganos K., 2002, A&A, 389, 1068
Sauty C., Trussoni E., Tsinganos K., 2004, A&A, submitted
Shibata K, Uchida Y., 1990, PASJ, 42, 39
Shang H., Glassgold A.E., Shu F.H., Lizano S., 2002, ApJ, 564, 853
Tsinganos et al., 1996, MNRAS, 283, 811

STANDARD COLOR–COLOR AND COLOR–MAGNITUDE DIAGRAMS IN THE INFRARED AS A TOOL FOR TESTING STELLAR POPULATIONS*

P.Gavras(1) , L.Cambresy (3), E.Kontizas(2) , D.Sinachopoulos(2) , M.Kontizas(1)

1 University of Athens
2 National Observatory of Athens
3 Centre de Donnes Stellaires , Strasbourg

INTRODUCTION

The color - magnitude diagrams are good tools for studying stellar populations in galaxies. Although in the optical region these diagrams are well known in all other wavelengths similar tools are not always available. In this study we have produced reference library color-color and color-magnitude diagrams in the infrared using data from 2MASS, IRAS and MSX surveys and the theoretical ones (assuming "stars" with blackbody spectrum) for the wavelengths corresponding filters. The prototype set of standard stars has been selected from HIPPARCOS observations i) to cover all range of spectral type and luminosity classes and ii) their position in the sky to minimize the effect of the extinction.

The main goal of this project is to study the dependence of the colors derives from the carious surveys on the spectral type and/or luminosity class of stars or various astronomical objects. These diagrams can be used to distinguish different populations in galaxies observed in the IR and a multiwavelength study of the morphology of galaxies.

OBSERVATIONS

The catalogues we used came from the following ground based and space missions

- Hipparcos satellite (I/239/hip_main).Hipparcos was dedicated to measuring the positions and proper motion, and observed over 100000 stars 200 times more accurate than ever before.
- 2MASS (2 Micron All Sky Survey) started in 1997 with two 1.3 m highly automated telescopes. Each telescope was observing the sky at J (1.25 microns), H (1.65 microns) and K_s (2.17 microns). 2MASS surveys finished on January 15 2001 after observing more than 300 million stars and other unresolved objects and more than 1,000,000 galaxies and other nebulae.
- IRAS (Infrared Astronomy Satellite).IRAS did observations on the following channels 12, 25, 60, 100 microns
- MSX stands for Midcourse Space Experiment. The satellite launched on April 24 1996, and observed in 6 channels: B1 (4.29 microns) , B2 (4.35 microns), A (8.28 microns), C (12.13 microns), D (14.65 microns), E (21.3 microns).

REDUCTIONS

First of all we have selected a prototype set of stars from HIPPARCOS. The criteria for this selection were the spectral type, parallax, luminosity class and galactic latitude. So we have selected stars with parallax greater than 9 mas and galactic latitude greater than 10^o . The galactic latitude had to be greater than 10^o in order to avoid interstellar absorption and the parallax greater than 9 mas because Hipparcos parallax measurements are 3σ above the accuracy. Then we created subcatalogues of stars according the spectral type and luminosity class. This set of stars has been used as input at Vizier catalogue service at CDS for downloading the same set of stars from the selected catalogues.

The next step was to cross matching the stars from different catalogues by their coordinates. This step was done by creating several programs in FORTRAN and AWK. So we have created data sets

* *Proceedings of the 6th Hellenic Astronomical Society Conference, 15-17 September 2003,Penteli, Greece*

of the same stars. Each catalogue had the flux or magnitude in various wavelengths and the parallax if needed (in case of magnitudes).

So after creating the catalogues we were ready to create the color – color and color – magnitude diagrams of our choice.

For 2MASS and IRAS catalogues we have created the conventional two color diagrams. For MSX we had to create diagrams of our own. We choose MSX bands that showed indications of variation by the spectral type and the luminosity class. Fig. 1 shows on the x-axis the wavelength from 2 to 12 microns and on the y-axis the flux (Heras. A.M.et al,1999). In wavelengths between 6 and 12 microns we can see that there is a variation in the spectra of different spectral types. So we choose MSX bands in between these two wavelengths.

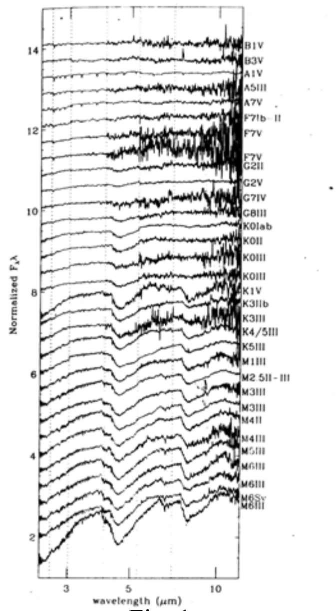
Fig. 1
(Heras. A.M.et al,1999)

DISCUSSION

i) With IRAS data we have produced color – color diagrams for four different cases Main Sequence stars, Giants, Super Giants, and the theoretical one. As it is expected from the theoretical diagram there is a weak dependence on spectral type for the observed accuracy. However these diagrams allow us to separate various objects such as stars from galaxies and star forming regions.

ii) The 2MASS data set in the color – magnitude diagram of Fig. 2 shows that we can discriminate the different spectral types in the main sequence. In this diagram we have superimposed a set of carbon stars (SMC).

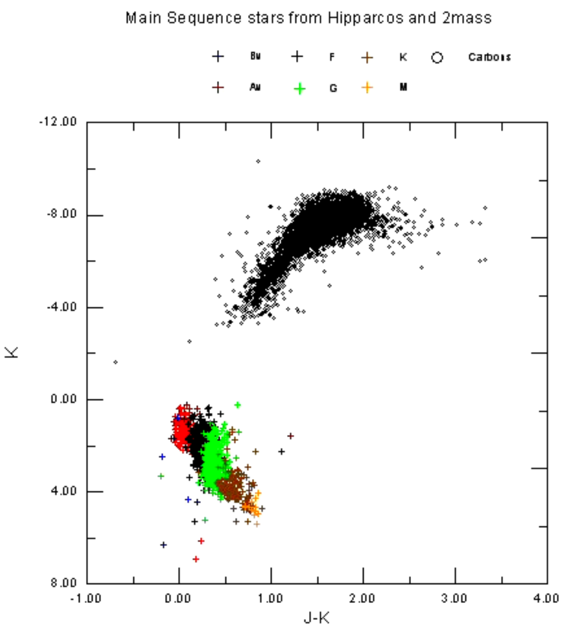

Fig. 2 Color – Magnitude diagram for 2MASS data for the main sequence and carbon stars.

iii) For MSX we produced a) Log(A/B1) Vs Log(C/B1) , b) Log(A/B1) Vs Log(C/D) and c) Log(C/A) Vs Log(D/A) all of those graphs are very sensitive to spectral type as expected from the theoretical ones (Fig3 a,b,c,d)

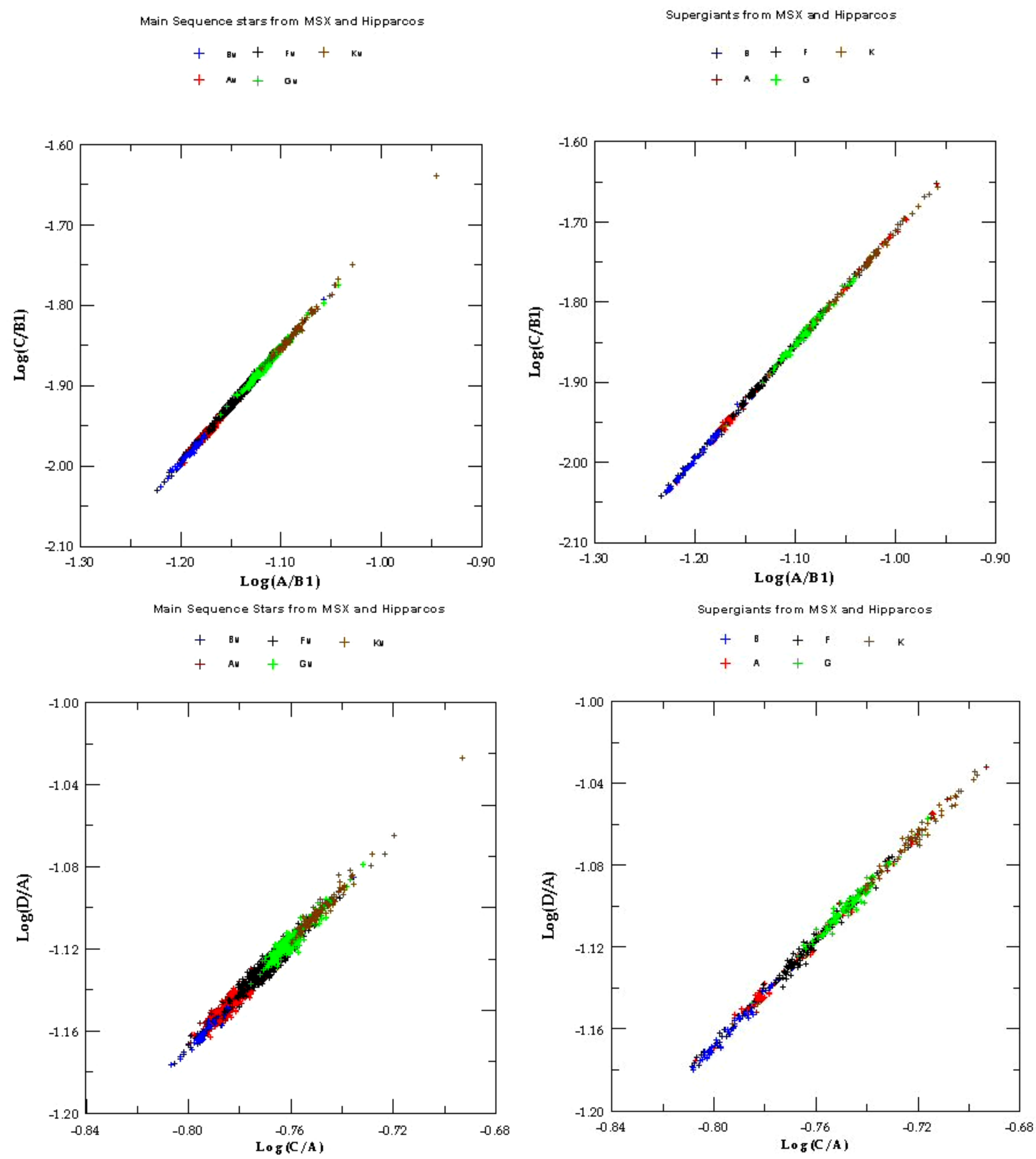

Fig. 3 Color – color diagrams for MSX data

As an example we used a CMD from 2MASS data for the SMC (Fig 4a,b) in K (vs) J-K. Comparison with Fig 2 allow us to isolate the B stars and the carbon stars of the SMC. The corresponding spatial distribution of these populations are shown in Fig 4b, confirming that the old stars are centrally concentrated (Maragoudaki et al, 2001)

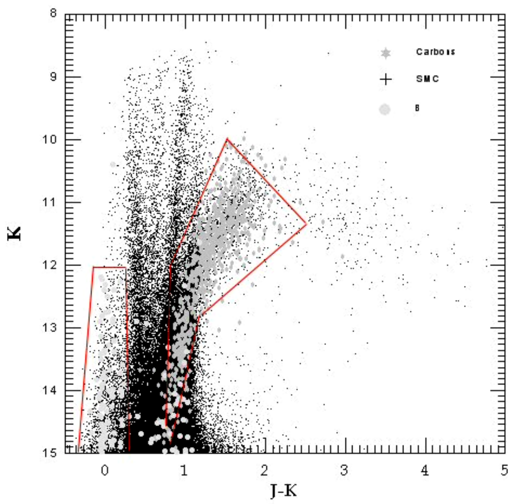

Fig.4a CMD from 2MASS of stars in the SMC region. The location of carbon and B stars is marked

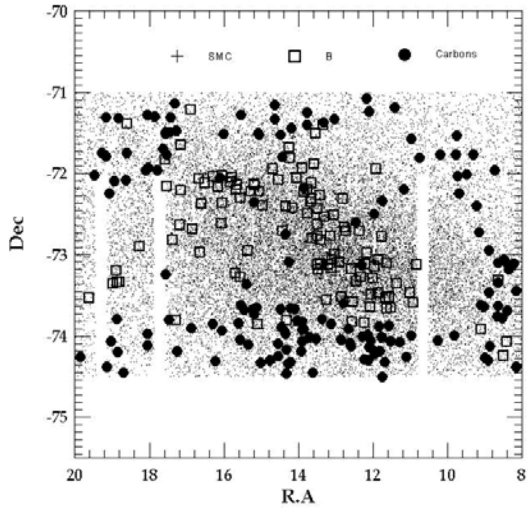

Fig. 4b The spatial distribution of carbon and B stars in the SMC

CONCLUSIONS

- The IR Color-Color & CMD diagrams are very important tools for studying stellar populations in stellar systems & galaxies
- IRAS has shown that the selected wavelengths are useful for classifying objects as stars, HII regions galaxies stellar complexes
- 2MASS colors (J-K,V-K) are good indicators of spectral type in stars
- MSX colors at 8.28 & 12.13 μm are very sensitive to spectral type
- A preliminary study for the SMC stars from 2MASS CMD confirm the spatial distribution

– Of carbon stars (elliptical distribution)
– Of B stars (bar concentrated)

Acknowledgments

The authors would like to thank CDS (Centre de Donnes Strasbourg) , ULP (Universite' Louis Pasteur) , ELKE of the University of Athens and the General Secretariat of Research & Technology for the financial support.

REFERENCES

Heras. A.M., Shipman R.F. et al, Proceedings of the conference "The Universe as seen by ISO" ,1999, eds P.Cox & M.F. Kessler , 329
Maragoudaki et al, 2001 A&A 379,864-869

MEAN GRAVITY OF BINARY COMPONENTS – LINES AND SURFACES OF CONSTANT GRAVITY*

Tsantilas S. and Rovithis-Livaniou H.

Astronomy, Astrophysics & Mechanics, Dept. of Physics, Athens University, Athens, Greece.

1. INTRODUCTION

The shape and geometry of a binary system are defined by the mass ratio, q, of the two components and the potential C. According to the Roche model, gravity acceleration can be computed from the following relation:

$$-\nabla\Psi(C,q,\vec{r}) = \vec{g} \tag{1}$$

where $\Psi(C,q,\vec{r})$ is the potential due to gravitational and centrifugal forces (e.g. Tsantilas et al. 2001). Using equation (1) gravity acceleration can be computed for every surface point. In this way, a mapping of the gravity and in consequence of the temperature field (e.g. von Zeipel 1924, Lucy 1967, Claret 2000) can be achieved.

2. EQUATIONS OF THE PROBLEM

Two are the basic equations: a) that of the Roche potential C at a point $\vec{r}(x,S,\eta)$ for a given mass ratio q, which in cylindrical coordinates takes the form:

$$C = \frac{2B_1}{\sqrt{x^2+S^2}} + \frac{2B_2}{\sqrt{(x-1)^2+S^2}} + (x-B_2)^2 + S^2\sin^2\eta \tag{2}$$

where $B_1 = \frac{1}{1+q}$, $B_2 = \frac{q}{1+q}$, $q = \frac{m_2}{m_1}$, (Binnendijk, 1977):

and b) the already given equation (1).

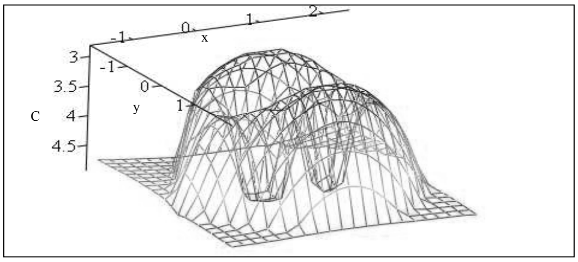

Fig.1. *Potential C as a spatial distribution on the (x,y) plane for q=0.6.*

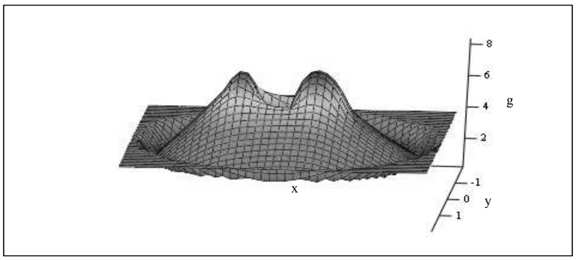

Fig.2. *Gravity g as a spatial distribution on the (x,y) plane for q=0.6.*

To solve the system of the foregoing mentioned equations, a computer program has been written that can be easily applied to any binary system. The basic output of the program is a data file with a large number of points (~30000), containing their coordinates and the values of the potential and gravity acceleration for each point. Among others, the program computes the mean gravity for the two members of a binary, and the ratio $\bar{g}_1/\bar{g}_2$.

Solving these two equations, one can get distributions like those presented in figures 1 and 2. While equation (1) -without any restriction for the potential C- yields to the surfaces of equal gravity (e.g. like those presented in Fig.3).

* *Proceedings of the 6th Hellenic Astronomical Society Conference, 15-17 September 2003, Penteli, Greece*

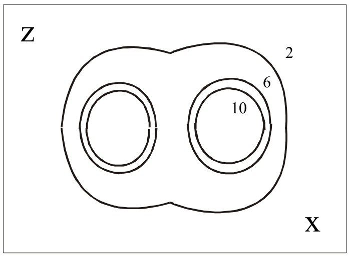

Fig.3. *Intersection on the z-x plane of the constant gravity surfaces for three g values for OO Aql (q=0.843). Notice that starting from a separated configuration, the decrease of g leads to a common surface surrounding the two components: The smaller the g, the larger the surface.*

3. Applications

Applications have been made to two binary systems: ***OO Aql*** and ***XY UMa***.

OO Aql is a contact binary of W UMa type. Following the procedure previously described and using the absolute elements of the system given by Hrivnak (1989), we computed the distribution of gravity (hence, that of temperature) over the photosphere of the system. In figure 4 (*a* and *b*) the system is presented edge on and pole on, respectively. The gravity values, normalized and real, are given in Table 1.

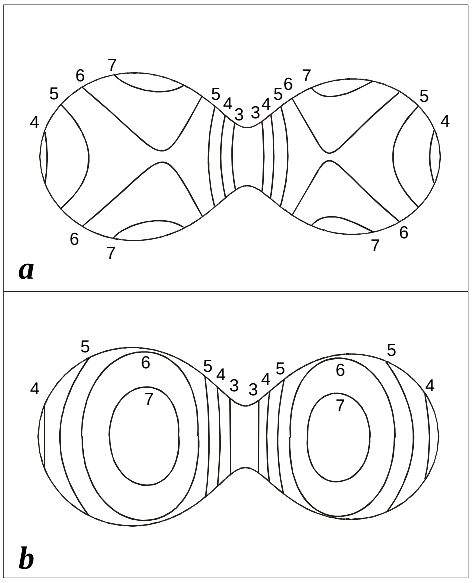

Fig.4. *Gravity distribution of OO Aql in normalized units:*
a. *OO Aql edge on* ***b.****OO Aql pole on*

Table 1

Values of gravity in normalized and physical units	
	m/s^2
g=4	96.6
g=5	120.7
g=6	144.9
g=7	169.0

XY UMa is a short period RC CVn's type binary (Pribulla et al. 2001). Following the same procedure as for *OO Aql*, our results are presented in figure 5 (*a* and *b*) and Table 2.

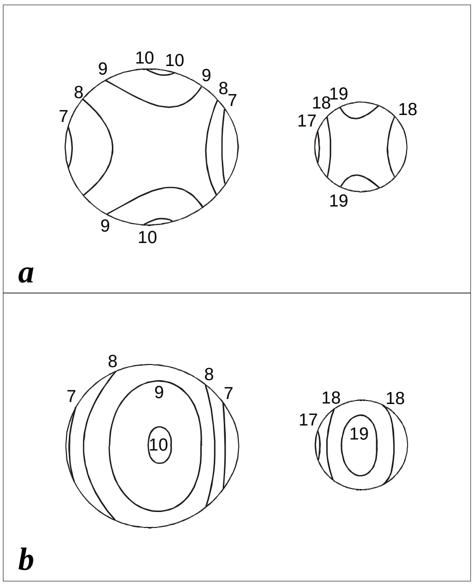

Fig.5. *Gravity distribution of XY UMa in normalized units.*
a. *XY UMa edge on* ***b.*** *XY UMa pole on*

Table 2

Values of gravity in normalized and physical units	
	m/s^2
g=7	174.8
g=8	199.7
g=9	224.7
g=10	249.6
g=17	424.4
g=18	449.4
g=19	474.3

4. Mean Gravity

As it has been shown, gravity presents a significant variation on the surface of binary stars. Nevertheless, in many cases it is more convenient to consider a mean value of gravity. The computation of mean gravity over the surfaces of the two components, can be done in two ways:

$$\textit{Statistically:} \qquad \overline{g}_s = \frac{1}{n}\sum_{i=1}^{n} g_i \tag{3}$$

$$\textit{Weighted:} \qquad \overline{g}_w = \frac{\int g\,dA}{\int dA}, \tag{4}$$

where $dA = -\dfrac{g}{f_y \sin\eta + f_z \cos\eta} S \cdot d\eta \cdot dx$

and $f_y = \dfrac{\partial C(x,y,z)}{\partial y}$, $f_z = \dfrac{\partial C(x,y,z)}{\partial z}$

Using formula (4), we computed the ratio $\overline{g}_1/\overline{g}_2$ for the two components, in 30 models of different C and q, of contact binaries. In particular, the following 3 cases were considered: a marginal contact configuration, a contact system filling its outer lobe (f=100%), and an intermediate case with filling factor f=50%. Figure 6 presents our results for $\overline{g}_1/\overline{g}_2$ versus q. The primaries show larger mean gravity in all three examined cases, with the intermediate configuration showing a tendency towards lower values.

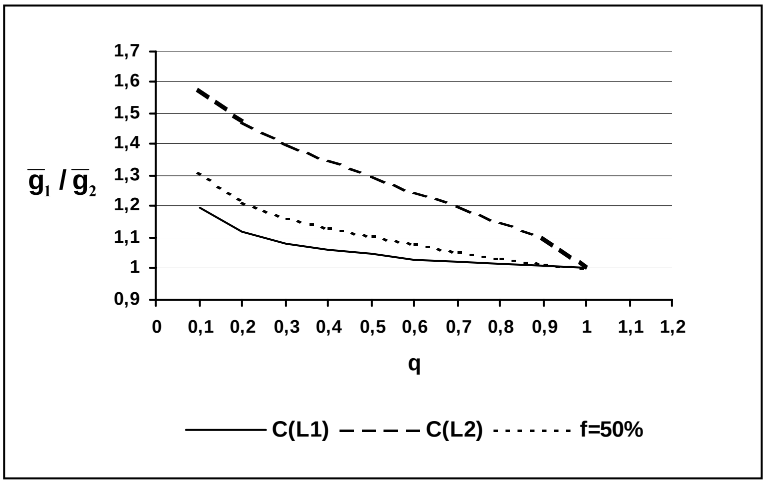

Fig.6. *Diagram of the ratio $\overline{g}_1/\overline{g}_2$ versus mass ratio, q, in three cases of different filling factor, for 30 models of contact binaries. (Continues line stands for a marginal contact binary, short-dash line is for a contact binary with f=50%, and the long-dash line is for a contact binary with f=100%).*

5. Temperature estimation

It is known that gravity is related to temperature with the relation: $T_{eff} \propto g^{\beta}$, where β can take different values (Claret, 2000). If T_1 and T_2 are the primary and secondary temperatures respectively, we have:

$$\frac{T_1}{T_2} = \left(\frac{\overline{g}_1}{\overline{g}_2}\right)^{\beta} \tag{5}$$

From equation (5) we ***can estimate*** the effective temperature T_2 of the secondary, given that T_1 has been accurately computed (e.g. spectroscopically). For example, by computing the value of mean gravity for the two components of *OO Aql*, we get $\overline{g}_1 = 5.668 \rightarrow 136.8\ \ m/s^2$ and $\overline{g}_2 = 5.560 \rightarrow 134.2\ \ m/s^2$. So, if we adopt for the gravity darkening exponent β the value of 0.08, appropriate for stars with convective envelopes (Lucy 1967, Djurasevic et al. 2003), we can estimate the effective temperature T_2 of the secondary, using the spectroscopically estimated temperature $T_1 = 5700^\circ$ K. Doing so, from equation (5) we get $T_2 = 5690^\circ$ K which is in very good agreement with the value $T_2 = 5635^\circ$ K obtained from the photometric solution (Hrivnak, 1989).

Moreover, if T_0 and g_0 are ***known values*** for temperature and gravity (e.g. at the poles) and T, g values at any other point, from relation:

$$\frac{T_0}{T} = \left(\frac{g_0}{g}\right)^{\beta} \tag{6}$$

we can obtain the temperature distribution over the whole surface of the binary. Nevertheless, deviations from this distribution may exist, caused by thermodynamical procedures (e.g. large scale circulation) taking place in the two components' interiors.

References

Binnendijk L., 1977, Vistas in Astron. 21, 359

Claret A., 2000, A&A 359, 289

Djurasevic G., Rovithis-Livaniou, H., Rovithis, P., Georgiades, N., Erkapic, S. & Pavlovic, R., 2003, A&A 402, 667

Hrivnak B. J., 1989, ApJ 340, 458

Lucy L.B., 1967, Zs. f. Ap. 65, 89

Pribulla T., Chochol D., Heckert P. A., Errico L., Vittone A. A., Parimucha S. & Teodorani M., 2001, A&A 371, 997

Tsantilas S., Livaniou -Rovithis H & Kalimeris A., 5th Hellenic Conference, 2001 (http://astrophysics.uoc.gr/conf/proceeding.htm)

Von Zeipel H.,1924, MNRAS 84, 702

*ABSTRACTS OF PAPERS POSTED DURING THE SESSION ON STARS AND STELLAR SYSTEMS**

DISCONTINUOUS STRUCTURES IN EARLY TYPE STARS' ATMOSPHERES

E. Danezis, E. Lyratzi, D. Nikolaidis, E. Theodossiou, M. Stathopoulou, C. Drakopoulos and A. Soulikias
Section of Astrophysics, Astronomy and Mechanics, Department of Physics, University of Athens,

Abstract: As it is already known, the spectra of many Oe and Be stars present Satellite Absorption Components (SACs), sometimes named Discrete Absorption Components (DACs). In this paper we present a mathematical model reproducing the complex profile of the spectral lines of Oe and Be stars that present SACs. This model presupposes that the regions, where these spectral lines are formed, are not continuous but consist of a number of independent absorbing density layers of matter, followed by an emission region and an external general absorption region. When we fit the spectral lines that present SACs, we can calculate, for the regions where the SACs are formed, the values of the apparent rotation and expansion / contraction velocities, as well as the values of ξ, which is an expression of the optical depth.

DISCONTINUOUS PHENOMENA IN MgII REGIONS OF BeV STARS

E. Lyratzi, E. Danezis, M. Stathopoulou, E. Theodossiou, D. Nikolaidis, A. Antoniou, C. Drakopoulos, A. Soulikias and M. Koutroumanou
Section of Astrophysics, Astronomy and Mechanics, Department of Physics, University of Athens,

Abstract: In this paper we present a statistical study of the UV Mg II resonance lines of 40 BeV stars' spectra, using the model proposed by Danezis et al. (2002, 2003). This model is based on the idea of independent density layers of matter in the regions where the spectral lines that present SACs (DACs) are created. We calculated the apparent rotation (V_{rot}) and expansion/contraction velocities (V_{exp}) of these density regions, as well as their ξ value, which is an expression of the optical depth. We also present the relation among these parameters and their evolution with the spectral subtype. The purpose of this statistical study is to check whether the evolution of these parameters follow some physical lows and to extract the limits of the values of these parameters.

* *Proceedings of the 6th Hellenic Astronomical Society Conference, 15-17 September 2003, Penteli, Greece*

*ABSTRACTS OF PAPERS POSTED DURING THE SESSION ON STARS AND STELLAR SYSTEMS**

DISCONTINUOUS PHENOMENA IN SiIV REGIONS OF BeV STARS

E. Lyratzi, E. Danezis, M. Stathopoulou, E. Theodossiou, D. Nikolaidis, A. Antoniou, C. Drakopoulos, A. Soulikias and M. Koutroumanou
Section of Astrophysics, Astronomy and Mechanics, Department of Physics, University of Athens,

Abstract: In this paper we present a study of the UV SiIV resonance lines of 42 BeV stars' spectra, using the model proposed by Danezis et al. (2002, 2003). This model is based on the idea of independent density layers of matter in the regions where the spectral lines that present SACs (DACs) are created. We calculated the apparent rotation (V_{rot}) and expansion/contraction velocities (V_{exp}) of these density regions, as well as their ξ value, which is an expression of the optical depth. We also present the relation among these parameters and their evolution with the spectral subtype. The purpose of this statistical study is to check whether the evolution of these parameters follow some physical lows and to extract the limits of the values of these parameters.

DISCONTINUOUS STRUCTURE AND SACS PHENOMENA IN THE Oe STAR'S HD 175754 ATMOSPHERE

E. Danezis, A. Antoniou, E. Lyratzi, E. Theodossiou, M. Stathopoulou, D. Nikolaidis, C. Drakopoulos, A. Soulikias & M. Koutroumanou
Section of Astrophysics, Astronomy and Mechanics, Department of Physics, University of Athens

Abstract: In this paper we present a study of the UV resonance lines SiIV, CIV, NV and the NIV line (λ 1718.80 Å) of the Oe star HD 175754, using 7 spectrograms, taken by IUE, between September 1978 and August 1981. We reproduced the above mentioned lines by the model proposed by Danezis et al. (2002, 2003), which is based on the idea of independent density layers in the regions where the spectral lines that present SACs (DACs) are created. We calculated the apparent rotation (V_{rot}) and expansion/contraction velocities (V_{exp}) of these density regions, as well as their ξ value, which is an expression of the optical depth. We also present the relation among these parameters and their evolution with time.

* *Proceedings of the 6th Hellenic Astronomical Society Conference, 15-17 September 2003, Penteli, Greece*

*ABSTRACTS OF PAPERS POSTED DURING THE SESSION ON STARS AND STELLAR SYSTEMS**

DISCONTINUOUS STRUCTURE OF SiIV REGIONS IN THE Oe STAR'S λ ORIONIS ATMOSPHERE

E. Danezis, M. Koutroumanou, E. Lyratzi, E. Theodossiou, M. Stathopoulou, D. Nikolaidis, A. Antoniou, C. Drakopoulos & A. Soulikias

Abstract: In this paper we present a study of the SiIV resonance lines in UV of the Oe star λ Orionis, using spectrograms, taken by IUE, in different epochs. We reproduced the above mentioned lines by the model proposed by Danezis et al. (2002, 2003), which is based on the idea of independent density layers in the regions where the spectral lines that present SACs (DACs) are created. We calculated the apparent rotation (V_{rot}) and expansion/contraction velocities (V_{exp}) of these density regions, as well as their ξ value, which is an expression of the optical depth. We also present the relation among these parameters and their evolution with time.

DOPPLER TOMOGRAPHY OF THE CATACLYSMIC VARIABLES AM HER, EX DRA AND V347 PUP

Christos Papadimitriou[1,2] and Emilios Harlaftis[3]
[1]Section of Astrophysics, Astronomy and Mechanics, Department of Physics, University of Athens Greece
[2]Institute of Astronomy and Astrophysics, National Observatory of Athens, Greece
[3]Institute of Space Application and Remote Sensing, National Observatory of Athens, Greece

Abstract: Cataclysmic variables (CVs) are close binary systems composed of a white dwarf, and a low mass companion on or near the main sequence. A general feature of CVs is that mass transfer is occurring from the companion star to the white dwarf, often via an accretion disk. Such a disk can dominate the optical light from the system. For this reason, and because the binary orbital motion (particularly in eclipsing systems) yields valuable spatial information about the disk, CVs are used as an observational test case of accretion disk theory.

We present Doppler maps of Ha of the magnetic cataclysmic variable AM Her from various epochs, using the 2.5m INT telescope, in order to constrain its emission components. The dominant emission for AM Her rises from the (-Vx, -Vy) velocity quadrant where the gas stream velocities lie in. During 3 epochs (low and high states), there is some minor emission in the –Vy axis at a velocity of (-100,-400) km/s and this may be the shock emission from the weaker, secondary pole. During the first and the second epoch, gas stream emission close to the ballistic trajectory is visible. The 3.5m NTT spectra of the eclipsing novalike V347 Pup are analysed to resolve the complex pattern of spiral shocks using its HeI Doppler maps. The eclipsing dwarf nova, EX Draconis, was observed with the 3.5m Calar Alto telescope during an outburst. The structure of trailed spectra (double peak separation) present strong evidence for spiral shocks on the disk. The gas stream emission along the ballistic trajectory is also visible.

* *Proceedings of the 6th Hellenic Astronomical Society Conference, 15-17 September 2003, Penteli, Greece*

ABSTRACTS OF PAPERS POSTED DURING THE SESSION ON STARS AND STELLAR SYSTEMS[*]

THE GALACTIC POPULATION OF CATACLYSMIC VARIABLES

B. Gänsicke[1], S. Araujo-Betancor[1], E. Harlaftis[2], C. Papadimitriou[2,3], D. Mislis[4], S. Kitsionas[2], O. Giannakis[2,3]

[1]Department of Physics and Astronomy, University of Southampton,
[2]National Observatory of Athens,
[3]Department of Physics, University of Athens
[4]Department of Physics, University of Thessaloniki

Abstract: The standard evolution theory of Cataclysmic Variables (CVs) makes several predictions which are in strong contrast to the statistics of the observed CV population. Some (if not all) of these discrepancies may be due to selection effects in the known CV sample. We are currently involved in two large-scale surveys for new CVs, selecting candidates from the Hamburg Quasar Survey and the ROSAT All Sky Survey. Here we report on time-resolved CCD photometry of 22 recently discovered CVs obtained at the Kryoneri Observatory during 26 nights in 2002 and 18 nights in 2003. The orbital period and the CV subtype could be determined for about 2/3 of the observed objects from the CCD photometry alone. The extreme variety of objects encountered in this survey is illustrated with the following examples. HS0220+06 is an eclipsing SW Sextantis-type CV with an orbital period of 215 min. HS1857+51 is a long-period CV (383 min) with no flickering and a large-amplitude reflection effect, indicating an extremely hot white dwarf in a recent post-nova system. RXJ0325-18 is a polar CV with an orbital period of 120 min. The observed modulation in these systems is caused by beamed cyclotron radiation in the footprint of the accretion stream impacting the white dwarf near its high-field (B>10MG) magnetic pole. RXJ1813+40 is an intermediate polar with an orbital period of ~190 min, containing a weakly magnetic white dwarf spinning with a period of ~25 min (Gänsicke, B.T., Araujo-Betancor, S., Hagen, H.J., Harlaftis, E., Fried, B., 2003, A&A, submitted). So far, only ~20 of these systems have been identified. HS2237+81 clearly reveals the photospheric emission of an 10000K white dwarf and an M4 main-sequence star at an orbital period of 178 min (pre-CV, or a CV just entering the period gap; Araujo-Betancor, S., Gänsicke, B.T., Engels, D., Harlaftis, E., Kitsionas, S., 2003, A&A, submitted). So far, we have measured orbital periods for 27 systems, and their distribution differs markedly from that of the previously known CVs. Our long-term goal is to establish in detail the properties of our entire sample of new CVs, and to compare these properties with the predictions of CV evolution theory.

---

[*] *Proceedings of the 6th Hellenic Astronomical Society Conference, 15-17 September 2003, Penteli, Greece*

*ABSTRACTS OF PAPERS POSTED DURING THE SESSION ON STARS AND STELLAR SYSTEMS**

DETECTION OF HIGH-FREQUENCY OPTICAL OSCILLATION DURING THE FLARE PHASE OF EV LAC IN 1999

Contadakis, M.E.(1), Avgoloupis S. (2), Seiradakis J. (2),Zhilyaev, B.E. (3), Romanyuk Ya. O. (3), Verlyuk I.A. (3), Svyatogorov, O.A. (3), Khalack, V.R. (3), Sergeev, A.V. (4), Konstantinova-Antova R.K. (6), Antov A.P. (6), Bachev R.S. (6), Alekseev I.Y. (5), Chalenko, V.E. (5), Shakhovskoy D.N. (5)

(1)Dpt. of Surveying and Geodesy, (2)Dpt. of Physics Section of Astronomy Astrophysics and Mechanics,Univ. Thessaloniki,Greece. (3)Main Astronomical Station, Ukraine. (4)Intern. Res. Center for Astronomy Medecine and Ecology, (5)Crimean Astrophysical Observatory, Ukraine (4)Bulgarian Academy of Sciences, Bulgary

Abstract: A program of Many-sites Multi Channel simultaneous observations of flare stars by a network of teleskops, was initiated in 1998. The purpose of this program is to investigate the fine structure of the flares light-curve in UBVRI, depressing atmospheric and instrumental noises. In this paper we present the results of the observations on the Flare star EV Lac in the B color, at the Stephanion observatory, during the campaign of 1999. The power spectra analysis of the B-light curve of the large flares, reveal high frequency small amplitude oscillations with periods ranging between 26s and 13s in around the flare maximum phase, in accordance with the results of 1998.Further analysis, in combination with the observations of all the network will reveal the color fine structure.

THE NEW VARIABLE STAR GSC 00323:00830

K.D. Gazeas, P.G. Niarchos
Section of Astrophysics, Astronomy and Mechanics, Department of Physics
University of Athens, Greece

Abstract: A new variable star was discovered during data reduction, in the frame of *BVRI* CCD observations of the eclipsing variable star *NN Vir*. Photometric data collected between March and May 2003 are used to determine the type of variation of *GSC 00323:00830*. Three times of minima were computed with the Kwee and van Woerden method and a new ephemeris is proposed:

$$\textbf{Min I (HJD)} = 2452767.3482(45) + 0^{d}.56717(11)\times E$$

Observations of four standard stars were obtained on April 8, 2003, in order to calculate the color index and the standard magnitude of the new variable. The observed color index (corrected for extinction and color) is found to be B-V=+0.587, classifying the new variable as a G0 type star. The standard magnitudes (at maxima) are: B=11.027, V=10.440, R=10.085 and I=9.705.

The results of the present analysis suggest two possibilities as far as the type of variability of the star is concerned. Although the possible pulsating behavior of the new variable was carefully examined, this possibility was excluded since its spectral type does not match with those of typical pulsators of A or F type. Therefore the new variable star *GSC 00323:00830* should be an eclipsing (*EW* type) binary, with very shallow partial eclipses or an ellipsoidal variable.

---

* *Proceedings of the 6th Hellenic Astronomical Society Conference, 15-17 September 2003, Penteli, Greece*

ABSTRACTS OF PAPERS POSTED DURING THE SESSION ON STARS AND STELLAR SYSTEMS[*]

INTENSITY OSCILLATIONS DURING A FLARE ON II PEG

S. Avgoloupis & J.H. Seiradakis
University of Thessaloniki, Department of Physics, Section of Astrophysics Astronomy and Mechanics, 54124, Thessaloniki, Greece

M. Mathioudakis & S.D. Bloomfield & J.McAteer
Department of Pure and Applied Physics, Queens University Belfast,
Belfast BT7 1NN, Northern Ireland, UK

Abstract: A very strong flare with energy in excess of 10^{36} ergs was observed on the RS CVn binary II Peg. One of the most conspicuous features of the flare is the oscillatory behaviour observed shortly after the impulsive phase. We have been prompted to investigate these results in view of the recent advancements on coronal loop models and the lack of oscillations associated with stellar flares. The observations were analysed using Fast Fourier Transform (FFT) and Wavelet analysis. The main advantage of Wavelets is that they can localise a signal in both frequency and time. Our analysis revealed a period of 220 seconds. This is the first time that such a long period oscillation has been observed during a stellar flare. The oscillation could be triggered by the flare or be a property of the flaring loop itself. The reliability of the oscillation was tested against Poisson noise and we found it to be reliable at the 99% confidence level. It was further tested against 1500 randomised time series with an identical distribution of counts. This criterion guards against random, pulsed like variations in the data that might be treated as real. We found that the oscillation is reliable at 99.9%. We have combined the amplitude and period of the oscillation with models of kink or torsional modes and have derived the temperature (10^8 K), electron density (4×10^{11} cm^{-3}) and magnetic field strength (1000 Gauss) for the flaring loop. We find no evidence for oscillations in the pre-flare quiescent state of the binary.
The observations were carried out at Stephanion Observatory using the 0.75m Cassegrain reflector of the University of Thessaloniki.

A Scilab PROGRAM FOR COMPUTING ROTATING NEUTRON STAR MODELS

P. J. Papasotiriou

Department of Materials Science, University of Patras, Greece

Abstract: We implement a reliable method for computing relativistic models of neutron stars in slow or fast rotation. The nonrotating model is computed by solving the transformed Oppenheimer-Volkoff equations. This method removes some difficulties occurred in previous algorithms. The nonrotating model is used as the basis of Hartle's perturbative formalism for computing the corresponding rotating model. The program has been written in Scilab (copyright INRIA-ENPC), a matrix-oriented high-level programming language. We show that the method gives accurate results for all practical purposes and it should prove an efficient tool for computing rapidly rotating pulsars.

[*] *Proceedings of the 6th Hellenic Astronomical Society Conference, 15-17 September 2003, Penteli, Greece*

ABSTRACTS OF PAPERS POSTED DURING THE SESSION ON STARS AND STELLAR SYSTEMS[*]

CAN SPH SIMULATIONS OF CV ACCRETION DISCS PREDICT THE OBSERVED PERIODIC SIGNALS OF WZ SGE?

S. Kitsionas[1], H.M.J. Boffin[2], E. Harlaftis[3], C. Papadimitriou[1], W. Skidmore[4]

[1]IAA-National Observatory of Athens, Greece
[2]ESO, Garching, Germany
[3]ISARS-National Observatory of Athens, Greece
[4]University of California, Irvine, U.S.A.

Abstract: We have adapted the SPH-Particle Splitting algorithm of Kitsionas & Whitworth (2002) to simulate the formation of the accretion disc in cataclysmic variables by inserting particles in the Roche lobe of the white dwarf through the L1 point of the binary. We investigate the effect of causing a permanent tilt to the accretion disc by inserting particles at an angle to the orbital plane. It is anticipated that on real systems such a tilt would produce a clear periodic signal in photometric observations, similar to a "superhump". In this paper, we present preliminary results of a standard accretion disc simulation, as a first step towards simulating a tilted disc. We also present CCD photometry of the eclipsing dwarf nova WZ Sge one year after its outburst, using the 1.2 m telescope of the NOA at Kryoneri. The observations, preliminary, reveal a periodicity which is similar to the ``superhump" period of WZ Sge (~82.3 min; Patterson *et al*. 1981). This "superhump" period is the beat period of the orbital period of the system (~81.6 min) and the precession period of the elliptical disc (~7.1 d; Warner 1995). We intend to use these observations to constrain our tilted disc model.

THE TURNOVER SCENARIO FOR WHITE DWARFS WITH SEVERAL VALUES OF MASS, ANGULAR MOMENTUM, AND MAGNETIC FIELD

V.S. Geroyannis and P.J. Papasotiriou

Astronomy Laboratory, Department of Physics, University of Patras, Greece

Abstract: We present numerical results for the so-called "turnover scenario" of differentially rotating white dwarfs with poloidal and toroidal magnetic fields (full details on the theory and the numerical treatment of this issue are given in Geroyannis 2002, ApJS, 141, 485). According to this scenario, the magnetic symmetry axis of an initially almost axisymmetric white dwarf model inclines at a gradually increasing angle (the so-called "turnover angle") relative to the invariant angular momentum axis. Our numerical results show that such a model becomes "perpendicular rotator" (i.e., its turnover angle becomes ~90 degrees) on a "turnover timescale" ~10^6-10^8 yr for several typical values of mass, angular momentum, and magnetic field.

---

[*] *Proceedings of the 6th Hellenic Astronomical Society Conference, 15-17 September 2003, Penteli, Greece*

*ABSTRACTS OF PAPERS POSTED DURING THE SESSION ON STARS AND STELLAR SYSTEMS**

HIGH-RESOLUTION SIMULATIONS OF CLOUD-CLOUD COLLISIONS USING SPH WITH PARTICLE SPLITTING: II. FOLLOWING THE PROCESS OF STAR FORMATION EVEN FURTHER

S. Kitsionas[1], A.P. Whitworth[2], I. Bonnell[3], P. Clark[3]

[1]IAA-National Observatory of Athens, Greece
[2]Dept. of Physics & Astronomy, Cardiff University, U.K.
[3]Dept. of Physics & Astronomy, University of St. Andrews, U.K.

Abstract: Particle Splitting is an algorithm which allows SPH simulations to have their numerical resolution increased on-the-fly only where and when this is required (Kitsionas & Whitworth 2002). Particle Splitting is invoked in response to the violation of the ``Jeans condition'' (Bate & Burkert 1997), thus there is increased confidence that our results do not suffer from spurious and/or suppressed fragmentation.

We have used SPH with Particle Splitting to conduct simulations of Star Formation triggered by cloud-cloud collisions (Kitsionas & Whitworth 2001, in the 5th HEL.A.S. conference). The side-effect of the application of Particle Splitting has been the sudden decrease in the simulation time-step which results in simulations that quickly move into suspended animation. Bate, Bonnell & Price (1995) have shown that the use of sink (star) particles, replacing groups of high-density gas particles already collapsed in protostars, prevents the decrease in the time-step. This enables the simulations to run longer and thus lead to the formation of star clusters. We present preliminary results of a simulation that continues our original simulation with clump masses of 10 $M_{\odot}$, impact parameter 0.2 and Mach number 10, with two sink particles replacing the protostars formed at the end of the original simulation: in the extra 1600 yr that the simulation with sinks has evolved, the additional amount of mass accreted on the three protostellar objects (a third protostar has collapsed) is ~0.22 $M_{\odot}$. We note that, although there is no additional computational cost in terms of memory in the simulation with sinks, if the simulation without sinks had to reach this evolved stage, it would require 3-4 times more CPU time.

A Scilab PROGRAM FOR COMPUTING RADIAL OSCILLATIONS OF NEUTRON STARS

P. J. Papasotiriou
Department of Materials Science, University of Patras, Greece

Abstract: We implement a reliable method for computing the eigenfrequencies of the radial oscillations of neutron stars. The program has been written in Scilab (copyright INRIA-ENPC), a matrix-oriented high-level programming language. The program is used to compute several radial eigenvalues for specific neutron star models. We interpret our numerical results in various ways by extensively using the graphics environment of Scilab.

* *Proceedings of the 6th Hellenic Astronomical Society Conference, 15-17 September 2003, Penteli, Greece*

ABSTRACTS OF PAPERS POSTED DURING THE SESSION ON STARS AND STELLAR SYSTEMS[*]

THE SYMBIOTIC-ECLIPSING BINARY AR PAVONIS

H. Rovithis-Livaniou[(1)] and A. Jones[(2)]

(1) Section of Astrophysics-Astronomy & Mechanics, Athens University, Greece
(2) Carter Observatory, Wellington, New Zealand

Abstract: AR Pav is an S-type symbiotic and eclipsing binary consisting of a M3-4 (III-II) star, filling its Roche lobe and transferring mass to its compact companion. In this work we present and discuss some new light curves of AR Pav, based on the observations obtained by one of us (A.J.) at Carter Observatory from 1995 to 2003. These correspond to the epochs from 65 to 68, according to the light elements of the system. From this observational material, differences in the depths and duration of the minima were noticed, as well as in the out of eclipse regions. After the low activity observed during cycles 66 and 67, it seems that AR Pav inserted into an active phase again during the 68th cycle. The orbital period of the system seems to have changed, too. More observations are needed to confirm the continuation of the system's activity and its period variation.

MONITORING THE NOVAE V2274 CYGNI AND V2275 CYGNI 2001

Voloshina I.[(1)], Rovithis-Livaniou H.[(2)], Metlova N. [(1)] and Papadopoulos A. [(2)]

(1) Sternberg Astronomical Institute, Moscow State University, Moscow, Russia.
(2) Section of Astrophysics, Astronomy & Mechanics, Dept. of Physics, Athens University, Greece.

Abstract: The two novae appeared in the constellation of Cygnus on July and August 2001 – namely V2274 Cyg and V2275 Cyg, respectively– were monitoring after their discovery. More analytically: our observations of V2274 Cyg started on July the 19th 2001 and carried out with the 60cm telescope of Sternberg Astronomical Institute at Crimea. In the beginning, a classical photometer (with UBV filters) was attached to the telescope, while later –when the nova became too faint– a CCD camera, in the V, R & I bands. Using our and others data we constructed the light curve of V2274 Cyg; and, since the nova is not included on the DSS images (limited magnitude 21), we can conclude that its outburst amplitude exceeded the 8 magnitudes.

Observations of the nova V 2275 Cyg started only two months after its discovery. They were performed with the same photometer and the 60cm telescope at Crimea, and lasted till December 2001. Moreover, this nova was re-observed with a CCD camera –in B, V, R, I bands– attached to the 120cm Cassegrain reflector at the Kryonerion Astronomical Station of the Athens National Observatory during two nights (4 & 5) August 2002. At that time the nova was monitoring for many hours each night. As a result, changes in its brightness of the order of about 0.45 magnitude in all observational bands was found.

[*] *Proceedings of the 6th Hellenic Astronomical Society Conference, 15-17 September 2003, Penteli, Greece*

ABSTRACTS OF PAPERS POSTED DURING THE SESSION ON STARS AND STELLAR SYSTEMS[*]

ON THE GAIA EXPECTED HARVEST ON ECLIPSING BINARIES

P.G. Niarchos

Section of Astrophysics, Astronomy and Mechanics, Depart. of Physics, University of Athens, Greece

Abstract: GAIA, the approved cornerstone 6 ESA mission, will observe up to a billion stars in our Galaxy and obtain their astrometric positions on a micro-arcsec level, multi-band photometry as well as spectroscopic observations. The GAIA large-scale photometric survey will have significant intrinsic scientific value for the study of variable stars of nearly all types, including detached eclipsing binaries, near-contact or contact binaries and pulsating stars. It is expected that about one million Eclipsing Binaries (EBs) (with V up to 16 mag) will be discovered. The number of photometric points in the five-year mission lifetime is estimated to be ~ 100 to 150 and the observing fashion will be quite similar to Hipparcos/Tycho mission operational mode. On the other hand, GAIA's spectrograph will be able to secure useful radial velocities for binaries down to V ~ 17. The combined astrometric, photometric and spectroscopic data will be used to compute the physical parameters of the observed EBs. Even if for only 1% of the observed EBs reliable physical parameters could be derived, this would be a great contribution to stellar astrophysics and a giant leap in comparison with what has been obtained so far from ground-based observations. From a study of a small sample of EBs, it is shown that the agreement between the fundamental stellar parameters, derived from ground-based and Hipparcos (GAIA-like) observations is more than satisfactory. The percentage difference between the absolute elements derived from GAIA-like observations and those from ground-based observations is of the order 2% or lower. These first results are encouraging and demonstrate that GAIA data will be suitable to obtain accurate binary solutions

[*] *Proceedings of the 6th Hellenic Astronomical Society Conference, 15-17 September 2003, Penteli, Greece*

HELLENIC ASTRONOMICAL SOCIETY

INVITED REVIEW

WHAT CAN WE LEARN FROM NEAR-INFRARED OBSERVATIONS OF SPIRAL GALAXIES

Preben Grosbøl

European Southern Observatory

WHAT CAN WE LEARN FROM NEAR-INFRARED OBSERVATIONS OF SPIRAL GALAXIES*

Preben Grosbøl

European Southern Observatory Karl-Schwarzschild-Str. 2 D-85748 Garching, Germany

ABSTRACT

The main differences between visual and near-infrared observations of spiral galaxies and benefits of the latter are illustrated using a sample of 54 spiral galaxies observed in the K filter. The small attenuation by dust at NIR wavelengths makes it possible to measure the distribution of luminous matter in the galaxies which otherwise is difficult to estimate for spiral galaxies with their high content of dust. Although the K band images mainly display the distribution of the old stellar disk population, light from young objects also contributes. A majority (~60%) of the disk galaxies has a symmetric, grand-design two-armed spiral pattern in their inner parts which often splits up into multiple arms in the outer regions. Around 10% of the galaxies show complex structures in the central parts. Non-axisymmetric perturbations in the disks were analyzed by 1D Fourier transform techniques. Relative amplitudes of bar components showed a continuous distribution down to the detection limit of ~3% with only 5 of 35 SA galaxies with no bar at this level. The main two-armed spiral structures displayed a lack of tight, strong spiral. Such patterns may have so high radial forces that non-linear dynamic effects would become important and damp them.

1. INTRODUCTION

Most classical studies of galaxies were done in the visual B band due to the high sensitivity of photographic plates in this band. With the arrival of CCD detectors, it became possible to extend investigations to the full visual spectrum. Although this gave access to many broad band colors, it was still impossible to safely separate population effects from attenuation by dust as the corrections are very similar and the detailed geometry of dust and stars in the galaxies is unknown. First with array detectors in the near-infrared (NIR) region of 1-2.5μ, available in the early 1990's, it become feasible to observe galaxies (Block & Wainscoat 1991) at wavelengths where dust attenuation starts to be insignificant. It also opened the possibility of direct studies1[1] of properties of spiral density waves (Lin & Shu 1964) in disk galaxies.

This paper shows some of the additional information one can obtain from NIR observations of spiral galaxies. It is illustrated by a sample of nearby spiral galaxies for which K-band (at 2.1μ) photometry was obtained.

---

* Hel.A.S. Invited Review
Proceedings of the 6th Hellenic Astronomical Society Conference, 15-17 September 2003, Penteli, Greece
Based on observations collected at the European Southern Observatory, La Silla, Chile.

[1] Πάντες άνθρωποι του ειδέναι ορέγονται φύσει (Αριστοτέλης)

2. VISUAL vs. NEAR-INFRARED

Observations in the NIR present several challenges compared to those in visual bands. The night sky levels are significantly higher especially in K (approx. 13 mag/□″) where thermal emission starts to be a major component. This has to be compared with the typical surface brightness of disks in spiral galaxies which is in the range of K = 16-19 mag/□″. Both absorption and emission associated to a number of atmospheric molecules (such as H_2O, CO_2, OH and O_2) are important and make the sky level vary at a time scale of minutes. A number of different array detectors are now available with sizes up to 2k×2k pixels. Although the stability and cosmetic quality of these NIR detectors2[2] have improved significantly, they still do not reach the standards for CCD's used for visual bands.

The rapid varying sky and high background levels demand an elaborate observing technique including short integration times to avoid saturation of detector pixels and sequences of exposures with small offsets to ensure that the full sky area is measured even with groups of bad detector pixels. For extended objects, like galaxies, one needs to interleave target frames with exposures of blank sky fields to correct for variation in background level.

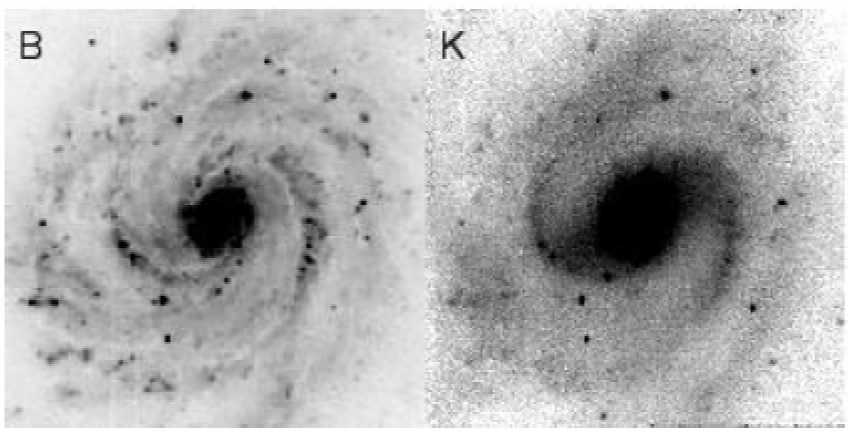

Figure 1 Direct images of NGC 5085 in B and K bands

Visual images of spirals are often dominated by the light from young objects which outline the spiral arms. Especially for late-type spirals, strong absorption by dust is also seen. This is illustrated in Fig. 1 where both B- and K-band images of the spiral galaxy NGC 5085 of type Sc(r)I-II are shown. Whereas the galaxy in B has a patchy appearance, mainly due to dust and young stars, the K frame shows the smooth variation associated with the old stellar disk population. The dust make the bulge look smaller and the spiral arms seem to reach further in than the NIR image indicates.

For studies of the distribution of luminous matter in galaxies, the NIR bands, especially K, are much more suitable as the attenuation of dust is very small. There are still population effects as seen on Fig. 1 where several bright knots in arm regions on the B map also appear enhanced in the K-band. Although the major part of the light in K originates from old stellar populations, a

---

[2] τυφλάς εν αυτοίς ελπίδας κατώκισα (Αισχύλος)

fraction (up to 30%) may come from younger objects such as red super-giant (Rix & Rieke 1993).

The detailed mass distribution in disks of spiral galaxies is important for the study of their dynamic structure and possible secular evolution. For these purposes, the K band is the better choice.

3. DATA AND REDUCTIONS

A sample of 54 non-barred spiral galaxies was observed in the K' band with the SOFI instrument on the 3.5m NTT telescope at La Silla to study their spiral structure and estimate the fraction of bars in ordinary spirals (Grosbøl et al. 2003). The galaxies was selected to represent a wide range of morphological types with a subset of 35 SA galaxies for which no bar perturbation could be identified in visual bands. Further, they were chosen to have inclination angles <65º and systemic velocities <5000 km/s to allow the detailed study of perturbations in their disks.. The typical seeing was 1" and the limiting magnitude was around 21 mag/□″ in K' for a signal-to-noise ratio of 3.

Before the internal structure of the galaxies could be analyzed, their sky projection parameters had to be determined3[3]. This was done by minimizing the constant phase component in the region of the disk occupied by the main spiral structure using 2D Fourier transforms on the polar maps of the galaxies.

4. GENERAL PROPERTIES

With the projections parameters fixed, the axisymmetric parts of the galaxies were fitted by a spherical bulge and a flat exponential disk. First the disk parameters were estimated for the region occupied by the main spiral pattern using only the inter-arm regions which better represent to old stellar disk population. Typical differences in the estimates of 10% were seen when compared to those using the full disk as they were biased by young object in the arms (Grosbøl & Patsis 1998).

The distribution of central surface brightness and linear scale length (assuming H = 75 km/s/Mpc) is shown in Fig. 2. There is a lack of centrally bright disks with long scale length which may be due to a limit in total angular momentum available during formation. Latetype spiral (i.e. T>4) are, on average, fainter while the distribution of linear scale length show little correlation with type.

The central region was then fitted with a bulge component after the contribution from the main disk was subtracted. Both a modified Hubble law (Binney & Tremaine 1987) and a Sérsic $n^{1/n}$ power law (Sérsic 1968) were used for the spherical bulge. For most galaxies, the latter gave a better fit with the power law index n in the range of 1-2. Addition of a central point source improved the fit in several cases. Further, it was tried to include a steep central exponential disk component with projection parameters identical to those of the main disk. The fits for the

[3] τέτλαθι δή, καρδίη· καί κύντερον άλλο ποτ' έτλης (Όμηρος)

majority of galaxies got better which suggests that the bulges often are oblate rather than spherical. However without detailed kinematic data, it is not possible to derive the actual 3D shape[4] of the bulge component.

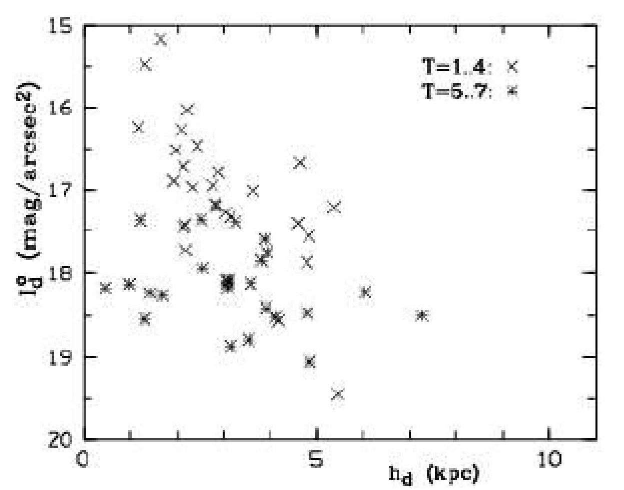

Figure 2 Distribution of the central surface brightness of the exponential disk as function of the scale length as measured in the K band.

5. MORPHOLOGY OF BARS AND SPIRALS

To analyze the perturbations in the disk, it is necessary to subtract the spherical bulge component which otherwise would give raise to an artificial bar feature when the galaxy is deprojected. Deviations from the assumed bulge shape can still leave traces such as constant phase features in the central parts. Problems in defining the exact shape of the PSF and pixel interpolation errors in high gradient region in the center made the analysis of the inner 2" uncertain which therefore was omitted.

The general morphology of bars and spirals was checked visually on direct face-on, bulge-subtracted images in the K band. The large dynamic range of exponential disks makes it difficult to view small perturbation. Thus, relative intensity maps were used in which the intensities were normalized by the average radial profile. Most spiral arms can be approximated by logarithmic spirals which appear as straight segment on logarithmic polar maps. Both of these types of maps are shown for three galaxies in Fig. 3-5.

The majority of the spiral galaxies (~60%) show a grand design spiral structure in their inner parts while this pattern often breaks up into multiple arms in the outer regions. One such galaxy is NGC 6118 shown on Fig. 3 and classified as Sc(s)I.3 in RSA. It displays a typical s-shaped spiral where the arms smooth increase pitch angle towards the center and finally almost become a bar. Although the galaxy is classified as non-barred in the visual a small bar is clearly seen on the K direct map. The main two-armed spiral pattern splits up in the outer parts.

[4] πολλάκις γάρ συνερχόμεθά τινές εις ταυτόν παραπλησιίαν ηλικίαν έχοντες, διασώζοντες την παλαιάν παροιμίαν (Πλάτων)

Many bright knots along the arms can also be seen indicating the presence of young objects and star formation.

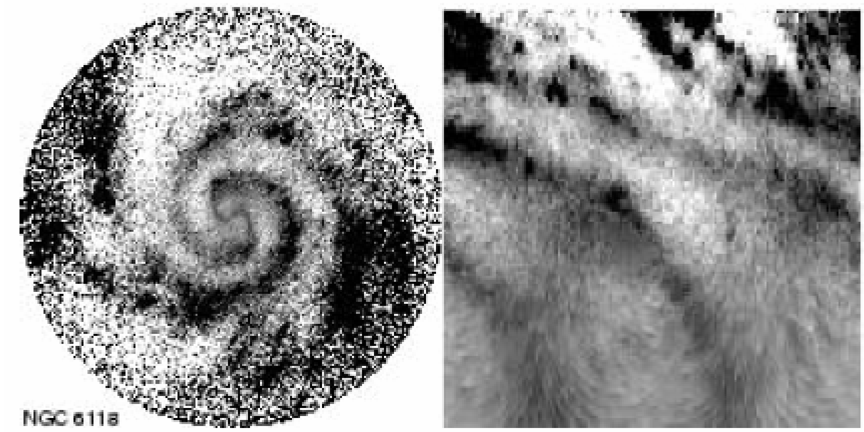

Figure 3 Direct face-on image and logarithmic polar θ-ln(r) map of the relative K band variation in the disk of NGC 6118. Dark areas represent enhanced intensity with black being +30% and white -30%.

Another example of a grand design spiral is NGC 1566 (see Fig. 4). Even though it is classified as a non-barred, s-shaped spiral galaxy with Hubble type Sc(s)I in the visual, its K image show an oval distortion in the central parts having a phase offset of ~30º relative to the inner ends of the spiral arms. This offset suggests that bar and spiral pattern constitute different modes with possibly separate pattern speeds (Sellwood & Sparke 1988). The spiral arms are quite symmetric and show many knots indicating strong star formation. As seen on the logarithmic polar map, one of the arms is well approximated by a logarithmic spiral while the other has a slightly more open pitch angle and displays a sudden change in its outer part. Around 10% of the galaxies in the sample have complex central regions[5] with several different structures of bars or spirals. NGC 4939 is one such case as seen on Fig. 5. It has the Hubble type Sbc(rs)I according to RSA. A central bar structure can be seen on the K map. At the ends of the bar a set of small arcs are location which could be associated to the T-regions seen in N-body models by Patsis & Athanasoula (2000). Just outside, there are two additional sets of arcs or tight spirals each offset by 90º. The main two-armed spiral starts from the last set of arcs. Although arms continue to larger radii, a phase shift can be observed on the polar map. Also in this galaxy many knots are seen along the arms. In general, spiral structure in disk galaxies looks smoother on K images than in visual bands reflecting better the surface brightness variations in the old stellar disk population. As dust do not obscure the view in NIR, it is also easier to estimate the density perturbation in the disk although some light from young objects still may be contribution even in the K band.

[5] καί διά τάς μαρμαρυγάς αδύνατοι καθοράν εκείνα ών τότε τάς σκιάς εώρα (Πλάτων)

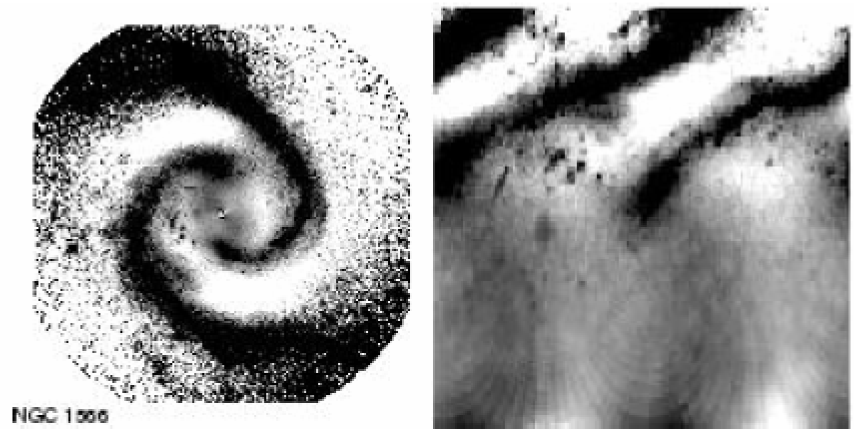

Figure 4 Direct face-on image and logarithmic polar map of the relative K band variation of the disk of NGC 1566. Density scale as in Fig. 3.

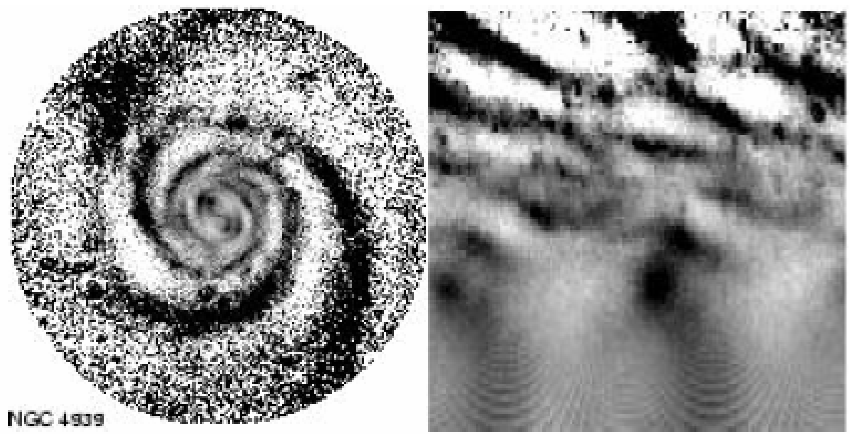

Figure 5 Direct face-on image and logarithmic polar map of the relative K band intensity variation in the disk of NGC 4939. Density scale as in Fig. 3.

6. BAR AND SPIRAL PERTURBATIONS

The quantitative distribution of non-axisymmetric perturbations in the disks were studied using 1D Fourier analysis of the azimuthal K intensity variation within 1" wide, consecutive annuli in the plan of the disk. Although 2D Fourier transforms yield more information, 1D FFT technique was preferred as 2D transforms are more difficult to interpret if the spiral arms do not follow a simple mathematical form (e.g. a logarithmic spiral) and may depend on the choice of radial region. To reduce the effects of young objects in the arms, a median filter was applied before the 1D Fourier transform was done. Bars or oval distortions were identified by their almost constant phase of the m=2 harmonics as function of radius whereas spiral structures show a systematic variation.

Several investigations have found that the frequency of bars in disk galaxies is higher in NIR than in visual bands (see e.g. Seigar & James 1998, Eskridge et al. 2000). Thus, it is of interest to quantify the distribution of weak bars and check if there is a group of truly non-barred disk galaxies or if all have some oval distortions in their central parts. The galaxies in the present sample are a selection of SA/SX type systems (i.e. classified as either non-barred or weakly barred) and should therefore provide the lower part of the distribution of bar amplitudes.

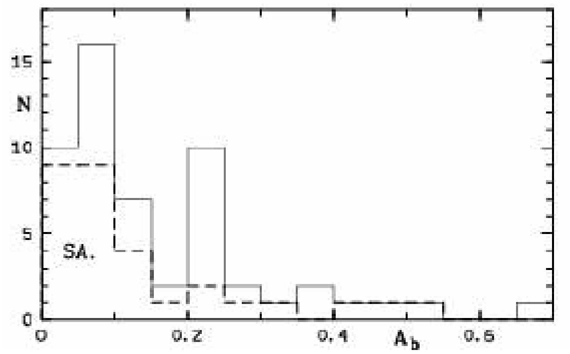

Figure 6 Histogram of bar amplitudes.

Bars in the galaxies were identified manually by inspecting the radial phase variations of the m=2 Fourier harmonic. The distribution of mean bar amplitudes is given in Fig. 6 where the inner 2" were omitted to reduce possible effects from an inadequate bulge subtraction. It shows a continuous distribution of amplitudes down to the detection limit of ~3% with only 5 galaxies below this limit. As expected, galaxies classified as non-barred have weaker bars on average than those of SX type. This suggests that 85% of the SA galaxies have detectable bar perturbation which would indicate that the fraction of truly non-barred6 [6]disk galaxies is as low as 5% of all spirals.

The extent of the main symmetric, two-armed spiral structure in the galaxies was also estimated manually from both the phase variations and the logarithmic polar maps. The average relative amplitude of the m=2 component and the pitch angle were derived (see Fig. 7). The amplitudes may be overestimated compared to the true variation of the old stellar disk population due to light from young objects in the arms. The two galaxies, NGC 1566 and NGC 2997, with the highest amplitudes both show traces of significant star formation in their arms

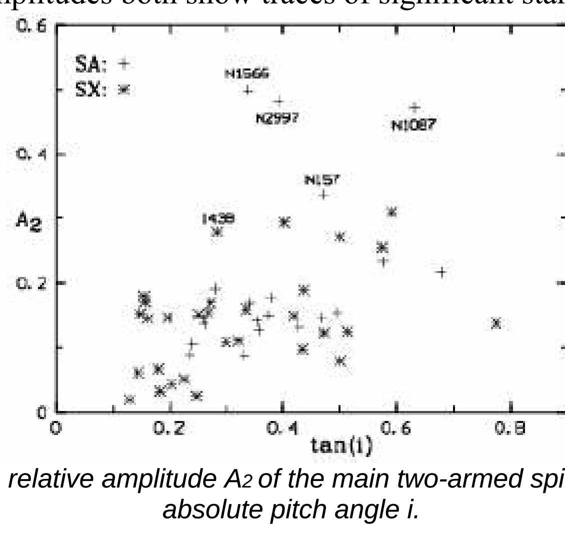

Figure 7 Distribution of the relative amplitude A_2 of the main two-armed spiral pattern as function of the absolute pitch angle i.

6 Τί ην είναι (Αριστοτέλης)

The pitch angles are mostly in the range of 5-30º where spirals tighter than 5º are very difficult to detect due to their small inter-arm distance. The amplitudes are generally less than 20% but there is a lack of strong, tight spiral patterns. Such spirals would have a high relative radial force perturbation ΔFr and therefore be subject to non-linear dynamic effects which could damp such patterns. This is expected to happen for ΔFr > 5% (Grosbøl 1993).

7. CONCLUSION[7]

The surface photometry of spirals in the NIR K band gives a good estimate of the mass distribution of luminous matter in them with only minor population effects. The smooth appearance of spiral arms suggests that spiral arms seen on visual images are caused by density waves.

The axisymmetric parts of the disk galaxies are well represented by a bulge and an exponential disk. The bulge component is best approximated by a Sérsic power law with a power in the range of 0.5-1. The bulge fit was improved in many cases by adding a steep exponential disk component which could indicate that many bulges are oblate.

Most spiral galaxies (~60%) have a two-armed, grand-design spiral structure in their inner parts while multi-arm patterns frequently are seen in the outer regions. A small fraction of the galaxies (~10%) display a complex structure in their central parts with multiple bars, arcs or spirals.

Bar amplitudes show a continuous distribution down to the detection limit of ~3% with 5 galaxies for which no bar structure could be identified. This suggests that only ~15% of ordinary spirals classified as SA are non-barred at this limit corresponding to 5% of all spirals.

The distribution of amplitudes and pitch angles of the main two-armed spiral structure shows a lack of strong, tight patterns. Such spirals would have the highest relative radial force perturbations and therefore possibly be damped by non-linear dynamic effects.

8. REFERENCES

Binney, J. & Tremaine, S. 1987, Galactic Dynamics (Princeton: Princeton Univ. Press)
Block, D.L. & Wainscoat, R.J. 1991, Nat, 353, 48
Eskridge, P.B., Frogel, J.A., Pogge, R.W. et al. 2000, AJ, 119, 536
Grosbøl, P. 1993, PASP, 105, 651
Grosbøl, P. & Patsis, P.A.1998, A&A, 336, 840
Grosbøl, P., Patsis, P.A. & Pompei, E. 2003, A&A, (in preparation)
Lin, C.C. & Shu, F.H. 1964, ApJ, 140, 646
Rix, H.-W. & Rieke, M.J. 1993, ApJ, 418, 123
Patsis, P.A. & Athanasoula, E. 2000, A&A, 358, 45
Sandage, A. & Tammann, G.A. 1981, A Revised Shapley-Ames Catalog of Bright Galaxies (Washington: Carnegie Inst.) [RSA]
Seigar, M.S. & James, P.A. 1998, MNRAS, 299, 672
Sellwood, J.A. & Sparke, L.S. 1988, MNRAS, 231, 25
Sérsic, J.L. 1968, Atlas de galaxia australes (Cordoba: Obs. Astron. De Cordoba)

[7] εγώ δέ, ώσπερ ουν ουκ οίδα ουδέ οίομαι· (Πλάτων)

Session III

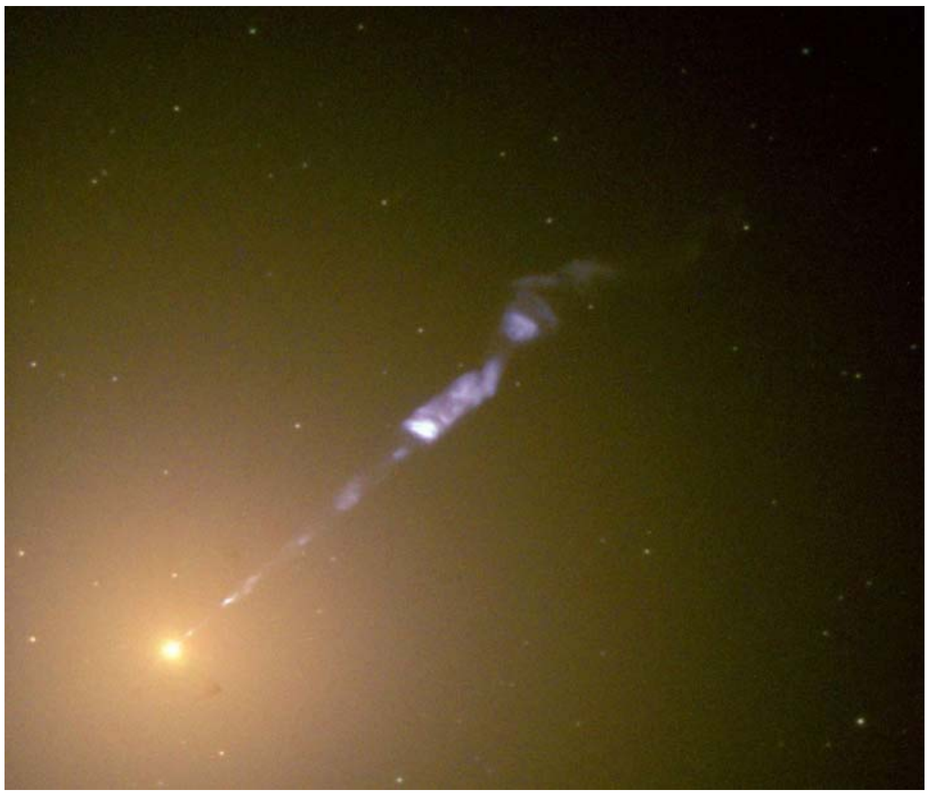

EXTRAGALACTIC ASTRONOMY

Conveners: K. Tsinganos and M. Kontiza

DISCS IN ACTIVE GALACTIC NUCLEI*

Evlabia Rokaki

Section of Astrophysics, Astronomy and Mechanics, Department of Physics,
University of Athens, Greece

ABSTRACT

Accretion discs around massive black holes are expected to be optically thick and radiate much of their emission in the UV band. Quasi-blackbody emission consistent with such discs is observed in many AGN. The harder, rapidly variable, X-rays emission from AGN objects must originate above the disc, probably from non-thermal processes involving magnetic fields. Photoionization, and fluorescence from the irradiated disc produce also line emission. Spectral and statistical signatures of such discs in the central region of active galactic nuclei are briefly reviewed.

1. INTRODUCTION

Our current working scenario for active galactic nuclei (hereafter, AGN) includes a central engine which is likely to be powered by accretion of gas, although its detailed nature is obscure. The heart of the AGN central engine is thought to be supermassive black hole which accretes matter from the host galaxy. By analogy with stellar accretion-powered systems such as cataclysmic variables and low-mass X-ray binaries, the accretion flow very close to the black hole is thought to form an equatorial accretion disc. The presence of accretion discs had received limited and indirect observational support until very recently. Models for the thermal emission from an accretion disc have provided a reasonably good description of the "big blue/UV bump" observed in the spectra of quasars (section 2). The most direct, dynamical evidence for the presence of accretion discs in the central engines of active galaxies comes from observations of very broad, double-peaked emission lines in optical and X-ray emission lines (section 3) . Finally there is also statistical evidence for line and continuum disc emission in radio loud AGN (section 4).

2. UV BUMP: THERMAL EMISSION OF DISC

The emission spectrum of an accretion disc was first derived by Lynden Bell (1969) and elaborated upon in numerous AGN studies since the UV/optical continuum was first plausibly associated with disc emission (Shields 1978; Malkan & Sargent 1987). The principal improvements attempted in the multitude of disc models introduced over the last decades are related to the relativistic effects of the gravitational field of the central black hole (e.g. Cunningham 1975) and/or the radiative transfer in the disc atmosphere (e.g. Sun & Malkan 1989; Laor & Netzer 1989; Ross, Fabian & Mineshige 1992)

---

* Main Session Invited Speaker

Proceedings of the 6th Hellenic Astronomical Society Conference, 15-17 September 2003, Penteli, Greece

adopting for the most part the standard Shakura & Sunyaev (1973) "α" for the disc viscosity.

In its simplest version, the stationary disc is assumed to radiate the viscously dissipated energy as a blackbody at the effective

$$T_{eff}(r) \cong (5x10^5 K)(\frac{\dot{M}}{0.1 M_{sol} yr^{-1}})^{1/4} M_8^{-1/2} r^{-3/4} \Im^{1/4}$$

where r is the radial distance expessed in Schwarzschild radii, M_8 is the black hole mass in units of $10^8 M_{sol}$, $\dot{M}$ is the mass accretion rate, and $\Im$ is a term that includes effects of the disc boundary conditions (Novikov & Thorne 1973). Most of the emission originates close to the black hole and it emerges in the UV when M_8 is in the range $10^{-2} - 10$, and $\dot{M}/\dot{M}_{Edd}$ between $10^{-2} - 1$ ($\dot{M}_{Edd} = 0.22 M_8 / \eta \quad M_{sol} yr^{-1}$). The emergent spectrum is then determined by integrating the Planck function $B_\nu \{T_{eff}(r)\}$, over the whole disc surface. It is characterized by a broad spectral emission with a flux density rising as $\nu^{1/3}$ and a high energy cut-off that is characteristic of the peak temperature.

Quasi-blackbody emission consistent with such discs is observed in the UV band in many Seyfert 1 galaxies and in quasars. Figure 1 shows an accretion-disc fit to the UV continuum of NGC 5548. The solid line is the thermal spectrum of a face-on disc fit with an accretion rate of $0.007 M_{sol} / yr$. The mass of the black hole is 8.3 $10^7 M_{sol}$ and has the maximum possible spin.

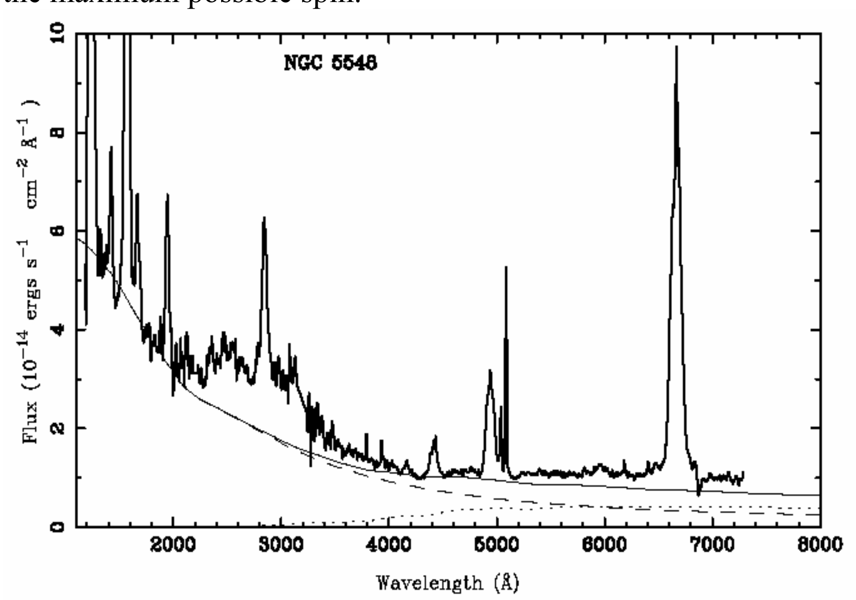

Figure 1.

A fit (solid line) of the optical to the UV continuum of NGC 5548 which sums a disc (dashed line) and a stellar component (dotted line). Physical parameters are given in the text.
From Rokaki & Boisson (1999).

3. DOUBLE PEAKED EMISSION LINE PROFILES

a. Optical lines

The broad emission lines are quite distinctive features of AGN spectra (see Figure 1), and since their generation involves well-understood processes (atomic physics), a wealth of information has been produced, using standard astronomical methods. The basic assumption of current broad line region (BLR) studies is that the line emission is due to photoionization by the continuum. Since the BLR resides well outside the central engine, the observed effects may be regarded as somewhat secondary, being due to reprocessing.

The most direct, dynamical evidence for the presence of accretion discs in the central engines of active galaxies comes from observations of very broad, double-peaked emission lines. These "exotic" line profiles are found in about 20% of the radio-loud AGNs surveyed by Eracleous & Halpern (1994, 2003) and in about 4% of (radio-loud and radio-quiet) objects from the SDSS studied by Strateva et al. (2003). About 40-50% of double-peaked Hα profiles can be described quite well by the relativistic, circular, Keplerian disc model. Doppler boosting and gravitational and transverse redshifts cause observable asymmetries (the blue peak appears much brighter than the red one, and a net redshift of the high-velocity portions of the profile, Chen, Halpern, & Filippenko 1989) when the velocity is of the order of 0.02 c. Figure 2 shows an example in which the broad double-peaked Hα line of Arp 102 B is fitted by a photoionized accretion disc (Collin- Souffrin & Dumont 1989). As a result several parameters of the BLR can be determined from the line profile fit, included the inclination angle.

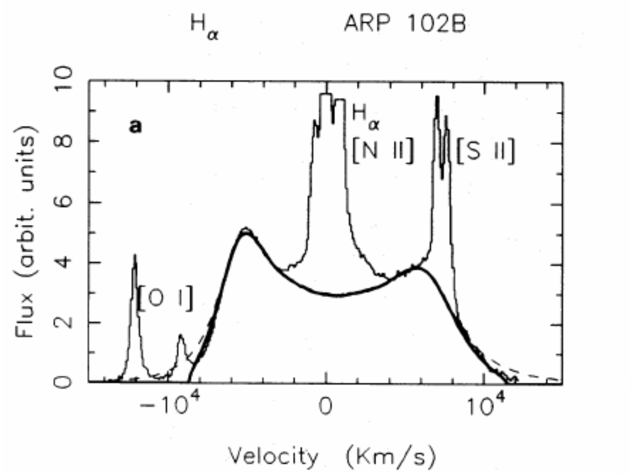

Figure 2.

Fit (solid line) of a relativistic Keplerian disc model to the double-peaked Hα line of Arp 102B. The observed line profile asymmetries constrain the disc inclination at 32±1 degrees. (From Rokaki et al 1992).

The remaining double-peaked line profiles require more sophisticated models, in which the disc is not axisymmetric . The candidate scenarios include bright spots orbiting in the disc, precessing eccentric discs, discs with spiral waves, and even a binary broad-line region associated with a binary black hole. At this time, the spiral wave scenario appears to be the most promising: it has been successfully applied to NGC 1097 by Storchi-Bergmann et al. (2003). This scenario not only explains the variability trend, but it also leads to an estimate of the precession period that is consistent with the black hole mass inferred from stellar kinematics.

It is noteworthy that several alternatives to accretion disc emission have been proposed and discussed in the literature. However, accretion disc emission is the interpretation favored by the data available today (see Eracleous & Halpern 2003 for a description of alternative scenarios and their comparison with observations).

b. Fe Kα (6.4 keV) Line in the X-Ray Spectra of Seyfert Galaxies

Early X-ray observations of mainly low-luminosity Seyfert 1 galaxies suggested that the spectra in hard X-rays (2-20 keV) in general conform to a power law with an index ~ 0.7. Subsequent Ginga observations revealed that the emission in the 1-30 keV range has a multicomponent structure, including an incident power law with a spectral index α^{int} ~ 0.9 and an excess above 10 keV. With the advent of ASCA and the capability for high-resolution X-ray spectroscopy the profiles of the Fe Ka lines in the X-ray spectra of AGNs were found to be extremely broad and asymmetric, with full widths at zero intensity approaching a third of the speed of light (Mushotzky et al. 1995; Tanaka et al. 1995). In most cases the line profiles can be described very well by models attributing the emission to the inner parts of a highly relativistic accretion disc (Tanaka et al. 1995; Nandra et al. 1996, Fabian et al 2002).

4. STATISTICAL EVIDENCE

In radio loud AGNs there are clear indications that the distribution and kinematics of emission line gas is related to symmetry axis of the central engine as defined by the radio jet. These jets originate at nuclear distances < 0.1 pc – similar to the highest velocity emission line gas. Significant correlations have been for quasars between the line widths (FWHM) of broad Hβ emission line and R (e.g Wills & Browne 1986, Corbin 1997), the radio core flux density to the extended radio lobe flux density. In the relativistic beaming model for radio sources, R is related to the angle between the radio axis and the line of sight, and the correlations are then consistent with motion of the emission-line gas being confined predominantly to a plane perpendicular to the radio axis.

VLBI expansion lets us derive another physical measurement, the angle of the jet axis to our line of sight, θ. Rokaki et al. (2003) use this approach to derive jet angles for a sample of radio-loud quasars for which they also measure Hα FWHM and equivalent widths (EW). Strikingly they find angles up to 40 degrees, well away from the region (θ < 10) where a beamed continuum dominates the quasar spectrum. Rokaki et al. find that more edge-on objects have on average broader FWHM (H α) (see Figure 3a), implying ordered rotation around the jet axis. Similar correlations with radio core-to-lobe ratio, which is a proxy for θ , find the same result, but proxy measurements cannot compare model predictions. Having θ, Rokaki et al. can do so, and they find that pure rotation is not a good fit, and that another component of amplitude ~2000 km is needed. The EW(Hα) vs θ plot (Figure 3b) also shows a correlation. If Hα were from a attened disc, as we expect the continuum to be, then as we view the disc at larger and larger angles both would suffer the same geometric and limb darkening, and so no change in EW. Instead larger θ objects have larger EW(Hα). Rokaki et al. find that the EW vs. θ relation is just as expected if the continuum comes from a disc and suffers cos θ and limb darkening, but the Hα is isotropic. So the BLR is not only rotating, it also has a large scale height, rising well above the continuum producing disc.

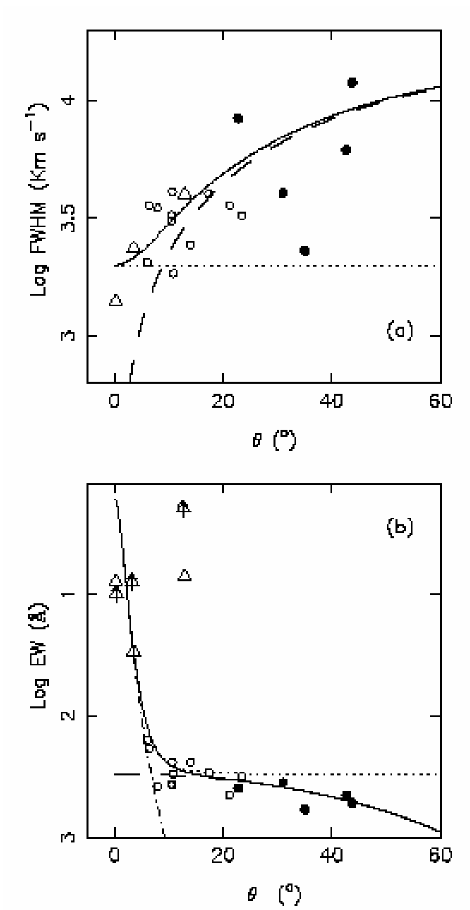

Figure 3

(a) FWHM of broad Hα emission line in a sample of 22 superluminal quasars versus θ compared with models. The dashed curve shows an axisymmetric component (V = 13 000 sin θ km/ s) and the solid curve gives its quadrature sum with an isotropic one (V = 2000 km/ s., the dotted curve).

(b) EW of broad Hα emission line of the versus θ compared with models. The dot-dashed curve shows the expected effect of Doppler enhancement for a jet with Lorentz factor γ = 30. The dashed curve shows the predicted effect for a flat accretion disc with a standard limb darkening, and the solid curve combines disc and beamed components. The dotted curve combines isotropic and beamed components

REFERENCES

Collin-Souffrin, S., & Dumont, A. M. 1989, A&A, 213, 39
Corbin M. R., 1997, ApJS, 113, 245
Chen, K., Halpern, J. P., & Filippenko, A. V. 1989, ApJ, 339, 742
Cunningham, C. 1975, ApJ, 202, 788.
Eracleous, M. & Halpern, J. P. 1994, ApJS, 90, 1
Eracleous, M. & Halpern, J. P. 2003, ApJ, 599, in press (astro-ph/0309149)
Fabian A.C. et al 2002, MNRAS 335, L1
Laor A. & Netzer H.,1989 MNRAS 238, 897
Lynden Bell , 1969 Nature 223, 690
Malkan M.A. & Sargent W.L.W, 1982, ApJ 254, 22
Mushotzky R. F et al., 1995 M.N.R.A.S., 272, P9
Nandra K., George I.M., Mushotzky R.F., Turner T.J., & Yaqoob, T., 1997, ApJ 477 602
Novikov I.D. & Thorne K.S, 1973 in Black Holes, ed. C. DeWitt & D. DeWitt

(New York: Gordon & Breach), p. 342
Rokaki E., Boisson C. & Collin-Souffrin S., 1992 A&A, 253, 57
Rokaki E., Boisson C., 1999, MNRAS, 307, 41
Rokaki E., Lawrence, Economou F. & Mastichiadis A., 2003, MNRAS 340, 1298
Ross R.R, Fabian A.C. & Mineshige S., 1992, MNRAS 258, 189
Shakura N.I. & Sunyaev R.A., 1973, A&A 24, 337
Shields G.A., 1978, Nature 272, 706
Storchi-Bergmann, T., et al. 2003, ApJ, 598, in press (astro-ph/0308327)
Strateva, I. V., et al. 2003, AJ, 126, 1720
Sun W.H. & Malkan M.A., 1989, ApJ 346, 68
Tanaka, Y., et al., 1995, Nature, 375, 659 .
Wills B. J., Browne I. W. A., 1986, ApJ, 302, 56

SHOCK FORMATION IN RELATIVISTIC JETS*

K. Tsinganos[1] and S. Bogovalov[2]

[1]Section of Astrophysics, Astronomy and Mechanics, Department of Physics, University of Athens, [2]Moscow Engineering Physics Institute, Moscow 11549, Russia

ABSTRACT

To account for the observation of collimated jets with relatively high fluxes, we have proposed a two-component model consisting of (a) an inner relativistic wind-type out-flow from a central source and (b) a nonrelativistic wind from the surrounding disk. By using a numerical code for a direct solution of the MHD problem we show that in this two-component model it is possible to collimate into two cylindrical jets all the mass and magnetic fluxes which are available from the central source. The collimation of the plasma is accompanied by the formation of oblique shock fronts. The nonrelativistic disk-wind not only plays the role of the jet collimator, but it also induces the formation of shocks as it collides with the initially radial inner relativistic wind and as it is reflected by the system axis. At such internal shocks particle acceleration may give rise to observed radiation emission from jets across the spectrum.

THE MODEL

In the following Figure 1 we sketch the initial (t=0) state of the two-component outflow model. A non-rotating central relativistic radial outflow originates in the hot corona surrounding an accretion dominated advection flow (ADAF) while a nonrelativistic rotating disk-wind originates in a surrounding Shakura-Sunyaev disk (SSD). For simplicity, the launching boundary of the inner outflow from the ADAF corona is taken at a spherical surface surrounding the ADAF while the boundary of the SSD on a rectangular slab attached to the spherical surface around the ADAF. The thin solid lines indicate lines of the poloidal magnetic field. The relativistic 4-velocity $U=\gamma v/c$ (γ is the Lorentz factor, v is the bulk flow speed and c the speed of the light) is sketched in the following right figure as a function of the magnetic flux ψ, such as the flow is relativistic ($\gamma=5$, $v=0.97979c$) at the inner part of the flow around the rotation axis and nonrelativistic at the surrounding disk wind ($\gamma=1.044$, $v=0.288c$).

SHOCK FORMATION

In Figure 2 and in more detail in the following Figures 4-5 are shown the results of the numerical simulation of the previous MHD outflow configuration after the system relaxes to an equilibrium state. The poloidal magnetic field lines of the outflow are plotted for intervals of equal magnetic flux. A notable feature in this case is the compression of the part of the inner relativistic flow from the central source into a thin jet of enhanced poloidal magnetic field, by the magnetic hoop stress of the surrounding azimuthal magnetic field which is generated by the rotation of the disk. During this interaction and collision of the two components of the outflow a shock wave is formed at the interface of the two components of the outflow.

* *Proceedings of the 6th Hellenic Astronomical Society Conference, 15-17 September 2003, Penteli, Greece*

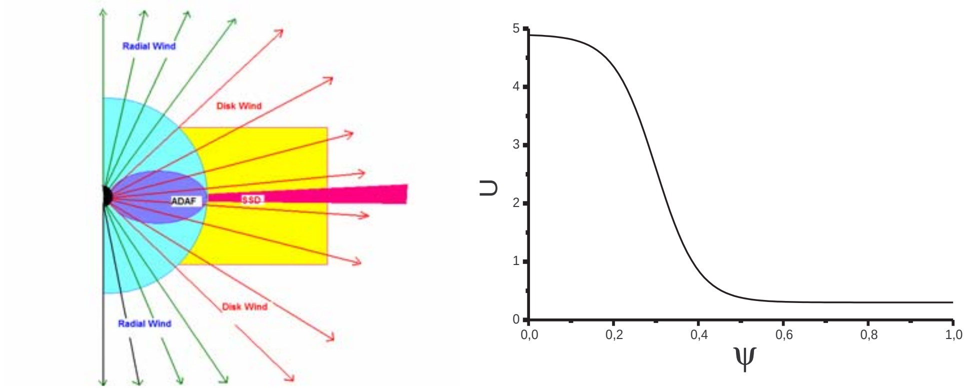

***Fig. 1**. Left: Sketch of initial state of a two-component outflow with part of the poloidal magnetic field rooted on the accretion disk and the remaining coming from the central object. Right: Dependence of 4-velocity on magnetic flux ψ, with relativistic values at small ψ and nonrelativistic ones further away.*

The magnetic flux between adjacent field lines is constant. In the same figure, before rotation starts there is no concentration of magnetic flux and collimation around the system axis for a monopole-like magnetic field wherein $\psi=(1-\cos\theta)/r$, if we plot the flux in intervals of equal magnetic flux.

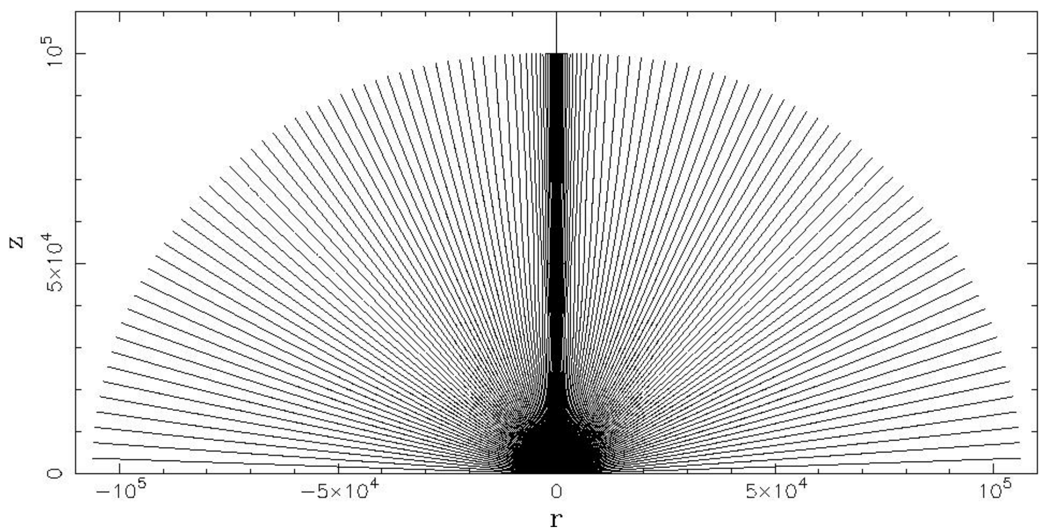

***Fig. 2**: An initially radial poloidal magnetic field becomes tightly collimated after rotation starts and the external component of the disk-wind forces the inner relativistic component to collimate.*

The collimation of the relativistic outflow from the central source is performed by the tension of the toroidal magnetic field which is generated by the rotating disk-wind. This wind which compresses the outflow from the central source, in general induces the formation of two shocks. The first oblique shock indicated by (1) in the Fig. 3 arises as the nonrelativistic collimated external part of the flow collides with the uncollimated relativistic inner component and forces this to collimate too. The second, is a reflection shock indicated by (3) in figure 3 and arises because of the existence of the symmetry z-axis which forces the supersonic flow to change direction and propagate parallely to the z-axis after it emerges from the shock (1) which directs the outflow towards this axis.

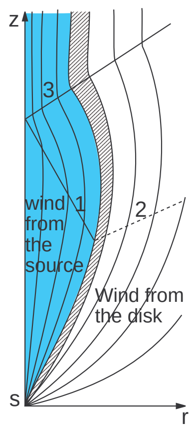

***Fig. 3**: Schematic illustration of predicted formation of compression shock (1) and reflection shock (3).*

The left panels of Figures 4-6 show the distribution of the various pressure components across the jet at various distances from the source. The collision shock (1) is first formed at a distance R ~ 100 from the source. Initially, close to the source the post-shock pressure is mainly provided by the pressure of the poloidal magnetic field, because there the poloidal magnetic field is still sufficiently strong. Thus, a layer of enhanced poloidal magnetic field is formed in the flow and this may be seen in Fig. 4b as a black ribbon. In Fig. 4a showing the pressure distribution along a surface crossing the z-axis at the distance z=400, shock (1) has not hit the z-axis yet, and the thermal pressure plays a dominant role in the post-shock region. The farther away from the source we move, the weaker the poloidal magnetic field becomes. Starting at a distance around z=400, the poloidal magnetic field is not able any longer to provide the needed pressure in the post shock region. This role is now taken by the gas pressure, i.e., the total post-shock pressure becomes mainly of thermal origin, as shown in Fig. 4a.

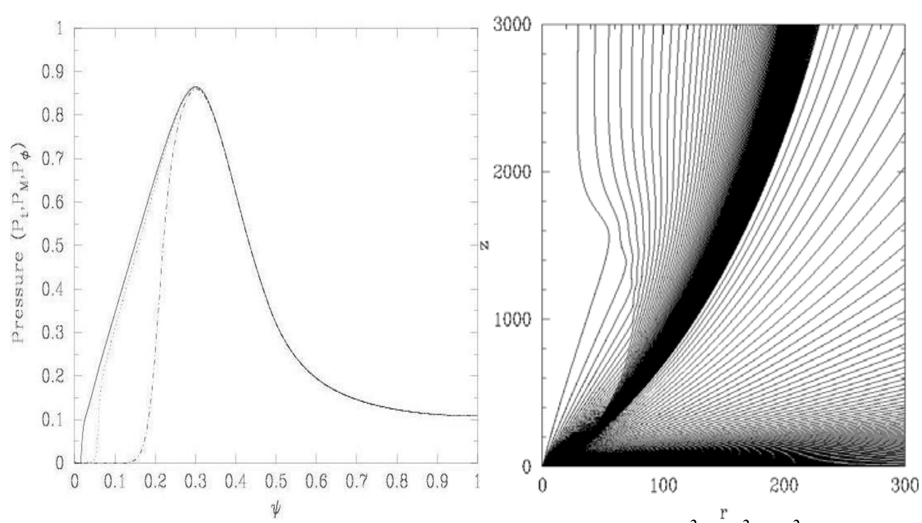

***Figure 4.** Left: Distribution of the total pressure $P_t = P_{gas} + (B_p^2 + B_\varphi^2 - E^2)/8\pi$ (thermal + electromagnetic) (solid line), total electromagnetic pressure $P_M = (B_p^2 + B_\varphi^2 - E^2)/8\pi$ (dotted line) and pressure of the toroidal field $P_\varphi = (B_\varphi^2 - E^2)/8\pi$ (dash-dotted line) along a sphere at z=400. Right: View of the poloidal fieldlines of the near zone of the flow up to z=3000.*

At intermediate distances z=20.000, the jet has been compressed to its minimum radius. The pressure distribution corresponding to this moment is shown in Fig. 5b. In this stage the overpressure of the flow at the axis produces the reflecting shock wave (3). This distribution of the pressure will turn now the flow off the z-axis. The reflecting shock wave (3) is well seen at relatively large distances from the axis, since the amplitude of the reflecting shock grows as the magnetic pressure decreases, an effect similar to what happens when a sound wave propagates in a region of decreasing density, wherein it is transformed into a shock wave. Indeed, at the beginning this distribution of the pressure creates a smooth motion of the plasma away from the z-axis. But at larger distances where the total magnetic field decreases, this motion results into the formation of a reflecting shock wave which corresponds to the predicted shock (3) in the sketch of Fig. 3.

At the far distances $z=10^5$ we distinguish the following regimes:

(i) At the inner jet around the outflow's axis, $0<\psi<0.05$, the total pressure is uniform across the jet. In fact the pressure there is thermally dominated by the heated post shock plasma, although initially the plasma was cold.

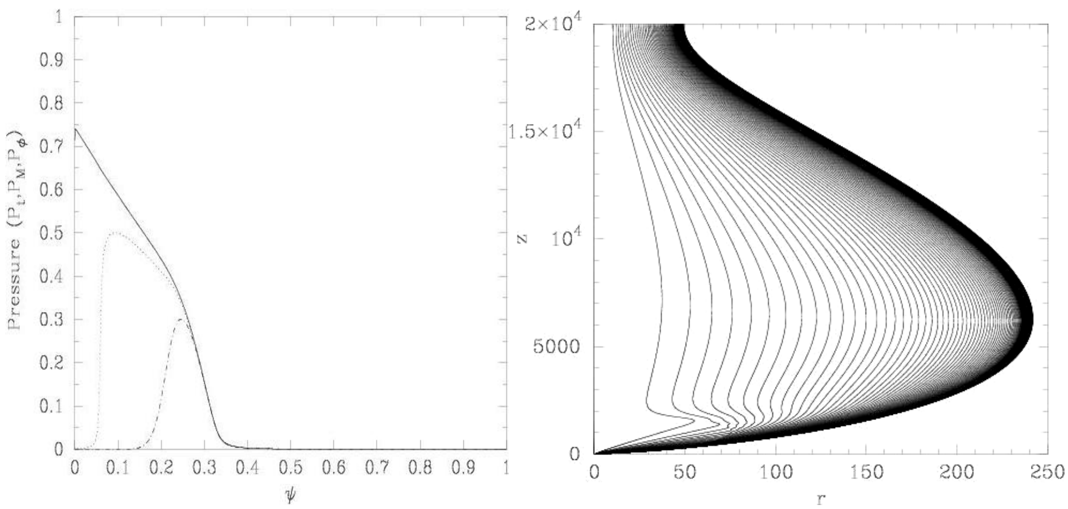

Figure. 5. *Left: Distribution of the pressure along a sphere at z=20.000. Right: View of the poloidal fieldlines of the flow up to z=20.000 .*

(ii) At an intermediate layer, say, $0.05<\psi<0.2$, the compression of the magnetic flux around the core of the jet contributes a dominant poloidal magnetic field pressure.

(iii) An outer layer, $0.20<\psi<0.4$ where the pressure associated with the toroidal field dominates the total pressure, since the toroidal field is peaked around $\psi = 0.25$.

(iv) The external layer at $\psi > 0.4$, where all pressure contributions have dropped to negligible values. Nevertheless equilibrium is maintained by the tension of the surrounding magnetic field.

It is worth to note that, all the plasma flux from the central source is collimated into the jet and thus the model under consideration can be applied to the modeling of observed jets from astrophysical objects.

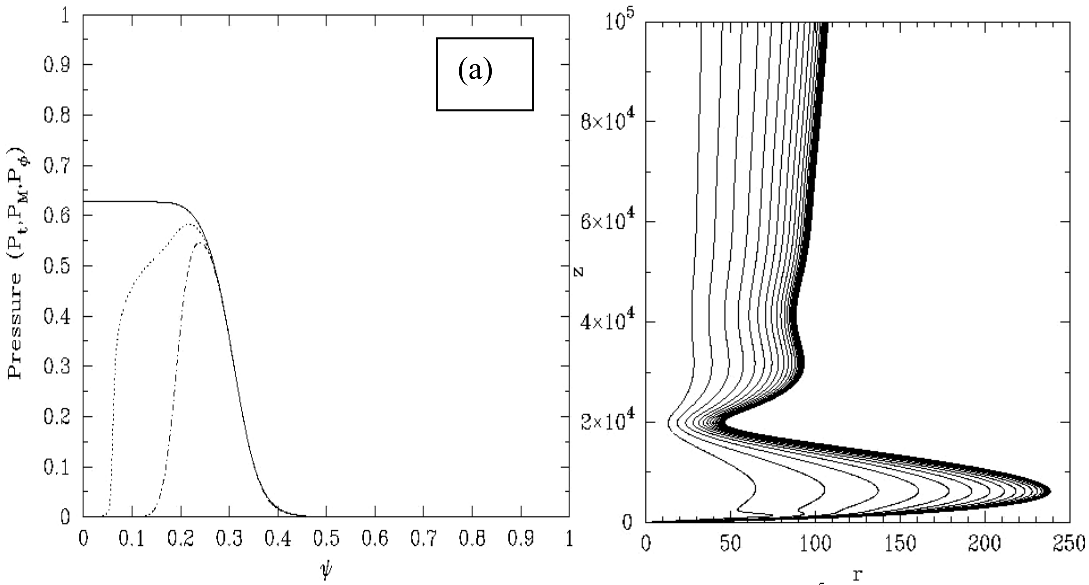

Figure 5. *Left: Distribution of the pressure along a sphere at z=10^5. Right: View of the poloidal fieldlines of the flow up to z=10^5.*

Bibliography

1. Bogovalov, S.. & Tsinganos, K. 2001, MNRAS, 325, 249
2. Tsinganos, K. & Bogovalov, S. 2002, MNRAS, 337, 553

DUST AND MID-INFRARED PROPERTIES OF LUMINOUS ACTIVE GALAXIES: FROM IRAS TO ISO TO SIRTF*

Vassilis Charmandaris

Abstract: Even though dust constitutes less than one hundredth of the mass of the interstellar medium it is now widely accepted that its influence on the energetics of galaxies, due to the heating of the gas via photoelectrons, as well as on their overall morphology because of obscuration/extinction effects is profound. Interactions between galaxies cause instabilities and lead not only to massive star formation over extended spatial scales where the properties of interstellar radiation field, gas and dust content vary substantially, but they also drive much of the gas into the central regions forming/fueling active galactic nuclei (AGN). We present a review of our current knowledge on the dust properties of active galaxies, using their emission in mid and far infrared wavelengths, focusing on the results obtained with the Infrared Space Observatory over the past few years. WE also present how, the soon to be launched Infrared Telescope Facility, will further revolutionize the field.

Main Session Invited Speaker

THERMAL OUTFLOWS IN GENERAL RELATIVISTIC MHD

Zakaria Meliani and Christophe Sauty

(Initially omitted, this paper can be found at the end, on page **389.** The Editor regrets the omission)**.**

DEEP SURVEYS OF OBSCURED AND HIGH REDSHIFT AGN

Eleni Chatzichristou,
Yale University

Abstract: The Great Observatories Origins Deep Survey (GOODS) is a multi-wavelength public survey that will yield an extremely deep view of two of the best ever studied fields, HDF-N and CDF-S. It will yiend the most uniform panchromatic data set (from X-rays to radio wavelengths) to study the distant Universe. I present the main AGN studies currently underway and the first exciting results from GOODS.

* *Proceedings of the 6th Hellenic Astronomical Society Conference, 15-17 September 2003, Penteli, Greece*

STAR-FORMING GALAXIES IN DENSE ENVIRONMENTS*

José M. Vílchez[1], Daniel Reverte-Payá
Instituto de Astrofísica de Andalucía - CSIC
18080 Granada, SPAIN
&
Jorge Iglesias-Páramo
Observatoire Astronomique Marseille-Provenze
13376 Marseille, FRANCE

ABSTRACT

The study of the population of emission line galaxies in nearby clusters is a necessary step towards our understanding of the evolution of galaxies in different environments and earlier epochs. We report here on the results of a long-term project devoted to the study of star-forming galaxies in nearby groups and clusters which is being carried out by our team.

1. Introduction.

The environment where galaxies are located plays an important role in their evolution. From theoretical grounds, it is expected that galaxies located in high density regions such as clusters can suffer tidal effects and interactions with other galaxies and with the intracluster medium (ICM). Environmental effects can also lead to important losses of gas and stars and subsequent redistribution of the material in the discs of the spirals and irregular galaxies in clusters. In addition, the interaction of galaxies with the ICM can produce ram pressure stripping and evaporation.

The effects of the environment on the star formation activity in galaxies are expected to be observable (e.g. Hashimoto et al. 1998; Iglesias-Páramo & Vílchez 1999 ; Balogh et al. 1998 ; Moss & Whittle 2000 ; Nakamura et al. 2003). This aspect is very relevant for the study of galaxy evolution since, for example, the existence of gas flows (either inflow or outflow) in galaxies has strong implications in the models of chemical evolution. In this respect, gas stripping and/or pressure confinement constitute relevant phaenomena for the study of the chemical evolution. Observational results have shown that there are significant differences in the observable HI gas content between spiral galaxies in the Virgo cluster and in the field, being Virgo galaxies deficient in HI (Cayatte et al. 1990).

In contrast, the results obtained for the content of molecular clouds located near the center of these galaxies show however that they remain in the discs (Kenney & Young, 1989; Boselli et al. 1997). Given that gas-rich dwarf galaxies are somewhat more fragile systems, the impact of environment is expected to be especially significant for these objects.

---

* *Proceedings of the 6th Hellenic Astronomical Society Conference, 15-17 September 2003, Penteli, Greece*
[1] Main Session Invited Speaker

For dwarf galaxies, the analysis of the spectroscopic properties of a sample of objects located in different density environments (e.g. Vílchez, 1995; 1999) suggested that the galaxies with the higher activity of star formation are always associated to the lower density regions. Recent work for dwarf galaxies in nearby voids does not seem to favour this behaviour (Popescu et al. 1999) though, on the large scale, the typical spectroscopic properties derived for emission line galaxies in large surveys (e.g. Hashimoto et al. 1998) are consistent with this view.

For Virgo spiral galaxies, previous results (Skillman et al. 1996 and references therein) have suggested they should have chemical abundances larger than field galaxies. Recent work (see Pilyugin et al. 2001) shows that this suggestion appears now tentative.

Up to date, there is no systematic project devoted to the study of a complete sample of star-forming galaxies in nearby ($z<0.05$) clusters. This kind of study may help us to understand the properties observed in more distant, star-forming objects discovered in deep surveys, as well as to establish a firmer local calibrator of the star formation activity of galaxies located in environments of different density. Here we report on the present stage of a long-term project devoted to the study of star-forming galaxies in a sample of nearby groups and clusters, that is being carried out by our team. We can anticipate here some of the implications of this ongoing study which are closely related to several classical issues on star formation in galaxies as e.g.:

-What are the triggering mechanisms of star formation bursts?
-Is the chemical evolution of SF galaxies (in clusters) affected by their environment?
-How is the observed galaxy spectral mix in groups & clusters produced?

Why is this study interesting? Clearly, one of the strongest reasons is because the environment of galaxies can affect their history of star formation (SFH).
Three fundamental results in the study of the evolution of galaxies and their environments were published in the 80's :

-The Butcher & Oemler effect (c. 1978)
-The Morphology-density relation (Dressler 1980)
-The Gas Deficiency of Cluster Galaxies (Haynes et al.1984)

Nonetheless, it is now clear that environmental effects are present at all the scales of star formation; from the spatial scale of the HII regions in the Milky Way, or the star formation regions in the galaxies of our Local Group, up to the scale of the most luminous starbursts in galaxies in groups and clusters, the environment is playing a key role.

2. Star Formation Activity in dense Environments.

What we have learned from recent work is that a high density environment is not one to one with an enhancement of star formation in the galaxies located there, as naively could have been expected in the past. Instead, there appears to be a two-fold effect operating on gas-rich disk galaxies located in these environments:

i) Inhibition of the "normal" star formation activity can be produced in very high density environments. This is a consequence of ram pressure stripping, gas removal, and partly also to the galaxy "Harassment" (Moore et al. 1996) operating especially in clusters. In these extreme environments part of the gas content of the galaxies can be displaced from their disks and, as a consequence, a "quenching" of the star formation activity can be produced. In some extreme situations, it may even produce a change of appearance and in the morphological type class of the galaxy (e.g. Koopman & Kenney 1996; Hashimoto et al. 1998; Iglesias-Páramo & Vílchez 1999; Verdes-Montenegro et al. 2001)**.** ***Observational fact:*** HI deficiency in spiral galaxies of nearby clusters (Virgo, Coma). Observations do show that galaxies with high HI deficiency inhabit the environments with the highest densities (e.g. Cayatte et al. 1990; Haynes et al. 1984; Solanes et al. 2001; Bravo-Alfaro et al. 2000). The question arises as to whether the Star Formation History or the Chemical Evolution of these galaxies can reflect these observational facts (e.g. Skillman et al. 1995; Pilyugin, Mollá, Ferrini & Vílchez 2002 and references therein).

ii) Enhancement of massive star formation, "starbursts", can be produced during strong galaxy interactions; in galaxy mergers; or, on a larger scale, also from subcluster merging (e.g. Abell 2125; Owen et al. 1999**).** These processes can give rise to localized accumulations of gas, inducing for example, (circum) nuclear starbursts; and/or the production of the so called tidal dwarf galaxies in the outermost tails of the merger (e.g. Moss & Whitle 1997; Vílchez & Iglesias-Páramo 1998; Rose et al. 2001).

On average, what it has been found is that the **present-day Star Formation Rate (SFR)** derived for groups of galaxies is similar to, or even slightly reduced than the SFR found for field galaxies. In their pionneering work, Larson & Tinsley (1978) suggested enhanced star formation as a consequence of the strong interactions seen in their sample of Arp objects. More recently, Moles et al. (1994) using UBV photometry studied the star formation history of a sample of Hickson compact groups of galaxies (HCG); they found that these very dense environments present similar or only slightly higher SFRs than the field. Present-day SFRs (derived using deep Halpha imaging) have been derived for a large sample of HCGs producing SFR values which are consistent with those found for field galaxies (Iglesias-Páramo & Vílchez 1999; Severgnini et al. 1999).

3. Studying Star-Forming Galaxies in Groups and Clusters.

We are carrying out a long term project on the activity of star formation and its effects in the chemical evolution for a sample of star-forming galaxies located in nearby groups and clusters. First, all northern HCGs with $z < 0.02$ where observed using deep Halpha and broad band imaging in order to derive structural properties and SFRs (Vílchez & Iglesias-Páramo 1998). Second, we are presently carrying out wide field (typically 1º x 1º) observations of a sample of all northern nearby ($z<0.05$) Abell Clusters in Halpha and broad band filters. Among these clusters, new results have been obtained for Virgo, Coma, A 1367, Hercules, A 634, A 400, A 2666, A 539, A 779, among others. Figure 1 shows the comparison of the Halpha Luminosity Functions of Virgo, Coma and A 1367

clusters (right) and the discovery of two Irregular galaxies falling towards the center of A 1367 showing 75Kpc long trails in Halpha (Left). Table 1 summarizes the work in progress or already done on this project, with references to recent publications.
In the following subsections, we present a report of some of the main results that we have found on the properties and evolution of star-forming galaxies in the Virgo cluster.

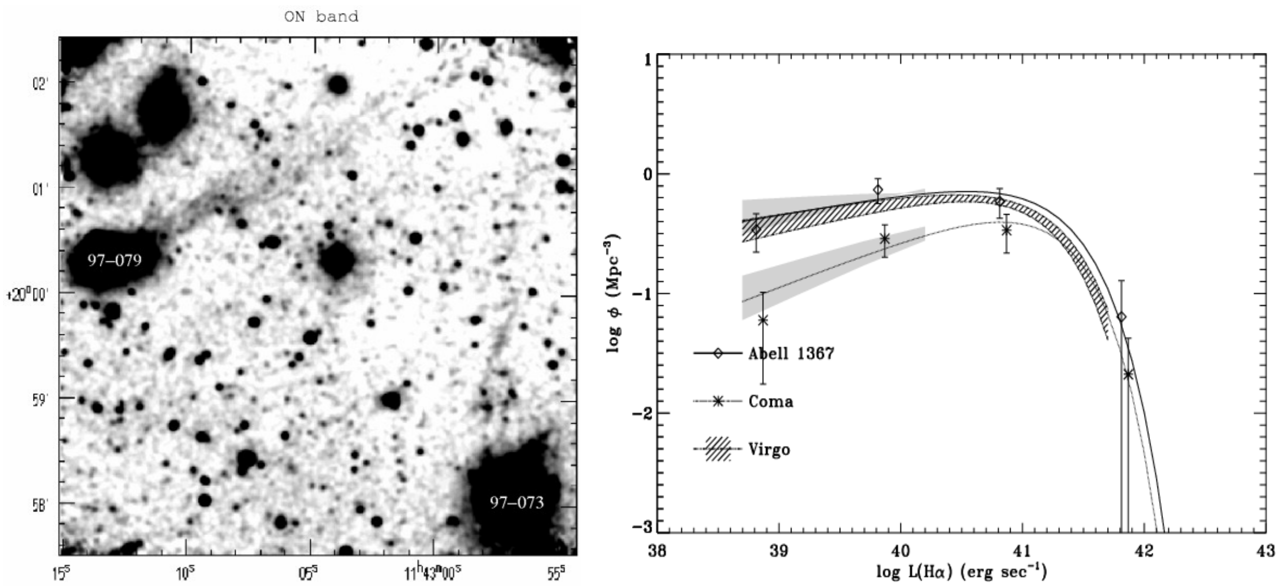

Figure 1.- Left : Detection of 75kpc Halpha trails of two dIrr from our deep Halpha survey of A 1367 (Gavazzi et al. 2001). Right: Comparison of the Halpha LFs derived for Coma, A 1367, Virgo. The three nearby clusters show similar slopes (Iglesias-Páramo et al 2002).

Table 1. Ongoing programs of our study of nearby clusters & references.

VIRGO	
Spectroscopic survey of 22 BCDs & dIrrs	(Vílchez & Iglesias-Páramo 2003 ApJ & ongoing)
Deep Ha, R Imaging of BCDs	(Boselli, Iglesias-Páramo,Vílchez, Gavazzi 2002 AA)
Chemical Evolution of Spirals vs. HI Deficency	(Pilyugin , Mollá,Ferrini, Vílchez 2002 AA)
COMA & A 1367:	
Deep Halpha survey: Halpha Lum. Functions	(Iglesias-Páramo,Boselli,Vílchez,Gavazzi, 2002 AA)
The r´ LF of A1367 & Coma vs. Field	(I-P, B, V, G 2003 AA)
Quantitative morphology of cluster galaxies	(Aguerri, I-P, V, CMT, Moles 2003 AJ & ongoing)
HERCULES:	
Deep surveys for star-forming dwarfs	(I-P, Duc, Papaderos, Vilchez et al . 2003 AA)
VLA HI search for dwarf galaxy candidates	(W.v. Driel, I-P, P, Balkowski, V, et al. 2003 AA)
Deep B,V,i Halpha imaging. V band LF	(R. Sánchez, Reverte, I-P, V, CMT ongoing)
A 2666, A 400, A 634, A 539, A 779 :	
Halpha & broad band (1 deg2 WFC): SFR & LF	(D. Reverte PhD, V, I-P, ongoing)

3.1. Chemical Abundance Segregation of Spirals in the Virgo Cluster

The chemical abundances of oxygen and nitrogen have been computed from the spectra of HII regions located in nine Virgo spiral galaxies (see Skillman et al. 1996) and in nine field spiral galaxies using the P-method (Pilyugin 2000). We have confirmed the existence of abundance segregation among the Virgo spirals; we have found that those gas deficient Virgo galaxies located near the core of the cluster show higher oxygen

abundances than the spiral galaxies located at the periphery of the cluster. At the same time, we have found that, from the chemical evolution point of view, the spirals of our Virgo sample are very similar to the nine spirals of our field sample. For both, Virgo periphery and Virgo core spirals, we can found counterpart galaxies among our sample of field spirals (see Pilyugin et al. 2002). Some field spirals show ratios of HI to optical radius similar to the ones shown by HI deficient Virgo core spirals.
These results have been analyzed using the multiphase chemical evolution models (Mollá et al. 1996) applied to the sets of galaxies located at the center, intermediate radii and the periphery of the Virgo cluster. An interesting prediction of these models is that the gas infall rate should have been stronger at earlier times for the Virgo core galaxies, whereas now it is observed to be quite low. Unenriched gas infall would produce the dilution of the elemental abundances, so chemical abundances lower than those expected from the closed box model of chemical evolution are predicted, in accordance to the gas fractions observed for the core spirals. Finally, the oxygen and nitrogen abundances derived for these Virgo spirals are found to be similar to the ones obtained for their counterpart field galaxies.

3.2. Virgo Star-Forming Dwarf Galaxies: Observations & First Results

Within an ongoing project combining deep Halpha imaging and spectra for all the BCD and Irregular galaxies in the VCC catalogue (Binggelli et al. 1985), a sample of 24 VCC objects clasified as blue dwarf galaxies (22 Virgo plus 2 background) was selected for our spectroscopic study, covering the VCC morphological classes: BCD, Im or Im/BCD (-pec). Long-slit spectra were obtained using the ISIS spectrograph at the cassegrain focus of the WHT 4.2m telescope (ING of Telescopes at the O.R.M., La Palma, Spain).
All the galaxies were selected across the Virgo central field (within 5 degrees from M87) for which the Halpha survey was carried out. The data reduction followed the standard procedures, and all the spectra were flux calibrated. Measurements of the flux in the [OIII] 4363 A line were obtained for 8 objects of the sample, for which a direct determination of the abundance was performed. For the rest of the objects chemical abundances were derived using semiempirical and model abundance calibrations.
Oxygen abundances and N/O abundance ratios were derived for 22 galaxies. We have obtained that the oxygen abundance of the sample of Virgo star-forming galaxies ranges from 1/25 to nearly 1 solar abundance, and the nitrogen to oxygen ratio, N/O, ranging from values typical of the low metallicity BCD galaxies up to solar metallicity ratios.
The abundances derived appear correlated with luminosity, color and total HI content of the galaxies. They are consistent with the overall shape of the metallicity-luminosity relation (e.g. Richer et al. 1998); though few outstanding exceptions to this general trend deserve further study (see Vílchez and Iglesias-Páramo 2003 for details).

3. Summary

The determination of the fraction of emission line galaxies in nearby clusters, their luminosity functions, star formation rates and metallicity is a necessary step for our progress to the understanding of the evolution of galaxies in different environments; as well as for the interpretation of the observations of higher redshift objects, which show a huge activity of star-formation. For nearby clusters, we are presently searching for their population of star-forming galaxies; deriving their chemical abundances and studying their Star Formation Histories. It is clear that the study of dwarf & gas-rich disc galaxies remains an *open question* for the issue of galaxy evolution in dense environments. In particular, the problem of *survival of star-forming dwarfs and disks* (Spirals) in rich clusters still remains a challenge for current models of galaxy formation and evolution.

Acknowledgements: JMV thanks the organizers of this magnificent HelAS Conference for their kind hospitality and support. This study was partially funded by the research project AYA2001-3939-C03 of the Programa Nacional de Astronomía y Astrofísica of the Spanish MCyT. JMV thanks the I.A.C. for hospitality during part of the preparation of this work

REFERENCES

Aguerri, J.A.L., Iglesias-Páramo, J., Vílchez, J.M., Muñoz-Tuñón, C. 2003 A.J. In press
Balogh, M.L., et al. 1998 Ap. J. 504, L75
Binggelli, B., et al. 1985 A. J. 90, 1681
Boselli, A. et al. 1997 A&A 327, 552
Boselli, A., Iglesias-Páramo, J., Vílchez, J.M., Gavazzi, G. 2002, A&A 386, 134
Bravo-Alfaro, H., et al. 2000 A. J. 119, 580
Cayatte, V., et al. 1990 A. J. 100, 604
Dressler, A., 1980 Ap.J. 236, 351
Gavazzi, G., et al. 2001 Ap.J. 563, L23
Hashimoto, Y., et al. 1998 Ap.J. 499, 589
Haynes, M., Giovanelli, R., Chincarini, G.L. 1984 A.R.A.A. 22, 445
Iglesias-Páramo,J.,Boselli,A.,Cortese,L., Vílchez,J.M., Gavazzi,G. 2002 A&A 384, 383
Iglesias-Páramo,J.,Boselli, A.,Gavazzi, G., Vílchez, J.M. 2003 A&A 397, 421
Iglesias-Páramo, J. et al . 2003 A&A 406, 453
Iglesias-Páramo, J. & Vílchez, J.M. 1999 Ap.J. 518, 94
Kenney, J., Young, J. 1989 Ap.J. 344, 171
Larson, R.B., Tinsley, B.M. 1978 Ap.J. 219, 46
Moles, M., et al. 1994 A&A 285, 404
Moore, B., et al. 1996 Nature 379, 613
Moss, C., Whittle, M. 1997 Rev. Mex. A&A C 6, 145
Moss, C., Whittle, M. 2000 MNRAS 317, 667
Mollá, M., et al. 1996 Ap.L. 466, 668
Nakamura, O., et al. 2003 astro-ph 0312519
Owen, F.N., et al. 1999 A.J. 118, 633
Pilyugin, L.S. 2000 A&A 362, 325
Pilyugin, L., Mollá, M., Ferrini, F., Vílchez, J.M. 2002 A&A
Popescu, C.C., Hopp, U., Rosa, M.R. 1999 A&A 350, 414
Richer, M., et al. 1998 Ap.J. 340, 67
Rose, J.A., et al. 2001 A.J. 121, 793
Severgnini, P., et al., 1999 A&AS 137, 495
Skillman, E.D., et al. 1996 Ap.J. 462, 147
Solanes, J.M., et al. 2001 Ap.J. 548, 97
van Driel, W., et al. 2003 A&A 399, 433
Vílchez, J.M. 1995 A.J. 110, 1090
Vílchez, J.M. 1999 ESO Astrophys. Symp. CEZHR Eds. J.R. Walsh & M.R. Rosa, p. 175
Vílchez, J.M., Iglesias-Páramo, J. 1998 Ap.J. S. 117, 1
Vílchez, J.M., Iglesias-Páramo, J. 1998 Ap.J 506, L101
Vílchez, J.M., Iglesias-Páramo, J. 2003 Ap.J.S. 145, 225

METRIC RADIO GALAXIES*

Gizani[1], Nectaria A.B. and Garrett[2], M.A.

1. Institute of Astronomy and Astrophysics, National Observatory of Athens, I. Metaxa & B. Pavlou, Lofos Koufou, Palaia Penteli, 15236 Athens, Greece
2. Director JIVE, Joint Institute for VLBI in Europe (JIVE), The Netherlands

ABSTRACT

We are investigating the pc-scale structure of two unique radio galaxies, namely 3C310 and Hercules A, in order to explain their unusual behaviour. These two AGN, which are classified as FR 1/2, present essential similarities and rather unusual characteristics with the obvious one being the presence of ring-like features which are interior to the source and not just phenomena of the boundaries. Global VLBI and EVN observations of 3C310 and Hercules A respectively, at 18 cm, have revealed a mas asymmetry characterised by a core-jet morphology and a large misalignment between the pc- and kpc-scale jets. Two compact components are detected at the core region of 3C310 at 4 mas and a NW extension. The corresponding total flux density is 9.5 and 8.8 mJy respectively. The small scale morphology of 3C310 seems complicated as the pc-scale jets present large misalignment with the NW (e.g. ~ 100 degrees) and NS kpc-scale jets. A faint but compact radio source was detected by the EVN at the core region of Hercules A at 18 mas resolution. The total flux density is 14.6 mJy. There is also evidence for extended emission in the NW-SE direction, most probably from the one-sided, eastern, pc-scale jet. If this is true then there is a misalignment between the direction of the pc-eastern and aligned large scale jets of about 35 degrees. The misalignment angles found which are relatively high compared to the ones found in other powerful radio galaxies is characteristic of quasars in the CSS class with steep spectrum cores. This result could be consistent with the suggestion that powerful radio galaxies are the unbeamed counterparts of quasars. However the misalignment could actually be small, but it is magnified when seen in projection.

1. Introduction

Both Hercules A (see Fig. 1) and 3C310 are nearby powerful, old radio galaxies with double optical nuclei. Baum et al., 1996 have also reported possible kpc scale rings of obscuration aligned near the radio axis of the first radiogalaxy. Hercules A is associated with the dimmer and larger optical galaxy. Both sources are classified as Fanaroff-Riley FR 1/2. Instead of hotspots they are probably the only two radio galaxies that show large multiple circular radio features (rings) that are interior to the lobes and not just phenomena of the boundaries. The rings have much flatter spectra than the surrounding diffuse lobes, suggesting that in both sources the jets are restarting. *We may be witnessing a renewed outburst from the active nucleus*. Inspite of being powerful and symmetrical in kpc-scales, their cores are very weak and there seems to be a substantial misalignment

* *Proceedings of the 6th Hellenic Astronomical Society Conference, 15-17 September 2003, Penteli, Greece*

between the pc- and kpc-scale jets. These misalignment angles are relatively high compared to the ones found in other powerful radio galaxies and are a characteristic of quasars in the compact symmetric sources (CSS) class with steep spectrum cores. This result could be consistent with the suggestion that powerful radio galaxies are the unbeamed counterparts of quasars. The direction of the probably one sided pc-scale jet of Hercules A seems to be in the direction of doppler beamed kpc-scale eastern jet. Recent Chandra X-ray observations (in collaboration with A. Wilson) show a preferred direction of the nuclear X-ray emission towards the smaller, brighter optical elliptical companion. *The core of Hercules A has a steep spectrum* and optically thin, which is apparently unusual. The thermal pressure at the distance of the radio lobes is larger than the lobe minimum pressure. Both sources are hosts of cooling flow clusters of galaxies. The X-ray brightness profile of both clusters can be described well if we assume contribution from a point source. However for 3C 310 we will take high resolution X-ray observations to clarify this. Hercules A has no strong emission lines although it is a powerful source. It is a weak line radio galaxy. The same might apply to 3C 310.

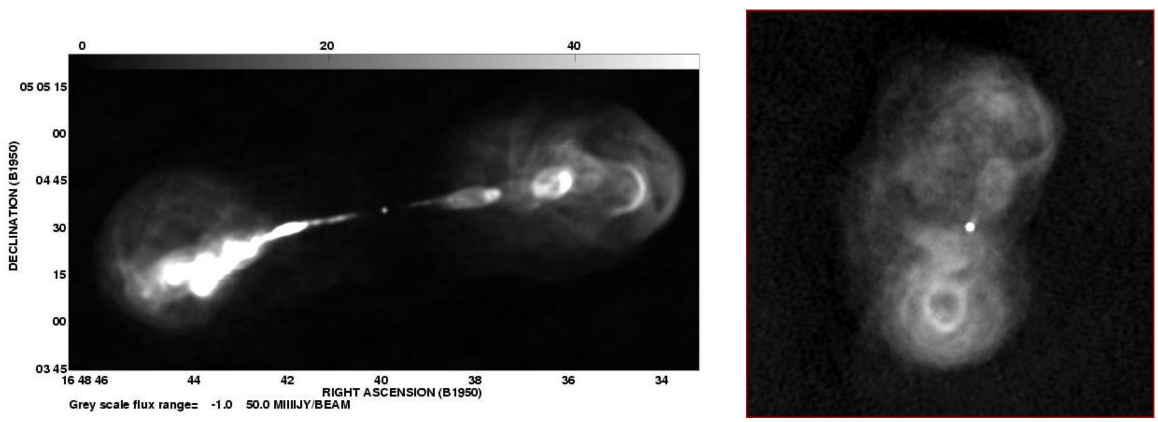

Figure 1. Grey scales VLA radio maps of Hercules A (left) and 3C310 (right). The ring-like structures are apparent. The total intensity VLA map of the 3C310 radio emission is at 21 cm, at 4 arcsec resolution (Van Breugel & Fomalont, 1984) and that of Hercules A is at 18 cm at 1.4 arcsec resolution (Gizani & Leahy).

2. The pc-scale structure

2.1. 3C 310

We made high resolution radio observations of the powerful extragalactic radio source 3C310 at ~ 4 milliarcseconds (mas), using the Global VLBI and employing the phase referencing technique (see Figure 2). At λ18 cm a faint but resolved radio source was observed with an unusual structure: Two compact components and an extended emission. The direction of this emission is NW, misaligned about 20 degrees with the direction of the larger scale north-western jet (cf. Fig.1, right). Model fitting to the three areas of emission detected in the core region of 3C 310 reveals that the component corresponding to the core of 3C 310 is the right of the two compact ones, since it has the highest brightness temperature of ~ 6.6 $\times 10^7$ K. The estimated core flux is ≅ 9.5 mJy. The core size is ≈ 8×7 mas and the position angle is 14.8 degrees. The values of the temperature brightness are typical of the core of low luminosity AGN (LLAGN).

There is also an indication of another extended emission in the NE/SW direction. The misalignment between pc- and kpc- jet structures is observed in many AGN, but such high values are not usual.

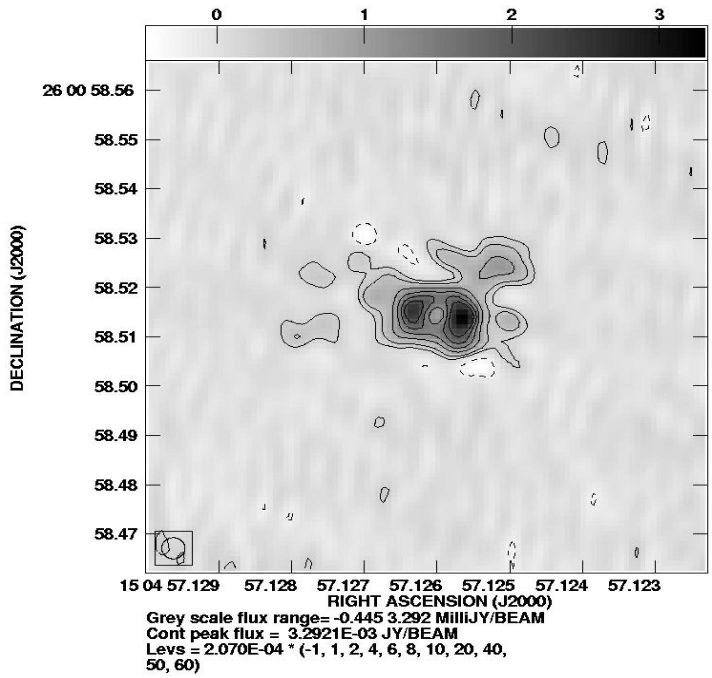

The Figure 2. The global VLBI map of the central region of 3C 310 at 18 cm at 4 mas resolution. A complicated structure is revealed. See text.

2.2 Hercules A

We have observed the core of Hercules A with the EVN at 18 cm employing phase referencing (Gizani & Leahy, 2003a; Gizani, Garrett & Leahy, 2001). Figure 3, shows the EVN map. Since the phase referencing did not work the axes of the map do not show absolute positions. The resolution obtained is ~18 mas corresponding to a linear size of 50 pc. A faint but compact source was detected coincident with the optical centre of Hercules A, but it is still unresolved as it is very weak. The flux density is ≅15 mJy, which indicates a radio power of 3.6×10^{22} W $Hz^{-1}sr^{-1}$. The size is ~ 18 × 7 mas and the position angle is ~ 139 degrees. The implied brightness temperature of the core is ≅ 2×10^7 K, typical of LLAGN. There is also an indication of emission from the core region in the NW/SE direction (see Figure 3). If this is indeed the case, then there is a misalignment between this direction (at least of the eastern pc-scale jet) with the kpc-scale jets of ~ 35 degrees.

It is possible that the extended structure we see is actually a one-sided, assymmetric core-jet structure. Gizani & Leahy 2003a,b suggest that the radio source is situated at the centre of a cooling flow cluster filled with a dense intracluster gas. The doppler boosted eastern jet is heading towards us at 50 degrees to the line of sight. Therefore the core in the EVN map should be situated at the extreme NW of the emission. The brightest component would then be identified with the inner pc-scale jet directed eastwards, towards the brighter larger scale jet. However the pc-scale jet also changes direction as it emerges from the core since it is decelerated. There is a gap between the pc- and kpc-scale jets indicating that the jets emanating from the nucleus are disrupted. This is probably because of the strong interaction between the energy flow and the environment. An alternative explanation of the lack of an extended counter-jet is free-free absorption of a circum-nuclear torus.

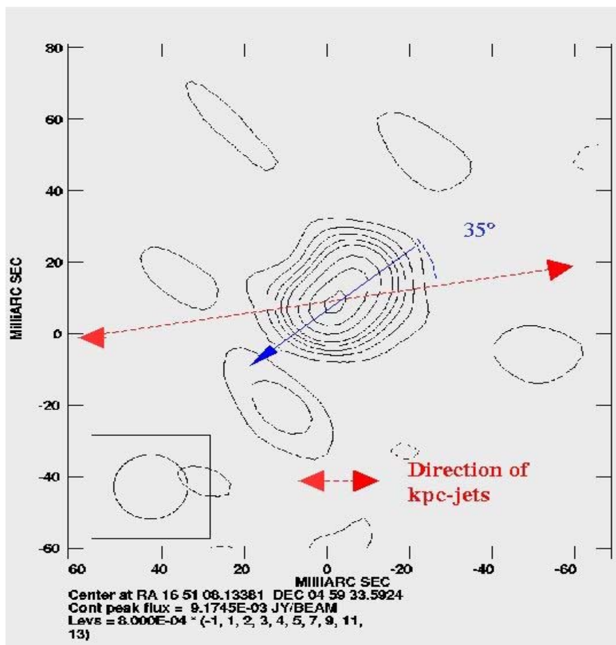

Figure 3. The EVN map of the core region at 18 cm at 18 mas resolution. There is evidence for extended emission in the NW/SE direction, see text.

3. Conclusions

We made high resolution Global VLBI observations of the core of the radio galaxy 3C 310 at 18 cm at 4 mas. An interesting and complicated structure was revealed consisting of two compact features and an extended NW emission. We assumes that the component with the highest brightness temperature and flux 9.5 mJy corresponds to the position of the central engine of 3C 310. We have also observed Hercules A in pc-scales with EVN at 18 cm at 18 mas. The core with ~ 15 mJy flux remains unresolved. In both sources there is evidence of a possible pc-scale asymmetry with a large misalignment between the pc- and kpc-scale jet. The resolution of the observations is not sufficient in order to find the most likely interpretation for this small-scale asymmetry in the case of Hercules A.

4. Acknowledgements

This research was supported by the European Commission's IHP Programme ``Access to Large-scale Facilities", under contract No. HPRI-CT-1999-00045. We acknowledge the support of the European Union -Access to Research Infrastructure action of the Improving Human Potential Programme. NG acknowledges the State Scholarships Foundation (IKY), Greece, for her current post-doctoral grant under contract 332 during which the current paper was written and published.

5. References

Baum S.A., O'Dea C.P., De Koff S., Sparks W., Hayes J. J.E., Livio M., Golombek D., 1996, ApJL, 465, 5

Gizani N. A., Garrett M. & Leahy J., 2001, PASA, 19, No 1, 69 (astro-ph/0111607)

Gizani N. A. & Leahy J., 2003a, MNRAS, 342, 399

Gizani N. A. & Leahy J., 2003b, MNRAS, accepted

van Breugel W. J.M., & Fomalont E. B., 1984, ApJL, 282, 55

ACTIVE AND NON-ACTIVE SPIRAL GALAXIES: OBSERVATIONS AND MODELING*

Xilouris E., CEA/SACLAY, FRANCE
Papadakis I., University of Crete, GREECE
Prantzos N., IAP, FRANCE

Abstract: We present preliminary results of a project that we have recently initiated, with the aim of investigating the possible relation between the star formation history of the disks and the appearence of central active nuclei in nearby spiral galaxies. Recent studies have provided strong evidence for the presence of super-massive black holes in the center of nearby galaxies. It is possible that most, even all, of nearby galaxies host a super-massive black hole in their central region. However, only ~ 10% of the nearby galaxies show evidence for the presence of a "classical" Seyfert-like nucleus. Furthermore, most of these nuclei reside in disk-systems. A potentially important factor that may influence the appearence of an active nucleus in a spiral galaxy, is the disk star formation history. Most of the gas may still be consumed in forming stars in the disks of galaxies with no AGN-like central activity, while galaxies with active nuclei may have undergone the phase of intense star formation in the distant past. In order to test this possibility, we have selected a sample of 60 spiral galaxies, with and without active nuclei, from the Palomar optical spectroscopic survey catalogue of Nearby galaxies. Using broad band B and I imaging from the 1.3 m telescope at Skinakas telescope, we aim at constructing radial colour profiles. When used as input to recent detailed chemo-spectrophotometric evolution models of spiral galaxies, these radial colour profiles can give us accurate information about the star formation history in the disks of these galaxies, hence, allowing us to examine the dependence of the appearence of central activity on the disk star formation history of these objects (if any).

GALAXIES IN THE XMM/2DF SURVEY

A. Georgakakis [1], I.Georgantopoulos [1], M. Plionis [1], G.C. Stewart[2], T. Shanks[3], B. J. Boyle[4]

([1]) NOA, ([2]) Leicester, ([3]) Duhram, ([4]),AAT

Abstract: We explore the X-ray properties of `normal' (i.e. non-AGN dominated) galaxies using a wide field (2.5 deg^2) shallow (2-10 ks) XMM-Newton survey (the XMM/2dF survey). The surveyed area overlaps with the 2dF Galaxy Redshift Survey (2dFGRS) and therefore, high quality optical spectroscopic observations are available for all galaxies to ≤ 19.5 mag. We find that only <1 % of the X-ray detections are "normal" galaxies at the flux limit f(0.5-2 keV) ~ x 10^{-15} cgs. Also, using stacking analysis we estimate the mean X-ray properties (i.e. mean X-ray flux, X-ray-to-optical flux ratio) of 2dFGRS galaxies to z ~ 0.1. The implications of our results to the X-ray evolution of spiral galaxies are also explored.

* *Proceedings of the 6th Hellenic Astronomical Society Conference, 15-17 September 2003, Penteli, Greece*

MORPHOLOGICAL EVOLUTION OF THE MAGELLANIC CLOUD AND THE EFFECT ON STAR FORMATION *

M.Kontizas, P.Gavras
Section of Astrophysics Astronomy & Mechanics,
Department of Physics, University of Athens, GR-157 84 Athens, Greece
E.Kontizas
Institute of Astronomy and Astrophysics,
National Observatory of Athens, P.O Box 20048, GR-188 10 Athens, Greece

Introduction

The Magellanic Clouds are an ideal laboratory for studying the consequences of galaxy interactions on the formation and evolution of stellar populations. It is believed that they have been bound to the Galaxy for at least the last 10 Gyr (Murai & Fujimoto 1980; Fujimoto & Murai 1984), during which time significant interactions between the LMC and the SMC as well as between the Clouds and the Galaxy have led to structural and kinematical peculiarities (Westerlund, 1997). In particular, the structure of the SMC is considered to have been severely affected by the previous SMC perigalactic passage which coincided with a close encounter between the Clouds 1.5 Gyr ago, and also by the more recent close encounter between the Clouds some 0.2 to 0.4 Gyr ago (Gardiner & Noguchi 1996; Kunkel et al. 2000).

The LMC has also suffered a violent star formation event, which has created large star formation regions revealed in wide-field observations (Maragoudaki et al, 1998).

In order to understand better the star formation mechanisms that govern the galaxies, it is of vital importance to study their various large stellar structures and their spatial distribution. It is well known that there are various such systems from single to multiple ones, which are often related to the parent galaxy's morphology and are known as stellar complexes.

Stellar complexes are typical large-scale structures where recent star formation has occurred. They are dominated by recently formed stars, young stellar clusters, OB-associations and all kinds of young objects with ages up to 5x 10^8 yr, (Efremov & Chernin 1994; Elmegreen et al. 1994; Efremov 1989, 1995; Elmegreen and Efremov, 1996) and have dimensions of the order of 200-1200 pc. Kontizas et al. (1996) have examined selected regions in the LMC and showed that large stellar complexes can be revealed from star count and spectral classification of their stars. The detected structures are found with sizes within the expected values.

In this work we search for stellar complexes in the LMC and the SMC in order to study their morphology and their properties and examine how the complexes can give evidence of star formation mechanisms.

* *Proceedings of the 6th Hellenic Astronomical Society Conference, 15-17 September 2003, Penteli, Greece*

Observations

The large-scale structures in nearby galaxies require extended field observational material in order to be treated homogeneously. Therefore plates taken with the 1.2 m UK Schmidt Telescope are ideal tools to detect and map the stellar complexes in the LMC. We used direct photographic plates taken with the UK 1.2m Schmidt Telescope, in various wavebands: U, R and HeII (λ=4686Å) down to a magnitude limit of 19-20 mag for the LMC and U,V,I for the SMC (centered on $1^h\ 06^m$,-75.0^o). The plates cover an area of 60x60 in the plane of the sky. These plates were digitised using the fast measuring machines APM and SuperCosmos. Objective prism plates from the same telescope were also used, in order to investigate the distribution of early type stars. The main problem is then to deconvolve such spectral window from the observed power spectrum of the star to distinguish the real peaks from the aliases. We present a mathematical method that could be helpful in cases of very close real frequencies and very bad quality spectral window.

Reductions

The U plate is ideal for showing the young blue stars of the upper main sequence and the I plate provides a good picture of the old stellar component. The V plate is, of course intermediate between these showing both main sequence stars and large numbers of giants and supergiants. All the plates were digitised using the fast measuring machine SuperCOSMOS in Edinburgh and catalogues of detected images were generated. For the SMC we calibrated the instrumental stellar magnitudes for the U, V and the I plate.

The (U , U -V) and (V , V - I) colour magnitude diagrams were used to select different stellar populations, the main sequence and the red giants/supergiants.

We then divided the stellar catalogues into sub catalogues according to the apparent magnitude of the stars and population type Maragoudaki et al (2001). We assigned an age to each magnitude ``slice'' from the empirical CMD of main sequence stars (Zombeck 1990) as given by the U magnitude (after allowing for the distance modulus of the SMC m-M=19.0mag and m-M=18.5mag for the LMC according to Westerlund 1997). Using theoretical isochrones with various metallicities, we derived a range of ages which expresses the error given for each magnitude slice's age. The slice corresponding to the red giants was selected to represent stars older than 2 Gyr (Zombeck 1990). The derived isocontours for each slice display the spatial distribution of the stellar content at the determined time for the corresponding magnitude slice. The SMC and LMC morphological evolution are illustrated in Figs 1 and 2 respectively.

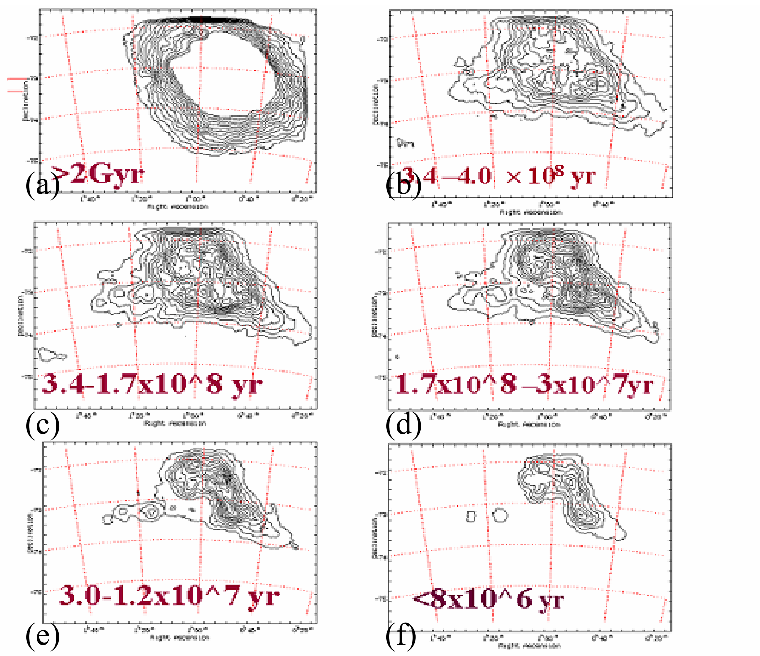

Fig 1 Isodensity contours of SMC a) giants $17<V<20$ and $0.4<V-I<-1.8$ b)MS stars with $19<U<20$ and $-0.4<U<1.2$ c) MS $18<U<19$ and $-0.8<U-V<0.7$ d) MS with $17<U<18$ and $-1.1<U-V<0.2$ e) MS with $16<U<17$ and $-13<U-V<-0.2$ and f)MS $U<15$ and $-1.5<U-V<-0.8$

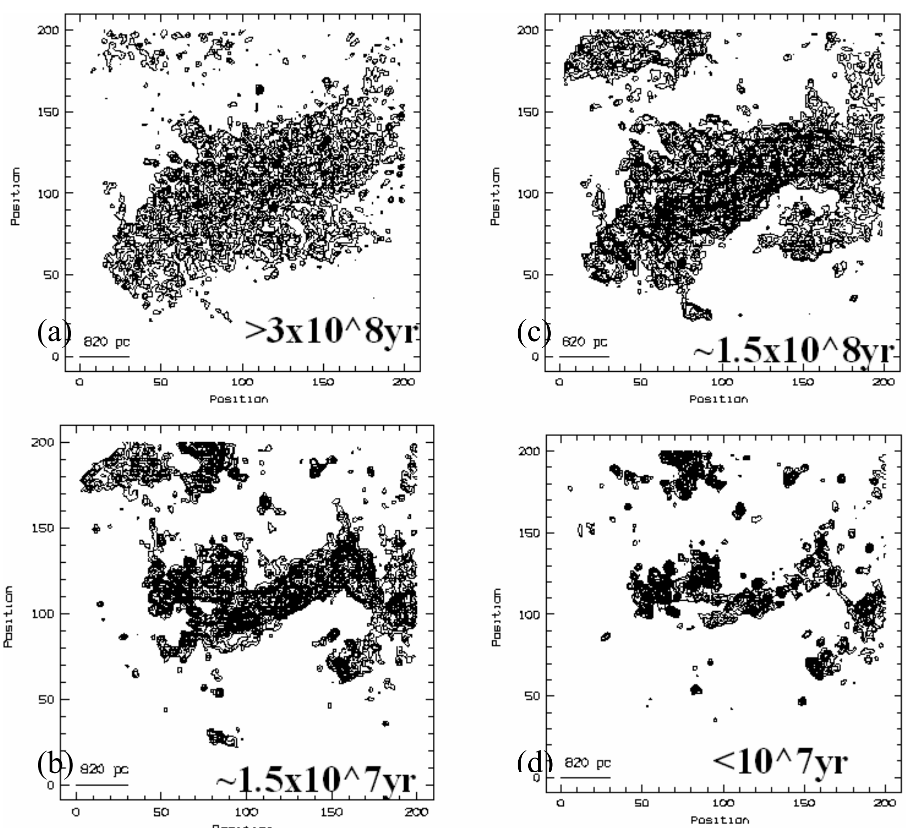

Fig 2 Isodensity contour map of LMC stars with a)$U>18.7$ and SpT ~B8-A0 b)$17<U<17.7$ and B7-B6 c)$16.4<U<15.2$ and B2-B4 and K ,M supergiants and d)$U<15.2$ and B1,B2 and G supergiants

Stellar Complexes

The star forming regions as revealed in this study are large stellar complexes mainly dominated by early type stars. We have examined the ones found in the LMC and in most cases these structures are found within each other and all of them contain the known LMC stellar associations (Lucke & Hodge, 1970). The known Shapley LMC Constellations (Shapley 1956) and the super-associations reported by Martin et al. (1976) have been found to be associated with the stellar complexes found here.

From the IRAS catalogues we calculated a total flux for each complex as the sum of the fluxes corresponding to the pixels, which cover the predetermined complex area. These total fluxes were corrected from the background.

Conclusions

From the morphological evolution of the LMC, SMC since $4x10^8$ yr to the present, the interaction of the LMC-SMC has produced:

In the SMC a bar-like structure which has taken shape about >> 10^7 yr ago. Whether the tidal tail and wing are formed during this interaction or earlier on it is not clear. If the formation of the bar is going on, then we have to accept that special geometry during the recent interaction has produced the slow-down of the angular velocity, giving an explanation on why we find no observational evidence of rotation in the SMC.

In the LMC it appears that at the same period intense star formation, started but it is obvious that the bar already existed as a feature in this galaxy. An earlier event may be responsible for the LMC bar formation, most probably the one that happened >>1-2 $x10^9$ yr ago and coincides with the approach of the LMC-SMC orbits with the Milky Way. The observed rotation in the LMC shows a normal rotating disc.

Acknowledgments.

The authors would like to thank CDS (Centre de Donnes Strasbourg), ULP (Universite Louis Pasteur), ELKE of the University of Athens and the General Secretariat of research & Technology for financial support

References

Efremov, Yu.N., 1989, Sov. Sci. Rev./Section E, 7, Part 2,
Efremov, Yu.N., 1995, AJ 110, 2757
Efremov, Yu.N., Chernin, A.D., 1994, Vistas in Astronomy, 38, 165
Elmegreen B.G. \& Efremov Yu.N., 1996, ApJ, 466, 802
Elmegreen D.M., Elmegreen B.G., Lang, C. \& Stephens, C., 1994, ApJ, 425, 57
Filipovic, M.D., Pietsch, W., Haynes, R.F. et al., 1998, A\&AS, 127, 119
Fujimoto, M., & Murai, T. 1984, in IAU Symp. 108, ed. S. van den Bergh, & K. S. de Boer (Reidel, Dordrecht), 115
Gardiner, L. T., & Noguchi, M. 1996, MNRAS, 278, 191
Haberl, F \& Pietsch, W., 1999, A\&AS, 139, 277

Kontizas, M., Maravelias, S.E., Kontizas, E., Dapergolas, A., Bellas- Velidis I. 1996, A&A, 308, 40
Kunkel, W. E., Demers, S., & Irwin, M. J. 2000, AJ, 119, 2789
Lucke, P.B., Hodge, P.W. 1970, AJ, 75, 171
Maragoudaki, F., Kontizas, M., Kontizas, E., Dapergolas, A., Morgan, D.H., 1998, A\&A, 338, L29.
Maragoudaki ,F., Kontizas, M., Morgan, D.H., et al., Kontizas, E., Dapergolas ,A., Livanou, E., 2001, A\&A, 379, 864.
Martin, N., Prevot, L., Rebeirot, E., Rousseau, J., 1976, A\&A, 51, 31
Murai, T., & Fujimoto, M. 1980, PASJ, 32, 581
Rowan-Robinson, M. \& Crawford, J., 1989, MNRAS, 238, 523
Rowan-Robinson, M., et al., 1997, MNRAS, 289, 490.
Sasaki, M., Haberl, F., Pietsch, W., 2000, A\&AS, 143, 391
Shapley, H. 1956, Amer. Scientist, 44, 73
Westerlund, B.E. 1997, The Magellanic Clouds, Camb. Astr. Ser., 29
Williams R., Murphy, R., Chu, Y., et al.,

The M64 Spiral Galaxy (the Sleeping Beauty). Picture of the Hubble Space Telescope

THE DYNAMICS OF MAGNETIZED GAMMA-RAY BURST OUTFLOWS*

Nektarios Vlahakis

Section of Astrophysics, Astronomy & Mechanics, Department of Physics, University of Athens

Abstract. According to the internal/external shock scenario, the GRB prompt/afterglow emission comes from the conversion of the kinetic energy of a highly relativistic multiple-shell outflow to nonthermal radiation, while – as it follows from afterglow fits – the outflow is collimated to opening angles of the order of a few degrees. The existence of a large-scale electromagnetic field, which is strongly supported by recent polarization measurements, is a natural way to explain both the acceleration and collimation of the flow. By using relativistic, axisymmetric, ideal MHD, we examine the motion of the baryon/electron-positron/photon fluid that emanates from a stellar-mass compact object/debris-disk system (a common outcome of many progenitor models). We demonstrate, through exact self-similar solutions, that the flow is first thermally and subsequently magnetically accelerated up to Lorentz factors >100 required in order to solve the compactness problem. Moreover, an initially neutron-rich outflow that undergoes decoupling between neutrons and protons at Lorentz factor <<100, could significantly alleviate the baryon contamination problem. We show that, in contrast to the hydrodynamic case, such a decoupling can occur in an MHD flow.

1. Introduction

It is generally accepted that the internal/external shock scenario provides an adequate explanation for the observed light curves of gamma-ray burst (GRB) prompt/afterglow emission. According to it, the central engine ejects a multiple-shell outflow. All the shells move practically with the speed of light (Lorentz factors $\gamma \sim 10^{2-3}$ required to evade the compactness problem). As a result, the distances between the shells remain constant and the pancake moves as a frozen pulse (constant width). Nevertheless, even small differences in the Lorentz factors of neighboring shells will end up in collisions. These are the internal shocks which – by converting the kinetic energy of the outflow to nonthermal radiation – produce the GRB prompt emission (also explaining the time variability). As the pancake continues to move and accumulate mass from the environment, gradually decelerates. The resulting external shock produces the afterglow. Moreover, the outflow is highly collimated to opening angles of the order of a few degrees (the collimation explains the panchromatic break in the afterglow light curves which happens when the beaming angle $1/\gamma$ equals the opening angle).

The most difficult problem is related to the progenitor; the central engine should be able to accelerate and collimate the flow, extracting energy $E \sim 10^{51}$ergs. The msec time variability and the highly relativistic motion suggest that a compact object is involved. Also, the two time scales (variability and total duration) and the energetics suggest accretion. Not surprisingly, a common outcome of many progenitor models is a stellar-mass compact object/disk system. The binding and the rotational energy of the system are available for extraction, and the question is how this can happen. One possibility is that a thermal fireball is formed (either by viscous dissipation or by dissipation of magnetic fields). The fireball expands under its own pressure, reaching final Lorentz factors

* *Proceedings of the 6th Hellenic Astronomical Society Conference, 15-17 September 2003, Penteli, Greece*

$\sim E/M_b c^2$, where M_b is the baryonic mass. This picture has several weak points: 1) It is difficult to explain the collimation. 2) The high luminosity implies high M_b, decreasing the final γ (the baryon contamination problem). 3) If the whole energy had been deposited as thermal fireball energy, the photospheric emission would have been detectable (contrary to the observations). The second and more promising possibility is magnetohydrodynamic (MHD) extraction, corresponding to an initial energy flux that is mainly Poynting.

2. The model

We examine the outflow originating from the vicinity of the compact object/disk system, taking into account baryonic matter, electrons (which neutralize the protons), $e^{\pm}$ pairs in thermodynamic equilibrium with photons, and large-scale electromagnetic field. Using ideal MHD the task is to solve the system consisting of the Maxwell and Euler equations together with the conservations of baryonic mass and specific entropy. We assume axisymmetry, highly relativistic poloidal motion ($V_p \approx c$) and steady poloidal magnetic field. This last assumption is equivalent to a zero toroidal electric field and implies that the poloidal streamlines and fieldlines coincide. Each shell that is ejected from the disk at time s/c, moves along a fieldline and at time t is located at a distance $\ell = \int_{s/c}^{t} V_p dt \approx ct - s$, which means that the distance between two shells $\ell_2 - \ell_1 = s_2 - s_1$ remains constant (this is the mathematical expression of the frozen-pulse approximation). The coordinate s can be used as a label for each shell. Eliminating t in terms of s we can show that all terms containing derivatives with respect to s are negligible compared with other terms in each MHD equation. For example, the operator d/dt can be written as $(c-V_p)\partial/\partial s + \mathbf{V}\cdot\nabla_s$, where ∇_s acts keeping s constant (i.e., following a particular shell). It is easily shown that $(c-V_p)\partial/\partial s \ll \mathbf{V}\cdot\nabla_s$, so we get the steady-state expression $d/dt = \mathbf{V}\cdot\nabla_s$. By doing this for all terms containing $\partial/\partial s$ (details can be found in Vlahakis & Königl 2003) we find the same mathematical forms as for the steady-state MHD equations.[8] It is well known that the steady MHD equations can be partially integrated to yield five fieldline constants: the mass-to-magnetic flux ratio, the field angular velocity, the specific angular momentum, the total energy-to-mass flux ratio μc^2, and the adiabat, all are functions of the poloidal magnetic flux function A. The only difference is that here, all these functions also have an s-dependence, allowing us to examine different initial conditions for each shell.

We integrate the two remaining equations (the Bernoulli and the transfield force-balance equations) following the r self-similar assumption $A = r^F f(\theta)$, where it is possible to separate the (r, θ) spherical coordinates.[9] The remaining task is to integrate ordinary differential equations and find solutions crossing the Alfvén and modified-fast magnetosonic singular points. A representative solution is shown in Figure 1. Looking at panel (a), which shows the acceleration, we distinguish three different regimes:

1) $\varpi_1 < \varpi < \varpi_6$ is the fireball phase. The specific enthalpy ξ decreases, resulting in increasing $\gamma \propto \varpi$ ($\xi\gamma \approx$const, a characteristic of hydrodynamic acceleration), while the specific Poynting flux remains constant (force-free field). The electromagnetic field only guides the flow; the significant part of the collimation happens in this regime.

8 The substitution $\nabla \rightarrow \nabla_s$ makes them physically different, though.

9 Our model is the "hot" generalization of the exact solution found independently by Li, Chiueh, & Begelman (1992) and Contopoulos (1994).

2) $\varpi_6<\varpi<\varpi_8$ is the magnetic acceleration regime. The fluid is cold ($\xi\approx1$), but γ continues to increase (close to $\gamma\propto\varpi$) due to the decreasing specific Poynting flux.
3) $\varpi=\varpi_8$ is the cylindrical asymptotic regime. The final Lorentz factor is of the order of the final specific Poynting flux, meaning that half of the total energy $\mu M_b c^2$ (which initially resides predominantly in the electromagnetic field) is transferred to baryonic kinetic energy, $\gamma_\infty\approx\mu/2$. Shell collisions can occur in this regime.

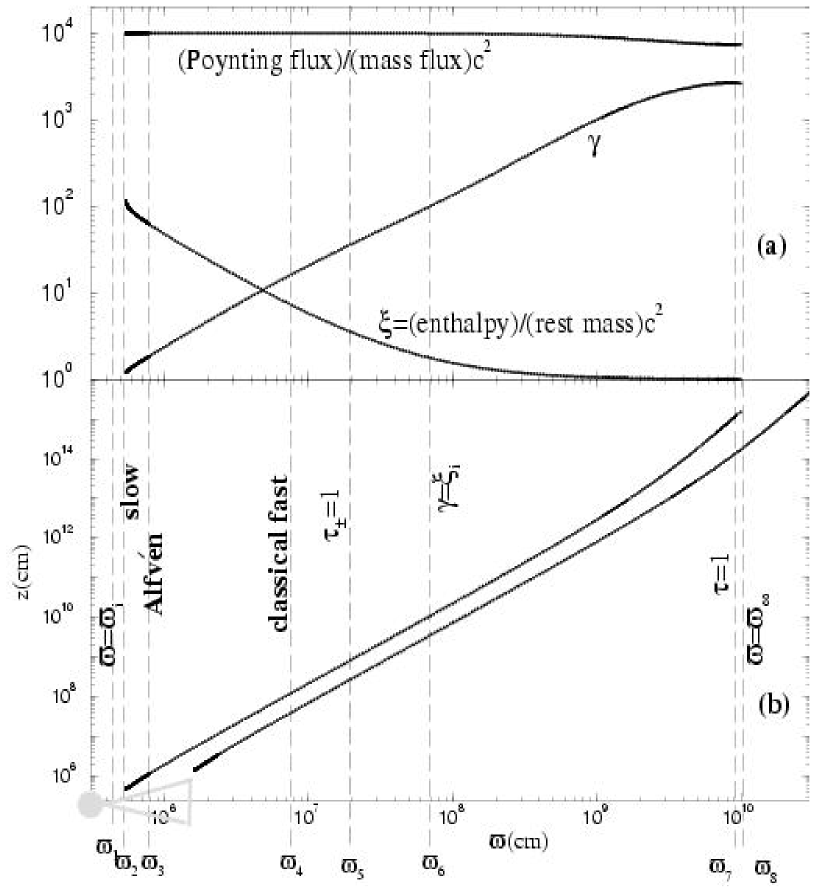

Figure 1. (a) The Lorentz factor γ, the ratio ξ of the enthalpy to the rest energy, and the ratio of the Poynting flux to the rest-energy flux (*top* curve) are shown as functions of ϖ, the distance from the axis of rotation, along the innermost fieldline. (b) The meridional projections of the innermost and outermost fieldlines are shown on a logarithmic scale, along with a sketch of the central object/disk system. The fieldlines have parabolic shape $z\propto\varpi^2$ for $\varpi\leq10^9$cm and become asymptotically cylindrical. The vertical lines mark the positions of the various transition points along the innermost fieldline (details can be found in Vlahakis & Königl, 2001).

The presented solution concerns one particular shell, corresponding to one specific value of s. By giving s-dependence in the initial conditions we may examine the whole pancake and recover the time dependence of the pulse. For example, the s-dependence in the total energy-to-mass flux ratio $\mu(s)c^2$ corresponds to differences in the final Lorentz factors of the various shells $\gamma_\infty(s)\approx\mu(s)/2$.
Summarizing, we found that the flow is first thermally and subsequently magnetically accelerated. Contrary to the Michel's (1969) solution, here the fieldline shape is nonradial and the classical fast magnetosonic point is located at a finite distance. The bulk of the magnetic acceleration happens after that point, and asymptotically $\gamma_\infty(s)\approx\mu(s)/2>>\mu(s)^{1/3}$. Thus, not only the magnetic acceleration is close to ~50% efficient, but also the stronger dependence of $\gamma_\infty(s)$ on the initial conditions – through $\mu(s)$ – can lead to larger $\Delta\gamma_\infty$, increasing the internal shocks efficiency. The self collimation (which happens relatively close to the source) is consistent with the observational indications for GRB jets and could be very helpful in reducing the source energy requirements to plausible values. Thus, the observationally inferred properties of GRB outflows can be attributed to magnetic driving.

3. Neutron-rich outflows

A promising proposal to alleviate the baryon loading problem (how the baryon loading of the jets remains so low even as the energy deposition in the flow is highly efficient) was made by Fuller et al. (2000), who suggested that, if the source of the outflow is neutron-rich, then the neutrons (which are only very weakly affected by the electromagnetic field and are accelerated primarily by collisional drag with ions) could in principle decouple from the flow before the protons attain their terminal Lorentz factor. If the mass source for the flow is a neutron star then it will clearly be neutron-rich, and this is the case also for outflows fed by a black hole debris disk (Pruet at al. 2003). However, it turns out that the decoupling Lorentz factor γ_d in a purely hydrodynamic outflow is of the order of the inferred value of γ_∞, which has so far limited the practical implications of the Fuller et al. (2000) proposal. Vlahakis et al. (2003) demonstrated that in a *hydromagnetic* neutron-rich outflow neutron decoupling can occur with $\gamma_d \ll \gamma_\infty$ (see fig. 2).

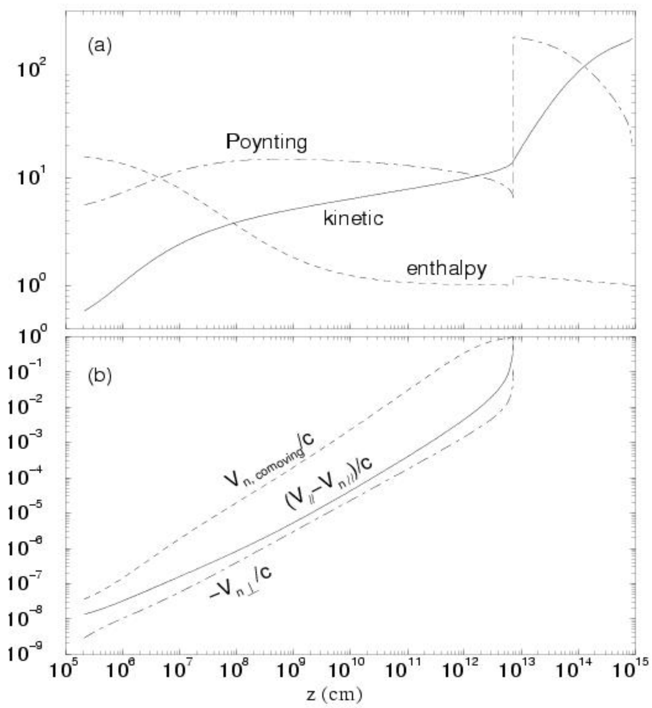

*Figure 2. S*olution for a neutron-rich outflow with neutron-to-proton mass ratio ρ_{0n}/ρ_{0p} =30. (a) The three components of the total energy flux, normalized by the mass flux $\times c^2$: kinetic (=γ-1; *solid*), enthalpy (*dashed*), and Poynting (*dot-dashed*), *vs* height (z) along the innermost fieldline. Decoupling occurs at a Lorentz factor $\gamma_d \approx 15$ in the presented example, a value that is significantly lower than the terminal γ of the protons γ_∞= 200. The Poynting and enthalpy curves are discontinuous at the decoupling point, where the mass flux decreases by a factor 1+ ρ_{0n}/ρ_{0p}. (b) Proton-neutron drift velocity along the poloidal magnetic field (*solid*), in the transfield direction (*dot-dashed*), and in the comoving proton frame (*dashed*).

In the presented solution the total baryonic mass is $\sim 10^{-4} M_\odot$ (although a significant part of the energy $E \sim 10^{51}$ergs is carried by the much fewer protons after the decoupling). This could significantly alleviate the baryon-loading problem in GRB source models.

References

Contopoulos, J. 1994, ApJ, 432, 508
Fuller, G. M., Pruet, J., & Abazajian, K. 2000, Phys. Rev. Lett., 85, 2673
Li, Z.-Y., Chiueh, T., & Begelman, M.C. 1992, ApJ, 394, 459
Michel, F. C. 1969, ApJ, 158, 727
Pruet, J., Woosley, S. E., & Hoffman, R. D. 2003, ApJ, 586, 1254
Vlahakis, N., & Königl, A. 2001, ApJL, 563, L129
Vlahakis, N., & Königl, A. 2003, ApJ, 596, 1080
Vlahakis, N., Peng, F., & Königl, A. 2003, ApJL, 594, L23

DETERMINING ACCURATE DISTANCES TO NEARBY GALAXIES*

Alceste Bonanos

Harvard-Smithsonian Center for Astrophysics, 60 Garden St., Cambridge, MA 02138

ABSTRACT

We have undertaken several projects with the purpose of determining accurate distances to nearby galaxies to calibrate the extragalactic distance scale. Specifically, I describe the DIRECT project which aims to derive the distance to M31 and M33 directly, using detached eclipsing binaries and the Baade-Wesselink method for Cepheids. I also present a ``hybrid'' method of discovering Cepheids with ground-based telescopes using image subtraction and then following them up with the *HST* to derive Cepheid period-luminosity distances.

1. Introduction

Distances to extragalactic objects are known with an accuracy of less than 10-15%. This is due to the fact that standard candles available to astronomers are not completely understood theoretically and most importantly, that there are large uncertainties in the current anchor galaxy of the extragalactic distance scale, the Large Magellanic Cloud (LMC). Cepheids are examples of such distance indicators: the periods of Cepheid variables are tightly correlated with their luminosities. The correlation seems to depend on metallicity, but this dependence is not well understood and is controversial. Also, the distances to the LMC obtained with the same technique but different calibrations disagree (see Benedict et al. 2002, Figure 8). The LMC has the advantages of being nearby and easy to observe, however it introduces problems as the anchor galaxy for the extragalactic distance scale. The sources of systematic error associated with the LMC include the differential reddening across the LMC, the elongation along the line of sight, the metallicity of the galaxy and the zeropoint of the Cepheid period-luminosity (PL) relation.

The uncertainty in the LMC distance not only translates into uncertainty in the Hubble constant, but also in the calibration of stellar luminosities and in constraining population synthesis models for early galaxy formation and evolution. We therefore propose to use other nearby galaxies, such as M31 and M33, as anchors of the extragalactic distance scale bypassing the LMC and the systematic errors associated with it.

2. Hybrid Method for Measuring Distances

We have proposed a "hybrid"approach for obtaining distances to nearby galaxies with Cepheids (Bonanos & Stanek 2003). Cepheids in nearby galaxies can be discovered

---

* *Proceedings of the 6th Hellenic Astronomical Society Conference, 15-17 September 2003, Penteli, Greece*

and characterized using large ground-based telescopes and then followed-up with the *HST* to obtain precise distances. We demonstrated this by re-analyzing the excellent 8.2 meter VLT data of M83, obtained by Thim et al. (2003), using the image subtraction method.

Blending must be taken into account in deriving the Cepheid distance to nearby galaxies. For example, at the distance of M83 which is ~4.5 Mpc (Thim et al. 2003), the median seeing of 0.76" of the VLT data corresponds to 17 pc. As first discussed by Mochejska et al. (2000), blending is the close association of a Cepheid with one or more intrinsically luminous stars, which is the result of the higher value of the star-star correlation function for massive stars, such as Cepheids, compared to random field stars. This effect cannot be detected within the observed PSF by usual analysis. In M83, a large fraction of the flux of a blended Cepheid could come from its companions and would result in a significant distance bias. The discovery of Cepheids in nearby galaxies can be done adequately from the ground given good signal-to-noise photometry; however, deriving the Cepheid PL distance requires high spatial resolution *HST* imaging.

With the image subtraction package ISIS (Alard & Lupton 1998; Alard 2000), we were able to detect 112 Cepheids, a nine-fold increase compared to the number detected by Thim et al. (2003) with the ``traditional" method of PSF photometry. We therefore demonstrate the power of image subtraction, which should especially be used in crowded fields. These additional Cepheids are valuable for determining the PL distance to M83 accurately. However, HST observations are necessary to resolve blending effects.

3. The DIRECT Project

Starting in 1996 we undertook a long term project, DIRECT (i.e. ``direct distances"), to obtain the distances to two important galaxies in the cosmological distance ladder, M31 and M33. These ``direct" distances will be obtained by determining the distance to Cepheids using the Baade-Wesselink method and by measuring the absolute distance to detached eclipsing binaries (DEBs). DEBs
(for reviews see Andersen 1991; Paczynski 1997) offer a single step distance determination to nearby galaxies and have the potential to establish distances to M31 and M33 with an unprecedented accuracy of 5%. However, DEBs are not easy to detect since they are intrinsically rare objects (massive unevolved stars) and only certain configurations produce eclipses. Now that large-format CCD detectors are available and that CPUs are inexpensive, the DIRECT project has undertaken a massive search for periodic variables, which is producing some good DEB candidates.

We have so far analyzed observations taken with the 1.2 meter FLWO telescope of six fields in M31, A-D, F (Papers I-VI, Kaluzny et al. 1998, 1999; Stanek et al. 1998, 1999; Mochejska et al. 1999; Macri et al. 2001) and recently field Y (Paper IX, Bonanos et al. 2003). A total of 674 variables, mostly new, were found in M31: 89 eclipsing binaries, 332 Cepheids, and 253 other periodic, possible long-periodic or non-periodic variables. We have analyzed two fields in M33, A and B (Paper VI, Macri et al. 2001) and found 544 variables: 47 eclipsing binaries, 251 Cepheids and 246 other variables. Follow up observations with the 2.1 meter KPNO telescope of fields M33A and M33B produced 280 and 612 new variables, respectively (Papers VII-VIII, Mochejska 2001a, 2001b).

Of the ~130 eclipsing binaries, we have found 4 DEB systems suitable for follow-up spectroscopy, 2 in M31 and 2 in M33. In October 2002, we obtained spectra of the two systems in M33 with ESI on Keck-II but did not have enough phase coverage (see Figure 1) to derive the radial velocity amplitude accurately. However, we concluded that M33A is a resolved double line eclipsing binary of early B type that is suitable for distance determination and obtained spectra with ESI on 3 more nights in September 2003. Deriving a radial velocity curve is challenging, because early type stars have few absorption lines in the visible part of the spectrum, which are often broadened and blended. We are currently analyzing these spectra and will soon have the first direct measurement of the distance to M33.

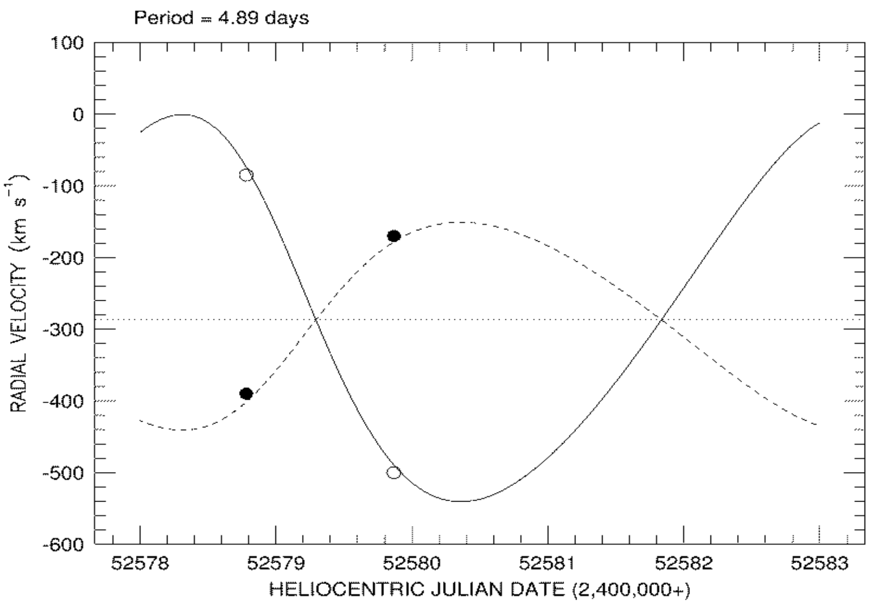

Fig. 1.- Radial velocity curve for the 4.89 day period DEB M33A, from two nights of data on Keck-II in October 2002.

We have also undertaken the first CCD variability study of the Draco dwarf spheroidal galaxy with the FLWO 1.2 m telescope, producing 163 variable stars, 146 of which were RR Lyrae (Bonanos et al. 2004). Using the short distance scale statistical parallax calibration of Gould & Popowski (1998) for 94 RRab detected in our field, we obtained a distance modulus of $(m-M)_0$ =19.40 +/- 0.02 (stat) +/- 0.15 (syst) mag, corresponding to a distance of 75.8 +/- 0.7 (stat) +/- 5.4 (syst) kpc to the Draco dwarf spheroidal galaxy.

4. Summary

The need for a new anchor galaxy or preferably for several anchor galaxies to calibrate the extragalactic distance scale is long overdue. The systematic effects introduced by using the LMC as the anchor galaxy can be avoided now that 10-meter class telescopes have become available. Large telescopes can be used for the detection of Cepheids from the ground and later followed-up with the *HST* to obtain accurate distances, as demonstrated in M83. The DIRECT project will determine geometric distances to M31 and M33 with an accuracy of 5% with DEBs and the Baade-Wesselink method for Cepheids. Both of these Local Group galaxies are excellent anchor galaxies for the calibration of the extragalactic distance scale.

REFERENCES

Alard, C., & Lupton, R. 1998, ApJ, 503, 325
Alard, C. 2000, A&AS, 144, 363
Andersen, J. 1991, A&AR, 3, 91
Benedict, G. F., McArthur, B. E., Fredrick, L. W., Harrison, T. E., Lee, J., Slesnick, C. L., Rhee, J., et al. 2002, AJ, 123, 473
Bonanos, A.Z., & Stanek, K.Z. 2003, ApJ, 591, L111
Bonanos, A.Z., Stanek, K.Z., Sasselov, D.D., Mochejska, B.J., Macri, L.M., & Kaluzny, J. 2003, AJ, 126, 175
Bonanos, A.Z., Stanek, K.Z., Szentgyorgyi, A.H., Sasselov, D.D., Bakos, G.A. 2004, AJ, *in press*
Gould, A., & Popowski, P. 1998, ApJ, 508, 844
Kaluzny, J., Stanek, K.Z., Krockenberger, M., Sasselov, D.D., Tonry, J.L., Mateo, M. 1998, AJ, 115, 1016 (Paper I)
Kaluzny, J., Mochejska, B.J., Stanek, K.Z., Krockenberger, M., Sasselov, D.D., Tonry, J.L., Mateo, M. 1999, AJ, 118,346 (Paper IV)
Macri, L.M., Stanek, K.Z., Sasselov, D.D., Krockenberger, M., Kaluzny, J. 2001, AJ, 121, 870 (Paper VI)
Mochejska, B.J., Kaluzny, J., Stanek, K.Z., Krockenberger, M., Sasselov, D.D. 1999, AJ, 118, 2211 (Paper V)
Mochejska, B.J., Macri, L.M., Sasselov, D.D., & Stanek, K.Z. 2000, AJ, 120, 810
Mochejska, B.J., Kaluzny, J., Stanek, K.Z., Sasselov, D.D., Szentgyorgyi, A.H. 2001a, AJ, 121, 2032 (Paper VII)
Mochejska, B.J., Kaluzny, J., Stanek, K.Z., Sasselov, D.D., Szentgyorgyi, A.H. 2001b, AJ, 121, 2032 (Paper VIII)
Paczynski, B. 1997, in The Extragalactic Distance Scale, ed. M. Livio, M. Donahue & N. Panagia (Cambridge: Cambridge Univ.Press), 273
Stanek, K.Z., Kaluzny, J., Krockenberger, M., Sasselov, D.D., Tonry, J.L., Mateo, M. 1998, AJ, 115, 1894 (Paper II)
Stanek, K.Z., Kaluzny, J., Krockenberger, M., Sasselov, D.D., Tonry, J.L., Mateo, M. 1999, AJ, 117, 2810 (Paper III)
Thim, F., Tammann, G.A., Saha, A., Dolphin, A., Sandage, A., Tolstoy, E., & Labhardt, L. 2003, ApJ, 590, 256

STUDY OF NONRELATIVISTIC AND RELATIVISTIC MHD JETS*

M. Lazaridis[1], C. Sauty[2], N. Vlahakis[1] and K. Tsinganos[1]

[1]Section of Astronomy, Astrophysics and Mechanics, Department of Physics, University of Athens, [2]Observatoire de Paris, Meudon, France.

Abstract

We model non-relativistic, meridionally self-similar outflows from a gravitating central object. Physical quantities, such as the Alfvén Mach number, the shape of the magnetic field and flow lines, the density, etc, are plotted and discussed, from the base of the outflow to infinity. These solutions can be applied, e.g., to jets from Young Stellar Objects.
We also model relativistic, radially self-similar disk-wind outflows. Physical quantities, such as the shape of the field and flow lines, the Lorentz factor and the density are plotted and discussed in the context of Gamma-Ray Bursts & Jets from Active Galactic Nuclei.

Main assumptions for obtaining analytical solutions:

- Ideal MHD, stationary equilibrium $\partial/\partial t = 0$.
- An MHD outflow may be described to a first approximation as an inviscid, compressible plasma of infinite conductivity.
- Axisymmetric outflow configurations, $\partial/\partial\varphi = 0$, in spherical ($r,\theta,\varphi$) and cylindrical ($z,\varpi,\varphi$) coordinates. A magnetic flux function A is introduced in terms of which the poloidal magnetic field is defined:

$$B_p = \nabla \times \left(\frac{A}{r\sin\theta} \mathbf{e}_\varphi \right) = \frac{\nabla A}{\varpi} \times \mathbf{e}_\varphi ,$$

  and a stream function Ψ_A, in terms of which we define the poloidal mass flux:

$$4\pi\rho \mathbf{V}_p = \nabla \times \left(\frac{\Psi}{r\sin\theta} \mathbf{e}_\varphi \right) = \frac{\nabla \Psi_A}{\varpi} \times \mathbf{e}_\varphi .$$

- The total angular momentum (L), mass-to-magnetic flux ratio (Ψ_A), and corotation frequency (Ω) are constant along magnetic flux surfaces $A=$const. Define $\alpha = \varpi_\alpha^2 / \varpi^2 = L/\varpi_o^2\,\Omega$, where ϖ_α is the cylindrical distance of the Alfvén point from the symmetry axis in each line and ϖ_o is constant.

* *Proceedings of the 6th Hellenic Astronomical Society Conference, 15-17 September 2003, Penteli, Greece*

Use the Alfvén Mach number M, and A as the *natural* variables and switch from poloidal coordinates (r,θ) to poloidal coordinates (M,α). Consider M and the cross-section of the outflow $G = \varpi/\varpi_\alpha$ as functions of a single variable χ :

$$M = M(\chi), \quad G = G(\chi).$$

This unifying scheme contains two large groups of exact MHD outflow models:

- $\chi \to r$: *meridionally* self-similar models with *spherical* critical surfaces and with prototype the Sauty & Tsinganos (1994) model

$$A \propto [r\sin\theta / G(r)]^2 ,$$

- $\chi \to \theta$: *radially* self-similar models with *conical* critical surfaces and with prototype the Blandford & Payne (1982) model,

$$A \propto [r\sin\theta / G(\theta)]^F ,$$

$F = $ const.

I. <u>Nonrelativistic Solutions</u>

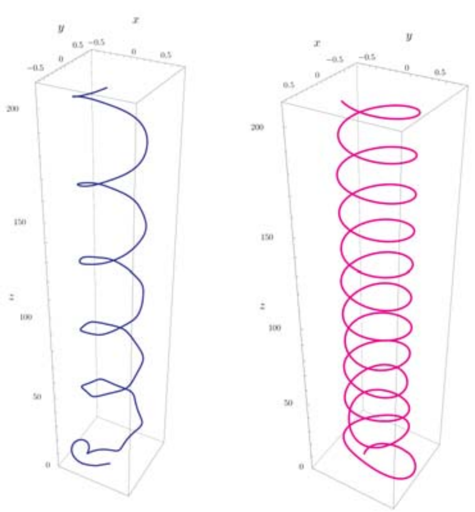

(a) (b)

Figure 1: (a) The 3D magnetic field line, (b) The 3D flow line. Space coordinates are measured in units of Alfvén radius. In the magnetic field line, oscillations of the poloidal field/flow produce "knees" near the beginning of the outflow. Away, both field and flow lines become cylindrical (collimation).

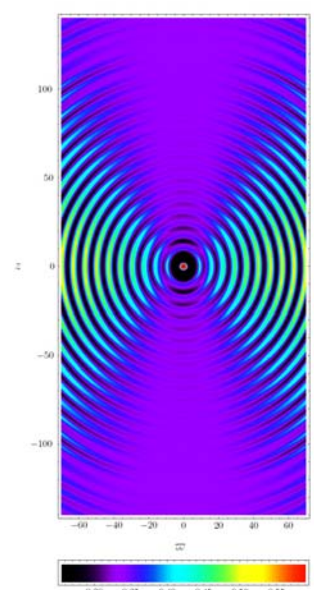

Figure 2: Density on the poloidal plane. Space coordinates are measured in units of Alfvén radius and density in units of Alfvénic density (density at the Alfvén radius). The outflow is less dense near the z-axis; this is a ``hollow''-jet model. Also, oscillations are evident.

1. The density can be written as a function of *α*,

$$\rho(r,\alpha)=\frac{\rho_*}{M^2(r)}(1+\delta\alpha),$$

where *δ* is a constant.

2. The pressure can be written in a similar way,

$$P(r,\alpha)=\frac{\rho_* V_*^2}{2}\Pi(r)(1+\kappa\alpha) \qquad .$$

The velocity of the flow and the magnetic field can be expressed as functions of the above quantities. For the three unknown functions, Π, G and *M*, three ordinary differential equations exist. These are quite complicated but they can be integrated numerically. Singular points occur though, and the integration must be done with caution.

II. Relativistic Solutions

1. The specific enthalpy ξ, which is defined in (Vlahakis & Konigl 2003),

$$\xi c^2 = c^2 + 4\frac{P}{\rho_o},$$

is a function of θ alone and ρ_o is the commoving matter density.

2. The plasma expansion is polytropic, with index 4/3, $P \propto \rho_o^{4/3}$,

For the magnetic field line:

$$\frac{\varpi d\phi}{B_\phi}=\frac{dz}{B_z}\Rightarrow dz=\frac{B_z\varpi}{B_\phi}d\phi.$$

But from the plots in figure 3:

$$\frac{B_z\varpi}{B_\phi}\propto\frac{\sqrt{z}\sqrt{z}}{z}=1\Rightarrow\frac{B_z\varpi}{B_\phi}=const.$$

so $d\phi / dz = const$ and the helix has a constant step.

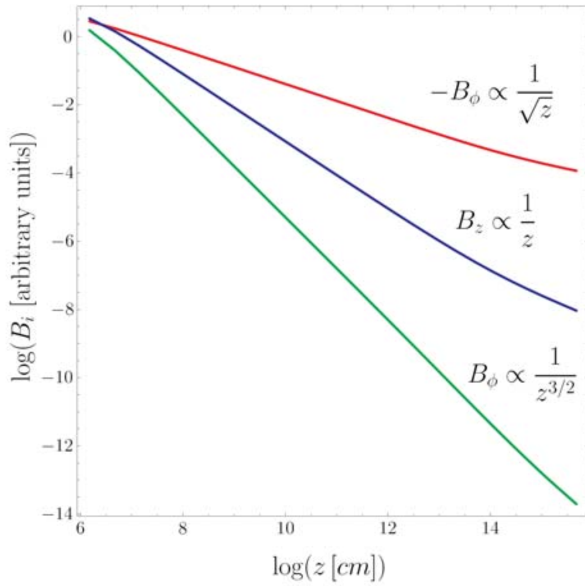

Figure 3:

Three components of the magnetic field along a poloidal field line (α =const) as a function of z. Notice that dependence of the components as functions of z.

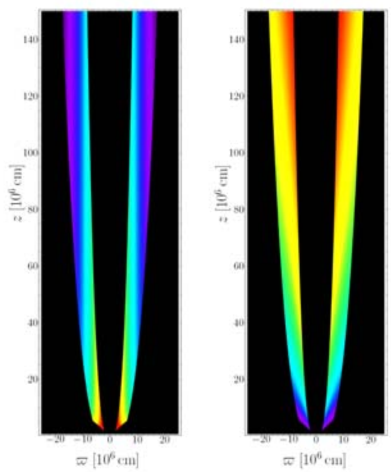

(a) (b)

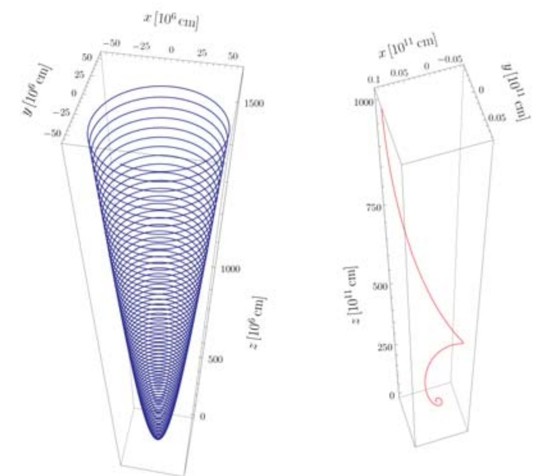

(a) (b)

Figure 4: (a) The density on the poloidal plane. (b) The Lorentz factor on the poloidal plane. Notice that both density and Lorentz factor are higher near the axis of the jet. (c) Profile of Lorentz factor in a cross-section of the jet (z=1.5). The material is more energetic in the center of the jet.

Figure 5: (a) The 3D magnetic field line. Notice that the step of the helix is constant in the magnetic field line (This is proved in poster). (b) The 3D flow line.

Bibliography

1. Blandford, R. D. & Payne, D. G. 1982, MNRAS, 199, 883
2. Sauty, C. & Tsinganos, K. 1994, A&A, 287, 893
3. Vlahakis, N. & Königl, A. 2003, ApJ, 596, 1080

DARK MATTER IN GALAXIES*

A.Bosma

Observatoire de Marseille, 2 Place Le Verrier, 13248 Marseille Cedex 4, France

Abstract: I discuss the observational side of the present state of the debate about the dark matter in galaxies, with emphasis on the core/cusp problem in low surface brightness galaxies.

1. The core/cusp problem in LSB galaxies

The WMAP results (Spergel et al. 2003) support the ΛCDM model for structure formation in the Universe, and underscore the need to understand galaxies in the framework of this theory. However, at the scale of galaxies, the "predictions" of the ΛCDM model depend on numerical simulations, which, despite their sophistication, suffer from inadequate resolution, and may miss some of the physics. Cosmological numerical simulations invariably produce cuspy dark halos, but the precise value of the inner slope α of the radial density profile $\rho \sim r^{\alpha}$ is debated. Moore et al. (1999) and Fukushige & Makino (2001) advocate α = -1.5, and Navarro, Frenk & White (1996, 1997) α = -1.0. New work by Hayashi et al. (2003) shows that there is no real convergence towards a unique value of the inner slope, the resolution prohibits predictions to be made inside a radius of ~ 1 kpc, but the pro_le remains cuspy, and there is some cosmic scatter (cf. also Fukushige et al. 2003). This new situation differs from a widespread perception until recently that the NFW profile, with inner slope -1.0, should be considered "universal", and the yardstick against which the observations should be discussed.

The observations in question are those of rotation curves and their associated mass models of low surface brightness galaxies, which are thought to be dark matter dominated, even in their inner parts (e.g. Bosma 2003). The radial density pro_les of these galaxies can thus directly be compared with those resulting from the cosmological numerical simulations. I will use the slope -1.0 here as a _ducial mark to see where the observations stand, and which is to be improved as the cosmological numerical simulations become more realistic, and better understood theoretically.

2. Inner slope values : technical and selection issues

Most observers conclude that α in LSB galaxies is closer to 0.0 than to -1.0, and almost all find that the decomposition mass models work better if the dark halo is modeled with a (pseudo-) isothermal sphere, rather than with the NFW profile. However, some authors maintain that the problem of determining the inner slope is fraught with systematic effects, which all contribute towards shallower slopes. The issue debated is not only about the best value for the inner slope, but also whether a slope of -1.0 can be excluded, so as to force a change of the ΛCDM picture at galaxy scales. On the selection side the

* *Proceedings of the 6th Hellenic Astronomical Society Conference, 15-17 September 2003, Penteli, Greece*

debate is about the quality and relevance of the data. As more galaxies are observed, stricter selection criteria are used to retain only galaxies with sufficiently "good" data. Thus one excludes 1) galaxies with poor angular resolution, requiring in most cases supplementary Ha data in addition to a HI rotation curve, so that the inner 1 kpc of a galaxy is well probed. This excludes galaxies far away or galaxies for which there is only low resolution HI data, and minimizes slit width effects; 2) edge-on galaxies, which are apparently too difficult to understand for some workers in the field, despite the findings by Bosma et al. (1992) and Matthews & Wood (2001) that small edge-on galaxies are transparent and have rotation curves which are slowly rising in the inner parts. The argument that somehow there is no emission at the tangent point leads to very peculiar Ha distributions in more face-on galaxies which are yet to be seen; 3) galaxies with large asymmetries, faint emission, etc., which have low quality rotation curves. De Blok, Bosma & McGaugh (2003) applied these criteria to data of McGaugh et al. (2001) and De Blok & Bosma (2002), and find for a restricted sample that the values of the inner slope are between 0.2 and -1.0. Swaters et al. (2003a), in a similar study, come to a similar conclusion. De Blok et al. (2003) also report about deliberate slit offsets and misalignments for one galaxy, UGC 4325, and conclude that these effects could not magically bring the slope from about -0.2 to -1.0, although of course scatter is introduced if the major axis is not observed correctly. Finally, for several galaxies there are more than one observation, done with different telescopes, and by different observers. Even though the error bars are sometimes unsatisfactory large, there is good agreement in general.

3. Inner slope values: astrophysical issues

There are also debates about the determination of the kinematical center, and the influence of non-circular motions on the rotation curves.

The rather irregular nature of some of the dwarf or LSB galaxies studied, and the faintness of particularly the near-infrared images makes the determination of the center of such galaxies difficult. Interestingly, HST data on central star clusters in late type spirals is available for a number of the galaxies used in the core/cusp studies, and comparison of these positions and the centers of the inner disks show agreement to ~ 1" – 2" (Böker et al. 2002).

For the galaxy IC 2574, I reanalyzed the HI data obtained by Walter & Brinks (1999), and deliberately varied the position of the center. In some cases I also carved up the galaxy into annuli, and allowed the center of each annulus to vary with respect to the next one. Despite the variation of the center positions with an r.m.s. scatter of about 250 pc, the determined slopes come out to be -0.15 ± 0.38, well away from the fiducial NFW slope of -1.0.

Bars could contribute to non-circular motions in the inner parts, thus leading to a poor quality rotation curve when long slit data are used, but also if a two-dimensional velocity field is not properly analyzed. Swaters et al. (2003a) assert that bars in their long slit data sample predominantly have shallow slopes, but inspection shows that UGC's 2259, 4499, and 5721, as well as F568-3 are also barred, in addition to the galaxies they identify as such. For the remaining unbarred galaxies, there is a wide variety of slopes. Swaters et al. (2003b) observe the galaxy DDO 39 with an integral field spectrograph permitting the construction of a twodimensional velocity _eld, which shows that the inner parts of this galaxy are affected by non-circular motion caused by a bar-like distortion. Several other studies of twodimensional Ha velocity _elds are underway. Garrido et al. (2002) report on data obtained with a Fabry-P´erot instrument, and Simon et al. (2003) report on Hα data obtained with an integral _eld spectrograph, combined with CO data obtained with BIMA. The results for NGC 4605 and NGC 2976 are that the inner slopes are rather shallow, and that the non-circular motions are mainly in the inner parts.

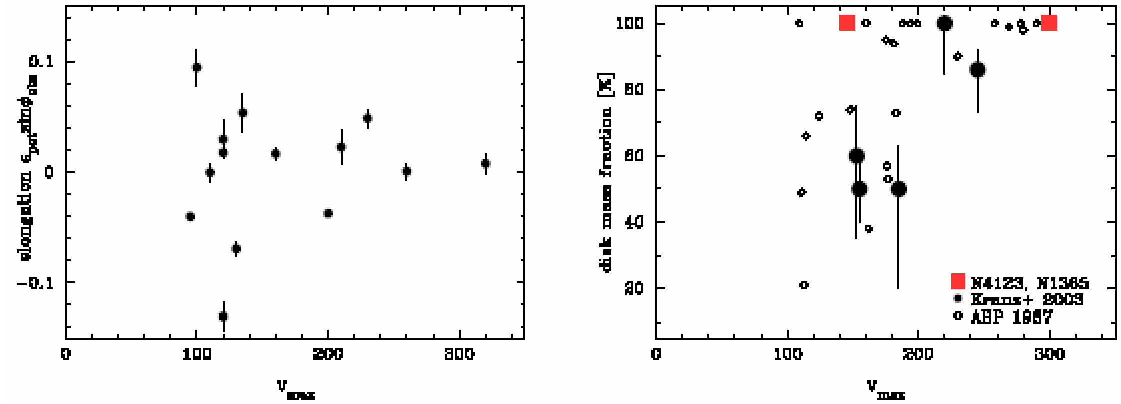

Figure 1: a) Disk elongation as function of Vmax, data extracted from Schoenmakers (1999). b) Disk mass fraction as function of Vmax, data from Kranz et al. (2003) with N4123 (left) and N1365 added. Faster rotators seem to have rounder disks, which are more self-gravitating.

One can look at bars in LSB galaxies in two ways: 1) they could be similar to bars in HSB galaxies, or 2) they could be just the response to the expected triaxiality of the dark halo. Since the reported non-circular motions are stronger in the inner parts for DDO 39 and NGC 2976, it seems likely that those galaxies behave like HSB's, where the disk is dynamically important in the inner parts. Yet it cannot be excluded that whole disks are elongated due to the triaxial halo. One way to study this further is to look at results of a Fourier analysis of velocity fields of a number of galaxies, performed by Schoenmakers (1999). From his work I have collected the results on disk elongation, which shows that the scatter in ε_{pot} sinφ is larger for galaxies with smaller maximum rotation velocity (see Figure 1a). Thus disks in small galaxies could be globally elongated due to the forcing of a triaxial halo.

In future, the effort will thus shift towards evaluating the importance of the disc component in LSB galaxies, using near-infrared surface photometry, and two dimensional velocity fields at high spatial resolution. Meanwhile, some evaluation of the importance of non-circular motions can be had by studying bars in HSB galaxies. Disk elongation can be constrained using the Tully-Fisher relation (Franx & de Zeeuw 1992). Early work on the barred spiral NGC 5383 (Athanassoula 1984) shows that the viewing angle is important: some angles are more favourable than others. Neither the mean rotation curve, nor the position velocity cut along the major axis can be trusted as a good representation of the true rotation curve, but the deviations scale with the strength of the bar. For the weak bars in LSB galaxies, it is not obvious how strong these effects are.

4. The importance of disk self gravity in HSB spirals

The so-called "maximum disk" problem is related to the core/cusp problem, since in the current LCDM picture the dark halo dominates the potential in the central parts also in high surface brightness spirals. Several ways have been explored to break the mass model degeneracy using other dynamical considerations concerning the importance of the disk in the inner parts of spiral galaxies. These have been discussed in Bosma (2003), and the reader is referred to that paper for further details. I have collected the main conclusion from these studies in Figure 1b, where I plot the disk mass fraction (the mass ratio between a given disk model and the maximum disk model) as function of V_{max} determined recently by Kranz et al. (2003), who compared their extensive modelling with previous work using swing amplifier criteria by Athanassoula et al. (1987). The overall conclusion of Figure 1 is that faster rotators have rounder disks, which are more self-gravitating.

Acknowledgements. I thank Lia Athanassoula for frequent discussions, and Erwin de Blok and Stacy McGaugh for fruitful joint work on LSB galaxies.

References:

Athanassoula, E. 1984, Physics Reports, 114, 319
Athanassoula, E., Bosma, A., & Papaioannou, S. 1987, A&A, 179, 23
Böker, T., et al. 2002, AJ, 123, 1389
Bosma, A. 2003, astro-ph/0312154
Bosma, A., Byun, Y.I, Freeman, K.C., & Athanassoula, E. 1992, ApJ, 400, L21
de Blok, W.J.G., & Bosma, A. 2002, A&A, 285, 816
de Blok, W.J.G., Bosma, A., & McGaugh, S.S. 2003, MNRAS, 340, 657
Franx, M., & de Zeeuw, P.T. 1992, ApJ, 392, L47
Fukushige, T., & Makino, J. 2001, ApJ, 557, 533
Fukushige, T. Kawai, A., & Makino, J. 2003, astro-ph/0306203
Garrido, O., Marcelin, M., Amram, P., & Boulesteix, J. 2002, aap, 387, 821
Hayashi, E. et al. 2003, astro-ph/0310576
Kranz, T., Slyz, A., & Rix, H.-W. 2003, ApJ, 586, 143
Matthews, L.D., & Wood, K. 2001, ApJ, 548, 150
Moore, B., Quinn, T., Governato, F., Stadel, J., Lake, G. 1999, MNRAS, 310, 1147
McGaugh, S.S., Rubin, V.C., & de Blok, W.J.G. 2001, AJ, 122, 2381
Navarro, J.F., Frenk, C.S., & White, S.D.M. 1996, ApJ, 462, 563
Navarro, J.F., Frenk, C.S., & White, S.D.M. 1997, ApJ, 490, 493
Schoenmakers, R.H.M, 1999, PhD Thesis, University of Groningen
Simon, J.D., Bolatto, A.D., Leroy, A., & Blitz, L. 2003, ApJ, 596, 957
Spergel, D. et al. 2003, ApJS, 148, 175
Swaters, R.A., Madore, B, van den Bosch, F.C., & Balcells, M. 2003a, ApJ, 583, 732
Swaters, R.A., Verheijen, M.A.W., Bershady, M.A., & Andersen, D.R. 2003b, ApJ, 587, L19
Walter, F., & Brinks, E. 1999, AJ, 118, 273

*ABSTRACTS OF PAPERS POSTED DURING THE SESSION ON "EXTRAGALACTIC ASTRONOMY"**

RINGS INSTEAD OF HOTSPOTS

Gizani[1], Nectaria A.B., Garrett[2], M.A., Morganti[3], R., Cohen[4], A., Kassim[5], N., Gonzales-Serrano[6], I. & Leahy[7], J.P.

1. Institute of Astronomy and Astrophysics, National Observatory of Athens, Greece
2. Joint Institute for VLBI in Europe (JIVE), The Netherlands
3. Netherlands Foundation for Research in Astronomy (NFRA),
4, 5. Naval Research Laboratory, Washington, USA
6. Universidad de Cantabria, Spain
7. Jodrell Bank Observatory, University of Manchester, UK

Abstract: We are studying the two powerful radio galaxies Hercules A and 3 C310 and their clusters. These radio galaxies present many essential similarities with the obvious one being the presence of rings which are internal to the source and not just phenomena of the boundaries. Employing a multiwavelength observational campaign across the electromagnetic spectrum we are trying to determine the origin of their similar and unusual structure (compared with the morphology of the AGN) and behaviour and to disentangle the physical mechanisms taking place interior and exterior to them. We are observing: -In the RADIO (VLA, VLBI & WSRT) in order, for example, to study the depolarization, map the Faraday rotation, estimate the intracluster magnetic field, investigate the spectral ageing, study the pc-scale environment, detect or not HI absorption against the nucleus and/or their lobes/ring-like features so that to study their central engine, the interstellar medium (ISM), and their environment. -In the (Near-) INFRARED (TNG & WHT) since as powerful radio galaxies they are expected to be strong emitters. We made JHK imaging and spectroscopy observations, for example, to map the spectral indices of the radio rings from the radio-to-NIR in order to understand radio-to-NIR alignments or associations, to constrain and compare the nature of their acceleration mechanism with the corresponding in the usual hotspots, probe the misalignment on pc- and kpc-scales found and determine the role of their double optical nuclei, calculate the minimum energy estimate of their magnetic field in an independent way, investigate the environment of the sources and the ISM, in order to shed light in their evolution. -In the X-RAYS, making higher resolution observations, for example, we will distinguish the AGN emission from the central thermal peak, study the intracluster medium (ICM), measure accurately pressure and density as a function of radius from the core, detect distortions in the gas distribution, investigate and identify possible interactions between the X-ray and radio emission also in the area of the radio rings.

* *Proceedings of the 6th Hellenic Astronomical Society Conference, 15-17 September 2003, Penteli, Greece*

*ABSTRACTS OF PAPERS POSTED DURING THE SESSION ON "EXTRAGALACTIC ASTRONOMY"**

STAR FORMATION REGIONS IN THE SMC

E. Livanou [1], M. Kontizas [1], E. Kontizas [2], D. Kester [3], U. Klein [4]

1. Section of Astrophysics, Astronomy & Mechanics, Department of Physics
2. Institute of Astronomy and Astrophysics, National Observatory of Athens
3. Space Research Organization of Netherlands, AV Groningen
4. Radioastronoomisches Institut der Uuniveritat, Bonn

Abstract: A multiwavelength study of the SMC is under progress in order to detect the active star formation regions, which are directly related to the close LMC-SMC encounter, a few times 10^8 yr ago. The SMC being almost adge-on does not easily reveal those structures, but multiwavelenght images such as optical, IR, (IRAS) and radio are a very useful tool for their study. We present here the method of detecting these star forming regions and their properties in the available wavelengths.

* *Proceedings of the 6th Hellenic Astronomical Society Conference, 15-17 September 2003, Penteli, Greece*

Hel.A.S. Invited Review

Relativistic Flows and Particle Acceleration

John G. Kirk

Max-Planck-Institut für Kernphysik, Heidelberg, Germany

RELATIVISTIC FLOWS AND PARTICLE ACCELERATION*

John G. Kirk

Max-Planck-Institut für Kernphysik, Heidelberg, Germany

Summary. Relativistic bulk motion is known to occur in several astrophysical contexts. In each case, nonthermal radiation from relativistic electrons is detected, requiring the acceleration of electrons to high energy in the local plasma frame. This situation has motivated the generalisation of the theory of diffusive particle acceleration to apply to the case of mildly relativistic flows, and, more recently, to flows of arbitrary Lorentz factor. The kinematic theory of particle acceleration at ultra-relativistic shocks leads to the prediction of a high-energy spectral index of -1.1 for the energy flux of synchrotron photons. However, several effects can change this picture. This paper summarises the basic theory and discusses some recent extensions. Application of the theory to the spectrum of the Crab Nebula suggests an additional acceleration mechanism is responsible for low energy electrons.

1 Introduction

In nonrelativistic flows, the first order Fermi process operating at a shock front has been applied in a wide variety of astrophysical situations and has been the subject of considerable theoretical effort — with interest currently focused on nonlinear aspects [1]. Fundamentally, this mechanism relies on the isotropisation of energetic charged particles in the vicinity of the shock front by magnetic fluctuations, which may be self-generated. In relativistic flows, magnetic fluctuations can also be expected to scatter energetic particles. However, simple kinematics dictates that the distribution function cannot be isotropised at the shock front. Seen from the upstream plasma, those particles which run ahead of a relativistic shock occupy a small cone in velocity space centred around the velocity of the shock. A small deflection quickly results in the particle being recaptured by the shock front. Consequently, in the absence of large-angle scattering events, most of velocity space remains unpopulated. Seen from the downstream frame, this translates into a hole in the angular distribution centred around the velocity of the upstream plasma. Under these conditions, the diffusion approximation cannot be applied close to the shock front; a different approach is needed, which is able to account for the intrinsic anisotropy of the particle distribution functions [2].

---

* Hel.A.S. Invited Speaker

Proceedings of the 6th Hellenic Astronomical Society Conference, 15-17 September 2003, Penteli, Greece

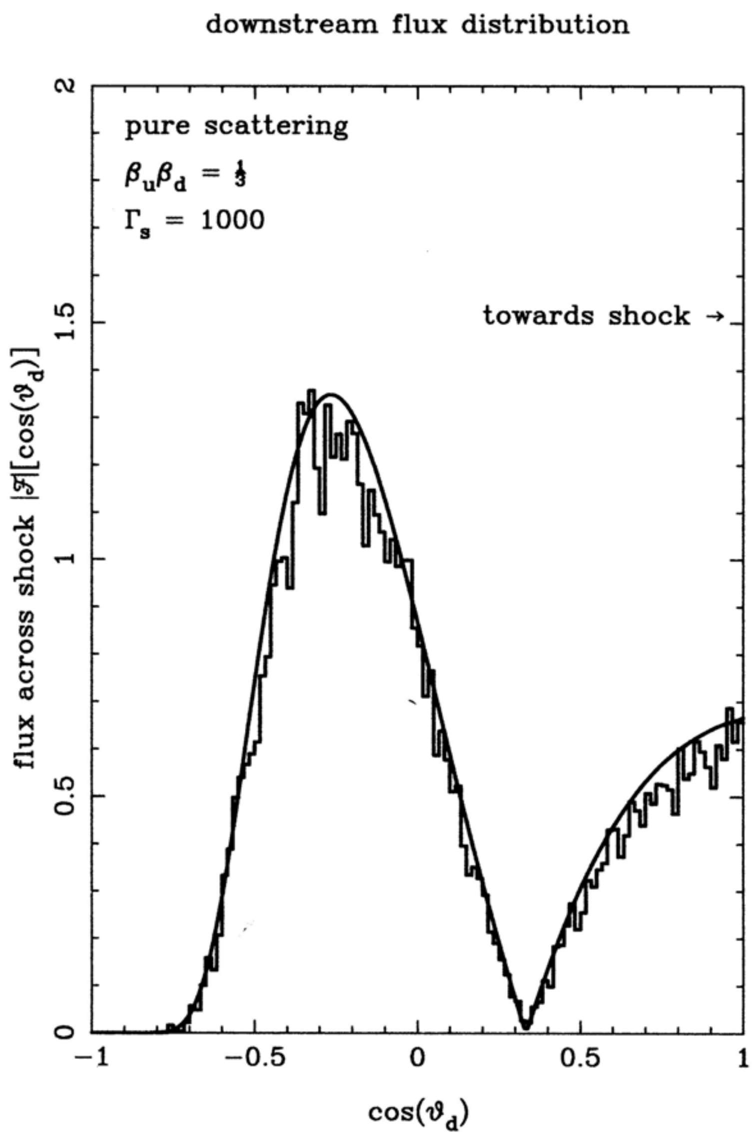

Fig. 1. A comparison (from [5]) between a Monte-Carlo simulation and the analytic result for the particle flux across a shock front as a function of the cosine of the angle θ_d between the particle velocity and the shock normal measured in the frame in which the downstream plasma is at rest. $\theta_d = 0$ corresponds to motion along the normal from downstream to upstream. Jump conditions for a relativistic gas are used and the upstream plasma has a Lorentz factor $\Gamma = 1000$.

2 Kinematics

The *kinematic* problem of particle acceleration at a relativistic shock, i.e., that of finding the distribution of a collection of test particles undergoing small-angle, random, elastic (in the plasma frame) deflections in the vicinity of a discontinuity in the (relativistic) plasma velocity is well-understood. An analytic method based on an eigenvalue decomposition is available which gives the spectrum and angular dependence of the distribution function at energies well above those of injection for

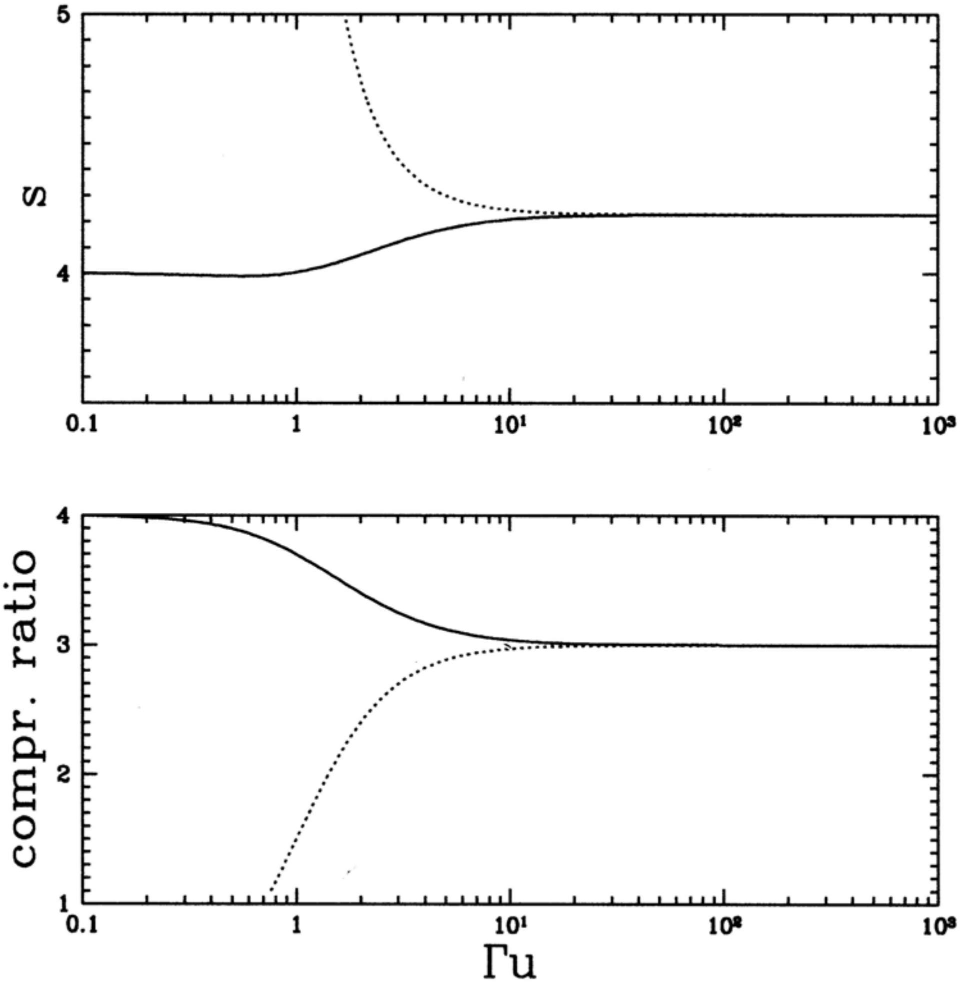

Fig. 2. The high-energy power-law index s (upper panel) and compression ratio (lower panel) as a function of the spatial component of the upstream four speed Γu. The dotted line refers to a shock in a gas with negligible rest-mass and the solid line to a strong shock (i.e., cold upstream medium) in an ideal gas with adiabatic index 5/3.

arbitrary shock speeds [3]. In addition, Monte-Carlo simulations have been performed, finding results which are in good agreement with the analytic approach [4, 5]. These results are illustrated in Figs. 1 and 2.

Well above the injection energy the phase-space density f is a power-law in momentum: $f \propto p^{-s}$ and at the shock front the angular dependence is well-approximated by the simple expression

$$f \propto (1 - \mu_s u)^{-s} \exp\left(-\frac{1+\mu_s}{1-\mu_s u}\right) \tag{1}$$

where μ_s is the cosine of the angle between the shock normal and the particle velocity cu measured in the frame in which the shock is at rest and the upstream plasma flows along the shock normal. This expression displays the expected hole in the angular distribution: $f \rightarrow \left(2\Gamma^2\right)^s \exp\left(-2\Gamma^2\right)$ for $\mu_s = 1$. In Fig. 1, which shows the particle flux $\mu \times f$ in the downstream reference frame, this is seen at $\cos\left(\theta_\mathrm{d}\right) = -1$.

Fig. 2 shows the compression ratio and the high-energy power-law index s as a function of the spatial component of the 4-speed Γu of the upstream plasma, where $\Gamma = \left(1 - u^2\right)^{-1/2}$. An interesting aspect of these results is that the power-law index tends asymptotically to the value $s \approx 4.23$ for large shock Lorentz factors (or, equivalently, upstream Lorentz factors), independent of the equation of state of the plasma. This asymptotic value is essentially fixed by the compression ratio of the shock and depends only weakly on the form of the scattering operator used to describe the small-angle deflections [3].

An isotropic small-angle scattering operator was used to compute the results shown in Figs. 1 and 2. This causes the particle's velocity vector to diffuse around on a sphere in a manner independent of its direction. Since shock crossings are the only events of relevance for acceleration, the transport equation contains only the angle between the velocity and the shock normal. In this case, the direction of the average magnetic field plays no role.

There is an important difference between this operator and the scattering operator conventionally used in nonrelativistic theory. The nonrelativistic picture assumes it is reasonable to define the trajectory of a particle between scatterings (the unperturbed motion) in terms of the motion of its guiding centre. Scatterings cause a change in the pitch-angle, leading to the diffusion of particles along magnetic field lines. Cross-field diffusion, on the other hand, is usually neglected in this picture (e.g., [6]). However, as seen in the frame of the downstream medium, the magnetic field carried towards a shock by an upstream plasma flowing at high Lorentz factor appears to lie almost in the plane of the shock front. As a consequence, highly relativistic shocks are *perpendicular* shocks [7] which cannot be multiply crossed by particles diffusing along field lines. Cross-field transport is essential to the operation of the first-order Fermi mechanism in this configuration.

In a uniform field, a particle which crosses a relativistic shock front from downstream to upstream will be recaptured by the front after executing a small fraction of roughly $\sim 1/\Gamma$ of a gyration, as illustrated qualitatively in Fig. 3. Thus, if scattering plays a role, it is reasonable to describe the unperturbed trajectory not as a helix, but as a straight line. This is especially true if, as expected (see next section), the field is highly nonuniform on the length scale of a gyro radius. In this case the role of the average field (if it exists) ceases to be important, and the description of the stochastic trajectory is in terms of deflections of the velocity, rather than changes in pitch angle. This is the form of operator used in the analytic approach. In Monte-Carlo treatments, on the other hand, it is possible to retain the effect of an average field [8, 5] but little difference is found, provided the turbulence remains strong. However, as expected, the acceleration mechanism becomes less effective as the turbulence diminishes [9]. Explicit calculations of particle motion in a random magnetic field have also been performed [10, 11] and used to compute the acceleration around a relativistic shock for Lorentz factors $\Gamma \leq 5$ [10] and, more recently, for $\Gamma \leq 100$ [12]. The latter find good agreement with the analytic result on the asymptotic power-law index.

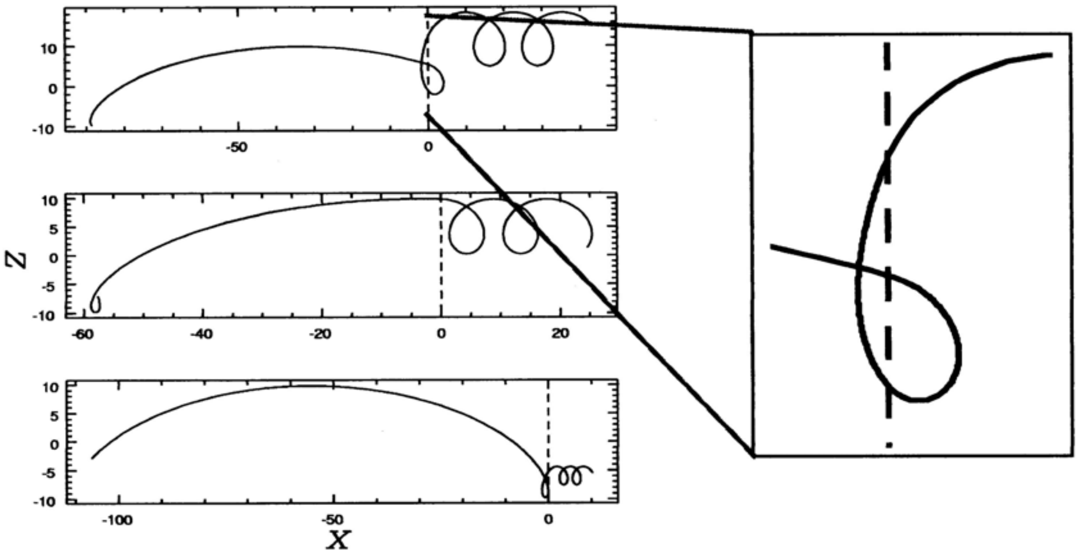

Fig. 3. Unperturbed (scatter-free) particle trajectories at a relativistic shock (located at $x = 0$), seen in the shock rest frame. The magnetic field is in the y direction and an electric field in the z direction causes particles to drift into and out of the shock with the plasma bulk speed. Depending on the initial phase, particles from upstream ($x < 0$) cross the shock one or more times, during which their gyrocentre shifts in z, causing an increase or decrease in the particle energy. The inset illustrates that a particle performs only a small fraction of a gyration upstream before being recaptured by the shock, even in this mildly relativistic example ($\Gamma = 5$).

3 Nonlinear effects and magnetic field generation

In contrast with the situation in nonrelativistic shocks [1], the nonlinear modification of relativistic shock does not affect the asymptotic power-law index at high particle energy, provided the scattering mean-free path of these particles increases with energy (as is to be expected for scattering off magnetic fluctuations). There are two reasons for this: firstly, isotropised, accelerated particles behave like a relativistic gas with adiabatic index 4/3, so that the overall compression ratio of an ultra-relativistic shock front remains unchanged, even when a significant part of the overall energy and momentum flux is carried by these particles. Secondly, the asymptotic power-law index in the test-particle picture is *soft* (i.e., $s > 4$). This means that it is possible to consider a Lorentz factor above which the test-particle approximation is valid, because the energy density in the remaining accelerated particles is indeed small. Nevertheless, a strong nonlinear effect can be exerted by particles of lower energies, whose mean free path to scattering is comparable to the size of internal structures in the shock transition [13].

The most promising mechanism of formation of relativistic shock in a collisionless plasma involves the nonlinear evolution of the Weibel instability [14, 15, 16], which generates magnetic field perpendicular to the relative streaming motion of the up and downstream plasmas i.e., in the plane of the incipient shock. A full simulation of this situation has not yet been performed, but recent 3D-PIC simulations of colliding plasma shells [17, 18, 19] suggest that a downstream magnetic field can be generated with a strength up to $\sigma \approx 1\%$. (Here the magnetisation parameter σ is defined as the ratio of the magnetic energy density to twice the total enthalpy density (including rest mass) as measured in the plasma rest frame). This is encouraging, since it is roughly the level implied by spectral modelling [20] of GRB after-glows.

The spectrum of accelerated particles is certainly closely tied to the evolution of the turbulent magnetic field. However, if we are interested only in high energy particles of long mean free path, the power-law index predicted by the first-order Fermi mechanism can be calculated simply by modifying the shock jump conditions to account for the generated field as a large amplitude wave in the downstream plasma. In a time averaged picture, linear functions of the wave fields vanish and the stress-energy tensor in the plasma frame is

$$T^{\mu\nu} = \left(w + \frac{B^2}{4\pi}\right) u^\mu u^\nu + \left(p + \frac{B^2}{8\pi}\right) g^{\mu\nu} - \frac{B^\mu B^\nu}{4\pi} \tag{2}$$

(for notation see [2]). The last term on the right hand side does not contribute to the fluxes across the shock front if the generated magnetic field lies in the shock plane. As a result, the jump conditions are the same as those of an unmagnetised fluid, provided the magnetic enthalpy density $B^2/4\pi$ and pressure $B^2/8\pi$ are taken into account [21]. For a relativistic gas, this gives an effective adiabatic index

$$\gamma_{\text{eff}} = \frac{4(1+\sigma)}{(3+\sigma)} \tag{3}$$

leading to an asymptotic compression ratio of $1/\left(\gamma_{\text{eff}} - 1\right)$ and a relative speed of the upstream medium with respect to the downstream medium corresponding to a Lorentz factor $\Gamma_{\text{rel}} = \Gamma\sqrt{(2-\gamma_{\text{eff}})/\gamma_{\text{eff}}}$ (where Γ is the Lorentz factor of the shock front seen in the upstream medium). As σ increases, the compression ratio of the shock decreases and the high-energy power-law softens, as shown in Fig. 4.

4 Application to the Crab Nebula

A relativistic wind carries energy from the Crab pulsar out to the Nebula. This energy is released into nonthermal particles at a termination shock, which is probably the best observed example of a relativistic shock in the universe. The average Lorentz factor of the upstream plasma can be estimated from the spin-down luminosity of the pulsar and the total number of electrons and positrons which have accumulated in the Nebula [22] to be between $\sim 10^4$ and 10^6. This is well into the asymptotic region of high Γ as far as the first-order Fermi process is concerned, and the X-ray synchrotron emission [23] indeed exhibits a power-law index of $s = 4.2$, as predicted for a plasma in which the magnetic energy plays no dynamical role [24].

However, the integrated synchrotron spectrum displays not only the expected "cooling break" at a frequency where the characteristic cooling time corresponds roughly to the age of the object, but also a second break at higher frequency [24]. This is presumably due to an intrinsic feature of the acceleration process and probably characterises the transition between two different mechanisms. One possibility is that the break energy reflects the different spatial scales associated with ions and electrons/positrons. Regarded as distinct fluids, these components would be

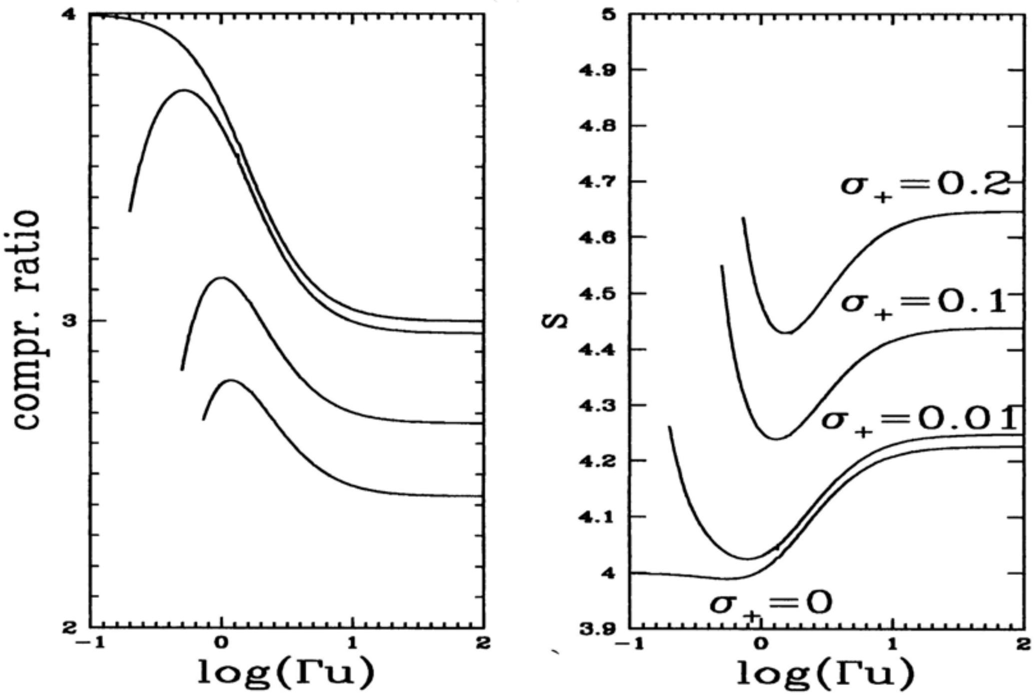

Fig. 4. The compression ratio and power-law index s for a gas of adiabatic index 5/3 in which a magnetic field is generated downstream to the level $\sigma = \sigma_+$ (see text for notation).

expected to produce shock structures each on the scale of the thermal gyro radius: $\Gamma Mc^2/eB$ and $\Gamma mc^2/eB$, respectively. However, strong heating of the electron/positron gas, perhaps via the maser mechanism proposed by Hoshino et al [25], should result in a smearing out of the smaller of these two scales. Below Lorentz factors of roughly $\Gamma M/m$, the hard ($s \approx 3$) maser mechanism should dominate over the first-order mechanism for electrons and positrons. An alternative explanation, which assumes the ions in the Crab wind carry very little of the energy flux, is that magnetic field dissipation within the shock front is responsible [21].

Although it is at present not known which (if any) of these theories is correct, the implications for modelling the spectra of sources which display relativistic bulk motion are clear: nonthermal electrons are likely to be injected with an intrinsic spectrum exhibiting a break. Hard spectra ($s < 4$) that concentrate energy at the highest Lorentz factors arise in connection with maser mechanisms and with reconnection [26], but are not predicted from the first-order Fermi mechanism at a relativistic shock. The signature of the latter, which should emerge at higher electron energy, is a soft spectrum with a power law index of the phase space distribution ranging from 4.2 to about 4.4, depending on the efficiency of magnetic field generation.

References

1. M. Malkov, L.O'C. Drury: Rep. Prog. Phys. **64**, 429 (2001)

2. J.G. Kirk, P. Duffy: J. Phys. G: Nucl. Part. Phys. **25**, R163 (1999)
3. J.G. Kirk, A.W. Guthmann, Y.A. Gallant, A. Achterberg: ApJ **542**, 235 (2000)
4. J. Bednarz, M. Ostrowski: Phys. Rev. Letts. **80**, 3911 (1998)
5. A. Achterberg, Y.A. Gallant, J.G. Kirk, A.W. Guthmann: MNRAS **328**, 393 (2001)
6. J.G. Kirk, A.F. Heavens: MNRAS **239**, 995 (1989)
7. M.C. Begelman, J.G. Kirk: ApJ **353**, 66 (1990)
8. M. Ostrowski: 1983 MNRAS **264**, 248 (1993)
9. M. Ostrowski, J. Bednarz: A&A **394**, 1141 (2002)
10. K.R. Ballard, A.F. Heavens: MNRAS **259**, 89 (1992)
11. F. Casse, M. Lemoine, G. Pelletier: Phys. Rev. D **65**, 023002 (2002)
12. M. Lemoine, G. Pelletier: ApJ **589**, L73 (2003)
13. D.C. Ellison, G.P. Double: Astroparticle Phys. **18**, 213 (2002)
14. T.Y.B. Yang, Y. Gallant, J. Arons, A.B. Langdon: Physics of Fluids B – Plasma Physics **5**, 3369 (1993)
15. T.Y.B. Yang, J. Arons, A.B. Langdon: Physics of Plasmas **1**, 3059 (1994)
16. M.V. Medvedev, A. Loeb: ApJ **526**, 679 (1999)
17. J. Sakai, T. Nakayama, Y. Kazimura, S. Bulanov: J. Phys. Soc. Japan **69**, 2503 (2000)
18. R.A. Fonseca, L.O. Silva, J.W. Tonge, W.B. Mori, J.M. Dawson: Physics of Plasmas **10**, 1979 (2003)
19. L.O. Silva, R.A. Fonseca, J.W. Tonge, J.M. Dawson, W.B. Mori, M.V. Medvedev: ApJ **596**, L121 (2003)
20. A. Panaitescu, P. Kumar: ApJ **571**, 779 (2002)
21. Y. Lyubarsky: MNRAS, **345**, 153 (2003)
22. J.G. Kirk, O. Skjæraasen: ApJ **591**, 366 (2003)
23. R. Willingale, B. Aschenbach, R.G. Griffiths, S. Sembay, R.S. Warwick, W. Becker, A.F. Abbey, J.M. Bonnet-Bidaud: A&A **365**, L212 (2001)
24. Y. Gallant, E. van der Swaluw, J.G. Kirk, A. Achterberg: Modelling plerion spectra and their evolution. In: *Neutron Stars in Supernova Remnants* ASP conference series **271**, eds: P.O. Slane, B.M. Gaensler p. 161
25. M. Hoshino, J. Arons, Y.A. Gallant, A.B. Langdon: ApJ **390**, 454 (1992)
26. S. Zenitani, M. Hoshino: ApJ **562**, L63 (2001)

Session IV

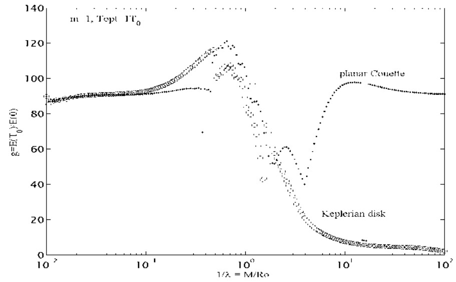

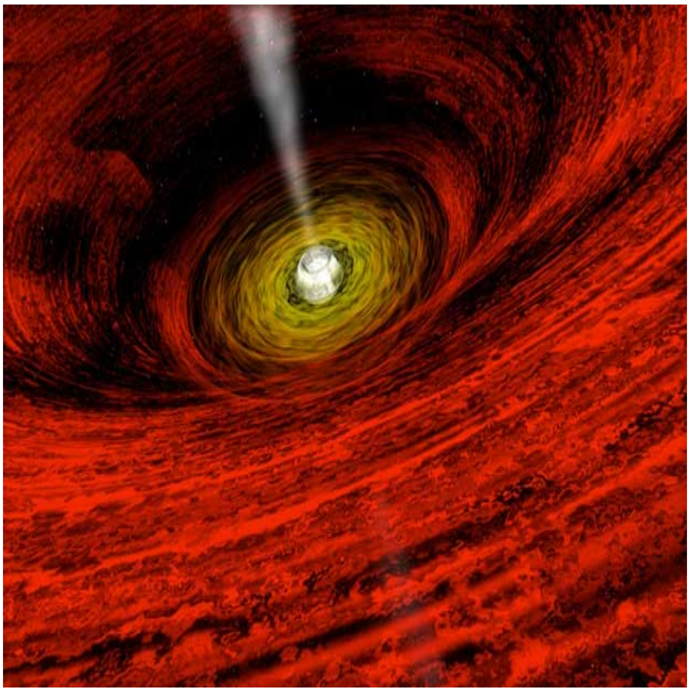

HIGH ENERGY ASTROPHYSICS

Conveners: N. Kylafis and A. Mastichiadis

ANGULAR MOMENTUM TRANSPORT IN KEPLERIAN ACCRETION DISCS*

A. Kakouris, G. I. Kefaliakos, P. J. Ioannou

Section of Astrophysics, Astronomy and Mechanics
Department of Physics, University of Athens, Greece

1. INTRODUCTION.

The traditional picture of accretion disks is that in the absence of magnetic fields they are quiescent, without energetic fluctuations, and coherent features (Balbus & Hawley, 1996). It has been argued also that such disks remain laminar despite their large Reynolds number ($\approx 10^{14}$) unless magnetic fields couple to the motions to allow the instigation of the Balbus-Hawley instability (Balbus & Hawley 1991). However, recent numerical simulations of purely hydrodynamic accretion disks have demonstrated that the disks are full of coherent vortices (Godon & Livio, 1999, 2000). It has been also argued, based on similarities with Rayleigh-Taylor laboratory experiments, that unmagnetized Keplerian disks should become turbulent at sufficiently high Reynolds number (Richard & Zahn, 1999; Longaretti 2002). This results call for reexamination of the stability properties of unmagnetized Keplerian disks. In this note we apply methods of generalized stability analysis (Farrell & Ioannou, 1996) to identify the perturbations that are expected to emerge in purely hydrodynamic accretion disks. This work extends the work of Ioannou & Kakouris (2001) to compressible Keplerian disks and the transient growth analysis performed by Chagelishvili et al (1997).

2. PERTURBATION DYNAMICS.

In order to study the stability of a non-magnetized Keplerian accretion disc, we will adopt the shearing sheet approximation (Goldreich & Tremaine 1978). In this approximation the perturbation dynamics of the disk are approximated in local Cartesian frame in which *x* is the radial direction and *y* the azimuthal. The perturbation variables are assumed in the form:

$$[p', u', v'](x, y, t) = [p, u, v](t) \exp\{i(kx + my)\} \quad , \qquad (1)$$

(p is the pressure perturbation, *u* the radial velocity perturbation and *v* the azimuthal velocity perturbation), with time-varying radial wavenumber, $k(t) = k_0 + (3m/2)t$. The linearized non-dimensional perturbation equations in the local rotating frame of reference are then:

$$\frac{dp}{dt} = -\frac{i\lambda}{M}(ku + mv) \quad ,$$
$$\frac{du}{dt} = -i\lambda k\, Mp - \left(K^2 + \frac{k^2}{3}\right)\frac{Ro}{\mathrm{Re}}u + \left(f - \frac{mkRo}{3\,\mathrm{Re}}\right)v \quad , \qquad (2)$$
$$\frac{dv}{dt} = -i\lambda m\, Mp - \left(-\frac{3}{2} + f + \frac{mkRo}{3\,\mathrm{Re}}\right)u - \left(K^2 + \frac{m^2}{3}\right)\frac{Ro}{\mathrm{Re}}v \quad ,$$

* *Proceedings of the 6th Hellenic Astronomical Society Conference, 15-17 September 2003, Penteli, Greece*

where $f=2$ is the Coriolis parameter and $K^2=k^2+m^2$ is the square of the total wavenumber. The equations have been rendered non-dimensional. The typical perturbation length and velocity are chosen as L and V and the Rossby number, Ro, the Mach number, M, the ratio λ, and the Reynolds number, Re, are defined as:

$$Ro = \frac{V}{\Omega_0 L} \quad , \quad M = \frac{V}{c_s} \quad , \quad \lambda = \frac{Ro}{M} \quad , \quad \mathrm{Re} = \frac{VL}{\nu} \quad , \qquad (3)$$

where Ω_0 is the local angular velocity, c_s is the velocity of sound and ν is the coefficient of the kinematic viscosity. The linear evolution of the perturbation state vector $\mathbf{Y}=[Mp,u,v]^{\mathrm{T}}$ obeys the equation $\mathrm{d}\mathbf{Y}(t)/\mathrm{d}t=\mathbf{A}(t)\ \mathbf{Y}$ where $\mathbf{A}(t)$ is the operator corresponding to the linear system (2). In this notation the perturbation energy is E = (1/4) $|\mathbf{Y}^2|$.

We note that the governing operator $\mathbf{A}(t)$ is non- normal, i.e. $\mathbf{A}\mathbf{A}^+ \neq \mathbf{A}^+\mathbf{A}$ where the dagger denotes the hermitian transpose, and generalized stability methods are adopted to study the stability of the perturbations (cf Farrell & Ioannou 1996a, 1996b). If the propagator matrix of the dynamical system is denoted by $\Phi(t)$ the maximum possible perturbation energy growth at time t is given by $||\mathbf{\Phi}(t)||^2$ where $||\bullet||$ denotes the Euclidian norm. The corresponding initial perturbation that gives the maximum energy growth, referred as the optimal perturbation, is identified from a singular value decomposition of the propagator $\mathbf{\Phi}(t)$=$\mathbf{U\Sigma V}^+$ as the column of $\mathbf{V}$ corresponding to the maximum singular value (the largest element of the diagonal matrix $\mathbf{\Sigma}$**)**.

It can be shown from that the potential vorticity of the perturbations, Q, is a constant:

$$Q = \frac{M^2}{Ro} p - \frac{i}{f-3/2}(kv - mu) = \text{constant} \quad . \qquad (5)$$

Using (5) of the radial and azimuthal kinetic energy density tendency can be written as (the brackets denote azimuthal averaging):

$$\begin{aligned} \frac{d}{dt}\left\langle \frac{u^2}{2} \right\rangle &= \left(\hat{k}^2 + f\right) < uv > - \hat{k}\hat{m} < u^2 > - ik\lambda^2 < uQ > \quad , \\ \frac{d}{dt}\left\langle \frac{v^2}{2} \right\rangle &= \left(\frac{3}{2} - \hat{m}^2 - f\right) < uv > + \hat{k}\hat{m} < v^2 > - im\lambda^2 < vQ > \quad , \qquad (6) \end{aligned}$$

$$\text{with} \quad \left(\hat{k},\hat{m}\right) = \sqrt{\frac{\lambda^2}{f-3/2}}(k,m) \quad .$$

The last relations imply that for a positive Reynolds stress, <uv> > 0, the azimuthal perturbation energy increases due to the shear while an amount of energy is transferred from the azimuthal term to the radial due to the Coriolis influence (which does not influence the overall energy tendency). The remaining terms represent work by the pressure; the radial energy term increases by $\hat{k}^2$ and the azimuthal decreases by

$\hat{m}^2$ which introduces an overall energy gain since $\hat{k}^2 > \hat{m}^2$. Analysis of the dynamics of fast show that despite the claims of Balbus et al. 1996, Hawley et al. 1999, a simultaneous increase in the kinetic energy in the radial and azimuthal directions is possible. The typical linear response of the Keplerian flow is shown in Fig. 1 where the energy evolution for a one-revolution optimal perturbation is plotted for both an inviscid and a viscous (Re=10^4) Keplerian disc. After the energy maximum for t=1T$_0$, a linear increase in energy occurs due to the evolving sound waves (Chagelishvili et al. 1997). The linearly increasing sound waves are dissipated in a viscous disc (Farrell & Ioannou 2000).

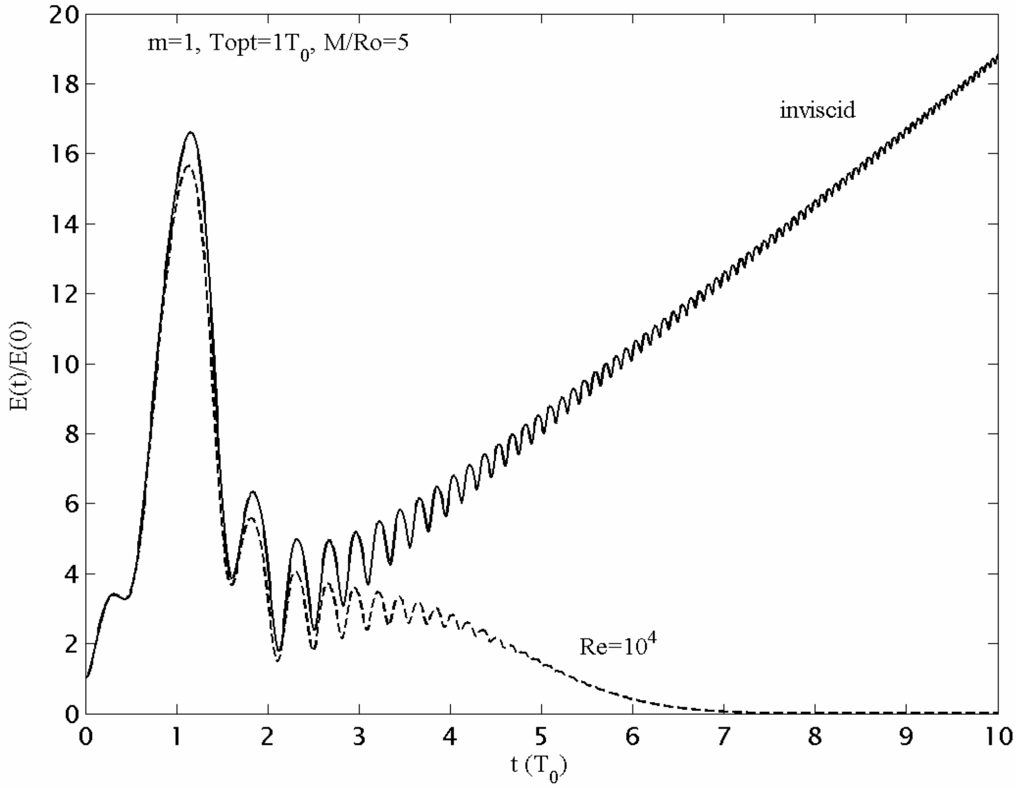

Fig. 1. *Perturbation energy evolution in a Keplerian disc for a one-rotation optimal perturbation. The solid line is for an inviscid disc and the dashed is for a viscous with Re=10^4.*

The dependence of the optimized growth in one rotation upon the parameter λ is shown in Fig. 2 in comparison with the planar Couette flow where the Coriolis force is absent. The energy growth is robust for λ >1. For large Mach numbers the Keplerian growth diminishes due to the domination of the inertial oscillations and in contrast to the planar Couette flow. The local maximum for $\lambda \approx 2$ indicates that the most efficient perturbations, which will carry angular momentum outwards, have a radial extent comparable to the local height of the accretion disc.

2. CONCLUSIONS.

In this work we revisit hydrodynamic processes as a source for anomalous viscosity in compressible Keplerian accretion discs. We found that locally subsonic perturbations with a radial extent of the order or less than the local height of the disc

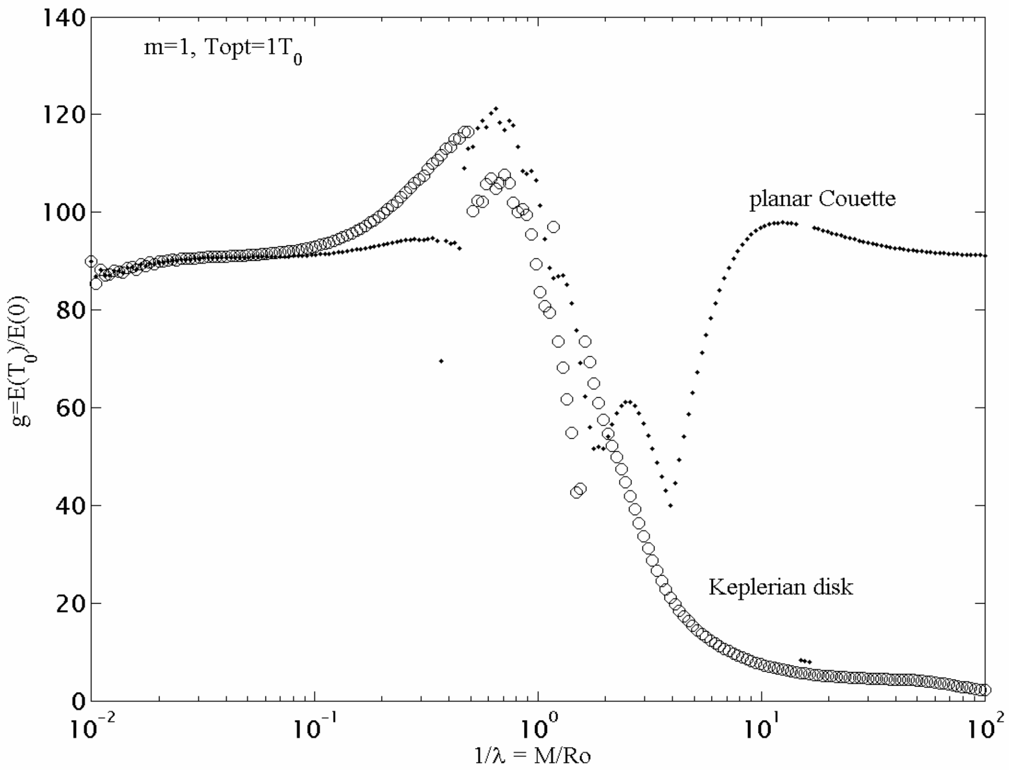

Fig. 2. *One rotation optimal energy growth for an inviscid Keplerian disc (circles) and for an inviscid planar Couette flow (dots).*

grow efficiently in energy and carry angular momentum outwards. In addition, the sound wave field, which we expect to evolve nonlinearly as spiral shock waves (Spruit 1987), transfers angular momentum outwards making the accretion procedure possible in non-magnetized Keplerian discs.

REFERENCES

Balbus, S.A., Hawley, J.F., 1991, ApJ 376, 214
Balbus, S. A., Hawley, J. F., 1996, Rev. Mod. Phys., 70,1
Balbus, S.A., Hawley, J.F., Stone, J.M., 1996, ApJ 467, 76
Chagelishvili, G.D., Tevzadze, A.G., Bodo, G., Moiseev, S.S., 1997, Phys. Rev. Let. 79, 3178
Farrell, B.F., Ioannou, P.J., 1996a, J. Atm. Sci. 53, 2025
Farrell, B.F., Ioannou, P.J., 1996b, J. Atm. Sci. 53, 2041
Farrell, B.F., Ioannou, P.J., 2000, Phys. Fluids 12, 3021
Ferreira, J., 1997, A&A 319, 340
Fleming, T.P., Stone, J.M., Howley, J.F., 2000, ApJ 530, 464
Godon, P., Livio, M, 1999, ApJ, 523, 350
Godon, P., Livio, M, 2000, ApJ, 537, 396
Goldreich, P., Tremaine, S., 1978, ApJ **222**, 850
Hawley, J.F., Balbus, S.A., Winters, W.F., 1999, ApJ 518, 394
Ioannou, P.J., Kakouris, A., 2001, ApJ 550, 931
Longaretti, P.Y., 2002, ApJ 576, 587
Menou, K., 2000, Science 288, 2022
Spruit, H.C., 1987, A&A 184, 173
Richard, D, Zahn, J-P, A&A, 347, 734
Tagger, M., 2001, A&A 380, 750

MODELING THE TEV GAMMA-RAY SPECTRUM OF THE TWO LOW REDSHIFT AGNS: MKN 501 & MKN 421*

A. Mastichiadis
Department of Physics, University of Athens, Panepistimiopolis, GR 15783, Zografos, Greece

A. Konopelko, J. Kirk
Max-Planck Institut fuer Kernphysik, Postfach 10 39 80, Heidelberg. Germany

O.C. de Jager
Unit for Space Physics, Potchefstroom University, 2520, South Africa

F.W. Stecker
Laboratory for High Energy Astrophysics, NASA Goddard Space Flight Center, Greenbelt, MD 20771, USA

1. INTRODUCTION

Ground based Cherenkov detectors have already identified several cosmic sources in the TeV γ-ray energy domain. Among the best studied of these are two nearby Active Galactic Nuclei: Mkn 421 (z=0.0031) (Punch et al. 1992) and Mkn 501 (z=0.0034) (Quinn et al 1996) which are commonly known as the 'TeV blazars'. The observations suggest that their spectrum is non-thermal in origin and therefore requires particle acceleration to energies of at least the same energy as the γ-rays observed.

X-ray observations of these objects show that both the X-ray and the TeV fluxes are well correlated, strongly suggesting that it is the same population of relativistic particles that produces the radiation in these two very different energy bands. At the same time the observed high fluxes and rapid variability make the modeling of these two objects very challenging.

Despite the fact that many theoretical models have been put forward to explain the high energy emission of the TeV blazars, the most successful so far have been the leptonic synchro self-Compton (SSC) models (Maraschi et al. 1992, Marscher & Travis 1996). These models attribute the radio to X-ray emission to synchrotron radiation from a population of relativistic electrons and the Mev to TeV γ-ray emission to inverse Compton scattering of the same electrons on the aforementioned synchrotron photons.

2. IR OPACITIES

A point that was, until recently, neglected is that the TeV photons emitted from the TeV blazars are subject to absorption from the Cosmic Infra-Red Background (CIRB) photons en route to us. Indeed, γ-rays from 300 GeV to 20 TeV interact most efficiently with photons of wavelength between 1-50 μm producing electron-positron pairs and therefore the measured TeV spectrum is not the intrinsic source spectrum but has been modified by absorption. Thus in order to find the intrinsic spectrum one needs first to calculate the optical depth of a photon of energy E_γ against photon-photon pair production on the CIRB photons and then de-absorb the observed spectrum. The required opacity can be calculated by integrating over the photon interaction angle, the redshift and the energy of the soft photon field according to the prescription given in Konopelko et al. 1999, 2003.

* *Proceedings of the 6th Hellenic Astronomical Society Conference, 15-17 September 2003, Penteli, Greece*

A difficulty arises due to the lack of direct measurements of the CIRB in the wavelength range 1-50 μm (Hauser & Dwek 2001). Thus, a computation of the opacity of the intergalactic medium to TeV γ-rays must be based on theoretical models of the diffuse radiation field. Such models are given, amongst others, by Malkan & Stecker (2001) and are consistent with all currently measured lower and upper limits in the mid-IR range as well as with the COBE-FIRAS fluxes given at 140 μm and 240 μm.

In order to deal with this uncertainty, we calculated opacities which correspond to two 'extreme' models of Malkan & Stecker. Applying these two sets of opacities to the measured spectra we interpreted the results as upper and lower values of the de-absorbed intrinsic flux, as 3σ deviations from the true value and added this error to the one attached to the original TeV point.

2. DATA

The HEGRA system of 5 imaging Cherenkov telescopes has achieved a very good energy resolution of about 10% for each individual γ-ray shower (Hofmann et al. 2000) using stereoscopic observations. This unique energy resolution allowed to deliver the high precision spectral data for Mkn 501 (Aharonian et al. 1999) during its outburst in 1997, and Mkn 421 (Aharonian et al. 2002) in its high and low states during the 2000-2001 observational period. In addition, we use here the data taken with BeppoSAX in the observation period of April 1977 (Pian et al. 1977) for Mkn 501 and X-ray spectra of Mkn 421 measured with the BeppoSAX in 2000 for the low and high states of the source (Fosatti et al. 2002). These two BL Lac objects have rather different intrinsic features which are summarized in Table 1. Mkn 421 is extremely highly variable source, whereas Mkn 501 has an extremely hard X-ray spectrum.

Table 1

Source	Mkn 501	Mkn 421
Time variability	20 min	15 min
Relative flux variability	~10	~10
Peak of synchrotron emission	~ 100 keV	~1 keV
Peak of intrinsic IC emission	~7 TeV	1-2 TeV

3. SSC MODEL

To model the multi-wavelength spectra of the TeV blazars in a homogeneous SSC scenario we use an approach described by Mastichiadis & Kirk (1997). This method involves prescribing an injection function for relativistic electrons and solving the two time-dependent kinetic equations for the electron and photon distribution functions. All relevant physical processes are taken into account, i.e., synchrotron radiation, inverse Compton scattering, photon-photon pair production and synchrotron self-absorption.

Seven model parameters are required to specify a source in a stationary case. These are

1. the Doppler factor $\delta=1/\Gamma(1-\beta\cos\theta)$, where Γ and cβ are the Lorentz factor and speed of the source, and θ is the angle between its direction of motion and the line of sight to the observer,
2. the radius R of the source (in its rest frame, in which it is assumed spherical) or, equivalently, the crossing time $t_{cr} = R/c$ .This is related to the observed minimum variation timescale in the galaxy frame by $t_{var} = R/(\delta c)$,
3. the magnetic field strength B,

4. the index s of the electron injection spectrum, for which we take $Q_e = q_e\gamma^{-s}e^{-\gamma/\gamma_{max}}$ where γ is the electron Lorentz factor,
5. γ_{max} , the Lorentz factor at the cut-off of the injection spectrum,
6. q_e , the amplitude of the injection spectrum, which is expressed in terms of the electron injection parameter $l_e = \frac{1}{3} m_e c\sigma_T R^2 \int_1^\infty d\gamma(\gamma-1)Q_e$ (here m_e the electron mass and σ_T the Thomson cross section),
7. t_{esc} , the effective escape time of relativistic electrons, which can be identified as the timescale over which adiabatic expansion losses limit the accumulation of relativistic electrons within the source.

In attempting to optimize a fit to a particular data set, it is essential to use a physically motivated strategy to arrive at reasonable starting values for these seven parameters, This is done by identifying six scalars which characterize the typical blazer spectrum:

1. the peak frequency $\nu_{s,18}$ of the synchrotron emission expressed in units of 10^{18} Hz,
2. the peak frequency $\nu_{c,27}$ of the inverse Compton emission expressed in units of 10^{27} Hz,
3. the total nonthermal luminosity L
4. the approximate ratio η of the total flux in the inverse Compton part to that in the synchrotron part of the spectrum
5. the break frequency ν_{br} in the synchrotron part of the spectrum, where cooling and electron escape timescale are comparable
6. the low frequency spectral index

Together with an estimate of the fastest variability timescale t_{var} these roughly estimated quantities or observables enable one to find reasonable starting values of the seven parameters of the SSC model. However, this method is reliable only if the intrinsic spectrum is available. In particular, it is not possible to estimate quantities $\nu_{c,27}$ (2) or η (4) unless the observed spectrum has been unfolded using an absorption model.

4. RESULTS

Using these starting values we find the best fit models for Mkn 421 (high and low states) and Mkn 501 as given in Table 2. The spectra are shown in Fig. 1. We can make the following comments:

- The χ^2 values, given the uncertainties in the intergalactic absorption, are unusually small. This indicates that the SSC model gives a reasonably good fit even though the X-ray and TeV γ-ray features of the two Mkn's are very different.
- The observed rapid variability of a few thousands of seconds imply high Lorentz factors of order of 50 in order to fit the data.
- The energy spectra of Mkn 421 in high and low states can be fitted by changing the γ_{max} and luminosity parameters, whereas the Doppler factor and the magnetic field remains unchanged.

Table 2

Source	State	δ	R(cm)	s	γ_{max}	l_e	B (Gauss)	t_{cr} / t_{esc}	χ^2 / dof
Mkn 421	High	55	4.8×10^{13}	1.75	5.0×10^{5}	1.23×10^{-5}	0.1	1.1	0.53
Mkn 421	Low	55	4.8×10^{13}	1.75	3.0×10^{5}	0.82×10^{-5}	0.1	1.1	0.61
Mkn 501		50	3.5×10^{15}	1.60	1.2×10^{6}	3.50×10^{-5}	0.04	1.2	0.90

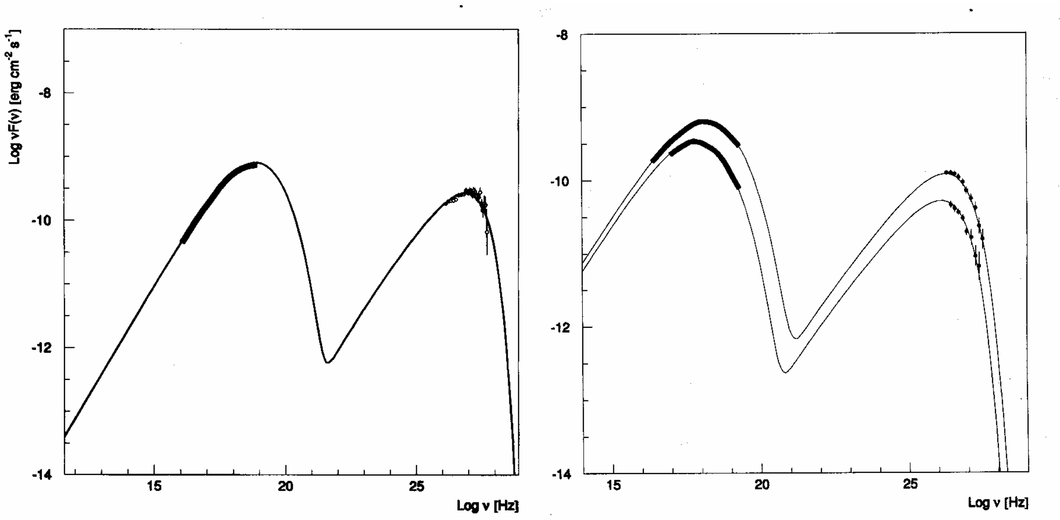

Figure 1: The combined multiwavelength spectra of Mkn 501 (left) and Mkn 421 together with the best fit models for both the high and low states (right).

5. REFERENCES

Aharonian, F., et al. 1999, A&A 349, 11
Aharonian, F., et al. 2002, A&A 393, 89
Fosatti, G. et al. 2002, April APS/HEAD Meeting, Albuquerque, B17
Hauser, M., Dwek, E., 2001, ARA&A, 29, 249
Hofmann, W. et al. 2000, Astropart. Phys, 12, 207
Konopelko, A. et al. 1999, ApJ, 518, L13
Konopelko, A. et al. 2003, ApJ, 597, 851
Malkan, M., Stecker, F., 2002, ApJ, 555, 641
Maraschi, L., Ghisellni, G., Celotti, A. 1992, ApJ, 397, L5
Marscher, A., Travis, J., 1996 A&AS, 120, 537.
Mastichiadis, A., Kirk, J. 1997, A&A, 320, 19
Pian, E. et al. 1997, ApJ. 486, 784
Punch, M., et al, 1992, Nature, 358, 477
Quinn, J. et al., 1996, Apj, 456, L83

THE EFFECT OF ABERRATION ON POLARIZATION POSITION ANGLE OF PULSARS*

D. Mitra[1] and J. H. Seiradakis[2]

[1]Max-Planck-Institut für Radioastronomie, Auf dem Hügel 69, 53121 Bonn, Germany
[2]University of Thesseloniki, Department of Physics, Section of Astrophysics, Astronomy and Mechanics, GR-54124 Thessaloniki, Greece}

Abstract. The linear polarization position angle (PPA) of pulsar emission shows a wide variety of structures, which deviates from the classical rotating vector model. In this study we investigate the effect on the PPA due to emission arising from a range of heights. We demonstrate that by appropriately choosing the emission height we can reconstruct the PPA sweep across the integrated pulse profiles.

1. Introduction

Pulsars exhibit broad-band coherent radio emission ranging from tens of MHz to tens of GHz and is highly polarized. It is usually observed that pulse widths at higher frequencies are smaller than that at lower frequencies (see Mitra & Rankin 2002 for a recent review). This phenomenon is termed as radius to frequency mapping (RFM) according to which emission at progressively higher frequencies arise closer to the stellar surface. The polarization position angle (PPA) of the linear polarization for several pulsars is seen to execute a smooth `S-shaped' curve which has been interpreted as evidence for highly beamed emission arising from dipolar magnetic field lines as per the rotating vector model (RVM) proposed by Radhakrishnan & Cooke (1969). Fitting the RVM model to the PPA traverse can be used to find the geometrical angles of the neutron star namely α the angle between the rotation axis and the dipolar magnetic axis and β the angle between the rotation axis and the observers line-of-sight. RVM and RFM together has been extensively used to find radio emission heights in pulsars and the shape of the pulsar beam. Canonical values for emission heights are found to be 50 times the stellar radius and the emission beam is thought to be organized in the shape of nested cones of emission, with a central core emission.

Whilst RFM is more commonly observed in pulsars (barring a few exceptions) there are significant deviations from the RVM observed in PPA traverses in pulsars. In some cases across the pulse the PPA traverse is seen to have 90º jumps and/or two orthogonal PPA tracks. Careful study has shown that each of the PPA track are in agreement with the RVM (Gil & Lyne 1994). The other kind of deviation is in the form of wiggles and kinks (non-orthogonal departures) observed in the PPA traverse. In this

* *Proceedings of the 6th Hellenic Astronomical Society Conference, 15-17 September 2003, Penteli, Greece*

paper we will concentrate on the latter kind of deviation observed and put forward a possible scenario which can explain such deviations.

2. The BCW model and the RVM curve

The RVM model has been further advanced by Blaskiewicz et al. (1991, hereafter BCW) where they included first order special relativistic effects into account. The model predicts that due to aberration and retardation (A/R) effects the PPA traverse depends on the emission height r_{em} and the pulsar period P (in sec) as,

$$\psi = \psi_0 + \arctan\left(\frac{\sin\alpha \sin(\phi - \phi_0) - (6\pi / P)(r_{em} / c)\sin\xi}{\sin\xi \cos a + \sin\alpha \cos\xi \cos(\phi - \phi_0)}\right) \tag{1}$$

Here ψ_0 and φ_0 are arbitrary position angle and longitude phase offsets and φ is the longitude of the pulse. The angle $\xi = \alpha + \beta$. Note that the above equation reduces to the RVM for $r_{em} = 0$. It is immediately obvious from the above equation that changes in r_{em} across the pulse will result in distortion of the PPA traverse. Also if r_{em} is fixed, then the distortions will be larger for faster pulsars, as expected from the A/R effects.

However r_{em} across the pulse is an unknown. It is thought that the central core emission arises much below the conal emission. In Figure 1 we show an example of how the PPA curve will be distorted if emission from different parts of the pulse originated from two distinctly different heights. To refine the above concept of emission arising from different heights we put forward the following model,

(a) We note a pulse profile can be decomposed as a set of Gaussians (Kramer 1994). Further each Gaussian can be attributed to either cone or core emission. These core and cone can arise from different heights.

(b) For every i^{th} longitude in the pulse, the resultant emission height $r_{em}(i)$ is an intensity (I) weighted quantity given as,

$$r_{em}(i) = \frac{\sum_{c=1}^{N}(I(i,c) \times r(c))}{\sum_{c=1}^{N} I(i,c)} \tag{2}$$

Here the index c refers to the Gaussian component and r(c) corresponds to the height attributed to that component (which corresponds to height of the cone or core component). In Figure 1 we show an example on how the PPA traverse behaves when equation 2 is applied. It should be noted that the PPA traverse strongly depends on the parameters α, β and r_{em} which are highly correlated to each other.

3. Application of BCW model to pulsars

Most of the time the distortions in the PPA traverse seem to occur below the central core component in pulsars. While it is seen in a few normal pulsars (NP), it is more commonly seen in millisecond pulsars (MSP). Also in MSP's the PPA traverse is seen to be flat.

PSR J1022+1001 a millisecond pulsar with a period of 16 msec at 408 MHz is a classical example where the PPA traverse shows distortions below the central core component, as shown in Figure 2 (left plot). The kinky nature of the PPA traverse seen below the central core component. This pulsar can be adequately described by fitting three gaussians, two outer ones comprising of one cone and the inner core. On the right hand plot

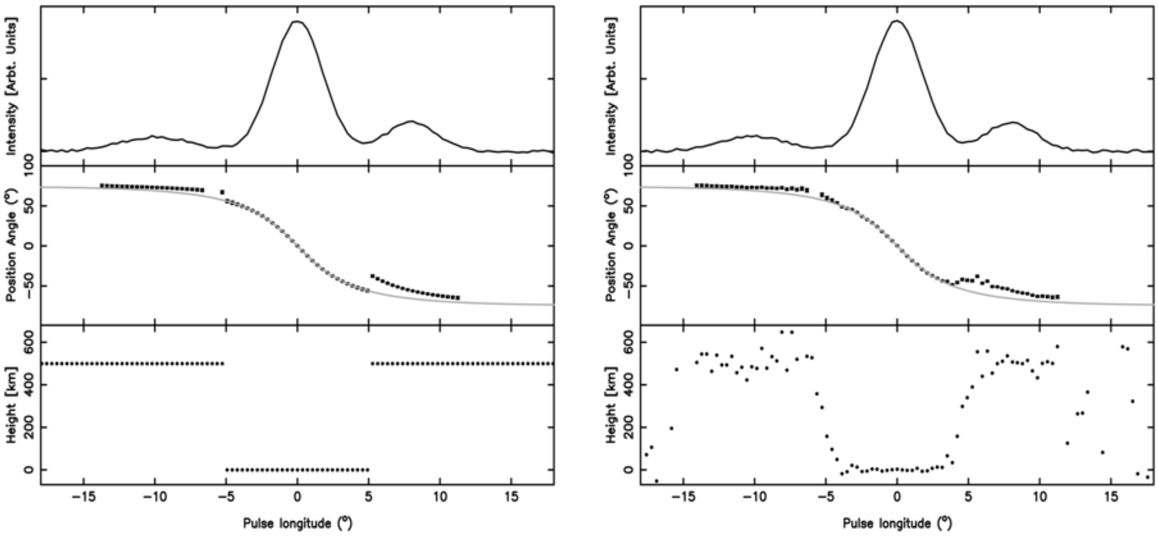

Fig. 1. The above plot shows the total intensity (top panel) the PPA traverse (middle panel) and the emission height (bottom panel) for a SIMULATED pulsar of period 0.7 sec, $\alpha = 39^o$, $\beta = 2^o$ and can be adequately described by three gaussian component giving rise to a central core and outer cone. The middle panel also shows the PPA traverse corresponding to the RVM model in solid line where as the points correspond to the BCW model. The left panel correspond to the case where two discrete emission height is considered. The right panel corresponds to the case where equation 2 has been applied to obtain the PPA traverse. Note that in both the case deviations in form of kinkiness appears in the PPA traverse (see text for further details)

of Figure 2 we show simulation of the PPA traverse using equation 2 assuming that the central core emission arises lower than the outer cone emission. This way we are able to generate the kinky feature in the PPA traverse. However we emphasize here that given the simple model that is being used we are only able to match the gross properties of the PPA traverse and do not claim to find the exact solution for α, β and r_{em}. For this a more sophisticated model needs to be considered.

4. Conclusion

Using a simple model we have been able to produce the kinkiness in the PPA traverse towards the central region of the pulse profiles which is quite often observed. As a consequence we are able to conclude the following:

(a) The central (or core) emission arises lower than the outer conal emission confirming a suggestion put forward by several people (see for example Rankin 1993).

(b) The PPA travese results from emission arising over a broad range of heights as has been recently suggested by Mitra & Li (2003).

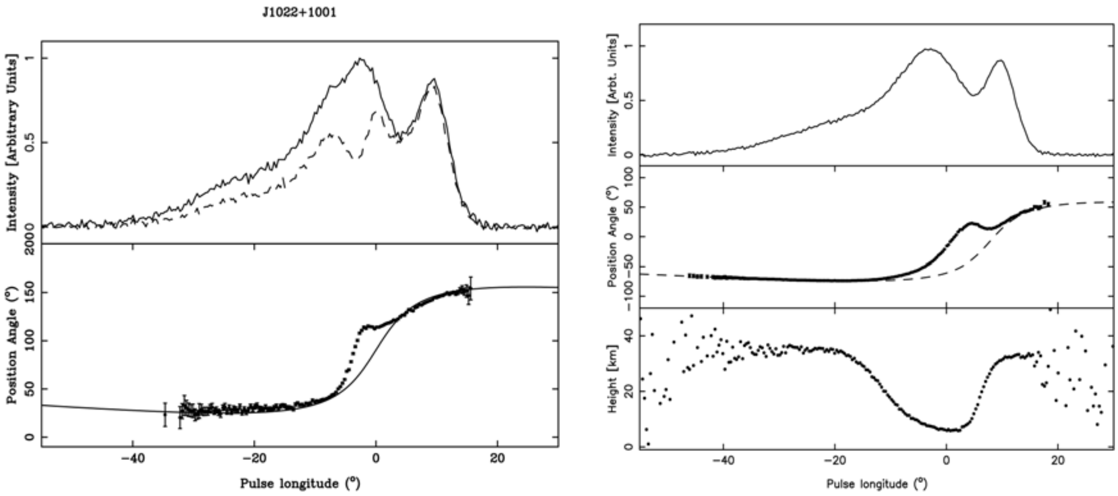

Fig. 2. The top panel of the left plot shows the total intensity profile (solid line) and linear polarization (dashed line) of PSR J1022+1001 at 410 MHz (data from Gould & Lyne 1998 as obtained from the EPN archieve maintained by MPIFR Bonn). The bottom panel shows the PPA traverse and the dashed line shows the RVM curve described by α = 3º and β =0.3º. The right plot is a simulation and application of equation 2. The meaning of the panels are the same as in Fig. 1.

Recently the central kinky feature seen in PSR J1022+1001 was interpreted as evidence for `return currents' in pulsars by Ramachandran & Kramer (2003). Here we show that by considering height dependent emission regions similar kinky features can be obtained and it is not necessary to invoke return currenteffects to explain this feature.

References

Blaskiewicz, M., Cordes, J. M., & Wasserman, I. 1991, ApJ, 370, 643
Gil, J. A. & Lyne, A. G. \ 1995, MNRAS, 276, L55
Gould, D. M. & Lyne, A. G. 1998, MNRAS, 301, 235
Mitra, D. & Li, X. H., 2003, A&A in press
Mitra, D. & Rankin, J. M. 2002, ApJ, 577, 322
Kramer, M. 1994, A&AS, 107, 527
Radhakrishnan, V.~\& Cooke, D.~J.\ 1969, ApJL, 3, 225
Ramachandran, R. & Kramer, M., 2003, A&A, 407, 1085
Rankin, J. M. 1993, ApJ, 405, 285

PULSAR SCIENCE WITH THE SQUARE KILOMETER ARRAY*

Aris Karastergiou[1] and Michael Kramer[2]
[1]School of Physics, University of Sydney, NSW 2006, Australia
[2]University of Manchester, Jodrell Bank Observatory, Macclesfield SK11 9DL, UK

ABSTRACT
The Square Kilometer Array, SKA, is the next generation radio telescope which will be built to have unprecedented sensitivity at radio frequencies. With a collecting surface of ~1 square kilometer, it is expected to make enormous advances in current fields of radio astronomy, as well as lead to new discoveries. We briefly summarize the specifications of this telescope and proceed to give a number of examples as to how pulsar astronomy will benefit from this instrument.

1. THE IMPORTANCE OF RADIO ASTRONOMY

The significance of radio astronomy stems from a few basic facts. First of all, radio-astronomical observations can be used as a diagnostic of matter in different phases, by means of the characteristic signatures of synchrotron radiation, maser emission and bremsstrahlung from thermal gas. The astrophysical information that is carried by radio frequencies can easily penetrate dust and gas, which absorbs and scatters light at most other wavelengths. Also, polarimetric radio observations provide information on cosmic magnetic fields. Finally, Very Long Baseline Interferometry using multiple radio telescopes still provides the highest resolution images in all astronomy. The brief history of radio astronomy is one of continuous, important astrophysical discoveries such as: cosmic microwave background radiation, quasars and radio galaxies, the cosmological evolution of radio sources, gravitational lenses, jets and super-luminal motions, dark matter in spiral galaxies, strong magnetic fields near the Galactic Centre, interstellar molecules and GMCs, masers and megamasers, the mass of the central object in an AGN, pulsars and their association with supernovae, gravitational radiation loss in a binary pulsar, the first extra-solar planetary system, GR time delay by planetary radar, slow rotation rate of Venus and the spin-orbit locking of Mercury.

2. THE SKA SPECIFICATIONS

The SKA will be designed to have 50 to 100 times the sensitivity of the VLA at the same frequency, with a brightness sensitivity of ~1K. As far as the frequency coverage is concerned, the aim is to span between ~150 MHz and ~22 GHz. The vastness of this band, only 2% of which is reserved for radio astronomy, will require the development of successful interference mitigation techniques to tackle the problem of interference.

One of the goals of the SKA will be to study transient objects as well as perform high spatial resolution observations. The intention is that the specifications will include a 1 square degree field-of-view, which, according to the predictions of the Hubble Deep Field, would include a surface populated by ~10^6 galaxies, not taking the effects of dust obscuration into account. At the same time a maximum resolving capacity of <0.1 arcsec is desirable, which exceeds the resolving power of HST, NGST and ALMA. The SKA

* *Proceedings of the 6th Hellenic Astronomical Society Conference, 15-17 September 2003, Penteli, Greece*

will not be a single 1 km^2 aperture telescope, but a radio interferometer consisting of a number of antennas. There are two basic design concepts: the large population, small aperture concept and the large aperture small population concept, each offering a number of advantages and disadvantages. Currently, a large number of designs are being tested for implementation. The schedule is to have a fully functional telescope by the year 2015.

3. OBSERVING PULSARS WITH THE SKA

In the 35 years since the discovery of pulsars, these unique objects have been invaluable in the study of a wide variety of physical and astrophysical problems. Most notable are studies of gravitational physics, the structure of the Milky Way and stellar and binary evolution, as well as studies of the structure of neutron stars themselves. Most, but not all, of the results in these fields have been obtained by pulsar timing. Other “uses” of pulsars depend on measuring their emission properties and/or the interaction of the radiation with an ambient medium. All such results will be measurable with the SKA to unprecedented precision. Pulsar astronomy will benefit hugely from the SKA, mainly because of the shear number of sources that will be discovered and studied. Searching for pulsars is a prime example where quantity results eventually in quality by discovering a large number of exotic objects that probe extreme physics. We list a number of areas of interest where the SKA is expected to provide the means for great advances.

3.1 PULSAR SEARCHES

Before we can time pulsars, we have to find them first. The sensitivity of the SKA makes this a particularly exciting research area. The straw man design of the SKA provides one with a sensitivity of S_{min} ~4 μJy in only 1 min integration time (assuming a detection threshold of 8σ, a system temperature of T_{sys} of 25K, and a bandwidth of $\Delta\nu \sim 0.5\nu$). This corresponds to the luminosities listed in the following Table.

Where	D (kpc)	L (mJy kpc^2)
Galactic Centre	8.5	0.1
Opposite Side of Galaxy	24	0.8
Magellanic Clouds	50-60	4.2
M31	690	660

Luminosities of pulsars detectable in a 1-min search with the SKA at various distances.

At 1.4 GHz, the currently **observed** luminosities range from 0.01 mJy kpc^2 to 10,000 mJy kpc^2 with a (logarithmic) median of ~25 mJy kpc^2. Clearly, the luminosity limits achievable with the SKA at the low end will not only provide an essentially complete census of the Milky Way pulsars but reasonable integration times even allow the discovery (and study!) of pulsars in nearby galaxies. We will firstly consider the implications resulting from the large number of pulsars that will be discovered.

3.2 TIMING

Studying the rotational behaviour and the propagation of the pulses in curved space-time is achieved by pulsar timing. In this mode of observing the arrival times of the pulses are measured with the highest possible precision. The special property of the SKA will be its unique sensitivity, about 10 times better than Arecibo or 100 times better than the Lovell telescope, Effelsberg or the GBT. An observed random-like variation in the pulsar’s spin-down properties (timing noise) has been studied for slowly-rotating pulsars, but is also now observed in some faster-rotating millisecond pulsars (e.g.~Lange et al.~2001, Lommen 2001). Newly developed techniques may help to circumvent this possible limitation (Hobbs et al.~2003), and further studies will show how commonly it will be observed in millisecond pulsars. Exciting results are expected in the array of gravitational physics by the use of timing (see section 3.5).

3.3 PULSARS AS NEUTRON STARS

The observations of relativistic effects in binary pulsars allow the measurements of neutron star masses. Most straightforward is the detection of a Shapiro time delay due to a companion for nearly edge-on orbits. Currently, the number of binary systems with such fortuitously aligned orbits is rather limited, but the combination of number of binary pulsars discovered and the sensitivity with the resulting timing precision will allow the measurement of many more neutron star masses. A manifold increase in the available statistics will allow us to study the amount of matter accreted during a spin-up process and will also help in studying the neutron star equation-of-state.

The study of the latter will also benefit from the vastly improved statistics of observed pulse periods. Currently, pulsar periods range from 1.5 ms to 8.5 s. The discovery of faster or slower pulsars will have implications on the neutron star structure and the connection of radio pulsars to magnetars, Soft-Gamma ray Repeaters (SGRs) and Anomalous X-ray Pulsars (AXPs).

3.4 PULSARS AS PROBES

The emission of radio pulsars interacts with the ionized magnetized medium it propagates through. The pulses become dispersed and scattered while the position angle of the linearly polarized emission component undergoes Faraday rotation depending on the electron density and magnetic field. At present, the best model for the electron density distribution in the Galaxy by Cordes \& Lazio (2002) demonstrates impressively how information about dispersion and scattering measures for a large number of independent line-of-sights to pulsars located in different parts of the Milky Way can be used to establish an increasingly detailed understanding. A Galactic Census of pulsars will provide so many lines-of-sight that, in particular with a combination of HI absorption measurements, distances, electron densities and scattering measures will be determined in such numbers that very detailed modelling becomes possible and a complete 3-D map of the Galaxy unfolds.

3.5 GRAVITATIONAL PHYSICS

One of the most exciting motivations to find lots of new pulsars is the prospect of finding some very exciting and exotic systems. We should find more planetary systems, we may find (over-determined!) double pulsar systems and perhaps even exotic or strange stars. Studying regions of high stellar density with an increased probability of stellar interactions, such as globular clusters and the Galactic centre (which is particularly interesting due to its conditions favouring more massive stars) should provide us with “the holy grail” of a pulsar-stellar black hole system, perhaps even a millisecond pulsar orbiting a black hole. For the first time it would be possible to probe the properties of a black hole predicted by Einstein’s theory of gravity as well as perform more stringent tests of GR (e.g.~Weisberg \& Taylor 2003, van Straten et al. 2001, Kramer 1998).

Monitoring a large sample of millisecond pulsars in a so-called Pulsar Timing Array (PTA) offers the means to detect the stochastic gravitational wave background that is expected in various cosmological theories (e.g.~Foster \& Backer 1990). The PTA would be used to search for (correlated) structures in the timing residuals of millisecond pulsars distributed across the sky. It will be sensitive to long-wave gravitational signals and is therefore complementary to current ground-based gravitational wave detectors such as GEO600 or LIGO and even future detectors such as LIGO-II or LISA. With a rough estimate of about 1000 millisecond pulsars to be discovered, the SKA would not only provide the necessary dense PTA but also the means of achieving the necessary sub-μs timing precision that will be needed to extract the weak signal.

4. CONCLUSIONS

The SKA will provide pulsar science with a number of opportunities. Apart from the ones listed above, we can also mention studies of the unsolved emission mechanism problem in pulsars, studies of the gravitational interactions in globular clusters by means of accurate parallax measurements and even black hole studies by means of the GR effects on the companion neutron star, were such a system to be found. Pulsars are transient objects on which we already have accumulated knowledge. However, the probability that there are other types of transient phenomena which have not yet been identified is quite large, since the means have not existed to investigate the transient phase space. The SKA, therefore, is expected not only to expand our knowledge on pulsars and how we can use them, but also to discover fundamentally new phenomena. Global planning for the SKA is well underway and when completed, this telescope will provide us with new, unique information about the Universe.

Acknowledgements

The science case is developed in collaboration with many colleagues across the world, and in particular Joe Lazio (chair), Don Backer, Jim Cordes, Justin Jones, Michael Rupen, and Jill Tarter.

REFERENCES

Cordes, J.M., Lazio, J., 2002, astro-ph/0007310

Foster, R.S., Backer, D.C., 1990, ApJ, 361, 300

Hobbs, G., Lyne, A.G., Kramer, M., 2003, in Radio Pulsars, ASP Conf.~Ser., eds.~M.~Bailes, D.~Nice, \& S.~Thorsett

Kramer, M. 1998, ApJ, 509, 856

Lange, Ch., et al., 2001, MNRAS, 326, 724

Lommen, A., 2001, PhD-thesis, University of California at Berkeley

van Straten, W., et al., 2001, Nature, 412, 158

Weisberg, J., Taylor, J.H., 2003, in Radio Pulsars, ASP Conf..Ser., eds. M. Bailes, D. Nice, & S. Thorsett

GAMMA RAY BURSTS: SOME NEW DEVELOPMENTS*

Demosthenes Kazanas

NASA/GSFC

Abstract: The field of Gamma Ray Bursts has moved in the past ten or so years from totally uncertain, to vexing, to certain and more recently to well established field of astrophysics, as observations of increasing quality and relevance became available which determined their distance and emission at frequencies other than gamma rays. Nonetheless, as these questions have been answered other questions have arisen which still remain uncertain, most notably the GRB engine and its relation to observations across the electromagnetic spectrum. Some of the more recent facts and models will be reviewed with emphasis on the remaining problems.

* Main Session Invited Review

*ABSTRACTS OF PAPERS POSTED DURING THE SESSION ON HIGH ENERGY ASTROPHYSICS**

RADIATIVE SIGNATURES OF THE 'BOX' MODEL OF SHOCK ACCELERATION

K. Moraitis & A. Mastichiadis

Section of Astrophysics, Astronomy and Mechanics, Department of Physics, University of Athens, Greece

Abstract: We study the time evolution and emission of the so-called "box" model of shock acceleration (*Drury et al, 1999, A&A, 347, 370*). The novelty of this acceleration scheme is that it can be written in the form of a time-dependent kinetic equation which allows particle diffusion in an energy dependent region around the shock, i.e. it addresses the possibility that the diffusion coefficient might be energy-dependent. We solve the continuity equation analytically assuming constant injection of particles at low energies and including a term for energy losses due to synchrotron radiation and inverse Compton scattering in the Thomson limit. We find that the accelerated particles form a power-law up to some energy which, in steady state, depends on the balance between the acceleration and energy loss timescales. From the electron distribution function we calculate the radiated spectra and discuss possible applications to the X- and gamma-ray spectra observed recently from the young supernova remnant SN 1006.

QSO PHOTOMETRIC REDSHIFT ESTIMATION FOR THE XMM-NEWTON/2DF SURVEY

S. Kitsionas[1], E. Hatziminaoglou[2], I. Georgantopoulos[1], A. Georgakakis[1], O. Giannakis[1]

[1]IAA-National Observatory of Athens, Greece

[2]Instituto de Astrofisica de Canarias, Tenerife, Spain

Abstract: The technique of estimating redshifts using photometric rather than spectroscopic observations has recently received great attention due to its simplicity and the accuracy of the results obtained. In this work, we estimate photometric redshifts for an X-ray selected QSO sample. This is the first time this technique is applied on such a sample. We first calculate the accuracy of the results obtained by comparing photometric to spectroscopic redshifts for a sub-sample of our QSO sample: for the majority (~67%) of the objects in this sub-sample, photometric redshift estimates are correct within $\Delta z<0.3$. We then derive the photometric redshift distribution for the whole QSO sample. In the future, we expect to use the photometric redshift distribution in order to derive the distributions of properties such as the Hardness Ratio and hence the hydrogen column density, the luminosity function etc. As an example, we estimate here the dependence of the Hardness Ratio of the QSO sample on photometric redshift.

* *Proceedings of the 6th Hellenic Astronomical Society Conference, 15-17 September 2003, Penteli, Greece*

Session V

COSMOLOGY, RELATIVITY and RELATIVISTIC ASTROPHYSICS

Conveners: M. Plionis, S. Persides and K. Kokkotas

MAGNETIC TENSION, CURVATURE AND GRAVITATIONAL COLLAPSE*

Christos G. Tsagas

Department of Mathematics and Applied Mathematics, University of Cape Town
Rondebosch 7701, South Africa
DAMTP, Centre for Mathematical Sciences, University of Cambridge, Wilberforce Road Cambridge
CB3 0WA, UK

ABSTRACT: We investigate the physics of magnetised gravitational collapse by studying the behaviour of a timelike congruence of worldlines in the presence of a magnetic field. We show that the general relativistic coupling between magnetism and geometry, and the tension properties of the field, lead to magneto-curvature stresses that can prevent an initially converging congruence from focussing. We provide, in the form of a lemma, a geometrical requirement sufficient for preventing caustic formation without violating the standard energy conditions.

The behaviour of magnetic and of electromagnetic, fields in strong gravity environments has been a matter of considerable interest for many researches over the years. To the best of our knowledge, however, most of the available studies address the possible gravitational effects on the Maxwell field and relatively few look into the implications of magnetic fields, in particular, for the gravitational collapse itself. Perhaps the most intriguing result has been that obtained by Thorne in his elaborate analysis of Melvin's cylindrical magnetic universe [1]. There, by introducing and developing the concept of 'cylindrical energy', the author reached the conclusion that "a strong magnetic field along the axis of symmetry may halt the cylindrical collapse of a finite cylinder before the singularity is reached" [2]. However, Thorne's results, though remarkable in their own right, remained more of a mathematical curiosity. In this article we revisit the issue of the magnetic impact on gravitational collapse from an apparently entirely different viewpoint. We consider the non-spherical (but not necessarily cylindrical) collapse of a magnetised fluid element, by looking into the behaviour of two neighbouring and initially converging particle worldlines. As it turns out, we arrive at the same qualitative result as Thorne did, namely that the gravitational collapse of a magnetised fluid element will stop before the singularity is formed when certain criteria are satisfied. In our analysis, however, the reason the collapse of the magnetised matter will never reach its endpoint is seemingly unrelated to the cylindrical energy of the Melvin universe. Instead, we find that it is the intricate coupling between magnetism and geometry and the tension properties of the magnetic field, namely the elasticity of the magnetic forcelines, which can prevent the ultimate collapse from happening. We start with a general spacetime containing a single perfect fluid of very high (effectively infinite) conductivity and allow for the presence of a magnetic field. Throughout the paper we consider standard conventional matter with positive gravitational mass and pressure. The infinite conductivity assumption means that there is no electric field and that the magnetic field is "frozen in" with the matter. This is the well known MHD approximation [3]. In what follows we examine the implications of the magnetic presence for the gravitational collapse of the fluid. We do so by testing the convergence of the timelike congruence that represents the worldlines of the matter particles.

When looking into the dynamics of gravitational collapse Raychaudhuri's formula is probably the most important equation, as it covariantly describes the volume evolution of a selfgravitating fluid element. Consider, in particular, a congruence of timelike worldlines tangent to the 4-velocity field u_a (with $u_a u^a = -1$). These are the worldlines of the fundamental observers, namely of the observers

---

*_Main Session Invited Review_

Proceedings of the 6th Hellenic Astronomical Society Conference, 15-17 September 2003, Penteli, Greece

that follow the motion of the fluid. The Raychaudhuri equation determines the proper-time evolution of $\Theta = \nabla_a u^a$, the scalar that measures the average contraction (or expansion) between two neighbouring worldlines of the congruence [4]. In a magnetised environment Raychaudhuri's formula reads [5]

$$\dot{\Theta} = -\frac{1}{3}\Theta^2 - \frac{1}{2}\kappa(\mu + 3p + B^2) - 2(\sigma^2 - \omega^2) + D_a\dot{u}_a + \dot{u}_a u^a, \qquad (1)$$

where $\kappa = 8\pi G$, μ and p are respectively the energy density and pressure of the fluid, $B^2 = B_a B^a$ measures the energy density and the isotropic pressure of the magnetic field (B_a), σ^2 and ω^2 are the respective magnitudes of the shear and the vorticity associated with u_α and $\dot{u}_a = u^b \nabla_b u_a$ is the 4-acceleration. The latter satisfies the momentum-density conservation law, which for a highly conductive perfect fluid takes the form [5]

$$(\mu + p + \frac{2}{3}B^2)\dot{u}_a = -D_a p - \in_{abc} B^b curlB^c - \Pi_{ab}\dot{u}^b, \qquad (2)$$

where $D_\alpha = h_\alpha \nabla_\alpha$ is the covariant derivative operator orthogonal to u_α and $\Pi_{\alpha b} = -B_{<\alpha}B_{b>}$ is the symmetric trace-free tensor that describes the magnetic anisotropic pressure and also conveys the tension properties of the field.[1] Note that we consider a non-geodesic worldline congruence, since the motion of the particles is dictated by the combined Einstein-Maxwell field and not by gravity alone. Also, the worldlines of the fluid are not hypersurface orthogonal which explains the presence of the vorticity term in (1).

The right-hand side of Eq. (1) determines the dynamics of the average volume evolution. Terms that are positive definite lead to expansion, while negative definite terms cause contraction. It becomes clear then that, when the standard energy conditions are satisfied, all the right-hand terms have a clear-cut role with the exception of $D_a\dot{u}^a$, namely of the projected divergence of the 4-acceleration, which in principle can go either way. For the rest of this letter, we will focus our attention on $D_a\dot{u}^a$ and examine its potential implications for the final fate of collapsing magnetised fluid element.

The magnetic Lorentz force (per unit mass) propagates via the associated acceleration vector $a_a = -\in_{abc} curlB^c$, where $\in_{abc}$ is the alternating tensor orthogonal to u_a and $a_a u^a = 0$. Using the 3-Ricci identity (see Eq. (5) below), the projected gradient of aa decomposes as

$$D_b a_a = -D_b(\in_{acd} B^c curlB^d) = -\frac{1}{2}D_b D_a B^2 + D_b B^c D_c B_a + B^c D_c D_b B_a + \Re_{acbd}B^c B^d, \qquad (3)$$

where $\Re_{acbd}$ is the Riemann tensor of the subspace of the tangent space orthogonal to u_α. In the absence of rotation the latter is the 3-dimensional space orthogonal to our worldline congruence. Note the last three terms on the right-hand side of the above, which convey the magnetic tension effects, and in particular the magneto-curvature stress at the far end of Eq. (3). This term reflects the special status of vectors, as opposed to that of scalars, in general relativity. This special status stems from the geometrical nature of the theory and it is manifested in the Ricci identity

$$2\nabla_{[a}\nabla_{b]}B_c = \Re_{dcba}B^d, \qquad (4)$$

[1] We use angled brackets to indicate the symmetric and trace-free part of projected second-rank tensors. Thus, $B_{\langle a}B_{b\rangle} = B_a B_b - \left(B^2/3\right)h_{ab}$, where $h_{ab} = g_{ab} + u_a u_b$ projects orthogonal to u_a.

applied here to the magnetic field vector, with $\Re_{dcba}$ being the spacetime Riemann tensor. When projected orthogonal to u_a, the above expression leads to what is commonly referred to as the 3-Ricci identity [4]

$$2D_{[a}D_{b]}B_c = \Re_{dcba}B^d - 2\omega_{ab}h_c{}^d\dot{B}_d\,, \tag{5}$$

where ω_{ab} is the vorticity tensor associated with the fluid flow. The Ricci identity (in either form) plays a fundamental role in the mathematical formulation of general relativity. Essentially, it is the definition of spacetime curvature itself. The Ricci identity also argues for a direct interaction between vector sources and curvature, which adds to the standard interlay between matter and geometry as we know it from the Einstein field equations. In the case of a magnetic field, this direct coupling brings into play the tension properties of the latter, namely the elasticity of the magnetic force lines, and couples it in an intricate way with the geometry of the space. This unique feature, the magnetic tension, manifests the well known fact that the field lines do not like to bend and react to any attempt that distorts them. Indeed, within the Newtonian theory the magnetic tension is known to trigger restoring stresses which depend on the strength of the field and on the deformation of the magnetic force lines, as measured by their curvature radius [3]. What the general relativistic expression (3) shows, is that deviations from Euclidean geometry will lead to analogous tension stresses, which are also proportional to the magnetic strength and to the amount of curvature distortion. This time, however, it is the curvature of the space itself that causes part of the magnetic deformation. The effects of the aforementioned tension stresses are generally counter-intuitive because of the nature of the property itself and its subtle coupling with the geometry of the space. The latter, in particular, means that even weak magnetic fields can lead to a strong overall effect under favourable circumstances. Some of the implications of the field's presence for magnetised cosmologies have been discussed in [6]. Here, we will examine the role of the same tension stresses during the gravitational collapse of a magnetised fluid.

Let us assume that both the fluid and the magnetic field have a spatially homogeneous energy density distribution, namely set $D_a\mu = D_a p = 0 = D_a B^2$. In physical terms this means that any inhomogeneity that might be present is relatively small. Then, Eq. (2) ensures that $\dot{u}_a B^a = 0$ and subsequently it reduces to

$$\left(\mu + p + B^2\right)\dot{u}_a = -D_a p - \in_{abc} B^b curl B^c\,, \tag{6}$$

Taking the projected divergence of the above, using the trace of (3), with $D_a B^a = 0$ due to the absence of electric fields, and substituting into Eq. (1) we arrive at

$$\dot{\Theta} + \frac{1}{3}\Theta^2 = -\frac{1}{2}\kappa\left(\mu + 3p + B^2\right) + 2\omega^2 - 2\sigma^2 - 2W^2 + 2\Sigma^2 + \frac{1}{\in}\Re_{ab}B^aB^b + \dot{u}_a\dot{u}^a\,, \tag{7}$$

where $\in = \mu + p + B^2, W^2 = \left(D_{[a}B_{b]}\right)^2/2\in, \Sigma^2 = \left(D_{\langle a}B_{b\rangle}\right)^2/2\in$ and $\Re_{ab} = \Re_{acb}$ is the Ricci tensor of the spatial sections. Consider the magneto-curvature term $\Re_{ab}B^aB^b$ in Eq. (7), which measures the curvature of the 3-space along the direction of the magnetic force lines. Then, using the Gauss-Codacci equation one can show that when there is only the magnetic field present $\Re_{ab}B^aB^b = 0$ [7]. So, despite the magnetic energy input, the geometry of the space in the direction of the field lines is flat; a result independent of the magnetic strength. Technically speaking, it is the negative pressure of the field, along its own direction, which cancels out the positive contribution of the magnetic energy density. More intuitively, however, it is the inherit tendency of the magnetic force lines to remain 'straight' which is responsible for the aforementioned null result. In general of course

$\Re_{ab}B^aB^b \neq 0$. In that case the magneto-curvature effect on Θ is rather unexpected. According to (7), when $\Re_{ab}B^aB^b < 0$ the magneto-geometrical stresses bring the worldlines of the particles closer to each other, but push them apart if the field lines are 'positively curved', that is for $\Re_{ab}B^aB^b > 0$. This is clearly in contrast with the common perception which always associates positive curvature with contraction and gravitational collapse. The reason behind this counter-intuitive behaviour is the tension properties of the magnetic force lines. The same tension stresses are also responsible for the much unexpected behaviour exhibited by some magnetised cosmological models [6].

Consider the tensors $\Sigma_{ab} = D_{\langle a}B_{b\rangle} / \sqrt{\in}$ and $W_{ab} = D_{[a}B_{b]} / \sqrt{\in}$ which have been introduced in Eq. (7) so that $2\Sigma^2 = (D_{\langle a}B_{b\rangle})^2 / \in$ and $2W^2 = (D_{[a}B_{b]})^2 / \in$. The former describes distortions in the magnetic field distribution, while the latter is the magnetic twist tensor. Note that, although Σ_{ab} and W_{ab} have the shear and the vorticity as their respective kinematical analogues, their effect on Θ is exactly the opposite of that normally associated with the shear and the vorticity (see also [8]). Again, this counter-intuitive magnetic behaviour is down to the fact that both Σ and W carry the tension properties of the field. In what follows we will assume that the effect of Σ and W is cancelled out by that of their respective kinematic counterparts. In other words, we will consider the case where $\omega^2 + \Sigma^2 = W^2 + \sigma^2$. Although it may not seem so, this assumption is much less restrictive that it looks. We will return to it a little later, but for the moment we would like to note that, in addition to counteracting each other, the pairs ω^2, W^2 and σ^2, Σ^2 are of the same nature and quadratic in D_au_b and D_aB_b. The latter ensures that the aforementioned terms, unlike $\Re_{ab}B^aB^b$ for example, become appreciable only in highly inhomogeneous configurations. Under these conditions the Raychaudhuri equation reads

$$\dot{\Theta} + \frac{1}{3}\Theta^2 = -\Re_{ab}u^au^b + c_{\mathrm{a}}^2\Re_{ab}n^an^b + \dot{u}_a\dot{u}^a\,, \tag{8}$$

where $c_{\mathrm{a}}^2 = B^2 / \in$ is the Alfvén speed and $\Re_{ab}$ is the Ricci tensor of the spacetime with $\Re_{ab}u^au^b = \kappa\left(\mu + 3p + B^2\right)/2 > 0$. The latter ensures that the strong energy condition is satisfied. Note that $n_a = B_a / \sqrt{B^2}$ is the unit vector along the magnetic force lines.

The assumption of a spatially homogeneous energy density distribution for the sources means that $D_ap = 0$, which in turn guarantees that the 4-acceleration vector $\dot{u}^a$ depends entirely on the magnetic field (see Eq. (6)). Therefore, when the field is absent all the positive definite terms in the right-hand side of (8) vanish and an initially converging congruence (i.e. one with $\Theta_0 < 0$) will focus within a finite amount of time, unless the energy conditions are violated. This is a fundamental and well known result about gravitational collapse, which forms the basis of all the singularity theorems of the 1960's and 70's (e.g. see [9]). In the magnetic presence, however, the two positive definite terms in the right-hand side of (8) will resist the collapse. Thus, ignoring the supporting effect of $\dot{u}_a\dot{u}^a$, we arrive at the following lemma: *In a spacetime filled with a magnetised perfect fluid of infinite conductivity and with a homogeneous energy distribution of the sources, the magneto-curvature effects can prevent an initially converging congruence of non-geodesic worldlines from focusing, without violating the standard energy conditions, if*

$$c_{\mathrm{a}}^2 \Re_{ab} n^a n^b \geq \Re_{ab} u^a u^b \tag{9}$$

Obviously, the above also holds when the assumption $\omega^2 + \Sigma^2 = W^2 + \sigma^2$ is replaced by $\omega^2 + \Sigma^2 \geq W^2 + \sigma^2$. It still holds when $\omega^2 + \Sigma^2 < W^2 + \sigma^2$, provided that $\dot{u}_a\dot{u}^a / 2 > W^2 + \sigma^2 - \omega^2 - \Sigma^2$. So, our conclusions hold for a variety of combinations between ω^2, Σ^2, W^2 and σ^2. This means that the earlier restriction placed on these quantities is not essential for the validity of the lemma. It helps, however, to demonstrate the role of the curvature terms in Eq. (7), which should decide the fate of the collapse anyway. Finally we note that, in addition to the usual matter fields, gravitational waves and tidal forces also contribute to $\Re_{ab} B^a B^b$ (e.g. see [4, 7]). The latter, in particular, are expected to increase dramatically as we approach the singularity.

From the physical point of view, we arrived at the above lemma by focusing on the two geometrical quantities in the right hand side of Eq. (7) at the expense of the rest. At first this may appear too drastic but a closer look shows that it is not. To begin with, not all of these five quantities support the contraction. In fact most of the terms (three) resist the collapse, which means that they are more likely to support against further contraction rather than the opposite. Even if we assume that the two terms favouring collapse are stronger (and we have no reason to assume that), their overall effect should be nearly balanced by the counteraction of the remaining three terms. Indeed, given that all these quantities are of the same perturbative order and nature, it is rather implausible to argue that one or two of them will completely dominate the rest. The opposite, namely that $\dot{u}_a\dot{u}^a / 2 + \omega^2 + \Sigma^2 > W^2 + \sigma^2$, seems more likely. However, the key physical argument for focusing on the geometrical quantities of Eq. (7) is that, as the collapse proceeds, we expect a dramatic increase in the curvature distortion. In fact, it is common belief that at the late stages of the collapse the curvature diverges. On these grounds, one expects that near the singularity the geometrical terms will completely dominate the right hand side of (7). In other words, the ultimate fate of the collapsing magnetised fluid should be decided by the balance between the two quantities in (9).

This lemma opens a number of new possibilities. The first implication is that, despite the general perception, violating the energy conditions to prevent an initially converging congruence from focusing is not necessary when magnetic fields are present and certain geometrical conditions are met. In other words, nonspherical magnetised collapse (the magnetic presence will inevitably distort spherical symmetry to a larger or lesser degree) does not necessarily lead to a singularity. Whether this mathematical lemma applies to physical situations, such as the gravitational implosion of a massive star for example, depends on whether the magnetic field of the star, or part of it, survives until the later stages of the collapse. Then, if condition (9) is met, the contraction can stop and massive magnetised stars could bounce before they actually reach the final singularity. Similarly, if one evolves a magnetised universe backward into the past, they may find, instead of a big-bang singularity, a nonsingular high density phase which may re-expand into the past. If this were to occur, general relativity could provide a conventional, nonsingular closed magnetised cosmological model with potentially unlimited cycles of expansion, contraction and bounce. Note that by itself the above lemma is not enough to guarantee a singularity-free spacetime, at least under the current consensus of what a singularity is [9]. For example, condition (9) does not seem to interfere with the geodesic completeness, or not, of a magnetised spacetime. However, any singularities due to geodesic incompleteness that might still exist will be of limited influence if most of the matter can successfully avoid them. Overall, in view of (i) the central role played by the Raychaudhuri equation in the formulation of all singularity theorems; (ii) the probable physical irrelevance of purely geodesic particle motions in the magnetic presence; (iii) the widespread presence of magnetic fields in the universe, this lemma poses the question as to whether and up to what extent magnetism can modify some of the standard views on singularity formation and of their physical consequences.

The main issue, however, is not so much the existence of magnetic related stresses, which resist gravitational collapse and can potentially prevent the formation of caustics. In fact, whenever we deal with worldline congruences which are not hypersurface orthogonal or geodesics, supporting stresses will always appear due to rotation or due to pressure gradients. The second and, in our opinion, the key point made by the above analysis is that, when magnetic fields are involved, one of the supporting stresses depends (in fact it is proportional) on the distortion of the curvature itself. In other words, the further the collapse progresses the stronger the resistance of the magneto-curvature stresses grows. The presence of these stresses is a direct and inevitable consequence of the vector nature of magnetic fields and of the geometrical interpretation of general relativity, while their counter-intuitive effects are the result of the tension properties of the field. It is the elasticity of the magnetic force lines, their inherit tendency to remain 'straight', which manifests itself as a reaction to curvature distortions that is proportional to the amount of the distortion itself. In a sense, it appears as though the elastic properties of the field have been injected in to the fabric of the space, which behaves as if it has acquired tension of its own.

AcknowledgmentsThe author wishes to thank George Ellis for numerous helpful discussions and Leon Mestel for many insightful comments. This work was supported by NRF, Sida and DAA.

References

[1] M.A. Melvin, Phys. Letters 8, 65 (1964); M.A. Melvin, Phys. Rev. 139, B225 (1965).
[2] K.S. Thorne, Phys. Rev. 138, B251 (1965); K.S. Thorne, Phys. Rev. 139, B244 (1965).
[3] E.N. Parker, Cosmical Magnetic Fields (Oxford University Press, Oxford 1979); L. Mestel, Stellar Magnetism (Oxford University Press, Oxford 1999).
[4] G.F.R. Ellis, in Carg`ese Lectures in Physics, Ed. E. Schatzmann (Gordon and Breach, New York, 1973), Vol. VI, p. 1; G.F.R. Ellis and H. van Elst, in Theoretical and Observational Cosmology, Ed. M. Lachiéze-Ray (Kluwer, Dortrecht, 1999), p. 1.
[5] C.G. Tsagas and J.D. Barrow, Class. Quantum Grav. 14 2539, (1997); C.G. Tsagas and R. Maartens, Phys. Rev. D 61, 083519 (2000).
[6] D.R. Matravers and C.G. Tsagas, Phys. Rev. D 62, 103519 (2000); C.G. Tsagas, Phys. Rev.Lett. 86, 5421 (2001); C.G. Tsagas, in Modern Theoretical and Observational Cosmology,Eds. M. Plionis and S. Cotsakis (Kluwer, Dortrecht, 2002), p. 45 (gr-qc/ 0112077).
[7] C.G. Tsagas, Class. Quantum Grav. 19, 3709 (2002).
[8] D. Papadopoulos and E.P. Esposito, Astrophys. J. 257, 10 (1982).
[9] S.W. Hawking and G.F.R. Ellis, The Large Scale Structure of Spacetime (Cambridge University Press, Cambridge 1973); R.M. Wald, General Relativity (University of Chicago Press, Chicago 1984).

SIMULATING SOURCES OF GRAVITATIONAL WAVES WITH NUMERICAL RELATIVITY*

Nikolaos Stergioulas

Department of Physics, Aristotle University of Thessaloniki,
Thessaloniki 54124, Greece

ABSTRACT

With several new gravitational-wave detectors being already online, there is a growing need for accurate predictions of the waveforms for different promising sources of gravitational waves. Through numerical relativity, such waveforms can now be computed for cases such as the pulsations of rapidly rotating neutron stars and their collapse to Kerr black holes. We give a brief summary of recent and ongoing research on these topics.

INTRODUCTION

The long-awaited new generation of gravitational-wave detectors is now online, setting new uppers limits on the strength of gravitational waves from specific sources. In the next few years the new detectors are expected to reach their design sensitivity, bringing the detection gravitational waves very close to becoming reality. For several interesting sources, the successful detection and/or the extraction of source parameters from the detected signal, requires a prior knowledge of the expected waveform with high accuracy. Although part of the signal for some sources is being treated very successfully with post-Newtonian techniques, for most sources the full nonlinear solution of the Einstein's field equations is required. For several decades now, numerical techniques have been applied for this purpose and in recent years new formulations and an increase in supercomputing power have finally enabled the first robust predictions of gravitational waveforms via 3D nonlinear simulations.

The breakthrough in 3D numerical relativity came after the traditional 3+1 equations were formulated in a conformal-traceless approach, initially by Nakamura, Oohara and Kojima (1987). Particular variants of this approach are now commonly called the BSSN formulation, after Shibata and Nakamura (1995) and Baumgarte and Shapiro (1999). The long-term stability of this formulation is by far superior to the ADM formulation, which was plagued by numerical instabilities. Since then, several new versions and formulations for stable evolutions have appeared, but the so-called BSSN formulation has been applied already to numerous specific problems with success (for examples, see e.g. Alcubierre et al. 2000, Font et al. 2002, Duez et al. 2003, Shibata, Taniguchi and Uryū, 2003, and references therein). The conformal-traceless formulation is based on the introduction of a conformal factor ϕ and a redefinition of the basic evolution variables of the $3+1$ approach. Of central importance is the introduction of the conformal connection functions $\tilde{\Gamma}^i$, which are evolved with separate evolution equations. The number of equations required to evolve the spacetime is thus increased by five. The new system of equations shows improved stability properties only when certain supplementary conditions are fulfilled (see Alcubierre et al. 2000 for details).

RAPIDLY ROTATING NEUTRON STARS

* Main Session Invited Review

Proceedings of the 6th Hellenic Astronomical Society Conference, 15-17 September 2003, Penteli, Greece

Both the spacetime and the hydrodynamical evolution need to be modelled accurately, in order to study gravitational waves from rapidly rotating neutron stars. For the hydrodynamics, the HRSC finite-volume method with a 3rd-order PPM reconstruction has been proven very successful in maintaining long-term equilibrium for stars rotating even at the mass-shedding limit (Font, Stergioulas and Kokkotas, 2000). For the spacetime evolution, it is important to use boundaries that are sufficiently far away from the star and a shift condition such as the Gamma-freezing shift (Alcubierre et al. 2002). An example of the long-term evolution of the rotational velocity profile for a rapidly rotating star can be found in Stergioulas and Hawke (2003). A review of recent results concerning the evolution of rotating stars in numerical relativity can be found in Stergioulas (2003).

GRAVITATIONAL WAVES FROM PULSATIONS

Pulsations in rotating neutron stars can be excited after core-collapse or accretion-induced collapse and after the merger of two neutron stars. In core-collapse, the proto-neutron star quickly settles into quasi-equilibrium after core-bounce, with excited oscillations surviving for several oscillation periods (see e.g. Dimmelmeier et al. 2001). It is expected that the dominant oscillation modes excited in rotational core collapse are the quasi-radial ($l = m = 0$) mode and the quadrupole ($l = 2, m = 0$) mode. Due to rotational couplings of nonradial terms in its eigenfunction, the quasi-radial mode becomes a strong emitter of gravitational waves in rapidly rotating stars (it could, in fact, become the dominant mode in which gravitational waves are emitted). The amplitude of the oscillations is estimated as several percent at the centre of the star. In the simulations of binary neutron star mergers by Shibata and Uryū (2000), quasi-periodic oscillations are excited, through which strong gravitational waves are emitted. The frequency range of these oscillations suggests that they could correspond to specific non-axisymmetric normal modes of the star. In addition to the non-axisymmetric modes, the axisymmetric quasi-radial mode could also be excited. The first computation of the quasi-radial modes in full general relativity was recently obtained via 3D nonlinear evolutions by Font et al. (2002).

In both protoneutron stars and hypermassive neutron stars created in binary mergers, gravitational radiation can drive several modes unstable, through the CFS mechanism (for a review, see e.g. Friedman and Lockitch, 2001), provided the star is rotating sufficiently rapidly. In relativistic stars, the $l = m = 2$ f-mode becomes unstable when $T/|W| > 0.07$ for uniform rotation (Stergioulas and Friedman, 1998, Morsink, Stergioulas and Blattnig, 1999) and at somewhat larger $T/|W|$ for differentially rotating stars (Yoshida et al. 2002). The $l = m = 2$ r-mode can become unstable at considerably lower rotation rates (for a review see Kokkotas and Andersson, 2001). Nonlinear 3D simulations (in the Cowling approximation) of the $l = m = 2$ r-mode in rapidly rotating relativistic stars by Stergioulas and Font (2001) have shown that this mode is indeed a discrete mode. More recently, these modes have been computed in full general relativity, including nonlinear spacetime evolution and gravitational-wave emission (see Stergioulas and Hawke, 2003, see Goodale et al. 2002, Baiotti et al. 2002 for a description of the numerical code). The frequency of the relativistic r-mode is very close to the frequency computed in the Cowling approximation, even for very rapidly rotating stars. Both the spacetime and the hydrodynamical variables oscillate with the same discrete frequency everywhere (as measured by a coordinate observer). We extract gravitational waves by first matching

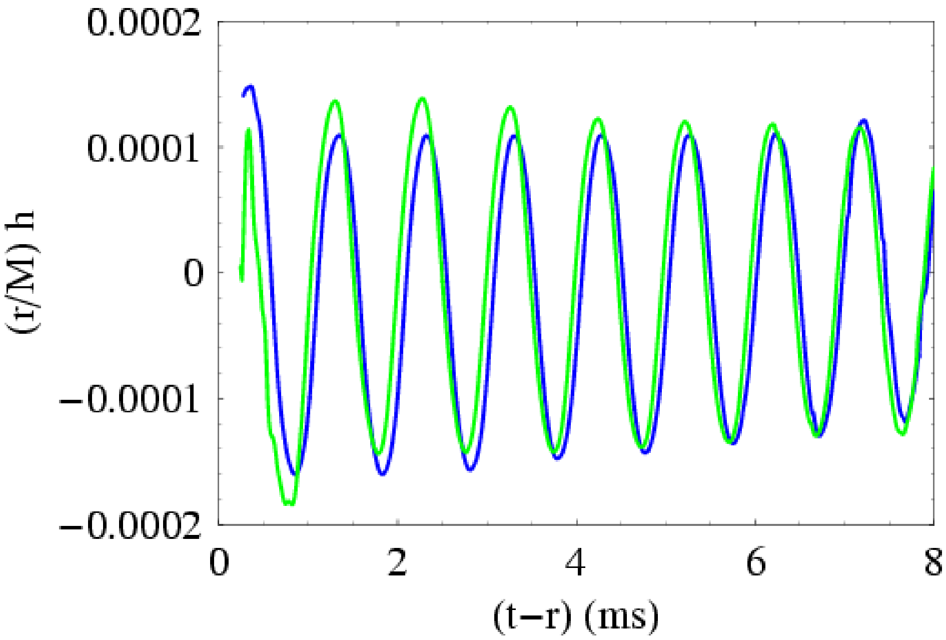

Figure 1. *Gravitational wave corresponding to the odd-parity Zerilli function* $\Psi^{(22)}$*, for an* $l = m = 2$ r*-mode in a rapidly rotating relativistic star, extracted at two different locations. Non-wave parts have been eliminated using their known radial dependence.*

the nonlinear evolution at some distance from the star to linear perturbations of a Schwarzschild background (see e.g. Abrahams et al. 2002, Allen et al. 1998). Since the rotating star is not spherical, stationary axisymmetric multipole-moment terms appears in the extracted Zerilli functions. . When the extraction is done in the near-zone, the non-wave parts in the Zerilli functions can be comparable to or larger than the actual gravitational wave. These non-wave parts can be eliminated, to a large degree, when their radial behaviour is known (see Kawamura, Oohara and Nakamura, 2003, for details). Applying this technique, we have obtained the first fully-relativistic gravitational-wave forms for r-modes. An example is shown in Figure 1, where the equilibrium star is the same as in Stergioulas and Font (2001). The two curves show the gravitational wave corresponding to the $l = m = 2$ odd-parity Zerilli function, as extracted at two different locations from the star, after the non-wave part has been eliminated. The amplitude of the wave is scaled by M/r. When plotted against retarded time $t - r$, the extracted waveforms at the two locations nearly coincide, verifying that non-wave parts have been nearly eliminated. Gravitational waves from pulsations of rapidly rotating stars also contain higher-order terms, which are currently under investigation (Stergioulas et al. 2003).

COLLAPSE TO KERR BLACK HOLE

The axisymmetric collapse of an unstable neutron star to a black hole can become a source of gravitational waves, if the neutron star is supramassive (i.e. its rest mass exceeds the maximum allowed rest mass for nonrotating configurations) and rotating rapidly. Instability can set in at least in two ways: after spin down along a constant rest-mass sequence, or after a hypermassive neutron star, that is created in a core-collapse or binary merger and is supported against collapse by differential rotation, becomes uniformly rotating. In the latter case, the star could collapse before becoming exactly differentially rotating. However, the mass-shedding limit for rotating neutron stars is very sensitive to differential rotation, so that collapse should set in when the

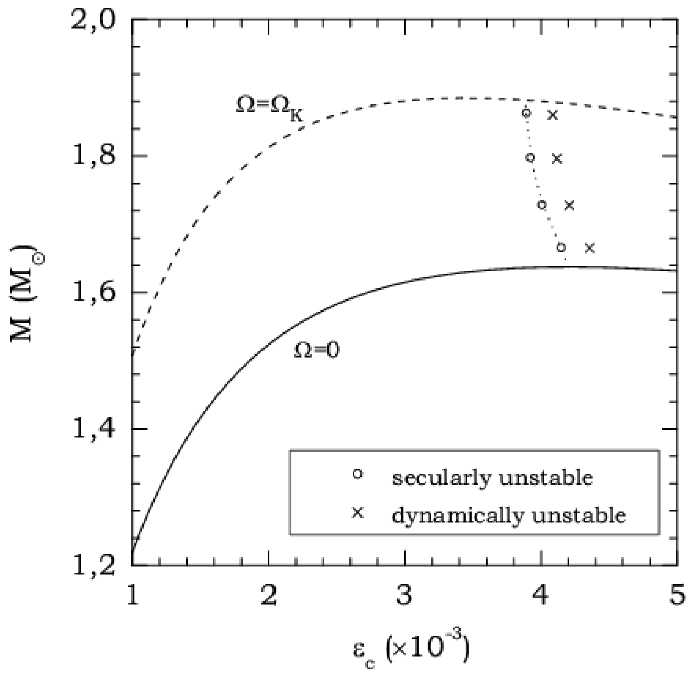

Figure 2. *Secularly and dynamically unstable initial models in a mass vs. central energy density graph. The solid, dashed and dotted lines correspond to the sequence of nonrotating models, the sequence of models rotating at the mass-shedding limit and the sequence of models that are at the onset of secular instability to axisymmetric perturbations, respectively.*

bulk of the star is already rotating nearly uniformly. Figure 2 shows a graph of gravitational mass vs. central energy density for various equilibrium models constructed with a relativistic $N = 1.0$ polytropic equation of state. The solid line is the sequence of nonrotating models while the dashed line is the sequence of models rotating at the mass-shedding limit for uniform rotation. The dotted line marks the onset of the secular instability to axisymmetric perturbations. Several individual models are shown that are either secularly or dynamically unstable to collapse.

The initial neutron star in unstable equilibrium has a stationary quadrupole moment that is given by

$$Q = -a\frac{J^2}{M}, \tag{1}$$

where J and M are the angular momentum and gravitational mass, respectively, and $a > 1$ is a parameter that depends on the equation of state (Larrakkers and Poisson, 1999). For a Kerr black hole, $a = 1$. Thus, part of the difference in the quadrupole moment will be radiated in gravitational waves, during the transformation of the rapidly rotating neutron star to a Kerr black hole. Using the same wave-extraction method as described in the previous section, we have extracted the gravitational waves emitted during the collapse, up to the horizon formation. In Figure 3, the gravitational-wave amplitude is shown (scaled by M/r) as a function of retarded time, for an observer located at $r = 19M$. The initial neutron star rotates close to the mass-shedding limit in Fig. 2. Several oscillations in the gravitational-wave amplitude

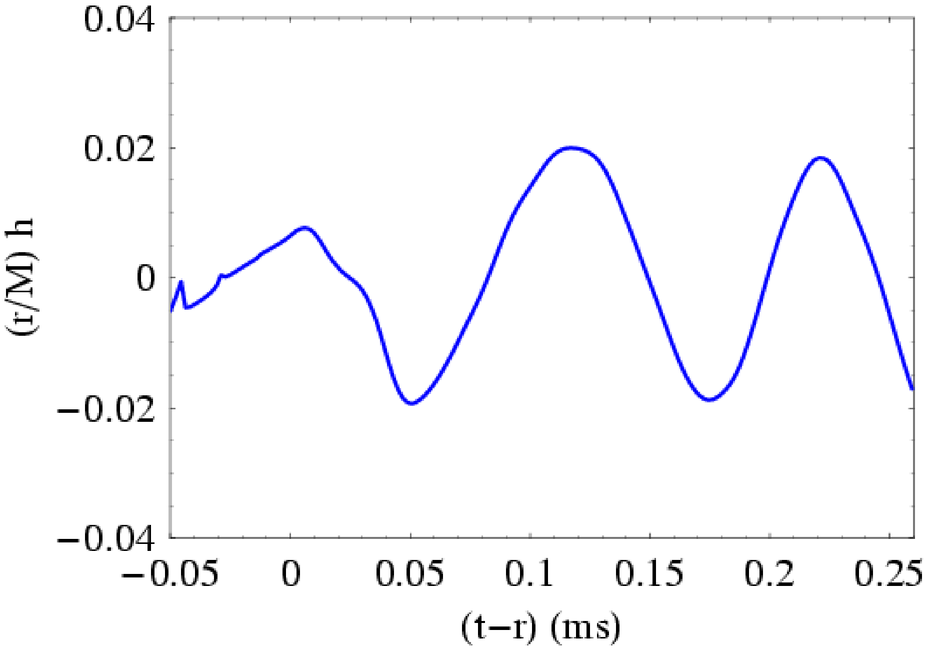

Figure 3. *Gravitational waves from the collapse of a rapidly rotating polytropic star to a Kerr black hole (see text for details).*

are observed. However, the signal is not monocromatic. As the collapse proceeds, the spacetime is continuously changing. The part of the signal before the horizon formation (at coordinate time of $\sim 0.2\,\mathrm{ms}$) corresponds to the excitation of the $l = 2, m = 0$ polar w-mode of the initial neutron star. After horizon formation, the gravitational waves are due to the oscillations of the black hole, having somewhat higher frequency. The waveform shown in Figure 2 should be compared to waveforms obtained in the pioneering simulations by Stark and Piran (1985). In the latter work, however, the initial neutron stars were still spherical and rapid rotation was imposed only in the velocity field, but not in the structure of the star itself. The simulations in Stark and Piran thus correspond to a transition of a star with zero initial quadrupole moment to a Kerr black hole, while our simulations show the realistic collapse of a rapidly rotating star, with an initial quadrupole moment much larger than that of the final Kerr black hole. An extensive survey of the rotational collapse to black holes for a range of initial models and rotation rates will be presented in Baiotti et al. 2003.

Acknowledgments

Work in progress reported here is in collaboration with L. Baiotti, J.A. Font, I. Hawke, F. Löffler, K. D. Kokkotas, P. Montero, A. Nerozzi and L. Rezzolla. Special thanks to Gab Allen for writing the subroutines for the Zerilli-function extraction. This work has been supported by the EU Programme 'Improving the Human Research Potential and the Socio-Economic Knowledge Base' (Research Training Network Contract HPRN-CT-2000-00137), KBN-5P03D01721 and the Greek GSRT Grant EPAN-M.43/2013555. The computations were carried out on the IBM Regatta at the Leibniz Rechenzentrum in Garching.

REFERENCES

[1] Abrahams, A., Bernstein, D., Hobill, D., Seidel, E., Smarr, L., 1992, Phys. Rev. D, 45, 3544

[2] Alcubierre, M., Brügmann, B., Dramlitsch, T., Font, J. A., Papadopoulos, P., Seidel, E., Stergioulas, N., Takahashi, R., 2000, Phys. Rev. D, 62, 044034
[3] Alcubierre, M., Brügmann, B., Diener, P., Koppitz, K., Pollney, D., Seidel, E., Takahashi, R., 2002, gr-qc/0206072
[4] Allen, G., Camarda, K., Seidel, E., gr-qc/9806036
[5] Baiotti, L., Hawke, I., Montero, P. J., Rezzolla, L., 2002, Mem. S.A.It., Vol. 73, 1
[6] Baiotti, L., Montero Muriel, P., Rezzolla, L., Stergioulas, N. Font, J.A., Hawke, I., Löffler, F., Seidel, E., Nerozzi, A., 2003, in preparation
[7] Baumgarte, T. W., Shapiro, S. L., 1999, Phys. Rev. D, 59, 064037
[8] Dimmelmeier, H., Font, J. A., Müller, E., 2001, Astrophys. J., 560, L163
[9] Duez, M. D., Marronetti, P., Shapiro, S. L., Baumgarte, T. W., 2003, Phys. Rev. D, 67, 024004
[10] Font, J. A., Goodale, T., Iyer, S., Miller, M., Rezzolla, L., Seidel, E., Stergioulas, N., Suen, W.-M., Tobias, M., 2002, Phys. Rev. D, 65, 084024
[11] Font, J. A., Stergioulas, N., Kokkotas, K. D., 2000 MNRAS, 313, 678
[12] Friedman, J. L., Lockitch, K. H., 2001, in Proc. 9th Marcel Grossman Meeting, eds. Gurzadyan, V., Jantzen, R., Ruffini, R., gr-qc/0102114
[13] Goodale, T., Allen, G., Lanfermann, G., Massó, J., Radke, T., Seidel, E., Shalf, J., 2002, *Proceedings of Vector and Parallel Processing - VECPAR'2002*, Lecture Notes in Computer Science, Springer, Berlin, see http://www.cactuscode.org
[14] Kawamura, M., Oohara, K., Nakamura, T., 2003, astro-ph/0306491
[15] Kokkotas, K. D., Andersson, N., 2001, in Proc. SIGRAV XIV, Genoa 2000, Springer-Verlag, gr-qc/0109054
[16] Laarakkers, W. G., Poisson, E., 1999, Astrophys. J., 512, 282
[17] Morsink, S. M., Stergioulas, N., Blattnig, S. R., 1999, Astrophys. J., 510, 854
[18] Nakamura, T., Oohara K., Kojima, Y., Prog. Theor. Phys. Suppl., 1987, 90, 1
[19] Shibata, M., Nakamura, T., 1995, Phys. Rev. D, 1995, 42, 5428
[20] Shibata, M., Uryū, K., 2000, Phys. Rev. D, 61, 064001
[21] Shibata, M., Taniguchi, K., Uryū, K., 2003, Phys. Rev. D, 68, 084020
[22] Stark, R. F., Piran, T., 1985, Phys. Rev. Lett., 55, 891
[23] Stergioulas, N., 2003, Living Rev. Relativity, 6, 3
[24] Stergioulas, N., Font, J. A., 2001, Phys. Rev. Letters, 86, 1148
[25] Stergioulas, N., Friedman, J. L., Astrophys. J., 1998, 492, 301
[26] Stergioulas, N., Hawke, I., Proceedings of the 10th Hellenic Relativity Meeting, eds. Kokkotas, K. D., Stergioulas, N., World Scientific, pg. 185, 2003
[27] Stergioulas, N., Hawke, I., Kokkotas, K. D., Seidel, E., 2003, in preparation
[28] Yoshida, S., Rezzolla, L., Karino, S., Eriguchi, Y., 2002 Astrophys. J., 568, L41

A CLASSICAL TREATMENT OF THE DARK-MATTER AND FLAT-ROTATION-CURVES PROBLEMS*

N.K.Spyrou

Astronomy Department, Aristoteleion University of Thessaloniki,
541.24 Thessaloniki, Macedonia, Hellas (Greece)

ABSTRACT

In the context of the Newtonian theory of gravity, the isentropic hydrodynamical flows in a bounded, gravitating perfect-fluid source are dynamically equivalent to geodesic motions in a generalized, scalar potential. This potential is explicitly expressed in terms of the source's standard gravitational potential and baryon-mass density, pressure and internal thermodynamic energy. On the other hand, the masses of cosmological structures, assumed as gravitating perfect fluids, are usually determined observationally with the aid of geodesic motions. Quite generally, the above two facts imply that the baryonic mass of a cosmological structure is different from and can largely exceed its observationally determined mass. The extra mass density and mass, beyond the baryonic mass, involved, depend on the source's internal physical characteristics, are both negative, and provide a natural classical explanation of the dark-matter problem and of the flat rotation curves of disc galaxies.

1. OBSERVATIONAL INTRODUCTION

According to many current observational data, the realistic picture and morphology of an astrophysical-cosmological structure differs greatly from its corresponding optical picture. The Solar System for example, viewed as a star accompanied by a number of nearby small objects and planets, differs from the one observed embedded in the solar wind, the outer boundaries of which extend up to the corresponding outer boundaries of the winds from nearby stars. Also, far beyond the *Kuiper Comet Belt,* extending far out the orbits of the outer planets *Neptune* and *Pluto*, there is an enormous spherical array of icy worlds orbiting the Sun called the *Oort Comet Cloud*, whose linear dimensions are of the order of 10^5 AU. This means that the Solar System extends up to half the distance of *a proxima Centauri*, the nearest to the Sun star. Furthermore, according to far-ultraviolet spectroscopic observations of the properties of the highly-ionized oxygen of the hot gas and of the high-velocity clouds in the halo of the *Milky Way* galaxy [8], there exists an extended, hot ($T>10^6$ K) and sufficiently diffuse *Galactic Corona*, previously undetected by other means (e.g. X rays), far beyond the nearby *halo*, detected previously. This implies that the Galactic Corona, and hence the Milky Way galaxy itself, possibly extends out to the *Magellanic Clouds*, and so the expected linear dimensions of the Milky Way galaxy are at least 200 kpc, almost ten times larger than its optical linear dimensions (~30 kpc). If such a result could be considered as typical, then the mutual distance of the outer boundaries of the Milky Way and the nearby *Andromeda Galaxy*, at a distance of approximately 600 kpc from it, is of the order of their linear dimensions, approximately 200 kpc. Such a result for neighboring galaxies is generally believed to be valid for typical *clusters of galaxies*, in which the mutual distances of neighboring members is of the order of *a few hundred kpc.* Under such conditions, the linear dimensions of galaxies with haloes and coronas (in the range 0.1 kpc - 1Mpc, depending on the type of galaxies, e.g. ellipticals, spirals, irregulars) *is not necessarily* much smaller than their mutual distances. As a consequence, the dynamical description of the observed motions in a typical cosmological structure is not that of a system of gravitating point masses (namely, no tidal interactions), but rather of the form of hydrodynamical flows in a more or less continuous gravitating source.

Furthermore, the structure of the interstellar medium itself in elliptical galaxies and of the intracluster medium in cluster of galaxies present special interest. Thus on the one hand the interstellar medium consists primarily of hot ($T> 10^6$ K) plasma; several molecular clouds with

* *Proceedings of the 6th Hellenic Astronomical Society Conference, 15-17 September 2003, Penteli, Greece*

dimensions 20-50 pc and masses ~10^6 solar masses (m^) in it are partly associated with HII regions and embedded in a lower-density interstellar medium; the masses (~10^8 –10^9 m^) of the central dark objects in elliptical galaxies are only a few percent of the molecular-gas mass in the sub one kiloparsec region. On the other hand a cluster of galaxies can be treated as an approximately isothermal sphere of hot ionized hydrogen (of dimensions a few Mpc, temperature ~10^8 K, number density of electrons ~10^{-4} cm^{-3}, and number density of molecular clouds ~10^{-4} to 10^{-3} cm^{-3}); the intracluster gas contains x-rays, fills the space between the galaxies, occupies much of the cluster's volume, and the x-ray luminosities fall in the range 10^{43} to 10^{45} erg. sec^{-1}; the mass of the intracluster medium exceeds the total mass of the luminous parts of the cluster's galaxies by a factor of several. (However, one must not forget that the surveys for the largest cosmological features so far cover only 0.001% of the observable universe!!!). In this spirit, it is interesting that, as a consequence of the improvement of the observing techniques, currently we witness (see e.g. [2,7,9]) continuous observational detections of many new galaxies, of intergalactic globular clusters and even stars, and also of hot filamentary networks connecting the galaxies of a cluster of galaxies, seen in the ultraviolet but unseen in the optical, infrared and radio wavelengths.

According to all the above the morphology of galaxies is very different from the simple picture of spiral, elliptical, or, even irregular galaxies, in the sense that the galaxies (as well as the clusters of galaxies, and the second-order clusters (superclusters) of galaxies) are almost spherically symmetric, very complex, practically continuous, and of much larger linear dimensions cosmological structures than previously assumed**.** This situation becomes even more interesting, considering, in particular, the shapes of *galactic dark-matter haloes* derived from *gravitational-lensing studies*, *N-body simulations*, *stellar tracers* (e.g. globular clusters), *HI studies and polar rings*, *studies of satellites* (e.g. various tails), as well as from *X-ray*, and *absorption lines* studies ([4]; in the same volume see, particularly, the contributions by Fillipi and Sepulveda, Ryden and Tinker, Zepf, Sparke, Johnston, Buote, Bowen). The observable Universe differs very much from the simple picture of a collection of galaxies (or higher-order cosmological structures) in which the mutual distances of the neighboring members are much larger than their linear distances. Consequently, the *constituent elements of the Universe and the Universe as a whole, can quite satisfactorily be treated as continuous gravitational systems and, more specifically, bounded, gravitating perfect-fluid sources, the physical-dynamical description of which is very well established at both the Newtonian and the general-relativistic levels.* So, we arrive at the very crucial result, that the motions of and in these constituents should be considered as as hydrodynamical flows rather than geodesic motions. It is exactly this result, that enables us, through the *dynamical-equivalence approach,* to recast the geodesic motions, taking into account now the contribution to the observationally determined mass of the fluid source of all of its internal physical characteristics.

Finally we recall that according to the observations of the cosmic microwave background by the *Wilkinson Microwave Anisotropy Probe* (WMAP), the *Cosmos* is composed of *heavy elements (*0.03 %)*, ghostly neutrinos* (0.3 %), *stars* (0.5 %), *free hydrogen and helium* (4%), *dark matter (22* %), and *dark energy (73* %*).*

In view of the above we feel that we can apply the model of a bounded, continuous, gravitating perfect-fluid source of classical hydrodynamics in order to describe the motions in the large-scale cosmological structures, and, in this way, to present a classical explanation of the dark-matter problem and of the flat-rotation curves of disk galaxies. Thus, in the next Section 2 we outline briefly the dynamical equivalence of the hydrodynamic flows and geodesic motions. Then we apply the result to typical cosmological large-scale structures, in order to examine the dependence of the observationally determined mass on the baryonic-mass density and on the internal physical characteristics of the fluid source. This enables us to prove that the baryonic mass of the structure generally differs from and actually it is much larger than its observationally determined mass, and so to propose a classical explanation of the *dark-matter problem*. Additionally, the above distinction between the baryonic and the observationally determined masses, and the use of planar, equatorial, circular geodesics in disk galaxies, allows us to propose a classical explanation of *the flat-rotation curves problem*.

2. DYNAMICAL EQUIVALENCE AND CONSEQUENCES

It has been recently suggested [5] that, in both the Newtonian and the general-relativistic theories of gravity, and at all levels, namely, cosmological [5,15,16,17], galactic [5,10,11,13,14,15,16], and stellar [5,10,12,14], it is possible to give to the equations of the hydrodynamical flow motions in the interior of a bounded gravitating perfect-fluid source the *form* of the equations of the geodesic motions in it. In the simplest possible case of the non-magnetized fluid and under adiabatic conditions [3], the *Euler's equations* for the hydrodynamical flow motion of a *fluid volume element* can be written in the form of the Newton's equation of motion of a *test particle-fluid volume element* (geodesic motion)

$$\frac{d\vec{\upsilon}}{dt} = \vec{\nabla} V, \tag{2.1}$$

where $\upsilon(\vec{x},t)$ is the three-velocity vector of the test particle-fluid volume element, and the *generalized potential* V is defined as

$$V = U - \left(\Pi + \frac{p}{\rho}\right), \tag{2.2}$$

where the *Newtonian gravitational potential* U obeys the standard *Poisson's equation*

$$\nabla^2 U = -4\pi G\rho \tag{2.3}$$

and ρ, p, and $\rho\Pi$ are, respectively, the *rest-mass* (baryonic-mass) *density, isotropic pressure,* and *internal specific energy density* of the fluid source. For consistency and similarity reasons, V is assumed to obey the field equation

$$\nabla^2 V = -4\pi G\rho_{v} \tag{2.4}$$

of the type of the Poisson equation. Then it is straightforward to prove, that the *generalized density* ρ_v is

$$\rho_{v} = \rho + \rho_i \tag{2.5}$$

where

$$\rho_i = \frac{1}{4\pi G}\nabla^2\left(\Pi + \frac{p}{\rho}\right) = \frac{1}{4\pi G}\vec{\nabla}\cdot\left(\frac{1}{\rho}\vec{\nabla}p\right) \tag{2.6}$$

is the *internal-mass density.* Furthermore, the volume integrals of ρ, ρ_i, and ρ_v will be, respectively, the *rest (or baryonic) mass,* m, the *internal mass*, m_i, and the *generalized mass*, m_v, so that

$$m_{v} = m + m_i \tag{2.7}$$

Obviously, it is the geodesic motions in the potential V that must be used rather than those in the gravitational potential U, because in the former all the internal physical characteristics of the gravitating source are taken into account. In other words, for simply physical reasons, as mass determined on the basis of geodesic motions, the mass m_v must be used, not the mass m. According to Eq. (2.7), the mass m_v, namely, the mass, determined observationally via the geodesic motions, differs from the baryonic mass

2.1 THE DARK-MATTER PROBLEM

Now we assume, for simplicity, that the gravitating perfect-fluid source of *absolute temperature* T and *mean molecular weight* μ is spherically symmetric of radius R, and is characterized by an adiabatic and isothermal (adiabatic index γ=1) equation of state, such that

$$p = \frac{kT}{\mu m_H}\rho \tag{2.8}$$

where k and m_H are the *Boltzmann constant* and *rest mass of the atomic hydrogen*, respectively, and where for the rest-mass (baryonic-mass)-density distribution law we shall adopt a *Plummer-type density,* namely,

$$\rho(r)=\rho_0\left(1+\frac{r^2}{r_0^2}\right)^{-\frac{n}{2}} \quad (r_0>0,\ \rho_0>0,\ \text{n: a positive integer}) \qquad (2.9)$$

Then, we verify that

$$\rho_i(r)=-\frac{n}{4\pi G r_0^2}\frac{kT}{\mu m_H}\frac{3+\frac{r^2}{r_0^2}}{\left(1+\frac{r^2}{r_0^2}\right)^2}<0, \qquad (2.10)$$

$$m(r)=4\pi\rho_0 r_0^3\left[\frac{1}{\sqrt{2}}-\ln\left(1+\sqrt{2}\right)-\frac{\frac{r}{r_0}}{\left(\frac{r^2}{r_0^2}+1\right)^{\frac{1}{2}}}+\ln\left(\frac{r}{r_0}+\sqrt{\frac{r^2}{r_0^2}+1}\right)\right], \qquad (2.11)$$

$$m_i=-\frac{nkT}{G\mu m_H}\frac{R^3}{r_0^2\left(1+\frac{R^2}{r_0^2}\right)}<0, \qquad (2.12a)$$

whence

$$m_i(R>>r_0)=-\frac{nkT}{G\mu m_H}R<0, \qquad (2.12b)$$

and, for n=3, we find

$$\frac{-m_i}{m}=1.9460\times10^{-6}\frac{x_{\max}}{\ln x_{\max}}\frac{T_{(7)}}{\mu} \qquad (2.13)$$

where

$$x=\frac{r}{r_0},\ x_{\max}=\frac{R}{r_0},\ r_0=3R_s \qquad (2.14)$$

R_s being the *Schwarzschild radius* of the structure's central dark object, and $T_{(7)}$ is the region's temperature in units 10^7 K. Therefore, *the internal mass is definitely negative and it diverges with the source's linear dimensions*. Also,

$$m=m_v+(-m_i)>m_v \qquad (2.15)$$

namely, *the rest (baryonic) mass, m, determined with the aid of the geodesic motions in simply the gravitational potential U, is larger than the generalized mass, m_v, determined with the aid of the geodesic motions in the generalized gravitational potential V.* In other words, *the rest mass of the source (baryonic mass) m is larger than the mass* m_v *determined observationally up to now*. This is exactly the very significance, cosmological, galactic, and stellar, of the above result (2.15) in complete agreement with the current belief on the relative abundance of the baryonic matter (rest-mass) and the observationally determined (dynamical) mass of a structure.

The application of the above results to galactic and cosmological levels is straigtforward [16]. Thus, in the case of *masering galaxies* (e.g. NGC 4258 and NGC 1068) and *nonmasering galaxies* (e.g. NGC 4261) we find that, depending on the linear dimensions of the *circumnuclear region* considered (ranging from the subparsec up to kiloparsec), $-m_i$ is not always negligible compared to the mass M of the central dark object ($10^{-5}<-m_i / M<10^{-2}$). On the other hand, $-m_i$ can be *comparable* to the total rest-mass, m, of the circumnuclear region ($10^{-3}<-m_i / m<0.6$; the upper bound 0.6 corresponding to the mass of the black hole believed to lurk in the Milky Way's nuclear region).

Specifically, in the case of the Milky Way, for the linear dimensions (R) of the region considered being in the range 0.1 pc and 100 kpc, the ratio $-m_i/m$ falls in the range (10^2 to 10^3) $T_{(7)}/\mu$. This means that e.g. in the innermost region of dimensions 0.1 pc, this ratio can be *larger than* unity, provided that the temperature there is at least 10^8 K, and also that considering the broader region of dimensions 100 kpc, the same ratio can be at least 10^3 for temperature of the order 10^2 K.

Also, in the case of typical clusters of galaxies with dimensions of a few Mpc, the ratio $-m_i/m$ falls in the range (10^3 to10^5) $T_{(7)}/\mu$ and so it can be larger than unity, provided that $T/\mu > 10^4$ to10^5 K. Finally, in the case of a second-order cluster (cluster of clusters) of galaxies, the ratio $-m_i/m$ is of the order of $10^3 T_{(7)}/\mu$, and so it can exceed unity, for $T/\mu > 10^3$ K. As it has been said in the *Introduction*, all the above conditions are met in the Universe, and, hence, *the internal mass (m_i) can be larger (absolutely) than the baryonic mass, and, as such, it cannot be ignored*. Since m_i is negative, the observationally determined mass is much smaller than the baryonic mass, and, hence, *there is plenitude of baryonic matter in the cosmological structure.*

.

2.2 THE FLAT-ROTATION-CURVES PROBLEM

In the case of a spherically-symmetric perfect-fluid source of generalized density ρ_V (r), the total velocity, V_c (r), of an equatorial, circular geodesic orbit at a distance r from the center, resulting from the continuous fluid distribution and a central dark object, is given (in units of 100 km/s) by the expression

$$V_c\left(100\frac{km}{s}\right) = 2.99\times 10^2 \left\{ \sqrt{2}\frac{1}{x}\ln\left(1+\sqrt{x^2+1}\right) - \frac{\sqrt{2}}{\sqrt{x^2+1}} - \frac{1}{x}\left[\ln\left(1+\sqrt{2}\right) - \frac{1}{\sqrt{2}}\right] - \gamma\frac{x^2}{x^2-1} + \frac{1}{6x} \right\}^{1/2} \tag{2.16}$$

in which the newly introduced here dependence of the total velocity on the source's absolute temperature and mean molecular weight is described through the parameter

$$\gamma = \frac{3kT}{\mu m_H c^2} = 2.75\times 10^{-13}\frac{T}{\mu}\,. \tag{2.17}$$

It is straightforward to verify that, for T/μ of the order 10^6 ($\gamma \sim 10^{-7}$), as indicated by recent observations, the circular velocity V_c (in units of 100km/s) remains flat for practically the whole optical part of the galaxy, and continues so up to a radial distance of at least 200 kpc ($x \sim 10^{11}$-10^{12}) retaining a constant value in the range ~1-2, in agreement with standard observational data (see e.g. [2]).

3. CONCLUDING REMARKS

From all the above we conclude that, if we insist in using the geodesic motions (inside and outside) of the cosmological structures for the observational determination of masses, in conjunction with the results of the dynamical equivalence, then *the internal mass m_i, due to the internal physical characteristics of the source, is revealed to be there*, it is negative and, in many cases, absolutely it can largely exceed the rest (baryonic) mass of the gas of the (corresponding region of the) large-scale cosmological structure under consideration. It is interesting that this negative extra mass "shows up", when, in the context of the dynamical equivalence, the geodesic motion in the generalized potential V is used, and *not* when the standard geodesic motion of a test particle in the original gravitational potential U is used. Moreover, since the internal mass m_i is negative, the observationally determined mass of the cosmological structure is smaller than its baryonic mass. These two general results give a very simple, classical solution to the dark-matter and the flat-velocity-curves problems. Finally, it must be stressed that the derivation of the these results is valid also in the exact general-relativistic theory of gravity [18], and that in this derivation nor any modifications of Newton's law of gravitational attraction is required, neither any other theories are introduced and used [1]. Further detailed results will be published elsewhere. We conclude with the remark that the explicit expression (2.10) for the internal–mass density may be helpful in answering the open question of the specific form the density-law distribution of dark-matter haloes in relation to the mutual importance of galactic disc and cuspy haloes [6]. Problems like the above are currently under consideration.

Acknowledgements

It is a pleasure to express, from this position also, my sincere thanks to the organizers for their nice organizing and warm hospitality during the Conference.

BIBLIOGRAPHY

[1]. Battersby, S. 2003, *Dark Matter Special: The New Dark Age*, New Scientist, Issue 25, January 2003, p.p. 28-37 (see also *www.astro.umd.edu/ssm/mond/index.html*).
[2]. Begeman, K., Broeils, A., and Sanders, R.H. 1991, *MNRAS,* **249**, 523-537.
[3]. Chandrasekhar, S.1969. *Ap.J.* **158**, 45-54.
[4]. Ellis, R.S. 2002, in *The Shapes of Galaxies and Their Dark Halos,* Yale University Workshop, Ed. P. Natarajan, World Scientific Publishing Pte. Ltd.,pp.254-262.
[5] Kleidis, K., and Spyrou, N.K. 2000, *Class. Quantum Grav.* ***17**, 2965-2982.*
[6.] Mcgough, S.S. 2002, in *The Shapes of Galaxies and Their Dark Halos,* Yale University Workshop, Ed. P.Natarajan, World ScientificPublishing Pte. Ltd., pp. 186-193.
[7]. Navarro, J.F. 2002, in *The Shapes of Galaxies and Their Dark Halos,* Yale University Workshop, Ed. P.Natarajan, World Scientific Publishing Pte. Ltd.,pp.114-118.
[8] Sembach, K. 2002, Space Telescope Science Institute *Newsletter,* Vol. **19**, Issue 02,1920.
[9].Simon, J.D.,Robishaw, T. and Blitz, L. 2003, *Dark Matter in Dwarf Galaxies: The First Dark Galaxy?* in *Satellites and Tidal Streams,* ASP Conference Series, Eds. Prada, F.,Martinez-Delgado, D., and Mahoney, T. (in press).
[10]. Spyrou, N.K.1997a, in *The Physics of Ionized Gases,* Proceedings of the 18thSummer School and International Symposium on the Physics of Ionizes Gases (Kotor, Jugoslavia, 2-6 September 1996), eds.B.Vujicic, S.Djurovic and I.Puric, Institute of Physics, Novi Sad University, Yugoslavia, pp.417-446.
[11]. Spyrou, N.K. 1997b, in *The Earth and the Universe,* Volume in HonoremL. Mavrides, eds. G. Asteriadis, A. Bandellas, M. Contadakis, K. Katsambalos, A. Papademetriou and I. Tziavos, Thessaloniki**,** Greece, pp. 277-291.
[12]. Spyrou, N.K. 1997c*, Facta Universitatis*, **4**, 7-14.
[13]. Spyrou, N.K. and Kleidis, K. 1999a, "On the Nature of Nuclear Galactic Masses" Proceedings of JENAM 1999, Samos.
[14]. Spyrou, N.K. 1999b, in *Current Issues of Astronomical and Planetary Environmental Concern*, Proceedings of International Seminar (Thessaloniki, 6-7 April 1999) ed. N,K.Spyrou, Astronomy Department, Aristoteleion University of Thessaloniki, Thessaloniki, Greece, pp.23-35.
[15]. Spyrou, N.K. 2001a "Conformal Invariance and the Nature of CosmologicalStructures", Invited Talk, Proceedings of The Conference on Applied Differential Geometry-General Relativity, and The Workshop on Global Analysis, Differential Geometry, Lie Groups, (Thessaloniki, 27 June-1July 2001) eds. G. Tsagas, C. Udriste, and D. Papadopoulos, pp. 101-107.
[16]. Spyrou, N.K 2002a, in *Modern Theoretical and Observational Cosmology,*Proceedings of the 2nd Hellenic Cosmology Meeting (Athens, 19-20 April 2001), eds. M.Plionis and S.Cotsakis, Kluwer Academic Publishers, Dordrecht, Vol. **276**, pp.35-43.
[17]. Spyrou, N.K. 2003a, in Proceedings of the 10th Conference *New Developments in Gravity*, eds. K. Kokkotas and N. Stergioulas, Kluwer, Academic Publishers, Dordrecht, (in press).
[18]. Spyrou, N.K., and Tsagas, C.G. 2003, *Astrophysical consequences of the dynamical equivalence between geodesic motions and hydrodynamic flows: A covariant approach, (*in preparation).

COSMOLOGICAL EXPANSION BY VIBRATING EXTRA DIMENSIONS*

L. Perivolaropoulos
Department of Physics, University of Ioannina, Greece

ABSTRACT

Recent observations have indicated that the universe is undergoing a period of accelerated expansion. Attributing this acceleration to a cosmological constant or to an arbitrary dynamical scalar field (quintessence) is faced with naturalness problems (coincidence problem, unnatural potentials etc). Here we propose a model that is based on the existence of compact extra dimensions and has the potential to resolve these problems. Extra dimensions are predicted by all theories that attempt to quantize gravity and unify it with the other interactions. We show that the size of extra dimensions (the radion field) stabilized by an appropriate potential for phenomenological consistency, necessarily oscillates due to its coupling to the density of redshifting matter. Depending on the power law of the stabilizing potential near its minimum, the energy of these oscillations can behave either as dark matter, or as dark energy with negative pressure inducing the observed accelerated expansion of the universe.

I. INTRODUCTION

Observations of the magnitude-redshift relation of distant Type Ia supernovae [1] and CMB measurements [2] have indicated that the universe is undergoing a period of accelerated expansion. A possible cause of this acceleration is the existence of a small a cosmological constant. This possibility however is not completely satisfactory (see e.g. [3]) because fine tuned initial conditions are required in order to solve the coincidence problem (why the vacuum energy is dominating the energy density right now). Thus, acceleration is attributed to the influence of a redshifting non-luminus form of energy with negative pressure called by many authors 'dark energy' or 'quintessence' [4]. The origin of this form of energy remains unknown. Several types of scalar fields [4] have been proposed as sources of dark energy including the dilaton, the inflaton, supersymmetric partners of fermions, Brans-Dicke (hereafter BD) scalars [5], etc. The dynamical evolution of these scalars is determined by specially designed potentials so that the scalar field energy density tracks the radiation-matter component at early times while at late times it dominates and leads to acceleration. The main drawback of these models is that there is usually no physical motivation for the proposed scalar fields and potentials.

Cosmological theories with extra dimensions generically contain a scalar field of geometrical origin which describes the size of extra dimensions. This is known as the radion field. These theories have the potential of providing a physically motivated solution to the hierarchy problem by postulating that the fundamental Planck mass M_* is close to the *TeV* scale [6–8]. This is possible in theories with extra dimensions [7] because Gauss's law relates the Planck scales of the 4+D-dimensional theory M_* and the long distance 4-dimensional theory M_{pl} by

$$M_{pl}^2 = b_0^D M_*^{D+2} \tag{1.1}$$

where b_0 is the present stabilized size of the extra dimensions.

* *Proceedings of the 6th Hellenic Astronomical Society Conference, 15-17 September 2003, Penteli, Greece*

According to observations, the internal space should be static or nearly static at least from the time of primordial nucleosynthesis[9]. This means that at the present evolutionary stage of the Universe only small fluctuations over stabilized or slowly varying compactification scales (conformal scales/geometrical moduli) are possible. Thus the size of the extra dimensions $b(t)$ (the radion field) is usually assumed to be stabilized to its present value b_0 by a 'radion stabilizing potential' $V(b)$. Observational constrains require this stabilization and theoretical models[10] have been proposed to justify it. In order to study the cosmological effects in the setup of compact extra dimensions we consider a flat $4+D$ dimensional spacetime $R^1 \mathrm{x} R^3 \mathrm{x} T^D$ with toroidally compact D extra dimensions. The metric may be written as

$$g_{MN} = diag\left[1, -a^2(t)\tilde{g}_{ij,} -b^2(t)\tilde{g}_{mn}\right] \tag{1.2}$$

where M,N run from 0 to D+3; i, j run from 1 to 3 and m, n run from 4 to D + 3. Also $a(t)$ is the scale of the non-compact 3-dimensional flat space (the scale factor of the universe) and $b(t)$ is the radius of the compactified toroidal space (the radion field).
The nonzero components of the energy-momentum tensor are given by

$$\begin{aligned} T_{00} &= \rho_{tot} g_{00} \\ T_{ij} &= -p_a g_{ij} \\ T_{mn} &= -p_b g_{mn} \end{aligned} \tag{1.3}$$

The energy density ρ_{tot} and the pressures p_a, p_b are derivable from the internal energy $u = u(a, b)$ as

$$\rho_{tot} = \frac{u}{v}, p_a = -\frac{a\partial u / \partial a}{3v}, p_b = -\frac{b\partial u / \partial b}{Dv} \tag{1.4}$$

where $v = a^3(t)\Omega_D b^D(t)$ is the volume of the (D+3) space $\left(\Omega_D = 2\pi^{\frac{D+1}{2}} \Big/ \Gamma\left(\frac{D+1}{2}\right)\right)$.

Consider now an internal energy of the form

$$u = a^3\left(V(b) + \rho\right) \tag{1.5}$$

$V(b)$ in equation (1.5) is the radion potential which can produce [12] sufficient primordial inflation to solve the horizon, flatness, homogeneity, and monopole problems and can stabilize b at

$$b_0 = \left(\frac{M_{pl}^2}{M_*^{D+2}}\right) \tag{1.6}$$

with a vanishing cosmological constant. The energy density $\rho = \rho(a)$ in (1.5) is due to mater and radiation. Using the metric ansatz (1.2) and the energy-momentum components (1.3), it is straightforward to obtain the following set of evolution equations for the scale factors a and b from the Einstein equations

$$6\frac{\dot{a}^2}{a^2}+D\left(D-1\right)\frac{\dot{b}^2}{b^2}+6D\frac{\dot{a}}{a}\frac{\dot{b}}{b}=\frac{V+\rho}{M_*^{D+2}b^D}$$
$$\frac{\ddot{b}}{b}+\left(D-1\right)\frac{\dot{b}^2}{b^2}+3\frac{\dot{a}}{a}\frac{\dot{b}}{b}=\frac{1}{M_*^{D+2}b^D}\left(\frac{2V}{D+2}-\frac{b}{D\left(D+2\right)}\frac{\partial V}{\partial b}+\frac{\rho-3p_a}{2\left(D+2\right)}\right) \tag{1.7}$$
$$\frac{\ddot{a}}{a}+2\frac{\dot{a}^2}{a^2}+D\frac{\dot{a}}{a}\frac{\dot{b}}{b}=\frac{1}{M_*^{D+2}b^D}\left(\frac{b}{2\left(D+2\right)}\frac{\partial V}{\partial b}-\frac{D-2}{2(D+2)}V+\frac{\rho+(D-1)p_a}{2(D+2)}\right)$$

For a stabilizing potential

$$V=\rho_v\left(\frac{b}{b_0}-1\right)^2 \tag{1.8}$$

$$\frac{\dot{a}^2}{a^2}+\frac{D(D-1)}{6}\frac{\dot{b}^2}{b^2}+D\frac{\dot{a}}{a}\frac{\dot{b}}{b}=\frac{\overline{m}^2(b-1)^2+\frac{1}{a^3}}{b^D} \tag{1.9}$$

$$\frac{\ddot{b}}{b}+(D-1)\frac{\dot{b}^2}{b^2}+3\frac{\dot{a}}{a}\frac{\dot{b}}{b}=\frac{3}{(D+2)b^D}\left[4\overline{m}^2(b-1)^2-\frac{4\overline{m}^2b(b-1)}{D}+\frac{1}{a^3}\right] \tag{1.10}$$

The term $1/a^3$ is the dimensionless and properly rescaled redshifting matter density which comes from the trace of the energy-momentum tensor (radiation has traceless energy momentum tensor and does not contribute here). The presence of this term implies that the static ansatz for a $b = 1$ and $\dot{b} = 0$ is not a solution of the above equations and therefore redshifting matter necessarily induces oscillations to the size $b(t)$ of the extra dimensions (the radion field).

These oscillations have been studied in Ref. [11] where the following points were demonstrated for the parabolic potential of the form (1.8):

- Radion oscillations are generically induced at late times by redshifting matter.
- For low radion masses ($m \approx 10$ - $100\ H_0$) these oscillations could provide a solution to two important cosmological problems: *the coincidence problem* (why do we live at the special time when the universe's expansion begins to accelerate) and *the apparent periodicity of galaxy distribution* with spatial period $\simeq 128$ $h^{-1}Mpc$. However, fifth force constraints based on solar system and terrestrial observations may not be consistent with this range of radion masses.
- For high radion masses ($m_b > 10^{-3}\ eV$) radion oscillations are consistent with fifth force and other constraints and they can provide the source of a new type of dark matter which has many similarities with axions (they are both a result of oscillating scalars).

Clearly for a parabolic potential, radion oscillations can play the role of dark matter but they can not induce accelerating expansion in the phenomenologically consistent range of high frequency oscillations. We are thus led to generalize the form of the stabilizing potential to an arbitrary power law of the form

$$V(\delta b)=\lambda\left|\,\delta b\,\right|^n \tag{1.11}$$

where $n > 0$ is a new power law parameter. It is straightforward to show [11] that the substitution

$$\phi = b^D$$

$$\omega = -1 + \frac{1}{D}$$

transforms the dynamical equations (1.9) to those of a Brans-Dicke scalar ϕ which is easier to analyze. This analysis [13] leads to the rescaled Friedman equation

$$\frac{\dot{a}^2}{a^2} \simeq \frac{\omega}{6} \delta\dot{\bar{\phi}}^2 + \bar{\rho}_\upsilon \delta\bar{\phi}^n \simeq B a^{-3\Gamma} \tag{1.12}$$

where B is a constant and Γ determines the redshift rate of $\bar{\rho}_\phi$ and is given by

$$\Gamma = \frac{2n}{n+2} \tag{1.13}$$

This equation leads to

$$a \sim t^{\frac{2}{3\Gamma}} \sim t^{\frac{n+2}{3n}} \tag{1.14}$$

which implies accelerated expansion for $1 > n > 0$. Notice that the power law dependence of a implied by (1.14) is independent of D and reduces to 2/3 (dark matter) in the case of a parabolic stabilizing potential $n = 2$ as anticipated from the results of Ref. [11]. A numerical simulation of the oscillating radion in the form of a Brans-Dicke scalar is shown in Fig. 1 where the analytical expectation [13] of the oscillation amplitude $\delta\phi_{max}$ time dependence

$$\delta\phi_{max} \sim t^{2/n} \tag{1.15}$$

is verified numerically.

In conclusion we have shown that extra dimension oscillations are generically induced by redshifting matter. An oscillating extra dimensions size (the radion field) can play the role of dark matter (parabolic stabilizing potential) or dark energy (generalized stabilizing potential).

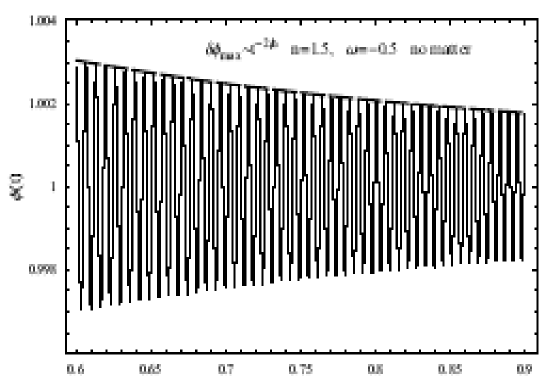

Figure 1: *The numerically obtained evolution of the $\delta\phi_{max}$ is in good agreement with the analytical prediction $\delta\phi_{max} \sim t^{2/n}$ for $n = 1.5$.*

Acknowledgements: This work was supported by the European Research and Training Network HPRNCT- 2000-00152

REFERENCES

[1] A. G. Riess *et al.* [Supernova Search Team Collaboration], Astron. J. 116, 1009 (1998) [arXiv:astroph/ 9805201]; S. Perlmutter *et al.* [Supernova Cosmology Project Collaboration], Astrophys. J. 517, 565 (1999) [arXiv:astro-ph/9812133].
[2] P. de Bernardis *et al.*, Astrophys. J. 564, 559 (2002) [arXiv:astro-ph/0105296].
[3] V. Sahni and A. A. Starobinsky, Int. J. Mod. Phys. D 9, 373 (2000) [arXiv:astro-ph/9904398].
[4] P. J. Peebles and B. Ratra, Astrophys. J. 325, L17 (1988); R. R. Caldwell, R. Dave and P. J. Steinhardt, Phys. Rev. Lett. 80, 1582 (1998) [arXiv:astroph/ 9708069];I. Zlatev, L. M. Wang and P. J. Steinhardt, Phys. Rev. Lett. 82, 896 (1999).
[5] C. Brans and . H. Dicke, Phys. Rev. 124, 925 (1961).
[6] I. Antoniadis, Phys. Lett. B 246 (1990) 377.
[7] N. Arkani-Hamed, S. Dimopoulos and G. Dvali, *Phys. Lett.* B 429*(1998) 263* [hep-ph/9803315], *Phys. Rev.*D 59 *(1999) 086004* [hep-ph/9807344].
[8] L. Randall and R. Sundrum, Phys. Rev. Lett. 83, 4690 (1999) [arXiv:hep-th/9906064]; Phys. Rev. Lett. 83, 3370 (1999) [arXiv:hep-ph/9905221].
[9] U. G¨unther and A. Zhuk, Class. Quant. Grav. 18, (2001), 1441 - 1460, hep-ph/0006283.
[10] W. D. Goldberger and M. B. Wise, Phys. Rev. Lett. 83, 4922 (1999) [arXiv:hep-ph/9907447].
[11] L. Perivolaropoulos and C. Sourdis, Phys. Rev. D 66, 084018 (2002) [arXiv:hep-ph/0204155].
[12] N. Arkani-Hamed, S. Dimopoulos, N. Kaloper and J. March-Russell, Nucl. Phys. B 567, 189 (2000) [arXiv:hep-ph/9903224].
[13] L. Perivolaropoulos, Phys. Rev. D 67, 123516 (2003) [arXiv:hep-ph/0301237].

MODELLING THE TWO POINT CORRELATION FUNCTION OF GALAXY CLUSTERS AND COSMOLOGICAL IMPLICATIONS*

Spyros Basilakos and Manolis Plionis

Institute of Astronomy and Astrophysics, National Observatory of Athens

Abstract: We study the clustering properties of the recently compiled SDSS cluster catalog using the two point correlation function in redshift space. Comparing the SDSS cluster correlation function with the predictions from various flat cosmological models ($\Omega_{\rm m}=0.3$) with dark energy (quintessence), we find that the ΛCDM model fits well the observational results.

ON THE ROTATIONAL INSTABILITIES OF RELATIVISTIC STARS*

K.D. Kokkotas

Section of Astrophysics, Astronomy and Mechanics, Department of Physics, University of Thessaloniki, Greece

Abstract: Rotational instabilities of relativistic stars are important both for their evolution and as sources of gravitational waves. We briefly discuss the prospect of detecting gravitational waves from such instabilities.

* *Proceedings of the 6th Hellenic Astronomical Society Conference, 15-17 September 2003, Penteli, Greece*

INTERPRETATIONS OF COSMOLOGICAL MODELS AND GEOMETRIC EQUATIONS OF STATE*

Michael Tsamparlis
Section of Astrophysics, Astronomy and Mechanics, Department of Physics, University of Athens, Greece

Einstein's field equations (EFE) result in an open system of PDFs. To make the system closed (i.e. to be able to solve it) one has to supplement extra equations, called *Constitutive Equations* or, in simple cases, *Equations of State*.

These equations are either indicated by analogues in Newtonian Physics or are written for a specific class of observers (=cosmological fluid). This situation is unsatisfactory because:

1. It destroys the "objectivity" in relativistic physics.
2. Makes cosmology having a "personal" and Newtonian aspect - it is observer dependent.
3. Leads to simple choices only - e.g. linear equations of state.
4. Makes impossible the comparison of the "physics" of two different classes of observers.

PROPOSED METHOD OF SOLUTION

We propose a solution to that problem in two steps:

1. In any given spacetime look for a geometric condition which will take a specific form for each class of observers. Take these equations as equations of state. This makes possible the comparison of the physics of two different classes of observers because the differences will be due only to the observers.
2. Choose this geometric condition to be the equation defining a collineation, that is a symmetry of the form $\mathcal{L}_X A_{ab} = B_{ab}$ where A_{ab} large is any tensor defined in terms of the metric and B_{ab} is any tensor with the same index symmetries as A_{ab}.

WHAT IS AN EQUATION OF STATE?

In spacetime choose a coordinate system $\{x^a\}$ and the general metric g_{ab}. Then consider EFE $G_{ab} = T_{ab}$. The left hand side can be written in terms of the metric components plus its derivatives. Until the right hand side is given in terms of components, no equations can be written. The right hand side is defined by "physics".

HOW ONE DOES PHYSICS IN SPACETIME?

1. By analogy with Newtonian Physics.

2. By personal taste or judgment or inspiration of "try lucky".

PRINCIPLES:

Proceedings 6th Hellenic Astronomical Society Conference, 15-17 September 2003,Penteli, Greece

1. Physics without observers does not make sense.
2. The "description" of matter is done in terms of the energy-momentum tensor.

METHOD OF WORK

1. Introduce observers (=Cosmological fluid): u^a ($u^a u_a = -1$).
2. Define the u^a–projection operator:

$$h_{ab} = g_{ab} + u_a u_b$$

3. Mathematical identity (1+3 decomposition):

$$T_{ab} = T_{ab} = \mu u_a u_b + p h_{ab} + 2q_{(a}u_{b)} + \pi_{ab} \tag{1}$$

where:

$$\mu = T_{cd}u^c u^d, \quad p = h^{cd}T_{cd}, \quad q_a = h_a^c u^d T_{cd},$$

$$\pi_{ab} = \left(h_a^c h_b^d - \frac{1}{3} h^{cd} h_{ab} \right) T_{cd}.$$

Using this decomposition of T_{ab} we can write the EFE as a system of 10 pdfs. However it contains too many unknown and we need supplementary equations. These are called "*constitutive equations*" or "*equations of state*". We must note that these equations involve the physical variables μ, p, q_a, π_{ab}!

HOW TO WRITE AN EQUATION OF STATE?

Using the same principles as above there are problems which arise i.e.:

1. Simple choices (linear equations, very few non-zero terms etc).

2. Equations observer dependent because they involve μ, p, q_a, π_{ab}, which are defined by the decomposition of T_{ab} w.r.t. u^a!

Therefore physics depends on personal choice and on specific class of observers and consequently physics of different classes of observers is not comparable. For example for spatially homogeneous tilted spacetimes we have two "natural" choices of u^a. However the question which arises is "*can we do better?*" We note that personal choice will stay but dependence on observers can be dealt.

PROPOSED PRINCIPLE OF "PHYSICAL COVARIANCE"

Consider a geometric condition inherent on the metric. Take this condition as the generator of equations of state. For each class of observers the generator will produce a related equation of state. Then the physics (=solution of the EFE) will have a common background structure and will depend only on the observers chosen.

ONE REASONABLE PROPOSAL

Take the geometric condition to be a collineation i.e. a relation of the form:

$$\mathcal{L}_X A_{ab} = B_{ab}$$

This choice means that **we let geometry to make physics**! However we do it anyway at the level of Killing vectors!

EXAMPLE

Equations of state in FRW cosmological models.

1. Metric (chosen by its symmetries):

$$ds^2 = S^2(\tau)\left[-dr^2 + U^2(k,\mathrm{x})\left(\mathrm{dx}^2 + \mathrm{dy}^2 + \mathrm{dz}^2\right)\right]$$

$$U(k,\mathrm{x}) = \frac{1}{1+\frac{k\mathrm{x}^2}{4}}$$

2. Observers (chosen by the symmetries of metric):

$$u^a = \delta_0^a$$

These assumptions give the following:

<u>KINEMATICS</u>

Hubble's parameter $\qquad H = \frac{1}{3}\theta = \frac{S_{,\tau}}{S^2}$

Deceleration parameter: $\qquad q = 1 - \frac{SS_{,\tau\tau}}{\left(S_{,\tau}\right)^2}$

<u>DYNAMICS</u>

$$T_{ab} = \mu(t)u_a u_b + p(t)h_{ab} \qquad \Rightarrow$$

$$T_{00} = \mu S^2(\tau), \qquad T_{11} = T_{22} = T_{33} = pS^2(\tau)U^2(k,x^a).$$

<u>FIELD EQUATIONS</u>

$$\mu = 3\frac{\left(S_{,\tau}\right)^2 + kS^2}{S^4}, \qquad p = \frac{-2SS_{,\tau\tau} + \left(S_{,\tau}\right)^2 - kS^2}{S^4}$$

Remains the variable S(τ). To fix it we need one equation of state. But how do define them? Choose as symmetries the matter collineations:

$$\mathcal{L}_X T_{ab} = 0$$

We compute the resulted equation of state using a technique developed by Apostolopoulos and Tsamparlis (**gr-qc**/**0110042** and *Gen. Rel. Grav.* 2004 **36**, 277-292). We restrict our considerations to k = 0 and we observe (Table IV of that paper) that there are two cases to consider, that is, T_1 = A = constant and $T_1 = \varepsilon A^2 e^{-2\overline{\tau}(\tau)/A}$. This means that we can define two families of geometric equations of state. We consider for demonstration only the case T_1 = A = constant (k=0). The results of the calculations are given in the following Table 1.

Table 1. The FRW models with k=0 which admit the MCs $P_{\hat{\tau}}, M_{\mu\hat{\tau}}$ and B,C are arbitrary integration constants.

Case	$S(\tau)$	$\mu(\tau)$	$p(\tau)$	$H(\tau)$	$q(\tau)$	Restrictions
1	$Ce^{\alpha\tau}$	$-\frac{3A}{C^2e^{2\alpha\tau}}$	$\frac{A}{C^2e^{2\alpha\tau}}$	$\frac{3a}{Ce^{\alpha\tau}}$	0	ε_1=-1, $A<0$
2	$B\cos^2\frac{\alpha\tau}{2}$	$\frac{12A(1-\cos\alpha\tau)}{B^2(1+\cos\alpha\tau)^2}$	$\frac{4A}{B^2(1+\cos\alpha\tau)^2}$	$\frac{2a\sin\alpha\tau}{B(1+\cos\alpha\tau)^2}$	$\frac{1+\cos\alpha\tau}{\sin^2\alpha\tau}$	ε_1= 1, $A<0$
3	$B\sinh^2\frac{\alpha\tau}{2}$	$-\frac{3A}{B^2}\frac{\coth^2\frac{\alpha\tau}{2}}{\sinh^4\frac{\alpha\tau}{2}}$	$\frac{A}{B^2}\sinh^{-4}\frac{\alpha\tau}{2}$	$\frac{a}{B}\frac{\coth\frac{\alpha\tau}{2}}{\sinh^2\frac{\alpha\tau}{2}}$	$\frac{1}{2\cosh^2\alpha\tau}$	ε_1=-1,$A<0$ $\left(\frac{S_{,\tau}}{S}\right)^2>a^2$
4	$B\cosh^2\frac{\alpha\tau}{2}$	$-\frac{3A}{B^2}\frac{\tanh^2\frac{\alpha\tau}{2}}{\cosh^4\frac{\alpha\tau}{2}}$	$\frac{A}{B^2}\cosh^{-4}\frac{\alpha\tau}{2}$	$\frac{a}{B}\frac{\tanh\frac{\alpha\tau}{2}}{\cosh^2\frac{\alpha\tau}{2}}$	$-\frac{1}{2\sinh^2\alpha\tau}$	$\left(\frac{S_{,\tau}}{S}\right)^2<a^2$

It can be shown that $\mu > 0$, $\mu \pm p > 0$, $\mu + 3p > 0$, i.e. all the energy conditions are satisfied. A posteriori (because we know the solution!) determination of geometric equation of state is possible and we can work either directly with the scale factor S(τ) or better with the energy conservation equation:

$$H = \frac{\sqrt{3}}{3}\left(\mu - \frac{3k^{1/2}}{S^2}\right) \quad \text{(Friedmann equation).}$$

The symmetry condition $\mathcal{L}_X T_{ab} = 0$ can be written:

$$2HSp = -p_{,\tau}$$

Eliminating S(τ) from the last two equations we find:

$$\frac{dp}{d\mu} = \frac{p_{,\tau}}{\mu_{,\tau}} = \frac{2}{3}\frac{p}{p+\mu}$$

This equation has two solutions:

$$p = \frac{1}{3}\mu$$

and

$$\mu - \frac{3B}{a}|p|^{3/2} + 3p = 0.$$

For B=0 we obtain a linear equation of state with γ = 2/3. It corresponds to the solution of case 1 of Table 1 whose metric is:

$$ds^2 = -dt^2 + t^{\frac{4}{3\gamma}}\left(dx^2 + dy^2 + dz^2\right).$$

This spacetime admits a HVF given by the vector $P_{\bar{\tau}}$. The rest three vectors are *proper* MCs. The other solution (B ≠ 0) leads to a non-linear equation of state and corresponds to the solutions 2,3,4, of Table 1. Similarly we work with the other case $T_1 = \varepsilon A^2 e^{-2\bar{\tau}(\tau)/A}$.

On the existence of self-similar tilted perfect fluid Bianchi class A cosmological models

Pantelis S. Apostolopoulos

Department of Physics, Section of Astrophysics-Astronomy-Mechanics, University of Athens, Panepistemiopolis 157 83, Athens, GREECE

February 25, 2004

Abstract

We present some results concerning the existence of transitively self-similar spatially homogeneous (Bianchi) cosmological models admitting a 3-dimensional group of isometries acting on 3-dimensional spacelike surfaces. In order to describe the effects on the Geometry and the Dynamics of tilted perfect fluid (PF) models, coming from the existence of a Homothetic Vector Field (HVF), we use the so-called *metric approach* and show that the Field Equations (FE) and the induced physical restrictions are incompatible with types VII_0, VIII, IX. This result indicates that it is high plausible, tilted PF models of types VII_0, VIII and IX are not self-similar at the asymptotic regimes (i.e. near to the initial singularity or into the future). In addition we prove that type VI_0 self-similar models are necessarily rotating and give the *general self-similar solution.*

Although, on a sufficiently large observational scale, the present state of the Universe is described by the Friedmann-Lemaître (FL) model which is isotropic and spatially homogeneous, more general cosmological models which, in some dynamical sense, are "close" to FL models but not isotropic on any spatial scale can be used to understand the presence and the form of small (local) expansion anisotropies. In addition, it is of cosmological importance to investigate the constraints that observations impose on the geometry of space-time and to classify all possible asymptotic states near to the cosmological initial singularity (i.e. near the Planck time) that are permitted by the Field Equations (FE), with a view to explaining how the real Universe may have evolved. The complexity of the system of partial differential equations, followed from the FE, initiated the examination of the dynamics of general cosmological models using more sophisticated and predictive methods. In this direction the theory of dynamical systems is a most promising method in order to solve many of these open questions. The value of these methods is that they lead to mathematically well-defined, though not proved, conjectures about the asymptotic behaviour of the studied models i.e. at early and late times as well as in the intermediate period of their evolution [1]. In the symmetry-based hierarchy of cosmological models [2] the simplest generalizations of the FL models are the spatially homogeneous (SH) models filled with non-tilted or tilted perfect fluid (PF). One of the striking results of the dynamical systems approach was that *transitively self-similar* SH models are important in describing the asymptotic states of the evolution for more general models. This is due to the fact that transitively self-similar models arise as equilibrium points in the dynamical state space of more general SH models and determine various stable and unstable submanifolds which may be identical to some of the invariant sets of their evolution orbits, consequently providing a way to gain deeper insight into their asymptotic behaviour [1]. At the same time the assumption of self-similarity has the advantage of reducing the FE to a purely algebraic (closed) form which, if not can be solved explicitly, is used for doing numerical simulations in SH cosmologies.

Although in the vacuum and non-tilted PF models considerable information are available regarding their asymptotic states [3], in the case of tilted PF models the situation is more complex. The overall goal of the present work is to provide a concise presentation of the known results about the existence of self-similar SH models of class A filled with a titled PF. In the rest of the article we follow the notations and conventions used in [4].

Transitively self-similar SH models admit a proper Homothetic Vector Field (HVF) $\mathbf{H}$ acting *simply transitive* on space-time:

$$\mathcal{L}_{\mathbf{H}} g_{ab} = 2\psi g_{ab} \tag{1}$$

where ψ =const. is the homothetic factor which essentially represents the (constant) scale transformation of the geometrical and dynamical variables. The full four dimensional metric g_{ab} is given by:

$$ds^2 = -dt^2 + g_{\alpha\beta}(t)\boldsymbol{\omega}^\alpha\boldsymbol{\omega}^\beta \tag{2}$$

where $\boldsymbol{\omega}^\alpha$ is the dual of the invariant basis $\mathbf{e}_\alpha$.

In addition the invariant basis $\mathbf{e}_\alpha$ and its dual $\boldsymbol{\omega}^\alpha$ satisfy the commutation relations:

$$[\mathbf{e}_\alpha, \mathbf{e}_\beta] = -C^\gamma_{\alpha\beta}\mathbf{e}_\gamma \qquad , \qquad d\boldsymbol{\omega}^\gamma = \frac{1}{2}C^\gamma_{\alpha\beta}\boldsymbol{\omega}^\alpha \wedge \boldsymbol{\omega}^\beta \tag{3}$$

where d stands for the usual exterior derivative of 1-forms, $\wedge$ denotes the usual exterior product and $C^\gamma_{\alpha\beta} = -C^\gamma_{\beta\alpha}$ are the structure constants of the 3-dimensional group of isometries.

Under the assumption of self-similarity it has been shown that there are no tilted dust SH models [5] indicating the possibility that for the values of the state parameter $\gamma \leq 1$ the self-similar non-tilted SH models are stable and global future attractors for the entire class of SH models. Furthermore, due to the non-existence of self-similar models for the types VII_0,VIII,IX and irrotational type VI_0 [4, 6], their analysis in the asymptotic regimes is still open and may lead to some interesting new phenomena. For example and, at least for the type VIII,IX models, we expect that their behaviour may be similar to the corresponding vacuum and non-tilted models in which, although not asymptotically self-similar, have a oscillatory (chaotic-like) behaviour near to the initial singularity. Among other, these facts may revealed the role that the vorticity could play in their evolution. Concerning the remaining type VI_0 of SH models the only known solution was due to Rosquist and Jantzen (RJ) [7] who have found a family of type VI_0 models in which the state parameter γ lies in the interval $(1.0411, 1.7169)$ $(\gamma \neq 10/9)$. Although these models are known over a decade it seems that their importance were not fully understood. These models belong to the class $n^\alpha_\alpha = 0$, they are rotating and consequently there are extra degrees of freedom adding to the difficulty of qualitatively analysing general type VI_0 models. Furthermore it was not known if this family represents the most general self-similar tilted perfect fluid type VI_0 solution.

Proposition 1 *In the most general tilted PF type VI_0 self-similar solution the frame components of the metric and the fluid velocity are given by (4)-(5) and the state parameter satisfies the inequality $\frac{6}{5} \leq \gamma < \frac{3}{2}$.*

Proof

In [4] the form of the transitively self-similar type VI_0 metric, the normalized tilted fluid velocity and the HVF are given in terms of a set of arbitrary integration constants $c_{\alpha\beta}, v_\alpha, a, b, D, \psi$ (equations (3.29)-(3.31) of [4]) where ψ is the homothetic factor. Setting $a = (p_1 + p_2)\psi + 4\psi - b$ and $D = (2 - p_2) - b$ the *frame* components of the self-similar metric and the fluid velocity become:

$$g_{\alpha\beta} = \begin{pmatrix} c_{11}t^{2(p_2-1)} & c_{12}t^{p_1+p_2-2} & c_{13}t^{2p_1} \\ c_{12}t^{p_1+p_2-2} & c_{11}t^{2(p_1-1)} & c_{23}t^{2p_2} \\ c_{13}t^{2p_1} & c_{23}t^{2p_2} & c_{33}t^2 \end{pmatrix} \tag{4}$$

$$\Delta_1 = v_1 t^{p_1-1}, \qquad \Delta_2 = v_2 t^{p_2-1}, \qquad \Delta_3 = v_3 t \tag{5}$$

whereas the HVF assumes the form:

$$\mathbf{H} = \psi t\partial_t + [(2-p_2) - b]\,\partial_x + [(p_1+p_2)\psi + 4\psi - b]\,y\partial_y + bz\partial_z. \tag{6}$$

In terms of the Ricci tensor, the FE and the Bianchi identities can be written:

$$R_{ab} - \gamma\tilde{\mu}u_a u_b - \frac{(2-\gamma)}{2}\tilde{\mu}g_{ab} = 0 \tag{7}$$

$$\tilde{\mu}_{;a}u^a + \gamma\tilde{\mu}\tilde{\theta} = 0 \tag{8}$$

$$(\gamma - 1)\tilde{h}^k_a\tilde{\mu}_{;k} + \gamma\tilde{\mu}\dot{u}_a = 0. \tag{9}$$

In contrast with the existence of two hypersurface orthogonal Killing Vectors (KVs) in type II models, self-similar type VI_0 models are necessarily rotating and admit only one hypersurface orthogonal KV ($\mathbf{X}_1$ or $\mathbf{X}_3$) [2]. Therefore it is convenient to divide our analysis according to whether $X_1^k R_{k[a}X_{1b]} = 0$ or $X_3^k R_{k[a}X_{3b]} = 0$ (since the KVs $\mathbf{X}_1$,$\mathbf{X}_2$ form an Abelian subgroup of the G_3 group of isometries the $\mathbf{X}_2$-case is similar).

Case $X_1^k R_{k[a}X_{1b]} = 0$

We employ a new constant s which is defined by the equation:

$$p_1 + p_2 = 2\,(s+1)\,. \tag{10}$$

Equation (8) implies that the state parameter γ is related with s via the relation:

$$\gamma = \frac{2}{2s+1}. \tag{11}$$

From (7) (or equivalently the existence of the hypersurface orthogonal KV $\mathbf{X}_1$) it follows that $v_1 = 0$ and, in order to avoid the orthogonal case, we assume $v_2, v_3 \neq 0$. The resulting system consists of a set of 10 highly non-linear algebraic equations (7) in 13 unknowns augmented by the system of equations (9). Imposing the physical restrictions:

$$\tilde{\mu} > 0, \quad \Gamma^2 > 0, \quad \sigma^2 > 0, \quad \omega^2 > 0, \quad \dot{u}^a\dot{u}_a > 0 \tag{12}$$

we can determine analytically the exact form of the self-similar metric and the fluid velocity [8].

The constant p_2 is related with the "state parameter" s according to:

$$p_2 = \frac{\sqrt{4s^2 - 36s + 17}\,|3s-1| - 42s^2 - 17\,(s-1)}{17 - 36s}. \tag{13}$$

The kinematical and dynamical quantities of this family of self-similar models are:

$$\tilde{\mu} = \frac{(2s+1)\,(2s+1-p_2)}{t^2} \tag{14}$$

$$\dot{u}^a\dot{u}_a = \frac{(p_2 - s - 1)\,[p_2 + 2\,(s-1)]\,(2s-1)^2\,[3p_2 - 2\,(2s+1)]}{t^2\,(p_2 - 2s - 1)\,[3p_2 - 2\,(3s+1)]} \tag{15}$$

$$\Gamma^2 = \frac{3p_2^3 - p_2^2(s+8) - p_2\left(10s^2+2s-7\right) + 2\left(4s^3+8s^2+s-1\right)}{(p_2-2s-1)\left[3p_2 - 2(3s+1)\right]} \tag{16}$$

$$\begin{aligned} \sigma^2 &= \left\{3p_2^3\left(100s^2-50s^2+13\right) - p_2^2\left(100s^3+1020s^2-369s+95\right) - \right. \\ &\quad -2p_2\left(500s^4-492s^3-647s^2+191s-38\right) + \\ &\quad \left. +4\left(200s^5+192s^4-328s^3-95s^2+36s-5\right)\right\} \times \\ &\quad \times \left\{12t^2\left[3p_2^2 - p_2(12s+5)+12s^2+10s+2\right]\right\}^{-1} \end{aligned} \tag{17}$$

$$\omega^2 = \frac{s\left[p_2+2(s-1)\right]^2}{2t^2\left[3p_2-2(3s+1)\right]}. \tag{18}$$

The positivity of the above quantities is ensured provided that:

$$s \in \left(\frac{1}{6}, \frac{1}{3}\right) \Leftrightarrow \gamma \in \left(\frac{6}{5}, \frac{3}{2}\right). \tag{19}$$

It is easy to show that this solution belongs to the subclass of SH models satisfying the constraint $n_\alpha^\alpha = 0$ hence it represents a family of models which has a four dimensional stable manifold [9]. We also note that for the case where $n_\alpha^\alpha \neq 0$ there is a solution of the FE (7) in which the constants $c_{\alpha\beta}$ are all non-vanishing. For these models the state parameter γ takes the values $\left(1, \frac{6}{5}\right) \cup \left(\frac{3}{2}, 2\right)$. However *none* of these solutions is physically acceptable i.e. they do not satisfy the inequalities (12) [8].

Case $X_3^k R_{k[a} X_{3b]} = 0$

In this case $v_3 = 0$ and the solution of the FE implies that $p_1 = p_2 = \frac{4}{3}$ which by means of (10) and (11) the state parameter $\gamma = \frac{6}{5}$. We note that this model also belongs to the subclass $n_\alpha^\alpha = 0$ and admits the hypersurface orthogonal KV $\mathbf{X}_3$. Furthermore it was recognized as an equilibrium point of the dynamical state space of the $\gamma-$law perfect fluid type VI_0 models [7]. $\square$

The family of self-similar models found in the present paper could play a similar role (as in the case of type II models) in the asymptotic behaviour of general type VI_0 models. In fact Barrow and Hervik [10] have studied the (local) stability of tilted SH models at late times (in the neighborhood of the non-tilted equilibrium point) and have shown that in type VI_0, the non-tilted Collins solution [1] (future attractor for nearby trajectories) is stable whenever $\gamma \in \left(\frac{2}{3}, \frac{6}{5}\right)$. Therefore for $\gamma = \frac{6}{5}$ the tilt destabilises the Collins model i.e. there is a bifurcation which is associated with the stability change of the equilibrium points (Collins model and the present solution). In addition for $\gamma \in \left(\frac{6}{5}, \frac{3}{2}\right)$ the present family of models is asymptotically tilted ($v_3 \neq 0$) and has a four dimensional stable manifold [9] hence it is possible to play the role of the future attractor at least for the subclass of tilted type VI_0 models satisfying $n^\alpha_\alpha = 0$ (we recall that for general type VI_0 models i.e. when $n^\alpha_\alpha \neq 0$ the dynamical state space is seven dimensional). In view of the above results and the similarities between types II and VI_0 one may conjecture that the subclass $n^\alpha_\alpha = 0$ of type VI_0 models are possible to be asymptotically tilted at late times for $\gamma \in \left(\frac{6}{5}, 2\right)$. Furthermore a preliminary analysis on this class of tilted type VI_0 models indicate that whenever $\gamma \in \left(\frac{3}{2}, 2\right)$, the tilt is becoming extreme at late times [9].

References

[1] C. B. Collins, 1971 Commun. Math. Phys. **23** 137-156; C. B. Collins and J. M. Stewart, 1971 Mon. Not. R. Astron. Soc. **153** 419-434; J. Wainwright and G. F. R. Ellis (eds), *Dynamical Systems in Cosmology* (Cambridge University Press, Cambridge 1997).

[2] C. G. Hewitt, R. Bridson and J. Wainwright, 2001 Gen. Relativ. Grav. **33** 65-94; C. G. Hewitt, 1991 Class. Quantum Grav. **8** L109-L114.

[3] J. Wainwright and L. Hsu, 1989 Class. Quantum Grav. **6** 1409-1431; C. G. Hewitt and J. Wainwright, 1993 Class. Quantum Grav. **10** 4242-4252.

[4] P. S. Apostolopoulos, 2003 Class. Quantum Grav. **20** 3371-3384.

[5] M. Bradley, 1988 Class. Quantum Grav. **5** L15-L19.

[6] P. S. Apostolopoulos and M. Tsamparlis, 2003 Gen. Rel. Grav. **35** 2051-2056.

[7] K. Rosquist and R. T. Jantzen, 1985 Phys. Lett. A **107** 29-32; R. T. Jantzen and K. Rosquist, 1986 Class. Quantum Grav. **3** 281-309.

[8] P. S. Apostolopoulos, 2004 Gen. Rel. Grav. (*to appear in August issue*; **preprint gr-qc/0310033**).

[9] S. Hervik, in preparation (2004).

[10] J. D. Barrow and S. Hervik, 2003 Class. Quantum Grav. **20** 2841-2854.

SOME COSMOLOGICAL MODELS AND THE AGE OF THE UNIVERSE*

Evangelos Chaliasos

365 Thebes Street GR-12241 Aegaleo, Athens, Greece

1. Prevailing model

The purpose of this section is to criticize the prevailing model of the Universe ($\lambda > 0$ & $k = 0$) with regard to the resulting age of the Universe on the one hand, and the plausibility of the small cosmological constant implied by the observations on the other hand.

The characteristics of the prevailing model are the following two ones. First, the Universe is "accelerating" ($q_0 < 0$),as implied by the observations of very distant supernovae. This property of $q_0 < 0$ can be secured by taking $\lambda > 0$. In fact, from the relation

$$\Omega_{M0} = 2q_0 + 2\left(\frac{\Lambda c^2}{3{H_0}^2}\right) \tag{1}$$

[6], we see that we can take q_0 negative if we choose Λ to be positive and large enough.

The second characteristic is that $k = 0$, that is the space is "flat", in order for the inflation theory to hold.

We take for the Hubble constant the value $H_0 = 73$ (km/sec)/Mpc [9] throughout. This value has resulted from observations of the Hubble telescope in 1999. Then for the model being examined an age of the Universe $t_0 \cong 1.25\times10^{10}$ yr is obtained, as we will see in what follows. This has to be contrasted to the estimated value $t_0 \cong 1.34\times10^{10}$ yr [8]. (For comparison, the age of the oldest stars is estimated to be $t \cong 1.2\times10^{10}$ yr [8] only).

We proceed to find q_0. The equations governing the matter-dominated era are

$${H_0}^2 + \frac{kc^2}{{S_0}^2} - \frac{1}{3}\lambda c^2 = {H_0}^2\Omega_{M0} \tag{2}$$

and

$$(1-2q_0){H_0}^2 + \frac{kc^2}{{S_0}^2} - \lambda c^2 = 0 \tag{3}$$

[6], where S_0 is the scale factor. From eqn (2) we find in our case ($k = 0$)

$$\Omega_{M0} = 1 - \frac{\lambda c^2}{3{H_0}^2} \tag{4}$$

and from eqn (3)

$$q_0 = \frac{1}{2} - \frac{1}{2}\frac{\lambda c^2}{{H_0}^2}. \tag{5}$$

If we set

$$\Omega_{\Lambda 0} \equiv \frac{\lambda c^2}{3{H_0}^2}, \tag{6}$$

we see that eqn (4) can be written as

* *Proceedings of the 6th Hellenic Astronomical Society Conference, 15-17 September 2003, Penteli, Greece*

$$\Omega_{M0} + \Omega_{\Lambda 0} = 1. \tag{7}$$

From observations we find that $\Omega_{M0} = 1/3$, so that, because of eqn (7), we conclude that $\Omega_{\Lambda 0} = 2/3$. Then from eqn (5) it follows that $q_0 = -0.5$.

Proceeding now to the determination of the age of the Universe t_0 in the prevailing model, we start from the equation of motion

$$H^2 \equiv \left(\frac{\dot{a}}{a}\right)^2 = \frac{8\pi G}{3}\rho_M + \frac{\Lambda c^2}{3} - \frac{kc^2}{a^2}, \tag{8}$$

where a is now the scale factor. Setting k = 0, and knowing that

$$\rho_M a^3 = \rho_{M0} a_0^{\ 3} = \text{const.}, \tag{9}$$

it can be shown that

$$t_0 = \frac{\sqrt{3}}{H_0} I, \tag{10}$$

where

$$I \equiv \int_0^1 \frac{dx}{x\sqrt{\dfrac{1}{x^3}+2}}. \tag{11}$$

We find numerically that I = 0.540331. Thus $t_0 = 1.25\times10^{10}$ years.

Let us now examine the plausibility for the introduction of the λ-term. This is meant as interpreting a vacuum energy, which is thought as resulting out of the quantum mechanical particle-antiparticle pair creations taking place. It is supposed of course that the mass of an antiparticle is the same with the mass of the corresponding particle (i.e. both positive). But then it is possible to be estimated [1, 5] that $\Omega_{\Lambda 0} \approx \approx 10^{120}$ (!). This of course gives rise to an unpleasant situation. But there is an exit from this big problem, if we assume that the mass of an antiparticle is the opposite (negative) of the mass of the corresponding particle (positive). Of course then it results in $\Omega_\Lambda = 0$. But, now, *the situation changes radically,* as we will see in what follows.

2. Negative mass and antiparticles

We know from Mechanics that the orbit of a particle is given by the action integral

$$S = \int_{t_A}^{t_B} L dt, \tag{12}$$

which must become a minimum. It is supposed that $t_A < t_B$. L is the Lagrangian, which for a free particle is given by

$$L = \frac{1}{2} m v^2. \tag{13}$$

Here m is a constant of proportionality called the *mass* of the particle. It is obvious that m > 0 in order for S to have a minimum (if m < 0, then we could make S negative and so small as we want by simply taking v sufficiently large [3]).

For particles moving *backward in time,* which we call *retrons,* we would have analogously

$$S = \int_{t_B}^{t_A} L' dt, \tag{14}$$

with L′ the new Lagrangian and now $t_B > t_A$. This must become again a minimum. The new Lagrangian is given by

$$L' = \frac{1}{2} m' v^2, \tag{15}$$

from which we now see that m′ < 0 in order for S to have a minimum.

Let us now come to Electrodynamics. The Lagrangian of a particle in an electromagnetic field is given by

$$L = -mc^2 \sqrt{1 - \frac{v^2}{c^2}} + \frac{e}{c} \vec{A} \cdot \vec{v} - e\phi, \tag{16}$$

where (φ, **A**) is the potential, and e the charge of the particle. Analogously for retrons

$$L' = -m'c^2 \sqrt{1 - \frac{v^2}{c^2}} + \frac{e'}{c} \vec{A} \cdot \vec{v} - e'\phi. \tag{17}$$

Now, if we demand that L′ = -L, because m′ = -m we will obtain also e′ = -e.

The equation of motion (Lorentz force) for a particle in an EM field is

$$mc \frac{du^i}{ds} = \frac{e}{c} F^{ik} u_k, \tag{18}$$

where u^i is its four-velocity and F^{ik} the electromagnetic field tensor. For our very well known *antiparticles,* supposed to have the same mass (m) with their corresponding particles and opposite charge (e′ = -e), we will have as the equation of motion (in the same field), analogously to eqn (18),

$$mc \frac{du^i}{ds} = \frac{e'}{c} F^{ik} u_k. \tag{19}$$

Feynman [2] was the first who realized that antiparticles should be particles moving *backward in time.* Thus, letting the charge to be e again but changing ds to ds′ = -ds (with m *unchanged*), he took effectively for antiparticles the equivalent to eqn (19) equation of motion

$$mc \frac{du^i}{ds'} = \frac{e}{c} F^{ik} u_k. \tag{20}$$

But in this way, since we have called retrons the particles moving backward in time, it is evident that we must *identify* antiparticles with retrons. However, we know that for retrons m′ = -m & e′ = -e. Thus we have to simultaneously change the sign of both m & e in eqn (20), so that we take for antiparticles the, equivalent to eqn (20) (and to eqn (19)), *correct* equation

$$m'c \frac{du^i}{ds'} = \frac{e'}{c} F^{ik} u_k. \tag{21}$$

Coming now again to the Universe, we have to observe that the time symmetry implied before is completely equivalent to matter-antimatter symmetry, according to our interpretation of antiparticles. And since the Universe we know that is homogeneous and isotropic (at large scale), we are led to the conclusion that matter must be uniformly mixed with antimatter (at large scale). Thus we have to take as density: $\rho = \rho_M + \rho_A = \rho_M - \rho_M = 0$ (!).

3. A new cosmological model

The Einstein equations for a homogeneous and isotropic universe (with a cosmological constant) are [7]:

$$\frac{\dot{R}^2}{R^2} - \frac{8\pi G\rho}{3} = -\frac{kc^2}{R^2} + \frac{\Lambda c^2}{3} \tag{22}$$

$$\frac{\dot{R}^2}{R^2} + 2\frac{\ddot{R}}{R} + \frac{8\pi Gp}{c^2} = -\frac{kc^2}{R^2} + \Lambda c^2, \tag{23}$$

where R is the scale factor now. If we take $\Lambda = 0$ (mainly for theoretical reasons [4]), these reduce to the Friedmann equations. Also, for matter-antimatter symmetry we must set $\rho = p = 0$ in the above equations.

To solve them, we observe that from eqn (23), because of eqn (22), we immediately take $R'' = 0$, so that

$$q \equiv -\frac{\ddot{R}R}{\dot{R}^2} = 0. \tag{24}$$

Note the excellent agreement of the $q_0 = 0$ curve with the observational data (see, e.g., Fig. 3 of S. Perlmutter *et al: Nature,* **391,** 51, 1 January 1998).

We also observe that in eqn (22) it must be $k = -1$, that is we apparently have a hyperbolic space. Then eqn (22) gives simply $R'^2 = c^2$, so that the solution for the scale factor R is $R = \pm ct$. Then it is obtained that $H \equiv R'/R = 1/t$, so that we finally find for the age of the Universe simply $t_0 = 1/H_0$. As an application we thus find $t_0 = 1.34\times10^{10}$ years, in complete agreement with the estimated value [8].

REFERENCES

1. Carroll, S.M., Press, W.H. & Turner, E.L. (1992) *ARA&A,* **30,** 499
2. Feynman, R.P.: "Theory of Fundamental Processes", Addison-Wesley, Reading (Massachusetts), 1961
3. Landau, L.D. & Lifshitz, E.M.: "Mechanics" (3rd edn), vol. 1 of "Course of Theoretical Physics", Pergamon Press, Oxford, 1976
4. Landau, L.D. & Lifshitz, E.M.: "The Classical Theory of Fields" (4th edn), vol. 2 of "Course of Theoretical Physics", Pergamon Press, Oxford, 1975
5. Michael, Eli: http://super.colorado.edu/~michaele/Lambda/phys.html (plausibility)
6. Narlikar, J.V. : « Introduction to Cosmology », Cambridge University Press, Cambridge, 1993
7. Rose, W.K.: "Astrophysics", Holt, Rinehart & Winston, Inc.,New York, 1973
8. http://www.abs.net.au/science/news/stories/s2664.htm
9. http://science.nasa.gov/newhome/headlines/ast25may99_1.htm

NON-LINEAR DYNAMICS OF DIFFERENTIALLY ROTATING RELATIVISTIC STARS*

T. A. Apostolatos[(1)], N. Stergioulas[(2)], and J. A. Font[(3)]

[(1)]Department of Physics, University of Athens, Panepistimiopolis, Athens 15784, Greece
[(2)]Department of Physics, University of Thessaloniki, Thessaloniki 54124, Greece
[(3)]Departamento de Astronomia y Astrofisica, Universidad de Valencia,
46100 Burjassot (Valencia), Spain

ABSTRACT

Sequences of neutron-star models with differential rotation, but with different rotation rates, have been constructed, perturbed axisymmetrically, and evolved. A fully general-relativistic code has been used for their evolution, in the Cowling approximation. By analyzing the time series we have studied the effects of differential rotation on the axisymmetric modes of NSs. Since differential rotation modifies the internal structure of our models, allowing them to be less compact near the center, it makes it possible to create much more oblate objects, than with uniform rotation, which pulsate with much lower frequencies. Besides this interesting result, a new mode showed up that is more pronounced in the fast rotating models and comes about as a splitting of the fundamental quasi-radial mode. If such a pulsation is detected by gravitational waves, it will give us independent information about the amount of differential rotation of the source.

1. INTRODUCTION

The formation of a neutron star, either as the end product of a supernova explosion, or an accretion-induced collapse of a white dwarf, or as the final merger of a binary neutron star, is quite a violent event. Thus, a newly formed neutron star will be a wildly pulsating object. Conservation of angular momentum, in the case of collapse, or the form of the initial configuration, in the case of a merger, are expected to lead to a differentially rotating star. The simplest realistic configurations that could be studied in order to yield valuable information about the initial phase of the life of neutron stars are pulsating and highly rotating neutron stars with differential rotation. Instead of relying on expensive and time-consuming 3D relativistic codes that are nowadays under development, we have used a well-tested 2D non-linear, fully relativistic, and shock capturing hydrodynamical code that is able to evolve any axisymmetric perturbations of the fluid assuming a fixed spacetime background. The assumption of axisymmetry is partly justified, since rotational collapse excited mainly axisymmetric oscillations.

Knowing how differential rotation affects the spectrum of neutron-star pulsations will be valuable for extracting information about the structure of the neutron star from any corresponding detected gravitational-wave signal, since the spectrum of each model is related to its rotation and the equation of state of its fluid. In the case of differential rotation a new mode shows up that seems to be degenerate with the fundamental mode when rotation is very slow. As the amount of rotation increases the two peaks move apart from each other. Therefore, the frequency separation between the two peaks is related to the amount of rotation, while the rate of differential rotation determines the balance of

* *Proceedings of the 6th Hellenic Astronomical Society Conference, 15-17 September 2003, Penteli, Greece*

excitations of the two modes. The new mode has a completely different eigenfunction from the other modes of low order and shows up as a splitting of the fundamental quasi-radial mode when differential rotation is induced, or it could just be an artifact of the Cowling approximation.

Another new feature that has been explored is the damping of pulsations, due to mass shedding. The faster the neutron star rotates, the more weakly bound is the fluid at the surface of the star near the equator, due to centrifugal force. Thus, pulsations lead to shocks that heat up the surface of the star, which absorbs energy from the pulsations.

Our study shows that the prospects of detection of gravitational waves from newly formed neutron stars is higher than expected, since higher rotation rates for the stars are allowed, due to differential rotation, and hence the corresponding pulsations exhibit much lower frequencies. This is very important for detection, at least for the first generation of interferometric gravitational wave detectors, since the most sensitive region of these detectors is of the order of 100 Hz, while the lowest order modes of a non-rotating neutron star is of the order of 2 kHz, well beyond the high-sensitivity window of such detectors. The fastest rotating neutron stars with differential rotation that we have studied have a fundamental l=2 mode with characteristic frequency of order 800 Hz. Since in the Cowling approximation the eigenfrequencies are higher than in the real case, chances for detection of gravitational radiation from pulsating young neutron stars are even better.

2. PREPARATION OF THE PERTURBED CONFIGURATIONS

The models we have used are constructed with a polytropic equation of state with polytropic index N=1 ($p = K\rho_0^{1+1/\mathrm{N}}$). The line element inside the star is assumed to have the following stationary axisymmetric form

$$ds^2 = -e^{\gamma+\rho}dt^2 + e^{\gamma-\rho}r^2\sin^2\theta(d\phi-\omega dt)^2 + e^{2\alpha}(dr^2 + r^2 d\theta^2)\,. \qquad (2.1)$$

All functions $\gamma, \rho, \omega, \alpha$ are functions of r, and θ. Differential rotation is implemented by the following one-parameter law[1]:

$$\Omega_c - \Omega = \frac{1}{A^2}\left[\frac{(\Omega-\omega)r^2\sin^2\theta\, e^{-2\rho}}{1-(\Omega-\omega)^2 r^2\sin^2\theta\, e^{-2\rho}}\right] \qquad (2.2)$$

where Ω_c is the rotation rate at the center of the star. The A parameter is the length scale for the variation of rotation rate. The higher the parameter A is, the more uniform the rotation rate Ω of the interior of the star. We have parametrized our models with the non-dimensional parameter $\widetilde{A} = A/R_e$, where R_e is the equatorial radius of the star. The equilibrium models have been constructed with a numerical code[2] that is able to construct equilibria even extremely close to the mass-shedding limit.

These equilibrium models have been excited by adding either a density perturbation ($l = 0$ modes), or a velocity perturbation ($l \neq 0$ modes). The profile of the initial perturbation is similar to the corresponding non-rotating eigenfunction[3]. Since the unknown eigenfunctions of our models should be quite different from the ones of non-rotating stars, the initial perturbations, which we implement, are expected to excite a number of modes. Actually, the spectrum is more complex for the fastest rotating models which differ significantly from the non-rotating case.

3. MODIFICATIONS OF THE SPECTRUM AND CONSEQUENCES

In order to obtain a clear picture of the effect of differential rotation on the pulsations of rotating neutron stars, we have constructed and explored three sequences of neutron star models. The first sequence consists of stars with the same axes-ratio and central density, but with different differential-rotation parameter $\widetilde{A}$, ranging from infinity (uniform rotation) to 1. By comparing the spectra of all models of this sequence we found that the frequencies are not modified by more than 20% through the whole range of $\widetilde{A}$'s. This means that differential rotation does not have a direct strong effect to the spectrum. The second and the third sequences consist of models with $\widetilde{A}=1$, and with varying axes-ratios (ranging from 1 to the lowest allowable value that an equilibrium could form). The former of these sequences was constructed assuming a constant mass of 1.4 $M_{\odot}$, while the latter consists of stars with constant central density. The outcome of our spectral analysis of all these models is the following.

With respect to the first of these two sequences, the more oblate the model is (lower axes-ratio), the lower the frequencies of their spectra are. This is a general conclusion irrespective of the uniform or non-uniform rotation of the stars. This happens because the higher the rotation rate is, the less centrally compact the star is and thus the frequencies are lower. Moreover, if differential rotation is assumed the frequencies do not drop as steep as when the star is uniformly rotating. The reason for that is that a differentially rotating star is rotating much slower than the corresponding uniformly rotating star with the same oblateness, and thus the former one is more centrally compact. On the other hand, since the same oblateness is achieved with much slower rotation rate, the differentially rotating models could rotate at much higher rates before they reach the mass-shedding limit. Therefore, the most extreme eigenfrequencies of differentially rotating models become much smaller than for their uniformly rotating counterparts. The other sequence, the one with constant central density, does not exhibit such a strong dependence of frequencies with oblateness. Now, the mass is increasing with rotation rate and the average density remains almost constant throughout the sequence and so do the frequencies.

A new feature of differential rotation is the new mode that appears near the fundamental mode and departs from the latter one with increasing $\widetilde{A}$. This was found by studying the spectrum of the first sequence with varying $\widetilde{A}$, but with constant central density and axes ratio. The eigenfunction of the new mode has a completely different shape from the fundamental mode and it is excited to large amplitude in the fastest rotating models.

The consequences for detecting gravitational waves from newly formed pulsating neutron stars is that differentially rotation leads to lower frequencies that could be easier detected with the ground-based interferometric detectors like LIGO, or VIRGO. Without the assumption of the Cowling approximation one would obtained to even lower frequencies, within the sensitive window of detectors. Our observation with respect to the new mode, if confirmed without the Cowling approximation, could be used in the future to obtain information about the internal rotation of newly-born neutron stars.

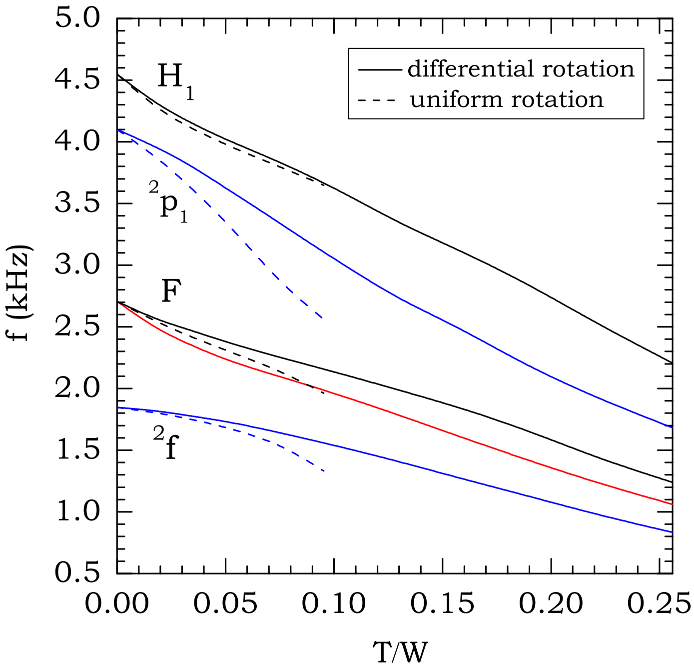

Figure 1. *This diagram shows how the frequencies are affected by the rotation rate of the differentially-rotating models. The T/W parameter (the ratio of kinetic to gravitational energy) is used to parametrize the rotation rate. The solid lines correspond to differentially rotating bodies with* $\tilde{A}$. *The dashed lines correspond to uniformly rotating bodies; although the latter frequencies decrease much faster with T/W the mass shedding limit ends these sequences much sooner. The lower line that bifurcates from the F-mode at T/W=0 corresponds to the new mode. The higher the rotation rate the more this mode departs from the F-mode.*

Acknowledgments

Financial support for this research has been provided by the the EU Network Programme (Research Training Network Contract HPRN-CT-2000-00137). T.A.A. acknowledges financial support from the Special Accounts for Research Grants (grant 70/4/4056), and J.A.F. acknowledges financial support from the Spanish Ministerio de Ciencia y Tecnologia (grant AYA 2001-3490-C02-01).

References

1. H. Komatsu, Y. Eriguchi, and I. Hachisu *MNRAS*, **237**, 355 (1989), and *MNRAS*, **313**, 678 (2000).
2. N. Stergioulas, and J. L. Friedman, *Ap. J.* **444**, 306 (1995).
3. J. A. Font, H. Dimmelmeier, A. Gupta, and N. Stergioulas *MNRAS* **325**, 1463 (2001).

LARGE SCALE POWER IN THE CMB AND NEW PHYSICS: AN ANALYSIS USING BAYESIAN MODEL COMPARISON*

Anastasia Niarchou, **Andrew Jaffe and Levon Pogosian**

Blackett Laboratory, Imperial College, London SW7 2AZ, UK

Abstract: The newly released WMAP data have revealed an intriguing lack of power at large scales that cannot be accounted for in the context of standard cosmology. We discuss alternative cosmological models that fit the data better than the standard ΛCDM model. We find that low power models such as a flat universe with a cutoff in the primordial power spectrum or a closed universe are only marginally preferred by the data. However, a hypothesis about the discrepancy originating in theoretical or data analysis methodology is more likely; we conclude that possibly no model will ever improve the fit to the large scales by more than 2.7σ.

1. INTRODUCTION

The first year data from the WMAP satellite seem to be consistent with a flat ΛCDM model with a nearly scale invariant spectrum of adiabatic primordial fluctuations [1]. However, the anisotropy power spectrum of the standard ΛCDM model contradicts the observations at large scales (fig.1).

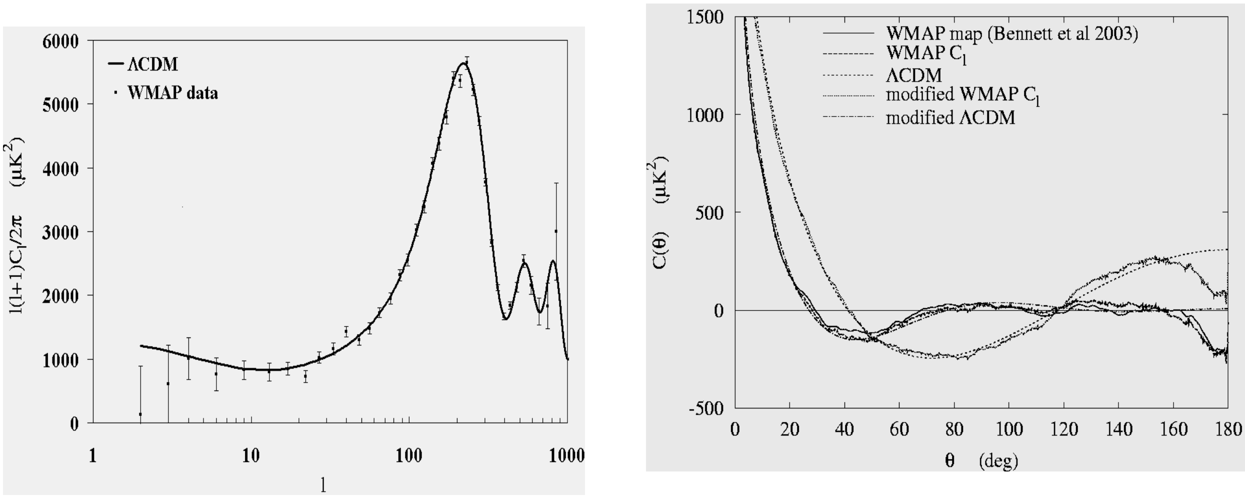

Figure 1. *Left*: The WMAP data exhibit a lack of power at lower multipoles. *Right*: The anisotropy correlation function calculated from the ILC map (long line), from the WMAP C_l (long dashed line), from the best-fit ΛCDM C_l (short dashed line), from the WMAP C_l with C_2 and C_3 matching those of the ΛCDM (dotted line) and from the ΛCDM C_l with C_2 and C_3 matching the observed values (dot-dashed line).

* *Proceedings of the 6th Hellenic Astronomical Society Conference, 15-17 September 2003, Penteli, Greece*

This phenomenon is particularly manifest in the anisotropy correlation function (fig.1):

$$
\begin{aligned}
C(\theta) &= \langle T(\hat{\mathbf{n}})T(\hat{\mathbf{m}})\rangle \quad \text{with} \quad \hat{\mathbf{n}}\cdot\hat{\mathbf{m}} = \cos\theta \\
&= \sum_l \frac{2l+1}{4\pi} C_l P_l(\cos\theta)
\end{aligned} \tag{1}
$$

The second expression is valid for a Gaussian distribution with enough samples and defines an estimator if one interprets the ensemble average as a spatial or pixel average. This function is practically zero for $\theta > 60^{\mathrm{o}}$. in contrast to what would be expected for a ΛCDM model. If, however, one lowers the theoretical values of C_2 and C_3 to their observed levels (or, vice versa, raises the values in the observed spectrum), the theoretical and experimental curves come into good agreement. Therefore, the difference between the two is due to the low observed values of the quadrupole and octopole alone. Our aim is to estimate the statistical significance of this observation and infer whether it points to the direction of new physics or can simply be attributed to experimental systematics. This is a review of the work presented in [3] which the reader is referred to for a more detailed analysis.

2. BAYESIAN MODEL COMPARISON

In order to carry out our analysis, we employ the technique of Bayesian model comparison [4]. Bayes' theorem gives the posterior probability of a set of parameters θ given a set of data D under the assumption that a model m is valid:

$$
P(\theta \mid DI_m) = P(\theta \mid I_m)\frac{P(D \mid \theta I_m)}{P(D \mid I_m)} \quad \text{with} \quad P(D \mid I_m) = \int P(\theta \mid I_m) P(D \mid \theta I_m) d\theta \tag{2}
$$

where $P(A \mid B)$ is the probability of A given B and I_m refers to the background information about m. $P(D \mid \theta I_m)$ is the likelihood function and $P(\theta \mid I_m)$ is the prior probability of the parameters θ. The normalization factor $P(D \mid I_m)$ is also called "evidence".

In order to discriminate amongst two models m and n we use the ratio of their likelihoods:

$$
\frac{P(m \mid DI)}{P(n \mid DI)} = \frac{P(m \mid I)}{P(n \mid I)}\frac{P(D \mid I_m)}{P(D \mid I_n)} = \frac{P(m \mid I)}{P(n \mid I)} B_{mn} \tag{3}
$$

The first factor on the rhs of Eq. (3) depends on the prior information regarding the likelihood of a model, while the second term (also known as the "Bayes factor") is determined by the experimental data. Therefore, if we have no prior information that would favour one model over another, the only way to decide which is the most likely is to estimate the Bayes factor. The latter tends to favour models with a more compact parameter space, unless more complicated ones fit the data significantly better. The Bayes factor is related to the "number of sigma" (by which a model or hypothesis is favoured) through $\nu = \sqrt{2 \,|\ln B_{mn}|}$, ν being the number of sigma.

In the following we select some alternative models that present a better fit to the WMAP data at large scales than standard ΛCDM and calculate the Bayes factor for each model with respect to the standard model. The evidence for the latter is just the value of the likelihood function, which is equal to 0.00094.

3. REMOVING THE DISCREPANCY

A simple way to account for the deficit of power at large scales is to consider a flat ΛCDM model with a power spectrum that would truncate at large scales. This model has been considered in [5], where the cutoff was imposed by fiat.

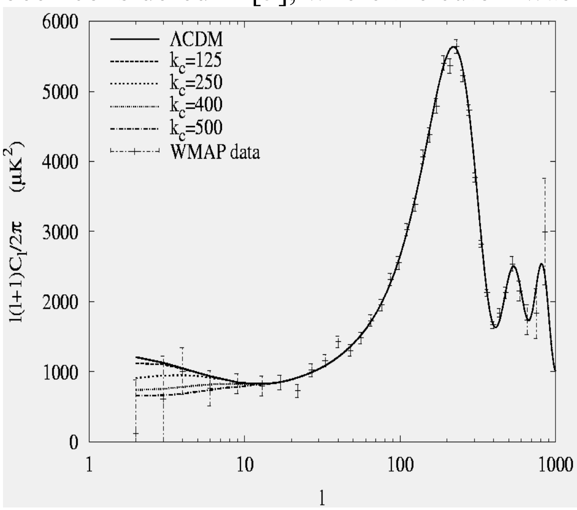

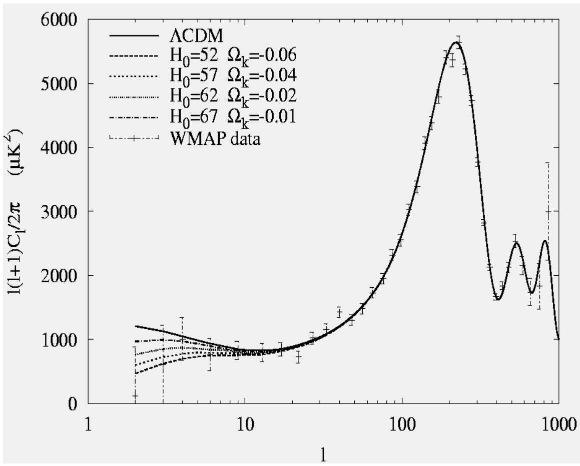

Figure 2. *Left*: Temperature anisotropy power spectra for various values of the cutoff scale k_c measured in units of 10^{-6} Mpc^{-1}. *Right*: Temperature anisotropy power spectra for various values of H_0 (in km/sec/Mpc) and the corresponding curvature values (Ω_k).

We can let the cutoff scale k_c be the free parameter of this model and calculate the evidence according to Eq. (3). We set $k_c \in [0, 0.001]$ Mpc^{-1}. For a flat prior in the aforementioned region, the evidence is 0.0025.

Another possible solution to the problem would be a slightly closed universe, which is allowed by the WMAP data. Its main drawback is the absence of a robust theory extending the notion of scale invariance to scales comparable to the curvature scale. Ref. [6] suggested that the primordial power spectrum would truncate on these scales, which could result in the observed lack of power at low multipoles. The anisotropy power spectrum can be adjusted to fit that of the ΛCDM at smaller scales thanks to the geometric degeneracy of the power spectrum described in [7]. It is fairly straightforward to produce a degeneracy line on the (Ω_k, h) plane so that models that lie on this degeneracy line have power spectra identical to that of the ΛCDM model. Differences are only manifest at large scales, where the truncation of the primordial power spectra of closed universes induces a decrease in power (fig.2). If we set h as the free parameter of the closed universe model and impose a Gaussian prior with mean $\bar{h} = 0.72$ and variance $\sigma = 0.10$ with $h \in [0.52, 0.72]$, the evidence is equal to 0.0034. It is worth noting that adding more free parameters to this model, namely the spectral index and σ_8, dramatically decreases the evidence.

New physics is not the only scenario that could account for the discrepancy between theory and observation at large scales. This problem may arise purely from data analysis methodology. A simple idea would be that of an underestimation of the error bars at low multipoles. However, we have firm evidence that the results reported from WMAP at large scales are likely to be reliable. An alternative interpretation of this suggestion is that the measurements at large scales are correct, but C_2 and C_3 have an origin outside the standard cosmology. We implement the idea of increasing the error bars on C_2 and C_3 by multiplying the corresponding diagonal elements of the likelihood curvature matrix by 2 constants, r_2 and r_3. The evidence is relatively insensitive to the upper limit of the prior on r_2 and r_3 and to whether the prior is uniform in the r_i or $\ln r_i$. If we assume $r_i \to \infty$, the evidence is equal to 0.041.

4. SUMMARY AND CONCLUSIONS

We summarize our results in the table below:

model	**parameters**	**Priors**	**Bayes factor**	**# σ** $\left(\sqrt{2\left\|\ln B_{mn}\right\|}\right)$
best fit	------	------	1	------
flat with cutoff	k_c	uniform in [0, 0,001] Mpc^{-1}	2.66	1.40σ
closed	H h n σ_8	h: gaussian $(\overline{h} = 0.72, \sigma_h = 0.1)$ n: gaussian $(\overline{n} = 0.99, \sigma_n = 0.07)$ σ_8: gaussian $(\overline{\sigma}_8 = 0.95, \sigma_{\sigma_8} = 0.05)$	3.62 0.85	1.60σ 0.57σ
data analysis	r_2 r_3	r_2: uniform in [1,200] r_3: uniform in [1,150]	41.2	2.73σ

We see that based on the WMAP observations alone, alternative cosmological models are only marginally preferred by the data. It is also worth emphasizing that the low power models are contrived; they have been fine-tuned to fit the observed power spectrum, a fact that lowers their prior and renders them even more unlikely. The possibility of a systematic error in the estimation of the error bars at large scales may not seem very plausible considering the work done by the WMAP team and the data from other experiments. Nevertheless, this concept leads us to an important conclusion: taking the $r_i \to \infty$ has the effect of disregarding the information provided by C_2 and C_3, which has an evidence equal to 0.041, corresponding to roughly 2.7σ. Therefore, it is evident that as far as power at large scales is concerned no model is ever likely to fare better than 2.7σ. Consequently, we will have to resort to other methods to probe the large scales which take into account details not probed by the power spectrum, such as considering the effects of the topology of the Universe, making accurate measurements of the polarization of the CMB and its correlation with the temperature, etc.

REFERENCES

[1] C. L. Bennett, M. Halpern, G. Hinshaw, N. Jarosik, A. Kogut, M. Limon, S. S. Meyer, L. Page, D.N. Spergel, G. S. Tucker et al., ArXiv e-prints (2003), astro-ph/0302207
[2] D. N. Spergel, L. Verde, H. V. Peiris, E. Komatsu, M.R. Nolta, C. L. Bennett, M. Halpern, G. Hinshaw, N. Jarosik, A. Kogut et al., ArXiv e-prints (2003), astro-ph/0302209
[3] A. Niarchou, A.H. Jaffe, L. Pogosian, ArXiv e-prints (2003), astro-ph/0308461
[4] E. T. Jaynes, *Probability theory: The Logic of Science* (Cambridge University Press, Cambridge, UK, 2003); T. J. Loredo in *Maximum-Entropy and Bayesian Methods, Dartmouth,1989,* edited by P. Fougere (Kluwer Academic Publishers, 1990), pp. 81-142
[5] C. R. Contaldi, M. Peloso, L. Kofman and A. Linde, Journal of Cosmology and Astro-Particle Physics **7**, 2 (2003)
[6] G. Efstathiou, ArXiv e-prints (2003), astro-ph/0303127
[7] G. Efstathiou and J. R. Bond, Mon. Not. R. Astr. Soc. **304**, 75 (1999)

Session VI

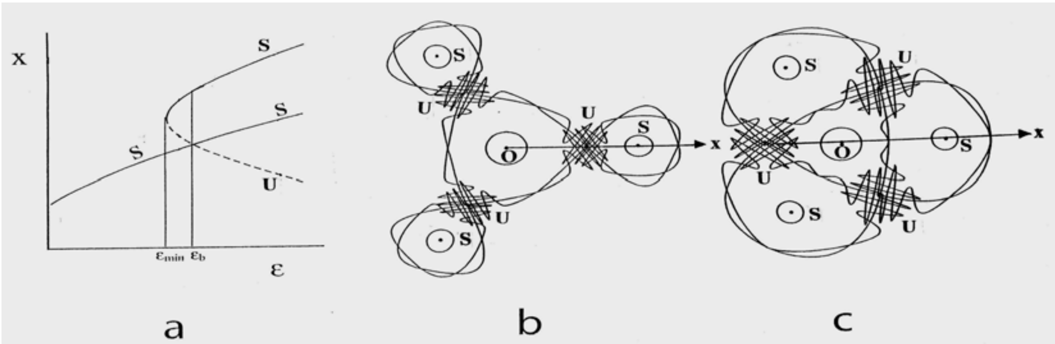

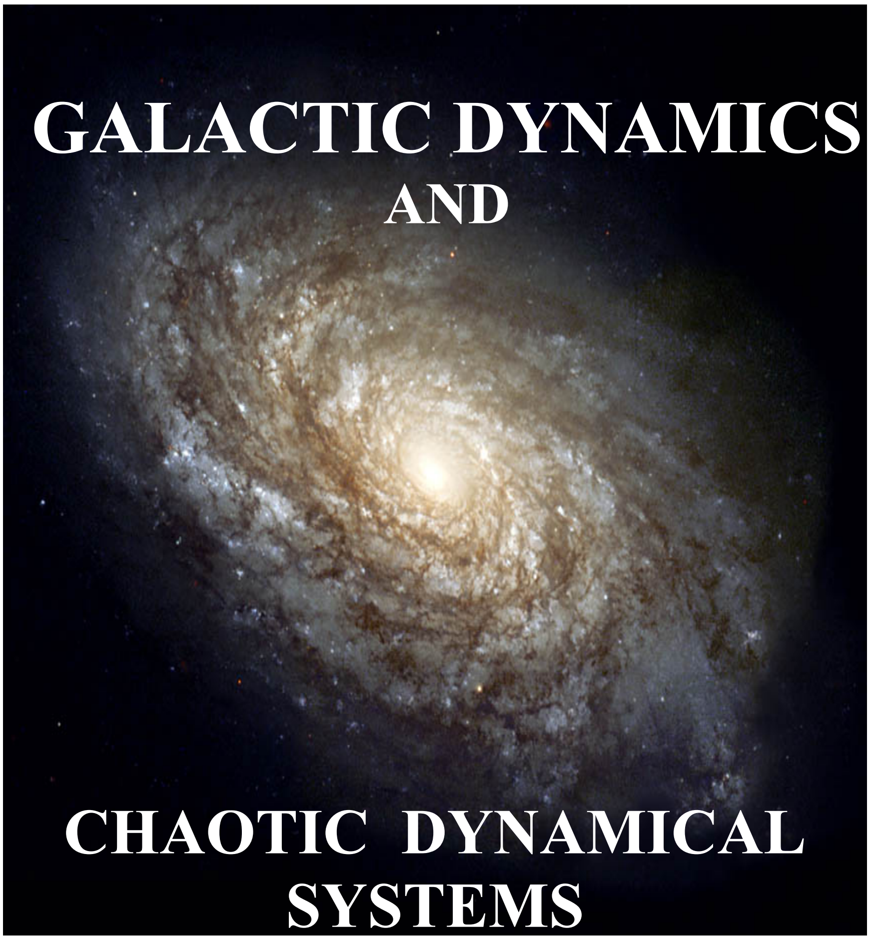

Conveners: N. Voglis and P. Patsis

THE STRUCTURE OF CHAOS*
(A Classification of the Homoclinic Tangles)

Contopoulos, G. and Dokoumetzidis, A.

Abstract

The structure of chaos in a particular dynamical system is found by studying the forms of the asymptotic curves of its unstable periodic orbits. We classify these tangles by the topology of the underlying periodic orbits. We study in more detail the tangencies of various orders of the asymptotic curves. Then we find the forms of the asymptotic curves in cases of recurrence of the homoclinic lobes, and in cases with escapes.

1. Introduction

The chaotic domains of a dynamical system are not populated in a random way. They have a well defined structure that is governed by the characteristic curves of the main (i.e. the simplest) unstable periodic orbits in every domain. The intersecting characteristic curves of the same periodic orbit form the corresponding homoclinic tangle, while the intersecting characteristic curves of different periodic orbits form heteroclinic tangles.

As an example, (Contopoulos and Voglis 1999) in Figs 1,2 we compare the phase spaces of two simple nonlinear maps, the standard map (Fig. 1a,b)

$$\begin{aligned} x' &= x + y', \\ y' &= y + \frac{K}{2\pi}\sin 2\pi x \end{aligned} \qquad (\text{mod } 1) \qquad (1)$$

and the Hénon map (Fig.2a,b)

$$\begin{aligned} x' &= 1 - K'x^2 + y \\ y' &= x \end{aligned} \qquad (\text{mod } 1) \qquad (2)$$

When K, K' are large, chaos is dominant over the whole phase space. For K=10, K'=7.407 no islands of stability were found in Figs 1a,b and if they exist they should be extremely small. The distribution of 10000 consequents of the same initial condition is practically the same and by the above choices of K, K' the Lyapunov characteristic number is the same, LCN=1.62.

However the underlying structure of the phase space in the two cases is very different. Figure 1c contains the asymptotic curves of the main periodic orbit of the standard map, which is ($x_0=y_0=0$), while Fig.1d contains the corresponding asymptotic curves of the Hénon map, starting at the simple periodic orbit ($x_0=y_0=0.256444$). The two structures are very different. If we start an orbit close to (x_0,y_0) along the unstable asymptotic curve in each case we find very different successions of points. These differences produce very different dynamical spectra (Contopoulos and Voglis 1999) in the two cases.

In particular the stretching numbers (Lyapunov characteristic numbers (LCN) after one iteration), although they have the same average, which is equal to LCN, they have substantially different distributions around this average.

---

* Main Session Invited Review

Proceedings of the 6th Hellenic Astronomical Society Conference, 15-17 September 2003, Penteli, Greece

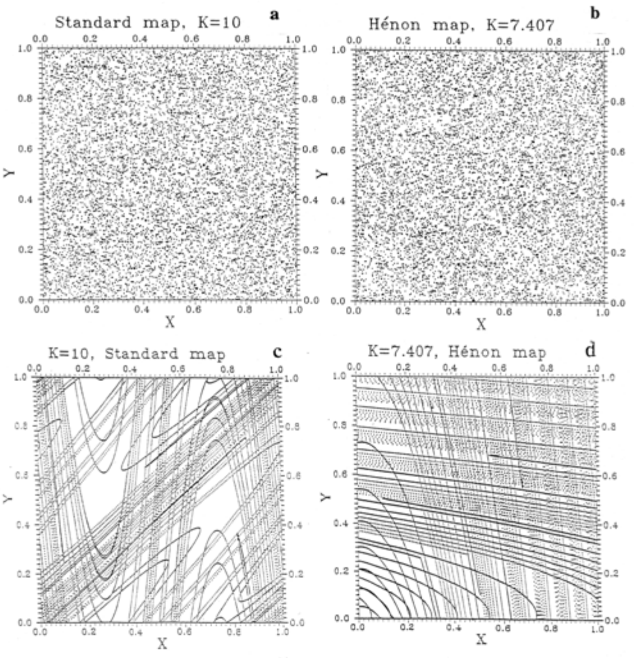

Figure 1

Distributions of 10000 consequents in the standard map (a) and in the Hénon map (b), and the corresponding unstable and stable manifolds of the main periodic orbit (x_0,y_0) (c and d).

Therefore, in order to understand the structure of the chaotic domain it is not sufficient to use just one quantity like the LCN (or any similar quantity, like the Kolmogorov entropy). It is necessary to study also the structure of the underlying homoclinic and heteroclinic tangles.

The importance of the asymptotic curves of the unstable periodic orbits was emphasized already by Poincaré (1899). These curves form a tangle so complicated that Poincaré stated “I shall not even try to draw it”.

However nowadays the use of fast electronic computers allows us to depict the forms of these curves and find their topological characteristics.

There are certain theorems, due to Poincaré, about these asymptotic curves that explain some of their basic characteristics. E.g. the asymptotic curves appear in pairs (stable-unstable). In the case of conservative two dimensional maps, or conservative Hamiltonian systems of two degrees of freedom there are two unstable curves U and UU, starting in opposite directions, and two stable curves, S and SS, also starting in opposite directions (Fig.6a below). The main theorems of Poincaré are: (1) that the curves U, UU do not intersect themselves, or each other, and the same applies to S and SS, (2) the areas on the plane of the map (in the Hamiltonian case the areas on a Poincaré surface of section) are preserved.

These theorems are necessary but not sufficient in order to understand the structure of the asymptotic curves. Thus several people have tried to formulate laws about the structure of the asymptotic curves (Meiss 1992 and references therein). A most important problem is the “transport” of particular regions of the phase space to other regions, that produce the mixing properties of the system (Bensimon and Kadanoff 1984, MacKay et al. 1984).

In particular Easton (1986,1991), Wiggins (1990), Rom-Keddar and Wiggins (1990) and Rom-Keddar (1990,1994) have classified various homoclinic tangles and studied their properties. However these studies are mostly restricted to a particular class of tangles, generated by the perturbation of an integrable system containing one stable and one unstable point (Figs 9a,b below).

In the present paper we classify more general types of homoclinic tangles of conservative dynamical systems of two degrees of freedom. In section 2 we discuss the homoclinic tangles in conservative Hamiltonians without escapes when the unperturbed case has only one stable invariant point (the "central" point on a Poincaré surface of section). At the end of this section we refer also briefly to some simple heteroclinic tangles. In section 3 we study the details of the tangles of a single unstable point with particular emphasis on the tangencies between the stable and unstable manifolds. In section 4 we find the Poincaré recurrences of the lobes generated by the asymptotic curves and in section 5 we study briefly the asymptotic curves in cases with escapes.

2. General Topology of the Homoclinic Tangles

A homoclinic tangle is generated by the asymptotic curves of a particular unstable periodic orbit. The periodic orbits are separated into regular or irregular (Contopoulos 1970a,b). Regular families of periodic orbits are generated by bifurcation from families existing also in the unperturbed (integrable) case, while irregular families are independent of the above; they appear by tangent bifurcations (stable-unstable pairs) inside lobes formed by the asymptotic curves of other periodic orbits.

A classification of the main bifurcations of the families of periodic orbits was provided by Hénon (1965), and it was completed by Contopoulos (1970b). A summary of the various types of bifurcations is provided by Contopoulos (2002).

A general case of a Hamiltonian of two degrees of freedom is of the form

$$H=H_2+\varepsilon H_\varepsilon \tag{3}$$

where

$$H_2=\frac{1}{2}\left(\dot{x}^2+\omega_1^2x^2\right)+\frac{1}{2}\left(\dot{y}^2+\omega_2^2y^2\right) \tag{4}$$

while H_ε is a polynomial, or a series, starting with terms of degree at least 3. The unperturbed Hamiltonian H_2 has two basic periodic orbits, y=0 and x=0. If ω_1/ω_2=n/m=rational, all the unperturbed orbits are periodic. If $\varepsilon\neq 0$, and ω_1/ω_2=n/m there are two families of periodic orbits near y=0 and x=0 and two more families of resonant periodic orbits (one stable and one unstable). All these orbits are regular. The families of periodic orbits bifurcating from these orbits, corresponding to particular resonances, are also regular.

If H_ε is even in y, e.g.

$$H_\varepsilon=-xy^2 \tag{5}$$

the plane y=0 is a Poincaré surface of section. The central periodic orbit ($x=x_0$, $y_0=0$) is stable for small ε and is surrounded by closed invariant curves. At a particular value of $\varepsilon=\varepsilon_{n/m}$ two resonant families of type n/m bifurcate from the central family. Their orbits close after n oscillations along the x-axis and m oscillations along the y-axis. One of these families is stable and the other unstable (e.g. Figs 2a,3a,4a). The asymptotic curves from the unstable periodic orbits join to form separatrices only in integrable cases. In general nonintegrable cases these asymptotic curves form homoclinic tangles near the unstable invariant points (Figs 2a,3a,4a).

In Figs 3a, 4a m is even. In the first case (Fig.2a) two stable invariant points are on the x-axis. In the second case (Fig.3a) two unstable points are on the x-axis. In the third case (Fig.4a) m=odd; then one stable and one unstable point are on the x-axis.

The corresponding characteristics are shown in Figs 2b, 3b, 4b. The central family is stable before and after the bifurcation. There are two bifurcating families in each case, and their stability is indicated in the figures.

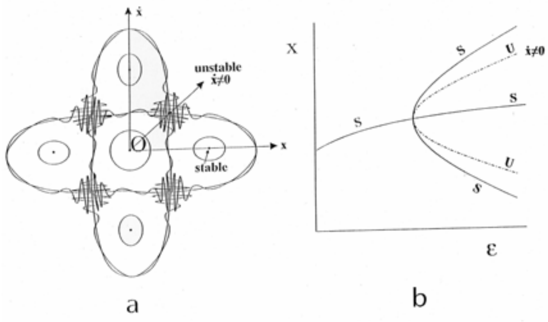

Figure 2
(a) Four islands of stability of the resonant type n/m=1/4 and four unstable invariant points together with their asymptotic curves that form a homoclinic tangle. Two stable points are on the x-axis.
(b) The corresponding characteristics of the central periodic orbit O and of the bifurcating families (—) stable, (-.-.-.-) unstable with $\dot{x} \neq 0$.

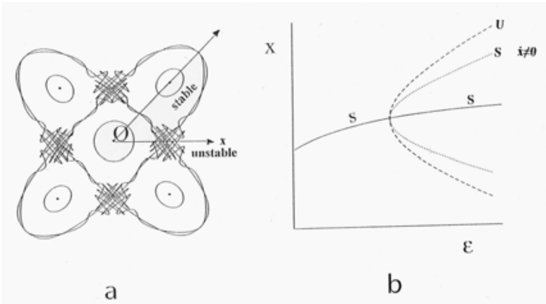

Figure 3
(a) As in Fig.2 but with the unstable bifurcating points on the x-axis.

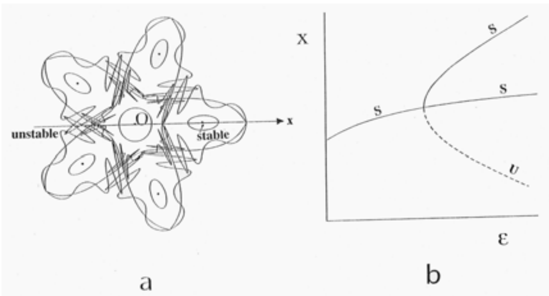

Figure 4
(a) Five islands of the resonant type n/m=1/5 and 5 unstable invariant points with their asymptotic curves.

In all cases the homoclinic tangles generated by the asymptotic curves of the unstable points have an approximate m-tuple symmetry.

In the particular case that the bifurcating families are of multiplicity m=1 there is only one stable and one unstable point on the x-axis besides the central point (Fig.5). The corresponding characteristics are similar to Fig.4b. In this case there is a homoclinic tangle around the unstable point, surrounding the island of stability from both sides.

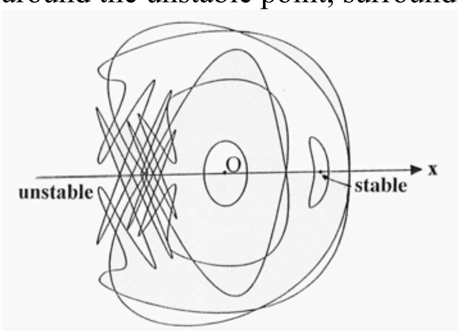

Figure 5
An island of stability in the case m=1, together with the corresponding unstable orbit and its homoclinic tangle.

If m=even and n=even we have a resonance n:2/m:2 but there are two pairs of stable-unstable orbits. E.g. if n/m=2/4=1/2 two opposite points in Fig.2a, or 3a (and in Figs 2b,3b) form one family. Thus there are two couples of unstable orbits. The tangles of these orbits form homoclinic and heteroclinic tangles, but their overall form is similar to Fig.2a, or Fig.3a.

If the central periodic orbit becomes unstable we have the bifurcation of a double period family (Fig. 6a, or a similar figure formed by rotating Fig.6a by 90º), or of two equal period families (represented again by Fig 6a, or a figure with a 90º rotation of the axes). In Fig.6a the bifurcating families have invariant points along the x-axis, while in the rotated case the bifurcated invariant points are outside the plane (ε, x), i.e. they have $\dot{x} \neq 0$. The corresponding characteristics are shown in Fig. 6b. The homoclinic tangle around the central point surrounds both islands.

Each bifurcation consists either of one family of double period represented by two points for every ε in Fig.6b, or of two families of equal period, each of them represented by one point for every ε (in Fig.6b one above and one below the original family, which is then unstable).

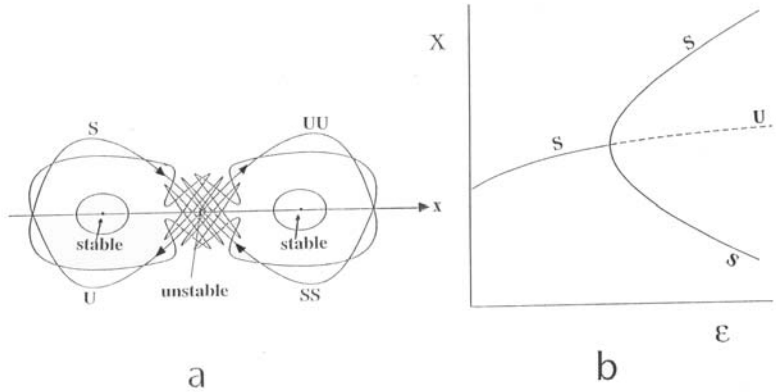

Figure 6
(a) When the central periodic orbit becomes unstable there are two islands of stability corresponding to a double period orbit, or two different equal period orbits. The asymptotic curves of the central unstable orbit are U,UU (unstable) and S, SS (stable).
(b) The corresponding characteristics. Symbols as in Fig.3b.

The case n/m=2/3 is special (Contopoulos 1968). In this case we have an oblique intersection of the characteristic of the triple orbits with the stable characteristic of the central periodic orbits. The bifurcating family is unstable on both sides of the central family (Fig.7a). The unstable family joins another stable family for $\varepsilon=\varepsilon_{min}$ further away from the central family. Then the structure of the asymptotic curves before the bifurcation point between $\varepsilon=\varepsilon_{min}$ and $\varepsilon=\varepsilon_b$, is shown in Fig.7b and beyond the bifurcation point in Fig.7c. There is a homoclinic tangle with approximate triple symmetry.

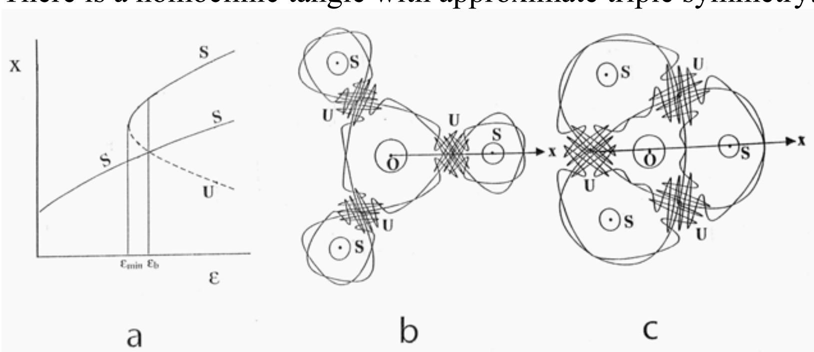

Figure 7
Bifurcation of an unstable triple family.
(a) The characteristics.
(b) The asymptotic curves of the triple unstable orbit for ε between ε_{min} and ε_b.
(c) The asymptotic curves for $\varepsilon>\varepsilon_b$.

Similar cases appear when we have an inverse bifurcation (Contopoulos 2002). This case appears when the stable central family becomes unstable and the new family has a maximum perturbation $\varepsilon=\varepsilon_b$ at the bifurcating point (Fig.8a). The bifurcating family is stable, but usually it joins another stable family away from the central family (unless it extends all the way up to the boundary of the system, i.e. y=0). In the case of Fig.8a the joining of the unstable and the new stable family occurs at a tangent bifurcation, at a minimum $\varepsilon=\varepsilon_{min}$. The corresponding Poincaré surface of section for ε between ε_{min} and ε_b is shown in Fig.8b and for $\varepsilon>\varepsilon_b$ in Fig.6a. In Fig.8b there are two unstable points, while in Fig.6a there is only one unstable point.

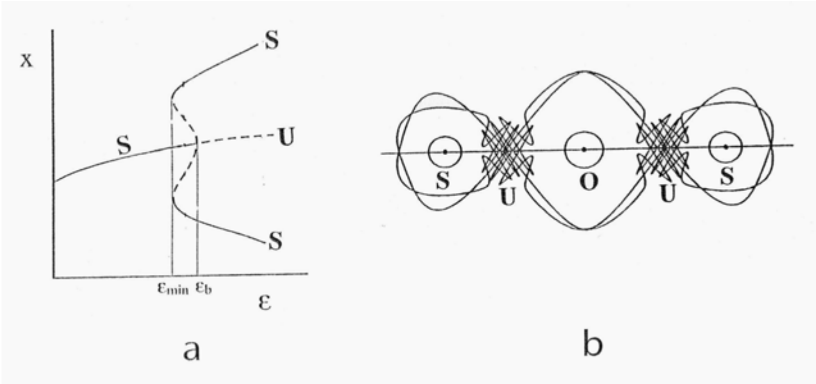

Figure 8
(a) The characteristics near an inverse bifurcation, when the central family becomes unstable.
(b) The asymptotic curves for ε between ε_{min} and ε_b.

Similar figures appear if the inverse bifurcation generates families outside the plane (ε,x), i.e. with $\dot{x}\neq 0$. We have also similar configurations whenever the characteristics of various families pass through other maxima, or minima.

In the special case when the ratio of frequencies is rational $\omega_1/\omega_2=n/m$ we have two resonant families of periodic orbits, one stable and one unstable. In the limiting case, when ε tends to zero, the stable and unstable points are located as in Figs 2a, 3a, 4a, but instead of a tangle we have exact separatrices. However when ε becomes different from zero a homoclinic tangle appears (Figs 2a, 3a, 4a).

A different form of the homoclinic tangle appears when the asymptotic curves extend to infinity (curves UU and SS in Figs 9a,b).

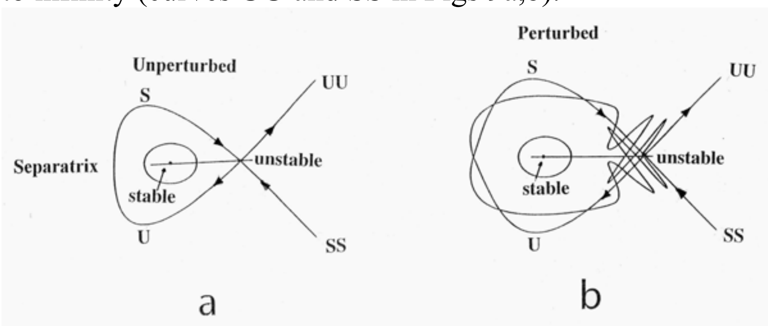

Figure 9
(a) Asymptotic curves from an unstable point in an integrable case, when two asymptotic curves (UU,SS) extend to infinity and the other two (U,S) form a separatrix.
(b) As in Fig.9a when a perturbation is added, that generates a homoclinic tangle.

In this case the unperturbed problem has a stable and an unstable periodic orbit (Fig.9a). The asymptotic curves that do not extend to infinity join into a separatrix (the curves U and S join into one curve). In the perturbed case (Fig.9b) the asymptotic curves U and S form a homoclinic tangle around the unstable point, which surrounds the stable point. Tangles generated by perturbing an integrable case with one stable and one unstable point, like Figs 9a,b, have been studied extensively by Easton (1986,1991), Wiggins (1990), Rom-Keddar and Wiggins (1990) and Rom-Keddar (1990,1994). These authors have classified particular subcases of this case. In their cases the asymptotic curve UU does not intersect S, nor does U intersect SS. However, in Hamiltonian systems of the general form (3) unstable points are generated, when the perturbation ε increases, by bifurcation of resonant invariant points from the central point (Figs 6a,b) and the asymptotic curves U, UU intersect S, SS in all possible ways (U,S), (U,SS), (UU,S) and (UU,SS).

The tangles with one unstable periodic orbit will be discussed in more detail in section 3.

A different type of tangle is the standard map without modulo 1 for values of K smaller than a critical value $K_{cr}=0.97$. In such cases the homoclinic tangle from the point ($x_0=y_0=0$) does not reach the tangles from the points (x_0=integer, $y_0=\pm1$). In fact the tangles near the axis y=0 are separated from the tangles near y=1 (and also the tangles near y=-1) by invariant curves extending indefinitely from left to right (from $x=-\infty$ to $x=+\infty$). However the asymptotic curves from ($x_0=y_0=0$) extend indefinitely to the right and to the left. In the case with modulo 1 the periodic orbits ($x_0=\ldots-2,-1, +1,+2\ldots, y_0=0$) coincide with ($x_0=y_0=0$) and their tangles form a unique homoclinic tangle. However if we drop the modulo 1 in x the points ($x_0=\ldots-2,-1, +1,+2\ldots, y_0=0$) are different from ($x_0=y_0=0$) and we have not only a homoclinic tangle between the unstable and stable asymptotic curves from ($x_0=y_0=0$) but also heteroclinic tangles with the corresponding asymptotic curves from all the periodic orbits ($x_0=\ldots-2,-1, +1,+2\ldots, y_0=0$). This is shown schematically in Fig.10.

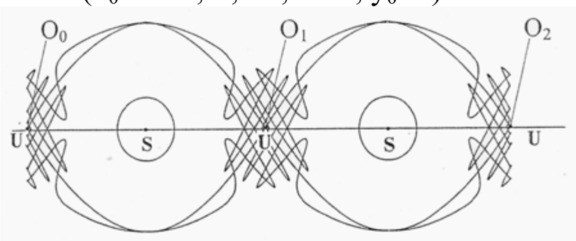

Figure 10
Asymptotic curves in the standard map when there is no modulo 1 and $0<K<0.97$. There are infinite unstable orbits O_n (x=n, y=0) and their asymptotic curves form both homoclinic and heteroclinic

In the limiting case $K\rightarrow0$ the asymptotic curves from ($x_0=y_0=0$) are separatrices reaching the points ($x_0=\pm1$, $y_0=0$), while if $0<K<K_{cr}=0.97$ they form tangles in the neighbourhood of ($x_0=0, \pm1, y_0=0$) but they extend further to the neighbourhood of ($y_0=\pm1$, $y_0=0$) and to any (x_0=integer, $y_0=0$) (Fig.10). In the case with $K>K_{cr}=0.97$ the asymptotic curves from ($x_0=y_0=0$) intersect also the asymptotic curves from ($x_0=\pm1$, etc, $y_0=\pm1$, etc) forming further heteroclinic tangles.

3. Details of the Tangles. Tangencies

The unstable and stable asymptotic curves from an isolated unstable orbit, represented by an isolated point in a map, or on a Poincaré surface of section, intersect each other at an infinity of homoclinic points, as shown schematically in Fig.6a.

Details about such homoclinic tangles were provided by Contopoulos and Polymilis (1993, 1996), and Polymilis et al. (2003). Of special interest is the study of tangencies between the unstable and stable asymptotic curves. If for a particular value of h an unstable and a stable asymptotic curve are tangent, for larger h these curves intersect, while for smaller h they remain separated close to the tangent point.

In Fig.11 we show the intersections of the asymptotic curves U and S in a realistic model, namely the system (3) with H_2 given by (4) and H_ε by (5). The values of the constants are $\omega_1^2=0.9$ $\omega_2^2=1.6$, $\varepsilon=0.08$ and $h=h_7=23.860$. In further cases below we fix ω_1^2, ω_2^2, ε and vary h.

The central intersection of the asymptotic curves U and S is the point P_0 at almost equal distances from O along U and S. The two arcs OP_0 along U and S form a region called resonance O_1. The continuation of U beyond P_0 intersects S at the points P_1', P_2', … inwards and the points P_1, P_2,… outwards from O_1. The arcs P_0P_1' along U and S define an outer lobe U_1' while the arcs $P_1'P_1$ along U and S define an inner lobe U_1. Similar definitions apply to outer lobes U_n' ($n\geq0$) and S_{-n} ($n\geq1$), and to inner lobes U_n ($n\geq0$), S_{-n}' ($n>0$). The areas of the lobes are equal according to the Poincaré theorem.

In Fig.11 we see that the inner lobes U_5 and S_{-2}' are tangent for $h=h_7=23.860$. Then the lobes U_i and S_j' are also tangent if $i-j=t_1$, where $t_1=7$ for the present value of h.

This can be described by saying the t_1=7 is the number of inner oscillations of the curve U beyond P_0, plus the number of inner oscillations of the curve S before P_0, until the curves U and S become tangent to each other (tangency of U_5 and S_{-2}' called first order tangency), Thus the number t_1=7 is the total number of inner oscillations of U and S that complete one rotation around the resonance O_1 forming the first order tangency.

For $h<h_7$ the lobes U_5 and S_{-2}' do not intersect while for $h>h_7$ these lobes intersect each other.

As h increases we reach another critical value $h=h_6=24.070$, at which the lobe U_4 is tangent to S_{-2}' and t_1=6. The critical values of h for various t_1 are given in Fig.13 (Polymilis et al.2003).

If we continue the curve U beyond U_5 we have further inner lobes and the lobe U_{12} is close to S_{-2}'. For $h=h_{14}^{(2)}=23.925$ the lobe U_{12} is tangent to S_{-2}' (second order tangency). At the same time U_i and S_j' are tangent if $i-j=t_2$ (=14 in this case) (Fig.12).

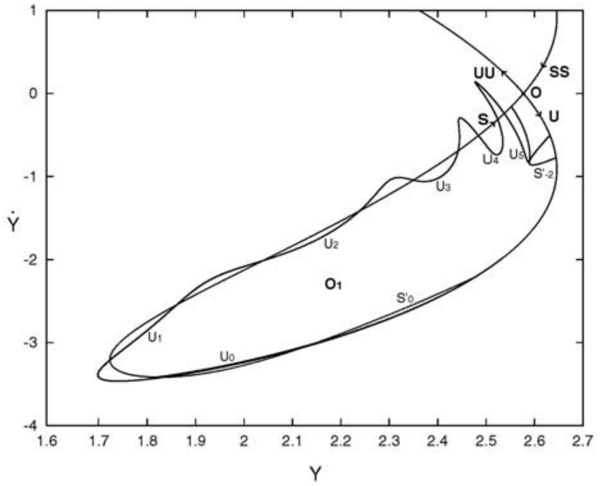

Figure 11
First order tangency in the homoclinic tangle of the system (3), for an energy h=23.860. This figure includes some low order lobes formed by the asymptotic curves U (unstable) and S (stable) from the invariant point O.

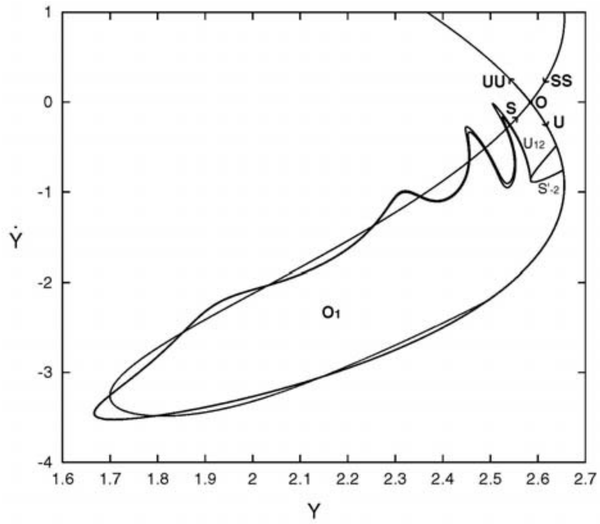

Figure 12
Second order tangency. The inner lobe U_{12} is tangent to S'_{-2} for h=23.925.

We notice that t_2 is equal to $t_2=2t_1$ for a value of $h_{14}^{(2)}$ close to h_7. This is to be expected because for the same value of h t_2 represents the total number of inner oscillations to form two rotations around O_1.

In the same way there are third order tangencies between U_i and S'_j if $i-j=t_3\approx 3t_1$.

The values of the energy h at first, second and third order tangencies for various values of t_1, t_2, t_3 are given in Fig.13 (Polymilis et al. 2003 The values of t_2 are, successively, along two nearby lines and the values of t_3 are, successively, along three nearby lines.

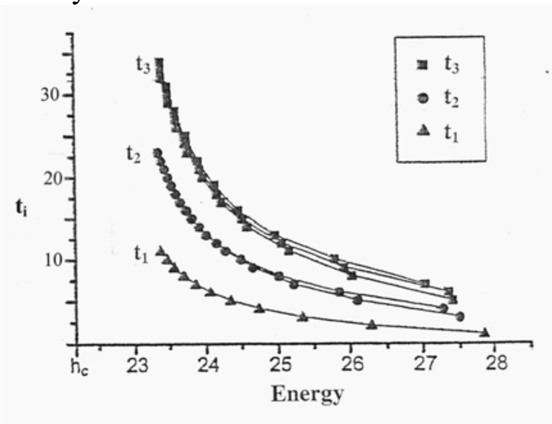

Figure 13
The values of t_1, t_2 and t_3 at which tangencies occur are plotted as functions of the energy. The values of t_1 lie on a smooth curve. The values of t_2 are divided into two sequences, each containing every second value, and follow two slightly different smooth curves. Similarly, the values of t_3 follow three slightly different smooth curves each containing every third value.

The values of t_i can be approximated by power laws of the form

$$t_i = b_i(h - h_c)^{-a_j} \tag{6}$$

where h_c is the value of the energy when the orbit O becomes unstable (h_c=22.16). The values of α_i are close to each other, while b_2 has two values close to $2b_1$, and b_3 has three values close to $3b_1$ (Table 1).

Table 1

	a	b
t_1	1.35 (±0.0081)	14.3 (±0.055)
t_2	1.28 (±0.0075)	28.9 (±0.10)
	1.22 (±0.016)	28.4 (±0.23)
t_3	1.18 (±0.019)	43.2 (±0.42)
	1.21 (±0.018)	42.5 (±0.39)
	1.23 (±0.011)	42.0 (±0.24)
t_{rec}	1.43 (±0.008)	48.53 (±0.19)

4. Recurrence

Recurrence occurs when a given set is intersected by one of its images. The Poincaré recurrence time (Poincaré 1890) is the average number N of iterations for such an intersection of a given set of area m its Nth image. This time is of the order of

$$N = M/m \tag{7}$$

where M is the total area of the phase space. Of course N may vary for different sets, but its variations obey certain restrictions.

In a previous paper (Contopoulos and Polymilis 1996) we considered the minimum recurrence time for a lobe of the homoclinic tangle of the system (1-3) considered above.

An outer lobe, say U_1’ cannot be intersected by a higher order lobe U_i’ at the outer side U_1’ because the curve U cannot intersect itself. The intersections must be realized by an elongated arc of a higher order outer lobe that enters, first, inside the resonance O_1, and then reaches U_1’ from its inner side S_1’. Such a higher order outer lobe starts outwards at two points on the S curve very close to O. It makes first a complete turn around the upper resonance O_2, then a complete turn around the lower resonance O_1, and then it enters inside some inner lobes, inside O_1, like U_8 (Fig.14) that are long enough to extend beyond the neighbourhood of the point P_0 and enter inside the lobe U_1’.

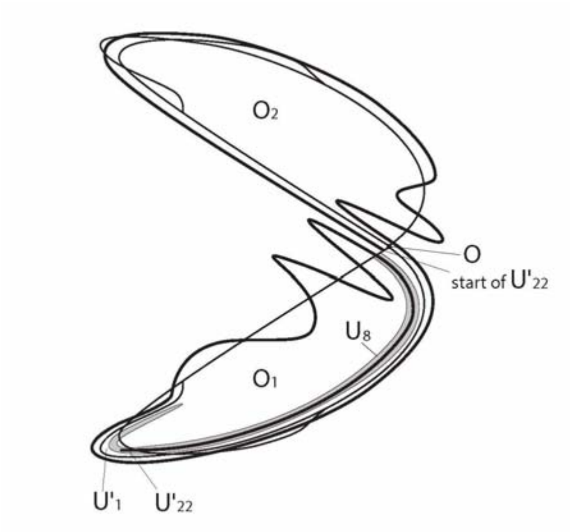

Figure 14
Recurrence in the homoclinic tangle for h=24 drawn schematically. The outer lobe U'_{22} (drawn as a thick line), starts at two points of the S asymptotic curve close to O. Then it makes a rotation around the resonance region O_2, and oscillates along the asymptotic curve SS. Some oscillations are so long that they make a rotation around O_1 (only one of them drawn) and come close to O from the left side, oscillating along the asymptotic curve U. One of these latter oscillations is long enough to reach U'_1 from its inner side, by entering the inner lobe U_8 (drawn in gray color).

The total number of oscillations for recurrence is equal to the sum of (a) half a rotation around O_1 to go from U_1' close to O, (b) one rotation around O_2, (c) one rotation around O_1 and (d) half a rotation around O_1 from the neighbourhood of O to U_1'. Therefore the minimum recurrence time t_{rec} is close to $t_3 \approx 3t_1$. The values of t_{rec} are given by Eq.(6) with a and b given in Table I.

It is remarkable that the minimum recurrence time t_{rec} exists even beyond the escape energy ($h=h_{esc}=25.31$ in the above model) although in this case the total area of the phase space is infinite and the (average) Poincaré recurrence time is not defined (Contopoulos and Polymilis 1993).

5. Escapes

When the energy of a Hamiltonian system is larger then the escape energy the equipotentials are open and some orbits escape to infinity. In general across the openings of the equipotentials there are periodic orbits, called Lyapunov orbits, reaching the equipotentials on both sides of the opening. Any orbit crossing a Lyapunov orbit outwards escapes from the system (Rod 1973).

The available phase space of escaping orbits is infinite. E.g. in Fig.9b the asymptotic curves UU and SS extend to infinity. In this case an opening is along the x-axis and the orbits can intersect this axis (y=0) for arbitrarily large x. But if a surface of section does not cross an opening the phase space on this surface is finite. E.g. in the case of the system of Eqs (3-5) the total area on the plane y=0 is finite, namely $\dot{x}^2+\omega_1^2x^2\leq 2h$. In such a case, if $h<h_{esc}$, the plane y=0 is a Poincaré surface of section and is intersected by all orbits that do not have $y=\dot{y}=0$. Then the areas of sets of successive intersections of orbits are preserved. However, if $h>h_{esc}$ the orbits crossing a Lyapunov orbit do not have any further intersections with the surface of section y=0. Therefore this surface is not a “Poincaré surface of section” and the areas on this surface are not conserved any more.

The initial conditions of the orbits on the surface y=0 ($h>h_{esc}$) leading to escape cover certain domains of the plane y=0 (Contopoulos 1990, Contopoulos and Polymilis 1993, Contopoulos and Efstathiou 2003). The asymptotic curves close to these regions form infinite spirals towards the boundaries of these regions and away from these boundaries. In Fig.15 we indicate the form of the asymptotic curve U of the system (3-5) when $\omega_1^2=1.6$, $\omega_2^2=0.9$, $\varepsilon=0.08$ and the energy is h=29. We note that the curves U and S start in the same way close to the invariant point O as in Fig.11, but beyond the homoclinic point P_0 the curve U, instead of forming a lobe, becomes a spiral approaching asymptotically the escape region.

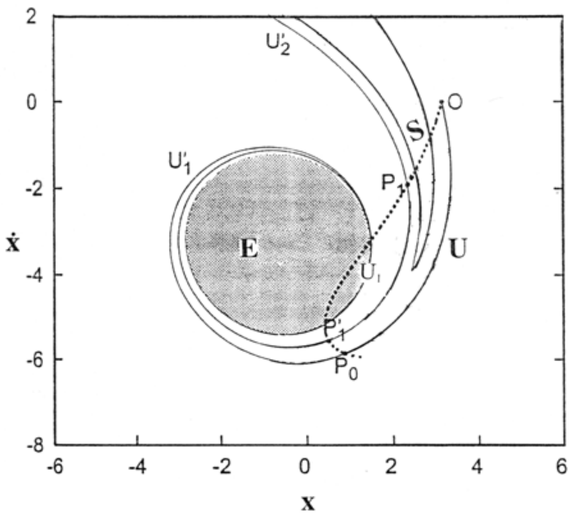

Figure 15
The asymptotic curve U in the case h=29 forms infinite spiral rotations clockwise around the escape region E beyond the homoclinic point P_0. Then another branch of the same curve forms infinite rotations around E counterclockwise before reaching the homoclinic point P'_1.

This example shows that the homoclinic tangle becomes even more complicated when a system contains escape regions. Further details on this problem are contained in a recent paper by Contopoulos and Efstathiou (2003).

6. REFERENCES

Bensimon, D. and Kadanoff, L.P.: 1984, *Physica D* **13**, 82.
Contopoulos, G.: 1968, *Astrophys. G.***153**, 83.
Contopoulos, G.: 1970a, *Astrophys. J.* **75**, 96.
Contopoulos, G.: 1970b, *Astrophys. J.* **75**, 108.
Contopoulos, G.: 1990, *Astron. Astrophys.* **231**, 41.
Contopoulos, G.: 2002, "Order and Chaos in Dynamical Astronomy", *Springer*, N. York.
Contopoulos, G. and Efstathiou, C.: 2003, *Cel.Mech.Dyn.Astr.* (in press).
Contopoulos, G. and Polymilis, C.: 1993, *Phys. Rev. E* **47**,1546.
Contopoulos, G. and Polymilis, C.: 1996, *Cel. Mech. Dyn. Astr.* **63**, 189.
Contopoulos, G. and Voglis, N.:1999, in Steves, B.A. and Roy, A.E. (eds) "The Dynamics of Small Bodies in the Solar System", *Kluwer,* Dordrecht, 429.
Easton, R.W.: 1986, *Trans. Am. Mat. Soc.* **224**,719.
Easton, R.W.: 1991, *Nonlinearity* **4**, 583.
Hénon, M.: 1965, *Ann. Astrophys.* **28**, 992.
MacKay, R.S., Meiss, J.D. and Percival I.C.:1984, *Physica D* **13**, 55.
Meiss, J.D.: 1992, *Rev. Mod. Phys.* **64**, 795.
Poincaré, H.: 1890, *Acta Math.* **13**, 1.
Poincaré, H.: 1899, "Methodes Nouvelles de la Mecanique Céleste", *Gauttieu Villeurs,* Paris, Vol.III.
Polymilis, C, Contopoulos, G, and Dokoumetzidis, A.: 2003, *Cel. Mech. Dyn. Astr.* **85**, 105.
Rod, D.J.: 1973, *J. Diff. Eq.* **14**, 129.
Rom-Keddar, V.: 1990, *Physica D* **43**, 229.
Rom-Keddar, V.: 1994, *Nonlinearity* **7**, 441.
Rom-Keddar, V. and Wiggins, S.: 1990, *Arch. Rat. Mech. Anal.* **109**, 239.
Wiggins, S.: 1990, "Introduction to Applied Nonlinear Dynamical Systems and Chaos", *Springer Verlag*, N. York.

ORIGIN OF SHORT-LIVED ASTEROIDS IN THE 7/3 KIRKWOOD GAP*

H. Varvoglis[1], K. Tsiganis[2] and A. Morbidelli[2]

[1] Section of Astrophysics, Astronomy and Mechanics, Department of Physics, University of Thessaloniki, GR-541 24 Thessaloniki, Greece
[2] Observatoire de la Cote d' Azur - Nice, UMR 6529 Cassini, CNRS, B.P. 4229, 06304 Nice Cedex 4, France

Abstract: A population of 23 asteroids is currently observed in a very unstable region of the main asteroid belt, the 7/3 Kirkwood gap. The small size of these bodies - with the notable exception of (677) Aaltje (~30 km) - as well as the computation of their dynamical lifetimes (<130 Myrs) shows that they cannot be on their primordial orbits, but were recently injected in the resonance. The distribution of inclinations, I, appears to be bimodal, the two peaks being close to 2 and 10 degrees repsectively. We argue that the resonant population is constantly being replenished, by the slow leakage of asteroids from both the Koronis (I ~ 2 degrees) and Eos (I ~ 10 degrees) families, due to the drift of their semi-major axes, caused by the Yarkovsky effect. Assuming previously reported values for the Yarkovsky mean drift rate, we calculate the flux of family members needed to sustain the currently observed population in steady state. The number densities with respect to semi-major axis of the observed members of both families are in very good agreement with our calculations. The fact that (677) Aaltje is currently observed in the resonance is most likely an exceptional event. This asteroid should not be genetically related to any of the above families. Its size and the eccentricity of its orbit suggest that the Yarkovsky effect should have been less efficient in transporting this body to the resonance than close encounters with Ceres.

* *Proceedings of the 6th Hellenic Astronomical Society Conference, 15-17 September 2003, Penteli, Greece*

SECULAR EVOLUTION OF ELLIPTICAL GALAXIES WITH CENTRAL BLACK HOLES*

Nikos Voglis[1] and Constantinos Kalapotharakos[1,2]

[1]Academy of Athens, Research Center for Astronomy and Applied Mathematics
[2]University of Athens, Department of Physics, Section of Astrophysics, Astronomy and Mechanics

Abstract

We examine the response of non-rotating N-body models of triaxial elliptical galaxies under the presence of a central black hole (CBH), or (more general) of a central mass concentration (CMC). The results show that for a massive CMC such systems become unstable, due to the large number of chaotic orbits. If the relative mass m of the CMC with respect to the mass of the galaxy exceeds the limit of $m \cong 0.005$, they enter a phase of remarkable secular evolution. The secular evolution proceeds by producing order out of chaos with a mechanism of self-organization, in which chaotic orbits are gradually converted to ordered orbits of a Short Axis Tube type. Equilibrium can be achieved in one Hubble time for $m \cong 0.01$ at least. For smaller values of m equilibrium can be achieved in time scales larger than a Hubble time. The equilibrium states correspond in general to oblate spheroidal configurations, but triaxial equilibrium configurations with CMC are also possible.

1. Introduction

Gravitational N-body simulations of cosmological disipationless collapses give systems that resemble non-rotating elliptical galaxies with smooth centers, i.e. the potential well near the center is approximately of a harmonic oscillator type. Such systems form triaxial configurations of particles. Let the cartesian coordinates x,y,z be oriented along the shortest axis (a), the intermediate axis (b) and the longest axis (c), respectively.

The majority of the ordered orbits of stars in such a smooth centre system can be classified in four types. Namely, **B**ox orbits, **I**nner **L**ong **A**xis **T**ube (**ILAT**) orbits, **O**uter **L**ong **A**xis **T**ube (**OLAT**) orbits and **S**hort **A**xis **T**ube (**SAT**) orbits. (de Zeeuw 1985; Statler 1987). A number of ordered orbits near higher order resonances can also appear. The box orbits fill a box resembling a parallelepiped with curved sides. The longest and the shortest dimensions of the box are respectively along the longest and the shortest axis of the system. A box orbit can pass arbitrarily close to the centre of the galaxy. The ILAT orbits fill a space elongated along the longest axis (z) of the system having a hole along the same axis. In many of them the hole is small and they resemble the box orbits. For this reason we call them box-like orbits (Contopoulos, Voglis and Efthymiopoulos 2002). Such orbits can also approach the centre.

The SAT orbits are roughly circular orbits surrounding the shortest axis x of the system. They fill a tube-like region not very extensive along the shortest axis. They support an oblate spheroidal configuration, or they can moderate the elongation of the triaxial figure created by the box and box-like orbits. Their frequencies of oscillation along the y and z axes have an 1:1 ratio. For this reason they are frequently called 1:1 resonant tube orbits so that they can be distinguished from other resonant tube orbits.

Triaxial systems with smooth centres develop a modest level of chaos. They contain a fraction of about 25%-35% of their total mass moving in chaotic orbits with Lyapunov

* *Proceedings of the 6th Hellenic Astronomical Society Conference, 15-17 September 2003, Penteli, Greece*

Characteristic Numbers (LCN) larger than $\approx 10^{-3}$ in units of the inverse radial periods of the orbits. These Lyapunov numbers rarely exceed the value of 10^{-1} and only a fraction less than 8% of the total mass has LCN>10^{-2} , that is, it belongs to orbits that can develop chaotic diffusion in a Hubble time (Voglis, Kalapotharakos and Stavropoulos 2002).
The chaotic orbits change their geometry in time, sometimes approaching the geometry of box and others times the geometry of SAT orbits and tend to fill the whole space inside the equipotential surfaces which are more round than the equidensity surfaces.
Galaxies, however, instead of smooth centres, may have developed cuspy central density profiles or Central Black Holes (CBH), (e.g. Kormedy and Richstone 1995; Kormedy et al. 1997; Faber et al 1997; Gebhardt et al. 2000) or more generally Central Mass Concentrations (CMC) composed by CBH, dense star clusters, large molecular concentrations etc. In this case the dynamics of the orbits cannot be the same as in the case of smooth centres, mainly because the geometry of the box orbits is not compatible with the spherical geometry of the gravitational field created by the CMC. Studies of galactic models with CMCs has been an active field of research in the last decade (e.g. Gerhard and Binney 1985; Merritt and Fridman 1996; Fridman and Merritt 1997; Merritt and Quinlan 1998; Valluri and Merritt 1998; Siopis and Kandrup 2000; Kandrup and Sideris 2002; Kandrup and Siopis 2003, Shen and Shellwood 2003).
As we will see bellow, if a massive CMC is inserted in an initially smooth centre model, most of the box and the box-like orbits are converted to chaotic orbits. Because of the diffusion of the chaotic orbits the system enters a phase of secular evolution in which the self-consistent potential changes in time towards a new equilibrium configuration.
In this paper we give some results of N-body simulations showing the effect of the presence of a CMC in triaxial self-consistent models of non-rotating elliptical galaxies.

2. The models

We start from two types of well-relaxed N-body systems with smooth centres created from Quite (Q model) and Clumpy (C model) cosmological initial conditions. The main difference of the two models is on the ratio of the kinetic energy of their bodies in radial and in tangential motion, being larger in the Q model than in the C model. Due to this difference the ellipticity of the Q model is larger. Most of the mass in the Q000 model moves in box or box-like orbits. The mass in SAT orbits is very small. This system is similar to an elliptical galaxy with ellipticity E7 in the inner parts and ellipticity E5 in the outer parts. The C model contains a good amount either of box or of SAT orbits. It has an ellipticity E4 in the inner parts and an ellipticity E2 in the outer parts.
A CMC is inserted in each of these models, with various values of the relative mass parameter $m=M_{cmc}/M_g$, where M_{cmc} is the mass of the CMC and M_g is the mass of the galaxy. In this way two families of models with CMC are created. We call these families Qxxx and Cxxx where Q and C stand for the parent model and xxx stands for the adopted value of m multiplied by 10,000. (E.g. Q100 is the name of the model derived from Q with m=0.01). The model of the potential field due to the CMC is given by the formula

$$V_{cmc}(r) = \frac{GM_{cmc}}{a}[\arctan(\frac{r}{a}) - \frac{\pi}{2}] \quad , \qquad (1)$$

where *a* is a softening length defined as

$$a = 0.05\frac{M_{cmc}}{M_g}R_g = 0.05mR_g \quad , \qquad (2)$$

where R_g is the radius of the galaxy.
This model, proposed by Allen, Palmer and Papaloizou (1990), is so designed that the softening length *a* does dot affect seriously the global behaviour of the system. An orbit approaching the centre undergoes a Keplerian scattering only if its pericentre is larger than

a. If it is smaller than *a* the scattering is moderated. Notice that for the needs of our problem this model is adequate, given that only a very small number of orbits can have such a small pericentre, thus the global behaviour of the model is not seriously affected by the softening.

3. Results

The secular evolution of our galactic models can be seen in terms of their maximum ellipticity E_{max} and their triaxiality index T. In order to measure these quantities we consider the triaxial equidensity surface with longest axis equal to the radius containing the half mass of the system. If a,b,c are respectively the lengths of the shortest, imtermediate and longest axes of this equidensity surface we can define the ellipticity on every main plain of it, as

$$E_{xy}=10(1-a/b),\ E_{yz}=10(1-b/c),\ E_{xz}=10(1-a/c)\ . \qquad (3)$$

The maximum ellipticity is on the xz plane, i.e. $E_{max}=E_{xz}$. In terms of a,b,c we can also define the triaxiality index T

$$T=\frac{c^2-b^2}{c^2-a^2}\quad . \qquad (4)$$

Notice that T is defined in the range [0,1] and the system tends to a prolate spheroidal configuration if T tends to 1, or to an oblate spheroidal configuration if T tends to 0 and to a maximally triaxial configuration if T is near to 0.5.

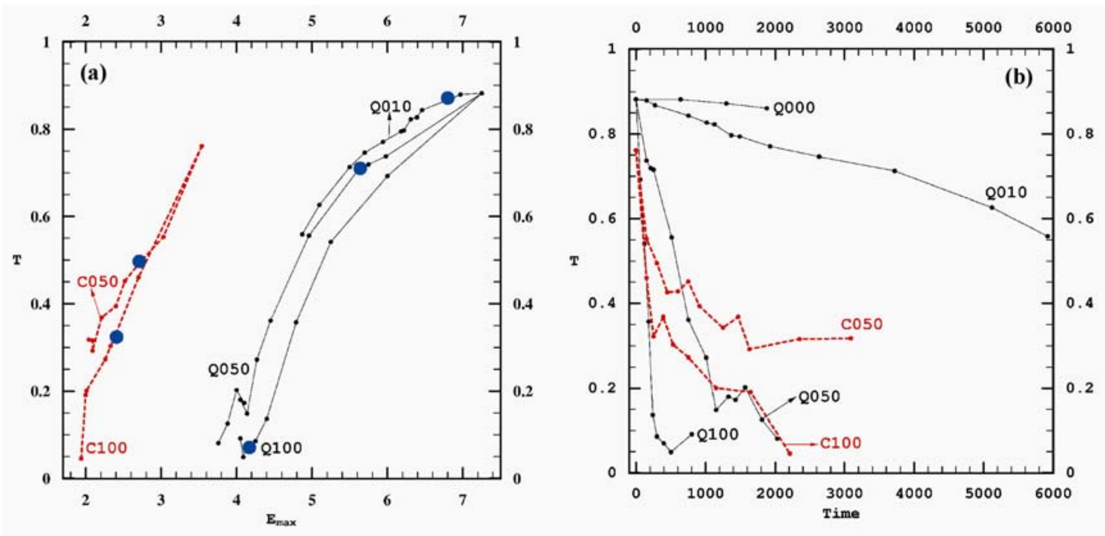

Figure 1. **(a).** The evolution of the models Q010, Q050, Q100 (solid lines) and the C050, C100 models (dashed lines) on the plane of the maximum ellipticity E_{max} and the triaxiality index T. A big dot on each curve gives the point reached by the corresponding model in one Hubble time. **(b).** The triaxiality index T of the models in (a) as a function of time.

In Fig.1a,b we show the evolution of the systems Q010, Q050 and Q100 (solid line) as well as the systems C050 and C100 (dashed line) on the plane of E_{max}-T. The Q family systems start from $E_{max}\ \cong\ 7$ and T $\cong$ 0.9 and they evolve in time by decreasing both these two quantities. The rate of evolution is quite slow for small values of the relative mass parameter *m*. E.g. for m = 0.001 the evolution during a Hubble time (indicated by a heavy dot upon these curves in Fig.1a) is small. (The maximum ellipticity has been reduced by less than 1.5 and the triaxiality index by less than 0.1 in this model in one Hubble time t=300).

Only the model Q100 (m=0.01) has reached an almost zero value of T, i.e. an oblate spheroidal configuration in one Hubble time, with a maximum ellipticity of about 4. The Q050 model (m=0.005) can also achieve a spheroidal equilibrium with about the same maximum ellipticity, but a much longer period of time is required in this case.
The C family systems C050 and C100 start from $E_{max} \cong 3.5$ and $T \cong 0.78$ and they evolve more slowly decreasing E_{max} by about 1 unit and T by about 0.25 and 0.45, respectively, in a Hubble time. A Hubble time is too short for these models to achieve a state of equilibrium. In much longer times, C100 can reach a spheroidal equilibrium configuration, but C050 reaches an equilibrium that preserves a good level of triaxiality, showing that triaxial equilibrium configurations can be compatible with massive CMCs in certain cases.

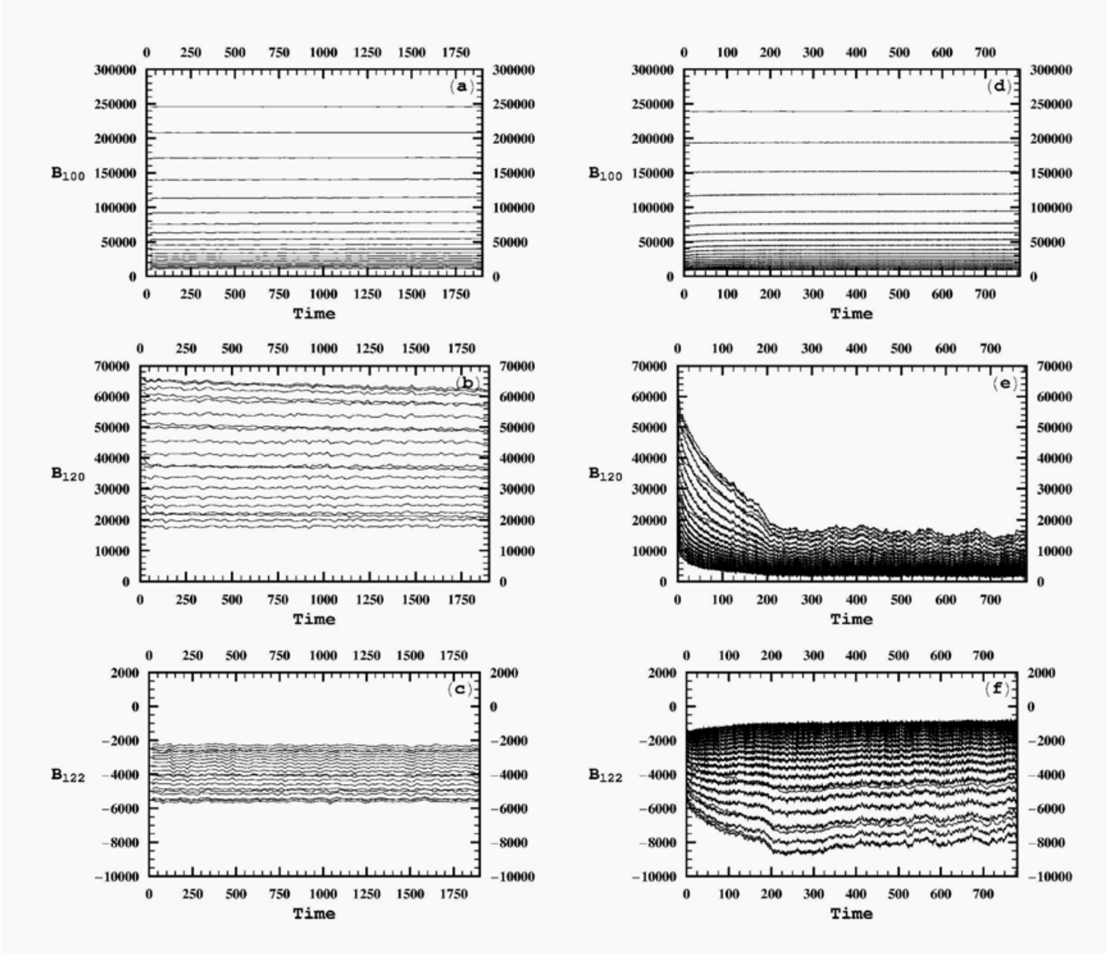

Figure 2. Time evolution of the most important coefficients of the monopole, the quadrupole and the triaxial terms the expansion of the potential for the Q000 model (left column) and for the Q100 model (right column).

The secular evolution of our models can also be seen in terms of the coefficients of the expansion of their self-consistent potential in terms of spherical Bessel functions and spherical harmonics.
This expansion is given, as a solution of the Poisson equation, by the conservative technique code that was designed by Allen et al. (1990) and it is used to run our systems self-consistently. The expansion of the potential contains 20 monopole terms with coefficients B_{l00}, 20 quadrupole terms with coefficients B_{l20} and 80 triaxial terms with coefficients B_{l21}, C_{l21}, B_{l22}, C_{l22}, *(l=0,1,2...19),* re-evaluated at small regular time steps during the run.

In Figs.2a,b,c,d,e,f the time evolution of the most important of these coefficients are shown in the Q000 model (left column, Figs.2a,b,c) and in the Q100 model (right column, Figs.2d,e,f). The coefficients of the monopole terms remain constant in time in both models (Figs.2a,d). However, the quadrupole coefficients decrease considerably in the Q100 model (Fig.2e), while they remain constant in the Q000 model (Fig.2b). This effect is only due to the presence of a CMC in the Q100.
The meaning of this decrease is that the prolate initial configuration along the z axis of the Q100 model is gradually transformed to a oblate configuration flatter along the x axis. This means that the bar along the z axis of the initial Q000 model cannot survive under the presence of a CMC of relative mass m=0.01. The system Q100 is initially unstable. It destroys the bar and changes towards a new equilibrium of an oblate spheroidal configuration.

4. Self-organization

The mechanism by which this transformation occurs is as follows. After the CMC is inserted most of the Box orbits in the system as well as a good number of ILAT orbits are converted to chaotic orbits. Using the method introduced recently (Voglis et al. 2002) we construct a library of particles in chaotic motion with LCN > $10^{-2.8}$. The fraction of this mass is initially on the level of 80% in the Q models and on the level of 50% in the C models almost independently of the mass of the CMC. For m < 0.005 this situation is quite constant in time scales of the order of a Hubble time. This is because the Lyapunov Numbers are not large enough to create considerable diffusion in a Hubble time. However, for m $\geq$ 0.005, diffusion is faster because the Lyapunov Numbers become larger. Such a diffusion causes time variations of the potential towards a form that allows smaller amount of chaotic orbits. As a consequence the mass in chaotic motion decreases in time, due to a self-organization of the system by converting gradually chaotic orbits in ordered orbits of the SAT type.

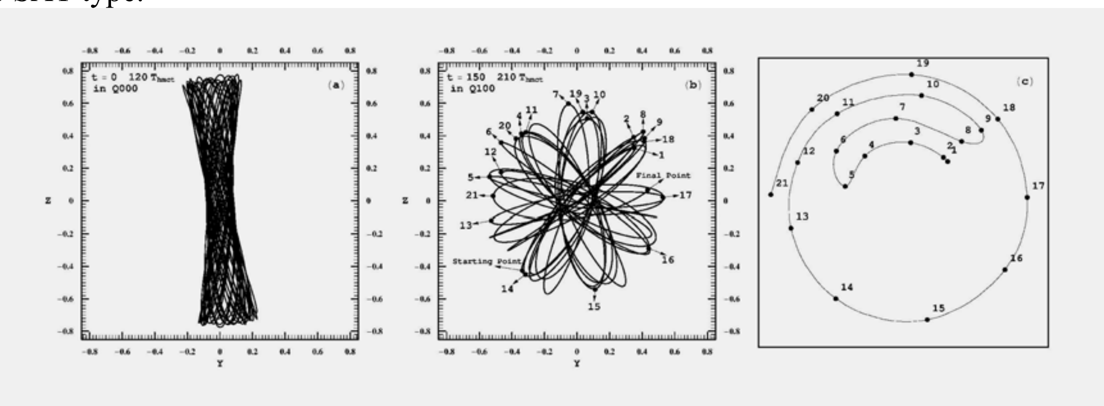

Figure 3. (a). A typical box orbits in the self-consistent Q000 model, projected on the yz plane. The major axis librates around a direction near to the z direction. **(b).** The major axis of the same orbit in the self-consistent model Q100 describes a chaotic libration with increasing amplitude for a period, but it is converted later on to an ordered rotation. **(c)**. A schematic diagram showing the successive orientations of the major axis of the orbit. The numbers 1 to 12 correspond to the chaotic libration, while the numbers larger than 13 correspond to the ordered rotation.

In Fig.3a we give an example of a typical box orbit in Q000 projected on the yz plane. The major axis of this orbit librates around a mean directrion near the z axis. By inserting the CMC (Q100 model), the libration of the major axis of this orbit becomes chaotic with increasing amplitude. At a given time this chaotic libration is converted to ordered rotation around the x axis. A projection of the orbits in this case is shown in Fig.3b. In Fig.3c the successive orientations of the major axis of the orbit are shown schematically, indicated by the numbers in this figure. The numbers 1 to 12 correspond to the orientations of the major axis of the orbit during the chaotic libration period, while the numbers larger than 13 correspond to the ordered rotation of the major axis of the orbit.

This process of self-organization occurs spontaneously in the system, driven by the scattering of the box or box like-orbits passing close to the CMC. When chaotic orbits are converted to SAT orbits the self-consistent potential is readjusted so that the equidensity contours change their shape towards a more spheroidal shape. The time variations of the self-consistent potential causes a redistribution of energy and entropy inside the system. Energy and entropy are transferred from the region of SAT orbits to the region of orbits that remain chaotic. Due to the second law of thermodymanics the remaining chaotic orbits become more chaotic, i.e. their Lyapunov numbers increase, so that, although their population becomes less, the total entropy of the system increases. Equilibrium is achieved when the remaining mass in chaotic motion becomes small enough so that its diffusion is no more able to alter the form of the potential established up to this time.

We have found that in the equilibrium configuration of the systems with $m \geq 0.005$ the mass left in chaotic motion is in the range of 12% in the C100 model to 25% in the Q050 model, while in the other two models it is in between.

References:

Allen A. J., Palmer P. L. and Papaloizou J., 1990, MNRAS, 242, 576

Contopoulos G., Voglis N., Efthymiopoulos C., 2002, SSRv, 102, 37

de Zeeuw T., 1985, MNRAS, 216, 273

Faber S. M. et al., 1997, AJ, 114, 1771

Fridman T., Merritt D., 1997, AJ, 114, 1479

Gebhardt K. et al., 2000, AJ, 119, 1157

Gerhard O. E., Binney J., 1985, MNRAS, 216,467

Kandrup H. E., Sideris I. V., 2002, CeMDA, 82, 61

Kandrup H. E., Siopis Ch., 2003, MNRAS, 345, 727

Kormendy J., Richstone D., 1995, ARA\&A, 33, 581

Kormendy J. et al., 1997, ApJ, 482, 139

Merritt D., Fridman T., 1996, ApJ, 460, 136

Merritt D., Quinlan., 1998, ApJ, 509, 933

Shen J., Shellwood J. A., 2003, astro-ph/0310194

Siopis Ch., Kandrup H. E., 2000, MNRAS, 319, 43

Statler T. S., 1987, ApJ, 321, 113

Valluri M., Merritt D., 1998, ApJ, 506, 686

Voglis N., Kalapotharakos C., Stavropoulos I., 2002, MNRAS, 337, 619

FORMATION AND EVOLUTION OF BARS*

E. Athanassoula

Observatoire de Marseille, 2 Place Le Verrier, F-13248 Marseille, Cedex 4, France

Abstract: Bars evolve by redistributing angular momentum within their galaxy. This is emitted at the resonances in the bar region and absorbed by the resonances in the outer disc and halo. Due to this redistribution, the bar gets stronger and slows down. A bar, or oval, can also be found in the halo. This is considerably shorter and weaker than the disc bar, and rotates with roughly the same pattern speed. I also briefly describe the orbital structure in the halo.

1 Introduction

Bars are a common feature of disc galaxies. Eskridge et al. (2000), using observations in near-infrared wavelengths, found that most disc galaxies are barred. Grosbøl, Pompei & Patsis (2002) studied the frequency of bars in a sample of 30 galaxies which had been classified as non-barred in the visual and found that approximately 75% of them showed a bar or an oval distortion longer than 5” and with a relative amplitude larger than 2%. This led them to suggest that roughly 95% of all spirals have some bar perturbation, albeit some times weak.

As early as the seventies, *N*-body simulations showed that bars form naturally in disc galaxies (e.g. Miller, Prendergast & Quirk 1970, Hohl 1971). The spectacular increase of computer power in the more than thirty years span since these very first simulations were made allowed for better resolution, more particles, a third dimension and the introduction of a live halo component. The more recent, higher quality simulations allowed us to study more thoroughly bar formation and what affects it, as well as to follow the evolution of the bar component over long times. Their results have been summarised in a number of review papers (e.g. Athanassoula 1984, 2002a; Sellwood & Wilkinson 1993; Martinet 1995). Here I will only discuss some very recent results which shed light on the physics of bar evolution, linking it with the angular momentum exchanged within the galaxy.

* Main Session Invited Review

2 Angular momentum exchange and bar evolution: The general picture

For an isolated galaxy, total angular momentum is a conserved quantity. Nevertheless, a galaxy can redistribute its angular momentum internally, between its various components, or parts. Lynden-Bell & Kalnajs (1972; hereafter LBK) show that it is mainly material at resonance that can gain or lose angular momentum. More specifically, they show that disc material at inner Lindblad resonance (hereafter ILR) can emit angular momentum, which can be absorbed by material at corotation (hereafter CR) and outer Lindblad resonance (hereafter OLR). Since the bar is confined to the region within CR (Contopoulos 1980), it is a negative angular momentum perturbation and by losing angular momentum it will grow stronger (Kalnajs 1971, LBK). In this early picture of bar evolution, angular momentum is emitted from the bar region (ILR) and absorbed at the outer disc, mainly by material at CR and OLR (LBK). The role of the halo in this picture was established by Athanassoula (2002b, hereafter A02; 2003, hereafter 2003). If the halo distribution function is a function of the energy only, then it is possible to show analytically that material at *all* halo resonances will absorb angular momentum. Thus, the LBK picture of bar evolution is now somewhat modified: Angular momentum is emitted from the bar region (ILR) and absorbed both at the outer disc (mainly disc material at CR and OLR) and by halo material (mainly material at all halo resonances). It is thus possible for the inner disc to shed more angular momentum than it would if the halo did not participate and thus to grow stronger. This explains the result of Athanassoula & Misiriotis (2002), namely that stronger bars can form in discs with heavier haloes. The amount of angular momentum that can be emitted, or absorbed, at a given resonance depends on the local density, but also on the local velocity dispersion, cold material being able to emit /absorb more angular momentum than hot one. By losing angular momentum the bar not only becomes stronger, but also reduces its pattern speed (e.g. Tremaine &Weinberg 1984; Weinberg 1985; Little & Carlberg 1991a, 1991b; Hernquist & Weinberg 1992; Athanassoula 1966; Debattista & Sellwood 2000; A03; O'Neill & Dubinski 2003).

3 Bar evolution and angular momentum exchange: Results from *N*-body simulations

The analytical results (LBK, Tremaine &Weinberg 1984,Weinberg 1985, A03) have been recently confirmed by *N*-body simulations (A02, A03). These showed that a considerable fraction of the particles are at near-resonance[1] even for the halo component (A02). They also showed that the resonances emit, or absorb, angular momentum in the way that theory predicted (A03). Finally,

[1] Exact resonance could only be established with infinite numerical precision

stronger and slower bars can be found in simulations where the resonances are able to emit/absorb more angular momentum (A03).

The analytical results lead us to expect a correlation between the amount of angular momentum exchanged and the bar strength, as well as an anti-correlation between the amount of angular momentum exchanged and the bar pattern speed. Unfortunately, it is very difficult to measure in a simulation the amount of angular momentum exchanged, so these correlations can not be directly tested. It is very easy, however, to measure the amount of angular momentum gained by the halo, and, if the outer disc absorbs only little angular momentum, the amount gained by the halo is roughly equal to the amount exchanged. Following A03, I plot in Fig. 1 the relation between the angular momentum gained by the halo and the bar strength and pattern speed. The upper panels contain the results of a very large number of simulations, with a relatively broad range of initial conditions. Even so, there is a very clear, strong correlation between the angular momentum gained by the halo and the bar strength, and a trend between this quantity and the pattern speed. In the lower panels I confine myself to simulations with a small core radius, for which most of the angular momentum emitted from the bar region is absorbed by the halo. In such cases, the angular momentum absorbed by the halo is a good estimate of the total angular momentum exchanged and there is thus a strong correlation between the pattern speed and the halo angular momentum.

4 A bar in the halo component

In simulations in which a strong bar is formed in the disc, the halo does not stay axisymmetric, but rather forms an oval, or bar, in its inner parts, which I will hereafter refer to as the halo bar. This is roughly aligned with the disc bar and turns with the same pattern speed. Its length grows with time, but it always stays considerably shorter than the disc bar. Since it has the same CR as the disc bar, it is what is generally called a slow bar, i.e. a bar terminating well before its CR.

As already mentioned, the halo has a number of near-resonant orbits. To investigate their properties, I calculated, in the potential of the simulation at a given time and with the appropriate pattern speed, the evolution of a number of orbits, using as initial conditions the positions and velocities of the halo particles in the simulation at that time. I find many orbits trapped around banana periodic orbits at CR, as well as a number of orbits trapped around the $l1$ family found by Skokos et al. (2002); i.e. around the $L1$ or $L2$ Lagrangian point. There are also many orbits trapped around the periodic orbits of the $x1$ tree[2], in particular orbits trapped around the x1v1 family[3]. I have also found orbits

[2] The $x1$ tree consists of the $x1$ family and of the families bifurcating from it (Skokos et al. 2002)

[3] Here I follow the nomenclature introduced by Skokos et al. (2002)

trapped around the *x*2 tree, albeit considerably fewer than those trapped around the *x*1 tree.

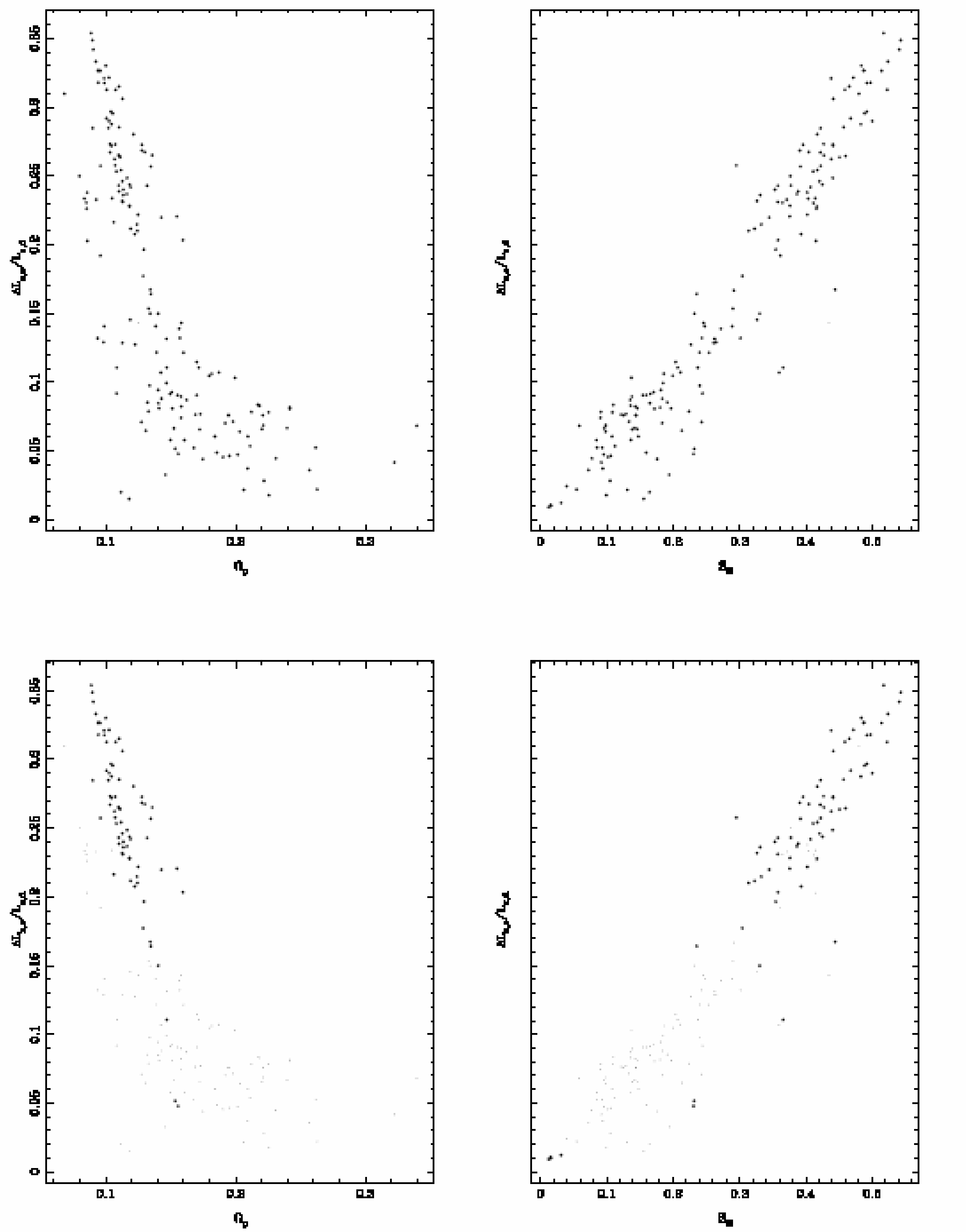

Figure 1: Relations between the angular momentum gained by the halo and the bar strength (right panels) and pattern speed (left panels). Each symbol represents the result of one simulation. In the lower row, large symbols represent simulations with a small initial core radius, and not too large extent. The angular momentum is normalised by the total angular momentum.

Although there are no chaotic orbits at the beginning of the simulation, several appear during the evolution, both in the disc and the halo component. For the case of a very strong disc bar, I find that it is possible that more than, or of the order of, one third of the halo particles are on chaotic orbits.

Acknowledgements

In this talk I included results from a number of my recent papers on secular evolution in barred galaxies. This work benefited from a number of interesting discussions with colleagues too many in numbers to be included here, but whom I would like to thank. Albert Bosma encouraged me all along. The work started in collaboration with A. Misiriotis, whose insightful questions often spurred me on. I also had the pleasure of collaborating with P. Patsis and Ch. Skokos on the 3D orbital structure in barred galaxies. The expertise from that work was most useful for me in the work presented here. The help of Jean-Charles Lambert and Angelos Misiriotis in many numerical aspects of this work is grateful acknowledged. I also thank Walter Dehnen for making his treecode and other related programs available to me. Finally, I thank IGRAP, the region PACA, the INSU/CNRS and the University of Aix-Marseille I for funds to develop the computing facilities used for the calculations discussed here. **5**

References

Athanassoula, E. 1984, Physics Reports, 114, 319

Athanassoula, E. 1996, in .Barred Galaxies., eds. R. Buta, D. Crocker and B. Elmegreen, PASP conference series, 91, 309

Athanassoula, E. 2002a, in “Galactic Disks : Kinematics, Dynamics and Perturbations”, eds. E. Athanassoula, A. Bosma, R. Mujica, PASP conference series, 275, 141

Athanassoula, E. 2002b, ApJ, 569, L83 (A02)

Athanassoula, E. 2003, MNRAS, 341, 1179 (A03)

Athanassoula, E. & Misiriotis, A. 2002, MNRAS, 330, 35

Contopoulos, G. 1980, A&A, 81, 198

Debattista, V. P., & Sellwood, J. A. 2000, ApJ, 543, 704

Eskridge, P. B. et al. 2000, AJ, 119, 536

Grosbøl, P., Pompei, E. & Patsis P. A. 2002, in .Galactic Disks : Kinematics, Dynamics and Perturbations., eds. E. Athanassoula, A. Bosma, R. Mujica, PASP conference series, 275, 305

Hernquist, L. & Weinberg, M. D. 1992, ApJ, 400, 80

Hohl, F. 1971, ApJ, 168, 343

Kalnajs, A. J. 1971, ApJ, 166, 275

Little, B. & Carlberg, R. G. 1991a, MNRAS, 250, 161

Little, B. & Carlberg, R. G. 1991b, MNRAS, 251, 227

Lynden-Bell, D. & Kalnajs, A. J. 1972, MNRAS, 157, 1, 1972 (LBK)

Martinet, L. 1995, Fundamentals of Cosmic Physics, 15, 341

Miller, R. H., Prendergast, K. H. & Quirk, W. J. 1970, 161, 903
O'Neill, J. K. & Dubinski, J. 2003, MNRAS, in press
Sellwood, J. A. & Wilkinson A. 1993, Rep. Prog. Phys., 56, 173
Skokos, Ch., Patsis, P. A. & Athanassoula, E. 2002, MNRAS, 333, 861
Tremaine, S. & Weinberg, M. D. 1984a, MNRAS, 209, 729
Weinberg, M. D. 1985, MNRAS, 213, 451

W-MODE INSTABILITY FOR ROTATING RELATIVISTIC STARS

Kostas D. Kokkotas

Section of Astrophysics, Astronomy, Mechanics, University of Thessaloniki, Greece

Abstract: The spacetime modes (or W-modes) of a fast rotating ultracompact star become unstable in stars with ergoregions. This instability is unique among all stellar instabilities because originates from the spacetime and not from the rotating fluid. The instability can grow in a timescale of seconds or minutes and damps out via the emission of gravitational waves.

ON THE NATURE OF INNER RINGS IN BARRED GALAXIES*

P. A. Patsis[1], Ch. Skokos[1] and E. Athanassoula[2]

[1] Academy of Athens, Research Center for Astronomy, GR-106 73 Athens, Greece
[2] Observatoire de Marseille, 2 Place Le Verrier, F-13248 Marseille,Cedex 4, France

Abstract: Inner rings in barred spiral galaxies are associated with specific 2D and 3D families of periodic orbits, which are found in the upper part of a type- 2 gap of the x1 characteristic. Using these orbits we reproduce the observed morphologies of inner rings and we explain why some of them are observed more frequently than others.

1 Introduction

Inner rings are ring-like structures, which surround the bars of barred spiral galaxies. Most inner rings are oval, sometimes with a somewhat lemon shape because of density enhancements at the bar major axis. As a typical case we mention NGC 6782. Some ovals have characteristic breaks or corners. In this latter case the ring becomes rather polygonal-like with sides roughly parallel to the bar's minor axis at its apocentra, and 'corners' close to the minor axis. This morphology is nicely demonstrated by the distribution of the HII regions in IC 4290 (Buta et al. 1998). In exceptional cases we encounter rings that are better described as pentagonal structures, while there is a single notable case, NGC 7020, with an inner hexagonal ring with cusps on the major axis of the bar and two sides parallel to it (Buta 1990).

We use a 3D Ferrers bar model to study the orbital structure of the rings. The model is described as "the fiducial case" in Skokos et al. 2002.

It consists of a Miyamoto disk, a Plummer bulge and a Ferrers bar. The potential of the Miyamoto disk (Miyamoto & Nagai 1975) is given by the formula:

$$\Phi = -\frac{GM_D}{\sqrt{x^2 + y^2 + \left(A + \sqrt{B^2 + z^2}\right)^2}}, \tag{1}$$

where M_D is the total mass of the disk, G is the gravitational constant, and the ratio B/A gives a measure of the flatness of the model.

The bulge is represented by a Plummer sphere, i.e. its potential is given by:

$$\Phi_S = -\frac{GM_S}{\sqrt{x^2 + y^2 + z^2 + \varepsilon_S^2}}, \tag{2}$$

where ε_S is the bulge scale length and M_S is its total mass.

* *Proceedings of the 6th Hellenic Astronomical Society Conference, 15-17 September 2003, Penteli, Greece*

Finally, the bar is a triaxial Ferrers bar with density

$$\rho(m)=\begin{cases}\dfrac{105M_B}{32\pi abc}\left(1-m^2\right)^2 & for \quad m\le 1\\ 0 & for \quad m>1\end{cases}\quad, \tag{3}$$

where

$$m^2=\frac{y^2}{a^2}+\frac{x^2}{b^2}+\frac{z^2}{c^2}, \qquad a>b>c. \tag{4}$$

In the above a, b, c are the principal semi-axes, and M_B is the mass of the bar component. For the Miyamoto disk we use A=3 and B=1, and for the axes of the Ferrers bar we set a:b:c = 6:1.5:0.6. The masses of the three components satisfy $G(M_D+M_S+M_B) = 1$. We have $GM_D = 0.82$, $GM_S = 0.08$, $GM_B = 0.10$ and $\varepsilon_S = 0.4$.

The length unit is taken as 1 kpc, the time unit as 1 Myr and the mass unit as 2 x $10^{11}\,M_\odot$. The bar rotates with a pattern speed Ω_b=0.054 around the z-axis, which corresponds to 54 km sec^{-1} kpc^{-1}, and places corotation at 6.13 kpc. The Hamiltonian governing the motion of a test-particle in our rotating with Ω_b system can be written in the form:

$$H=\frac{1}{2}\left(p_x^2+p_y^2+p_z^2\right)+V\left(x,y,z\right)-\Omega_b\left(xp_y-yp_x\right), \tag{5}$$

where p_x , p_y, and p_z are the canonically conjugate momenta of x, y and z respectively and V(x,y,z) is the total potential of the combined three components of the model: disk, bar and bulge.

2 Results

In our 3D Ferrers bar model, inner rings are due to orbits belonging to families in the upper part of the type-2 gap at the inner radial 4:1 resonance (Contopoulos & Grosbøl 1989). They are grouped in two orbital trees, which have as mother-families two planar families we call “f” and “s”. The orbits that make the rings belong in their vast majority to three-dimensional families of periodic orbits. These 3D families have large stable parts and thus they increase considerably the volume of the phase space occupied by ring-supporting orbits. The energy width over which we can find stable 3D orbits supporting the rings is larger than the corresponding interval of 2D stable families.

The prevailing types of inner rings are variations of oval shapes and are determined by the way the f and s families are introduced in the system. This is the tangent bifurcation mechanism. In such a bifurcation (also known as saddle-node bifurcation) one of the newborn sequences of orbits is unstable (the saddle), while the other is stable (the node) (see Contopoulos 2002, pg. 102). The characteristics of families f and s are of this

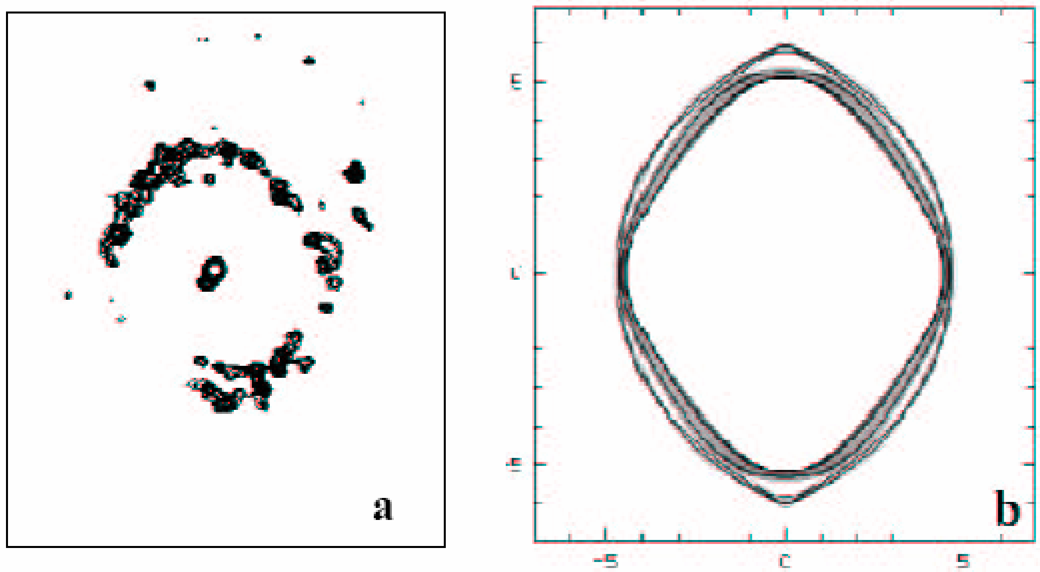

Figure 1: (a) The distribution of HII regions in IC 4290 as given in Buta et al. (1998). (b) The face-on view of a set of stable orbits belonging to the f- and s-trees. The HII regions outline the inner ring structure, and the set of the orbits we present reproduces the observed morphology.

type which means that these families are *not* bifurcated from any family belonging to the the x1-tree (Skokos et al. 2002). Furthermore, they build their own group of families, i.e. their own trees.

The orbits on the stable branch of their characteristic, together with their stable 3D bifurcations, support ovals with a more or less strong lemon shape, or oval-polygonal rings with 'corners' along the minor axis of the bar. These types of inner rings represent frequently observed morphologies.

In Fig. 1 we see at the left panel the distribution of the HII regions in IC 4290 (Buta et al. 1998) and at the right one a combination of weighted (see Patsis et al. 2003) stable orbits belonging to the f- and s-trees of families. These orbits can reproduce the distribution of the HII regions that outline the shape of the inner ring in this galaxy.

Pentagonal rings are rare because the families building them have small stable parts and usually come in symmetric pairs. These families belong to the f-tree. Thus, in order for these rings to appear, the symmetry must be broken and only one of the two branches be populated due to some particular formation scenario. Furthermore, considerable material should be on regular non-periodic orbits trapped around stable periodic orbits existing only in narrow energy ranges.

If orbits are trapped around stable s periodic orbits at the energy minimum of the s characteristic, then an NGC 7020 morphology can be reproduced. Although such a morphology is in principle possible, it should be rare, because it would necessitate that considerable amount of material be on regular orbits trapped around periodic orbits in a very narrow energy interval. Indeed the hexagonal orbits with cusps on the *major* axis are on the unstable branch of the tangent bifurcation.

Acknowledgements This work has been supported by the Research Committee of the Academy of Athens. Ch. Skokos was partially supported by the Greek State Scholarships Foundation (IKY). P.A.P and Ch.S. thank the Observatoire de Marseille for its hospitality during their stay in Marseille.

3 References

Buta R., 1990, ApJ, 356, 87

Buta R., Alpert A.J., Cobb M.L., Crocker D.A., Purcell G.B., 1998, AJ, 116, 1142

Contopoulos G., 2002, "Order and Chaos in Dynamical Astronomy", Springer-Verlag Berlin Heidelberg

Contopoulos G., Grosbøl P., 1989, A&A Rev., 1, 261

Miyamoto M., Nagai R., 1975, PASJ, 27, 533

Patsis P.A., Skokos Ch., Athanassoula E., 2003, MNRAS, 337, 578

Skokos Ch., Patsis P.A., Athanassoula E., 2002, MNRAS, 333, 847

*ABSTRACTS OF PAPERS POSTED DURING THE SESSION ON GALACTIC DYNAMICS AND CHAOTIC DYNAMICAL SYSTEMS**

CHAOS IN A GALAXY MODEL WITH A MASS TRANSPORT

N. D. Caranicolas and N. J. Papadopoulos.

Department of Physics, Section of Astrophysics,Astronomy and Mechanics, University of Thessaloniki, Greece

Abstract: We study the transition from regular to chaotic motion in an axially symmetric galaxy model with a disk-halo and a spherical nucleus. The mass of the nucleus increases exponentially because mass is transported from the disk to the nucleus while the total mass of the galaxy remains constant. Stars with values of angular momentum (Lz) less or equal to a critical value (Lzc), moving near the galactic plane, are scattered to the halo when approaching the nucleus. The corresponding orbits are chaotic. A linear relationship is found to exist between the critical angular momentum and the final mass of the nucleus (Mnf). Our results suggest that the stars in the central regions of disk galaxies with massive nuclei must be in chaotic orbits. Comparison with previous work is also made.

THEORETICAL PREDICTION OF THE EXISTENCE OF FAMILIES OF PERIODIC ORBITS IN THE N-BODY RING PROBLEM

Antonis. D. Pinotsis

Department of Astrophysics, Astronomy and Mechanics, Faculty of Physics, University of Athens, Panepistimiopolis, 157 84 Zographos, Athens, Greece

Abstract: In this work we theoretically investigate the existence of families of periodic orbits in the planar N-body ring problem and we give a qualitative picture of the periodic motions. We ascertained four families of periodic orbits which are valid for every value of the parameter N and β: Two families of periodic orbits around the central body, one sidereally retrograde which is also synodically retrograde and another sidereally and synodically direct and also two families around all the peripherals, one retrograde in the rotating and fixed system and another direct in the fixed system and retrograde in the rotating system. We also found numerically these families of simple and double 2-dimensional symmetric periodic orbits for N-1=7 and 4 and for some values of β. We did not find numerically direct family of symmetric periodic orbits with respect to the rotating and the fixed system in the case $r>r_p$, (r_p is the distance between each peripheral and the origin of the system) as we predicted theoretically. These four families of periodic orbits evolve for $|r| > r_p$ in the (x,y) plane (Pinotsis et.al. 2001, Pinotsis submitted). Also for $C\to\pm\infty$ the absolute value of x_o tends to $x_o\to\infty$, as we have theoretically predicted

---

* *Proceedings of the 6th Hellenic Astronomical Society Conference, 15-17 September 2003, Penteli, Greece*

*ABSTRACTS OF PAPERS POSTED DURING THE SESSION ON GALACTIC DYNAMICS AND CHAOTIC DYNAMICAL SYSTEMS**

DOUBLE PERIODIC ORBITS IN RING (N+1)- BODY MODELS

Tilemahos J. Kalvouridis

National Technical University of Athens
5, Heroes of Polytechnion Ave., Zografou, 15773, Athens, Greece

Abstract: During the last few decades much attention has been paid on the simulation of many body systems. One of the proposed models approximating certain types of N-body configurations is the so-called ring problem (Kalvouridis, 1999). The system consists of N coplanar big bodies, ν=N-1 of which have equal masses m, and are symmetrically arranged on the periphery of a circle, or, equivalently, at the vertices of a regular polygon. Another major body P_0 with different mass m_0 lies at the mass center of the system. A point-like body S of negligible mass moves under the resultant gravitational attraction of the big bodies. The system has two parameters, namely the number ν of the peripheral big bodies and the ratio $\beta = m_0/m$ of the central mass to a peripheral one. The evolution of the families of double periodic orbits, as well as their qualitative characteristics in two concrete configurations of the above problem, were the subjects of our investigation. Commenting briefly on some of the properties of these families and of the results obtained so far, we may make some general remarks: (1) The periodic solutions of a given configuration, are "accumulated" in some regions of the space of initial conditions (x_0, C), mainly between the characteristic curves of simple periodic orbits. (2) The characteristic curves are smooth and generally of very low curvature except when they develop near the asymptotes passing through the primaries that lie on the x-axis of the synodic coordinate system. (3) The period generally decreases as the Jacobian constant C decreases, and so does the size of the orbits. (4) The majority of the double periodic solutions are unstable.

* *Proceedings of the 6th Hellenic Astronomical Society Conference, 15-17 September 2003, Penteli, Greece*

*ABSTRACTS OF PAPERS POSTED DURING THE SESSION ON GALACTIC DYNAMICS AND CHAOTIC DYNAMICAL SYSTEMS**

ION INTERACTIONS WITH AN AURORAL POTENTIAL STUCTURE: HAMILTONIAN APPROACH

A.Anastasiadis[1], I. A. Daglis[2] and C. Tsironis[3]

[1]National Observatory of Athens, Institute for Space Applications and Remote Sensing, Penteli GR 15326, Greece.
[2]National Observatory of Athens, Institute for Space Applications and Remote Sensing, Penteli GR 15326, Greece.
[3]Aristotle University of Thessaloniki, Department of Physics, Thessaloniki GR 54006, Greece.

Abstract: We study the interaction of oxygen ions with an one dimensional auroral arc potential well of an exponential form with a characteristic length Lx, using the Hamiltonian formulation. The oxygen ions are drifting in the presence of a constant magnetic field Bz and a constant electric field Ey. The orbits of individual ions for different initial conditions (phase angle and kinetic energy) are traced. It is found that, depending upon the initial conditions, the ions can be either accelerated, decelerated or remain energetically unaffected. Furthermore, we perform a parametric study for the interaction of monoenergetic and Maxwellian type of ion disttributions, using random phase angle injection of the particles, with repect to our model parameter, the characteristic length of the potential Lx.

* *Proceedings of the 6th Hellenic Astronomical Society Conference, 15-17 September 2003, Penteli, Greece*

*ABSTRACTS OF PAPERS POSTED DURING THE SESSION ON GALACTIC DYNAMICS AND CHAOTIC DYNAMICAL SYSTEMS**

TRACING PERIODIC ORBITS IN 3D GALACTIC POTENTIALS USING THE PARTICLE SWARM OPTIMIZATION METHOD

Ch. Skokos[1,2], K. E. Parsopoulos[3], P. A. Patsis[1], and M. N. Vrahatis[3]

[1]Research Center for Astronomy, Academy of Athens, 14 Anagnostopoulou str. , GR-10673, Athens, Greece
[2]Department of Mathematics, Division of Applied Analysis and Center for Research and Applications of Nonlinear Systems (CRANS), University of Patras, GR-26500 Patras, Greece
[3]Department of Mathematics, University of Patras Artificial Intelligence Research Center (UPAIRC), University of Patras, GR-26110 Patras, Greece

Abstract: We investigate the efficiency of a numerical algorithm for locating periodic orbits in a Hamiltonian system. The algorithm has been applied successfully on a 3D potential of a barred galaxy. In particular, an appropriate scheme that transforms the problem of finding periodic orbits to the problem of detecting the global minimizers of a function defined on the Poincaré Surface of Section (PSS) of the Hamiltonian system has been developed. In the case of p-periodic orbits, this function is the square of the Euclidean distance on the PSS, between the initial point of the orbit and its p-th intersection with the PSS. The minimizers of the function are computed by applying the Particle Swarm Optimization (PSO) method. PSO is a population based algorithm, i.e., it exploits a population, called a *swarm*, of points to probe promising regions of the search space simultaneously. Each search point, called a *particle*, moves in the search space with a velocity, which is adapted by taking into consideration the 'best' position it has ever encountered as well as the 'best' position that has been attained by all the particles in a neighborhood of it. In our case, the search space is the PSS and the 'best' positions possess lower function values. Using the PSO method, several stable periodic orbits near the corotation of a 3D Ferrers bar potential that were not detected by other methods, have been located. In particular, families of 2D and 3D periodic orbits, associated with inner resonances higher than the 8:1 resonance have been found. Moreover, various p-periodic orbits with $p>1$, have also been detected.

Acknowledgements
Ch. Skokos was supported by the Research Committee of the Academy of Athens, the `Karatheodory' post—doctoral fellowship No 2794 of the University of Patras and the Greek State Scholarships Foundation (IKY).

* *Proceedings of the 6th Hellenic Astronomical Society Conference, 15-17 September 2003, Penteli, Greece*

*ABSTRACTS OF PAPERS POSTED DURING THE SESSION ON GALACTIC DYNAMICS AND CHAOTIC DYNAMICAL SYSTEMS**

FACE-ON VIEWS OF 3D BARRED GALAXIES

P. A. Patsis[1], Ch. Skokos[1], and E. Athanassoula[2]

[1]Research Center for Astronomy, Academy of Athens, 14 Anagnostopoulou str. , GR-10673, Athens, Greece
[2]Observatoire de Marseille, 2 Place Le Verrier, F-13248 Marseille Cedex 4, France

Abstract: We study the conditions that favour boxiness of isodensities in the face-on views of orbital 3D models of barred galaxies. Boxy isophotes are typical features at the end of the bars of early type (SB0, SBa) barred galaxies seen not far from face-on, as well as, in snapshots of N-body simulations. In order to explain the dynamical reasons for their appearance by means of the orbital theory, we study the face-on structures supported by stable periodic orbits in analytic 3D models of barred galaxies. The potentials of our models consist of three components, namely a Miyamoto disk, a Plummer sphere bulge, and a Ferrers bar. The models studied have different mass values for the three components of the potential, as well as different values of the bar pattern speed. In every model we find the families of periodic orbits belonging to the x1-tree and construct weighted profiles using only the stable orbits of these families. The basic result of our study is that boxiness in the face-on views of 3D barred models is an effect caused by the coexistence of several stable periodic orbits belonging to different families. The morphology of boxy isodensities/isophotes is not necessarily similar to the morphology of individual stable, rectangular-like orbits. The consideration of several families of orbits for building a face-on profile may lead to boxy features close to the end of bars, with the ratios of their projection on the major axis of the bar to the projection on the minor axis being different from the corresponding ratios of individual orbits or families of orbits. 3D orbits that are introduced due to vertical instabilities play a crucial role in the face-on profiles and enhance their rectangularity. This happens because at the 4:1 radial resonance region we have several orbits with boxy face-on projections, instead of few rectangular-like x1 orbits, which, in a fair fraction of the models studied, are unstable at this region. We also find that it is the pattern speed that mostly affects the elongation of the boxy feature, in the sense that fast bars are more elongated than slow ones.

Acknowledgements
Ch. Skokos was supported by the Research Committee of the Academy of Athens and the Greek State Scholarships Foundation (IKY).

* *Proceedings of the 6th Hellenic Astronomical Society Conference, 15-17 September 2003, Penteli, Greece*

NGC4631 The Whale Galaxy

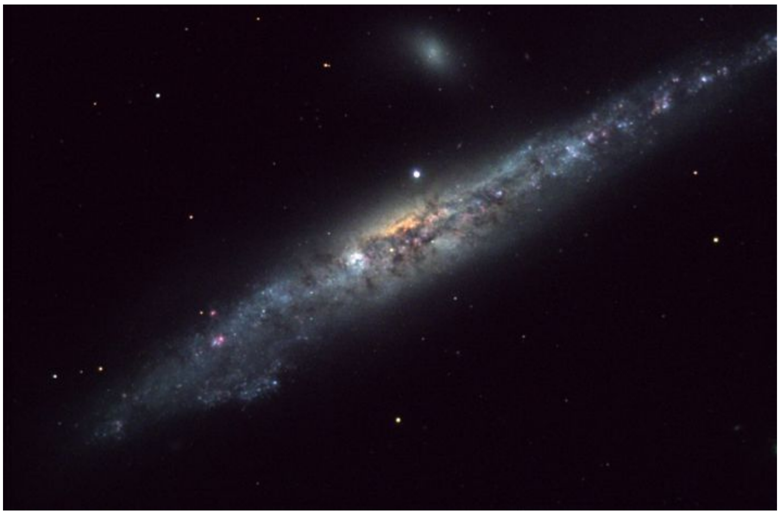

Session VII

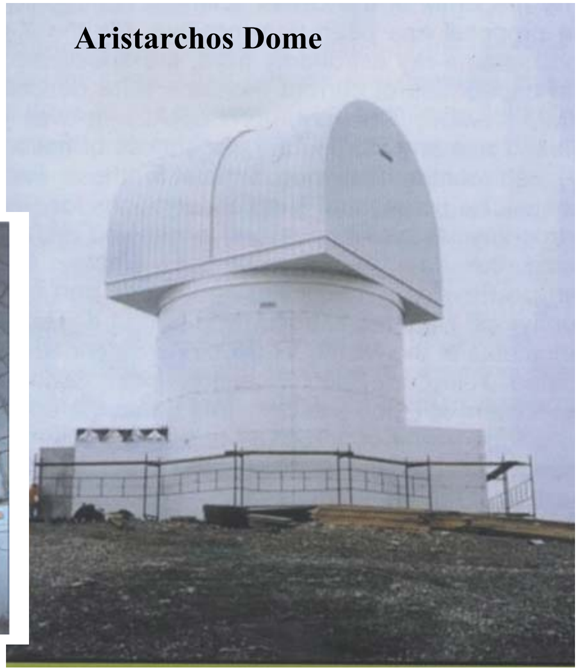

Aristarchos Dome

Skinakas Observatory

INFRASTRUCTURE OF ASTRONOMY IN GREECE

Conveners: C. Goudis and D. Hatzidimitriou

INSTITUTE OF ASTRONOMY AND ASTROPHYSICS (IAA): ACTIVITIES AND PERSPECTIVES*

C. Goudis, P. Hantzios, P. Boumis, A. Dapergolas and N.Matsopoulos
Institute of Astronomy and Astrophysics, National Observatory of Athens, Greece

STRATEGY

The main strategic target of the Institute of Astronomy and Astrophysics (IAA) at the National Observatory of Athens (NOA) is the triplet **R**esearch-**E**ducation-**C**ulture **(REC)**, a unified area of intellectual activity based on the innate co-lateral activities of our human potential and on the technological infrastructure we posses. The driving power of the scheme demands for a continuous source of energy ejecting euros in substantial amounts. Since the Greek State has championed over the past twenty years a sustained policy of low investment in Research and Development – we are the undisputed bottom of the list in the EU and the rest of the advanced nations of the planet – the chances for our adventurous effort to succeed are rather limited. But being Greeks, and been continuously inspired by the slogan "Greece never dies", we try our best.

Research is an area served by the Institute, which is mainly oriented in observational astrophysics and has strong international ties and collaborations, through two distinct channels. The one is the *ab initio* acquisition of data, i.e. through observations made in our own astronomical stations with our own instruments, and the other, not surprisingly the most succesful, through frontline observations obtained by having access in a number of international observatories and space probes pursuing astrophysical topics.

Spearheading our research effort, both in quantity and quality of production – in publications I mean, but we are all in a sense obliged to speak the language of the masters of this earth, the language of economists – are two scientifically interrelated groups, the X-ray Astronomy and the Cosmology groups. Indeed these two have been further developed after the approval of the project "X-ray Astrophysics with ESA's mission XMM' within the framework of the program 'Promotion of Excellence in Technological Development and Research. This program was funded with 350.000 euros over a period of three years, following a favourable report by an international peer review committee. Four (4) postdoctoral and two (2) postgraduate research associates are employed at the IAA within the framework of the above programme. Our research potential has also strengthened after the recent arrival – over the past year – of two talented younger observational astronomers, which opens wide the opportunity for the IAA to become very activily involved in the field of interstellar matter and the optical study of galaxies with emphasis in the area of the Active Galactic Nuclei (AGN).

To have however a distinct presence in the wider astronomical community, a modern nucleus, such us our new observatory on Helmos, is absolutely necessary. We will make our best to see the "Aristarchos" 2.3 m telescope becoming the international façade of Greek astronomy in the near future, by attracting viable long term international collaborations and give the younger generation of astronomers a chance to compete and collaborate with cleagues abroad on better terms than we ever did. It is an effort, the scientific gravity of which should be clearly understood by the Greek State. As a warning, we would like to stress that many third world countries have built in the past observatories and installed large diameter telescopes to boost their national pride. Eventually, these observatories became national mausoleums. In a sense, supporting scientists in order to obtain the proper function of such an observatory at international standards is a better civilization and development index for a country, than the anxious and extremely expensive effort to emerge as successful innkeeper of the so called Olympic Games.

* *Proceedings 6th Hellenic Astronomical Society Conference, 15-17 September 2003, Penteli, Athens, Greece*

Our second aim, the educational dimension, is served by establishing strong ties and shaping a productive interface with the academic world of the universities, a world deeply embedded in teaching with few facilities to transform astronomical knowledge into astronomical practice. In applying this strategy of integration, we have now host permanently in the Institute more than five students committed in active research, pursuing diplomas and postgraduate degrees (M. Sc. and Ph. D.) under the supervision of joined committees with the participation of members from both, our Institute and the universities they nominally belong. In parallel, we dominate as IAA the yearly Summer Schools organized by NOA, by offering introductory astrophysical courses and observational experiences to classes of senior high school pupils, an activity sine qua non for the attraction of brilliant young people to astronomy.

Culture, a far broader concept involving a combination of education and modern credos, is an area our Institute is active by disseminating proper scientific knowledge and clarifying obscure cases of modern mythology to people of various social and educational strata and of various ages, through a well organized Visitors Centre, a modern web site, a flux of related articles to journals and newspapers, the frequent appearance of our representatives in radio and television interviews and panels and the organization of public events bridging the gap between science and the arts. As a clear example of the last kind of communication with the public, we should mention last September's very successful "Night of Poetry and Astronomy" at the National Observatory of Athens, co-sponsored by the British Council, during which people under the full moon listened to poets and actors reading literary pieces related to Astronomy and visited the old atmospheric observatory at Thisseion.

After paying a brief tribute to our astronomical heritage of the past, by showing you snapshots of our historical telescopes, the Dorides refractor (40cm, f/12.5) at Thisseion I have just mentioned above, and the still very active within our Visitors Centre, Turner-Newall refractor (62cm, f/14) of the Pentele Astronomical Centre (PAC) - in which we are literary embedded right now - let us proceed with the more clinical aspects of our talk by presenting to you in some detail the infrastructure and the activities of the Institute.

OBSERVATORIES

Our main Astronomical Stations to pursue active research are the Kryonerion Astronomical Station and the newly built Helmos Astronomical Station. Let us outline the main features of the two observatories :

The **K**ryonerion **A**stronomical **S**tation **(KAS)**

The Astronomical Station at Kryonerion of Korinth is placed in Northern Peloponnese at an altitude of ~930m above see level. Its geographical coordinates are Longitude =22° 37.3' E, Latitude = 37° 58.4' N.

The station is equipped with the 1.2m Cassegrain telescope, made by Grubb Parsons Co., Newcastle, and installed in 1975. Its optical system consists of a paraboloidal primary mirror of 1.2m diameter with an f/3 focal ratio, and a hyperboloidal secondary mirror (31 cm). Both mirrors are made of Zerodur. The telescope's final focal ratio is f/13, its field of view is about 40 arcmin and the image scale is 12. 5 arcsec/mm.

The main scientific instrument of the 1.2m Telescope is the CCD camera, a Series 200 Camera System made by Photometrics, which it is mounted on the Cassegrain focus of the telescope.

CCD CAMERA FEATURES

CCD Type:	SI-502, Grade 1, UV-coated
	516 x 516 pixels
gain:	5.17e-/ADU (1x gain)
	1.23 e-/ADU (4x gain)
readout noise:	9.0 e- RMS (1x gain)

7.5 e- RMS (4x gain)
pixel size: 24μ x 24μ
dark current:1.03e-/pix/s
cooling: up to -40°C Peltier system (water circulation)

The field size of the CCD is about 2.5 X 2.5 arcmin with pixel size 0.30 arcsec.The Quantum Efficiency of the CCD versus wavelength is seen in the following table:

nm	300	320	340	360	380	400	450	500	550	600	650
QE	0.19	0.25	0.29	0.35	0.40	0.41	0.46	0.64	0.64	0.65	0.64

A set of 5 Bessel filters is provided (U,B,V,R,I). It is mounted on a computer-controlled filter wheel. The camera and the filter wheel are controlled by a dedicated PC (Windows). A PMIS control program is used for the CCD, while the filter is controlled by simple commands parsed to a serial port. Automated sequence of observations can be programmed using a simple script language. A GPS system (PCI-card) provides accurate time. Another PC (Windows and Linux) is used for image storage, processing, and analysis. Both PCs are time-synchronized. The computers are connected to a Local Area Network.

A characteristic example of the performance of the CCD camera in combination with the 1.2 m telescope, is its capacity to detect in the visual (through a V filter) a 15^{th} magnitude star (placed in 1.3 air masses) in a 1 minute exposure, with an error of 0.01 magnitude.

In the following table are seen the number of nights used for observations with the 1.2m telescope from 1998 – 2002:

Year	1998	1999	2000	2001	2002
Nights Used	64	120	201	121	167

The scientific output from observations taken with the 1.2m telescope for the same period has been the core of 25 refereed papers.

The **H**elmos **A**stronomical **S**tation **(HAS)**

The National Observatory of Athens completed the construction of the new astronomical station on the top of Mt. Helmos at an altitude of 2340 m (nearby the Kalavryta Ski Center). Its geographical coordinates are Longitude =22° 13' E, Latitude = 37° 59' N. Road access, infrastructure, meteorological conditions, darkness of the night sky and image quality were the criteria for the selection of the Helmos mountaintop.

These criteria guarantee the optimum utilization of telescope time, provided that the Greek state will:

a) realize the necessity for proper construction of a safe road from the ski centre to the top of the mountain,
b) provide the means to have it open during the winter period, and
c) support the electrification of the observatory,

by treating these urgent demands as top priorities. This new astronomical station is expected to strengthen significantly the research and its technological aspects in our country.

The Greek company PROTER A.T.E. constructed the telescope tower and the auxiliary buildings, performing a high quality work in record time. The astronomical station consists of two compartments: the telescope tower and the control room, with a distance of 35 meters between them. This way, human activity and the heat radiated from engines, computers, etc will not affect the performance of the telescope and particularly the image quality.

The Helmos Astronomical Station disposes the necessary infrastructure for the support of the observing activities and operation. In summary, the infrastructure of the astronomical station is analyzed as follows:

- Access: The closest small town is Kalavryta (~1,000 population, prefecture of Achaia), 25 km away. Access from Athens airport is within 4 hours by car (250 km). Bus and train connections to Kalavryta are also available from Athens. Patras (200,000 population) is within 100 km with port and airport facilities. The site location guarantees very easy access from all Balkan and East-European countries. Up to the base of the Kalavryta Ski Center (altitude 1700 m) there is an asphalt paved road which is kept open throughout the year. In summertime, the access from the base of the ski center to the mountaintop is taking place through the existing unpaved (and rather unsafe as it stands) road (length 8.5 km). For this reason the astronomical station disposes a 4x4 vehicle. During winter time the access to the mountaintop is taking place through the use of the ski center lifts as well as the snow vehicle of the astronomical station.

- Power: Two power generators of 75 kVA and 12 kVA will be used for powering the activities of the telescope tower and the control room respectively. Parallel to this, an initiative is moving forward for the connection of the astronomical station with the Public Electric Company network, but the financial cost we are facing is enormous.
- Communications: The connection of the astronomical station with the home of the Institute at Pentele will be effected through a microwave link. The capacity of the link is 2 Mb/s with the ability to be extended to 11 Mb/s.
- Computer Center: The astronomical station will be equipped with a computer network (server, work stations, PC.'s and related items, all of them already bought and stored) which will support the operation of the telescope, the astronomical instruments, communications, etc

THE ARISTARCHOS TELESCOPE

The station will be equipped with the new 2.3m ARISTARCHOS optical telescope which has been built by Carl Zeiss Jena (1998-2003) utilizing new technologies and techniques arising mainly as a spin-off from the development of the new generation of 8-metre optical/IR telescopes. The modern design of the telescope makes it unique in this class of telescopes, since technologies developed for the new, largest 8-10m telescopes are now applied to medium-size telescopes (2.3m ARISTARCHOS, 2m Liverpool telescope, 2.5m VST/ESO).The telescope has been assembled and factory tests are underway. Based on the progress of the telescope tests, delivery is expected during 2004.

MECHANICAL STRUCTURE

The alt-azimuth design makes the telescope lighter, thus cheaper and easier to construct, whereas at the same time offers a number of instrument stations which are easily accessible by a simple movement of a small flat mirror. It has four cassegrain side ports able to bear instruments up to a total of 300 Kg, while the weight of one instrument can be up to 100Kg, and one main cassegrain port sustaining an instrument up to 300 Kg (by distance of the center of gravity of the instrument less or equal to 300 mm from the instrument flange.). Despite the advantages just mentioned, the dimensions of the telescope are those of a huge structure (6.5 m when the telescope is placed horizontally, 9 m when in the vertical position). The total weight of the moving parts is 29.000 Kg rising to 34.000 Kg if the infrastructure is included. Regarding the resonant frequencies of the telescope, the first natural eigenfrequency of the fork is 16 Hz and the respective one of the tube 21 Hz.

OPTICS

The 2.3 m "Aristarchos" telescope, according to the specifications of the contract, is a Ritchey Chretien telescope, consisting of :

- a Sitall primary mirror of 2.3 meters in diameter with a focal ratio f/2.4, and
- a Sitall secondary mirror of 74 cm in diameter with focal ratio f/3.1.
- The final focal ratio of the telescope is f/8.

The optical design is such as to offer :
- an uncorrected field of view of the order of 10 arcmin
- a corrected field of view of the order of 1 degree
- image scale 1. 17 arcsec/mm
- The the image quality (80% encircled energy) on axis will be verified by a spreading less than 0.35 arcsec and less than 0.5 arcsec in a radius from 5 arcmin to 20 arcmin off axis, for all altitudes between 20 and 90 degrees and for the spectral range from 3.500 A to 10.000 A.
- The accuracy of focusing obtainable through the movement of the secondary mirror will be of the order of +/-0.005mm, whereas the travel range of the focusing mechanism will be +/- 50mm.

PERFORMANCE

Some useful parameters characterizing its expected performance are:

- Range of movement in azimuth : +/- 200 degrees
- Range of movement in altitude : +/- 90 degrees
- Rate of movement in azimuth : max 2 degrees per second
- Rate of movement in altitude : max 2 degrees per second
- Accuracy of pointing: < 4 arcsec up to zenith distances =70 degrees
- Accuracy of tracking in open loop : < 0.5 arcsec in 10 minutes
  < 2 arcsec in 1 hour
- Accuracy of tracking in closed loop : < 0.25 arcsec in 10 minutes
  < 0.5 arcsec in 1 hour
- Accuracy of rotator tracking : 0.25 arcsec in 10 minutes
  0.5 arcsec in 1 hour
- Radius of Zenith blind spot : 2 degrees
- Mean time between failures : 750 hours
- Mean time to effect repair : < 4 hours
- Operating temperature range : from – 10 C to + 35 C
- Operating humidity range : up to 80% relative humidity
- Wind tolerance : up to 15 m/s (in operation)
  >15 m/s (parked)
- Earthquake resistance: accelerations up to 2m/ square sec in any direction

As has already pointed out, the telescope building design is such as to minimize any heat trapped within the structure which could degrade the ambient ‘seeing’ (control room outside telescope building, oil cooling system, heat extractor, advanced ventilation of building, advanced shielding and insulation of building). The control system design is such as to offer remote-control operation of the telescope should this be required in the future.

The location of the telescope at the Neraidorahi peak of the 2.3 km mountain Helmos which is located between 3 other mountains exceeding 2 km altitude at the North-central Peloponnese, South Greece is one of the darkest locations in Europe.

- Preliminary seeing measurements have been conducted in the past couple of years (yielding 0.8 arcsec FWHM). More systematic measurements with a DIMM unit will commence as soon as the telescope starts getting installed.

The telescope has been so far equipped (in a very short time) with a number of instruments covering all standard needs in imaging (CCD cameras) and spectroscopy (a low/medium-dispersion and an Echelle high resolution spectrograph) but also a novel instrument for fast CCD photometry.

In particular, the following instruments will be available for the guest observers from 2005:

a. A back-illuminated 1kx1k CCD camera (SITeAB, liquid nitrogen cooling). The pixel size is 24 microns and thus the camera covers a 5 arcmin field-of-view on the sky. We estimate that the camera can reach B=24 in a 5 min exposure (S/N=5) on a dark night.

b. A low/medium dispersion spectrometer with a Red 1200 groove/mm grating centred on 6000Å to give 2.5 Å resolution and 103 Å/mm, a Green 1200 groove/mm grating centred on 5000 Å to give 2.5 Å resolution and 95 Å/mm and a 600 g/mm grating centred on 6000 Å but at 245 Å. The latter covers the wavelength range of 4270 Å -7730 Å. The spectrograph, sponsored by the Universities of Patras and Manchester is designed to work with a dedicated CCD camera (AP7 back-illuminated 0.5kx0.5k chip, thermo-cooled). The spectrograph is constructed by the University of Manchester, similar in design (but much better since 3 gratings will be available instead of one) with the spectrograph of the Liverpool Telescope 2-m in La Palma. The spectrograph can obtain sufficient quality spectra (signal-to-noise 10σ) down to B=19^{th} for point sources.

c. The Manchester echelle spectrograph (MES; R=10^5 for 30 micron pixel, 31.6 grooves/mm echelle grating, resolution ~6 km/s with a 70μm slit). The spectrograph can be used with a cross disperser (grism) or broad filters to isolate separate echelle orders while observations with a single slit or multi-slits can be performed with a maximum slit length of 30 mm (3.4 arcmin), covering the wavelength range of 3900 Å -7500 Å (Meaburn et al. 1984, MNRAS, 210, 463, Meaburn et al. 2003, RMAA, 39, in press).

d. A fast 3-CCD camera (ULTRACAM), designed by the University of Southampton. This obtains simultaneously images in 3 bands (covering a 5x5 arcmin field of view) with a time resolution of 0.1 seconds. Therefore the camera is ideal for probing flickering in transients and AGN.

In summary, the strengths of the new telescope in our Helmos observatory are:

- Modern alt-azimuth design based on new-generation 8-10m large telescopes
- Ability for simultaneously accomodating five (5) instruments
- Remote-control operation to be implemented in the near future
- Large amounts of observing time available using state-of-the art or unique instrumentation
- Increased use of target of opportunity programmes (transient sources)
- Open to specialized visiting instrumentation either for on-sky demonstration/ commissioning or general use
- 1.05 degrees field of view at main cassegrain port
- proximity to East-European Astronomers and neighbor astronomers from the Balkan countries in particular.

It should be stressed that the “Aristarchos” telescope is successfully involved in the OPTICON transnational access activities, together with the major European (some of them international) medium size (2-4m class) telescopes, These particular OPTICON activities, financially backed by the European Union, seek to create a European pool of observing time, to enhance the use of these telescopes by the wider European community and to generate ideas for greater integration programs, shared access to instrumentation and possibly shared strategy for the future.

RESEARCH

The Institute is active in :

- galactic and extra-galactic stellar work,
- optical astrophysics of interstellar matter and galaxies
- extra-galactic X-ray astronomy, and

- cosmology

Some details concerning our fields of interest :

GALACTIC AND EXTRAGALACTIC OPTICAL STELLAR WORK

Topics in these areas, traditionally pursued and currently under investigation by a number of our researchers in the Institute, include:

- **time resolving observations of cataclysmic variable stars, long term photometry of interacting binaries and symbiotic stars**,
- **astrometry of HIPPARCOS visual binaries,**
- **the star cluster system of the LMC, automatic spectral classification of stars in the Magellanic Clouds from objective prism plates, metallicity and age evolution of the Magellanic Clouds, stellar asssociations and stellar complexes in the Magellanic Clouds.**
- **star burst galaxies , star formation and starburst phenomena in galaxies, and**
- **reference multi-wavelength colour-colour and colour magnitude diagrams for stellar population studies in galaxies**

OPTICAL ASTROPHYSICS OF INTERSTELLAR MATTER & GALAXIES

New members of the Institute have been active in this field and will coordinate their activities as team members of a new group, focusing on the systematic study of :

- Dynamic phenomena in the interstellar medium. Ionized gaseous structures i.e. HII regions, ionized loops, supernova remnants (SNRs) and planetary nebulae (PNe), are of great interest because of their important role in the chemical enrichment history of the interstellar medium (ISM) and the star-formation and star-death history and evolution of our Galaxy. Despite the fact that SNRs emit strongly in optical emission lines (e. g. Hα, [O III], [S II], [N II]), a limited number of optical observations has been performed. Planetary nebulae are created during the final stages of evolution of low and medium mass stars. Their main characteristics are the mass loss due to several ejection episodes with different densities and velocities (winds), photoionization of the expanding envelope by the UV radiation of the central white dwarf and interaction between the winds emitted during different stages of evolution. The instrumentation of the 2.3m telescope (CCD cameras and spectrometers) will provide the opportunity to perform detailed optical imaging (through several narrow band filters) and spectroscopic (low dispersion and echelle) observations of a large number of known radio (and/or X-ray) supernova remnants and planetary nebulae (as well as to detect new) and help to study the physical and ionization structure of these nebulosities, detect faint haloes around PNe, find possible interaction with the interstellar medium and study their geometrical effects. Furthermore, due to the fine resolution of ARISTARCHOS instrumentation, detailed correlated maps with other wavelengths (radio, X-ray. Infrared) will provide extra clues concerning their nature...

- Micro-variability of Active Galactic Nuclei (AGN). The 2.3 m telescope will be linked to AGNs photometric monitoring campaigns of simultaneous observations from X-rays to radio wavelengths, in order to provide information of the optical micro-variability that these sources exhibit. Dense sampling and the establishment of light curves in different optical bands will permit the study of the intra-night flux and spectral variability of the source in detail. Both radio-loud (BL Lacs) and radio-quiet (Seyfert) objects will be monitored. Intensive, B, V, R, I observations of BL Lac objects will provide the means to study the intra-night variations and further understand the physical characteristics of their nucleus. The long term B, V, R, I monitoring observations of Seyfert galaxies will permit the study and correlation of X-ray/optical variability as well as the investigation of the origin of optical variations. Thus, optical observations with a sampling interval of ~1-2 min (using ARISTARCHOS/ULTRACAM) will offer us important clues on the acceleration and cooling mechanism of AGN's particles.

- Distribution of stars and dust in galaxies (optical and infrared view) Dust is but a small fraction of the mass of a galaxy, yet it plays a crucial role in galactic evolution. Thus it is of great importance to examine the dust content and the way that interstellar dust is distributed within galaxies. Using optical images we can see the effects of dust in diminishing the stellar light. Using far-infrared/Submillimeter maps of the galaxies – especially now that new and more advanced observing facilities like SIRTF (Space Infrared Telescope Facility) are becoming available – we can detect the dust in emission. Using state-of-the-art radiative transfer models for both the extinction of the stellar light by the dust and the dust emission, we can get a good description of the global properties of the galaxies.

- Active and non-Active galaxies (observations and modeling). Recent dynamical studies suggest that most, perhaps all, galactic bulges contain massive black holes. If so, then why some galaxies show AGN activity and others do not? It is shown that there are differences between active and non-active galaxies in terms of their central morphology. A work under progress deals with optical observations of galaxies (active and non-active) and their modeling using a stellar evolutionary model in order to detect possible differences in global galaxy parameters such as Star Formation Rates, metallicities and related topics.

EXTRAGALACTIC X-RAY ASTRONOMY

The observational X-ray Astronomy team works on the analysis of data from missions such as Chandra (NASA) and XMM (ESA) and, previously, from ROSAT, Ginga, ASCA, RXTE, BeppoSAX. The team has practically developed extensive experience on the data analysis from all X-ray Astronomy missions recently in space. There are strong links and collaboration with well known High Energy Astrophysics Centers worldwide such as, the Goddard Space Flight Center, the Harvard-Smithsonian Center for Astrophysics (US) and the University of Leicester (UK). Many of the research programs have the IAA as the PI which is quite prestigious considering that the above programs are allocated after international competition. The scientific topics studied by the X-ray group include:

- Obscured AGNs. One of the most active research topics is the spectral study of obscured Seyfert-2 galaxies. In particular spectral monitoring observations with the RXTE mission have revealed a wealth of information on the geometry and physical properties of the nuclear region. The team has shown that the column density in the well known Seyfert-2 galaxy Mrk 348 varies with time and that this variation is most probably due to cloud motions (the cloud's distance is less than 1 l.y. from the nucleus) in front of the X-ray source. The standard AGN unification models predict that the AGN with high levels of photoelectric absorption should also present large amounts of optical reddening (due to the molecular torus). This model nicely represents the differences in the optical and X-ray spectra between Seyfert-1 and Seyfert-2 galaxies. At higher redshifts there is now increasing evidence that these models may not hold in all QSOs. For example, an XMM X-ray spectral observation of a QSO at a redshift of z=0.67shows a high amount of photoelectric absorption (N_H~10^23 cm-2 corresponding to 70 magnitudes of optical reddening for a Galactic dust-to-gas ratio) while the reddening measured from the optical spectrum is only 3.5 magnitudes in striking contrast to the standard unification models.

- X-ray surveys. These have as main goal to reveal the nature of the extragalactic X-ray populations and their relation to the X-ray background. The team's survey with ASCA in the 5-10 keV band gave some nearby bright examples of the sources which produce the bulk of the X-ray background. These are obscured low luminosity AGN at low redshift. The work is continuing with the XMM mission. The high effective area of the XMM mission makes much easier the study of the X-ray spectral properties of these sources; moreover, XMM's good spatial resolution (6 arcsec FWHM) facilitates the location of the optical counterparts of the X-ray sources.

COSMOLOGY

Active research areas of the group include:

- Study of the cluster of galaxies internal dynamis, substructures and their cosmological evolution as well as relaxation processes, using multiwavelength observations (ROSAT, XMM, APM, SDSS, 2dF). The analysis of the group shows a large fraction of non-virialized clusters.
- Study of the evolution of density perturbations in different cosmological backgrounds and within different biasing schemes between the galaxy and dark-matter distributions. Furthermore, study of the virialization process of galaxy clusters in cosmological models with a cosmological constant.
- Study of the environment of different types of AGNs in order to identify relations between the AGN activity and the large-scale structure within which the AGNs may be embedded.
- Study of the density and velocity fields of galaxy clusters on large-scales in order to identify the extend and scales of validity of the linear approximation of perturbation theory.

NETWORK AND COMPUTER FACILITIES

Since 1996, the Institute of Astronomy and Astrophysics operates a Local Area Network (LAN) of computers at Pentele site. This LAN is a separate part of the NOANET, the Wide Area Network (WAN) of the National Observatory of Athens. Through the WAN facilities, the Institute is connected with 2Mbps (mega-bits per second) line to the Greek Research Network (GRNET) and, generally, to the Internet community.

There are more than 40 nodes connected to the central switch (CISCO) of the Institute LAN. A dedicated UNIX server (HP) provides network services to IAA and generally to the Internet community. Most used services are the e-mail and POP, the Domain Name System service, the terminal access (ssh, telnet), the file transfer (sftp, ftp), the World Wide Web service, Network Time Protocol, and Network Printing (with two network printers) services.

Few numbers follow as examples of our network services usage. The e-mail server processes about 40.000 incoming and about 20.000 outgoing mails per year. The web-server registered the last season about 5.000 requests per day and about 400 MB (mega-bytes) per day were transferred out.

The IAA LAN nodes include 10 UNIX workstations (HP and SUN), more than 20 desktop PCs (most of them running Linux) and few laptops. A Fiber Optics link connects two desktop PCs in the Newall Telescope Dome to the IAA LAN. We are extensively using general astronomical image processing systems as MIDAS and IRAF, as well as special packages for space observatories and telescopes data processing (XANADU from NASA, CIAO from CfA, and ESA's SAS) on these work places. Our own software is being developed here as well.

There is a small private network set up at Krionerion Astronomical Station. It is mainly used for servicing the observations there. Two desktop PCs, the one with a GPS and with a CCD-camera control system, a network printer and a switch are part of this network. A dial-up connection provides link to the Internet. Now we are setting up a Radio-link for Internet connection at 5.4 GHz and 11 Mbps between the IAA facilities at Pentele, the new Chelmos Observatory and the Krionerion Astronomical Station.
Our computing and network facilities are widely used not only for our research work, but also for educational purposes (students practice, Summer School) and for public outreach (Visitor Center, Almanac, e-Journal).

PUBLIC OUTREACH

The basic Institute windows to the public are the Visitors Centre and our Web site :
www.astro.noa.gr

VISITORS CENTRE

The Visitors Centre of the Institute of Astronomy & Astrophysics resides at Pentele Astronomical Centre (PAC) of the National Observatory of Athens. It was established in 1995 with the financial support of the Greek General Secretariat for Research and Technology (GSRT) under the wider project named “Open Gates”.

The activities of the Visitors Centre include:

- Presentations to elementary school pupils
- Presentations to high school pupils
- Presentations to University students
- Open nights for the public
- Open nights for organized groups
- Communication and science outreach to the mass media
- Organization of seminars and workshops for amateur astronomers
- Creation of educational material
- Astronomical observations of astronomical phenomena that have interest for the public

The Visitors Centre employs for its activities the building that houses the Turner-Newall refractor (62.5 cm, f/14) and a smaller building housing a cantina and a 6 inches Zeiss refractor. The average number of visitors is 12000 –15000 per year.

WEB SITE

One of the activities of the IAA is to provide high-quality educational and cultural services to the public. To this end we have upgraded our web-page **www.astro.noa.gr** to include information not only regarding the educational and research activities that we pursue, but also information regarding the daily celestial phenomena, the phases of the moon, the visibility and position of the planets as well as simulations of the daily motion of stars and constellations.

Furthermore, we have started the publication in Greek of an astronomical on-line journal, entitled "Cosmic Pathways", where astronomers mainly from the IAA, but also from other Greek or foreign institutes, publish edited articles related to modern astronomical issues.

ARISTARCHOS INSTRUMENTATION: Manchester Echelle Spectrometer (MES) and Aristarchos Transient Spectrometer (ATS/PatMan)*

P. Boumis[1], J. Meaburn[2], C.D. Goudis[1,3]

[1] Institute of Astronomy & Astrophysics, National Observatory of Athens, Greece
[2] Jodrell Bank Observatory, The University of Manchester, Macclesfield SK11 9DL, UK
[3] Astronomical Laboratory, Dept. of Physics, University of Patras, 26500 Rio-Patras, Greece

Abstract

We present the two spectrometers which will be installed on the new 2.3 m ARISTARCHOS telescope in Greece. The Manchester Echelle Spectrometer (MES) is a very well known instrument already used successfully at different astronomical sites (i.e. Anglo-Australian, La Palma and San Pedro Martir observatories). This high resolution spectrometer is dedicated to the investigation of extended line-emission phenomena (supernova remnants, planetary nebulae, HII regions, luminous blue variable star's nebulae etc.). On the other hand, the Aristarchos Transient Spectrometer, is a new low-medium resolution spectrometer, that has been developed in order to study relatively bright but transient phenomena like the variability of cataclysmic variable stars, active galactic nuclei, symbiotic stars, the optical flashes of gamma-ray bursts and novae etc.

1. Aristarchos Transient Spectrometer (ATS/PatMan)

Aim of the design: A low-medium dispersion spectrometer has been designed and manufactured specifically to obtain spectra of relatively bright (brighter than 18 mag) but transient phenomena. These can include gamma-ray bursts as soon after the events as possible, the variable spectra of Symbiotic stars, Cataclysmic variables, nuclei of nearby Seyfert galaxies, nearby nova events etc.

Design: To achieve these aims any of three gratings can be driven into the beam with present angles. These are: a Red 1200 groove/mm grating centred on 6000 Å to give 2.5 Å resolution and 103 Å/mm: a Green 1200 groove/mm grating centred on 5000 Å to give 2.5 Å resolution and 95 Å/mm: a 600 g/mm grating centred on 6000 Å but at 245 Å/mm. The detector is a thermo-cooled AP47p CCD with 1024x1024, 13 micron pixels. Ease of operation and rapid serendipitous response are traded for some loss in ultimate sensitivity i.e. the spectra will be dark-current limited rather than read-out noise limited as with a liquid nitrogen cooled CCD. The AP47p CCD can be driven using the parallel port of any Windows PC. The spectrometer's long slit input is fed by 50 fibres (each 50 micron diameter) in a 10 arcsec diameter bundle in the telescope's focal plane. Again, ease and rapid target acquisition are traded for some fibre losses when compared to a traditional long-slit spectrometer. Its optical layout as well as its interior can be seen in Fig. 1(a)-(b).

Outcome: A 'first-light' spectrometer has been designed and manufactured that can be left running permanently for opportunist over-ride observations of transient events. Survey programmes of relatively bright but transient phenomena can also be carried out. It is not intended for use as a traditional low-dispersion spectrometer found on most telescopes.

* *Proceedings 6th Hellenic Astronomical Society Conference, 15-17 September 2003, Penteli, Athens, Greece*

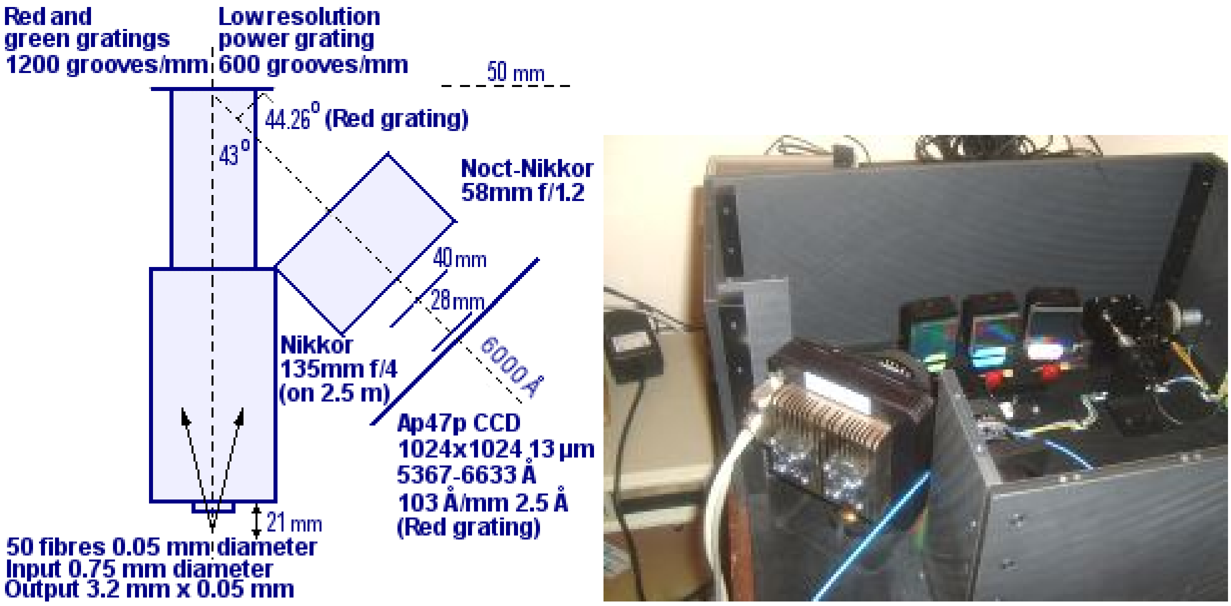

Fig. 1: (a) Optical layout of ATS, designed by J. Meaburn, (b) The interior of ATS

2. Manchester Echelle Spectrometer (MES)

The Manchester Echelle Spectrometer (MES) is a simple spectrometer dedicated to a narrow range of astrophysical phenomena. The first version of MES was commissioned in 1983 on the Anglo-Australian Telescope (AAT – Meaburn et al. 1984), the second version in 1986 and 1987, respectively on the 2.5 m Isaac Newton Telescope (INT) and 4.2 m William Herschel Telescope (WHT – Meaburn & Bryce 1993) and the last version in 1995 on the 2.1 m San Pedro Martir telescope (SPM – Meaburn et al. 2003). Its optical & mechanical layout is shown in Figs.2 & 3. In its primary mode, a single order of its echelle grating (nominally $\delta = 63.54^{o}$ with 31.6 grooves mm^{-1}) is isolated by a broad, efficient, three-period interference filter eliminating the need for cross-dispersion. Consequently, its primary use, is to obtain spatially-resolved profiles of individual emission lines from faint extended sources emitting in the range 3900-9000 Å with a spectral resolving power of $\lambda/\Delta\lambda \leq 10^5$. Several secondary modes are available. A direct image of the field can be obtained by both the insertion of a clear area to replace the slit and of a mirror before the grating. For one thing, precise slit positions against images of extended sources can be obtained using this facility. Also, insertion of a prism along with the plane mirror permits longslit, low-dispersion (76.3Å mm^{-1}) spectra to be obtained.

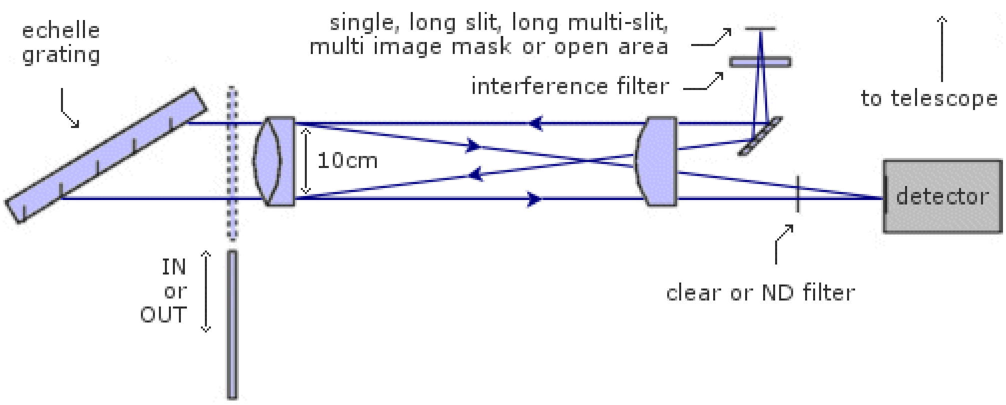

Fig. 2: Optical layout of MES

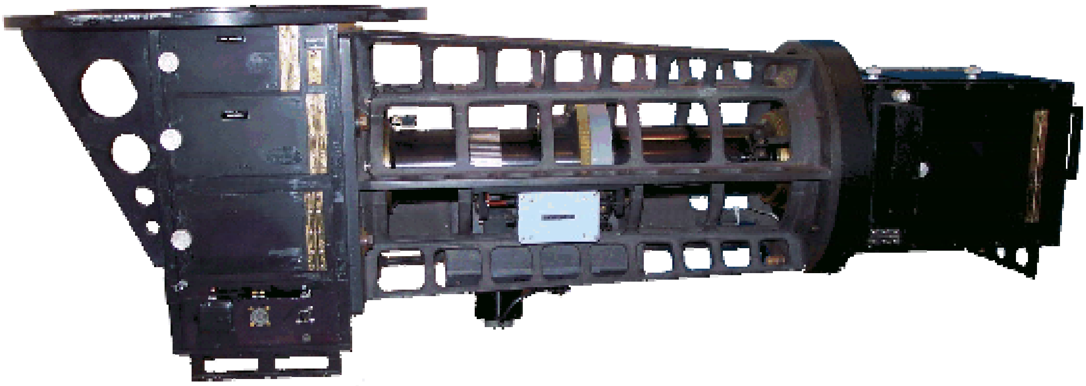

Fig. 3: Mechanical layout of MES

3. Recent Observations & Results using MES

In order to give an idea of what can be observed using MES, a sample of recent observations taken using this spectrometer combined with the AAT and SPM telescopes can be seen below.

3.1 "RX J08520.4622" A young X-ray Supernova Remnant in Vela

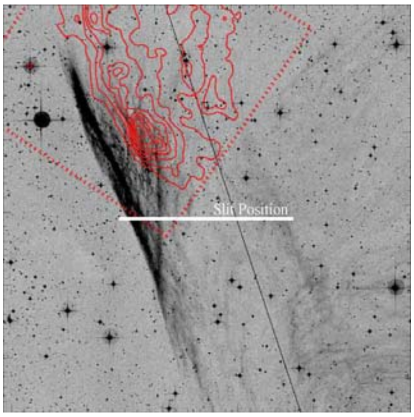

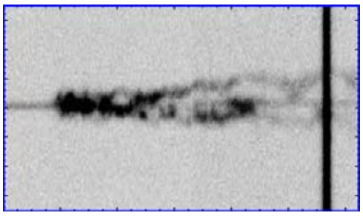

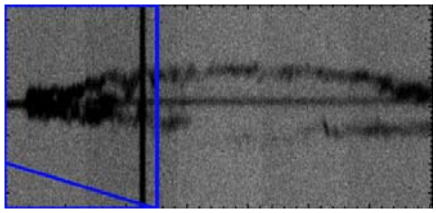

Fig. 4: (left) RCW 73 showing MES slit position and contoured Chandra ACIS X-Ray data.

(above): Combined [O III] 5007 Å pv-arrays of five overlapping slit positions shown in the left figure and zoomed region to show details in the brightest velocity components in the eastern edge of RCW 37.

3.2 The ellipsoidal planetary nebula Sa 2-21

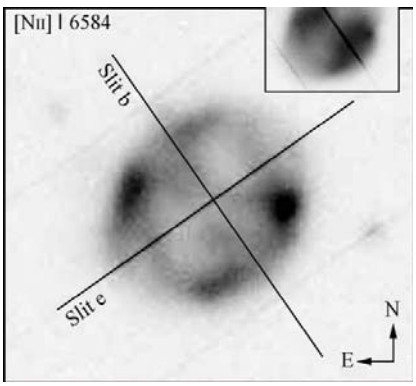

Fig. 5: (left) Observed MES images of Sa 2-21 showing slit positions. (right) Observed pv arrays of the first ellipsoidal planetary nebula known to have rings (Harman et al. 2003).

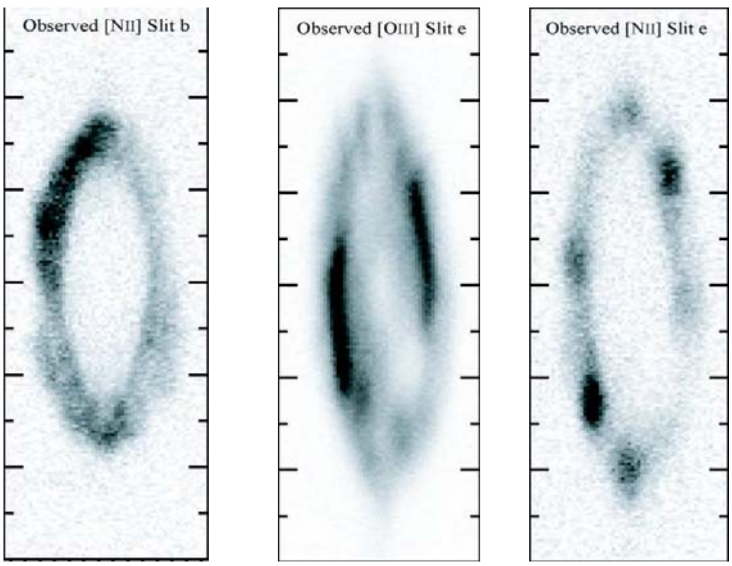

3.3 High-velocity knots in PN "MyCn 18"

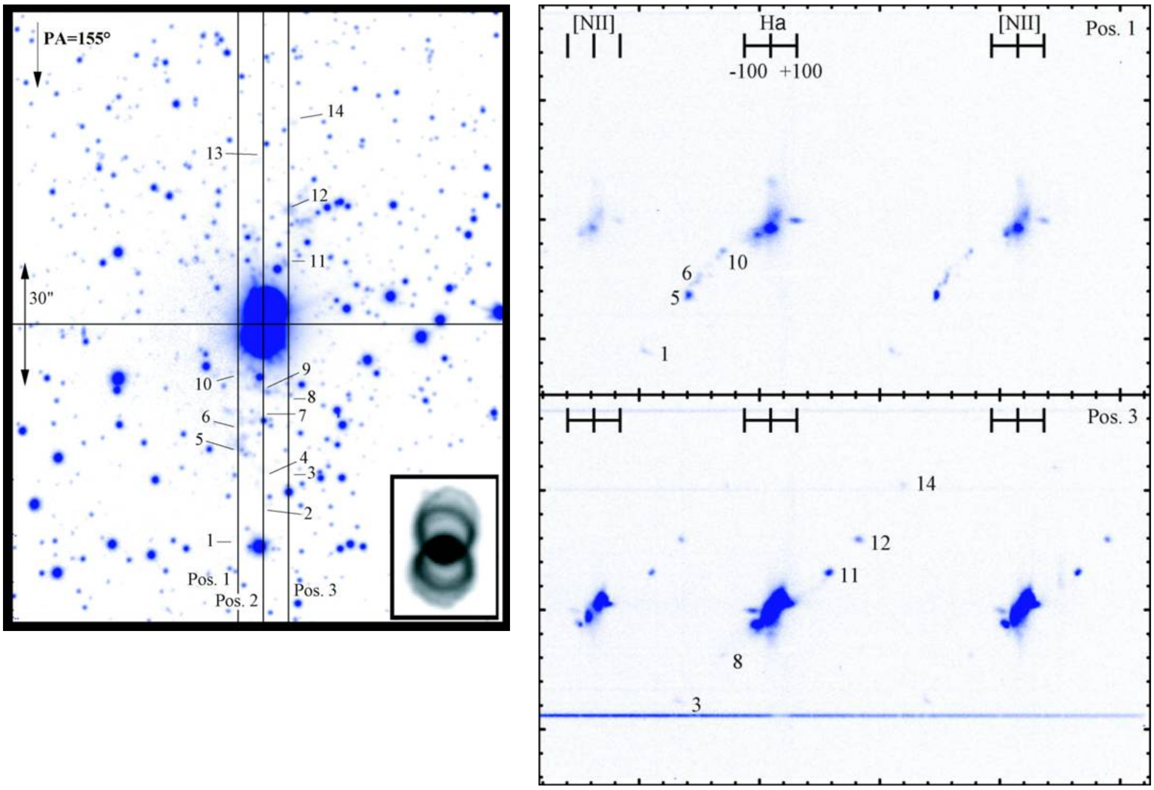

Fig. 6: (left) The PN MyCn 18 showing slit positions and hypersonic knots, (right) position-velocity (pv) data from the left (Pos. 1) and right (Pos. 3) slit (O'Connor et al. 2000)

References

Harman, D.J., Bryce, M., Redman, M.P. & Holloway, A.J., 2003, MNRAS, 342, 823

Meaburn, J., Blundell, B., Carling, R., Gregory, D.E., Keir, D.F. & Wynne, C.G., 1984, MNRAS, 210, 463

Meaburn, J. & Bryce, M., 1993, Opt. Astr., 32nd Herst.Conf., p.9

Meaburn, J., Lopez, J.A., Gutierrez, L., Quiroz, F., Murillo, J.M., Valdez, J. & Petrayez, M., 2003, RMAA, 39, 2, in press

O'Connor, J.A., Redman, M.P., Holloway, A.J., Bryce, M., Lopez, J.A. & Meaburn, J., 2000, ApJ, 531, 336

Redman, M.P., Meaburn, J., Bryce, M., Harman, D.J. & O'Brien, T.J., 2002, MNRAS, 336, 1093

SKINAKAS OBSERVATORY: INSTRUMENTATION AND HIGHLIGHTS*

I. Papamastorakis[1,2], D. Hatzidimitriou[1,2]

[1] Department of Physics, University of Crete, P.O. Box 2208, 710 03 Heraklion, Crete, Greece
[2] Foundation for Research and Technology, Hellas, Institute for Electronic Structure and Lasers, P.O. Box 1527, 711 10 Heraklion, Crete, Greece

Abstract

We present the facilities and research activities of the Skinakas Observatory**.** The Observatory is operated jointly by the University of Crete, the Foundation for Research and Technology-Hellas and the Max-Planck Institute for Extraterrestrial Physics in Garching, Germany. The operational instrumentation of the 1.3m Telescope includes an auto-guider, three CCD cameras and a focal reducer, which more than doubles the field of view of the telescope and which also allows low-resolution spectroscopic measurements. An adaptive optics system and a high resolution echelle spectrograph are under construction. Highlights of the main scientific results achieved with the Skinakas Observatory Telescopes are also described.

1. Skinakas Observatory – The site

1.1 The location

Skinakas Observatory (Longitude 24^o 53 ' 57 " East, Latitude 35^o 12 ' 43 " North) is located on the Ida mountain in Central Crete at an altitude of 1750m, 25km line-of-sight distance and 60km by road from the city of Heraklion.

In the figure to the right, an aerial photograph of the Skinakas Observatory is shown. On the right-hand side, one can see the 1.3m telescope building (white dome) and next to it the visitor-center building.
In the centre lies the guesthouse, to the left of it the 0.3m flat-field telescope building and further to the left the photovoltaic power plant.

1.2 Seeing measurements at Skinakas Observatory

Using a two-aperture Differential Image Motion Monitor (DIMM), it was shown that the Skinakas Summit is an excellent site from the point of view of atmospheric seeing – in fact one of the best known so far in the Mediterranean area. The seeing observations took place from the beginning to the end of randomly chosen astronomical nights from June to September 2000 and from May to June 2001. Extremely good seeing values were measured (0.4”) often, with the best being near 0.23”. The median seeing during the campaigns of years 2000 and 2001 was 0.64” and 0.69”, respectively.

* *Proceedings 6th Hellenic Astronomical Society Conference, 15-17 September 2003, Penteli, Athens, Greece*

2. Instrumentation

2.1 Brief Technical Description of Skinakas Observatory Telescopes

The 130cm telescope has a modified Ritchey-Chretien design and an equatorial mount.

The main mirror has an aperture of 129cm, while the secondary, of 45cm. The focal ratio of the telescope is 7.64. The mirrors were all constructed by Carl Zeiss Oberkochen, while the telescope mount by DFM Engineering.

The telescope is equipped with an autoguider, with an off-axis guiding system, constructed by Baader Planetarium.

The 30cm telescope is a Schmidt- Cassegrain flat field Telescope, with an equatorial mount. It has an aperture of 30cm, a focal ratio of 3.2, a field of view of 1.5 degrees, and it is also equipped with an autoguiding system.

2.2 CCD cameras

There are four nitrogen cooled CCD cameras:

(a) A front-illuminated Photometrics Thomson chip, 1024 x 1024, with 19 μm pixels,
(a) A back-illuminated ISA, SITe chip, 2000x800, with 15 μm pixels, and
(b) Two back-illuminated Photometrics, SITe chips, 1024x1024, with 24 μm pixels.

There are also three general purpose cameras (SBIG: ST4, ST 7, ST8).

2.3. Focal Reducer

A Focal Reducer is mounted to the 1.3m telescope. The Focal Reducer can be used in two different configurations:

1. In the imaging mode, the focal length of the telescope is reduced by a factor of 1.87, enlarging, by the same factor, the imaged area of the sky on the CCD. A Filter Wheel with 6 filter positions is integrated to the Focal Reducer.
2. In the spectroscopy mode, a reflection grating is introduced in the collimator path. Using different gratings, resolution ranging from ~1Å/pixel to ~20Å/pixel is achievable, with a 15μm pixel CCD camera. A Slit Wheel offering 6 positions with slit widths: 80μm, 160μm, 320μm and 640μm is part of this configuration.

2.4 Filters

A large selection of 27 filters can be used for imaging. These include standard *U, B, V, R, I* filters, Strömgren filters, and interference filters at specific lines (e.g. HeI5876, Ha 6563 etc).

2.5 Instruments under construction

An adaptive optics system and a high resolution fiber-fed echelle spectrograph with a Zeeman analyzer are currently under construction.

3. Highlights of Skinakas Research

Research at the Skinakas Observatory covers various fields of Astronomy. The main observing programmes include:

- Variability studies of Active Galactic Nuclei (AGN).

- Surface photometry of clusters of galaxies.
- Optical identification of X-ray sources.
- Gravitational lenses.
- Structure of spiral galaxies.
- Photometry of star clusters.
- RR Lyrae variables.
- Photometric and spectroscopic investigation of gaseous nebulae
- (Supernova remnants and planetary nebulae).
- Spectroscopic investigation of X-ray sources in Local Group Galaxies
- X-ray binary systems including high mass X-ray binaries,
- black hole candidates and cataclysmic variables.
- Search of extrasolar planets.
- Interaction of cometary tails with the solar wind.

Many of the Skinakas projects are pursued as collaborations between astronomers from Crete and from the Max-Planck Institut, but also with many other astrophysicists and observatories around the world. Forefront research in highly interesting objects like AGN, requires coordinated observations in several wavelengths. Especially important are simultaneous observations in X-rays and optical wavelengths. The Skinakas Observatory uses a significant percentage of the observing time for simultaneous observations with X-ray space observatories such as RXTE, XMM-Newton and CHANDRA.

3.1 Active Galactic Nuclei

'Active Galactic Nuclei' (AGN) exist in the central regions of approximately 10% of all the galaxies in the Universe. Their size is a few light years, i.e. comparable to the distance of the nearest star to the Sun. At visible wavelengths, the energy that they emit is 10-100 times more than the energy emitted by all the stars in our Galaxy. What is even more interesting is that their emission is variable, and the amplitude of the observed variations increases towards shorter wavelengths.

Today, we believe that the engine of the AGN consists of a massive black hole (106 – 109 solar masses) and a gaseous disk around it, which feeds it with matter (with an accretion rate of a few per cent of the Eddington limit). As the matter falls in, gravitational power is released and large amounts of energy are liberated in the form of radiation. However, many details are still missing.

One way to investigate the physical processes that operate in the central region of AGN is to study their variations in different wavelengths. Quite a few projects to this aim have taken place at the Skinakas Observatory the last few years. For example, the narrow-line Seyfert 1 galaxy Ark 564 was monitored in 2000 for a period of 20 days in the B, V, R, and I optical bands. When combined with simultaneous X-ray observations, the data showed a complex X-ray/optical correlation, a result that challenges recent reprocessing models of AGN. Furthermore, ten BL Lac objects (one of the most peculiar classes of AGN) were observed regularly in the years between 1999 and 2002. Each object has been observed for at least 4-5 nights, in more than one optical band (usually B and I). The observations resulted in almost evenly sampled light curves, with a sampling interval of a few minutes. Because of the dense sampling and the availability of light curves in more than one band, the acquired data give us the opportunity to study the intra-night flux and spectral variability of these objects in great detail. Skinakas Observatory has also participated in many international observational campaigns of radio loud AGN, like the WEBT (Whole Earth Blazar Telescope) campaigns of

BL Lac (1999-2002), of S5 0716+714 (2000), and the recent campaigns of AO 0235 and 3C66A (2003). Finally, monitoring observations of 12 radio-quiet quasars and 12 compact steep-spectrum radio-loud quasars were carried out in 2003. The observations lasted for a few weeks, and the objects were observed in various optical bands. The resulting light curves will allow us to investigate accurately the variability dependence on luminosity, redshift and rest-frame wavelength.

3.2 Unknown X-ray sources identified from Skinakas Observatory

X-ray observations can only be carried out at very high altitudes because of absorption of X-rays by the Earth's atmosphere. Thus, the exploration of the X-ray sky started in the beginning of the 60's, only after rockets capable of lifting scientific payloads above the atmosphere became available. The sources that were first observed had not been predicted by astrophysicists. First detections included supernova remnants, neutron stars and black holes in Galactic binary systems, active nuclei in distant galaxies and the enigmatic X-ray background radiation which fills the whole Universe. Since then, great effort has been devoted to the study of the nature of the discrete sources that make up the X-ray background radiation.

Deep B and R observations of 35 regions in the sky were performed at Skinakas Observatory in the period between 2001 and 2002. These regions were selected from the ASCA 5-10 keV 'SHEEP' survey, and have already been observed by the NASA X-ray satellite 'CHANDRA'. The Skinakas observations allowed us to identify the optical counterpart to the X-ray source, and measure its magnitude. Subsequent optical spectroscopic observations at CTIO and KPNO will allow us to understand the nature of the X-ray sources in these regions. So far, most objects appear to host an AGN, but the optical observations reveal an interesting variety of properties.

3.3 Transparency of spiral galaxies: A definitive answer to a long standing question

Dust is but a small fraction of the mass of a galaxy, yet it plays a crucial role in galactic evolution. It is on the surface of dust grains that molecules form. This gives rise to the giant molecular clouds, which are a prominent component of the interstellar medium in spiral galaxies. Dust plays a crucial role in the collapse and cooling of clouds and the subsequent formation of stars. Thus, the study of how much dust there is in a galaxy and how it is distributed, forms a key part of any detailed study of galactic evolution, since the star-forming process is so fundamental.

For many years, the effects of dust on our understanding of the global properties of spiral galaxies have been a matter of debate in the astronomical community. Using optical observations taken from Skinakas Observatory and analyzing them with a realistic model of spiral galaxies, we were able to give definite answers to these long standing questions.

Our analysis has shown that typical spiral galaxies, galaxies like our own Galaxy, would be transparent if viewed face-on, meaning that dust has little effect on our understanding of the global properties of galaxies. It has also shown that the total amount of dust in galaxies is about ten times more than previously thought. This has now been confirmed by recent observations in the infrared by the ISO satellite and at submillimeter wavelengths by the SCUBA bolometer. Finally, another important result is that the dust properties are similar to those in our own Galaxy, which indicates a universal behavior of the dust.

3.4 Globular clusters of stars in our Galaxy

Globular clusters are massive, almost spherical conglomerates of hundreds of thousands of stars of different mass, which were created almost at the same time and from the same original giant molecular cloud. These objects are amongst the oldest stellar systems in our own Galaxy and in the Universe in general. They are therefore treated as fossils for the study of the early stages of galaxy formation and evolution.

At Skinakas Observatory we have initiated a comprehensive photometric study of globular clusters in the Milky Way Galaxy with the purpose of improving our knowledge of the basic physical parameters that characterize these objects (i.e. age, metal abundance, distance, reddening). Additionally we have launched a survey of a specific type of variable stars in these systems, named RR-Lyrae variables, which provide valuable information on the local distance scale.

During this project, we have discovered one of the most metal poor and oldest globular clusters (namely NGC 6426) in our Galaxy. This discovery has important implications for the formation of the Milky Way and for the age of the Universe in general.

3.5 Supernova remnants: New detections from Skinakas Observatory

The shell of gas produced by a supernova explosion is traveling for tens of thousands of years, with an ever decreasing velocity, until it mixes with the interstellar medium and its surface brightness becomes so low that we cannot detect it anymore. Modeling the observed radiation is a difficult problem since it involves radiation physics, hydrodynamics, and the interstellar environment. The existing models allow us to compare the observational data with their predictions. Observations of supernova remnants at various wavelengths allow us to study their evolution and the related physical processes. The physical conditions studied are unique and cannot be reproduced in any laboratory. In addition, we can study the physical and chemical state of the interstellar medium and how a supernova explosion influences the recycling of heavy elements in galaxies and star formation.

Observations from Skinakas Observatory have led to the discovery of optical emission from several supernova remnants (e.g. CTB 80, G65.3+5.7), as well as to the detection of a few previously unknown remnants.

3.6 Planetary Nebulae: Mapping their physical structure

A program was initiated at Skinakas Observatory to observe in detail planetary nebulae (PNe) and construct maps of the projected two-dimensional distribution of the electron temperature and electron density. In addition, the optical images have been used to study the ionization state and structure of the nebula, to search for possible abundance variations, and also for small scale structures (e.g. NGC 6781). Also, deep images of aging PNe have been successfully used to study their interaction with the ambient interstellar medium.

3.7 New Planetary Nebulae in the Galactic Bulge

Many new Planetary Nebulae (PNe) were discovered at Skinakas Observatory during an oxygen emission line ([OIII]5007 Å) survey of the Galactic Bulge and resulted in increasing the already known number of PNe in the northern Galactic Bulge by 40%. The 0.3 m telescope was used to detect the objects and the 1.3 m telescope to study them in detail.

The galactic PNe are always under intensive investigation because of the intrinsic difficulties in determining their properties (such as their number, distance, chemical composition, morphology and kinematics). They play a very important role in the chemical enrichment history of the interstellar medium as well as in the star formation history and evolution of our Galaxy. The Galactic Bulge extends over a region of galactic longitude l~±150 and galactic latitude b~±100. Most PNe emit strongly in the optical (such as in the Hα and [OIII] 5007 Å emission lines). The [OIII] line was chosen for our survey, taking into account the fact that a

PNe survey in the bulge of our Galaxy has never been done in the past using this emission line except for a limited number of images.

3.8 X-Ray binary star systems

X-ray binaries consist of a compact, collapsed object orbiting a normal star, i.e., a star still converting hydrogen into helium through thermonuclear reactions. The compact companion can be a blackhole, a neutron star, or, a white dwarf. Be/X-ray binaries belong to the category of massive X-ray binaries where the normal star is significantly more massive than our Sun. Their X-ray emission is highly variable and most of them are transient. The two observational properties in the optical band that characterize a Be star are the presence of emission lines in their spectra, and an infrared excess when they are compared to B stars of the same spectral type.

At Skinakas Observatory we have been performing long term, photometric and spectroscopic monitoring observations of these systems since 1999. Together with X-ray observations, the Skinakas Observations showed that the long-term (several months) optical photometric variability is dominated by the loss and re-formation of the circumstellar disk, which correlates with the X-ray emission. Therefore, for the first time, we were able to determine the structure and distribution of the circumstellar material in Be stars. Furthermore, spectroscopic observations allowed us to study the variations in the profiles of the emission lines in the spectra of Be/X-ray binaries. We were able to confirm that profile variations are caused by the precession of a density perturbation in the circumstellar envelope of the Be star as suggested by current theoretical models.

In summary, the Skinakas Observatory photometric and spectroscopic observations of Be/X-ray binaries allowed us to investigate in detail the structure, the motion and the evolution of density perturbations in the circumstellar disks of these systems.

3.9 Flaring light from a black hole reveals a new phenomenon

Very high time resolution, simultaneous measurements in X-rays from space and in the optical from Skinakas Observatory revealed new insight in the immediate proximity of a stellar black hole in our Galaxy. The object, XTE J1118+480, is in the constellation of Ursa Majoris at a distance of 6,000 light years. It is presumably a black hole 6 times the mass of our Sun. The black hole is a member of a binary star system. Material streams from the other member of the system, which is a normal star, to the black hole and builds an accretion disk around it. At the same time, there is an outflow of gas material perpendicular to the accretion disk under the influence of magnetic fields. When larger gas clouds fall down to the black hole, giving rise to the X-ray light, waves are built in the up-streaming gas, which radiates the flaring optical light.

X-ray flashes from this system have been recorded by the Rossi-XTE Space Telescope, whereas optical flashes with about a tenth of second delay have been observed from Skinakas, using the 1.3 m telescope and the high resolution timing detector OPTIMA of the Max-Planck-Institut für Extraterrestrische Physik.

The interpretation of these observations is that the out-streaming gas should have a speed of less than 10 percent of the speed of light and the optical emission should originate in about 20,000 km distance from the black hole. The time delay of the optical light to the X-ray eruption arises through a time of flight delay.

This is the first observation of a relatively slow gas out-streaming from the vicinity of a black hole. Until now, only strongly collimated ultrafast jets were known.

3.10 The interaction of cometary tails with the solar wind

As the magnetized plasma of the solar wind interacts with the ionized (plasma) tail of the comet, long living regular structures of knots and density enhancements are produced.
High quality consecutive CCD images of the plasma tails of the comets Austin and Hale-Bopp taken with the 0.3 m Skinakas telescope and special filters, have been successfully used to get new significant insight into the relevant physical processes in the cometary tails, as the formation and dynamics of the plasma structures.

4. Student Education in Astronomy

The facilities of the Skinakas Observatory are widely used for student education in Astronomy. Many undergraduate and graduate students take advantage of the opportunity to participate in research projects based on optical observations performed at Skinakas. In fact, most of the projects highlighted above have had active student participation.

5. Observatory Open Days

Skinakas Observatory offers a number of open days each year. This gives the opportunity to visitors to be introduced to the operation of the observatory, to get informed about the latest achievements in Astrophysics and to observe through the telescope.
The open days of Skinakas Observatory have found enthusiastic response: More than a thousand people visit the observatory each year, where they are offered conducted tours. This way, not only a great number of people get more familiar with modern science and technology, but also the research done in Greece becomes widely known.
The observatory open days are announced at the Skinakas web site http://www.skinakas.org.gr

Acknowledgements

The matter presented in this paper is the result of long-standing collaborative work of several astronomers, engineers and technicians over the past years. Their efforts are most sincerely acknowledged by the authors.

THE IMPORTANCE, USEFULNESS, AND NECESSITY OF A RADIO TELESCOPE IN GREECE
Vision, Perspectives, and National Response*

N.K.Spyrou

Section of Astrophysics, Astronomy and Mechanics, Department of Physics, University of Thessaloniki, 41.24 Thessaloniki Greece

ABSTRACT

The importance, usefulness and necessity of the installation of a radio telescope in Greece are explained, the efforts made up to now towards such an installation are described, the response of the Greek scientific community is analyzed, and the vision and perspectives of such a project are emphasized.

Στο πρόσωπο του συναδέλφου Καθηγητή κ. Χ. Γούδη εκφράζω, και από την θέση αυτή, τις ευχαριστίες μου προς τους αρμοδίους και υπευθύνους της θεματικής ενότητας Infrastructure of Astronomy in Hellas (Greece) του σημερινού συνεδρίου της *Ελληνικής Αστρονομικής Εταιρείας* (ΕΛ.ΑΣ.ΕΤ.) και προς όλα τα μέλη του *Ινστιτούτου Αστρονομίας και Αστροφυσικής* του Εθνικού Αστεροσκοπείου Αθηνών για την πρόσκλησή τους γι' αυτήν την ομιλία.

Σύμφωνα με τον τίτλο της, η ομιλία μου θα έχει ως αντικείμενο τη γενική ιδέα, φιλοσοφία και οραματισμό για την εγκατάσταση ενός Ραδιοτηλεσκοπίου (Ρ/Τ) στην Ελλάδα, για τις μέχρι τώρα ακαδημαϊκές ενέργειες προς την κατεύθυνση αυτής της εγκατάστασης, για την μέχρι τώρα πράγματι αισιόδοξη και ελπιδοφόρα εθνική ανταπόκριση και, τέλος, για τις πιθανές μελλοντικές ενέργειές μας.

Δεν θα σας απασχολήσω με ειδικότερα προβλήματα τεχνικής φύσεως, τα οποία και εμπίπτουν στις υποχρεώσεις ειδικότερων συναδέλφων-ομιλητών. Ανεξάρτητα, όμως, από το θέμα της ειδίκευσης του καθενός, ένα μέλος της επιστημονικής κοινότητάς μας είναι σε θέση, θα μπορούσα να πω *πρέπει* να έχει άποψη για τα ενδιαφέροντα την ευρύτερη επιστημονική κοινότητα θέματα και προβλήματα.

Βέβαια, αυτά τα προβλήματα δεν είναι ούτε λίγα ούτε ασήμαντα και η προτεραιότητα του καθενός εξαρτάται από το την οπτική γωνία θεώρησής του και από τα ενδιαφέροντα και επιδιώξεις του θεωρούντος. Από συζητήσεις που είχα και με άλλους συναδέλφους μου και του δικού μας *Εργαστηρίου Αστρονομίας* αλλά και άλλων Πανεπιστημίων και Ερευνητικών Ινστιτούτων της χώρας μας και της αλλοδαπής, φάνηκε ότι ένα γενικότερου ενδιαφέροντος ανοιχτό πρόβλημα, το οποίο θα έπρεπε να απασχολήσει όχι μόνον την αστρονομική αλλά την ευρύτερη επιστημονική κοινότητα της χώρας μας, είναι η εγκατάσταση ενός ραδιοτηλεσκοπίου στην χώρα μας και αυτό, φυσικά, ανεξάρτητα από το τηλεσκόπιο «Αρίσταρχος».

Από τις ίδιες αυτές συζητήσεις προέκυψαν, τελικά, και μερικές ιδέες για τη διαδικασία που θα έπρεπε να ακολουθηθεί και τη στρατηγική που θα έπρεπε να εφαρμοσθεί κατά την διεκδίκηση ενός ραδιοτηλεσκοπίου. Αυτά θα σας τα περιγράψω εν συντομία.

Δεδομένης, λοιπόν, της προϊστορίας του θέματος, κάποιος έπρεπε να αναλάβει την πρωτοβουλία, ώστε να αρχίσει *εκ νέου* η διαδικασία κάπου, π.χ. στην Θεσσαλονίκη. Και ποιό αρμοδιότερο για την περίπτωση σώμα στην Θεσσαλονίκη από τον *Τομέα Αστροφυσικής Αστρονομίας και Μηχανικής* (ΑΑΜ) του Πανεπιστημίου Θεσσαλονίκης;

Έτσι, ως πρώτο βήμα, ήλθε ως θέμα η έκφραση γνώμης των μελών του Τομέα ΑΑΜ για την αναγκαιότητα και χρησιμότητα της εγκατάστασης ενός ραδιοτηλεσκοπίου στην χώρα μας. Η απόφαση της Γενικής Συνέλευσης των μελών του Τομέα ΑΑΜ, μετά από διεξοδική συζήτηση, ήταν ομόφωνη και θετική, το ενδιαφέρον δε και εν πολλοίς αναμενόμενο χαρακτηριστικό της συζήτησης ήταν η ομόθυμη υποστήριξη της πρότασης, ανεξάρτητα από την χρηματική αξία, τον τόπο εγκατάστασης, τον τρόπο διοίκησης του ραδιοτηλεσκοπίου και άλλα ανάλογα ερωτήματα, τα οποία, όμως, αν και σοβαρότατα, θεωρήθηκαν ως μεταγενέστερα προβλήματα. Αντικειμενικός σκοπός της συζήτησης ήταν

* *Proceedings 6th Hellenic Astronomical Society Conference, 15-17 September 2003, Penteli, Athens, Greece*

το να εξετασθεί αν η εγκατάσταση ενός ραδιοτηλεσκοπίου στην χώρα μας είναι χρήσιμη, αναγκαία και επιβεβλημένη, κάτι που στη συγκεκριμένη συνέλευση επετεύχθη.

Στην ίδια συνέλευση και στο ανωτέρω πνεύμα συζητήθηκαν και τα επόμενα βήματα, η περαιτέρω στρατηγική που έπρεπε να ακολουθηθεί. Είναι προφανές, ότι το Εργαστήριο Αστρονομίας του Πανεπιστημίου Θεσσαλονίκης, μπορεί μεν να επανέφερε το όλο θέμα, μόνο του, όμως, δεν ήταν δυνατόν και ούτε θα έπρεπε να επωμισθεί την όλη ευθύνη της διεκδίκησης. Πράγματι, για την υλοποίηση ενός σχεδίου σαν κι αυτό, κατ' εξοχήν ισχύει το «Η ισχύς εν τη ενώσει». Άρα έπρεπε να ακολουθήσει η ενημέρωση όλων των κατ' αρχήν ενδιαφερομένων για την εγκατάσταση ενός ραδιοτηλεσκοπίου στην χώρα μας. Αυτό σημαίνει, ότι έπρεπε να ενημερωθεί όλη, *και το τονίζω αυτό, όλη* η αστρονομική κοινότητα της χώρας μας.

Αλλά, από πλευράς στρατηγικής, και αυτό, αν και είναι το πρώτο απαραίτητο εκτός Εργαστηρίου Αστρονομίας βήμα, δεν θα έφθανε. Επειδή, προφανώς, ένα ραδιοτηλεσκόπιο είναι ένα διεπιστημονικό όργανο ενδιαφέροντος και άλλων επιστημονικών περιοχών πέραν της αστρονομικής, θα έπρεπε και όσοι ανήκουν σε μη αστρονομικές περιοχές ενδιαφερόμενες για ένα ραδιοτηλεσκόπιο, να ενημερωθούν για το θέμα αυτό και να ζητηθεί η γνώμη και η συμπαράστασή τους. Και στην περίπτωση αυτή, ακόμη πιο έντονα ισχύει το «Η ισχύς εν τη ενώσει».

Στο σημείο αυτό θέλω να τονίσω, ότι η γνώμη μου είναι, χωρίς αυτό να σημαίνει ότι δεν υπάρχουν και άλλοι τρόποι ενέργειας, όπως αυτός που ακολουθήθηκε στην επιτυχή διεκδίκηση του τηλεσκοπίου «Αρίσταρχος», ότι για ένα πρόγραμμα αυτής της εμβέλειας, δεν θα ήταν αποδοτικό, ο Τομέας ΑΑΜ να απευθυνθεί κατ' ευθείαν στις αρμόδιες κυβερνητικές αρχές και μάλιστα μόνον σ' αυτές.

Με απόφαση, λοιπόν, του Τομέα ΑΑΜ εστάλη μια σχετική επιστολή του Διευθυντή του Τομέα ΑΑΜ σε αστρονομικούς φορείς αλλά και σε διάφορους μη κυβερνητικούς-πολιτικούς-κομματικούς, κατά τη γνώμη μας κατ' αρχήν και εν δυνάμει ενδιαφερόμενους φορείς.

Πριν σας διαβάσω αυτήν την επιστολή, ακριβώς για να φανεί η διαχρονικότητα του εξεταζόμενου θέματος, θα ήθελα να σας θυμίσω δύο γεγονότα:

1) Πριν από δέκα χρόνια ακριβώς, γιορτάσθηκαν τα πενήντα χρόνια του Εργαστηρίου Αστρονομίας του Πανεπιστημίου Θεσσαλονίκης (*Φέτος είναι η επέτειος των εξήντα χρόνων λειτουργίας του*). Κατά την επίσημη τελετή του εορτασμού, ως Διευθυντής του Τομέα μας τότε, είχα αναφέρει δύο μελλοντικούς στόχους του Εργαστηρίου Αστρονομίας, από τους οποίους

α) Ο ένας ήταν η δημιουργία ενός *Πλανηταρίου*, κάτι που έλειπε στη Βόρεια Ελλάδα και το οποίο ήταν τόσο μεγάλης σημασίας για την ενημέρωση του ευρύτερου κοινού. Ήδη, αυτή η δημιουργία είναι πλέον γεγονός, στο πλαίσιο της πραγματοποίησης ενός πολύ μεγαλύτερου και φιλόδοξου έργου στην Θεσσαλονίκη, που λέγεται *Κέντρο Διάδοσης Επιστημών και Μουσείο Τεχνολογίας*, περιλαμβάνει *Πλανητάριο, Κοσμοθέατρο* και *Προσομοιωτή* και στην πραγματοποίηση του οποίου το Εργαστήριο Αστρονομίας είχε και έχει σημαντική συνεισφορά .

β) Ο δεύτερος ήταν η εγκατάσταση ενός ραδιοτηλεσκοπίου στη Βόρεια Ελλάδα με πιθανές περιοχές εγκατάστασης, είχα αναφέρει τότε, το Πανεπιστημιακό Κτήμα στο Χολομώντα, τα Πιέρια και το Βέρμιο. Είναι ελπιδοφόρο το γεγονός, ότι δέκα χρόνια μετά, το θέμα συζητείται επισήμως στο επίσημο Συνέδριο των Ελλήνων Αστρονόμων.

2) Το δεύτερο γεγονός που επιθυμώ να σας θυμίσω είναι , ότι η εγκατάσταση ενός ραδιοτηλεσκοπίου στην Ελλάδα είχε απασχολήσει την Ελληνική αστρονομική κοινότητα και παλαιότερα. Το 1999 στο συνέδριο «Αστρονομία 2000+» της Εθνικής Αστρονομικής Επιτροπής, η εξωτερική επιτροπή ειδικών στην αναφορά της προς την Εθνική Αστρονομική Επιτροπή ως μία από τις κύριες προτάσεις της (Major Recommendations) για την ενίσχυση της *Παρατηρησιακής Αστρονομίας* είχε συμπεριλάβει και την εγκατάσταση ενός ραδιοτηλεσκοπίου στην Ελλάδα. Η σχετική αναφορά στη σελίδα 12 ήταν**:** *Greece should also participate in international collaborations such as the new European Very Long Baseline Array research by constructing a radio telescope, possibly on the island of Crete, to provide the longest baseline. A study of Greece's participation should be conducted. (*As it is known) *Very Long Baseline Interferometry (VLBI) is the world's foremost technique to achieve unprecedented angular resolutions in the study of radio emitting cosmic sources and would provide Greece with participation in forefront research. Such a project can indeed be interdisciplinary since it can also be useful for the study of geology (movement of tectonic plates) and seismology. A radio telescope with dimensions of 30 to 40 meters would be desirable, since such an antenna could also be used as a stand alone useful instrument*

and can also participate in space VLBI. Such a project would use talents of electrical engineers from Greece and would create a beneficial cooperation in various disciplines, including industry.

Μετά από αυτήν τη σύντομη ιστορική αναδρομή, μπορώ να σας διαβάσω τη σχετική επιστολή μου. Από όσους γνωρίζουν το περιεχόμενό της ζητώ και τη συγγνώμη τους αλλά και την υπομονή τους, ώστε να ενημερωθούν και οι υπόλοιποι σύνεδροι.

Θα σας διαβάσω την επιστολή, την οποία έστειλα πρώτα στον Πρόεδρο της ΕΛ.ΑΣ.ΕΤ. Παρόμοια επιστολή εστάλη αργότερα και στον Πρόεδρο της *Εθνικής Αστρονομικής Επιτροπής* και σε άλλα σε άλλους, όπως θα διαπιστώσετε, φορείς και άτομα.

Σε όλους, όσοι μου απάντησαν στην επιστολή μου, μια καθαρά ακαδημαϊκή ενέργεια, εκφράζω τις ευχαριστίες μου από την θέση αυτή, διότι δεν είχα την ευκαιρία να απαντήσω στον καθένα χωριστά. Αντιλαμβάνομαι, ότι ορισμένους παραλήπτες ο φόρτος εργασίας και η τριβή με τα καθημερινά θέματα δεν τους επέτρεψαν, γι' αυτό το τόσο σημαντικό πρόβλημα, να εκφράσουν τη γνώμη τους έστω και αρνητική (Η επιστολή παρατίθεται αυτούσια στο τέλος).

Η εθνική ανταπόκριση στην ανωτέρω επιστολή, ήταν άμεση, θετική και θερμή.

Θέλω να επισημάνω, ότι απαντητικές, όλες θετικές, επιστολές υποστήριξης της πρότασης ελήφθησαν και από τους επίσημους εκπροσώπους φορέων και ατομικά από μέλη των φορέων αυτών, από όπου αυτή εστάλη. Είναι σημαντικό, ότι θετική ήταν η ανταπόκριση στο, τα σχόλια για, και η αντιμετώπιση του περιεχομένου-προτάσεων της επιστολής και από παρατηρησιακούς και από θεωρητικούς αστρονόμους και, μάλιστα, ανεξάρτητα από τη συγκεκριμένη επιστημονική περιοχή που ο καθένας εμπίπτει και ανεξάρτητα από τα ερευνητικά ενδιαφέροντα του καθενός και της καθεμιάς. Είναι πολύ ενδιαφέρον και σημαντικό, ότι όσοι μη αστρονόμοι απάντησαν, εμπίπτουν σε μια εξαιρετικά ευρεία περιοχή θεματικών-ερευνητικών, αμιγώς μη αστρονομικών ενοτήτων, όπως *σεισμολγία, γεωφυσική, γεωλογία, γεωδαισία και τοπογραφία, φυσική και περιβαλλοντική γεωγραφία, εγγύς διαστημικό περιβάλλον, μετεωρολογία και κλιματολογία, φυσική της ατμόσφαιρας, αστροσωματιδιακή φυσική και έρευνα βαθείας θαλάσσης.*

Η συνολική εθνική ανταπόκριση στην πρόταση εγκατάστασης ενός Ραδιοτηλεσκοπίου στην χώρα μας συνοπτικά φαίνεται στον παρακάτω *Πίνακα.*

Από τα ανωτέρω προκύπτει το συμπέρασμα, ότι ο η ελληνική επιστημονική κοινότητα, αστρονομική και μη αστρονομική, θεωρεί, ότι η εγκατάσταση ενός ραδιοτηλεσκοπίου είναι και χρήσιμη και αναγκαία Από διοικητικής δε πλευράς επίσης υπάρχει υποστήριξη, από όπου αυτή ζητήθηκε.

Ως αποτέλεσμα όλων των ανωτέρω, τι θα πρέπει να γίνει από εδώ και πέρα και ποιές είναι οι πιθανές επιβαλλόμενες ενέργειές μας;

Το πρώτο απαραίτητη μέτρο είναι, ότι η παρούσα συνεδρία (*Infrastructure of Astronomy in Greece*) αποδέχεται την αναγκαιότητα και χρησιμότητα της εγκατάστασης ενός Ραδιοτηλεσκοπίου στην χώρα μας, εγκρίνει ομόφωνα και ομόθυμα τη σχετική πρόταση και τη συνταχθείσα *Declaration*, η οποία παρατίθεται αυτούσια στο τέλος, και προωθεί τα ανωτέρω θέματα προς το Διοικητικό Συμβούλιο της Ελληνικής Αστρονομικής Εταιρείας (ΕΛ.ΑΣ.ΕΤ.) για έγκριση από τα μέλη της Γενικής Συνέλευσης της ΕΛ.ΑΣ.ΕΤ., οι εργασίες της οποίας αρχίζουν στην αίθουσα αυτή αμέσως μετά το τέλος των εργασιών του παρόντος συνεδρίου. (*Αυτή η ομόφωνη και ομόθυμη έγκριση πράγματι ελήφθη*).

Επίσης, εντελώς συνοπτικά, για χρήση στη σύνταξη της σχετικής έκθεσης κατά τα μελλοντικά στάδια διεκδίκησης του Ραδιοτηλεσκοπίου, απαιτείται η κωδικοποίηση και χρησιμοποίηση των μέχρι τώρα αποτελεσμάτων και η δημιουργία σχετικού φακέλλου, ο ακριβής καθορισμός των τεχνικών χαρακτηριστικών του Ραδιοτηλεσκοπίου, ο προσδιορισμός των πιθανών θέσεων εγκατάστασης του Ραδιοτηλεσκοπίου, ο ορισμός-σύσταση *Επιτροπής Διεκδίκησης του Ραδιοτηλεσκοπίου (πράγμα το οποίο ανετέθη στον γράφοντα*), η προώθηση της ιδέας σε εθνικό και διεθνές επίπεδο από όλους μας ανεξάρτητα, ατομικά και σε συνεργασία με την ανωτέρω επιτροπή με κατάλληλες δημοσιεύσεις εντός και εκτός Ελλάδος, η προσέγγιση και ενημέρωση των μελών άλλων, μη αμιγώς αστρονομικών θεματικών περιοχών, ενδιαφερόμενων για την εγκατάσταση του Ραδιοτηλεσκοπίου και συνεργασία μ' αυτά, η πιθανή διεύρυνση της *Επιτροπής Διεκδίκησης του Ραδιοτηλεσκοπίου* με εκπροσώπους άλλων θεματικών περιοχών, η πιθανή έγκριση-υιοθέτηση της *Declaration* από αρμόδια όργανα άλλων θεματικών περιοχών και, τέλος, η προσέγγιση και κατάλληλη ενημέρωση των αρμόδιων εθνικών πολιτικών, κομματικών και κυβερνητικών οργάνων και φορέων αλλά και των αρμόδιων διεθνών οργανισμών και φορέων, κατ' αρχήν από την ΕΛΑΣΕΤ σε συνεργασία με τις ανωτέρω επιτροπές, αλλά και ατομικά από τον κάθε ενδιαφερόμενο.

Είναι φανερό, ότι απαραίτητη προϋπόθεση επιτυχίας των μελλοντικών ενεργειών είναι το πνεύμα συνεργασίας και η συνεχής αμοιβαία ενημέρωση όλων μας.

ΠΑΡΑΡΤΗΜΑ 1

(Η Επιστολή προς τον Πρόεδρο της ΕΛ.ΑΣ ΕΤ.)

Θεσσαλονίκη 14 Μαρτίου 2003

Αρ .Πρωτ.:10

Κ ^{ον} Π. Λασκαρίδη
Καθηγητή-Διευθυντή
Τομέας Αστροφυσικής, Αστρονομίας και Μηχανικής
Τμήμα Φυσικής
Εθνικό και Καποδιστριακό Πανεπιστήμιο Αθηνών

Θέμα*: Εγκατάσταση Ραδιοτηλεσκοπίου στην Ελλάδα.*

Αγαπητέ Κ^{ε} Λασκαρίδη,

Με την επιστολή αυτή θα ήθελα να ενημερώσω εσάς και τα μέλη της επιστημονικής μονάδας σας για μια πολύ πρόσφατη πρωτοβουλία του *Τομέα Αστροφυσικής, Αστρονομίας και Μηχανικής (ΑΑΜ)* του Πανεπιστημίου Θεσσαλονίκης.

Πρόσφατα ο Τομέας μας, στη συνεδρίασή του Αρ.2/22-1-2003 και με πλήρη ομοφωνία των μελών του, αποφάσισε ότι είναι αναγκαία και χρήσιμη η εγκατάσταση ενός *ραδιοτηλεσκοπίου* (Ρ/Τ) στην Ελλάδα.

Οι αντικειμενικοί στόχοι της εγκατάστασης ενός Ρ/Τ στην Ελλάδα είναι πολλοί, πρέπει, όμως, να τονισθούν ιδιαίτερα οι εξής:

1. Η *εκπαίδευση* Ελλήνων μεταπτυχιακών υποτρόφων και η *ερευνητική ή/και τεχνολογική εργασία* επιστημόνων σε επιστημονικό όργανο που μέχρι τώρα *δεν υπάρχει* στην χώρα μας. Η διεξαγωγή αυτής της εκπαίδευσης και εργασίας στο εσωτερικό της χώρας μας αναμένεται αφενός μεν να μειώσει αισθητά το ρυθμό, με τον οποίο οι ανωτέρω νέοι επιστήμονες και ερευνητές αναγκάζονται να καταφεύγουν στην χρήση αντίστοιχων επιστημονικών οργάνων του εξωτερικού, αφετέρου δε να ανακουφίσει το σχετικό προϋπολογισμό της χώρας μας,
2. Η συμπλήρωση του *Ευρωπαϊκού Δικτύου Συμβολομετρίας* με ένα Ρ/Τ εγκατεστημένο εκεί ακριβώς όπου υπάρχει έλλειψη, δηλαδή, στην *νοτιοανατολική Ευρώπη*. Ίσως δεν είναι σε όλους γνωστό, ότι όλα τα εν χρήσει ευρωπαϊκά ραδιοτηλεσκόπια υψηλών συχνοτήτων συμβαίνει να βρίσκονται επί μιας νοητής κατά προσέγγιση ευθείας, με διεύθυνση από νοτιοδυτικά (Ισπανία) προς βορειοανατολικά (Φινλανδία). Συνεπώς, η εγκατάσταση ενός Ρ/Τ υψηλών συχνοτήτων και προηγμένης τεχνολογίας στην χώρα μας, *πέραν και αρκετά εκτός της ανωτέρω ευθείας*, είναι εκ των πραγμάτων επιστημονικώς απαραίτητη, θα αυξήσει σημαντικά τις δυνατότητες και την απόδοση του *Ευρωπαϊκού Δικτύου Συμβολομετρίας* και θα επιτρέψει την ενεργό συμμετοχή της χώρας μας στο γενικότερο Ευρωπαϊκό επιστημονικό γίγνεσθαι,
3. Επειδή ένα Ρ/Τ θα εξυπηρετεί τα επιστημονικά ενδιαφέροντα και σκοπούς όχι μόνον της *αστρονομικής κοινότητας* αλλά επί πλέον και των επιστημόνων των ασχολούμενων με άλλες επιστήμες όπως *η σεισμολογία, η εφαρμοσμένη γεωφυσική, η γεωδαισία, το εγγύς διαστημικό περιβάλλον και η ατμόσφαιρα,* η εγκατάστασή του θα μπορούσε να συμβάλει, μέχρις ενός σημείου, στην ενίσχυση ή και έναρξη συνεργασίας επιστημόνων-ερευνητών *διάφορων επιστημονικών ενδιαφερόντων και ειδικοτήτων*, στο συντονισμό των αντίστοιχων επιστημονικών προγραμμάτων και, συνεπώς, στην αποδοτικότερη χρηματοδότησή τους,
4. Ο κατά τεκμήριον διεθνής ρόλος ενός Ρ/Τ και η χρησιμοποίησή του από επιστήμονες από όλον τον κόσμο θα συμβάλει στην αναβάθμιση της επιστημονικής παρουσίας της χώρας μας σε Ευρωπαϊκό αλλά και παγκόσμιο επίπεδο.

Όπως, ίσως, γνωρίζετε, η εγκατάσταση ενός Ρ/Τ στην Ελλάδα, είχε απασχολήσει την Ελληνική αστρονομική κοινότητα και παλαιότερα. Πιο συγκεκριμένα, το 1999 από την *Εθνική*

Αστρονομική Επιτροπή είχε διοργανωθεί στην Πεντέλη των Αθηνών το συνέδριο «*Αστρονομία 2000+*». Στο συνέδριο αυτό, η ορισθείσα διεθνής, εξωτερική επιτροπή ειδικών, στην αναφορά της (με τίτλο *Astronomy in Greece At the Gates of the 21st Century)* προς την Εθνική Αστρονομική Επιτροπή, είχε προτείνει, ως μία από τις προτεραιότητες της επιστήμης της Αστρονομίας στην χώρα μας, την εγκατάσταση ενός Ρ/Τ στην Ελλάδα. Οι ερευνητικοί στόχοι της πρότασης αυτής ήταν ουσιαστικά οι προαναφερθέντες αντικειμενικοί στόχοι της εγκατάστασης του Ρ/Τ στην Ελλάδα. Η ανωτέρω πρόταση του συνεδρίου είχε τύχει τότε της ευμενούς αποδοχής από τους συμμετέχοντες στο συνέδριο. Ενόψει, όμως, του γεγονότος ότι τότε είχαν ήδη ξεκινήσει οι διαδικασίες εγκατάστασης του τηλεσκοπίου *Αρίσταρχος*, είχε κριθεί ότι αυτή η πρόταση εγκατάστασης ενός Ρ/Τ θα έπρεπε να συζητηθεί και πάλι, όταν θα είχε ολοκληρωθεί η εγκατάσταση του τηλεσκοπίου *Αρίσταρχος*. Ήδη, όπως είναι γνωστό, οι κτιριακές εγκαταστάσεις του τηλεσκοπίου *Αρίσταρχος* είναι έτοιμες, το τηλεσκόπιο αυτό αναμένεται να παραδοθεί από την κατασκευάστρια εταιρεία στο αμέσως προσεχές μέλλον, ώστε είναι πλέον δυνατό να αρχίσει η διαδικασία εγκατάστασης του Ρ/Τ στην χώρα μας.

Είναι μάλλον προφανές ότι, λόγω των πολλαπλών χρήσεων και δυνατοτήτων ενός Ρ/Τ και λόγω του σχετικά μεγάλου κόστους κατασκευής και λειτουργίας του, το πρόγραμμα εγκατάστασης ενός Ρ/Τ δεν μπορεί να είναι αρμοδιότητας μόνον ενός Εργαστηρίου Αστρονομίας, ή ενός Τομέα, ούτε ενός Τμήματος, ούτε, ακόμη, ενός Πανεπιστημίου. Αυτό θα είναι ένα πρόγραμμα πανελλήνιας (τουλάχιστον) εμβέλειας, στο οποίο καθοριστικός θα είναι ο ρόλος κατ' αρχήν του Ελληνικού κράτους και της Ευρωπαϊκής Ένωσης, αλλά και διεθνών σχετικών υπηρεσιών και οργανισμών (π.χ. NASA, European Space Agency, Max Planck Gesellshaft) και, οπωσδήποτε, των Ελλήνων και φιλελλήνων μελών της διεθνούς επιστημονικής κοινότητας. Επομένως, το εν λόγω πρόγραμμα εγκατάστασης απαιτεί, *σε εθνικό επίπεδο*, την ευρύτερη δυνατή και, αν αυτό είναι δυνατό, την ομόφωνη αποδοχή και υποστήριξή του, ώστε με αξιώσεις να επιδιωχθεί η πραγματοποίησή του σε εθνικό και διεθνές επίπεδο. Το δικό μας Εργαστήριο Αστρονομίας ΑΑΜ/ΑΠΘ απλώς αναλαμβάνει την πρωτοβουλία, με σκοπό να διερευνηθεί η δυνατότητα διαμόρφωσης αυτής της ευρύτερης δυνατής συμφωνίας.

Όπως, ήδη αναφέρθηκε, η πρόταση για την εγκατάσταση ενός Ρ/Τ στην Ελλάδα συζητήθηκε στην ανωτέρω συνεδρίαση του Τομέα μας, η δε ομόφωνη γνώμη των μελών του Τομέα είναι η πρόταση αυτή να προωθηθεί για συζήτηση προς *όλους τους ενδιαφερόμενους φορείς*, των οποίων και πρέπει να ζητηθεί η γνώμη και βοήθεια, με κύριο, *προς το παρόν*, στόχο τη διαμόρφωση συμφωνίας ως προς την αναγκαιότητα και χρησιμότητα εγκατάστασης ενός τέτοιου οργάνου στην χώρα μας. Εφόσον κάτι τέτοιο επιτευχθεί, θα ήταν δυνατό κατόπιν να συζητηθεί και η δημιουργία μιας επιτροπής πανελλήνιας εμβέλειας και πολυθεματικής σύνθεσης, έργο της οποίας θα ήταν μια πρώτη αντιμετώπιση μεταγενέστερων θεμάτων όπως π.χ. ο συντονισμός των ενεργειών των μελών της επιστημονικής κοινότητας, μια αξιολόγηση των πιθανών θέσεων εγκατάστασης του Ρ/Τ, το σχήμα διοικητικής υποστήριξης και το νομικό καθεστώς λειτουργίας του Ρ/Τ κ.λ.π.

Με βάση όλα τα ανωτέρω, με την επιστολή αυτή, πέραν της κατ' αρχήν ενημέρωσής σας και αυτής των μελών της επιστημονικής μονάδας σας, επιθυμώ, εκ μέρους των μελών του Τομέα ΑΑΜ/ΑΠΘ, να ζητήσω, σε ένα πνεύμα ανοικτής συνεργασίας, τις απόψεις, παρατηρήσεις-υποδείξεις και την επίσημη γνώμη της μονάδας σας για την αναγκαιότητα και χρησιμότητα εγκατάστασης ενός Ρ/Τ στην χώρα μας. Είναι πλέον ή φανερό, ότι η έκφραση μιας τέτοιας θετικής αλλά και κρίσιμης, αναμφισβήτητα, για το μέλλον γνώμης με κανένα τρόπο δεν υποδηλώνει ανάληψη οποιασδήποτε μορφής δέσμευσης, οικονομικής ή άλλης μορφής, της μονάδας σας και των μελών της, πέραν και απλώς του γεγονότος της σύμφωνης, αυτής καθ' εαυτήν, γνώμης όλων σας για την αναγκαιότητα και χρησιμότητα εγκατάστασης ενός Ρ/Τ στην χώρα μας.

Με τιμή
Ο Διευθυντής του Τομέα ΑΑΜ/ΑΠΘ

Νικόλαος Κ. Σπύρου, Καθηγητής Αστρονομίας

Υ.Γ. Η ανωτέρω απόφαση του Τομέα ΑΑΜ/ΑΠΘ έχει ήδη υποστηριχθεί (κατά χρονολογική σειρά):

1. Κατά τη Γενική Συνέλευση Αριθμ.2 της 22ας Ιανουαρίου 2003 των μελών του *Τομέα Αστροφυσικής, Αστρονομίας και Μηχανικής του Πανεπιστημίου Θεσσαλονίκης*.

2. Κατά την κοινή συνεδρίαση του Διοικητικού Συμβουλίου της *Ελληνικής Αστρονομικής Εταιρείας* και των μελών της *Εθνικής Αστρονομικής Επιτροπής* της 5ης Φεβρουαρίου 2003.
3. Κατά τη Γενική Συνέλευση της 8ης Φεβρουαρίου 2003 των μελών του *Τομέα Αστροφυσικής, Αστρονομίας και Μηχανικής* του Καποδιστριακού Πανεπιστημίου Αθηνών.
4. Κατά τη Γενική Συνέλευση Αριθμ.6 της 3ης Μαρτίου 2003 των μελών του *Τμήματος Φυσικής* της Σχολής Θετικών Επιστημών του Πανεπιστημίου Θεσσαλονίκης.

ΠΑΡΑΡΤΗΜΑ 2

(*Πίνακας Εθνικής Ανταπόκρισης****)***

ΠΙΝΑΚΑΣ

ΕΘΝΙΚΗ ΑΝΤΑΠΟΚΡΙΣΗ

ΣΤΗΝ ΕΓΚΑΤΑΣΤΑΣΗ ΡΑΔΙΟΤΗΛΕΣΚΟΠΙΟΥ ΣΤΗΝ ΕΛΛΑΔΑ

(*Υπογραμμίζονται όσοι απάντησαν στην επιστολή***)**

1. ΜΕΛΗ ΤΟΥ ΤΟΜΕΑ ΑΑΜ/ΣΘΕ/ΑΠΘ (**Ν.Κ.Σπύρου**, Ι.-Χ. Σειραδάκης, Ι. Χατζηδημητρίου, Στ. Αυγολούπης, Χ. Βάρβογλης, Λ. Βλάχος , Σ. Ιχτιάρογλου, Ν. Καρανικόλας, Κ. Κόκκοτας, Δ. Παπαδόπουλος,*Φ. Γρηγορέλης,* Γ. Βουγιατζής, Ν. Στεργιούλας)

2. ΕΛΛΗΝΙΚΗ ΑΣΤΡΟΝΟΜΙΚΗ ΕΤΑΙΡΕΙΑ (ΕΛΑΣΕΤ) (Π. Λασκαρίδης)

3. ΕΘΝΙΚΗ ΑΣΤΡΟΝΟΜΙΚΗ ΕΠΙΤΡΟΠΗ (ΕΑΕ) (Ι.-Χ. Σειραδάκης)

4. ΚΟΙΝΗ ΣΥΝΕΔΡΙΑ ΕΛΑΣΕΤ ΚΑΙ ΕΑΕ

Μέλη Δ.Σ. / ΕΛΑΣΕΤ (**Π. Λασκαρίδης**, **Ε. Αντωνοπούλου**, Κ. Τσίγγανος, Ε. Θεοδοσίου, Ξ. Μουσσάς)

Μέλη Εθνικής Αστρονομικής Επιτροπής (ΕΑΕ) (**Ι.-Χ. Σειραδάκης**, **Ε. Κοντιζάς**, **Ε. Πλειώνης**, Δ. Χατζηδημητρίου, Αιμ. Χαρλαύτης)

5. ΑΡΙΣΤΟΤΕΛΕΙΟ ΠΑΝΕΠΙΣΤΗΜΙΟ ΘΕΣΣΑΛΟΝΙΚΗΣ

Σχολή Θετικών Επιστημών

Κοσμητεία (Α. Φιλιππίδης)

Τμήμα Φυσικής (Δ. Κυριάκος)

Τομέας Αστροφυσικής, Αστρονομίας και Μηχανικής (Ν.Κ. Σπύρου)

Τομέας Εφαρμογών Φυσικής και Φυσικής Περιβάλλοντος (Αλκ. Μπάης)

Τμήμα Γεωλογίας(Γ. Τσόκας)

Τομέας Γεωφυσικής (Π. Χατζηδημητρίου)

Τομέας Μετεωρολογίας και Κλιματολογίας (Χ. Μπαλαφούτης)

Τομέας Φυσικής και Περιβάλλοντικής Γεωγραφίας (Α. Ψιλοβίκος)Πολυτεχνική Σχολή

(Σχολή Τοπογράφων και Αγρονόμων Μηχανικών)

Τομέας Γεωδαισίας και Τοπογραφίας (Δ. Ρωσσικόπουλος)

6. ΙΝΣΤΙΤΟΥΤΟ ΤΕΧΝΙΚΗΣ ΣΕΙΣΜΟΛΟΓΙΑΣ ΚΑΙ ΑΝΤΙΣΕΙΣΜΙΚΩΝ ΚΑΤΑΣΚΕΥΩΝ (ΙΤΣΑΚ)

(Β Λεκίδης, Θεσσαλονίκη)

7. ΕΘΝΙΚΟ ΚΑΠΟΔΙΣΤΡΙΑΚΟ ΠΑΝΕΠΙΣΤΗΜΙΟ ΑΘΗΝΩΝ

Τμήμα Φυσικής ***Τομέας Αστροφυσικής, Αστρονομίας και Μηχανικής*** **(**Π. Λασκαρίδης**)**

Τμήμα Γεωλογίας (Κ.Μακρόπουλος)

Εργαστήριο Φυσικής της Ατμόσφαιρας και Κλιματολογίας (Χ.Ζερεφός)

Τομέας Γεωγραφίας και Κλιματολογίας (Γ. Λειβαδίτης)

Τομέας Γεωφυσικής και Γεωθερμίας (Ε. Λάγιος)

Τομέας Δυναμικής Τεκτονικής και Εφαρμοσμένης Γεωλογίας (Σ. Λέκκας)

8. ΠΑΝΕΠΙΣΤΗΜΙΟ ΠΑΤΡΩΝ

Τμήμα Φυσικής

Τομέας Θεωρητικής και Μαθηματικής Φυσικής
και Φιλοσοφίας της Επιστήμης (Ι. Μπάκας)

Εργαστήριο Αστρονομίας (Χ. Γούδης)

9. ΠΑΝΕΠΙΣΤΗΜΙΟ ΚΡΗΤΗΣ

Τμήμα Φυσικής (Ν.Κυλάφης)
10.ΠΑΝΕΠΙΣΤΗΜΙΟ ΙΩΑΝΝΙΝΩΝ
Τμήμα Φυσικής
Τομέας Αστρογεωγραφίας (Κ.Αλυσσανδράκης)
11. ΕΘΝΙΚΟ ΜΕΤΣΟΒΕΙΟ ΠΟΛΥΤΕΧΝΕΙΟ
Τμήμα Αγρονόμων και Τοπογράφων Μηχανικών (Α. Γεωργόπουλος)
Τομέας Τοπογραφίας (Δ. Παραδείσης Κ. Παπαζήση)
Τμήμα Εφαρμοσμένων Μαθηματικών και Φυσικών Επιστημών (Γ. Σπαθής)
12. ΔΗΜΟΚΡΙΤΕΙΟ ΠΑΝΕΠΙΣΤΗΜΙΟ ΘΡΑΚΗΣ
Τομέας Τηλεπικοινωνιών και Διαστημικής (Ε. Σαρρής)
13. ΕΘΝΙΚΟ ΑΣΤΕΡΟΣΚΟΠΕΙΟ ΑΘΗΝΩΝ
Πρόεδρος του Διοικητικού Συμβουλίου (Δ. Λάλας)
Ινστιτούτο Αστρονομίας και Αστροφυσικής (Χ. Γούδης, Αντί του Προέδρου Δ/Σ)
Γεωδυναμικό Ινστιτούτο (Γ. Σταυρακάκης)
Ινστιτούτο Διαστημικών Εφαρμογών και Τηλεπισκόπησης (Π. Μαθιόπουλος)
Ινστιτούτο Ερευνών Περιβάλλοντος και Βιώσιμης Ανάπτυξης (Μ.Πετράκης)
Ινστιτούτο NESTOR (Λ. Ρεσβάνης)
14. ΑΚΑΔΗΜΙΑ ΑΘΗΝΩΝ
Κέντρο Ερευνών Αστρονομίας και Εφαρμοσμένων Μαθηματικών (Γ.Κοντόπουλος)
Κέντρο Ερευνών Αστρονομίας και Εφαρμοσμένων Μαθηματικών (Ν. Βόγλης)
Κέντρο Έρευνας Φυσικής της Ατμόσφαιρας και Κλιματολογίας (Χ.Ρεπαπής)
Κέντρο Έρευνας Φυσικής της Ατμόσφαιρας και Κλιματολογίας (Π. Λιγομενίδης)
Δ.Νανόπουλος ("Οίκαδε")
Λ. Μαυρίδης (Ομότιμος Καθηγητής ΑΠΘ - Αντεπιστέλλον Μέλος της Ακαδημίας Αθηνών)

ΠΑΡΑΡΤΗΜΑ 3

DECLARATION
FOR THE INSTALLATION OF A RADIO TELESCOPE
IN HELLAS (GREECE)

- We, the participants of the 6th Hellenic Astronomical Conference and the participants of the subsequent General Assembly of the Hellenic Astronomical Society, would like to publicly assert that Astronomy is one of the most fundamental, attractive and educational sciences, and that, with its beauty and its message of our place in the Universe, is a precious treasure of humanity, on which we rely for our knowledge and understanding of our origins and destiny. Its cultural, historical, philosophical and aesthetic values help to establish a better understanding between natural sciences, arts and humanitarian sciences.
- We strongly believe that astronomical education and research in all the regions of the electromagnetic spectrum are equally important for the development and promotion of Science and Technology.
- We note that in Hellas, astronomical research is actively pursued, both theoretically and observationally, in many areas. However, observational research of radio-emitting cosmic sources can only be performed abroad. This is due to the fact that, although modern optical telescopes exist (or are being constructed) in our country, a radio telescope does not exist, neither in Hellas nor in its broader surrounding region of southeastern Europe.
- *With this*

  we declare

  our strong wish for the installation of a radio telescope in Hellas.
- We believe that the installation of a radio telescope will be to the benefit of scientific research nation-wide from both the observational point of view and that of the necessary interaction

between theory and observation, as well as from the technological point of view. Also, according to the warm response and encouragement we have received up to now, a large number of colleagues from a wide range of other scientific and technological disciplines believe that they could use such an instrument in our country in their research activities, and benefit from its use. Such disciplines are seismology, geophysics, geology, geography, geodesy and topography, physical and environmental sciences, near-Earth space environment, astroparticle physics, meteorology and climatology, atmospheric physics, deep sea research; and the benefits will be raised from the mutual collaboration of these disciplines with astronomy and from a better coordination of research programs of common interest and a more effective financial funding and expenditure.

- We note that crucial discoveries have been made with radio telescopes to advance our knowledge of the universe, such as the detection of the cold neutral hydrogen content of the galaxy, the discovery of the remnant radiation of the hot early universe, the discovery of quasars and pulsars, and of the complex interstellar molecules. Four Nobel Prizes have been awarded to scientists involved in these discoveries during the last few decades.

- We are aware that the installation of a radio telescope in southeastern Europe will be a very important addition to the European and intercontinental network of Very Long Baseline Interferometry (VLBI). It will significantly increase the space resolution of the European VLBI network and will improve its coverage. The international cooperation that will be initiated will provide our country with leading participation in forefront research, thus upgradinge research and education, in our country, and will creating a beneficial cooperation in various disciplines, including industry.
- We understand (realize) that the installation of a modern radio telescope in Hellas is not a national project, but, in reality, a multinational project to be addressed in the first place to the Hellenic authorities and political parties and also to intergovernmental organizations.
- We urge the Hellenic government and the political parties to endorse this declaration as one of their first priorities of the national research policy in the immediate future.
- We are ready to collaborate and offer our help, knowledge and skills in every possible way towards the realization of our suggestion.
- We also urge the European Union, the International Astronomical Union, the International Council of Scientific Unions and all relevant scientific societies to support our cause and use all means at their disposal to assist the installation of a radio telescope in Hellas.
- We strongly believe that the installation of a radio telescope in Hellas is a precious investment for the future, which will undoubtedly assist and promote scientific research in astronomy and many other disciplines at both national and international level.

FULLY OPTICAL SIGNAL PROCESSING SYSTEMS IN SUPPORT OF EFFECTIVE ROBOTIC TELESCOPE OPERATION*

Nikolaos H. Solomos [1,2]

[1] Electrooptics Laboratory, Physics Sector, Hellenic Naval Academy, Piraeus - 18503, Greece

[2] EUDOXOS National Observatory, Mount Ainos, Kefallinia Island, Greece

STAR-FIELD PATTERN RECOGNITION IN ROBOTIC ASTRONOMY: DEFINITION-SOLUTION APPROACHES

Robotic Astronomy faces the following problem: as we go deeper aiming at much fainter objects (AGN, quasars, faint stars) taking photometric advantage of the high quantum efficiency and the 2D format of the CCDs, we are forced to cross the *12-mag confusion barrier* [3]: The increase of the sensitivity quickly leads us to a situation where the detected sky-portions are so much crowded by stars (see Fig-1) that obviously becomes mandatory to device robust methodologies for star-field pattern recognition and object identification. Consequently, the remotely controlled or robotic observatories -where no confirmation by the human observer is possible- should incorporate embedded *engines*, properly constructed for real time generation and issuing of *indexes* i.e *confidence estimators* that the desired object is observed. The pattern-recognition problem under consideration is *to find the best similarity measure of two patterns that is subject to a fast computation*. In other words it maybe stated as follows: device optimum unique representations of a star-pattern in such a way that comparisons with reference ones can be efficiently carried out in real time. For this purpose we conceptualy proposed and specified ([2] Solomos, 1995) a two element solution: an Image intensified CCD tracker-camera with Incorporated Serial, Artificial Intelligence (AI) or Optical Signal Processing (OSP) tools ([1], [2], [3]). These, should perform identification of faint objects by comparison with either prestored or simulated sky images generated from combined Hubble Guide Star and other catalogues. The final processing element aims in the generation of the seeked increased-confidence indexes which directly follow the results of the identification process on the observed star pattern.

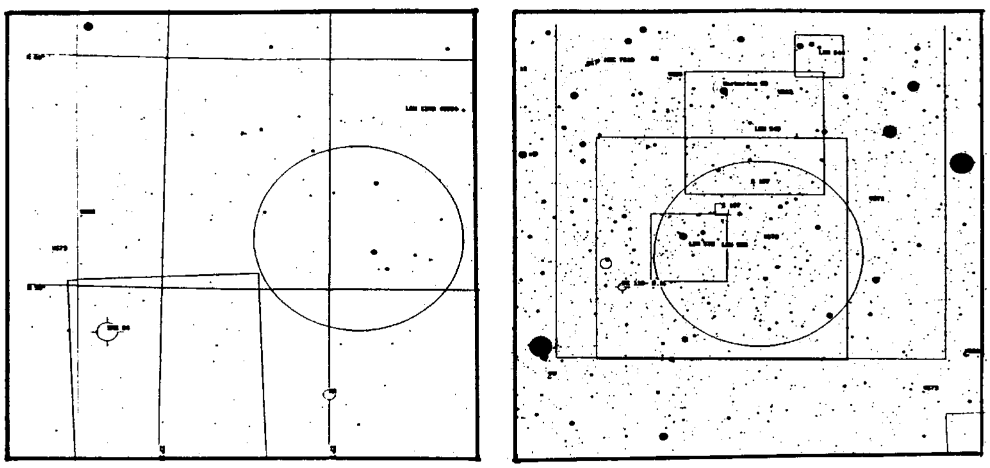

Fig-1: sky simulation with CCD detection threshold at 5^{mag} (a) and 12^{mag} (b) respectively

The basic structure of a wide-field camera for star-field acquisition plus subsequent field recognition can be found schematically in the block diagram of Fig-2 of [1].

* *Proceedings 6th Hellenic Astronomical Society Conference, 15-17 September 2003, Penteli, Athens, Greece*

THE PROPOSED FULLY OPTICAL SIGNAL PROCESSING APPROACH:

In a previous paper ([1] and refs. therein) we further described and analyzed the two identification approaches (Serial Processor & Artificial Intelligence Processor) and suggested a third (Optical Superprocessor) which is the subject we focus on, in the present work. (A more robust solution based on a hybrid configuration, will be presented in a subsequent publication). Here, we summarize the basic concepts behind the suggested novel solution i.e. to use linear optics means for rapid and efficient calculation of needed quantities. We essentially rely upon the inherent Fourier Transform properties of thin lenses [5] which we utilize to correlate the observed field with a reference star-field pattern generated computationally using the Hubble Guide Star Catalogue. The correlation procedure is thus used for comparing a (serial or not) sequence of templates from an image bank with real imagery or vice-versa.

Consider the observed and reference patterns as two-variable scalar functions $f_1(x,\psi),\ f_2(x,\psi)$ of the spatial coordinates x,ψ . As an efficient measure of similarity between the two patterns f_1,f_2 we adopt the cross-correlation function

$$f_1(x,\psi)\oplus f_2(x,\psi)=\int\int_{-\infty}^{+\infty} f_1^*(x,\psi).f_2(x+a,\psi+\beta).dxd\psi \qquad (1)$$

Cross-correlation reduces to multiplication from the well known important property

$$F(\,f_1(x,\psi\,)\oplus f_2(x,\psi\,))=F_1^*(\,p,\ q\,)F_2(\,p,\ q\,) \qquad (2)$$

where $F_1^*,\ F_2$ represent the Fourier Transforms of $f_1^*,\ f_2$ respectively which are functions of the spatial frequencies p,q and f_1^* is the complex conjugate of $f_1(x,\psi)$. The last relation shows that if we manage to optically produce $F_1^*(p,q)$ and $F_2(p,q)$, we could also generate the cross-correlation function simply by taking the inverse Fourier Transform of the product of the right side in equation (2). This is essentially the concept behind the coherent '4f' correlator depicted in Fig-2.

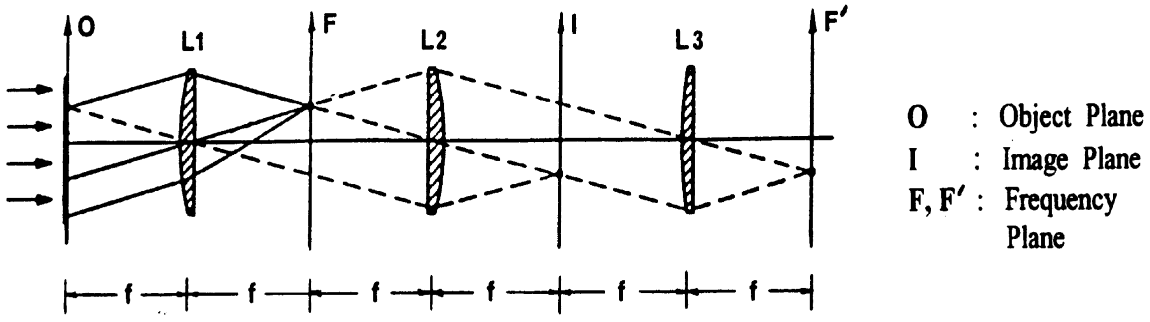

Fig-2: Schematics of the "4f" correlator principle

Although $F_2(p,q)$ can materialized in real time with a Fourier Lens, production of $F_2^*(p,q)$ i.e. of a transparency having transmittance proportional to the complex Fourier transform of the object to be recognized, requires a holographic filter mask [4], The relatively complicated construction processes of the latter, will eventually lead to non real-time operation. Several other drawbacks also exist:

- system size is very large

- laser must provide a good plane wave and good degree of coherence
- a dynamic mask is necessary for the system to operate at useful speeds
- the correlation peak is very susceptible to small changes in scale and rotation differences between the object to be recognized and its appearance in the scene to be interrogated.

These disadvantages can be partially overcome with a Joint Transform Correlator (JTOC) [6] whose structure is shown schematically in Fig-3.

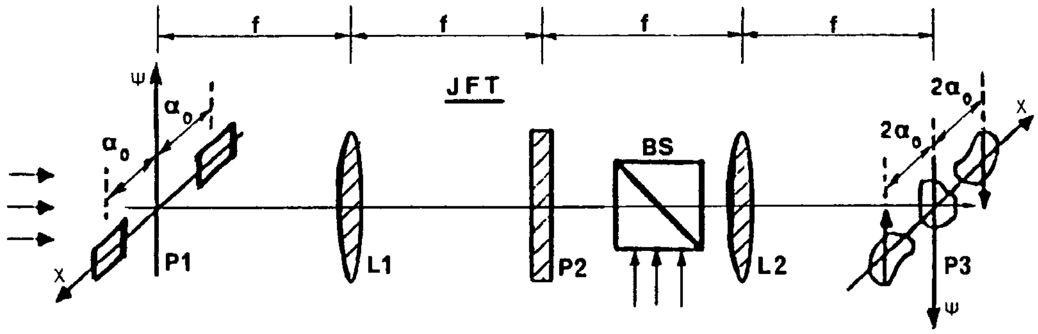

Fig-3: The principle of the Joint Transform Optical Correlator

Assume for simplicity two slightly displaced but identical object functions $F(x-\alpha_0,\psi)$ and $f(x+\alpha_0,\psi)$ as shown in Fig-7. After illumination of this joint scene with a coherent plane wave, the complex light distribution (Joint Fourier Transform 'JFT') arriving at a square law converter element (e.g. CCD) placed at Fourier Plane P2 of the Fourier lens L_1, will be:

$$E(p,q)=F(p,q)e^{-i\alpha_0 p}+F(p,q)e^{+i\alpha_0 p} \tag{3}$$

where $F(p,q)$ denotes the Fourier transformed $f(x,\psi)$ and p,q are the angular spatial frequencies. The corresponding irradiance at the input end (P2) of the square-law detector is:

$$I(p,q)=2\,\|\,F(q,p)^2\,\|\,(1+cos\,2\alpha_0 p) \tag{4}$$

We then send a coherent readout beam at the beam-splitting element (BS) to get the inverse fourier transform of the JFT, with the aim of the second lens L_2 to image the JFT (which we display on a Liquid Crystal Television (LCTV) located at its front focal plane) on its real focal plane (P3). The complex light distribution at plane P3 is then:

$$g(x,\psi)=2f(x,\psi)\oplus f^*(x,\psi)+f(x,\psi)\oplus f^*(x-2\alpha_0,\psi)+f^*(x,\psi)\oplus f(x+2\alpha_0,\psi) \tag{5}$$

The first term of (5) is clearly the autocorrelation function diffracted at the origin of the output plane and the last two are autocorrelation terms diffracted around $\alpha=2\alpha_0$ and $\alpha=-2\alpha_0$. We therefore physically implement the correlation integral in the time the light takes to cross the optical system.

Concluding Remarks: We propose the following feasible architecture implementing a JTOC, to assist the solution of the well known star field identification problem in robotic astronomy. We suggest that the experimental optical layout shown in Fig-4 can perform real time linear operations on 2D images and perform target recognition and location at near TV frame rates (~15/sec).

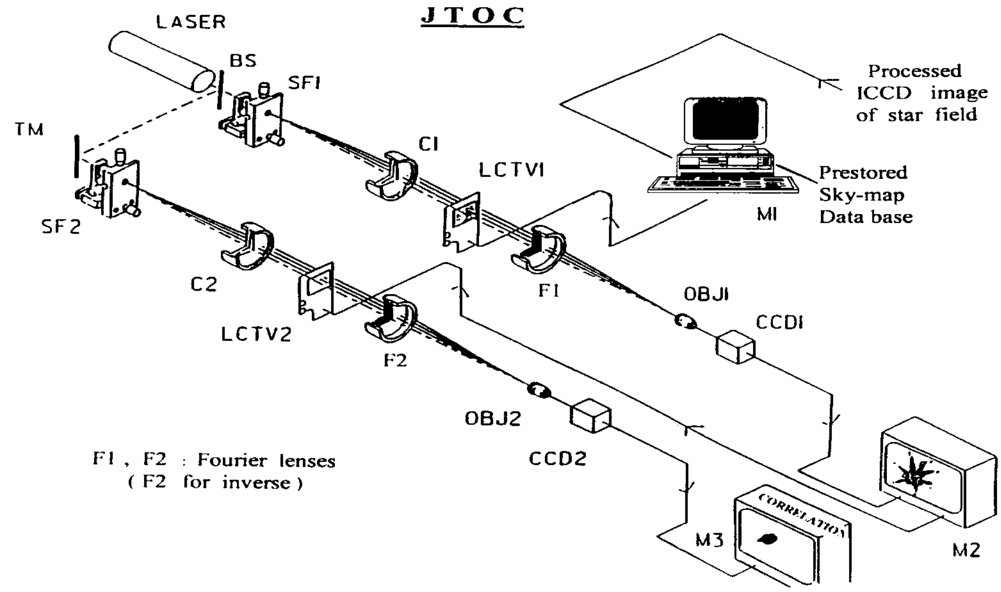

Fig-4: the suggested herein JTOC implementation as a star-field identifier

A splitted, spatially filtered (SF1,2) and collimated by C1, C2 lenses input coherent beam, enters the 'direct' and 'inverse' FT arms of the system. Correlations are performed between digitized optical imagery from the ICCD camera and multiple sequential references inserted in the front focal plane of F1, using a PC to address the LCTV image forming spatial light modulators (limiting system speed and space-bandwidth). The liquid crystal modulates the polarization of the coherent readout beam, so an analyzer (not shown) should be used to create an intensity modulated output beam. CCD1,2 are low noise miniature CCD detectors upon which the JFT (by F1) and the correlations (by F2) are properly projected by OBJ1,2 respectively. Matches between an input star-field and one of the stored 'sky'-filters are indicated by the appearance of a bright correlation spots at CCD2. Correlation plane data displayed by output monitor M3 are to be digitally sampled and statistically analyzed using a DSP frame grabber. Among the other advantages of the suggested JTOC are the real time processing speed, no need for preprocessing of the reference image, the allowance of the user to change objects in real time and the capacity for object tracking since the JTOC retains the shift invariant property of the FT. The remaining scale and rotation sensitivity, as S/N ratio degradation considerations in the correlation plane, as well as the quite large system size, put certain limits in its performance. We currently investigate, advances in scale invariant Mellin Transform type correlators to device a hybrid design incorporating specific advantages of both systems and, also, possible ways to deal with the problem of the absence of appreciable energy at low spatial frequencies in the power spectrum of a celestial image.

References

[1] Solomos, N. (2002): in NATO ASI on "*Optics in Astrophysics*". www-Proc., Eds. R. Foy, Y. Balega, Obs. de Lyon, France.

[2] Solomos, N. (1995) EAS 4th JENAM, Catania Astroph. Observatory Special Publication, pp.69-

[3] Solomos, N., Hatzilau, I. (1997) in "*Circuits Systems & Computers' 96*" Proceedings, Ed. N. Mastorakis pp.673-680

[4] VanderLught, A., (1964): IEEE Trans. Inf. Theor., IT-10, 139.

[5] Goodman, J. W., (1966): *Introduction to Fourier Optics*, McGraw-Hill, New York.

[6] Weaver, C.S. Goodman, J.W., (1966): Appl.Opt. 5, 1248.

OPTICON: GREECE'S PARTICIPATION IN A PROJECT AIMING TOWARD THE INTEGRATION EUROPEAN ASTRONOMICAL INFRASTRUCTURE*

Seiradakis J.H.
University of Thessaloniki

Abstract: OPTICON is a large European project (80 partners) designed to support the European infrastructure of Optical and Infrared Astronomy. It consists of three main elements: (i) Networking (11 projects), (ii) Transnational Access (1 project with 20 partners) and (iii) Joint Research Projects (8 projects). Greece participates in the Managerial Board (Greek National Committee for Astronomy) and in the Access project (National Observatory of Athens - Aristarchos telescope). OPTICON is the largest among the Integrated Infrastructure Initiative projects for Astronomy supported by the European Research Area.

PLANS FOR CONSTRUCTING A RADIO TELESCOPE IN GREECE

Seiradakis J.H.
University of Thessaloniki

Abstract: Preliminary plans for constructing a radio telescope in Greece are presented. The advantages and disadvantages of the project are investigated from several perspectives: operating frequency, location, compatibility with existing facilities, technological aspects, multidisciplinarity of the project, cost effectiveness, etc.

OBSERVATIONS FROM X-RAY AND GAMMA-RAY ASTROPHYSICS MISSIONS

I.Georgantopoulos[1], A. Georgakakis[1], I. Papadakis[2] and M. Plionis[1]

1Institute of Astronomy and Astrophysics, National Observatory of Athens
[2]University of Crete

Abstract: We summarize the specifications and capabilities of the recent X-ray and gamma-ray astrophysics missions (XMM-Newton, Chandra, INTEGRAL). All these missions are open for observations for astronomers regardless of their nationality. Moreover, all data after a period of 12 months become publicly available. We discuss the potential of these observations for the Greek Astronomy as well as the ways of accessing the data.

CURRENT STATUS OF THE NESTOR EXPERIMENT

Leonidas K. Resvanis

NESTOR Institute

Abstract: The NESTOR experiment is continuing its activities in Pylos. The current status of the project is presented. Emphasis is given in the ability of NESTOR to detect neutrinos of astrophysical origin.

---

* *Proceedings of the 6th Hellenic Astronomical Society Conference, 15-17 September 2003, Penteli, Greece*

THE IMPROVED MULTICHANNEL SOLAR RADIOSPECTROGRAPH ARTEMIS IV*

P.Kontogeorgos[4], P. Tsitsipis[4],C. Caroubalos[1], X. Moussas[2], C. E. Alissandrakis[3], A. Hillaris[2], P. Preka-Papadema[2], J. Polygiannakis[2], J.-L. Bougeret[5], G. Dumas[5], C. Perche[5]

[1] Dep. of Informatics, Un. of Athens

[2] Section of Astrophysics, Astronomy and Mechanics, Dept.. of Physics, Univ. of Athens

[3] Section of Astro-Geophysics, Department of Physics, University of Ioannina,

4 Department of Electronics, TEI of Lamia, Lamia, Greece

5 LESIA, Observatoire de Paris, Meudon, France

Abstract: We present the lately (2003) improved solar radiospectrograph of the University of Athens/LESIA Observatoire de Meudon operating at the Thermopylae Satellite Station (OTE) since 1996. Observations now cover the whole frequency range from 20 to 650 MHz. The spectrograph has the old 7-meter moving parabolic antenna for 110 to 650MHz and a new stationary antenna for the 20 to 110 MHz. There are two receivers operating in parallel, one sweep frequency for the whole range (10 spectrums/sec, 600 channels/spectrum) and one acousto-optical receiver for the range 270 to 470 MHz (100 spectrums/sec, 128 channels/spectrum). The data acquisition system consists of two PCs (equipped with 12 bit, 225ksamples/sec DAC, one for every receiver, DVD writer) Windows operating system, connected through Ethernet. The daily operation is fully automated: pointing the antenna to the sun, starting and stopping the observations at preset times, data acquisition, and archiving on DAT tapes and CDROM. We can also control the whole system through modem or Internet. The instrument can be used either by itself to study the onset and evolution of solar radio bursts or in conjunction with other instruments including the Nancy Decametric Array, the WIND/WAVES, and the under construction STEREO/ WAVES and LOFAR low frequency receivers to study associated interplanetary phenomena.

* *Proceedings of the 6th Hellenic Astronomical Society Conference, 15-17 September 2003, Penteli, Greece*

*ABSTRACTS OF PAPERS POSTED DURING THE SESSION ON INFRASTRUCTURE OF ASTRONOMY IN GREECE**

HIGH TIME RESOLUTION MEASUREMENTS OF THE NUCLEONIC COMPONENT OF COSMIC RAYS WITH THE UNIVERSITY OF ATHENS NEUTRON MONITOR STATION

C. Sarlanis, G. Souvatzoglou, X. Moussas, H. Mavromichalaki, S. Tatsis and M. Gerontidou,

Department of Physics, National and Kapodistrian University of Athens, Panepistimiopolis GR 15783, Zografos, Athens, Greece

Abstract: We have constructed a new acquisition system for the neutron monitor of the National and Kapodistrian University of Athens (Super neutron monitor NM-64) which enable us to record the count rates of all 6 counters every second. The Athens Neutron monitor station is located at the Department of Physics at Panepistimiopoli, Athens, Greece. It has a cut-off rigidity 8.53 GV and provides measurements of the hadronic component of the cosmic ray intensity continuously real time. The data are available real time at the web. http://cosray.phys.uoa.gr. We study the distribution of count rates with time. We hope that we might record major solar events or major cosmic events which could appear as sudden increases of the recorded count rate. If we combine many neutron monitor stations of the world wide network recording at this high rate we can construct a new type inexpensive universal detector covering all the Earth. Such a combination of many stations with high time resolution will permit triangulation of high energy sources.

LABORATORY MEASUREMENTS FOR THE CHARACTERIZATION OF BACK- ILLUMINATED CCDS IN THE EUDOXOS OBSERVATORY

Solomos, N.[1,2], Georgopoulos, P.[2], Solomos, I.[2]

[1]Physics Sector, Hellenic Naval Academy, Piraeus,

[2]EUDOXOS National Observatory, Ainos, Kefallinia, Greece

Abstract: We have applied laboratory methods for the characterization of a SITE 512x512 back-illuminated CCD chip of the Ap7b CCD camera of the 0.62m AM Telescope of EUDOXOS Observatory and critically discussed the resulted measurements. Using very simple equipment we have precisely measured CCD camera Gain =1.97± 0.01 e^-/ADU, Readout Noise: R=13±4e. Given the gain, we measured the mean dark current production at 0^0C as 14.7 e^-. sec $^{-1}$.pix $^{-1}$ by averaging it over the central 1/4 area of the CCD, after a long (32 sec) exposure bias-subtracted dark frame was taken. By plotting the signal produced by the radiance of a very stable LED source vs exposure time, we also measured that the linearity of the SITE chip/electronics is exhibiting a max. deviation from the least squares fit line of only 0.3%. Interestingly, when the CCD signal saturates the ADC circuit, its output does not pin at (2^{16}-1), but returns to 0 value, and thereafter linearly re-increases). The exact cause (attributed to a fault in the ADC, or to soft. error) is unknown. Nevertheless, as was found, the consequences on the Ap7b photometry are minimal if avoiding the ADC saturation level. Finally, most interesting are the results on the photon transfer function (variance vs signal). The observed high linearity indicates good fixed-pattern elimination by the method applied.

* *Proceedings of the 6th Hellenic Astronomical Society Conference, 15-17 September 2003, Penteli, Greece*

*ABSTRACTS OF PAPERS POSTED DURING THE SESSION ON INFRASTRUCTURE OF ASTRONOMY IN GREECE**

OPTICAL DESIGN AND CONSTRUCTION OF A 4-MIRROR 27CM TELESCOPE AND A COMPACT NARROW-BAND CCD PHOTOMETER

Nikolaos Solomos
Physics Department, Hellenic Naval Academy

Abstract: We present the conceptual design, the actual optical architecture and the main optical and mechanical parameters of the "NIOPTIR", an unusual 27cm 4-mirror telescope and the "POLYFIMOS" a lightweight narrow-band multi detector CCD/PMT photometer. The two instruments have been constructed and are now being used by the Electrooptics Laboratory of the Hellenic Naval Academy for various atmospheric studies, including experiments on laser guide star excitation. They were also designed as scaled-down models to help making realistic predictions on the expected performance of the Eudoxos' new instruments, namely the 1.1m Karatheodory Telescope and the High Speed three-beam photometer respectively.

FORECAST OF SOLAR FLARE PARTICLE EVENTS FROM THE NEUTRON MONITOR NETWORK IN REAL TIME

H. Mavromichalaki[1], C. Sarlanis[1], G. Souvatzoglou[1], S.Tatsis[1], M. Gerontidou[1], C. Plainaki[1] A. Belov[2], E. Eroshenko[2] and V. G. Yanke[2]

[1]. Nuclear and Particle Physics Section, Physics Department, University of Athens,
[2]. IZMIRAN, Russian Academy of Sciences, 142190. Troitsk, Moscow region, Russia

Abstract: Relativistic cosmic rays (galactic and solar) registered by neutron monitors at the Earth, bring valuable information on their interaction with the interplanetary disturbances. Therefore, they can play a useful role in forecasting space weather storms and in specifying magnetic properties of CME shocks and ejecta. The reconstruction of pitch-angle distribution of high energy particles may be derived from ground level cosmic ray (CR) observations well in advance the onset of geomagnetic storm. This can be used for forecasting aims. High energy solar particle events during powerful solar flares are registered at the Earth well before the main development of particle profiles recorded onboard GOES. This gives a good chance for a preventive prognosis of dangerous particle bulk by ground level observations. To produce real-time prediction of the phenomena, only real time data from Neutron Monitor Network (NMN) should be employed. The increased number of NM stations in real-time gives a good basis for using NMN as a single multidirectional tool and for improving the definition of the onset of GLE in powerful SPEs and to give an immediate forecasting of the arrival of the interplanetary disturbance at the Earth. The properties of the Neutron Monitor Network and its possibilities for Space Weather tasks are discussed in this paper. Different real time Neutron Monitor Network topologies, different synchronization methods and the ways of collecting data in a central data server accessible to the users, are also discussed.

* *Proceedings of the 6th Hellenic Astronomical Society Conference, 15-17 September 2003, Penteli, Greece*

ABSTRACTS OF PAPERS POSTED DURING THE SESSION ON INFRASTRUCTURE OF ASTRONOMY IN GREECE[*]

EXPERIMENTAL INVESTIGATION OF CCD CHARGE SPREADING AND ITS INFLUENCE ON THE DETERMINATION OF PSF

Georgopoulos, P.[1], Solomos, N. [2,1]
[1]EUDOXOS National Observatory, Ainos, Kefallinia, Greece
[2]Physics Sector, Hellenic Naval Academy, Piraeus, Greece

Abstract: An analysis on the physics involved in the phenomenon of charge spreading within CCD sensors was presented. We have examined the theoretical consequences of this being due to the charge diffusion in the field-free region, both with mathematical modeling and computer simulation methods. A simple statistical model is developed and extensive computer simulations for the prediction of the actual PSF have been carried out. An unexpected highly peaked PSF with a distinct departure from gaussianity occurs in the IR wavelengths. Moreover the validity of the theoretical modeling was checked by experiment. The MTFD and PSFD obtained experimentally were found to be in excellent agreement to the theoretical models reflected by the computer simulations. It has been demonstrated that the PSF is blurred by charge-spreading in every wavelength for a back-illuminated CCD, and this is what makes this phenomenon very important concerning the CCD's spatial resolution. Specifically in the Visual, the spreading is typically 1-2 pixels around the correct pixel and follows a distribution that can be very well approximated by a Gaussian. However, it has been found that the blurring is not as severe in IR light, where the PSF exhibits a very peaky, non-Gaussian, appearance. Nevertheless, a considerable percentage of the e^- are spread the same way (and same distance), as was in the visible light case.

THE HELMOS ASTRONOMICAL STATION, HOUSE OF THE 2.3M TELESCOPE

P. Hantzios
Institute of Astronomy and Astrophysics, National Observatory of Athens

Abstract: The Helmos Astronomical Station has been completed and is ready to accomodate the new 2.3m Aristarchos telescope. The new facilities are presented. The presentation includes information on the modes of operation, access, utilities, communications, and the entire relevant infrastructure for the operation of the 2.3m Aristarchos telescope.

[*] *Proceedings of the 6th Hellenic Astronomical Society Conference, 15-17 September 2003, Penteli, Greece*

Hellenic Astronomical Society

Invited Lecture

DEVELOPMENT OF ASTRONOMY AMONG SERBS FROM THE BEGINNING OF XVIII CENTURY UNTIL THE FIRST WORLD WAR

Milan S. Dimitrijević

Astronomical Observatory, Volgina 7, 11160 Belgrade,
Serbia and Montenegro

DEVELOPMENT OF ASTRONOMY AMONG SERBS FROM THE BEGINNING OF XVIII CENTURY UNTIL THE FIRST WORLD WAR

Milan S. Dimitrijević*
Astronomical Observatory, Volgina 7, 11160 Belgrade, Serbia and Montenegro
E-mail:mdimitrijevic@aob.bg.ac.yu

1. EIGHTEENTH CENTURY

In the eighteenth century, only Rudjer Bošković among Serbs worked as a scientist on astronomy. He investigated different astronomical problems, developed his theory on atoms and founded the Brera observatory in Milano. In the year 1739 he wrote: *De novo telescopii usu ad objectes coelestis determinanda.* He wrote works on optics and also on the construction and use of the optical instruments, telescopes, heliostats, on ocular adjusting, on meridian determination, on errors of meridian instrument etc.

Besides the theoretical work in the research field of astronomy, Rudjer Bošković also observed. So, he published results of his two observations of Mercury transit across the solar disc: *De Mercurii novissimo infra Solem transitu,* 1737 and *Osservazioni de ultimo passagio di Mercurio sotto il Sole*, 1753. He measured two degrees of the meridian circle between Rome and Rimini, together with Ch. Le Maire in order to determine more precisely the Earth's shape and the map of the Vatican state. Also, in 1736, Bošković wrote the book: *De maculis Solaribus* on solar spots and their observations. Later in 1777, he observed solar spots from France, and wrote on methods of observations and on his perceptions on the solar nature.

Comets also attracted his attention so that he observed them from 1744, and after that, in 1746, he wrote the article: *De cometis.* On the occasion of the comet of 1744, he also published a method for the determination of comet's orbit on the basis of his observations in three slightly distant positions.

In this period a Count from Bologna, Luigi [Aloysius] Ferdinandus Marsigli (1658-1730), performed astronomical observations from Serbian country. A soldier by profession, a scientist by voccation, an exceptional man with a universal spirit, he published the results of his investigations in Amsterdam in 1726 in the monumental work of six volumes: *Danubius Pannonico – Mysicus, observationibus geographicis, astronomicis, hydrographicis, historicis, physicis*. On the 35 pages in the second part of the first volume, he describes, with detailed drawings, results of his astronomical observations, performed in today Serbia (region Vojvodina) in June and July 1696. On the confluent of rivers Drava and Danube and in the Titel fortress, he determined, by using astronomical methods, the local geographical latitudes and the heights of the Sun on the meridian. He observed also Jupiter and his four satellites and sketched the Moon's appearance. Moreover, from the bridge on Crna Bara near Bačko Gradište he performed observations of Jupiter and his satellites and made drawings of the surface of the Moon. He observed again Jupiter and its satellites from Senta and in Žabalj he drew the map of the Moon (Jovanović, 1985). The work of Count Marsigli, a man of encyclopedical wideness, puts him among men of exceptional interest in the history of science of the eighteenth century in Serbian countries.

It is interesting also, that the great traveler, poet, theologian and at the end archimandrite Jovan Rajić (11. XI 1726 – 11. XII 1801) was teaching astronomy in the so called Latin school in Sremski Karlovci from 1749 up to 1768. The manuscript of his lectures is preserved (Janković, 1985). At the same time he was an observer, and his description of the observations of a comet of 1769 is also preserved. In Great Serbian orthodox grammar-school astronomy is taught according to Walch text-book of 1794 written in German. Elements of

---

* Hel.A.S Invited Speaker

astronomy are also included in the courses of mathematical geography and physics (Jovanović, 1990).

2. ENLIGHTENERS AND POPULARIZATORS

Other witnesses of interest to Astronomy are different translations and alterations of texts concerning this science. Besides, astronomical contents may be found in calendars, which start to be printed in Serbian in the second half of the eighteenth century. From 1765 up to the end of the XVIII century only a dozen of calendars have been printed, while in the middle of the XIX century a large number of different calendars is printed every year.

The scientific life in Serbian countries at the end of the eighteenth and the beginning of the nineteenth century is denoted by the "enlightener" spirit of Dositej Obradović. For him, the science was at first a mean to enlighten the people and to suppress the superstition. The most important among writers who followed such views of Dositej was Atanasije Stojković (1733-1832), doctor of philosophy and fellow of German scientific societies. He finished the so called Grammatical latin school in his native town Ruma and started to work as a teacher. He continued the studies of philosophy and law in Sopron, Szegedin and Pozhun. Also, he learnd physics and philosophy in Goettingen (Germany), where in 1799, he became a doctor of philosophy. The same year he returned to Serbia and wrote the first modern Serbian text-book on Physics, *Fisika* (Part I, 1801; Part II, 1802; Part III, 1803). He also published the books: *Kandor ili Otkrovenije egipetskih tajn* (Candor or the revelation of Egyptian secrets), 1800, which is written on the model of Voltair's *Candide, Aristid i Natalija* (Aristid and Natalie), 1801 and *Srpski sekretar* (Serbian secretary), 1802. In 1803 he was elected professor of physics at Kharkov University, where he arrived from Serbia in 1804 (Deretić, 1973). In Kharkov he was rector for two times (1807 and 1811) and he wrote his most important works (Milogradov-Turin, 2001a) as for example a book on meteorites: *O vozdushnykh kamnyakh i ikh proiskhozhdenii* (On air stones and their origin) 1807, and *Nachalnaya osnovaniya fizicheskoj astronomii* (Starting bases of physical astronomy), 1813. In honor of his scientific results concerning meteorites, Leonid Yakovlevich Kulik named a hill near the place of Tunguska event hill Stojkovich (Milogradov-Turin, 2001ab). In 1809 he was elected correspondent fellow of the Imperial Academy of Sciences in Sankt Peterburg (Milogradov-Turin, 2001a). He left Kharkov in 1813 and he spent his last years of life mainly in Sankt Peterburg.

3. SECOND HALF OF THE NINETEENTH CENTURY

In the second half of the nineteenth century a basis permitting to Astronomy to become a real science and to find a place in secondary schools and in Grand School is developed. In this period an Astronomical and Meteorological Observatory has been founded (1887), as well as the Chair for Astronomy and Meteorology. In this period the first scientific articles in today's sense are published, the first textbooks are appearing and the amateur astronomy starts to develop.

In 1849, Vuk Marinković (1807 - 1859) becomes by invitation professor of Lyceum. He was the first of physics teachers at Lyceum and he taught physics from 1849 up to 1859 and wrote his textbook: *Načela fizike* (Principles of Physics), published in 1851, and containing astronomical subjects. He taught astronomy probably from 1849 together with physical geography.

It is interesting that one priest, Djordje (Gavrilo) Popović (1811 Baja – 1871 Beograd) was also a popularizator of astronomy. In 1850 he published the book: *Astronomija ili nauka o zvezdama* (Astronomy or the science about stars).

During the considered period Amateur Astronomy appears among Serbs. Jovan (Julijan) Čokor (21.01/2.02 1810 Baja – 1/13.06 1871 Sremski Karlovci) can be considered as one of the first amateur astronomers in serbian countries (Janković, 1955). He made a small observatory in Sremski Karlovci and he also produced sun-dials. Among the Amateur Astronomers were also doctor Djordje Maksimović (1838 – 1881), officer and diplomat Petar

Manojlović Selim, the writer of the first serbian science fiction novel: *Jedna ugašena zvezda* (Beograd, 1902) Lazar Komarčić, Sreten Hadžić and others.

Jelenko M. Mihajlović (January 11, 1869 Vrbica near Knjaževac – October 30, 1956, Belgrade) is founder of modern Serbian seismology, and he published a large number of works related to geological and particularly seismological features of our country. Within the period 1893 - 1906 he was the coworker of Milan Nedeljković, the founder of Belgrade Astronomical and Meteorological Observatory (Banjac, 1999). He was also the author of the numerous textbooks, popular scientific books and articles, concerning spectroscopy, photometry and photography in astronomy.

Cousins Ivan and Ilija Milošević left also a trace in the history of Serbian astronomy of the nineteenth century. They are descendents of Boka Kotorska and they were both born in Venice – Ivan in 1850 and Ilija in 1848 (Protić-Benišek, 2002).

Ivan, devoted himself to mathematics and he left several astronomical works. The most known is: *O najskorijem prehodu Danice preko Sunčevog kola* (On the approaching Venus transit across the Solar disc), concerning the transit of Venus of 1874. This work is important for the history of astronomy since it is the first work on the Venus transit across the Solar disc on Serbian language.

Ilija Milošević, the son of Filip Milošević, sailor and merchant from Dobrota near Kotor, was a professor of astronomy in the Naval institute in Venice and during 1879-1902 vice director and director of the "Collegio Romano" Observatory. He worked on the theory of asteroid orbits and their perturbations. He drew Particular attention to the determination of the ephemerides' corrections for the transit of Venus across the solar disc on 8 December 1882 and the transit of Mercury on 6 May 1878. He discovered two asteroids, 303 Josephina and 306 Unitas (Protić-Benišek, 2002).

For the history of astronomy of this period important are also the articles *Soko-Banja, prvi meteorit u Srbiji* (Soko-Banja, the first meteorite in Serbia) by Josif Pančić (*Glasnik Srpskog učenog društva*, 1880, XLVIII) and *Jelički meteorit* (The meteorite of Jelica) by Jovan Žujović (*Geološki anali*, 1890).

4. STEVAN P. BOŠKOVIĆ AND ASTROGEODETICAL DETERMINATIONS IN THE KINGDOM OF SERBIA

Stevan P. Bošković was born in Zaječar in 1868. He finished the Military Academy in Belgrade in 1889 and in 1892, as a state scholarship holder, he was sent to Russia to study geodesy and astronomy. He was the first officer of Serbian army sent to specialize in advanced geodesy and positional astronomy, since the military authorities noticed the importance of the establishment of the state trigonometric network as the basis for an exact triangulation of Serbia (Dačić and Cvetković, 2002). After finishing the theoretical training in 1897, Bošković came to Pulkovo Observatory, where he learned fundamental astronomy and astrometry. In Pulkovo, Bošković calculated and prepared for the territory of Serbia ephemerides for stellar pairs for determination of time with the Tsinger method and for the determination of latitude by the Pevcov method, as well as Polar star ephemerides for the determination of the azimuth. He also prepared in Pulkovo the project of triangulation of Serbia and the program of astronomical observations. After his return from Russia in 1899 he became professor of geodesy at the Military Academy.

During his studies in Pulkovo Bošković suspected that the reason for geodetic and consequently cartografic, mainly longitudinal disagreement among countries in Panonical and Pontical pools, is probably the deviation of vertical from his normal position toward the ideally curved surface of Earth's geoid. He planned geodetical and astronomical projects in order to check his assumptions. He choosed for this a series of points on the highest mountains, and another series of points in river valleys, counting that in such a way he will examine and discover suspected attractive influences on the normal direction of the Earth's gravitational force intensity, and consequently the deviation of the vertical.

The first determinations on the first – north point of Paraćin's basis and on the highest top – Šiljak of the Rtanj mountain in 1900 gave very good results. Projects on trigonometrical triangulation, on topographical measurements for an 1:25000 map, on topographical measurements of regions liberated during Balkan wars 1912-1913 and the First World War, prevented him of working out of the huge astronomical material which is however preserved. It was transferred by the Serbian army to Krf , after in Saloniki, and after the victory, from Saloniki to Belgrade.

Academician and General Stevan P. Bošković gave great contribution to development of Serbian geodesy, topography and cartography. Also, he is one of the great names of serbian astronomy.

6. MILAN NEDELJKOVIĆ AND THE FOUNDATION OF THE CHAIR FOR ASTRONOMY AND METEOROLOGY

One of the most important personalities within the considered period is certainly the founder of the Chair for Astronomy and Meteorology and of the Belgrade Astronomical and Meteorological Observatory Milan Nedeljković (Belgrade 27. Sept. 1857 - Belgrade 27 Dec. 1950). As a junior lecturer of physics and mathematics at the Grand School (Belgrade University) he applied on August 16, 1878, at the Ministry of Education for continuing abroad his studies, specifically in physics and astronomy and besides analytical and rational mechanics and mathematics. Minister Bošković asked for the opinion of the rector, which arrived on June 12, 1879. According to this opinion the plan of Nedeljković's studies was as follows: 1) The first two years to attend lectures in infinitesimal calculus, probability calculus, mathematical physics, meteorology, rational and analytical mechanics, higher geodesy and astronomy; 2) The third year to dedicate to practical training at the Paris Observatory and to attend special lectures in astronomy and meteorology, mainly those treating the theory and the use of the astronomical and meteorological instruments; 3) The first half of the fourth year was to be spend in London and the second in traveling, visiting thereby the most important astronomical and meteorological establishments. This opinion was signed by Josif Pančić, Kosta Alković, Sima Lozanić, Ljubomir Klerić, Dimitrije Nešić and Dimitrije Stojanović (Janković, 1989). By this opinion Nedeljković was directed towards the astronomical and meteorological studies and on that account he, as a state scholarship holder, was sent to France.

The Grand School Organization Law, passed in 1863, does not refer to astronomy. Astronomy was introduced in 1880 by the Modifications and Supplements of the same Law as a separate subject at the Natural-Mathematical Department of the Philosophical Faculty of the Grand School, the lectures on which were to be attended also by the engineering students. This decision came into force only in 1884 when Milan Nedeljković was back from his studies in France.

On returning from his studies Milan Nedeljković was appointed junior lecturer of astronomy and meteorology, being at the same time entrusted with the Chair for Astronomy and Meteorology of the Grand School, the post he held forty years, until his retirement in 1924. The only break took place between 5th of July 1899 and 31st of October 1900, when he was sent into retirement for political reasons and the Chair for Astronomy and Meteorology has been entrusted to Djordje Stanojević.

7. DJORDJE STANOJEVIĆ THE FIRST SERBIAN ASTROPHYSICIST

Djordje Stanojević (Negotin, 7 April 1858 - Paris 24 Dec. 1921), the first Serbian astrophysicist, the second director of the Belgrade astronomical and meteorological observatory and later rector of Belgrade University, a great popularizator of astronomy and science in general, was the driving force in the introduction of electrical light in Belgrade, Užice, Čačak, Leskovac... He was the builder of the first hydro-electric power station in Serbia, a pioneer of industry of refrigerating appliances, the initiator of setting up a committee for cooling problems and of forming an international organization for cooling techniques in Paris in 1903. He was also the pioneer of the color photography in Serbia.

He finished the elementary school and lower secondary school in his native town Negotin, where today his memorial room is in exhibition. As a grant holder of the Ministry of Military affairs he was from 1883 up to 1887 on study, specialization and work on the most known astronomical and meteorological institutions in Europe in: Berlin (University), Potsdam (Astrophysical observatory), Hamburg (meteorological institute), Paris (Sorbonne), Meudon (Paris observatory for physical astronomy), Greenwich, London and Pulkovo. During this period Stanojević turns to astrophysics and chooses Solar physics as his research field.

In Meudon he works with the founder of this Observatory, the famous astrophysicist Jansen and there he begins the serious scientific work in solar physics and spectroscopy. In 1885 he publishes his first real scientific work: *Analyse spectrale des elements de l'atmosphere terestre* in the journal Communication *a l' Academie des Sciences de Paris*. In the next year, 1886, in this well known scientific journal he publishes the work: *Sur l'origine du resau photospherique Solaire* and *Sur le spectre d'absorption de l'Oxygene* (Trifunović, Dimić, 1976). In 1887 he publishes the scientific work: *Sur la photographie directe de l'etat barometrique de l'atmosphere Solaire*. These astrophysical scientific works, published in editions of the Paris academy of sciences, are the first real scientific works in the modern sense in astrophysics among Serbs.

At the end of his stay in Paris, in August of 1887, he participated as a representative of Paris observatory in the expedition for the observation of the total solar eclipse of 19 August 1887 in Russia (Petrovsk) and published his report (*L'eclipse totale du Soleil du 19 aout 1887, observe en Russie (Petrowsk)*) in the journal of Paris academy. Weather has not been favorable and only 20-25 seconds of observations were successful.

After his return in Serbia in 1887, he became a professor of Physics and Mechanics of the Military academy. He was invited by the Paris observatory to take part in French expedition for investigations of the Sun in Sahara, where he stayed for three months (1891 – 1892). In 1893, after the retirement of Kosta Alković, he became the professor of Experimental physics in Grand School, where he became the director of the Physical institute. From 1900 up to 1913 he was dean of the Philosophical faculty and from 1913 up to 1921 rector of the Belgrade University.

Between 5th of July 1899 and 31st of October 1900 Djordje Stanojević is director of Belgrade astronomical and meteorological observatory and on the head of the Chair for astronomy and meteorology in the Grand School.

His scientific results were so above the scientific level in Serbia that Serbian royal academy rejected the publication of his article on solar physics. Disappointed he practically leaves the scientific work in astrophysics. In editions of the Paris academy of sciences he publishes after that only a review: *L'etat actuel de la photographie du Soleil,* in 1889.

After this he works in physics and on practical problems of electrification and industrialization of Serbia. He performs electrification of Belgrade, Užice, Leskovac, Čačak, Zaječar... He takes part in the construction of the first hydro - electric power station in Serbia near Užice. In Grand School he organises a service for the repairment of electromotors. He introduces color photography in Serbia and publishes in 1901 the first book with such photos: *Srbija u slikama (fotografski snimci)* (Serbia in pictures (photographies)). He continues on serious scientific work in physics, and after a break of nine years his scientific articles appear again in *Communication a l' Academie des Sciences de Paris*, but now on experimental physics (Trifunović, Dimić, 1976).

8. FOUNDATION OF ASTRONOMICAL AND METEOROLOGICAL OBSERVATORY

The principal astronomical institution in Serbia is the Belgrade Astronomical Observatory, one of the oldest scientific organizations and the only autonomous astronomical institute in Yugoslavia. Its past development forms an important part of the history of science and culture in these regions. The decree of its founding conjointly with the Meteorological Observatory was signed on 20 March (7 April) 1887 by the Minister of Education and Church Affaires of Kingdom of Serbia Milan Kujundžić Aberdar on the initiative of Milan Nedeljković. He was appointed first director of the newly founded Observatory.

On the 1st of May of 1871 Nedeljković started his activity at the provisory Observatory in the rented Geizler family's house. Here, the Observatory was operating until the 1st of May of 1891, when it was moved into its own building constructed meanwhile - the one in which at present is Meteorological Observatory in the Karadjordje Park. In the minor museum section of this building there is, since the celebration of the Observatory's centenary in 1987, a room dedicated to the origins of astronomical science in Serbia and Montenegro.

Nedeljković was at the head of the Observatory from 26 March (7 April) 1887 until the 30st of January 1924. A break took place only between 5th of July 1899 and 31st of October 1900, when he was sent into retirement for political reasons.

Apart from its importance for astronomy and meteorology, the newly built Observatory, headed by Nedeljković, was a cradle of the seismic and geomagnetic researches in Serbia. In the course of its history the Belgrade Astronomical Observatory grew to an institution of great importance in the history of science and culture of the Serbian people. Linked to this institution are the names of the famous personalities in the history of science, who contributed to the Observatory and the scientific achievements of Serbian astronomers in general, having earned esteem in the international scientific community. Young people in our country have a good perspective, in engaging in this beautiful and challenging science, in an ambiance enabling them to achieve results of the highest value.

Acknowledgements: This work is a part of the project GA 1471 “The history of astronomy in Serbia” supported by the Ministry of Science, Technologies and Development of Serbia.

REFERENCES

Banjac N.: 1999, Serbian Astronomical Journal, **160**, 75.
Dačić M., Cvetković Z.: 2002, Publ. Astron. Obs. Belgrade, **72**, 25.
Janković N.: 1955, Astronomy with Serbs (in Serbian), Encyclopedia of Yugoslavia I, Leksikografski zavod FNRJ, Zagreb.
Janković N.: 1989, Publ. Obs. Astron. Belgrade, **36,** 107.
Jovanović B. D.: 1985, Publ. Astron. Soc. “Rudjer Bošković”, No. 4, Belgrade, 117.
Jovanović B. D.: 1990, We will not go to the XVIII century (in Serb.), Dnevnik, 14. VII, 2.
Milogradov - Turin, J.: 2001a, Flogiston, **11**, 15.
Milogradov - Turin, J.: 2001b, Vasiona, **49**, No. 1-2, 1.
Protić-Benišek V.: 2002, Publ. Astron. Obs. Belgrade, **72**, 147.
Trifunović D., Dimić M.: 1976, Bibliography of works of Djordje Stanojević (in Serbian), In: Stanojević Djordje M: Nikola Tesla and his discoveries, Beograd.

SESSION VIII

HISTORY OF ASTRONOMY

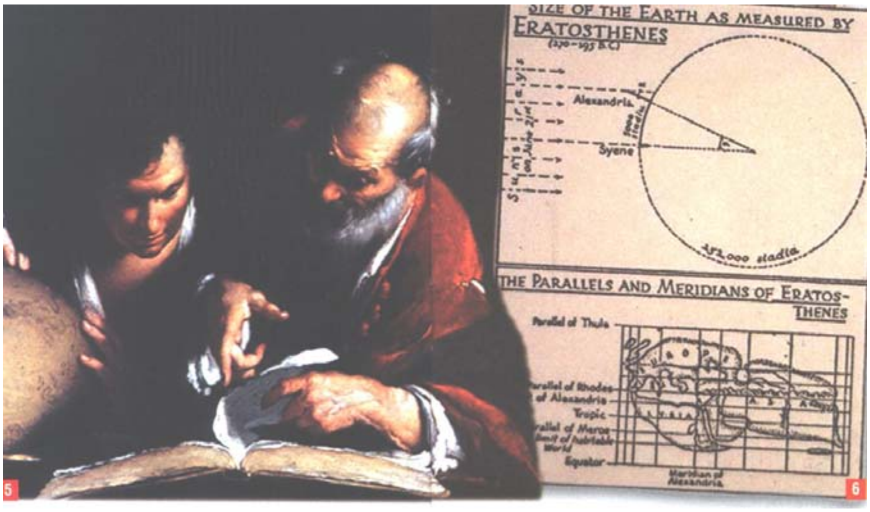

TEACHING OF ASTRONOMY

Conveners: E. Theodossiou and E.Danezis

ΜΕΛΕΤΗ-ΚΑΤΑΓΡΑΦΗ ΗΛΙΑΚΩΝ ΡΟΛΟΓΙΩΝ ΜΙΑ ΠΡΟΤΑΣΗ ΕΛΕΓΧΟΥ*

Στράτος Θεοδοσίου

Τομέας Αστροφυσικής-Αστρονομίας και Μηχανικής
Τμήμα Φυσικής-Πανεπιστήμιο Αθηνών

ΠΕΡΙΛΗΨΗ

Η έρευνά μας αυτή αποτελεί ένα μακροχρόνιο πρόγραμμα μελέτης και καταγραφής των αρχαίων, βυζαντινών-μεσαιωνικών και νεότερων ηλιακών ρολογιών της Ελλάδος.
Από τη στατιστική έρευνα της σχετικής Βιβλιογραφίας, αλλά και από επιτόπιες έρευνές μας, διαπιστώθηκε μια αριθμητική δυσαρμονία μεταξύ αφ' ενός των αρχαίων και νεότερων ηλιακών ρολογιών της Ελλάδος και αφ' ετέρου των βυζαντινών-μεσαιωνικών ηλιακών ρολογιών. Ουσιαστικά μιλάμε για ένα μεγάλο πλήθος ηλιακών ρολογιών στις δύο πρώτες κατηγορίες και ένα ελάχιστο αριθμό ηλιακών ρολογιών στη Βυζαντινή περίοδο. Σ' αυτήν ακριβώς την αριθμητική δυσαρμονία και τις πιθανές εξηγήσεις της επικεντρώθηκε η μελέτη μας.

1. Η ΚΑΤΑΓΡΑΦΗ ΤΩΝ ΗΛΙΑΚΩΝ ΡΟΛΟΓΙΩΝ

Ερευνώντας αρχικά τα ηλιακά ρολόγια στην Αρχαία και τη Νεότερη Ελλάδα διαπιστώσαμε ότι υπήρχαν και υπάρχουν πολλά απ' αυτά με χαρακτηριστικά παραδείγματα: τα οκτώ κατακόρυφα ηλιακά ρολόγια στο μνημείο του Ανδρονίκου του Κυρρήστου (Αέρηδες) κ.ά. Άλλωστε η Sharon Gibbs στη μελέτη της *«Greek and Romans sundials»* (1976) αναφέρει δεκάδες κωνικά ηλιακά ρολόγια που βρέθηκαν από τις ανασκαφές και φυλάσσονται στα Μουσεία διαφόρων πόλεων της πατρίδας μας.
Ομοίως στη νεότερη Ελλάδα υπάρχουν δεκάδες ηλιακά ρολόγια, όπως αναφέρει ο Manfred Hüttig (2002), τα περισσότερα οριζόντια, που αποτελούν διακοσμητικά στοιχεία κήπων και πλατειών. Ως παραδείγματα αναφέρουμε το ηλιακό ρολόι στον Εθνικό Κήπο στην Αθήνα, το ηλιακό ρολόι στα Ψηλά Αλώνια στην Πάτρα και πλήθος άλλων.
Απέμενε, λοιπόν, ως ερευνητικός χώρος η περίοδος μετά την αρχαιότητα έως τη σύγχρονη εποχή. Ουσιαστικά η Βυζαντινή Ελλάδα, περίοδος που περιέχει και την αντίστοιχη Μεσαιωνική. Με έκπληξή μας είδαμε ότι τα ηλιακά ρολόγια αυτή τη χρονική περίοδο σπανίζουν στην Ελλάδα. Και γράφουμε με έκπληξή μας επειδή την αντίστοιχη περίοδο στη Μεσαιωνική Ευρώπη εκατοντάδες ηλιακά ρολόγια έχουν καταγραφεί στις ευρωπαϊκές χώρες. Μάλιστα αυτό συμβαίνει σε χώρες, που κατά τεκμήριο δεν φημίζονται για την ηλιοφάνειά τους. Θα περιμέναμε, λοιπόν, σε μια ηλιόλουστη χώρα, όπως η πατρίδα μας, να υπάρχει πλήθος ηλιακών ρολογιών. Δεν συμβαίνει όμως αυτό. Αντιθέτως λιγότερα από δέκα ηλιακά ρολόγια μελέτησε και κατέγραψε η ερευνητική μας ομάδα.

2. ΠΙΘΑΝΗ ΕΞΗΓΗΣΗ

Όλα τα Βυζαντινά ηλιακά ρολόγια της Ελλάδας βρίσκονται σε χριστιανικούς ναούς και είναι κατακόρυφα. Μελετώντας τα, είδαμε ότι πρόκειται είτε για αυτόνομα γλυπτά ενσωματωμένα στους νότιους τοίχους του αντίστοιχου ναού είτε πρόκειται για εγχάρακτα ηλιακά ρολόγια πάνω στον αντίστοιχο μονόλιθο, τον ενσωματωμένο στον τοίχο της

* *Proceedings of the 6th Hellenic Astronomical Society Conference, 15-17 September 2003, Penteli, Greece*

εκκλησίας. Αυτού του τύπου θεωρούμε ότι είναι το κατακόρυφο ηλιακό ρολόι στον ναό της Θεοτόκου στη Μονή του Οσίου Λουκά.
Τονίζουμε το γεγονός ότι παρά το μεγάλο πλήθος των βυζαντινών ναών της Ελλάδος, δεν είναι αντίστοιχος ο αριθμός των ηλιακών ρολογιών. Το ερώτημα είναι γιατί;
Η απάντησή μας είναι ότι τα Βυζαντινά ηλιακά ρολόγια κατασκευάστηκαν μόνο σε εκείνες τις περιοχές όπου εν γένει κατά καιρούς έδρασαν Φράγκοι ή Δυτικοί κατακτητές της Ελλάδας κατά τον Μεσαίωνα. Δηλαδή κατηγορηματικά αναφέρουμε ότι δεν υπάρχουν για παράδειγμα ηλιακά ρολόγια στον Βυζαντινό Μυστρά, ενώ υπάρχουν στην Αργολίδα: στα χωριά Αγία Τριάδα (Μέρμπακας) και Νέο Ηραίο, όπου είναι βέβαιο ότι έφθανε η δικαιοδοσία του δομινικανού καθολικού επισκόπου της Κορίνθου William of Moerbeke (1278-1286).
Αυτό σημαίνει ότι για κάποιο σοβαρό λόγο δεν τοποθετήθηκαν εξαρχής ηλιακά ρολόγια στις Ελληνικές Ορθόδοξες Εκκλησίες, όταν τούτο ήταν κάτι το σύνηθες στις αντίστοιχες εκκλησίες της Δύσης.
Γιατί όμως; Η απάντηση, κατά τη γνώμη μας, πηγάζει από την όλη κοσμοθεωρία της Ανατολικής Ορθόδοξης Εκκλησίας. Πιθανότατα για την Ανατολική Εκκλησία η Αστρονομία ήταν κάτι το απαγορευμένο ή μάλλον χρήσιμο μόνον για κάποιους ιθύνοντες και για κάποιες γενικές γνώσεις, αλλά ουσιαστικά χωρίς ιδιαίτερη αξία ή ακόμη και απαγορευμένο για τους πολλούς;

Ίσως η όλη κοσμοθεωρία των Πατέρων της Ανατολικής Εκκλησίας απέρρεε από το ότι –σύμφωνα με τα απόκρυφα του Ενώχ – διδάσκαλος της Αστρονομίας στους ανθρώπους ήταν ο εκπεπτωκός άγγελος Ιλώτας, ο μετέπειτα δαίμονας Μπελιάλ; Γι' αυτόν τον λόγο η Αστρονομία ήταν η «απαγορευμένη» επιστήμη, αυτή που έπρεπε να βρίσκεται στα χέρια των ειδικά εκπαιδευμένων ιερωμένων-μυστών και μόνον. Είναι χαρακτηριστική η άποψη του Μ. Βασιλείου – που μολονότι ο ίδιος σπούδασε Αστρονομία στην Αθήνα – στις Ομιλίες του στην Εξαήμερο αναφέρει τα εξής: *Τι νόημα έχουν οι γεωμετρίες και οι μέθοδοι των μαθηματικών και οι στερεομετρίες και η πολυθρύλητη αστρονομία, όλη η πολυάσχολη ματαιότητα, αν όσοι ασχολούνται με ζήλο με αυτά έκαναν τη σκέψη ότι ο κόσμος που βλέπομε είναι συναΐδιος με τον κτίστη των όλων Θεό, εξισώνοντας στο μεγαλείο τον περιορισμένο και με υλικό σώμα κόσμο με την απεριόριστη και αόρατη φύση;(Ομιλία Α΄, γ΄).*

Επομένως, σύμφωνα με τον Μεγάλο Πατέρα της Εκκλησίας μας, είναι αδιανόητο ο κτιστός φθαρτός, και περιορισμένος χρόνος να αναχθεί και να συσχετιστεί με τον άκτιστο-αιώνιο χρόνο και τον Θεό Δημιουργό. Πιθανότατα, λοιπόν, ο Μέγας Βασίλειος έδωσε το στίγμα που αποτέλεσε και πάγια αρχή-άποψη της Ανατολικής Εκκλησίας: Η μελέτη της Αστρονομίας ίσως ήταν μία επικίνδυνη ενασχόληση (για τους αδαείς). Παρά το γεγονός ότι πολλοί Πατέρες της Εκκλησίας σπούδασαν Αστρονομία – όπως γίνεται φανερό από τη μελέτη των έργων τους – εντούτοις η τετρακτύς (Quatrivium): Αστρονομία, Αριθμητική, Γεωμετρία και Μουσική θεωρείτο κατώτερη από τις αντίστοιχες θεολογικές και φιλοσοφικές σπουδές και το Trivium (Γραμματική, Ρητορική και Διαλεκτική).
Ο Μέγας Βασίλειος (P.G. 29, 9) καλεί την Αστρονομία πολυάσχολη ματαιότητα. Ωστόσο, αλλού πάλι θεωρεί την παρατήρηση των άστρων αναγκαία, διότι δι' αυτής προβιβαζόμαστε στη γνώση της θείας σοφίας, και σωτήρια τα εξ αυτής συμπεράσματα. *«Τι άλλο μας διδάσκει η Σελήνη πλησιφαής γινομένη και πάλι φθίνουσα, παρά να μη μεγαλοφρονώμεν δια τας ευημερίας του βίου; Αρκεί μόνον να μη περιεργάζεταί τις τα υπό των άστρων σημεία πέραν του δέοντος».*

Επιπλέον ο Μέγας Βασίλειος έψεγε όσους θεωρούσαν ότι η γήινη ζωή εξαρτιόταν από την κίνηση των άστρων (P.G. 29, 128), ή εκείνους που ζητούσαν να μάθουν την τύχη των νεογέννητων από τα άστρα (P.G. 29, 128 εξ.).

Ο Γρηγόριος ο Θεολόγος χαρακτήριζε την Ασία ως *«ασεβείας διδασκαλείον»,* επειδή εκεί διδασκόταν η αστρονομία και η μετ' αυτής συνδεδεμένη *«γοητεία»* (P.G. 35, 557), ενώ τους αστρολόγους χαρακτήριζε ως *«των ουρανίων καταψευδομένους»* (P.G. 35, 669). Τόνιζε ακόμη το γεγονός ότι ο αδελφός του, ο Καισάριος, απέφυγε τις επικίνδυνες διδασκαλίες της Αστρονομίας που υποστήριζαν ότι από τα άστρα εξαρτώνται τα όντα και όλα τα επί της Γης γινόμενα (P.G. 35, 761).

Άξια μνείας είναι και η τοποθέτηση του νεότερου αδελφού του Μεγάλου Βασιλείου, του κοσμολόγου Αγίου Γρηγορίου Νύσσης (335-394), η θεολογία του οποίου εναρμονιζόταν άριστα με την ανθρωπολογία και την κοσμολογία με κέντρο τον Τριαδικό Θεό και την ενανθρώπιση του Χριστού, μέσω του οποίου μπορούμε να προσεγγίζουμε τη θεία υπόσταση.

Ο Γρηγόριος ο Νύσσης στον «Απολογητικό του εις την Εξαήμερον» (379), όπου συμπληρώνονται οι περί της Εξαημέρου Ομιλίες του Μεγάλου Βασιλείου θεωρούσε ότι ο χρόνος γινόταν αντιληπτός σαν ένα θετικό δημιούργημα του Θεού, μέσα από τον οποίο δημιουργήθηκε ο άνθρωπος.

Ο άνθρωπος είναι κέντρο του υλικού κόσμου και μεθόριος της ορατής και αόρατης κτίσης. Ωστόσο παραμένει κτίσμα και είναι απλώς μέτοχος της θείας ζωής. Η κτιστή φύση του έχει ως συνέπεια τη μεταβολή. Αντιθέτως, η θεία φύση είναι αναλλοίωτος και δεν υπόκειται στον νόμο της χρονικής μεταβολής. Εκτός της βασικής διάκρισης μεταξύ ακτίστου και κτιστού, δημιουργού και δημιουργημάτων, η φύση διακρίνεται σε υλική και πνευματική. Στη δεύτερη ανήκουν οι άγγελοι, ενώ ο άνθρωπος είναι «μεθόριος» της ορατής ή υλικής και της αόρατης ή πνευματικής κτίσης. Με το σώμα του μετέχει στην πρώτη, ενώ με την ψυχή του στη δεύτερη.

Ειδικά ο άνθρωπος γεννήθηκε με το χάρισμα να μπορεί να διακρίνει το καλό από το κακό. Η θνητότητά του είναι εκείνη που τον οδηγεί κάποιες φορές προς τον κόσμο της αμαρτίας και το κακό. Η θέση του Γρηγορίου Νύσσης ήταν ότι η διάρκεια της ζωής του ανθρώπου δεν είναι μια ισόβια καταδίκη – μέσα στην οποία πρέπει να υποφέρει – αλλά ένα δώρο συνεχούς καλυτέρευσης, ώστε τελικά να επιλέξει το καλό και να πλησιάσει τον Δημιουργό του στον αντιληπτό – από τον άνθρωπο – χρόνο. Και αυτό ακριβώς είναι το κομβικό σημείο. Δεν μπορεί ένα θνητό δημιούργημα του Θεού να συλλάβει την έννοια του άχρονου-χρόνου. Ο άνθρωπος δεν μπορεί να γίνει «αντιπρόσωπος» του Θεού, να σταθεί δηλαδή προς αυτόν «πρόσωπο προς πρόσωπο». Ο Θεός είναι υπέρβαση. Συνεπώς είναι περιττή, αν όχι βλάσφημη, η τοποθέτηση ηλιακού ρολογιού – που χρησιμοποιεί για τη μέτρηση του χρόνου τον εθνικό θεό Ήλιο – πάνω στον τοίχο του ορθόδοξου ναού για να μετρά τις ώρες αναβιβάζοντας τον επίγειο χρόνο και κάνοντάς τον να γίνεται αντιληπτός ως συναΐδιος χρόνος του Δημιουργού, όπως ακριβώς φοβόταν ο Μέγας Βασίλειος.

Ο Γρηγόριος ο Νύσσης θεωρούσε ότι ουδέποτε εκ των κτισμάτων της φύσεως αφορμώμενοι θα δυνηθούμε να εννοήσουμε την πρώτη αρχή. Η σκέψη μας κινείται πάντοτε εντός του πλαισίου του χρόνου και του χώρου. Η συνδιαλλαγή του Θεού προς τον άνθρωπο δεν περιορίζεται, σύμφωνα με τον Γρηγόριο, μόνον στον άνθρωπο, αλλά περιλαμβάνει ολόκληρη την *«εν χώρω»* και *«εν χρόνω»* κτίση. Αυτή θα συντελεστεί κατά την *«ογδόη»* ημέρα της Δημιουργίας, η οποία θα είναι ημέρα κειμένη *«επέκεινα»* των ημερών. Κατ' αυτήν θα παύσει η ροή του *«αισθητού χρόνου»*, ο οποίος κινείται κυκλικά. Η «ογδόη» ημέρα δεν θα επιδέχεται εν εαυτή τη διαδοχή του αριθμού, δεν θα εκπίπτει ο χρόνος εις το τρισδιάστατο συνεχές του παρελθόντος, παρόντος και μέλλοντος. Θα είναι ημέρα *«ουκέτι την του αριθμού διαδοχήν εφ' εαυτής δεχομένη»*. Κατ' αυτήν θα συντελεστεί η μεταμόρφωση του ροϊκού (αισθητού) χρόνου στον αδιαίρετο και ενιαίο «αιώνα».

Επιπροσθέτως, τονίζουμε το γεγονός ότι ο ορθόδοξος ναός ποτέ δεν εκλήφθηκε ως ένα «σκηνικό», ένα επίγειο θέατρο για την παρουσίαση κοσμικών γεγονότων, αλλά ως η κατοικία του Θεού, ο μικρόκοσμος της Βασιλείας των Ουρανών, όπου ο χρόνος είναι αιώνιος! Για τον λόγο αυτό δεν διακοσμήθηκε ποτέ με αγάλματα αγγέλων, ή με ηλιακά ρολόγια όπως πολλοί ναοί της Δύσης (ναός της Sartres).
Παρ' όλα αυτά, ειδικός κανόνας της Δ΄ Οικουμενικής Συνόδου (451) επιτρέπει την ελεύθερη ενασχόληση με την Αστρονομία. Πράγματι κατά τους Βυζαντινούς, όπως ήδη αναφέραμε, τα *μαθήματα* ήταν η Αριθμητική, η Γεωμετρία η Μουσική και η Αστρονομία, που υποδιαιρείτο – σύμφωνα με τον Φαίδωνα Κουκουλέ – στην καθ' αυτό Αστρονομία, που εξέταζε τη θέση, κίνηση, απόσταση κ.ά. των ουρανίων σωμάτων και επομένως μη απαγορευμένη και στην αστρολογία που εξέταζε τα απαγορευμένα και απόκρυφα μαθηματικά, και η οποία δίδασκε ότι τα ανθρώπινα δρώμενα εξαρτώνται από τα ουράνια σώματα. Η τελευταία εννοείται ότι απαγορευόταν και οι μ' αυτήν ασχολούμενοι αστρολόγοι, που καλούνταν και μαθηματικοί, καταδιώκονταν από την Πολιτεία και την Εκκλησία. Έτσι, σύμφωνα με τον Ιουστινιάνειον κώδικα που *πραγματευόταν De maleficis et mathematicis et ceteris similibus*, απαγορευόταν η άσκηση της μαθηματικής (Cod. Just. 9, 18, 2), μια διάταξη που ίσχυε συνεχώς και επαναλαμβανόταν και σε μεταγενέστερους αιώνες (Βασιλικά 60, 39, 23, Φωτίου Νομοκανόνων, 9, κεφ. 25). Τα δε βιβλία τους απομακρύνονταν από κάθε πόλη και συνήθως καίγονταν (Φωτίου Νομοκανόνων, 12, κ. 3).
Ωστόσο δεν είναι φανερή η διαφορά μαθηματικών και αστρολόγων ή μάλλον δεν ταυτίζονταν απόλυτα οι δύο αυτές έννοιες, αφού σύμφωνα με τον Θεόδωρο Βαλσαμώνα:

«Μαθηματικοί οι τα ουράνια σώματα δοξάζοντες έχειν την του παντός κυριότητα και κατά την κίνησιν αυτών διοικείσθαι τα καθ' ημάς. Αστρολόγοι οι δια των αστέρων μαντευόμενοι κατά δαιμονικήν συνέργειαν και τούτοις πιστεύοντες» (Ράλλη-Ποτλή, Σύνταγμα 3, 205).
Επιπλέον, η Σύνοδος της Λαοδικείας, με τον 36ο κανόνα της απαγόρευε στους κληρικούς να γίνονται μαθηματικοί (Ράλλη-Ποτλή, Σύνταγμα 3, 203) και η Διδαχή των δώδεκα Αποστόλων, στο τρίτο της κεφάλαιο, συνιστά να μη γίνεται κάποιος μαθηματικός: *«εκ γάρ τούτου ειδωλολατρεία γεννάται»* (Ευσέβιος Αλεξανδρείας, P.G. 86^1, 453).

Επίσης ο Ιεροσολύμων Κύριλλος χαρακτήριζε τα της Αστρονομίας ως *«παρανομώτατα πράγματα»* (P.G. 33, 501).
Όλα τα παραπάνω αντανακλούν το αδιαμφισβήτητο γεγονός ότι στην Ορθόδοξη Ανατολική Εκκλησία – εκτός ελαχίστων περιπτώσεων, που επιβεβαιώνουν τον κανόνα – τα ηλιακά ρολόγια θεωρούνταν περιττά ως προς τον άχτιστο χρόνο του Δημιουργού, αλλά και ανίερα στολίδια του ιερού χώρου. Οι ορθόδοξες εκκλησίες δεν ήταν κατ' ουδένα τρόπο τα κατάλληλα κτίρια για την τοποθέτηση ηλιακών ρολογιών.
Επομένως μετά βεβαιότητος μπορούμε να πούμε ότι όπου στη Μεσαιωνική-Βυζαντινή Ελλάδα υπάρχουν ηλιακά ρολόγια σε ναούς, υποδηλώνουν είτε ρωμαιοκαθολική επίδραση ή κατάκτηση της περιοχής – όπου υπάρχουν αυτοί οι ναοί – από Φράγκους ή Καταλανούς ή εν γένει κατακτητές ρωμαιοκαθολικούς το θρήσκευμα. Εξάλλου αυτοί θα είχαν μαζί τους και τους κατάλληλους τεχνίτες και γνώστες της Γνωμονικής, αφού – όπως φαίνεται – αυτή η τέχνη ήταν μάλλον άγνωστη στη Βυζαντινή-Μεσαιωνική Ελλάδα.

Ευχαριστίες

Ευχαριστούμε τον υποψήφιο διδάκτορα της Θεολογικής Σχολής κ. Ιωάννη Ρουσάκη για τα εποικοδομητικά του σχόλια στην εργασία μας.

Abstract

A systematic study of sundials-A new proposition
(Efstratios Theodossiou)
This investigation is a long-time study and listing program of the Ancient, Byzantine and Modern sundials in the whole Hellenic territory, from Constantinople to Crete and from Florina to Mystras. Studying the statistical contribution of all Greek sundials – from both the Bibliography and our local investigations – we found that there is a numerical discord between the ancient and Modern Greek sundials and the corresponding Byzantine.
Essentially we found that there is a great number of ancient and hundreds of modern sundials in Greece, while there are only ten sundials constructed during the thousand-year Byzantine period. We present here a new proposition on the construction of the ten Byzantine sundials and we try to explain the arithmetical discord.

ΒΙΒΛΙΟΓΡΑΦΙΑ

Βασιλείου του Μεγάλου, 1990, *Ομιλίες στην Εξαήμερο.* Μετάφραση Ιγνάτιος Σακαλής. Φιλοσοφικός Λόγος, Εκδ. Πολύτυπο, Αθήνα.

Γρηγορίου Νύσσης, *Απολογητικός εις την Εξαήμερο*. P.G. 44, 61-124 κ.ά.

Gibbs L. Sharon, 1976, *Greek and Romans sundials*, Yale University Press, New Haven and London.

Hüttig Manfred, August 2002, *Katalog der Sonnenuhren in Griecheland*, Wolfenbüttel (private communication).

Κουκουλέ Φαίδωνος, Μάιος 1948, *Βυζαντινών Βίος και Πολιτισμός*, Τόμος Α΄, ΙΙ, Εκδόσεις Παπαδήμα, Αθήναι, σελ. 144-146.

Νιάρχου Κωνσταντίνου, 1997, *Προβλήματα της Ευρωπαϊκής Φιλοσοφίας*, Εκδόσεις του Πανεπιστημίου Αθηνών, Αθήναι.

ANCIENT CELESTIAL SPHERES FROM THESSALY*

X. Moussas, V. Petoussis and S. Dimitrakoudis
Section of Astrophysics, Astronomy and Mechanics, Department of Physics, University of Athens

Abstract: We present some small finds (periapta) found in during excavations at the temple of Athena Itonia near Philia in Thessaly, which could be ancient celestial spheres as the ones described by Plato, or the first celestial sphere constructed by Chiron to be used by Jason and the Argonautes in their long journey to the unknown. The spheres have what seems to be an equator and several meridians (semi-circles), four, five or six. They all have a hole in their lowest part, possibly to accommodate a stick (axis) and another hole near the top which could accommodate another stick perpendicular to the axis. Such an instrument could be used to measure the time at a known place, or at a place of known latitude, as well as to measure the latitude at a given time (best at noon). These periapta might well be portable and universal (that can be used in every place) astronomical instruments as the ones used for centuries after.

* *Proceedings of the 6th Hellenic Astronomical Society Conference, 15-17 September 2003, Penteli, Greece*

ΜΑΘΗΜΑΤΙΚΟ ΚΑΙ ΑΣΤΡΟΝΟΜΙΚΟ ΜΥΣΤΗΡΙΟ ΤΩΝ ΠΥΡΑΜΙΔΩΝ*

Α. Δακανάλης και Ε.Θεοδοσίου

Τομέας Αστροφυσικής-Αστρονομίας και Μηχανικής
Τμήμα Φυσικής-Πανεπιστήμιο Αθηνών

ΠΕΡΙΛΗΨΗ

Στην εργασία αυτή δίνεται μια επιγραμματική παρουσίαση ορισμένων θεωριών που επιχειρούν να δώσουν απάντηση σε κάποια από τα ερωτήματα με τα οποία μας κατακλύζουν οι πυραμίδες της Αιγύπτου. Αυτές είναι η θεωρία της «Ταυτόχρονης Μετάβασης» της K. Spence, η μελέτη χωροθέτησης των πυραμίδων στην Γκίζα του J. Legon καθώς και η θεωρία του «Σημείου Φυγής» του S. Goodfellow. Τέλος, αφού γίνει αναφορά στην ανακάλυψη του R. Gantenbrink, παρουσιάζεται επιγραμματικά η θεωρία της «Συσχέτισης με τον Ωρίωνα» του R. Bauval.

ΕΙΣΑΓΩΓΗ

Στην Αίγυπτο υπάρχουν περίπου 90 πυραμίδες. Κοινή παραδοχή ανάμεσα στους Αιγυπτιολόγους αποτελεί το γεγονός πως δεν υπάρχουν στοιχεία για την ύπαρξη μιας μακράς προπαρασκευαστικής περιόδου ανάπτυξης ούτως ώστε να δικαιολογείται η αρχιτεκτονική και κατασκευαστική τελειότητα των πρώτων πυραμίδων. Δεύτερο παράδοξο αποτελεί το γεγονός πως έπειτα από την 4^{η} δυναστεία οι πυραμίδες είναι όχι μόνο μικρότερες σε μέγεθος, αλλά και πολύ κατώτερες σε ποιότητα. Οι Αιγυπτιολόγοι ακολουθώντας το δόγμα πως οι πυραμίδες ήταν τάφοι των φαραώ εκτιμούν πως οι λόγοι ήταν οικονομικοί έχοντας στο νου το τεράστιο κόστος που απαιτείται για το χτίσιμο μιας πυραμίδας. Η εξήγηση αυτή δεν μοιάζει να είναι ορθή διότι, θα περίμενε κανείς να διατηρηθεί τουλάχιστον η κατασκευαστική γνώση και απλώς να μικρύνει το μέγεθος της πυραμίδας.

Η διαδικασία εύρεσης του φαραώ στον οποίο ανήκει μια πυραμίδα είναι εξαιρετικά δύσκολη. Αυτό κυρίως οφείλεται στο γεγονός πως κάθε φαραώ είχε περίπου πέντε διαφορετικά ονόματα καθώς και στο γεγονός πως η ιερογλυφική γραφή απουσιάζει από τις πυραμίδες της 3ης και 4ης δυναστείας. Το πρόβλημα γίνεται εντονότερο όταν αναλογιστούμε τη μεγάλη αβεβαιότητα που υπάρχει για τη χρονολόγηση των συνολικά 30 δυναστειών, η οποία οξύνεται όσο βαδίζουμε στην αρχαιότητα. Το πρόβλημα χρονολόγησης ενός φαραώ μεταφέρεται και γίνεται πρόβλημα χρονολόγησης μιας πυραμίδας. Το γεγονός πως οποιοσδήποτε φαραώ 4ης δυναστείας θάφτηκε μέσα σε πυραμίδα παραμένει αναπόδεικτο. Υπάρχουν πολλά στοιχεία που υποστηρίζουν την άποψη πως οι πρώτες πυραμίδες δεν λειτουργούσαν ως τάφοι.

Εμείς υιοθετούμε την ορθότερη άποψη, δηλαδή πως δεν μπορούμε να προσπελάσουμε τα εμπόδια 4500 περίπου ετών και να μάθουμε την αντικειμενική αλήθεια για το εάν ήταν τάφοι ή όχι. Δεν αμφισβητούμε όμως τον ολοφάνερο νεκρικό χαρακτήρα τους.

ΟΙ ΘΕΩΡΙΕΣ

Κατά παράδοση, οι πυραμίδες χτίζονταν κατά τρόπο που η κάθε τους πλευρά προσανατολιζόταν στα τέσσερα σημεία του ορίζοντα με μεγάλη ακρίβεια και οι είσοδοι τους βρίσκονταν πάντα στη βορινή πλευρά. Κατά κανόνα, η είσοδος τους βρισκόταν ψηλότερα από τον υπόγειο κεντρικό θάλαμο και ο διάδρομος που ένωνε τα δύο μέρη ήταν κατηφορικός, με

* *Proceedings of the 6th Hellenic Astronomical Society Conference, 15-17 September 2003, Penteli, Greece*

κλίση περίπου 26 μοιρών. Ήταν πρακτικό γιατί ο θάλαμος μπορούσε να σφραγιστεί εύκολα τοποθετώντας ογκώδεις λίθους που έφραζαν τον διάδρομο. Είχε όμως και συμβολικό χαρακτήρα διότι η ψυχή του φαραώ βγαίνοντας από το θάλαμο και περνώντας χωρίς πρόβλημα μέσα από τα λίθινα εμπόδια, θα ανηφόριζε με κλίση γύρω στις 26 μοίρες και θα κατευθυνόταν προς τον πολικό αστέρα και τους αειφανείς αστέρες, δηλαδή προς τη θεία της πηγή. Εξαίρεση στον κανόνα αποτελεί η μεγάλη πυραμίδα, που θα εξετάσουμε λεπτομερέστερα αργότερα.

Ας εστιάσουμε τώρα το ενδιαφέρον μας σε μια θεωρία που αφορά στην τοποθέτηση των πυραμίδων έτσι ώστε να προσανατολίζονται προς τα 4 σημεία του ορίζοντα. Ονομάζεται θεωρία της Ταυτόχρονης Μετάβασης (Simultaneous Transition), προτάθηκε από την Δρ.Kate Spence του τμήματος Ανατολικών Σπουδών του Πανεπιστημίου της Οξφόρδης και δημοσιεύτηκε στο περιοδικό Nature (2000). Είναι μια προσπάθεια για χρονολόγηση των πυραμίδων από αστρονομικά δεδομένα.

Η Spence υποστηρίζει πως οι αρχαίοι Αιγύπτιοι καθόριζαν την ακριβή κατεύθυνση του βορρά ευθυγραμμίζοντας ένα αλφάδι με τη νοητή ευθεία που σχηματίζει ο μεγάλος κύκλος που περνά από τα αστέρια Kochab (β UMi) και Mizar (ζ UMa), καθώς και από τον άξονα που τρέχει από βορρά προς νότο και βρίσκεται επί των ανατολικών ή δυτικών πλευρών των πυραμίδων. Δεδομένου ότι η μέθοδος δεν άλλαξε ανά τους αιώνες, τότε θα πρέπει να παρουσιάζεται ένα συστηματικό σφάλμα στον προσανατολισμό των πυραμίδων, που οφείλεται στην απομάκρυνση της νοητής αυτής ευθείας από τον πολικό αστέρα, η οποία οφείλεται στο φαινόμενο της μετάπτωσης.

Ο John Legon (2003), πτυχιούχος της Σχολής Εφαρμοσμένων Φυσικών Επιστημών και με μεγάλο ενδιαφέρον στην αρχαιολογία, μελέτησε εκτενώς και επέκτεινε την πρώτη τοπογραφική μελέτη που έγινε στην Γκίζα από τον W.M.F. Petrie (1883). Βασιζόμενος στα αποτελέσματα της μελέτης του, υποστηρίζει πως βρήκε τις μαθηματικές σχέσεις με τις οποίες οι κτίστες καθόρισαν το μέγεθος και τη χωροθέτηση των τριών πυραμίδων. Επίσης υποστηρίζει πως υπήρχε ένα ενιαίο σχέδιο που ακολουθήθηκε, και μελετά μέχρι και σήμερα την ύπαρξη κάποιου βαθύτερου συμβολισμού σε αυτό. Μιας και η εργασία του στον τομέα αυτό δεν έχει τελειώσει, δεν μπορούμε να παρουσιάσουμε τις ιδέες του για τον συμβολισμό αυτή τη στιγμή.

Μια άλλη ενδιαφέρουσα θεωρία είναι αυτή του «Σημείου Φυγής», εμπνευσμένη από τον τότε απόφοιτο της Σχολής Καλών Τεχνών Stephen Goodfellow (2003), ο οποίος συνεργάστηκε με τον John Legon. Σημείο φυγής του ζωγράφου σε ένα προοπτικό σχέδιο, είναι το σημείο τομής δύο ευθειών που στην πραγματικότητα είναι παράλληλες. Τρία σημεία ορίζουν ένα κύκλο. Εάν λοιπόν λάβουμε ως δύο τριάδες τις ΒΔ και ΝΑ γωνίες κάθε πυραμίδας, θα τις περιγράψουμε εντός ενός κυκλικού τομέα. Το προοδευτικά μικρότερο μέγεθός τους μας κατευθύνει στο σημείο τομής των δύο κύκλων, το οποίο δεν βρίσκεται κάπου μακριά, αλλά σε ένα πολύ ενδιαφέρον σημείο. Βρίσκεται πάνω στον περιβάλλοντα τοίχο της τρίτης πυραμίδας, ο οποίος παρουσιάζει κάποιες ανεξήγητες κατασκευαστικές ιδιομορφίες.

Ας εξετάσουμε τώρα λεπτομερέστερα τη μεγάλη πυραμίδα, που είναι ένα αληθινό κατασκευαστικό θαύμα. Αν και έχει ένα πέτρινο πυρήνα άγνωστων διαστάσεων, υπολογίζεται πως περίπου 2.300.000 ξεχωριστοί κατεργασμένοι λίθοι μάζας μεταξύ 2,5 και 15 τόνων χρειάστηκαν για την κατασκευή της.

Εξετάζοντας την κλίση των πλευρών, βρίσκει κανείς πως μια πυραμίδα με κλίση 51° 52΄ έχει τη μοναδική γεωμετρική ιδιότητα, ότι το ύψος της προς την περίμετρο της βρίσκεται στην ίδια αναλογία με αυτή της ακτίνας ενός κύκλου προς την περιφέρεια του, δηλαδή 1/2π. Η εμπλοκή του αριθμού π σε μια εποχή όπου υποτίθεται ότι δεν ήταν γνωστή η ύπαρξη του, έχει δώσει βάση σε πολλές συζητήσεις.

Ας εστιάσουμε το ενδιαφέρον μας περισσότερο σε δύο αγωγούς που ξεκινούν από τον βόρειο και τον νότιο τοίχο του θαλάμου του βασιλιά που διαπερνώντας την πυραμίδα, βγαίνουν έξω στο ίδιο ύψος, γεγονός που οδήγησε αρχικά τους αρχαιολόγους να πιστέψουν πως ήταν αεραγωγοί. Όταν όμως αναλογιστεί κανείς την ιδιομορφία της πυραμίδας, η σκέψη του κατευθύνεται αλλού. Η μεγάλη πυραμίδα είναι η μοναδική που έχει εσωτερική διαρρύθμιση και συνεπώς οι δύο αυτοί αγωγοί, διαστάσεων 20 x 20 cm, φέρνουν στο νου αυτό που αναφέραμε προηγουμένως, δηλαδή τους διαδρόμους που οδηγούσαν την ψυχή του φαραώ στον ουρανό. Εξετάζοντας κανείς τη μέση κλίση εισόδου και εξόδου τους, γίνεται αντιληπτό πως την εποχή που χτίστηκε η πυραμίδα, ο βορεινός σκόπευε προς το α του Δράκοντος (Thuban), τον τότε πολικό αστέρα, ενώ ο νότιος σκόπευε στα τρία άστρα της ζώνης του Ωρίωνα. Η ιδέα αυτή εμπνεύστηκε αρχικά από τον αρχαιολόγο R.O. Faulkner[1]. Δύο ανάλογοι κρυμμένοι αγωγοί βρέθηκαν και στο «θάλαμο της Βασίλισσας». Στον βορινό μάλιστα βρέθηκαν τρία περίεργα αντικείμενα, το ένα μάλιστα ξύλινο, που υπήρχαν εκεί σφραγισμένα από την εποχή που κτίστηκε η πυραμίδα. Για άγνωστους λόγους, το ξύλινο κομμάτι δεν κατέληξε σε κάποιο μουσείο και δεν χρονολογήθηκε ποτέ, γεγονός πολύ περίεργο μιας και ήταν το μοναδικό οργανικό στοιχείο εντός της πυραμίδας. Η χρησιμότητα τους παραμένει άγνωστη μέχρι σήμερα, αν και πιθανότατα έχουν συμβολικό χαρακτήρα και μπορεί να χρησιμοποιούνταν σε κάποιο τελετουργικό. Οι αγωγοί αυτοί ερευνήθηκαν διεξοδικά από τον Γερμανό μηχανικό Rudolf Gantenbrink (2003), ο οποίος είχε προσληφθεί για να βελτιώσει τον αερισμό της πυραμίδας. Εξερεύνησε τους αγωγούς με ένα ρομποτάκι, το Upuaut, που θυμίζει το Pathfinder, εξοπλισμένο με μια μικρή κάμερα, και έφτασε το 1993 σε αυτό που πολλοί θεωρούν τη μεγαλύτερη αρχαιολογική ανακάλυψη που έγινε τις τελευταίες δεκαετίες. Η κάμερα έδειξε ένα τοιχαλάκι με 2 χάλκινα πώματα, και ξεσήκωσε θύελλα στην αρχαιολογική κοινότητα διότι πιθανό να είναι πορτάκι προς ένα κρυμμένο μέχρι τώρα θάλαμο. Στον άλλο αγωγό βρέθηκε ένα ακόμη κομμάτι ξύλου, το οποίο δεν έχει φτάσει ακόμη στα χέρια των αρχαιολόγων και παραμένει εκεί μέχρι και σήμερα.

Μια πολύ ενδιαφέρουσα θεωρία έχει προταθεί από τον μηχανικό Robert Bauval, ο οποίος παρατήρησε πως η χωροθέτηση των τριών πυραμίδων μοιάζει έντονα με την ουρανογραφική θέση των τριών αστεριών της ζώνης του Ωρίωνα. Βασιζόμενος σε μετρήσεις του Gantenbrink (2003), υποστηρίζει πως οι δύο αγωγοί στο θάλαμο της βασίλισσας σκόπευαν στον Σείριο και στον Kochab. Μέχρι και σήμερα μαίνεται μια θεολογική διαμάχη μεταξύ του Bauval και των αντιπάλων του, για το εάν ο Ωρίωνας ήταν γνωστός στους αρχαίους κτίστες, εάν ήταν για αυτούς ένα ή περισσότερα αστέρια, καθώς και για το εάν η πυραμίδα είναι αστρικό η ηλιακό σύμβολο. Η διαμάχη βασίζεται στις διαφορετικές ερμηνείες των λεγόμενων «Κειμένων των Πυραμίδων» (Pyramid Texts), ιερογλυφικών κειμένων που αναφέρονται στη μετάβαση της ψυχής του φαραώ στον ουρανό και βρέθηκαν σε μεταγενέστερες πυραμίδες. Η θεωρία του βασίζεται όμως και σε άλλα στοιχεία που έχουν να κάνουν με την ευρύτερη διάταξη στην Γκίζα και καταλήγει στο ότι οι πυραμίδες μεταξύ άλλων, λειτουργούν και σαν δείκτες μιας συγκεκριμένης ημερομηνίας, το 10500 π.Χ. που πιστεύει ότι ήταν η χρονολογία που πίστευαν οι αρχαίοι Αιγύπτιοι ότι ξεκίνησε ο πολιτισμός τους. Επίσης πιστεύει πως η Γκίζα είναι το γήινο ανάλογο του νεκρικού βασιλείου στον ουρανό (Duat), δηλαδή πως είναι η εικόνα του ουρανού προβεβλημένη στη Γή.

Κλείνοντας, ας θέσουμε στους εαυτούς μας ένα ερώτημα που θέτει ο Bauval[2]: Τι ήταν αυτό που ανατέθηκε στον αρχιτέκτονα των πυραμίδων; Να σχεδιάσει ένα μνημείο για να εκφράσει τις αρχές των ιερών μαθηματικών ή να προμηθεύσει την πυραμίδα με χαρακτηριστικά που θα εξυπηρετούσαν τη λειτουργία της; Εμείς ασπαζόμαστε και τις δυο υποθέσεις. Πιθανόν όλες οι προαναφερθείσες θεωρίες να έχουν μια δόση της αντικειμενικής αλήθειας, άλλες περισσότερο και άλλες λιγότερο.

Στον αραβικό τύπο γράφτηκε πως οι αιγυπτιακές αρχές σκοπεύουν επιτέλους να ολοκληρώσουν τον Νοέμβριο του 2003 την εξερεύνηση των αγωγών στον θάλαμο της βασίλισσας, κάτι για το οποίο όλοι όσοι παρακολουθούν τις εξελίξεις προσμένουν τα τελευταία 10 χρόνια.

Abstract:

The astronomical and arithmetical mystery of the pyramids
(Aris Dakanalis and Efstratios Theodossiou)
The mystery of the ancient Egyptian pyramids is an unsolved problem for a great range of scientists, as archaeologists, historians and astronomers. In this study we tried to give some arithmetical and astronomical correlation of the dimensions of the pyramids, using an extensive and modern Bibliography, which refers to the "hidden" arithmetical (or astronomical) mystics of the eternal pyramids of Ancient Egypt. We also tried to explain this correlation on the pyramid's dimensions especially in the Great Pyramid of Cheops. Additionally, this paper presents all the current aspects on the so-called mystery – mathematical and astronomical – of the pyramids in Egypt.

ΑΝΑΦΟΡΕΣ

[1] R.O. Faulkner published this proposal in 1966 at the *Journal of Near Eastern Studies vol. 25*
[2] Bauval, Robert (1996) *The Orion Mystery,* Mandarin Paperbacks, London, Appendix 5 *Mathematical Astronomy or Astronomical Mathematics?* p.283

ΒΙΒΛΙΟΓΡΑΦΙΑ

1. Bauval, Robert & Hancock, Graham (1996) *The Message of the Sphinx,* Three Rivers Press, New York.
2. Bauval, Robert & Gilbert Adrian (1996) *The Orion Mystery,* Mandarin Paperbacks, London.
3. Bauval, Robert, (2003) *The official website of Robert Bauval,* (articles). http://www.robertbauval.com/
4. Edwards, I.E.S. (1996) *The Pyramids of Egypt*, Penguin Books, London.
5. Gantenbrink, Rudolph (2003) *The official website of Rudolph Gantenbrink.* http://www.cheops.org
6. Goodfellow, Stephen (2003) *Giza Pyramids; The Vanishing Point.* http://www.goodfelloweb.com/giza/
7. Legon, John (2003) *Giza Site Plan (official website).* http://www.legon.demon.co.uk/
8. Lehner, Mark (2001) *The Complete Pyramids,* Thames&Hudson Ltd, London.
9. Magli, Giulio (2003) *On the astronomical orientation of the IV dynasty Egyptian pyramids and the dating of the second pyramid,* Polytechnical University of Milan, department of Mathematics (on Simultaneous Transition Theory).
10. Mendelssohn,Kurt (1986) *Riddle of the Pyramids*, Thames&Husdon, London.
11. Trimble,Virginia (1964) *Astronomical Investigations concerning the so-called Air-Shafts of Cheops' Pyramid,* Mitteilungen des Institutes für Orientforschung Akademie der Wissenschaften zu Berlin, band x, Heft 2/3.

Η ΜΑΤΑΙΗ ΑΝΑΖΗΤΗΣΗ ΤΟΥ ΠΛΑΝΗΤΗ ΗΦΑΙΣΤΟΥ*

Βασίλειος Ν. Μανιμάνης και Ευστράτιος Θεοδοσίου

Τομέας Αστροφυσικής, Αστρονομίας και Μηχανικής,
Τμήμα Φυσικής, Πανεπιστήμιο Αθηνών

ΠΕΡΙΛΗΨΗ

Η έρευνα για έναν υποθετικό πλανήτη που με τις παρέλξεις του προκαλούσε μια μικρή μετατόπιση του περιηλίου του Ερμού, προσέλκυσε μεγάλο ενδιαφέρον κατά το 19ο αιώνα. Θα ήταν ο εγγύτερος στον Ήλιο πλανήτης και του είχε ήδη δοθεί το όνομα Ήφαιστος από τον Le Verrier (1811-1877). Διάσημοι παρατηρησιακοί αστρονόμοι της εποχής δαπάνησαν πολλές ώρες σε έρευνες για την ανακάλυψή του, μέχρι το 1915: Η ματαιότητα της αναζητήσεως του Ηφαίστου έγινε πλέον φανερή όταν ο A. Einstein με τη Γενική Θεωρία της Σχετικότητας ερμήνευσε το έλλειμμα των 43 arcsec στους υπολογισμούς του Le Verrier.

Μια από τις μεγαλύτερες αστρονομικές αναζητήσεις του 19ου αιώνα υπήρξε η προσπάθεια για την ανακάλυψη ενός πλανήτη που θα περιφερόταν περί τον Ήλιο εγγύτερα από ό,τι ο Ερμής. Την ύπαρξη ενός τέτοιου πλανήτη υπέθεσε πρώτος ο Γάλλος αστρονόμος Urbain Jean Joseph Le Verrier (1811-1877). Το Σεπτέμβριο 1846 ο Le Verrier είχε αποκτήσει παγκόσμια φήμη, όταν ο J.G. Galle (1812-1910) του Αστεροσκοπείου του Βερολίνου, βασιζόμενος σε υποδείξεις του, ανακάλυψε τον όγδοο γνωστό πλανήτη, τον Ποσειδώνα. Ο Le Verrier είχε μελετήσει (1845), μετά από υπόδειξη του Arago, ορισμένες ανωμαλίες που είχαν παρατηρηθεί στην κίνηση του Ουρανού κατά την περιφορά του και τις απέδωσε στις παρέλξεις ενός άγνωστου μέχρι τότε πλανήτη. Με βάση αυτή την παραδοχή υπολόγισε μαθηματικά τη θέση του άγνωστου πλανήτη και την υπέδειξε στον Galle, ο οποίος τον ανακάλυψε σχεδόν στο ίδιο σημείο που είχε προβλέψει ο Le Verrier. Το γεγονός είχε τότε χαιρετιστεί από την παγκόσμια επιστημονική κοινότητα ως μια απόδειξη για τη δύναμη των Μαθηματικών και θρίαμβος για την κλασική θεωρία βαρύτητας του Νεύτωνα.

Το 1858, βασιζόμενος σε ανάλογες ανωμαλίες που είχαν παρατηρηθεί στην κίνηση του Ερμού, ο Le Verrier πρότεινε και πάλι ότι ένας άγνωστος μέχρι τότε πλανήτης προκαλούσε με τις βαρυτικές του παρέλξεις τις ανωμαλίες αυτές, και συγκεκριμένα τη μετατόπιση του περιηλίου της τροχιάς του Ερμού κατά 43΄΄ ανά αιώνα *περισσότερο* από ό,τι προέβλεπε η Νευτώνεια θεωρία. Το άγνωστο σώμα θα ήταν εύκολο να διαφύγει της προσοχής των αστρονόμων, καθώς από τη Γη θα φαινόταν να βρίσκεται πάντα κοντά στο εκτυφλωτικό φως του Ήλιου. Ακόμα και ο Ερμής αποτελεί ένα δύσκολο στην παρατήρησή του πλανήτη εξαιτίας της εγγύτητάς του στον Ήλιο. Περίπου 13 φορές ανά αιώνα εμφανίζεται να περνά μπροστά από τον ηλιακό δίσκο ως μαύρη κηλίδα, και στις περιπτώσεις αυτές, τις διαβάσεις του Ερμού, η θέση του ως προς τον Ήλιο μπορεί να μετρηθεί με πολύ μεγάλη ακρίβεια, γεγονός που επέτρεψε την ανίχνευση της παραπάνω ανωμαλίας στην κίνησή του.

Εκτός από τον Le Verrier, ο Γερμανός Heinrich Schwabe, ελπίζοντας να ανιχνεύσει τον Ήφαιστο σε μια διάβασή του, εξέταζε τον ηλιακό δίσκο κάθε αίθρια ημέρα από το 1826 ως το 1838, συσσωρεύοντας παρατηρήσεις 3.500 και πλέον ημερών. Δεν

* *Proceedings of the 6th Hellenic Astronomical Society Conference, 15-17 September 2003, Penteli, Greece*

ανακάλυψε κάποιο νέο πλανήτη, εντούτοις κατέγραψε κάτι εξίσου σημαντικό: τον ενδεκαετή κύκλο της ηλιακής δραστηριότητας, μέσα από την περιοδική αυξομείωση στον αριθμό των ηλιακών κηλίδων.

Ωστόσο η ανακοίνωση του Le Verrier το Σεπτέμβριο του 1859 γνώρισε πολύ μεγαλύτερη δημοσιότητα, αφού περιελάμβανε τα στοιχεία της τροχιάς του άγνωστου πλανήτη με περίοδο περιφοράς 33 ημέρες (άρα και συχνότερες διαβάσεις), και σύντομα παρουσιάσθηκε μια αναφορά για μια μικρή μαύρη κηλίδα, που είχε παρατηρηθεί να κινείται κατά μήκος του ηλιακού δίσκου στις 26 Μαρτίου 1859, από τον ερασιτέχνη αστρονόμο Edmond Modeste Lescarbault, ο οποίος επί έτη επεδίωκε να ανακαλύψει τον εσωτερικό πλανήτη. Αρχικά ο Le Verrier αντέδρασε με σκεπτικισμό, όμως τελικά αποφάσισε να συναντήσει τον Lescarbault. Κατά την επίσκεψή του στο χωριό του ερασιτέχνη, του έθεσε μια σειρά από ουσιαστικές ερωτήσεις. Μετά από συζήτηση μιας ώρας, ο Le Verrier αναχώρησε πεπεισμένος ότι θα μπορούσε να εμπιστευθεί την ερασιτεχνική παρατήρηση. Ονόμασε τον, υποθετικό νέο πλανήτη Ήφαιστο (Vulcan) και μάλιστα επέμεινε να τιμηθεί ο Lescarbault με το παράσημο της Λεγεώνας της Τιμής από τον ανώτατο άρχοντα της τότε Γαλλίας Ναπολέοντα Γ΄.

Ο Le Verrier αποφάνθηκε ότι ο Ήφαιστος θα έπρεπε να κινείται περί τον Ήλιο σε μέση απόσταση 19×10^6 km και να εκτελεί 2-4 διαβάσεις ανά έτος, 1 ή 2 κατά τα τέλη Μαρτίου ή στις αρχές Απριλίου και 1 ή 2 κατά τα τέλη Σεπτεμβρίου ή στις αρχές Οκτωβρίου. Η κάθε διάβαση θα έπρεπε να έχει διάρκεια μέχρι 260 min. Εκτός από τις διαβάσεις, ευκαιρία για την ανακάλυψή του θα παρουσιαζόταν σε κάθε ολική έκλειψη Ηλίου. Αλλά όσοι προσπάθησαν να ανιχνεύσουν τον Ήφαιστο την άνοιξη του 1860, απέτυχαν. Ούτε και στην ολική έκλειψη του Ιουλίου 1860, ορατή από την Ισπανία, υπήρξε έστω και μία θετική παρατήρηση. Οι υποστηρικτές του Ηφαίστου άρχισαν να αμφιβάλλουν, ενώ όσοι ήταν ανέκαθεν δύσπιστοι άρχισαν να εκφράζονται με απόλυτο τρόπο. Κατά τα επόμενα έτη αναφέρθηκαν μερικές σποραδικές θετικές παρατηρήσεις από ερασιτέχνες, με την περίπτωση του Βρετανού Lumis να απολαμβάνει ιδιαίτερη δημοσιότητα. Ο Lumis ισχυρίσθηκε ότι είχε ανιχνεύσει με ένα διοπτρικό τηλεσκόπιο μια κινούμενη κηλίδα στον Ήλιο στις 20/3/1862.

Η ολική ηλιακή έκλειψη της 7/8/1869 υποσχόταν μια ακόμα πολύτιμη ευκαιρία για τον εντοπισμό του Ηφαίστου. Η σκιά της Σελήνης θα διέσχιζε διαγωνίως τη Β. Αμερική, από το Βερίγγειο Πορθμό ως τη Β. Καρολίνα. Ο Le Verrier παρέμενε σταθερός υπέρμαχος του αόρατου πλανήτη και το κύρος του μπορούμε να πούμε ότι συνέτεινε αρκετά στο να διατηρείται το θέμα στη σκέψη των περισσότερων παρατηρητών. Ο S. Newcomb (1835-1909) του Ναυτικού Αστεροσκοπείου των ΗΠΑ ήταν ένας από αυτούς. Θα συνόδευε μια αποστολή στο Des Moines της Iowa για να παρατηρήσει την έκλειψη. Ο Newcomb λοιπόν προσκάλεσε το Δανό αστρονόμο C.H.F. Peters (1813-1890), που είχε εγκατασταθεί στις ΗΠΑ από το 1854 και είχε ανακαλύψει πολλούς αστεροειδείς, να τους ακολουθήσει στην αναζήτηση του Ηφαίστου. Ο Peters του απάντησε απότομα: *«Δεν θα ενδιαφερθώ να ψάξω για τα μυθικά πτηνά του Le Verrier»*. Η απάντηση αυτή, κατά τους Baum & Sheehan (1997), είχε πιθανότατα ένα ενδιαφέρον βαθύτερο νόημα, που για να το αντιληφθούμε θα πρέπει να γνωρίζουμε κάποιες εμπειρίες από την προηγούμενη σταδιοδρομία του C. H. F. Peters.

Μερικές εβδομάδες πριν, ο Peters είχε δημοσιεύσει στο *Astronomische Nachrichten* («Αστρονομικά Νέα») μια εμπειρία από τότε που βρισκόταν στο Αστεροσκοπείο της Νεαπόλεως στην Ιταλία. Το Μάιο 1845 οι εκεί αστρονόμοι είχαν παρατηρήσει μικρά σώματα να περνούν μπροστά από το δίσκο του Ήλιου. Αυτή δεν ήταν η πρώτη παρόμοια αναφορά. Ο C. Messier (1730-1817) π.χ. παρατηρώντας από το Παρίσι το 1777 είχε παρακολουθήσει *«ένα μεγάλο αριθμό σκοτεινών σφαιριδίων»* να περνά μπροστά από τον Ήλιο μέσα σε 5 min. Η μεγάλη θύελλα διαττόντων των Λεοντιδών του 1833 είχε καταστήσει γνωστή την ύπαρξη μετεωρικών σωμάτων που εκινούντο σε πυκνά σμήνη ή (σύμφωνα με μια θεωρία της εποχής που είχε προτείνει ο Adolph Erman το 1839) περιφέρονταν περί τον Ήλιο σε διακριτούς δακτυλίους. Δεν θα ήταν μήπως πιθανό υπό συγκεκριμένες συνθήκες, όταν η Γη βρισκόταν κοντά στα σμήνη αυτά, μερικά από τα μικρά εκείνα σώματα (μετεωροειδείς) να εκτελούν διαβάσεις; Αρχικά οι αστρονόμοι από τη Νεάπολη υπέθεσαν ότι είχαν δει συμπυκνώσεις στο ρεύμα μετεωροειδών που προκαλεί την ετήσια βροχή διαττόντων «η Υδροχοΐδες» κάθε Μάιο και σήμερα γνωρίζουμε πως αποτελείται από υλικό του Κομήτη του Halley. Το γεγονός κίνησε το ενδιαφέρον του Peters, που θέλησε να επιβεβαιώσει τις παρατηρήσεις και να διαλευκάνει το μυστήριο. Στις 6/10/1845 ήρθε η επόμενη ευκαιρία: πολλά μικρά αντικείμενα έγιναν ορατά καθώς διάβαιναν με μεγάλη ταχύτητα μπροστά από τον Ήλιο, άλλα μεμονωμένα και άλλα κατά ζεύγη. Ο Peters χρονομέτρησε προσεκτικά τις διαβάσεις. Το φαινόμενο επαναλήφθηκε και τις επόμενες ημέρες, ώστε στις 17/10 ο Peters να γράψει: *«Ενώ μετρούσαμε τις ηλιακές κηλίδες, πέρασαν πολλά μικρά σώματα, λίγο-πολύ γρήγορα»*. Εκείνη τη νύκτα, με το τηλεσκόπιό του στραμμένο προς τη Σελήνη, μέτρησε 9 μικρά σώματα σε 15 min, κινούμενα οριζόντια μπροστά από το δίσκο της Σελήνης μία ημέρα μετά την πανσέληνο. Και, εντελώς ξαφνικά, η ταυτότητά τους έπαψε να αποτελεί μυστήριο.

«Ήταν πουλιά», έγραψε ο Peters, *«με όλα τα χαρακτηριστικά τους γνωρίσματα: ουρά, κεφαλή και πτέρυγες. Πέρασαν όλα μπροστά από το δίσκο της Σελήνης... ...παράλληλα ή σχεδόν παράλληλα ως προς τον ορίζοντα. Το καθένα εμφανίσθηκε σαν ένα μαύρο αντικείμενο επάνω στο δίσκο. Η νύκτα ήταν καθαρή και ο άνεμος ασθενής.»*

Ο Δανός επιστήμονας συμπέρανε ότι και τα σώματα που είχαν παρατηρηθεί τον προηγούμενο Μάιο ήταν επίσης πτηνά, καθώς μεγάλοι αριθμοί αποδημητικών πτηνών περνούσαν πάνω από την περιοχή κάθε Μάιο και Οκτώβριο, διατύπωσε μάλιστα και τη γνώμη ότι ήταν ορτύκια!

Επομένως όταν ο Peters αναφερόταν στα *«μυθικά πτηνά του Le Verrier»* φαίνεται ότι δεν μιλούσε μεταφορικά, αλλά πολύ συγκεκριμένα. Κατά τους Baum & Sheehan (1997) πολλοί από τους «Ηφαίστους» που παρατηρήθηκαν κατά καιρούς ήταν απλώς πουλιά. Ακόμα και οι εποχές που είχε προτείνει ο Le Verrier για τις διαβάσεις (άνοιξη και φθινόπωρο) ενισχύουν την παραπάνω υποψία, αφού αντιστοιχούν στις εποχές της αποδημίας. Τα περισσότερα χερσαία αποδημητικά ταξιδεύουν κατά τις αποδημίες τους σε ύψος μικρότερο των 1.500 m, αλλά μπορεί να υπερβούν και τα 4 km. Αν δεχθούμε άνοιγμα πτερύγων 20 cm και ύψος 2 km με το δίσκο του Ήλιου 3° πάνω από τον ορίζοντα, το πουλί θα βρίσκεται όταν περνά μπροστά από τον Ήλιο σε απόσταση 4 km από τον παρατηρητή και θα έχει φαινόμενο άνοιγμα πτερύγων περίπου 10΄΄. Συγκριτικά, ο Ερμής κατά τις διαβάσεις του έχει φαινόμενη διάμετρο 13΄΄. Με μικρές μεγεθύνσεις θα ήταν σχεδόν αδύνατο να αναγνωρισθεί η πραγματική φύση μιας τόσο μικρής μαύρης κηλίδας. Ωστόσο θα πρέπει να επισημανθεί ότι ένας πλανήτης, ακόμα και ο ταχύτατος Ήφαιστος, θα φαινόταν να διασχίζει τον ηλιακό δίσκο εκατοντάδες φορές πιο αργά από ό,τι ένα πουλί, ακόμα και το πιο μακρινό. Οι αστρονόμοι γνώριζαν ότι ο Ήφαιστος θα χρειαζόταν ώρες για να διασχίσει τον ηλιακό δίσκο. Η πορεία των αποδημητικών πτηνών έχει γενική κατεύθυνση Β-Ν. Αν τα περνούσαν για πλανήτη, αυτός ο πλανήτης θα έπρεπε να έχει μια τροχιά με μεγάλη κλίση ως προς την εκλειπτική, πολύ μεγαλύτερη από την κλίση των 12° που είχε προτείνει ο Le Verrier.

Η έκλειψη της 7/8/1869 απέτυχε να αποκαλύψει τον Ήφαιστο κοντά στον Ήλιο. Ο Le Verrier διακήρυξε ότι ή υπήρχαν πολλοί Ήφαιστοι ή δεν υπήρχε κανείς και ότι αν υπήρχε Ήφαιστος θα έπρεπε να διαβεί μπροστά από τον ηλιακό δίσκο στις 23/3/1877. Μετά το θάνατό του, στις 23/9/1877, υπήρχαν ακόμα αστρονόμοι που έλπιζαν στην ύπαρξη του Ηφαίστου, έστω και αν ο σκεπτικισμός αυξανόταν. **Ο λόγος ήταν ότι δεν υπήρχε άλλη εξήγηση για την ανωμαλία στην τροχιά του Ερμού**. Το αποκορύφωμα ήρθε με την ολική ηλιακή έκλειψη της 29/7/1878 στις ΗΠΑ. Ο Newcomb την παρατήρησε από το Wyoming συνοδευόμενος από τον J.C. Watson του Πανεπιστημίου του Michigan. Κατά τα 3 min της ολικής φάσεως ο Newcomb χρησιμοποίησε μικρό τηλεσκόπιο για να ερευνήσει το χώρο στα Α του Ήλιου, ενώ ο Watson με ένα μεγαλύτερο τηλεσκόπιο ερεύνησε μια ζώνη μήκους 15° και πλάτους 1,5° Α και Δ του Ήλιου. Με την ισχυρή μνήμη του, ο Watson είχε προηγουμένως απομνημονεύσει από τους χάρτες του ουρανού τις θέσεις όλων των αστέρων αυτής της ζώνης μέχρι ορισμένου m(V). Στα Δ του Ήλιου συνάντησε ένα «ερυθρωπό άστρο» που δεν υπήρχε στους χάρτες, ορατό με γυμνό μάτι. Ακόμα δυτικότερα, βρήκε έναν άλλο, φωτεινότερο, ερυθρό αστέρα, σημείωσε τη θέση του και έσπευσε να ειδοποιήσει το Newcomb, ώστε να υπάρχει ανεξάρτητη επιβεβαίωση από άλλο παρατηρητή. Ο Newcomb όμως ήταν απορροφημένος από την παρακολούθηση ενός δικού του υποψήφιου «Ηφαίστου», ενός αστέρα όπως αποδείχθηκε αργότερα. Τότε η ολική έκλειψη έλαβε τέλος. Ο Watson, που είχε ανακαλύψει πολλούς αστεροειδείς, ήταν πεπεισμένος ότι είχε δει τουλάχιστον έναν εσώτατο πλανήτη. Οι παρατηρήσεις του όμως δέχθηκαν αργότερα την κριτική του Peters, που θεώρησε ότι ο Watson είχε θεωρήσει τους θ και ζ Καρκίνου σαν «Ηφαίστους».

Ο Watson αρνήθηκε να εγκαταλείψει τις προσπάθειες και πέρασε την υπόλοιπη ζωή του κυνηγώντας τον υποθετικό πλανήτη. Αφού άφησε το Πανεπιστήμιο του Michigan στο Ann Arbor προκειμένου να επιβλέψει την κατασκευή του Αστεροσκοπείου Washburn του Πανεπιστημίου του Wisconsin στο Madison, επιδίωξε να ανακαλύψει τον Ήφαιστο κατά τη διάρκεια της ημέρας: ήθελε να τοποθετήσει ένα τηλεσκόπιο στον πυθμένα ενός φρέατος βάθους 7,3 m σε ένα λόφο κοντά στη λίμνη Mendota, ελπίζοντας ότι έτσι θα ήταν σε θέση να διακρίνει αστέρες κοντά στον Ήλιο. Η ιδέα χρονολογείται από την εποχή του Αριστοτέλους, ο οποίος είχε αναφέρει πως οι φωτεινότεροι αστέρες μπορούσαν να γίνουν ορατοί και κατά τη διάρκεια της ημέρας μέσα από βαθιά πηγάδια, πράγμα που είχε πάντως αποδειχθεί λανθασμένο ήδη πριν την εποχή του Watson. Μόνο με τηλεσκόπιο οι φωτεινότεροι αστέρες μπορούν να γίνουν ορατοί κατά τη διάρκεια της ημέρας, αλλά και πάλι όταν δεν βρίσκονται προς την πλευρά του Ήλιου, εκτός αν βρισκόμαστε σε μεγάλο υψόμετρο (>5 km).

Ο Watson πέθανε από επιπλοκές πνευμονίας το Νοέμβριο 1880, σε ηλικία 42 ετών, πριν ολοκληρώσει το σχέδιό του. Την επόμενη άνοιξη, όταν ο διάδοχός του, ο Edward S. Holden (1846-1914) έφθασε στο Madison για να αποπερατώσει το υπόγειο αστεροσκοπείο, ο Peters τον προειδοποίησε: *«Μη καθίσεις μέσα σε αυτή την υπόγεια τρύπα να παρακολουθείς μέχρι που να περάσει ο Ήφαιστος! Δεν φοβάμαι ότι ίσως τον ανακαλύψεις... ...αλλά μπορεί να καταστρέψει την υγεία σου και το καλύτερο που έχεις να κάνεις είναι να καλύψεις την τρύπα.»* Ο Holden πάντως διεξήγαγε λίγες παρατηρήσεις, ώστε να βεβαιωθεί και προσωπικά ότι ο Ήφαιστος θα ήταν αδύνατο να παρατηρηθεί κατά τη διάρκεια της ημέρας, και στη συνέχεια το υπόγειο αστεροσκοπείο εγκαταλείφθηκε για πάντα. Σήμερα δεν έχει απομείνει ίχνος του.

Μετά το θάνατο του Watson η ιδέα του Ηφαίστου περιέπεσε οριστικά σε δυσμένεια μεταξύ των αστρονόμων. Λίγοι αστρονόμοι, μεταξύ των οποίων και ο Holden, από όσους ταξίδεψαν μέχρι τη νήσο Καρολίνα στον κεντρικό Ειρηνικό Ωκεανό για να παρατηρήσουν την ολική έκλειψη του 1883 το έπραξαν με την ελπίδα να ανακαλύψουν τον Ήφαιστο. Στις 11/1/1891 ο Lescarbault ισχυρίσθηκε ότι τον ανακάλυψε στο Λέοντα, αλλά λεπτομερής έλεγχος απέδειξε ότι ο υποτιθέμενος Ήφαιστος ήταν ο πλανήτης Κρόνος!

Η επιπλέον μετατόπιση του περιηλίου του Ερμού εξηγήθηκε από τον Αϊνστάιν το Νοέμβριο 1915: η Γενική Σχετικότητα εξαφάνισε την ανάγκη για την ύπαρξη του Ηφαίστου, καθώς σύμφωνα με αυτή τη Θεωρία η τροχιά του Ερμού θα έπρεπε να μεταπίπτει ελαφρώς ταχύτερα, ακριβώς όσο χρειαζόταν για να εξηγήσει την επιπλέον μετατόπιση του περιηλίου.

Παρά το γεγονός αυτό, οι παρατηρήσεις του J.C. Watson κατά την έκλειψη του 1878 δεν εξηγήθηκαν ποτέ εντελώς. Ο Peters ίσως είχε δίκιο όταν υποστήριζε την πιθανότητα λάθους, αλλά μια πιο συναρπαστική πιθανότητα είναι ο Watson να είδε δύο μικρούς κομήτες από αυτούς που περνούν πολύ κοντά από τον Ήλιο και συνήθως πέφτουν επάνω του. Τέτοιοι κομήτες ανακαλύφθηκαν κυρίως από το SOHO τα τελευταία έτη. Π.χ. ο «κομήτης SOHO» που ανακαλύφθηκε στις 3/5/1998 και πέρασε σε ελάχιστη απόσταση 22×10^6 km από τον Ήλιο (περιήλιο) 5 ημέρες αργότερα (συγκριτικά, ο Ερμής δεν πλησιάζει τον Ήλιο περισσότερο από 46×10^6 km). Αν και τώρα έχει σχεδόν ξεχασθεί, ο Ήφαιστος μας υπενθυμίζει τη μεγάλη έφεση του ανθρώπου για εξερεύνηση και ανακάλυψη, καθώς και την τυχαία ανακάλυψη άλλων πραγμάτων, ίσως πιο σημαντικών, κατά τη διάρκεια των ερευνών για κάποιο δύσκολο στόχο: η αναζήτηση για τον Ήφαιστο οδήγησε τον H. Schwabe στο να ανακαλύψει τον ενδεκαετή κύκλο της ηλιακής δραστηριότητας.

Abstract:

The futile search for the hypothetical planet Vulcan.
(Vassilios Manimanis and Efstratios Theodossiou)
The search for a hypothetical planet, whose gravitational perturbations were causing a small extra precession of Mercury's perihelion, attracted considerable interest in the 19th Century. It would be the planet closest to the Sun and it had been already given the name Vulcan by the French astronomer Urbain Jean-Joseph Le Verrier (1811-1877). Famous observational astronomers of that era spent many hours searching for Vulcan, until the theoretical reason for its existence was eliminated in 1915, when Einsteinian Relativity explained with great precision the difference of 43 arcsec in Le Verrier's calculations.

ΒΙΒΛΙΟΓΡΑΦΙΑ

Δανέζης, Μάνος και Θεοδοσίου, Στράτος: *Το Σύμπαν που αγάπησα - Εισαγωγή στην Αστροφυσική*, τόμος Β΄, εκδόσεις Δίαυλος, Αθήνα 2000

Baum, Richard & Sheehan, William: *In search of planet Vulcan*, Plenum, 1997

Sheehan, William: «James Craig Watson, First Director of Washburn Observatory: His Obsession with the Intra-Mercurial Planet Vulcan», *BAAS,* **28**, 858 (1996)

GENDER ISSUE IN GREEK ASTRONOMY*

E. Kontizas
Institute of Astronomy and Astrophysics, National Observatory of Athens, Greece

Abstract: Astronomy has a long and honorable tradition of participation of women, who have made many valuable contributions to the field. We know that women and men are equally capable of producing excellent scientific work and they are supposed to be equally treated in promotions. I present some statistics on women in Greek astronomy from data gathered from the Hellenic Astronomical Society records, from the GNCA, and from the web pages of the Greek Universities and research Institutes, in order to examine the present situation. I wonder why there was never a woman full professor in Astronomy in any of the seven (7) Greek Universities, where Astronomy is taught, or a woman director in any of the two research centers in Greece.

THE AMOUNT AND QUALITY OF SCIENCE COMMUNICATION IN THE GREEK MASS MEDIA

Matsopoulos Nicolaos
Institute of Astronomy and Astrophysics, National Observatory of Athens, Greece

Abstract: During the last decade there is an increasing interest on how science is communicated by the mass media. Studies have been done in order to find out the amount and quality of science that is passing from the experts to the public through newspapers, radio broadcasts and TV programs. In this study, we’ve tried to find the amount of science presented in 4 Greek newspapers and 4 major TV channels. We've also done an initial evaluation on the quality of the science newspaper articles. The quality of the articles in the newspapers was studied under a relevant coding scheme. The results show that the amount of science in TV and newspapers in Greece is comparable to those in larger and more scientifically advanced countries as Canada, USA and Great Britain. They also show that most Greek scientists do not write popularizing articles but they play an important role as experts. The more serious newspapers provide more reliable information in the form of integrated articles and not as fragmentary science news. Furthermore, Greek newspapers avoid writing about controversial scientific issues and they present science as abstract and authoritative

* *Proceedings of the 6th Hellenic Astronomical Society Conference, 15-17 September 2003, Penteli, Greece*

APPLICATIONS AND ERRORS OF ERATOSTHENES' METHOD FOR THE MEASUREMENT OF THE EARTH'S MERIDIAN*

Antonios D. Pinotsis

Section of Astrophysics, Astronomy and Mechanics, Department of Physics, University of Athens, Greece.

ABSTRACT

In this study we describe and explain the method invented by Eratosthenes for the measurement of the size of the Earth based on texts by ancient authors. Furthermore, we analyze the errors which intruded into Eratosthenes' result and we point out the applications of his method to cartography, geography and astronomy. Finally, using curvature theory we apply the method to the determination of the form and the size of the Earth.

1. INTRODUCTION

In previous papers[4,8] we studied the development of cosmological ideas and mathematic models in ancient Greece between the 6th B.C. and 2nd A.C. century. Two diametrically opposite cosmological theories namely the Geocentric and the Heliocentric system were developed during the above period. According to our study it was Pythagoras who actually introduced the Geocentric system. Furthermore among other supporters of this system were Plato, Eudoxus of Knidus, Kallippus, Aristotle, Apollonius of Perga, Hipparchus and Claudius Ptolemy. Anaximander as well as Pythagoreans Philolaus, Hicetas and Ekphantus, Heraclides of Pontus, Seleucus and naturally Aristarhus of Samos were the first philosophers who introduced the idea of the Earth not being static but moving. A thorough study of ancient sources leads us to the conclusion that the novel theory of Heliocentric system, which was introduced by Aristarhus of Samos (310- 230 B.C.), did not arise as a peculiar mathematic model but was the final outcome of a long-lasting intellectual activity. Anaximander, Pythagoreans Philolaus, Hicetas and Ekphntus, Herakleides of Pontus were predecessors of Aristarhus of Samos who created a fervent atmosphere of blossoming ideas[4,8] which affected Aristarhus' thinking. Moreover, these ideas and theories whose development lasted until the time of Eratosthenes influenced not only Astronomy but all sciences.

After thoroughly studying ancient sources we have also collected valuable information about the methods developed in Antiquity for the measurement of the length of the Earth's meridian. Since the earliest times various attempts were made in order to measure several distances on the Earth's surface as well as its size. Anaximander, Aristotle, Dikaearchus, Archimedes, Eratosthenes, Posidonius of Rhodes were among those who made important contributions to that direction. The above have been extensively described elsewhere[5,7,9] where we also give the corresponding ancient texts. Among the methods used, two are the most important: the *geometrical* method of Eratosthenes and the *astronomical* method of Poseidonios of Rhodes[5,7]. In the paper on

* *Proceedings of the 6th Hellenic Astronomical Society Conference, 15-17 September 2003, Penteli, Greece*

Poseidonius we described and explained among others his astronomical method of measuring the length of a terrestrial meridian. In the present paper we describe and explain the method of Eratosthenes, we locate its errors and evaluate its significance.

2. THE METHOD OF ERATOSTHENES (276-194 B.C.)

Eratosthenes was born in the town of Kyrene in N. Africa. He was the first eminent geographer of antiquity; he was also mathematician, astronomer, philosopher and an outstanding orator[11]. He even occupied himself with poetry and literature study – *philology*, a term he invented himself. Thus Eratosthenes has been a broadly educated man. Eratosthenes wrote several works on geographical, astronomical, mathematical and philosophical topics, but also on poetry and literature and so he left behind him a manyfold scientific work, according to ancient posterior writers, for which he was called new Plato or Plato B' or *Πένταθλος* (dic. Suida). Archimedes (287 -212 B.C.) appreciated him very much and he dedicated to him certain of his writings. This is the reason why the king of Egypt Ptolemy III the Benefactor invited him to assume the directorship of the famous Library of Alexandria.

From his astronomical books the better known was "Katasterismoi". In one of his works he calculated the inclination of the ecliptic with an accuracy that amazes without the use of telescope. He found the value 23°51′ at a time when the real value was about 23°43′ while today's value is, as we know, approximately 23°27′.[9] Of equal importance was his opus "Geographika", consisting of three books and describing the whole world known in his era. Fragments of this work are saved in the writings of posterior geographers, such as Polyvios, Hipparchus, Poseidonios and Strabo[11], who found there much information but also criticized it. Eratosthenes derived a geographical map of the then known world, on which he had traced meridians and parallels[5,9]. We know that he used astronomical observations and the positions of the constellations in order to determine the distances of various places.

According to Cleomedes[1], Eratosthenes hypothesized that: i) The Earth is spherical. ii) Alexandria and Syene (a town in south Egypt) were on the same celestial -terrestrial meridian and, since meridians are great circles on the sky, the circles of the Earth that lie

---

[1] Ὑπό τῷ αὐτῷ κεῖσθαι φησί μεσημβρινῷ Συήνην καί Ἀλεξάνδρειαν.Ἐπεί οὖν μέγιστοι τῶν ἐν τῷ κόσμῳ οἱ μεσημβρινοί, δεῖ καί τοὺς ὑποκειμένους τούτοις τῆς γῆς κύκλους μεγίστους εἶναι ἀναγκαίως. Ὥστε ἡλίκον ἄν τόν διά Συήνης καί Ἀλεξάνδρειας ἥκοντα κύκλον τῆς γῆς ἡ ἔφοδος ἀποδείξει αὕτη, τηλικοῦτος καί ὁ μέγιστος ἔσται τῆς γῆς κύκλος. Φησί τοίνυν (ὁ Ἐρατοσθένης), καί ἔχει οὕτως, τήν Συήνην ὑπό τῷ θερινῷ τροπικῷ κεῖσθαι κύκλῳ.

Ὁπόταν οὖν ἐν τῷ Καρκίνῳ γενόμενος ὁ ἧλιος, καί θερινάς ποιῶν τροπάς, ἀκριβῶς μεσουρανήσῃ, ἄσκιοι γίνονται οἱ τῶν ὡρολογείων γνώμονες ἀναγκαίως, κατά κάθετον ἀκριβῆ τοῦ ἡλίου ὑπερκειμένου καί τοῦτο γίνεσθαι λόγος ἐπί σταδίους τριακοσίους τήν διάμετρον. Ἐν Ἀλεξανδρείᾳ δὲ τῇ αὐτῇ ὥρᾳ ἀποβάλλουσιν οἱ τῶν ὡρολογίων γνώμονες σκιάν ἅτε πρὸς ἆρκτῳ μᾶλλον τῆς Συήνης ταύτης τῆς πόλεως κειμένης…

Εἰς ταύτας οὖν παραλλήλους οὔσας ἐμπίπτει εὐθεῖα ἡ ἀπό τοῦ κέντρου τῆς γῆς, ἐπί τοῦ ἐν Ἀλεξανδρείᾳ γνώμονα ἥκουσα, ὥστε τάς ἐναλλάξ γωνίας ἴσας ποιεῖν...Δεῖ οὖν ἀναγκαίως καί ἀπό Συήνης εἰς Ἀλεξανδρείαν διάστημα πεντηκοστόν εἶναι μέρος τοῦ μεγίστου τῆς γῆς κύκλου καί ἔστι τοῦτο σταδίων πεντακισχιλίων. Ὁ ἄρα σύμπας κύκλος γίνεται μυριάδων εἰκοσιπέντε καί ἡ μέν Ἐρατοσθένους ἒφοδος τοιαύτη.

directly under them are also great circles. iii) The distance between Syene and Alexandria is 5000 stadia. iv) The rays of sunlight that encounter the various places on the surface of the Earth are parallel to each other, i.e. the solar rays falling on Alexandria and Syene are parallel. v) Syene lies on the summer Tropic, the Tropic of Cancer. vi) Straight lines intersecting parallel lines form equal alternate angles. vii) The arcs of circles corresponding to equal angles have the same length ratio to their respective circumferences.

Eratosthenes (according to Cleomedes) had the idea to measure the length of the shadow of a vertical stick (***gnomon***) in both Syene and Alexandria at the local noon (the moment of the upper culmination of the Sun) during the summer solstice in order to find the difference of the Sun's altitude between the two cities. More specifically, he observed that at the noon of the summer solstice the Sun did not create shadows in the city and at an area 300 stadia in diameter. He probably knew that in the vertical wells of Syene during the summer solstice, when the Sun has the maximum altitude above the horizon at local noon, the solar rays were reaching their bottom, so that the Sun was being reflected on the water of each well. He reasoned that the solar rays were falling vertically to the surface of the Earth in Syene and therefore the Sun was at the zenith (Figure 1), the end of the vertical line KS, which is the hypothesis (v). At the same moment it was also culminating in Alexandria and its rays were forming an angle φ with the gnomon, i.e. with the vertical line KA. By measuring the length of the stick's shadow and since the length of the stick was known he determined the angle φ. So the Sun was to the south of Alexandria's zenith by an angle φ. This angle is presumably equal − hypothesis (vi) − with the angle ω formed by the vertical KS of Syene and the vertical KA of Alexandria, which in turn equals the difference of the geographical latitudes of the two cities. KS and KA also define the celestial meridian passing over these cities, which lies exactly over the terrestrial meridian. Thus, from a known theorem of geometry we have[5,9]:

$$\frac{(\mathrm{SA})}{2\pi \mathrm{R}} = \frac{\mathrm{angle(SA)^o}}{\mathrm{cel.merid.} = 360^o} \tag{1}$$

where R is the radius of the Earth. The angle of the arc (SA) is measured by means of the epicentric angle ω. Therefore, since the length of the arc (SA) is known in stadia, equation (1) gives immediately the length of the terrestrial meridian as 2π times the radius of the Earth.

As we said, Eratosthenes measured with the aid of the gnomon the angle φ = ω and he found it equal to 7.2^o or 7°12′, with rather good accuracy. This value is exactly the 1/50 of the circle and so it corresponds to the 1/50 of the terrestrial meridian (see the ancient text). The length of the meridian corresponding to the angle ω is 5000 stadia, equal to the distance between Syene and Alexandria (Figure 1) and so from eq. (1) this distance must be the 1/50 of the length of the circumference of the Earth. Consequently, the circumference of the Earth is C = 5000 stadia x 50 = 250000 stadia. If we adopt for the stade used by Eratosthenes the value 1 stade = 157.5[3,5,9] m then the circumference-meridian of the Earth is 39375 km. Alternatively, if we consider a later value by Eratosthenes for the circumference of the Earth, 252000 stadia, this is 39690 km.

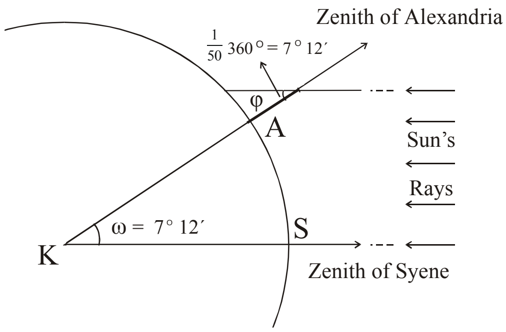

Figure 1

This value is very close to the true value of the circumference, which ranges from 40075 km (equatorial) to 39942 km (polar – a meridian). The corresponding radius of the Earth according to Eratosthenes is R = 6281 km or, if we adopt the value 252000 stadia, R = 6317 km. Thus, the radius calculated by Eratosthenes is only about 40 km smaller than the true value of the polar radius, which is 6357 km and about 61 km smaller than the true value of the equatorial radius (6378 km). This estimation by Eratosthenes is an excellent approximation of the true value [5,9].

3. FACTORS THAT AFFECTED THE ACCURACY OF THE METHOD

All the errors (factors) mentioned below have been studied analytically in our previous works[5,7,9].

a) It is difficult to determine the exact point in Syene as well as in Alexandria, where Eratosthenes placed the gnomon and therefore is difficult to ascertain the exact geographical coordinates of these two points. The latitude of Aswan, which is very near ancient Syene, is approximately 24°07′ and in ancient Syene is about 24°05′. As far as Alexandria is concerned, two were its cultural and scientific institutions, which were adorning it as buildings as well: the Museum and the Library. The geographical latitude of the Phare of Alexandria is about 31°14′, that of the Library 31°06′, while at the area of the Museum is about 31°11′. We suggest as the more probable place for Eratosthenes to have made his observations the area of the Museum, since the Museum not only had, among its other facilities, an observatory but also it had been the residence of famous scientists – many of whom were acknowledged as the best astronomers, mathematicians and philosophers. In such a case, the difference between the latitudes of Syene and Alexandria was approximately $\omega_\pi = 7°06'$.

b) The Earth in Antiquity was considered at best a perfect sphere, while in reality it is flattened towards its poles.

c) The rotation of Earth around its axis causes an additional error, which is different from the one due to the geoid shape of the Earth, because the direction and the magnitude of the gravitational field intensity $\overline{g}$ are influenced by its rotation.

d) The measurement of the length of the shadow thrown by the gnomon is not accurate, as happens also with a sundial, because of the existence of a penumbra.

e) The distance between Syene and Alexandria was not exactly 5000 stadia, but something like 800 km.

f) Syene was not exactly placed on the Tropic of Cancer at the age of Eratosthenes, but slightly to the north of it, since the inclination of the ecliptic was back then 23°43′, while Eratosthenes had determined it, as said earlier, at about 23°51′. With the value of 23°43′

Syene is located no less than 8 arc minutes while for the modern value of 23°27′ about 24′ to the north of the Tropic of Cancer.
g) Syene, with a geographical longitude of about 32°53′ and Alexandria (area of the Museum) with a geographical longitude of about 29°55′, do not lie on the same meridian, the latter being around $\Delta\lambda = 3$ degrees to the west.
h) In Syene and Alexandria, because of the phenomenon of atmospheric or astronomical diffraction, the solar rays are not parallel.

The number of 250000 stadia is given by Cleomedes[2], while Strabo[11,5,7,9] explicitly states that according to Eratosthenes the circumference of the Earth is 252000 stadia. Also Theon of Smyrna[12,5,9] reports that Eratosthenes demonstrated that the great circle of the Earth is 252000 stadia. The same number was adopted by Pliny[10,5,9] and is the most widely quoted in ancient writings. The different value given by Cleomedes has been the topic of a great discussion on the reason for this discrepancy. It seems more plausible that Eratosthenes himself or even a later author corrected the number 250000 to 252000 either due to a subsequent improvement of the approximate value of 5000 stadia, or because he wanted to adopt a number divisible with 60 or 360, i.e. 252000/60 = 4200 stadia, or 252000/360 = 700 stadia. This way the integer 4200 or 700 results as the number of stadia corresponding to 1° on the surface of the Earth[1,5,9].

It is not, however, certain that Eratosthenes himself knew the division of the circle into 360°. This division seems to have appeared for the first time in the 2nd century B.C.[9]. Hipparchus, like others before him, was dividing the circle into 360° and he introduced this division to the circumference-meridian of the Earth. In order to describe the celestial phenomena and to construct tables with astronomical data for every zone (band) of geographical latitude from the equator to the North Pole, he adopted the number 252000 stadia of Eratosthenes, which he considered accurate[11,5,9]. The division 252000/360° gives 700 stadia per 1°. So Hipparchus described the celestial phenomena per 1° of latitude or per 700 stadia.

Finally, it is not clear which is the exact length of the stade used by Eratosthenes. It appears that in ancient Greece various values were used in different periods[5]. A well-known stade was the Olympic one of 185 m, while another was the Ptolemaic or Royal stade of 210 m. But the stade used by Eratosthenes was[3,5,9], according to Pliny, shorter than the Olympic and equal to about 157.5 m while according to Rennell it was about 154 m (according to others 148,8m). The Eratosthenian stade was a wayfaring measure, used in Antiquity for distances counted with steps by professional steppers.

4. THE SIGNIFICANCE OF THE METHOD

Eratosthenes calculated with great accuracy the size of the Earth, making a relative error of approximately 1%, if we adopt the stade of 157.5 m as his unit of length; his method remained as a major achievement of the ancient Greek thought. This method causes admiration even today, since Eratosthenes did not have at his disposal modern instruments and since the errors we mentioned here are not due to his method but due to other causes.

As we have already mentioned, Hipparchus described the celestial phenomena for various zones of geographical latitude from the equator to the North pole, giving in the form of tables the astronomical data for every 1° of latitude[9]. However, he did not proceed to measure the lengths of various arcs in different latitudes along one meridian.

We suppose this was due to the belief of the ancient philosophers, astronomers and mathematicians since Pythagoras, that the Earth, like the planets, is spherical[7,9].

The method of Eratosthenes by itself is precise and is applied even today for the determination of the size and shape of the Earth. In our opinion, the work of Hipparchus combined with the method of Eratosthenes, who had calculated the latitudes and the distances of various places (such as the distance Alexandria-Rhodes as 3750 stadia[11,5]), were the factors that incited subsequent geographers to determine the size and shape of the Earth using better technology, which in turn supplemented the Eratosthenian method[9].

In order to apply the method of Eratosthenes for the determination of the shape of the Earth and its size we are based on curvature theory[6]. By measuring the length of various arcs of the same meridian which correspond to equal epicentric angles, corresponding to the closest circle (circle of curvature), at different geographical latitudes, it is proved that these lengths increase as we proceed from the equator to the poles[9]: The lengths of the arcs of the same meridian that correspond to an angle of 1^o are not equal. Thus it can be proved that the Earth is oblate at its poles. On the contrary, along the equator (and at sea level) these lengths are equal. So, it can be proved theoretically that the meridians of the Earth are ellipses, because the radius of the circle of curvature corresponding to the poles is larger than the respective radius of the circle of curvature that corresponds to the equator (the center of the ellipse does not coincide with the centers of the inscribed circles corresponding to the various points of the ellipse)[9].

REFERENCES

1. Berger, E.H.: *Geschichte der wissenschaftlichen Erdkunde der Griechen*, 1903
2. Cleomedes,: *Kyklikis Theorias Meteoron*, ed. car. Christ. Lips. 1832
3. Hultsch, F.L.: *Griechische und Romische Metrologie*, Ber. 1882
4. Pinotsis, A.: The reasons which led Hipparchus of Rhodes to adopt the Geocentric system and the models of epicycles and the eccentric circles, D. Chr., IE, Rhodes (1993),1998 [in Greek].
5. Pinotsis, A.: The Contribution of Poseidonios of Rhodes in Astronomy and Mechanics, D. Chr., IZ, Rhodes (1993),2000 [in Greek]
6. Pinotsis, A.: *A Mathematical Introduction to Theoretical Mechanics*, ed. Stamoulis, Athens 2002,(2000) [in Greek]
7. Pinotsis, A.: Comparison of Earth-size measuring methods in the ancient Greek world; in 5th Hellenic Astronomical Conference, 20-22 September 2001, Crete, Proc., ed. D. Hatzidimitriou et.al., Crete, Greece, 2002.
8. Pinotsis, A.: The development of cosmological ideas and mathematics models in ancient Greece; in Proceedings of the 4th Hellenic Conference Aristarhus of Samos, 17-19 October, Samos 2003, p. 279-307. .
9. Pinotsis, A.: The evolution of the methods for the measurement of the Earth's size and the significance and errors of Eratosthenes' method (submitted).
10. Pliny, S.: Naturalis Historia, Lip. 1865
11. Strabo,: *Geographika*, Kaktos, Athens
12. Theon of Smyrna,: *Astronomia*, E. Hiller, Teub. Lips. 1878

ADVENT AND FUTURE OF THE 'ΕΥΔΟΞΟΣ' OBSERVATORIES COMPLEX -III: TEACHING SCIENCE WITH "EUDOXOS"*

Solomos, N. [1,2,3] , Fanourakis, G. [2,3] , Zachariadou, K. [2,3] , Geralis, T. [2,3] , Georgopoulos, P. [3,2] , Sotiriou, S. [4] , Andrikopoulos, N. [4] , Kalkanis, G [5] , Angulo Rasco, F. [6] , Rodriguez Gonzalez, C. [6] , Garcia Cruz, E. [6] , Scheuermann, F. [7]

[1] Hellenic Naval Academy, Physics Sector, Piraeus, Greece. [2] Institute of Nuclear Physics, National Research Centre "Demokritos", Greece [3] National Observatory of Education "EUDOXOS" Kefallinia, Greece. [4] Ellinogermaniki Agogi School, Pallini, Greece [5] Pedagogical Department, Univ*ersity* of Athens, Greece [6] University of Cadiz, Spain, [7] Management Center Innsbruck, Austria

EUDOXOS: Educational Vision and Distant Learning Curricula

After the establishment of the 'ΕΥΔΟΞΟΣ' National Observatory of Education in 1999, the organization has been the common cradle from which two consequent educational e-learning initiatives -both bearing its name "EUDOXOS"- have emerged. The first (I) was funded by the Hellenic Ministry of Education (1999) and the second (II) by the European Commission (2002). Two different experimental curricula have been elaborated for different student ages in Greek and European Schools. Here we describe and analyze the pedagogical and learning strategies adopted in both cases but pay particular attention to the ongoing EUDOXOS (II) project. The current status of ΕΥΔΟΞΟΣ National Observatory of Education as the first robotic observatory of the country, its recent programs and its prospects in Science & Education are also very briefly described. EUDOXOS' elaborated development plans including several new telescope designs and instrumentation activities, summarized in the light of recent advances in astrophysics, are given in Solomos et.al (2002)-a The major teaching goal of the "EUDOXOS" establishment is to provide to promising pupils and undergraduate students Web-*access* to a variety of modern scientific instruments which allows them to acquire and analyze their own images and spectra, and help the acquisition of analytic skills to test astronomical hypotheses and theories. In EUDOXOS-I there is a strong emphasis on discovery (e.g. SN Type-Ia, microlensing event patrols) and advanced hands-on experimentation. The emphasis is put on building on the student's own curiosity to guide them into understanding the Universe using the scientific method of hypothesis, observation, and analysis, based on the fact that astronomy is so attracting that is particularly suited for such a purpose. More than 10 self contained exercises have been written covering modern Astrophysics by following the imaginary path from 'near' to 'far' (that is from Solar System to Cosmology) and also a parallel but symplectic path, largely based on the historic development of Astronomy. The material of this (ever expanding) curriculum can be downloaded by students in the form of self-contained classes and corresponding teacher guides written in Greek. In EUDOXOS-II project, the emphasis was transferred in improving the attractiveness of the user interface as well as in the elaboration of a new comprehensive less-demanding curriculum to be used on-line by younger pupils. The latter is written in English as the targeted user group is the pupils of the European schools. Moreover, it will be finally available in five European languages including Greek.

* *Proceedings of the 6th Hellenic Astronomical Society Conference, 15-17 September 2003, Penteli, Greece*

The system approach of the Eudoxos National Observatory of Education:

Plate-1: Air view of the 'Eudoxos' Observatories Complex an astronomical establishment operating since 1999. It was formed by a consortium of Greek institutes involving the National Research Center of Physical Sciences "Demokritos", the Hellenic Naval Academy, the Ministry of Education and the Prefecture of Kefalonia & Ithaki. It now belongs to the Research Foundation of Kefalonia (RFK) an establishment recognized by the Greek State. It is being operated by the same consortium with the addition of the University of Athens, Faculty of Primary Education and has already received substantial support from the Hellenic Air Force and the Ministry of Education. "Eudoxos" is a Web-accessible complex of optical and radio observatories whose administration and first facilities are located 10 miles SE of Argostolion, Kefallinia Island at a plateau 600m below the peak of mount Ainos (1628m). Its premises (a former military base of the Hellenic Air Force), have been donated to the "Eudoxos"/RFK establishment as a symbolic contribution to the progress of the Hellenic Youth.

Scientifically, EUDOXOS invested on the strength of the Robotic Astronomy which, in fact, is based on the inherent advantages of the small (<2m) telescopes emanating from: (a) the continuing existence of astrophysical problems where large collecting power and extreme sky quality are not critical or constraining factors for the success of the relevant observations and (b) the realization that there are still extremely significant research opportunities in astronomical issues the investigation of which is intimately associated with the factor of *time*. Such projects could be the long term monitoring of celestial objects the latter being stars or galaxies.

As it was shown (Solomos, 2002-a) automated telescopes under unattended operation are characterized by at least 1 order of magnitude higher throughput than ordinary ones.

These considerations combined with inherent advantages of Small Telescopes such as: less demand for time allocation, unique performance on repetitive tasks (low-inertia structures, rapid switching among astronomical objects), efficient and economical dedication to special purposes and experiments, photometry and spectroscopy from larger field of views and attractive capacity for co-ordinated observations, make them the ideal platforms of long-term continuous operation of astronomical instruments. This, in turn, implies dedicated Small Telescopes not conventional but pre-designed with capacity of executing repetitive tasks. Largely based on these grounds, we essentially introduced Robotic Astronomy in Greece with a series of studies (see Solomos, 1993, 1995, 2001, 2002 and references therein) culminated in the operation of our first telescope unit (“TAM”) in 1999. This advanced

Telescope was named to honor the memory of "*Andreas Michalitsianos*" (TAM) the eminent Cephalonian Astrophysicist and Director of the Laboratory for Astronomy & Solar Physics of NASA, not only symbolically -for his early contact with robotic astronomy at Kit Peak (in the-70s)- but for his scientific originality, experimental skills and steep rise in astronomy since the age of 16, which offers a unique bright paradigm to the younger generation

The pedagogical approach of the EUDOXOS scientific curricula

The 'Eudoxos' projects share a common educational axis: They take advantage of the thrill and magic of Astronomy and utilize the possibilities the Internet offers in order to transform the classroom into a research laboratory and improve learning. The projects provided platforms that allow the students and teachers to remotely control and use the "Andreas Michalitsianos" Robotic Telescope (TAM) and recently the "Apollon" Solar Telescope (HTA), in the framework of their school curriculum and beyond. The new Eudoxos' pedagogical approach cross cuts the traditional boundary between the classroom, home, scientific laboratories and research institutions as distinct learning environments. It aims at involving the users (students, teachers) in extended episodes of playful learning. One implication of this model is that students should are assigned activities that reflect the application of the content knowledge as it is practiced by scientists outside the classroom. The goal is to induce the learner into a "culture of practice" which makes the knowledge meaningful. Within this general framework the new technology application of Eudoxos-I project supports the pedagogical method of autonomous self-directed learning and allows for a self-directed acquisition of skills to meet users individual communication and learning needs. The self-learning method is supported by elements of entertainment (play and learn) in order to enhance learning by using the modern communication technologies to transfer the magic of an observatory into the classroom. The learning process is supported through an on-line manual that acts as an on-line tutor. In the framework of the European Project EUDOXOS-II a much friendlier web-based educational environment is being developed in order for the telescope to be operated via queue based scheduling by high school students and their teachers. The partnership has adopted a heavily user-centered approach in the development of the tool. In order to do so the project's implementation includes two cycles of school-centered work in real school environments. For the first cycle an adapted curriculum is developed around a solid educational framework that captures the main learning objectives of the project (observation of the moon, sun, planets, variable stars etc), while during the second cycle the students and teachers of the participating schools will have the chance to design and perform their own experiments by using the telescopes to carry out their own direct astronomical observations. The overall pedagogical framework includes the necessary adjustments to the normal school curriculum, teachers training (on-line seminars and workshop) and support, development of lesson plans for the project's implementation in the classroom and development of educational material (conventional and electronic).

In the framework of the previous EUDOXOS-I project, we have also carefully prepared, and proposed the *Eudoxos' Modern Telelaboratory Curriculum (EMTC)* tailored to the characteristics and special advantages of the TAM. 13 subjects are currently available to the participating schools and can be also available on demand to other interested Greek Universities. Further extension of the EMTC to the field of radioastronomy was also designed and is currently in preparation Another extension on astronomy-driven Interdisciplinary targets (data mining, informatics, radio science, astrobiology) is being planned (see suggestions by Kafatos, 2002). Eudoxos

Observatory is now working on collaboration plans with other institutes abroad as well as with the Univ. of Athens on GRBursts, Reverberation mapping of AGN, Symbiotic stars, AGN monitoring, time-series studies. Also, since 1997 we had conceived and push forward preparatory work on a visionary program aiming at the advancement of time-domain '*Ultra High Speed Astrophysics*' in Greece. For the latest status and presentation of our work on such a promising initiative see Solomos et. al.,(2002)-b and previous references therein.

Concluding Remarks

An updated account of the progress of the 'ΕΥΔΟΞΟΣ' project from the time of its conception to the operations period of today was given herein. Although the "Eudoxos project" is using sophisticated technological devices of the EUDOXOS National Observatory of Education, its aim is not to test this technology but to focus on its impact in the teaching procedure. The first project EYDOXOS-I, has been successfully completed (2001), the second project is now (May 2003) on its eighth month of operation involving Schools from Austria, Greece, Italy and Spain. The new lesson plans and the user interface have been developed and the first stage of the implementation and evaluation has already started. In conclusion, the "EUDOXOS" center, aims not only to fulfill its mission as the official National Observatory of Education accessible through the Web, but, also, to become and remain one of the country's rapidly evolving and competitive observational establishments, capable to contribute original high quality data for the study of a wide spectrum of well defined and timely astrophysical problems.

References

European Commission (2002): Preparatory and innovative actions – e-Learning action plan - DG EAC/25/01

Kafatos, M.: (2002) http://astrophysics.physics.uoc.gr/conf/sessions/Session08/S825/

Polykalas et. al. (2002) http://astrophysics.physics.uoc.gr/conf/sessions/Session08/S807/solomos19.ps

Solomos, N. et al (2001): "EUDOXOS" Final Report, Pedagogical Institute, Hellenic Ministry of Education

Solomos, N. (2002)-a:http://astrophysics.physics.uoc.gr/conf/sessions/Session08/S806

Solomos, N.(2002) b:http://astrophysics.physics.uoc.gr/conf/sessions/Session07/S712

Solomos, N. (1995).*"The Research Potential of Small Telescopes"* 2nd Hel. Astr. Soc. Conf., Ed. J.Seiradakis, 643-648

Solomos, N. (1995).*"Remotely controlled operation for repetitive data-acquisition: the future of the Korgialenios Astronomical Station of Kryonerion, Greece"* 2nd Hel. Astr. Soc. Conf., Ed. J.Seiradakis, 629-633

Solomos, N., Arageorgis, I., Madianos, I. (1993). *Korgialenios Telescope Upgrade Initiative*, Proposal to the National Observatory of Athens (NOA protocol No.663).

ASTRONOMICAL CALENDAR FOR 2003 WITH CELESTIAL MAPS*

Zafiropoulos Basil and Stavliotis Charalampos
Department of Physics, University of Patras

Abstract. An Astronomical Calendar with celestial maps has been compiled for the year 2003. Old constellations charts, made by well known artists (like Albrecht Dürer), famous astronomers (as J. Bode, J. Flamsteed and J. Hevelius), or distinguished mathematicians (like D' Alembert), have been chosen to be included in this calendar. In addition to every day rise and set of the Sun and the Moon, important astronomical data like: season's duration, lunar and solar eclipses, as well as meteorite showers, have been incorporated. The main procedure applied has been to restore the black and white prints (whenever this was necessary) and to prepare a proper copy of the restored map. Subsequently a mixed method has been followed to add colour to the copy by hand and by means of the computer. Finally, from the various colour versions created by the program, the most suitable to the era of the chart fabrication, has been adopted. This way the original black and white print remains untouched. All the stages of the professional printing procedure have been closely observed, to secure optimum result. From the massive work done, only a small fraction of 33 maps, have been included in the Astronomical Calendar. The rest charts will appear in a book to be published shortly.

1. INTRODUCTION

Old celestial maps constitute one of the most beautiful aspects of the human creativity. They depict the stars together with the mythological representation of constellations, combining the artistic merit with the scientific accuracy.

The calendar for 2003 includes mainly printed celestial maps. The first of this kind is considered to be the one by A. Dürer, dated since1515, followed in 1532 by the two planispheres made by Johann Honter. One of the very first efforts, which includes 1706 stars, is "Uranometria" (1603), the masterpiece by Johann Bayer. He employs the Tycho Brahe catalog, with its accurate positions of the stars and introduces 12 constellations, in addition to the 48 classical ones by Ptolemy.

Many astronomers followed the Uranometria of Bayer, like the polish Johann Hevelius, the Frenchmen Louis La-Caille and Philippe La-Hire, as well as, the English royal astronomer John Flamsteed. The first one in his unsurpassed Uranographia (1690), in 56 maps imprints the positions of 1564 stars and proposes the introduction of 11 new constellations. Celestial maps as well as astronomical and cosmological diagrams are including the atlas Coelestis (1742) of the distinguished German mathematician Johann Doppelmayr [5]. The astronomer Johann Bode accomplished the last great attempt in 1801. In his 20 gigantic celestial maps with dimensions 67cmx93cm each, he registered 17.240 stars and nebulae with unique accuracy. He also proposed the introduction of new constellations, setting boundaries to each of them.

Exceptionally esthetic and of great artistic value is the collection of the 29 maps incorporated in "Harmonia Macrocosmica" (1661) by Andreas Cellarius. This atlas includes two planispheres of Julius Schiller. The latter attempted in 1627, to Christianize the heavens by replacing the classic constellations with figures and symbols from the Holly Bible, but he failed. In 1930 the International Astronomical Union (IAU) put an end to the fair of representing on the sky heroes, myths and technological achievements. IAU restricted the number of constellations to 88 and established strict boundaries for each one.

2. HISTORY OF CELESTIAL MAPS

The contribution of ancient Greeks in celestial cartography has been very important. **Clemes** from Alexandria mentioned that **Centaur Chiron** is the first one who tried to settle the sky and did the first star grouping, in order to assist the Argonauts to their expedition. At about the beginning of the second millennium B.C. many constellations were known, as it can be seen from the **Orphic hymns**. The sixth hymn mentions seven zodiac constellations: Aries, Taurus,

* *Proceedings of the 6th Hellenic Astronomical Society Conference, 15-17 September 2003, Penteli, Greece*

Virgo, Aquarius, Pisces, Scorpio and Lion. In the famous epic poems **Iliad** and, mainly, **Odyssey**, **Homer** refers to the Sun, the Moon and the planets, such as Morning star "Avgerinos" and Night star "Esperos", (they didn't know at that time that they both were one and the same planet, namely Venus). Also he mentions Pleades, Yades, Orion, Ursa Major, Sirius, Arcturus and Bootes. Regarding Ursa Major he quotes (Odyssey ε283-285):

"And the Bear, which sometimes is called Wain,
and goes round and round starring at the Hunter,
and never dipping into the water of the Oceanus".

In the following extract Homer tells how Hefaestos forges his artistic creations on Achilles shield (Iliad, Σ 483-489):

"He wrought the earth, the heavens and the sea; the moon also at her full and the untiring sun, with all the signs that glorify the face of heaven- the Pleiads, the Hyads, huge Orion, and the Bear, which men also call the Wain and which turns round ever in one place, facing Orion, and alone never dips into the stream of Oceanus".

Our great poet **Isiodos** from Askry of Boeotia (8th century B.C.) in his poem "**Works and Days**" gave some advice to the farmers based on astronomical observation. He mentioned Ursa Major, Taurus, Bootes and Orion. A great step forward in naming the constellations is the poem by **Aratos of Soloi** (305-240 B.C.) "**Phenomena**" [1], where he glorifies the stars and their myths. It is said that Aratos turned into poems the works of **Eudoxus of Cnidus** (408-355 B.C.) "**Phenomena**" and "**Enoptron**". In this astronomical poem forty-three constellations and five bright stars are mentioned.

The greatest Greek astronomer of all times was **Ipparchos** (190-120 B.C.) born in Nicea of Bythinia. From a supernova discovery he made in 134 B.C. in Scorpio, he was inspired to compile a catalogue from 1020 stars and 43 constellations. Fortunately his discoveries were saved in the most important work of antiquity, "**The Mathematical Syntaxis**" by **Ptolemy** of Alexandria (108-170 A.D.) [10]. It consists of 13 books, which incorporate the whole astronomical and mathematical knowledge up to the era when this work was compiled. Apart from a table of 1028 stars, "**Almagest**" (the Greatest - as it was known to the West by its Arabic translation), it includes 48 groups of stars known as "the ancient 48 constellations". "Almagest" remained for almost 1500 years the greatest astronomical book.

Another work of antiquity is "**Katasterismoi**". It is attributed to **Eratosthenes** (276-194 B.C.) and deals with enlistment of constellations and the myths associated with them. One of the very first representations of the sky is the planisphere of **Dentera**, dated since 36 B.C. that includes the 12 zodiac constellations among others. It used to decorate the ceiling of a secret room in the temple of Isis. Today it is found at the entrance of Paris National Library.

Celestial maps and planispheres, which present artistically the real positions of the stars as well as the respective mythological forms of the constellations, constitute relatively recent applications, that appeared at sky atlases after 1500 A.D. One of the most remarkable representations of the sky appeared on the woodwork of the great German painter and engraver **Albrecht Dürer**, who in 1515 drew separately the north and south celestial hemispheres. It is considered to be the first printed map, followed by **Johann Honter's** planispheres in 1513. Stars combined with their respective mythological representation are first met on **Peter Apianus** charts, which included the 48 Ptolemy's constellations.

The death of the Danish astronomer **Tycho Brahe** (1546-1601) put an end to the pre-telescopic astronomy. Among other things, he had published a catalogue that included about a thousand stars as well as planet observations. The unsurpassed accuracy of Brahe's observations, created the basis for the extraction of the three laws of planetary motion by his student **J. Kepler** (1571-1630).

The first astronomical atlas, which combined great artistic value, scientific accuracy and originality, published in 1603 by the Bavarian lawyer **Johan Bayer** [2]. In his famous work "**Uranometry**", he introduces 12 new constellations, based on a celestial map of the south hemisphere, that the Dutch navigator **Peter Keyser** presented in 1595.

Many astronomers and mapmakers, who introduced a great number of new postclassical constellations, adopted Bayer's example. The most eminent among them are the polish **Johannes Hewel,** known with his Latin name **Johannes Hevelius,** [7] and the French **Luis La-Caille** [9]. The first one published in 1687 his masterpiece **Uranographia,** in which he proposes the introduction of seven new constellations. The latter, after his return from a trip to the Cape of Good Hope in South Africa, introduced, in 1715, fourteen new constellations.

In parallel with the two important celestial atlases reported above, there were also remarkable editions like the one by **Edmond Halley** in 1677, according to observations he made from the island of St. Helen. Another eminent publication is that of the English Royal Astronomer **John Flamsteed** (1725) [6]. The period of important celestial atlases ends with the work of **Johann Bode** (1747-1826) [3]. In his gigantic **Uranographia** he proposes a small number of new constellations that were never recognized as such.

Thus at the beginning of the 19^{th} century, the sky was flooded with a great variety of constellations, that represented various scientific instruments and technological achievements, like the printing press, pump, air balloon etc. This kind of chaos appears in the atlas of **Alexander Jameson** [8], which was published in 1822 and included almost all the constellations known up to that time. The most revolutionary attempt to Christianize the heavens was made by the cartographer **Julius Schiller** [11], in 1627. He created a celestial atlas in which he had replaced all the known classical figures with Christian saints, the twelve Apostles and symbols from the Holly Bible.

The most beautiful and unsurpassed set of celestial maps that had ever been published is that of **Andreas Cellarius** [4]. In twenty-nine charts of unique beauty, he presents four pairs of planispheres and various other figures of cosmological importance, which clarified the various astronomical theories of that era. All these maps were included in the atlas "**Harmonia Macrocosmica**" (1661), which also incorporates the two planispheres done by Julius Schiller.

Indicatively we present the month of September of this calendar.

REFERENCES

[1] Aratus Solensis. "Phainomena kai Diosemeia", Oxford, 1672.
[2] Bayer, Johann. "Uranometria", Augsburg, 1603.
[3] Bode, Johann Elert. "Uranographia Sive Astrorum Descriptio", Berlin, 1801.
[4] Cellarius, A. "Harmonia Macrocosmica sev Atlas Universalis et Novus", Amsterdam, 1661.
[5] Doppelmayr, Johann Gabriel. "Atlas Novus Coelestis", Nuremberg, 1742.
[6] Flamsteed, John. "Atlas Coelestis", London, 1729.
[7] Hevelius, Johannes. "Firmamentum Sobiescianum, sive Uranographia totum Coelum Stellatum", Gdansk, 1690.
[8] Jamieson Alexander, Celestial Atlas, 1822.
[9] La-Caille, Nicolas Louis de. "Planisphere contenant les constellations Celeste", Paris, 1756.
[10] Ptolemy. "Omnia quae Extant, Opera", Basel, 1541.
[11] Schiller, Jullius. "Coelum Stellatum Cristianum", Augsburg, 1627.

Τέσσερεις από τους 56 χάρτες του Johann Hevelius, Uranographia (1690).
α) Τοξότης, β) Ταύρος, γ) Ανδρομέδα, δ) Περσέας -Ηνίοχος.

ΑΥΓΟΥΣΤΟΣ 2003

ΠΑΡΑΣΚΕΥΗ	ΣΑΒΒΑΤΟ	ΚΥΡΙΑΚΗ	ΔΕΥΤΕΡΑ	ΤΡΙΤΗ	ΤΕΤΑΡΤΗ	ΠΕΜΠΤΗ
1 ☼ 5:28/19:35 ☾ 8:33/21:49	2 ☼ 5:28/19:34 ☾ 9:41/22:16	3 ☼ 5:29/19:33 ☾ 10:50/22:44	4 ☼ 5:30/19:32 ☾ 12:00/23:13	5 ☼ 5:31/19:31 ☾ 13:11/23:46 Πρώτο Τέτ. 9:29	6 ☼ 5:32/19:30 ☾ 14:24/—	7 ☼ 5:33/19:28 ☾ 15:37/0:24
8 ☼ 5:34/19:27 ☾ 16:46/1:10	9 ☼ 5:34/19:26 ☾ 17:49/2:06	10 ☼ 5:35/19:25 ☾ 18:42/3:09	11 ☼ 5:36/19:24 ☾ 19:26/4:17	12 ☼ 5:37/19:23 ☾ 20:01/5:27 Πανσέληνος 6:48	13 ☼ 5:38/19:21 ☾ 20:32/6:35 Περσείδες	14 ☼ 5:39/19:20 ☾ 20:58/7:41
15 ☼ 5:40/19:19 ☾ 21:22/8:43	16 ☼ 5:41/19:18 ☾ 21:45/9:43	17 ☼ 5:41/19:16 ☾ 22:09/10:43	18 ☼ 5:42/19:15 ☾ 22:34/11:41	19 ☼ 5:43/19:14 ☾ 23:02/12:41	20 ☼ 5:44/19:12 ☾ 23:34/13:41 Τελευτ. Τέτ. 2:50	21 ☼ 5:45/19:11 ☾ —/14:40
22 ☼ 5:46/19:10 ☾ 0:13/15:39	23 ☼ 5:47/19:08 ☾ 0:59/16:34	24 ☼ 5:47/19:07 ☾ 1:52/17:24	25 ☼ 5:48/19:06 ☾ 2:53/18:09	26 ☼ 5:49/19:04 ☾ 3:59/18:47	27 ☼ 5:50/19:03 ☾ 5:08/19:20 Νέα Σελήνη 19:27	28 ☼ 5:51/19:01 ☾ 6:18/19:50
29 ☼ 5:52/19:00 ☾ 7:29/20:18	30 ☼ 5:53/18:58 ☾ 8:39/20:46	31 ☼ 5:54/18:57 ☾ 9:50/21:15				☼ Αν/Δυσ Ηλίου ☾ Αν/Δυσ Σελ. Διάττοντες ★

Λέων: Johann Hevelius (Ουρανογραφία 1690)

<u>*PAPERS POSTED DURING THE SESSION ON HISTORY OF ASTRONOMY & TEACHING OF ASTRONOMY*</u>*

THE HELIOCENTRIC SYSTEM FROM THE ORPHIC HYMNS AND THE PYTHAGOREANS TO THE EMPEROR JULIAN

Efstratios Theodossiou and Vassilios N. Manimanis

Section of Astrophysics, Astronomy and Mechanics, Department of Physics, University of Athens

Abstract: The geocentric system, placing our small planet at the center, suited more to the self-centered thought of the ancient savants and dominated for centuries, adopted by the majority of philosophers and astronomers. But this does not mean that there weren't any views supporting the heliocentric system. Before Aristarchus of Samos, seeds of the heliocentric theory exist in the Orphic Hymns and in the teachings of Anaximander and the Pythagoreans. Later, Aristarchus laid the foundation of this theory, which unfortunately did not prevail while the geocentric system which was widely spread under the weight of the views of Aristotle and Ptolemy.

Nevertheless, it should not be assumed that the faith in the heliocentric system had been forgotten. During the 4th Century A.D., the Emperor Julian (A.D. 336-363), known as the Parabates or Renegade, was a supporter of it. Julian considered the Earth as a planet which, as the rest planets, was revolving around the Sun following a circular orbit. This fact indicates that the Aristarchean theory not only had not been forgotten, but in the 4th Century A.D. had still its followers.

THE PRE-ARISTARCHEAN PYTHAGOREANS: THE VIEWS OF PHILOLAOS OF CROTON

Efstratios Theodossiou, Vassilios N. Manimanis and Emmanuel Danezis

Section of Astrophysics, Astronomy and Mechanics, Department of Physics, University of Athens

Abstract: The Pythagorean School founded the philosophy of mathematics and physics, correlating the order and harmony of the sounds with the mathematics and the order and harmony of the universe. The Pythagoreans were basically astronomers, but they studied the planetary distances in analogy to a celestial musical harmony, which was being produced by the harmonical sounds.

The Pythagorean hypotheses were made known to a wider audience in the middle of the 5th Century B.C. by Philolaos (450-400 B.C.), who systematized Pythagorism and wrote a synopsis of the Pythagorean philosophy. Philolaos conceived the idea of the philosophy of the limit and the infinity, and of the harmony between them. He argued that the universe is one and it was created gradually starting from the middle, while he considered that the fire was at the center and beyond it he placed the *antichthon*, the Earth, the Moon, the Sun the five then known planets and the sphere of the fixed stars. Thus, around the central fire 'dance' ten celestial bodies, in order to reach the holy (for the Pythagoreans) number 10. Philolaos, by doubting the traditional geocentric cosmology, paved the ground for the heliocentric theory of Aristarchus, who with this theory would question clearly and totally the central role of our small planet in the universe.

---

* *Proceedings of the 6th Hellenic Astronomical Society Conference, 15-17 September 2003, Penteli, Greece*

PAPERS POSTED DURING THE SESSION ON HISTORY OF ASTRONOMY & TEACHING OF ASTRONOMY*

THE PRE-ARISTARCHEAN PYTHAGOREANS: THE VIEWS OF IKETAS, ECPHANTOS AND HERACLIDES OF PONTOS

Efstratios Theodossiou and Vassilios N. Manimanis
Section of Astrophysics, Astronomy and Mechanics, Department of Physics, University of Athens

Abstract: In addition to the hypotheses of Philolaos of Croton, who contributed with his work to a wider knowledge of the Pythagorean views, other students of Pythagoras, such as Hiketas of Syracuse, Ecphantos of Syracuse and Heraclides of Pontos, formulated pioneering views on the planetary issue.

Hiketas was the first who argued that the heavens, the Sun, the Moon and the stars are motionless and the only moving body is the Earth. Indeed, according to Cicero, he was supporting the theory of the rotation of the Earth on its axis. A true breakthrough for his era.

Moreover, it seems that this same theory was also supported by Ecphantos and Heraclides; both were considering the Earth as moving through space and rotating simultaneously. Therefore, the students of Pythagoras were the ones who assigned to our planet its true position and motions, while at the same time they supported a pyrocentric planetary theory, which at the very least facilitated Aristarchus of Samos to express his own heliocentric theory.

THE HELIOCENTRIC SYSTEM OF ARISTARCHUS OF SAMOS IN THE ANCIENT GREEK WRITERS AND THE MODERN GREEK REFERENCES IN FAVOR OF HIM

Efstratios Theodossiou
Section of Astrophysics, Astronomy and Mechanics, Department of Physics, University of Athens

Abstract: nitially, as a loan from the international bibliography, the heliocentric system was usually being referred to in the Greek bibliography as Copernican, in honor of the astronomer Nicolaus Copernicus who was considered as the introducer of the heliocentric theory. However, careful research by non-Greek astronomers, as well as the persistence of the Greek astronomer Eugene Antoniades (with excellent work in France during the early 20th Century) resulted in several Greek writers and astronomers citing Aristarchus as its first introducer in their pertaining publications.

In this paper it is presented a collection of the views of Greek writers from the ancient times to the present, which support the discovery of the true system of the world by Aristarchus. All the existing references of the ancient philosophers and doxographers are cited, from the Archimedean *Psammites* to the references by Aetius and Diogenes Laertius, as well as many of the references of the Modern Greek writers and astronomers.

From the large number of these references it seems logical that the contribution of Aristarchus must be recorded in the Greek astronomical manuals. All Greeks (and not only them) must know that the true introducer of the heliocentric theory was the great mathematician and astronomer Aristarchus of Samos, and that Copernicus was simply its reviver.

---

* *Proceedings of the 6th Hellenic Astronomical Society Conference , 15-17 September 2003, Penteli, Greece*

PAPERS POSTED DURING THE SESSION ON HISTORY OF ASTRONOMY & TEACHING OF ASTRONOMY[*]

THE HELIOCENTRIC SYSTEM OF ARISTARCHUS OF SAMOS IN THE MODERN INTERNATIONAL REFERENCES IN FAVOR OF HIM

Efstratios Theodossiou
Section of Astrophysics, Astronomy and Mechanics, Department of Physics, University of Athens

Abstract: In the international bibliography the heliocentric system is usually being referred to as Copernican, in honor of the Polish astronomer Nicolaus Copernicus. Nevertheless, today there are several writers and astronomers in the world who cite as its first introducer Aristarchus of Samos and Copernicus as its mere reviver. Here it is presented a collection of the views of writers in the international bibliography who support the discovery of the heliocentric theory by Aristarchus.

From the numerous references it is an undoubted fact that the contribution of Aristarchus is recognized not only by the Greek, but by the international astronomical community as well, and it is stated not only in scientific papers but also in the astronomical manuals. All astronomers and many other educated people know by now Aristarchus as the true introducer of the heliocentric theory, while Copernicus was simply its reviver. And, as the majority of the researchers and writers note, the heliocentric system must be referred to from now on as Aristarchean and not Copernican, and this term must also be used in the respective Greek manuals and books.

THE CONTRIBUTION OF THE ARABIC WORLD IN ASTRONOMY

Efstratios Theodossiou, Vassilios N. Manimanis and Emmanuel Danezis
Section of Astrophysics, Astronomy and Mechanics, Department of Physics, University of Athens

Abstract: The development of astronomy was, and still is, a continuous creation of both observations and theoretical calculations. This development continued even after astronomy's flourishment during the Classical and Hellenistic era of antiquity. It did not stop neither during the years of the Roman Empire, nor during the years of the Byzantine Empire.

In addition the important contribution of Arab astronomers must be presented, since it is in general unknown in the West. The Arabs offered much to astronomy during their hey-day and up to at least A.D.1600. Until the 16th Century A.D. the Arabic world was the world of Science, while nothing analogous existed in Europe which could be compared with the developments in the Arabic/Islamic world.

The Arabs assisted the transfer of the ancient Greek knowledge in the West. This knowledge first became known from the Arabic translations and subsequently from the prototype Greek texts (the ones that had not been lost). Moreover, the Arab scholars and scientists, along with the Christian scholars of Byzantium, contributed to the prosperity of science, art, medicine and philosophy for at least five centuries and in the large area from Ispahan to Sicily and Spain.

[*] *Proceedings of the 6th Hellenic Astronomical Society Conference , 15-17 September 2003, Penteli, Greece*

PAPERS POSTED DURING THE SESSION ON HISTORY OF ASTRONOMY & TEACHING OF ASTRONOMY*

ASTRONOMY IN BYZANTIUM AND THE WEST UNTIL COPERNICUS

Efstratios Theodossiou and Vassilios N. Manimanis
Section of Astrophysics, Astronomy and Mechanics, Department of Physics, University of Athens

For centuries before Nicolaus Copernicus (1473-1543) astronomy did not show any pioneering scientist, neither in Byzantium nor in Western Europe. Nevertheless, it is a fact that astronomical knowledge was preserved in Byzantium and that the Byzantines commented on and preserved many works of ancient Greek scholars. Especially eminent was the work of Nikephoros Gregoras (1295-1359), who is probably the greatest astronomer of the Byzantine era. Of course, one should not overlook other eminent astronomers of this period, such as Gregorios Khioniades and Constantine Lykites of Trebizon, and the exceptional figure of Georgios Gemistos or Plethon.

In parallel, at the same times in the West wrote Roger Bacon (1220-1292), Albert the Great (1200-1280), Jean Buridan (14th Century), Nicole d' Oresme (1323-1382), Nicolaus Cuzanus (1401-1464) and others. These scientists were the scholars who, after studying the ancient texts, gave with their works the necessary thrust to science in the Medieval Europe. With their astronomical writings, they essentially questioned the authority of Aristotle and the geocentric system, while they rekindled the ideas of Aristarchus about the heliocentric theory.

COSMOGONY AND COSMOLOGICAL VIEWS OF THE ANCIENT GREEKS AND OF THE ANCIENT EASTERN CIVILIZATIONS

Efstratios Theodossiou
Section of Astrophysics, Astronomy and Mechanics, Department of Physics, University of Athens

Abstract: From the most ancient times humans worshipped the cosmic duality of god Sun and mother Earth. Yet, in parallel his worship turned also towards the divine two, Heaven and Gaia/Earth, who were the first divine pair. The basic philosophical question was: who occupies the center of the universe, the Sun or the Earth?

At the same times were developed the cosmogony ideas of both the ancient Eastern people and the ancient Greeks. The other basic questions, what or who created the universe, the world in which they lived, ought to be answered. Almost all cosmologies of the Eastern people and the ancient Greeks accept the initial cosmic chaos, a formless entity without structure, an abyss or a non-decorated space. From this chaos was created the cosmic egg. The explosion of the cosmic egg, in conditions similar to these of the Big Bang, generated the whole Creation. The meaning of the cosmic egg in the cosmogony myths of all people corresponds to the symbol of totality from which the whole world comes from.

* *Proceedings of the 6th Hellenic Astronomical Society Conference , 15-17 September 2003, Penteli, Greece*

*PAPERS POSTED DURING THE SESSION ON HISTORY OF ASTRONOMY & TEACHING OF ASTRONOMY**

ASTRONOMICAL VIEWS OF THE ANCIENT EASTERN CIVILIZATIONS AND OF THE ANCIENT GREEKS

Efstratios Theodossiou
Section of Astrophysics, Astronomy and Mechanics, Department of Physics, University of Athens

The shape of the universe (of our world) is concrete for the ancient Eastern people, as well as the positions and the forms of Heaven and Earth. The Egyptians believed that the universe had the shape of a rectangular parallelepiped, at the center of which was Egypt, while the heaven was covered by the lengthy body of goddess Nut, or later of the goddess Athor, the divine cow. The sages of India believed that the universe was restrained over the vacuum by a vast snake, which supported a huge sea turtle, upon which were four elephants carrying the Earth on their backs. Similarly, the ancient Jews thought that the Earth was supported by four columns, without mentioning upon what these columns were standing.

The Homeric Earth was a flat circular disc surrounded by a vast, roughly circular river, the Ocean. The sky was a metallic dome made of copper or iron, supported by either columns or the Titan Atlas. For this reason the heaven in the Homeric epics is described as polychalkos and iron-made; however it is also full of life, offered by the stars that decorate it.

ΟΙ ΚΟΣΜΟΓΟΝΙΚΕΣ ΑΠΟΨΕΙΣ ΤΩΝ DOGON

Μανιμάνης Βασίλειος και Θεοδοσίου Στράτος
Τομέας Αστροφυσικής-Αστρονομίας και Μηχανικής, Τμήμα Φυσικής-Πανεπιστήμιο Αθηνών

Οι κοσμογονικές απόψεις των Dogon μιας νέγρικης φυλής στο Μάλι της Δυτικής Αφρικής για τη δημιουργία του Σύμπαντος παρουσιάζουν πολύ μεγάλο ενδιαφέρον γιατί εμπεριέχουν γνώσεις από τη σύγχρονη Αστρονομία. Οι γνώσεις τους αυτές έγιναν γνωστές στην επιστημονική κοινότητα όταν ο Γάλλος εθνολόγος Marcel Griaule και η συνεργάτις του Germain Dieterlen, τη δεκαετία του 1930, ηγήθηκαν μιας εθνολογικής-ανθρωπολογικής αποστολής στα χωριά τους και έζησαν μαζί τους τουλάχιστον για 20 έτη. Οι μύστες της φυλής του αποκάλυψαν τις μυστικές και απόκρυφες γνώσεις της φυλής. Έτσι, σήμερα γνωρίζουμε ότι οι πρωτόγονοι αυτοί κάτοικοι του Μάλι, γνωρίζουν πράγματα που «κανονικά δεν θα έπρεπε να ξέρουν».

Ανάμεσα στις ιδιόμορφες γνώσεις τους ξεχωρίζει η γνώση για την ύπαρξη του -αόρατου με γυμνό μάτι- συνοδού του λαμπρού αστέρα Σείριου, του Σείριου Β. Μήπως αυτοί οι μάλλον πρωτόγονοι κάτοικοι του Μάλι υπήρξαν κληρονόμοι μιας ξεχασμένη γνώσης;

* *Proceedings of the 6th Hellenic Astronomical Society Conference , 15-17 September 2003, Penteli, Greece*

*PAPERS POSTED DURING THE SESSION ON HISTORY OF ASTRONOMY & TEACHING OF ASTRONOMY**

STUDENTS' MISCONCEPTIONS ON BASIC ASTRONOMICAL MEANINGS

Aik. I. Flogaiti
University of Patras, Department of Physics, Sector of Theoretical and Mathematical Physics, Astronomy and Astrophysics

Abstract: This project concerns to the research of the basic knowledge of the students who are studying Physics and Mathematics in order possible astronomical misconceptions to be proved. The students had to answer a multiple choice questions referred to the basic knowledge of Astronomy. The analysis took place after considering the department of their studies (Physics or Mathematics), the sex, the environment of their living and studying and the resource of their knowledge (school, media and internet). Having in mind that this research refers to students who have just entered the University or some who had not attended any of the Astronomy lessons up to that moment, the results of the analysis give a picture of the knowledge that young people gain from their studies at Lyceum and, in general, the efficacy of education in Greece.

ATTALUS: AN UNKNOWN RHODIAN ASTRONOMER

Antonis. D. Pinotsis
Section of Astrophysics, Astronomy and Mechanics, Department of Physics, University of Athens

Abstract: In this work we study Attalus who was a not very well known Rhodian astronomer. The scientific work of Attalus is generally unknown since neither his texts (books) nor sufficient information about him from other writers have survived into modern times. We focus on giving a sketch of his scientific work based on secondary ancient sources (Pinotsis 1999)**.** Attalus was a Rhodian astronomer, mathematician and grammatical of the Alexandrian period. He lived and acted in Rhodes the 2nd B.C. century being thus contemporary with Hipparchus of Rhodes. He wrote comments in favour of the eminent poem (book) Phaenomena of the astronomer, poet and mathematician Aratus (315-240 B.C.). In these comments Attalus defended Aratus using scientific arguments as well as the famous astronomer and mathematician Eudoxus of Knidus against the criticisms from certain contemporary astronomers and mathematicians. Hipparchus seriously considered Attalus' comments and arguments which he also mentions repeatedly. After studying the relevant references we conclude that Hipparchus distinguished Attalus among all those studied and written comments on the Phaenomena of Aratus many of them being eminent mathematicians. Apparently Hipparchus highly appreciated Attalus and had strong sympathy for him because he was a serious and careful scientist and also because of his deep knowledge of astronomy and mathematics. In conclusion Attalus without doubt occupied a distinguished place among the scientists and philosophers of that period.

* *Proceedings of the 6th Hellenic Astronomical Society Conference, 15-17 September 2003, Penteli, Greece*

THERMAL OUTFLOWS IN GENERAL RELATIVISTIC MHD*.

Z. Meliani [1,2]; C. Sauty[1,2]

[1]*Université de paris 7, APC, 2 Place Jussieu, F-75005 Paris, France*

[2] Observatoire de Paris, LUTH, 92190 Meudon, France

Abstract: We study steady axisymmetric flows of a relativistic ideal magnetohydrodynamical (GRMHD) fluid in the magnetosphere of a Schwarzschild black hole surrounded by an accretion disk. We present a relativistic extension of meridional-self-similar models of jets outflowing from a hot spherical corona. This method gives a good description of the outflow close to the polar axis, conversely to radial-self-similar models. Using general relativity allows us to extend previous analyses from jets of young stellar objects (YSO) to galactic and extragalactic jets from compact sources. By increasing the mass of the central object, we increase the deep of gravitational potential in the launching region of the outflow which increases relativistic effects. The various solutions obtained for different types of objects tell us that indeed the same mechanisms may explain the acceleration and the collimation on such different scales. Relativistic effects are qualitatively unimportant but play an important quantitative role.

1. INTRODUCTION

The formation of relativistic jets around compact objects is one of the most intriguing and not yet fully understood phenomena observed in nature. Jets are observed in Young Stellar Objects (YSO) (Königl & Pudritz, 2000), Active Galactic Nuclei (AGNs) (Begelman et al., 1984), microquasars (Mirabel & Rodriquez, 1998), and possibly γ Ray Bursts (GRBs) (Mirabel, 2003). Most jets seem to be launched very close the central engine. In the case of YSOs, there is direct observational evidences of this fact (Burrows et al, 1996) as well as in some microquasars (Mirabel, 1998). Another evidence that the outflow may originate relatively close to the central object is that the observed asymptotic velocity of the jet is of the order of the escape speed at the vicinity of the central engine (see Livio, 1999).

In the last thirty years analytical and numerical studies of the formation and the propagation of jets have been developed to understand the mechanisms for their acceleration, their collimation and their asymptotic behavior (see Livio, 1999). The formation of collimated jets seems to be closely related to the presence of large scale magnetic fields and the existence of the gaseous disk around the central object (Königl & Pudritz, 2000; Livio, 2002). One of the key model developed extensively has been proposed by Blandford & Payne (e.g. Königl & Pudritz, 2000, for a review). In such disk wind models, ejection comes from the central part of a Keplerian disk where large scale magnetic fields anchored in a rotating disk force the ionized flow to follow the field lines and to accelerate it magneto-centrifugally. Such a model has been extended to (special) relativistic winds and applied successfully to AGN jets (Vlahakis & Konigl, 2003) but neglecting gravity, which may not be valid for the very central part of the ejection. The origin of relativistic jets could also be in the quasi spherical corona of the inner disk has suggested by Das (1999) who explored spherical relativistic winds (1D) but using a pseudo Newtonian gravitational potential. Note, however, that whether it is a coronal wind or a disk wind the accretion disk always remains the ultimate source of energy and matter.

Trying to understand the formation of the jet near the compact object where the contribution of the thermal energy in the initial acceleration may become comparable to magnetic energy, we present here a semi-analytical model of a jet emerging from a spherical corona surrounding the inner part of the compact object. We use a meridional self-similar technique to explore the global structure of the magnetic field, which allows us to describe in

* *Proceedings of the 6th Hellenic Astronomical Society Conference, 15-17 September 2003, Penteli, Greece*

a simple way variations with latitude θ of the different physical quantities.

2. CONSTRUCTION OF THE MODEL

We use the full set of relativistic MHD equations, assuming axisymmetry and a central black hole of negligible rotation. As a consequence, we can use Schwarzschild's metric.

$$ds = \alpha_G^2 dt + \frac{1}{\alpha_G^2} dr + r^2 d\theta + r^2 \sin^2\theta d\varphi \qquad \textbf{(1)}$$

where $\alpha_G = \sqrt{1 - \frac{2\,G\,M_\otimes}{r\,c^2}}$ is the redshift factor which measures the effects of gravity due to the presence of the central object of mass $M_\otimes$.

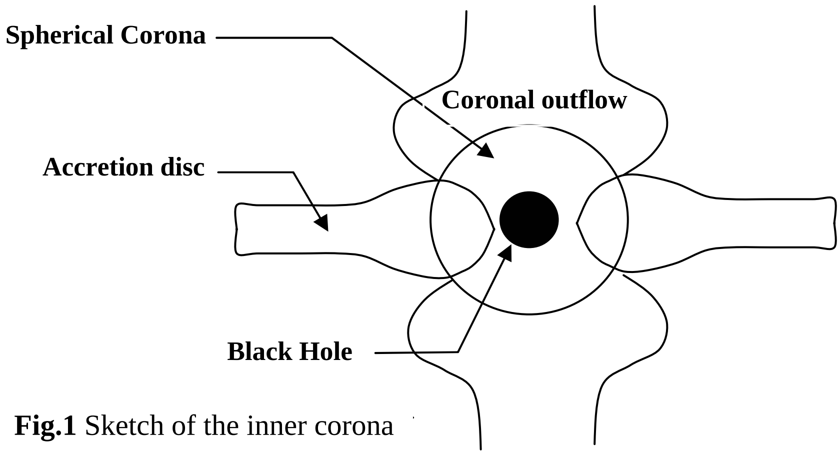

Fig.1 Sketch of the inner corona

We use the 3+1 splitting of space-time. It allows us to construct analytic solutions by separating the variables in the ideal MHD equations. In the 3+1 formalism, Maxwell equations, mass conservation and Euler equation are respectively,

$$\vec{\nabla}.\vec{E} = 4\,\pi\,\rho_e \quad , \vec{\nabla}.\vec{B} = 0, \quad \vec{\nabla} \wedge (\alpha_G \vec{E}) = \vec{0}, \qquad \vec{\nabla} \wedge (\alpha_G \vec{B}) = \frac{4\pi}{c}\alpha_G\,\vec{\Im}, \qquad \textbf{(2)}$$

$$\nabla(\alpha_G\,\gamma\,n\,\vec{v}) = 0 \qquad , \qquad \textbf{(3)}$$

$$\gamma^2\,n\frac{\xi}{c^2}\,\vec{v}\cdot\vec{\nabla}\vec{v} = -\gamma^2\,n\frac{\xi}{c^2}\,\vec{\nabla}\Phi + \gamma^2\,n\frac{\xi}{c^2}\,\vec{v}\,(\vec{v}\cdot\vec{\nabla}\Phi) - \vec{\nabla}P + \frac{1}{c}\vec{\Im}\times\vec{B} - \frac{\vec{v}}{c^2}(\vec{E}\cdot\vec{\Im}) + \rho_e\vec{E}\,. \qquad \textbf{(4)}$$

where $\xi = u + \frac{P}{n}$ is the specific effective enthalpy. This enthalpy represents the global enthalpy including the energy exchanged with the external medium via heating and cooling.

To reduce to a set of ODEs this set of equation, we assume self similarity in the θ direction (see Meliani & Sauty, 2003), recovering in the classical limit the model of Sauty et al. (2002). The splitting of the variables given in the classical case is not possible in the relativistic case because of the existence of the light cylinder which deforms the Alfvén singularity (Breitmoser & Camenzind, 2000). However, if we assume that the coronal outflow is close enough to the rotation axis and that rotation close to this axis is not relativistic, the effect of the light cylinder may be neglected. Then we can assume that the Alfvén Mach number is only a function of the spherical radius, $M(R,\alpha) = M(R)$, as in the classical model. Thus the angular speed (Eq. 5) takes almost the same form as in the classical limit, except for an extra multiplying term corresponding to the space curvature at the Alfvén surface, α_{G_*}. The angular velocity Ω, angular momentum *L*, pressure *P*, density *n* and the specific enthalpy ξ are function of radius *R* and magnetic flux α (N.B. $\gamma = (1 - V^2/c^2)^{-1/2}$ is the Lorentz factor),

$$\Omega = \alpha_{G_*} \frac{\lambda V_* / r_*}{\sqrt{1+\delta\,\alpha}}, \qquad L = \lambda \frac{r_* \gamma_* V_* \xi_*}{c^2} \frac{\alpha}{\sqrt{1+\delta\alpha}}, \tag{5}$$

$$P = \frac{\xi_*}{2c^2} n_* \gamma_*^2 V_*^2 \Pi_{(R)} (1+\kappa\alpha), \qquad \gamma n \alpha_G = \gamma_* n_* \alpha_{G*}^3 \frac{1+\delta\alpha}{M^2_{(R)}}, \qquad \gamma^2 n \xi = \gamma_*^2 n_* \xi_* \tag{6}$$

α_{G_*}, V_*, γ_*, n_* and ξ_* are quantities along the pole at the Alfvén radius.

To be consistent with the rotation law we should also neglect the effect of charge separation and the Ohmic term related to the light cylinder.

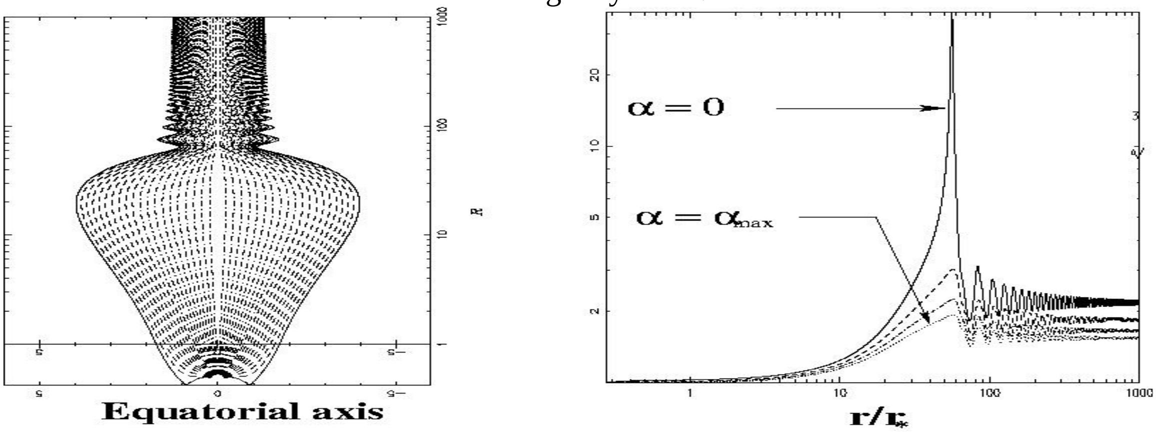

Fig. 2: In (a) morphology of the jet in the poloidal plane. In (b) the Lorentz factor of 4 different streamlines within the jet.

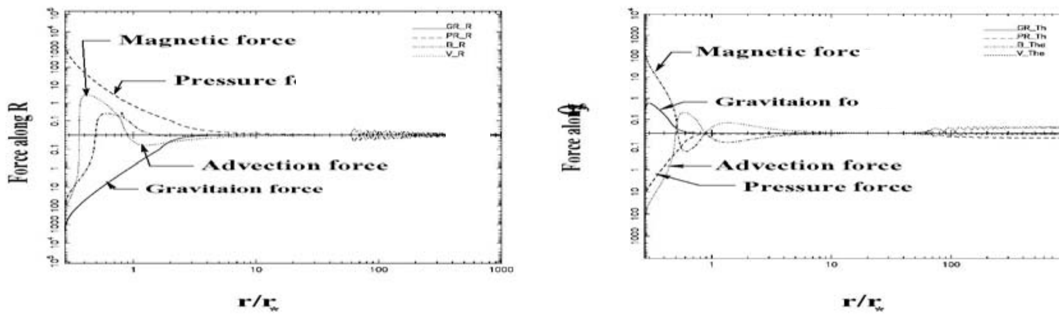

Fig. 3 (a) The force balance in the radial (R) direction along the last streamline of the jet; (b) The force balance in the θ direction along the same streamline.

3. EXAMPLE OF A RELATIVISTIC SOLUTION

We have selected among other one interesting solution of the model with large Lorentz factor comparable to that observed in some AGN, i.e. $\gamma > 10$. The solution has also a small κ (definition in Eq. 6) such that the jet is only weakly thermally confined by the external pressure (Fig. 3) and exhibits an important expansion factor. For this particular solution we have obtained a maximum Lorentz factor at the refocusing point in the outflow of 37. Beyond the recollimation point the Lorentz factor drops to 2 asymptotically (Fig. 2). The acceleration for this solution is of thermal origin as shown in Figs. 3 and 4. Enthalpy is transformed into kinetic energy, the Poynting flux being negligible, consistently with our initial assumption. The Lorentz factor along the axis of the jet is much larger than on the last line closer to the equator (Fig. 2). Thus the model is similar to the double component model proposed by Sol et al. (1989) with a highly relativistic inner jet surrounded by a slower and denser component (see also Tsinganos & Bogovalov, 2002). We note an increase of the thermal acceleration of the outflow when we increase gravity (i.e. when the Alfvén critical surface gets closer to the Black hole). This corresponds to an increase of the thermal energy of the corona to support gravity. Consequently the coronal temperature increases as well as the pressure gradient which accelerates the flow.

After the recollimation point, the collimation of the jet is mainly due to the external pressure and is not magnetic (Fig. 3). However other solutions have been obtained where the magnetic pinching force may be responsible for collimation. The jet radius becomes minimum at the refocalizing point at 1352 Schwarzschild radius from the Black hole. This represents for an AGN of $10^9 M_\otimes$ a distance of 0.13 pc from the central engine. This is rather close to the source but this value strongly depends on the chosen parameters.

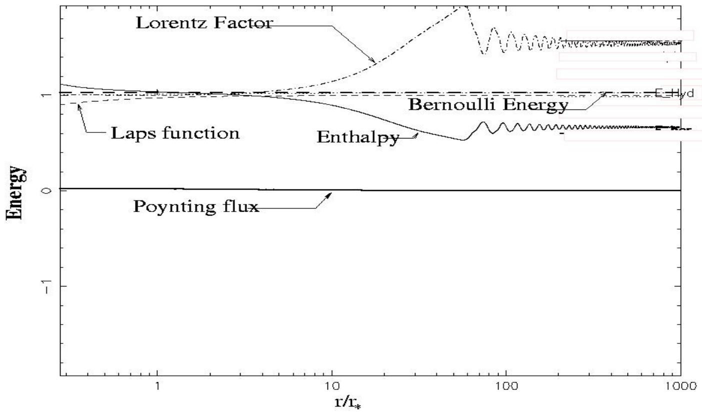

Fig. 4 Display of the different energies along the last streamline

4. CONCLUSION

We have presented here preliminar results of a new 2D self similar model for relativistic outflows from the corona of a Schwarschild black hole including consistently general relativity. This is an extension of previous classical meridionally self-similar solutions. The outflow is mainly thermally driven while collimation is of magnetic or thermal origin. We have selected one interesting solution among other which showes two main features. First the outflow expands almost radially from the source to 1352 Schwarzschild radius and then collimates cylindrically after refocusing. At this point the Lorentz factor reaches a maximum of 37 before the flow decelerates down to a Lorentz factor of only 2. This deceleration on large scale (usually between the parsec and the kiloparsec scale) is typical of FRI jets. We also show that an increase the effect of the gravity in our model leads to an increase of the thermal energy and thus of the efficiency of the acceleration. This is similar to the results obtained in the Parker relativistic wind (Meliani et al., 2004). Note also the diminution of the toroidal component when we increase gravity. This is a consequence of the increase of the thermal driving which gives larger terminal speeds in the flow and pushes the magnetic field lines. This may be correlated to the difference in AGN with fast jets and small toroidal magnetic fields and BL Lac which have slower jets but higher values of their toroidal magnetic field (Gabuzda , 2003).

References

Belgelman M. C. ,Blandford R. D., Rees M., 1984, Rev. Mod. Phy., 56, 255
Burrows C. J. et al, ApJ, 473, 437
Das,T. K., 1999, MNRAS, 308, 294
Konigl A., Pudritz R. E., 2000. In: Mannings V., Boss A. P., Russell S. S. (eds.) “Protostar and Planets IV”, Tucson : University of Arizona Press, p. 759.
Gabuzda D. C. ,2003, A&SS , 288, 39
Livio M., 1999, Physics Reports, 225, 245
Livio M., 2002, Nature, 417, 125L
Mirabel I. F., Rodriquez L. F., 1998, Nature, 392, 673
Mirabel I. F., 2003, NewAR, 47, 471
Meliani Z., Sauty C., 2003, Ap&SS, 287, 1, 241
Meliani Z., Sauty C., Tsinganos K., Vlahakis N., 2004, A&A, submitted
Sauty C ., Trussoni E., Tsinganos K., 2002, A&A, 389, 1068
Sol H.,PelletierG.,Asseo E.,1989,MNRAS,237, 411
Tsinganos K., Bogovalov S., V., 2002, MNRAS, 337, 553
Vlahakis N., Konigl A., 2003, ApJ, 596, 1080

6th ASTRONOMICAL CONFERENCE 2003

LIST OF PARTICIPANTS

Aggelis Evangelos
Aggelis Panagiotis
Akylas Athanassios
Alikakos Ioannis
Anastasiadis Anastasio
AndrikopoulosEvagel.
Antoniou Antonios
Antoniou Valsamo
Antonopoulou Eugenia
Apostolatos Theoch.
Apostolopoulos Pant.
Argyropoulos Stylian.
Arka Ioanna
Athanassoula Evagelia
Avgoloupis Stavros
Avguli Ursula
Basilakos Spyros
Bonanos Alceste
Bonanos Sotirios
Bosma Albert
Boumis Panayoitis
Boutsia Konstantina
Chaliasos Evangelos
Charmandaris Vassilis
Chrysostomou Anton.
Contadakis Michael
Contopoulos George
Dacanalis Aris
Daglis Ioannis
Dallas Efthymios
Danezis Manos
Dapergolas Anastasios
Dara Eleni
Delis Nikolaos
Dialynas Konstantinos
Dimaratou Maria
Dimitrakoudis Stavros
Doxas Isidoros
Efthimiopoulos Christ
Flogaiti Aikaterini
Gavras Panagiotis
Gazeas Kosmas
Georgakakis Antonis
Georganopoulos Mark
Georgantopoulos Ioan.
Georgiou Marina
Georgopoulos Petros
Georgoulis Manolis
Geranios Athanassios
Geroyannis Vassilis
Giannakis Omiros
Giannikakis Ioannis
Giorjiou Konstantinos
Gizani Nectaria
Gontikakis Costis
Goudis Christos
Gradoula Georgia
Grammenos Theophan.
Grosbøl Preben
Hantzios Panayotis
Harlaftis Emilios
Harsoula Mirella
Hatjidemetriou Despina
Hillaris Alexander
Hitzanidis Kyriakos
Ichitiaroglou Symeon
Kakouris Alexandros
Kalapotharakos Konst.
Kallio Esa
Kaltsa Maria
Kalvouridis Tilemahos
Kamaretsos Ioannis
Karanikola Irene
Karastergiou Aris
Katina Maria
Katsanikas Mathew
Katsiyannis Athanas.
Kazanas Demosthene
Kefaliakos Georgios
Kirk John
Kitsionas Spyridon
Kokkotas Kostas
Kontizas Evangelos
Kontizas Mary
Kontogeorgos Athan.
Korogiannis Ioannis
Koukouli Mary-Eliza
Koutoulas Thomas
Kylafis Nikolaos
Laskarides Paul
Lazarides Matthew
Lentis Bassileios
Livanou Evdokia
Lykou Fotini
Lyratzi Valia
Maganari Maria
Makris Demetrios
Malandraki Olga
Manimanis Vassilios
Manousakis Antonis
Marhavilias Panagioti
Mastichiadis Apostol
Matsopoulos Nicolao
Mavridis Lysimachos
Mavromatakis Fotis
Mavromichalaki Hele
Meliani Zakaria
Metallinou Fiori-Ana
Mitsakou Eleftheria
Moraitis Kostas
Moschovitis Vassilis
Moussas Xenophon
Nanouris Nikos
Nikolopoulou Aggel.
Nikolopoulou Aikater
Nikolaou Ioulia
Niarchos Panagiotis
Niarchou Anastasia
Nikolaidis Dimitris
Papadimitriou Christos
Papadopoulos Nikolaos
Papasotiriou Panayotis
Patsourakos Spiros
Papadopoulos Gregorio
Papaspirou Panagiotis
Patsis Panagiotis
Perivolaropoulos Leand
Persides Sotirios
Petoussis Vlassis
Petrie Gordon
Petsori Dimitra
Pinotsis Antonis
Plainaki Christina
Plionis Manolis
Pothitakis George
Poulou Victoria
Preka- Papadema Pana
Pyrlis Orestis
Resvanis Leonidas
Romeou Zaharenia
Rigos Alexandros
Rokaki Evlambia
Roumelioti Eleni
Rovithis Helen
Rovithis Petros
Sarlanis Christos
Sauty Chistophe
Seiradakis John-Hugh
Sergis Nikolaos
Skokos Charalambos
Solomos Nikolaos
Souvatzoglou George
Spyrou Nikolaos
Stathopoulou Mariell
Stavrinos Haralambo
Stavropoulos Ioannis
Stergioulas Nikolaos
Strikis Jakob
Theodossiou Efstratios
Tsagas Christos
Tsamparlis Michael
Tsantilas Sotirios
Tsiantis Konstantinos
Tsimilli Maria
Tsinganos Kanaris
Tsironis Christos
Tsiropoula Georgia
Tsitsipis Panagiotis
Tsokaros Antonis
Tsoutsis Panagiotis
Tziotziou Kostas
Varvoglis Harry
Vassiliou Christophoro
Ventura Joseph
Villchez Jose – Manuel
Vlahakis Nektarios
Vlahos Loukas
Voglis Nikos
Wagner Stefan
Xanthopoulos Emily
Xilouris Emmanuel
Zachariadis Theodoss
Zacharopoulou Olga
Zachilas Loukas
Zafiropoulos Basil
Zouganelis Ioannis

Index to Authors